NEW AGE

SECOND EDITION

Abhishek Chitnis

NUCLEAR PHYSICS

An Introduction

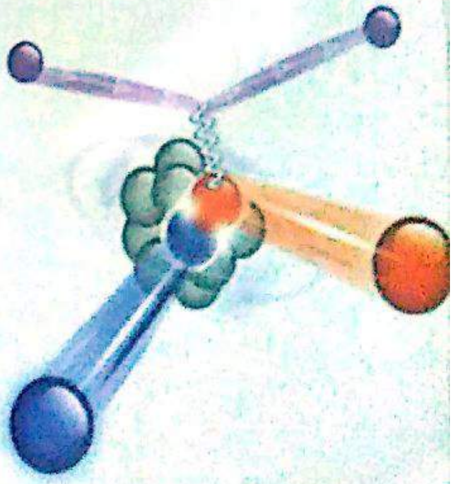

S.B. Patel

NEW AGE INTERNATIONAL PUBLISHERS

NUCLEAR PHYSICS

An Introduction

Second Edition

S.B. Patel
Emeritus Professor
University of Mumbai
Mumbai

PUBLISHING FOR ONE WORLD
NEW AGE INTERNATIONAL (P) LIMITED, PUBLISHERS
New Delhi • Bangalore • Chennai • Cochin • Guwahati • Hyderabad
Jalandhar • Kolkata • Lucknow • Mumbai • Ranchi
Visit us at www.newagepublishers.com

ABHISHEK V. CHITNIS

Preface to the Second Edition

For the past two decades, this book has received an excellent response from both, students and teachers of Nuclear Physics. Many of its readers have always missed a chapter on the fascinating world of "Elementary Particles". I am very happy to include in this Second Edition, Chapter 10, "Elementary Particles". This meets a long standing demand from the readers and attempts to give a flavour of the spectacular progress made in the field of High Energy Physics. This is particularly relevant today as the Large Hadron Collider (LHC) goes on stream at CERN, Geneva. Topics like, anti-particles and anti-matter, fundamental forces of nature, conservation laws, strangeness, isospin, the Quark Model, the QCD and the standard model are included in the discussion. Use of Feynman Diagrams is underlined whenever advantageous to the discussion.

It is hoped that, inclusion of the new chapter would make this book more useful to both, students and teachers of the subject. I would like to express my deep sense of gratitude to all the colleagues and students who have given vital inputs and encouraging response to this book. I would also like to thank the publishers, New Age International (P) Limited, for their very positive involvement and great patience with me. I sincerely hope that the book continues to motivate students to take up a study of the important field of Nuclear Physics.

Shriprakash B. Patel
Emeritus Professor,
University of Mumbai, Department of Atomic Energy Centre
for Excellence in Basic Sciences
Vidyanagari Campus, Santacruz (East)
MUMBAI–400 098.

Preface to the First Edition

There are broadly three classes of textbooks in the subject of nuclear physics. In the first type we have books which give an oversimplified introduction to the topic. Most of the books on modern physics give an introduction to nuclear physics and would fall in this category. On the other hand, we have the type which give a formal, advanced treatment of the subject. These books use quantum mechanics extensively. In between these two types, we have the bridge text which fills the gap between a course on modern physics and an advanced, formal treatise on nuclear physics. This book is an effort in this direction.

It is an introduction to nuclear physics suitable for any student who has been exposed to a college level course in modern physics and mathematical competence at the level of calculus and elementary vector analysis. The book is primarily meant to meet the needs of B.Sc. Physics students and those M.Sc. students who take a general course in nuclear physics. However, it can be used with advantage to motivate M.Sc. students wishing to take up a serious study of nuclear physics.

In the light of the author's long experience of teaching, both at the B.Sc. and M.Sc. levels an attempt is made to treat the topics in a less formal, simple and direct way. Physical ideas are given prominence and this is done by informal discussions and many analogies. For example, particular care is taken in treating the nuclear shell model. Here, the analogy with atomic and molecular physics is taken advantage of. The first chapter is entirely devoted to familiarize students with tools of nuclear physics, both physical and mathematical. This makes the book self sufficient at the level intended. An important feature of the book is illustrative examples given in every chapter. Also a set of problems and questions is given at the end of each chapter. These complement the text and should encourage problem solving habit.

The first chapter, also contains an introduction to modern gamma ray spectroscopy using compton-suppressed germanium detectors. The last chapter is devoted to an introduction to the NMR and Mössbauer techniques, which have originated from nuclear physics and are now widely used in different branches of science. Throughout this text of limited size, an attempt is made to sustain student's interest and he is motivated to read further. Excellent references are given at the end. It is hoped that this book will meet the needs of an introductory course in nuclea physics, both at the B.Sc. and M.Sc. levels.

The author wishes to thank all those who helped to shape this book, particularly the valuabl feedback from many students. Special thanks are due to Prof. R.D. Godbole, former head o the physics department, Ramnarain Ruia College, Bombay for going critically through much o the manuscript and making useful suggestions. Ms. Sridevi Subramaniam, former colleague of mine went through part of the manuscript. I am grateful to her for her comments. Last, but not the least, I am thankful to the publishers, New Age International (P) Ltd. for a nice job and to my colleague, Mr. S. Bose for the art work.

AUTHOR

Contents

Preface to the Second Edition v
Preface to the First Edition vii

1. TOOLS FOR DOING NUCLEAR PHYSICS 1–56

PART–I: PHYSICAL TOOLS

1.I.1 Introduction 1
1.I.2 Interaction Between Particles and Matter: A Brief Survey 2
1.I.3 Detectors for Nuclear Particles 7
1.I.4 Particle Accelerators 22
1.I.5 Beta Ray Spectrometer 33
1.I.6 Brief Account of Counter Electronics: Logic 35

PART–II: MATHEMATICAL TOOLS

1.II.1 Introduction 37
1.II.2 Particle in a One-Dimensional Infinite Square Well 38
1.II.3 One-Dimensional Potential Step 40
1.II.4 Parity 44
1.II.4A Particle in a One-Dimensional Square Potential Well 45
1.II.5 Harmonic Oscillator—Parabolic Potential Well 49
1.II.6 Angular Momentum Operator and its Eigenvalues 50
1.II.7 The Total Angular Momentum Vector $\vec{J}$ 53

2. RADIOACTIVITY 57–90
2.1 Introduction 57
2.2 Properties of Radioactive Rays 58

2.3 The Law of Radioactive Decay 60
2.4 Statistical Nature of Radioactivity 66
2.5 The Statistical Errors of Nuclear Physics 67
2.6 Radioactive Growth and Decay 70
2.7 Ideal Equilibrium 72
2.8 Transient Equilibrium and Secular Equilibrium 73
2.9 Radioactive Series 76
2.10 Radioactive Isotopes of Lighter Elements 81
2.11 Artificial Radioactivity 81
2.12 Determination of the Age of the Earth 84
2.13 Carbon Dating—Archaeological Time Scale 86

3. THE Q EQUATION 91–111

3.1 Introduction 91
3.2 Types of Nuclear Reactions 92
3.3 The Balance of Mass and Energy in Nuclear Reactions 94
3.4 The Q Equation 94
3.5 Solution of the Q Equation 97
3.6 Centre of Mass Frame in Nuclear Physics 105

4. THE NUCLEUS 112–177

PART–I: CONSTITUENTS OF THE NUCLEUS AND SOME OF THEIR PROPERTIES

4.I.1 Introduction 112
4.I.2 Rutherford Scattering and Estimation of the Nuclear Size 113
4.I.3 Measurement of Nuclear Radius 116
4.I.4 Constituents of the Nucleus and their Properties 118
4.I.5 Nuclear Spin, Moments and Statistics 124

PART–II: ALPHA RAYS: SPECTRA AND DECAY

4.II.1 Range of α-Particles 133
4.II.2 Disintegration Energy of Spontaneous α-Decay 137
4.II.3 Alpha Decay Paradox—Barrier Penetration 139

PART–III: BETA RAYS: SPECTRA AND DECAY

4.III.1 Introduction 144
4.III.2 Continuous β-Ray Spectrum—Difficulties in Understanding it 145
4.III.3 Pauli's Neutrino Hypothesis 146

4.III.4 Fermi's Theory of Beta Decay 149
4.III.5 The Detection of Neutrino 160
4.III.6 Parity Non-conservation in Beta Decay 165

PART–IV: INTRODUCTION OF GAMMA EMISSION

4.IV.1 Introduction 168
4.IV.2 γ-Ray Emission—Selection Rules 169
4.IV.3 Internal Conversion 171
4.IV.4 Nuclear Isomerism 174

5. THE LIQUID DROP MODEL OF A NUCLEUS 178–208

5.1 Introduction 178
5.2 Binding Energies of Nuclei: Plot of *B/A* Against *A* 180
5.3 Weizsacher's Semi-Empirical Mass Formula 182
5.4 Mass Parabolas: Prediction of Stability Against β-Decay for Members of an Isobaric Family 190
5.5 Stability Limits Against Spontaneous Fission 196
5.6 Barrier Penetration-Decay Probabilities for Spontaneous Fission 202
5.7 Nucleon Emission 205

6. NUCLEAR ENERGY 209–229

6.1 Introduction 209
6.2 Neutron Induced Fission 210
6.3 Asymmetrical Fission—Mass Yield 211
6.4 Emission of Delayed Neutrons by Fission Fragments 214
6.5 Energy Released in the Fission of ^{235}U 216
6.6 Fission of Lighter Nuclei 217
6.7 Fission Chain Reaction 218
6.8 Neutron Cycle in a Thermal Nuclear Reactor 220
6.9 Nuclear Reactors 225

7. THE SHELL MODEL OF A NUCLEUS 230–267

7.1 Introduction 230
7.2 The Evidence that Led to the Shell Model 233
7.3 Main Assumptions of the Single-Particle Shell Model 237
7.4 Spin-Orbit Coupling of an Electron Bound in an Atom 238
7.5 Spin-Orbit Coupling in Nuclei, for a Single Particle Shell Model 242
7.6 The Single Particle Shell Model—Parabolic Potential 244

7.7 The Single-Particle Shell Model—Square Well Potential 247
7.8 Predictions of the Shell Model 250
7.9 The Collective Model of a Nucleus 251

8. NUCLEAR FORCE 268–290
8.1 Introduction 268
8.2 The Ground State of the Deuteron 269
8.3 Magnetic Dipole and Electric Quadrupole Moments of the Deuteron 270
8.4 Square Well Solution for the Deuteron 271
8.5 Central and Non-Central Forces: The Tensor Force as an Example of Non-Central Forces 277
8.6 Exchange Forces: Meson Theory of Nuclear Force—A Qualitative Discussion 279
8.7 Qualitative Features of Nucleon–Nucleon Scattering 285

9. NUCLEAR PHYSICS IN OTHER AREAS OF PHYSICS 291–315
9.1 Introduction 291
9.2 The Technique of NMR (Nuclear Magnetic Resonance) 291
9.3 Some Experiments with NMR 298
9.4 The Mössbauer Effect 303
9.5 Some Experiments Using Mössbauer Effect 306
9.6 Natural Fusion—Energy Production in Stars 311
9.7 Possibility of Controlled Fusion 313

10. ELEMENTARY PARTICLES 316–343
10.1 Introduction 316
10.2 Antiparticles and Antimatter 317
10.3 Feynman Diagrams 320
10.4 Estimation of a Pion Mass 321
10.5 The Four Fundamental Forces of Nature 324
10.6 W Bosons and Gluons 325
10.7 Conservations Rules 326
10.8 The Nucleon Isospin 329
10.9 The Gell-Mann-Nishijima Relation: Isospin of Particles 330
10.10 The Quark Model 332
10.11 The "Beauty" and "Truth" 336
10.12 The Generations of Matter 336
10.13 The QCD—Colour Quantum Number 337
10.14 Colours for Quarks and Gluons 338

10.15 Why We Do Not See Free Quarks or Colour Particles? 339
10.16 The Standard Model: Quest for the Grand Unified Theory (GUT) 339

Appendix I: Fundamental Constants and Conversion Factors **345–346**
Appendix II: List of Elements **347–348**
Appendix III: Masses of Neutral Atoms **349–358**
Appendix IV: The Concept of Cross-Section for a Nuclear Reaction **359–361**

BIBLIOGRAPHY **363–364**
INDEX **365–372**

1

Tools for Doing Nuclear Physics

> "Science clears the fields on which technology can build."
>
> —*Werner Heisenberg*

PART–I: PHYSICAL TOOLS

1.I.1 INTRODUCTION

Imagine the plight of a hiker on hills not having a can-opener or knife to open cans of food. It is a terrible experience to be stranded without proper tools. In understanding nuclear physics also we need tools. During the past 100 years, many ingenious and powerful tools have been invented. Some of them have no longer remained part of nuclear exploration alone, but have acquired wide applications in fields like chemistry, biochemistry, biophysics, atomic and molecular physics and so on. For example, the technique of Nuclear Magnetic Resonance (NMR), which has its origin in Nuclear Physics, is increasingly being used in areas other than Nuclear Physics. In Chapter 9 we will consider some techniques of Nuclear Physics widely used in other areas of science.

It is equally important to learn the skills of using some mathematical tools, particularly some elementary wave mechanics, without which it is impossible to appreciate and understand Nuclear Phenomena. To familiarise the students with these tools, this chapter has been divided into two parts. Part I deals with Physical Tools like nuclear radiation detectors, accelerators, spectrometers, etc. On the other hand, Part II deals with Mathematical Tools like wave mechanics of a particle in a potential barrier or well. Both these parts deal with basic tools essential to the understanding of Nuclear Physics.

1.1.2 INTERACTION BETWEEN PARTICLES AND MATTER: A BRIEF SURVEY

The design of a nuclear radiation detector depends on our understanding of passage of radiation through matter. Strictly, this is governed by Atomic Physics. However, because of its importance in the design of nuclear detectors, we shall outline its main features.

When a collimated beam of monoenergetic particles passes through a piece of matter, there are two extreme cases of interest: (*i*) In the first case, a particle undergoes many interactions, every time losing a small amount of energy and suffering a small-angle scattering; (*ii*) In the second case the particle either passes unharmed through the material or is removed from the beam in one single 'catastrophic' encounter. These two cases are depicted in Figs. 1.I.1 (a) and (b).

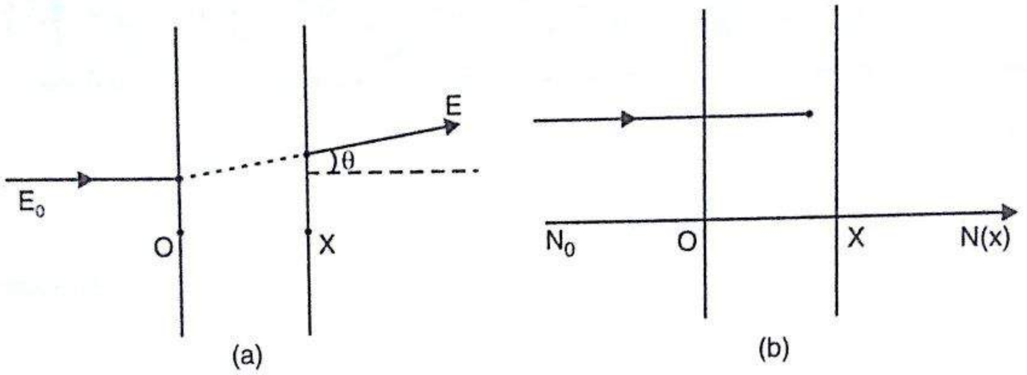

Fig. 1.I.1. Passage of a collimated beam of particles through matter.
(*a*) Each particle undergoes many interactions.
(*b*) A particle is either removed from the beam or passes unharmed.

We shall consider these two cases in some detail.

(*i*) When a particle undergoes many interactions, it progressively loses energy. A monoenergetic beam of such particles will show an energy spread as shown in Fig. 1.I.2.

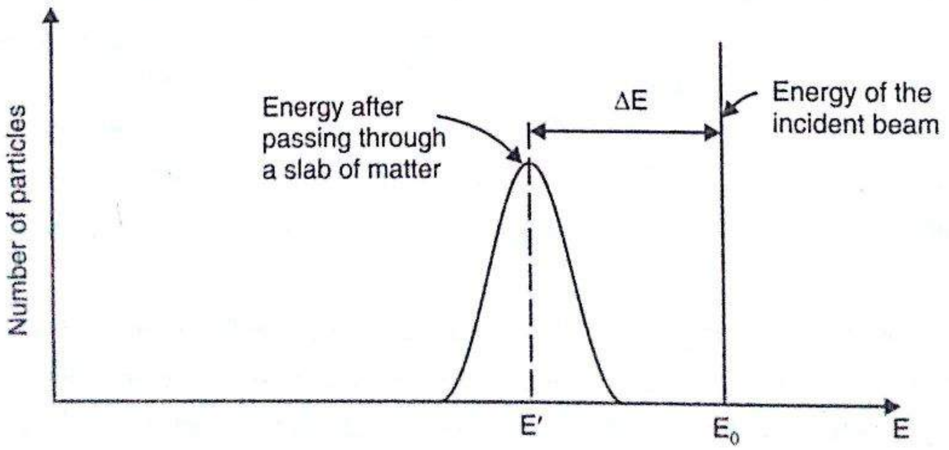

Fig. 1.I.2. Energy spread of a beam of monoenergetic, heavy and charged particles after passing through a slab of matter.

Figure 1.I.3 shows the behaviour of a number of particles transmitted through an absorbing piece of matter as a function of the absorber thickness.

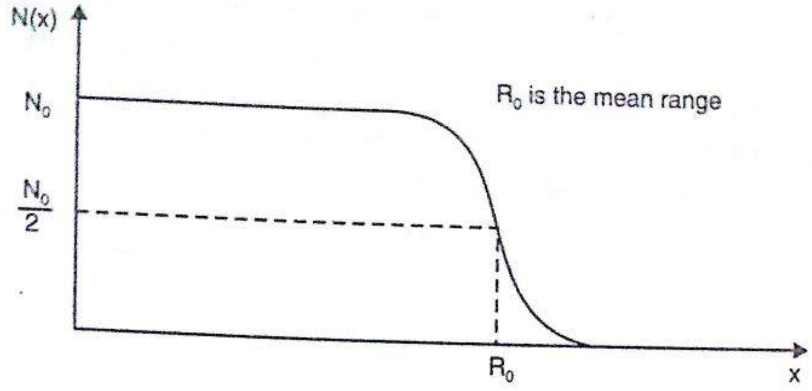

Fig. 1.I.3. Existance of range for a beam of heavy charged particles.

Clearly, all particles are transmitted up to a certain thickness. At a thickness R_0, half the particles get stopped. R_0 is the *mean range.* At a sufficiently large thickness, all particles get stopped. The fluctuation in range is called *straggling.*

Heavy charged particles like a proton, α-particle, fission fragment, etc. fall in this category. They all have a fairly definite *range* in a gas, liquid or solid. We repeat that the energy loss occurs in a large number of small interactions. The particle has such a large momentum that its direction is not significantly changed during its slowing process (see Fig. 1.I.1). The energy loss is mainly due to the excitation and ionisation of atoms in its path. These heavy charged particles lose more energy per unit length of the path near the end of their range, since they are moving more slowly and have more time to interact with the atoms which they pass by. This enables us to assume that the energy loss per unit length of the path is inversely proportional to the velocity, v.

$$\therefore \qquad \frac{-dK}{dx} = \frac{C}{v}$$

where C is a constant that depends on the absorbing material. For heavy charged particles like an α-particle, we can say: $K = \frac{1}{2}mv^2$ = kinetic energy.

$$\therefore \qquad -mv\frac{dv}{dx} = \frac{C}{v}$$

Let R be the range of the particle. Therefore, for $x = 0$, $v = v_0$ and for $x = R$, $v = 0$. Separating the variables we have,

$$\int_{v_0}^{0} -mv^2\, dv = \int_{0}^{R} C\, dx$$

This gives,

$$\frac{mv_0^3}{3} = CR$$

or

$$v_0^3 = C'R \qquad \ldots(1.I.1)$$

where C' is another constant depending on the absorbing material. Equation 1.I.1 is *Geiger's* rule. This rule is approximately correct for any charged, heavy particle in any medium and explains how the range R is related to the particle's energy. The measurement of the range of a heavy charged particle is a common method for measuring its energy. Figure 1.I.4 shows the ranges of α-particles and protons in air. Notice that the range of α-particle is much shorter than that of a proton with the same energy. This is because the α-particle is slower and is more charged than the proton with the same energy and so, is more ionising.

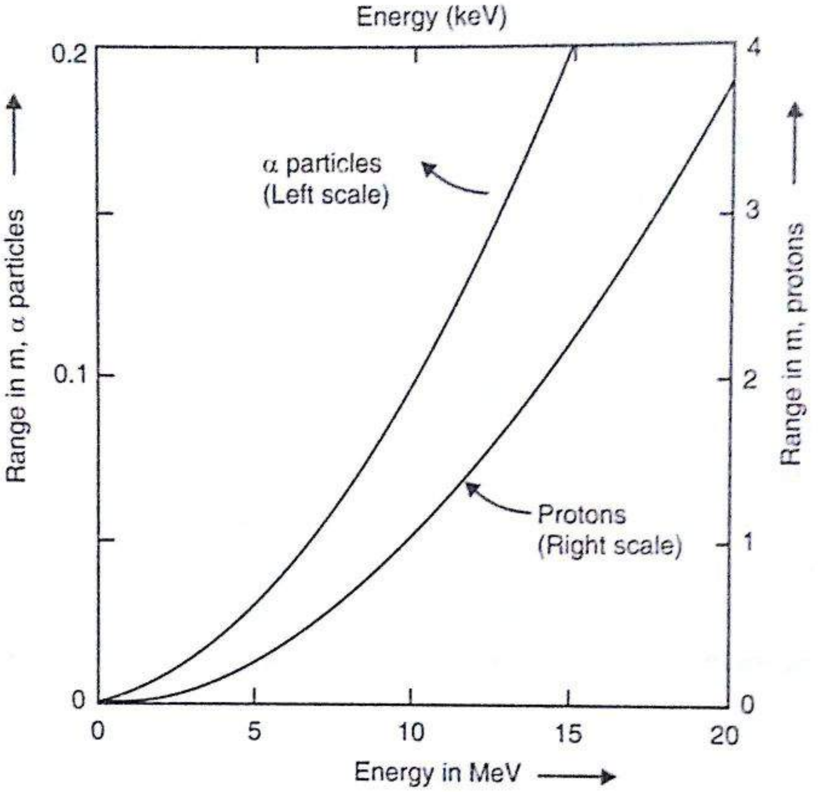

Fig 1.I.4. Ranges of α-particles and protons in air at 15°C and 76 cm Hg pressure. [From *Experimental Nuclear Physics*, Vol. I, E. Segre, ed., Wiley (1953)].

The energy loss rate $-dK/dx$ is called the *stopping power*. It varies from substance to substance because the atomic levels are different and so the energy loss in the ionisation process varies. A more significant factor affecting the stopping factor is the density of the absorber as the number of electrons in a unit volume is roughly proportional to the density. The more the number of electrons per unit volume, the more is the energy loss due to the excitation of these electrons. If we replace $-dK/dx$ by $-\left(\frac{1}{\rho}\right)\frac{dK}{dx}$ where ρ is the density, the stopping powers (now expressed in kg per m^2 of matter traversed) become comparable. For example, the range of 10 MeV protons is about 1.4 kg m^{-2} in air, 1.7 kg m^{-2} in aluminium and 2.1 kg m^{-2} in copper.

(*ii*) Let us now consider the second important case of interaction between a monoenergetic beam of particles and matter in such a manner that a particle in the beam is either unharmed in the absorber or is totally removed from the beam in a single "catastrophic" event (see Fig. 1.I.1).

If an interaction removes the particle from the beam then the features of the transmitted beam are quite different from those described before. Clearly, the transmitted beam has the same particle energy because those particles which have come out of the absorber (or are transmitted) have not undergone any interaction. For every material thickness dx, the number of particles undergoing interactions is proportional to the number of incident particles and so.

$$-\frac{dN}{dx} = \mu N(x)$$

where μ is the constant of proportionality called the *absorption coefficient.* This on integration yields.

$$N(x) = N_0 e^{-\mu x} \qquad \ldots(1.1.2)$$

i.e., the number of transmitted particles decreases exponentially. This is indicated in Fig. 1.1.5.

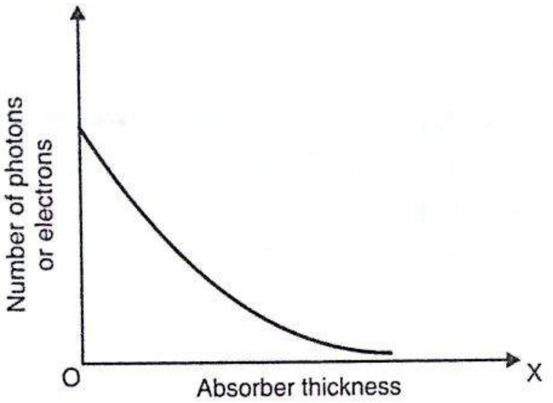

Fig. 1.1.5. Absorption of light particles like photons or electrons by matter.

In this case, no range can be defined, but one can talk about the mean free path defined as the average distance travelled by a particle before undergoing a collision. This mean free path is equal to 1/μ. Photons or electrons approximate this behaviour.

The slowing down of electrons with energies less than 1 MeV is like the slowing down of heavy charged particles. This is mainly due to the ionisation and excitation-collision processes. However, the electron does not exhibit a well-defined range because (*i*) it is much lighter than the proton (the mass of electron is 1/1836 the mass of proton) and so can be easily deflected from the direction of the main beam; and (*ii*) a few collisions are sufficient to stop an electron. At higher energies (K.E. > 1 MeV), the energy loss of an electron is chiefly due to *Bremsstrahlung* (production of continuous X-rays). The probability for this process increases with the energy.

Figure 1.1.6 depicts the Bremsstrahlung process.

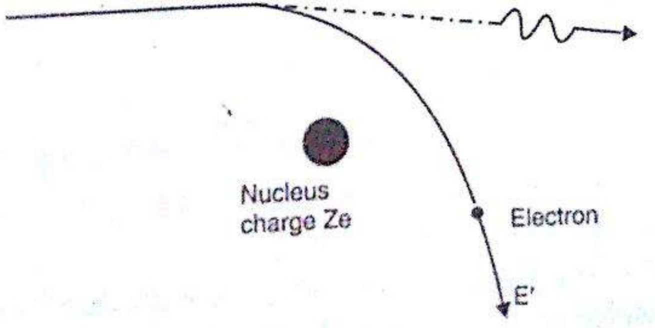

Fig. 1.1.6. The accelerated electron radiates and loses energy in the form of a photon (Bremsstrahlung).

We shall now outline the interaction between photons and matter. Photons interact with matter through three principal processes.

1. Photoelectric effect
2. Compton effect
3. Pair production.

In the photoelectric effect, an atom absorbs the photon and an electron from one of the shells is ejected. In the Compton effect, the photon gets scattered by an atomic electron. In pair production, the photon is converted into an electron positron pair. This last process can occur only in the presence of the nuclear Coulomb field which helps to balance energy and momentum.

The likelihood of the above three processes is energy dependent. At low energies below a few keV the photoelectric effect dominates, the Compton effect is negligible and pair production is energetically impossible.

The rest energy 2 m_0c^2 of the pair is 1.02 MeV, and so the γ-ray must have at least an energy of 1.02 MeV to produce a pair. If the energy of the incident γ-ray is 3.02 MeV, for example, the electron and positron would share 2.00 MeV of kinetic energy. If this kinetic energy can be measured, it would tell us the γ-ray energy.

Equation 1.1.2 is also valid for γ-ray absorption (like for electron absorption).

Recall that this equation is a direct consequence of the fact that photons do not lose energy in small steps; a photon is either scattered out of the beam or is absorbed. The attenuation of a monochromatic beam of photons follows Eq. 1.1.2.

The absorption constant μ for γ photons of various energies is illustrated in Fig. 1.1.7.

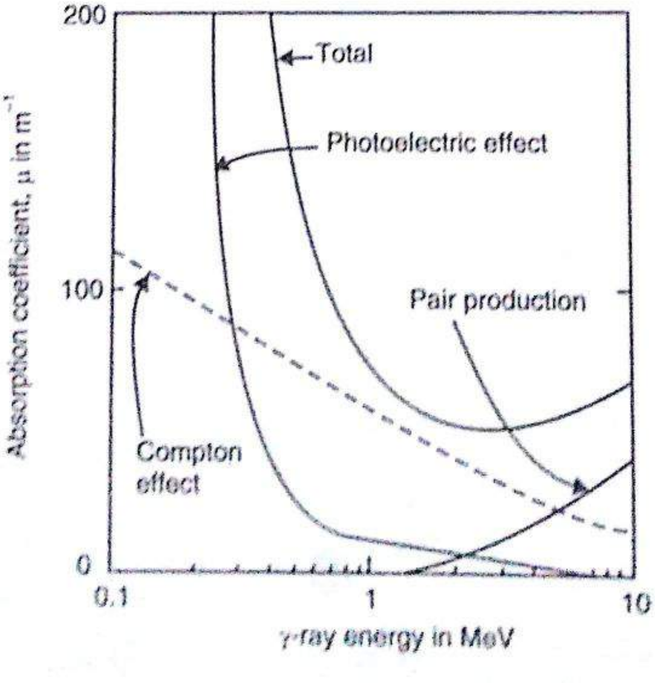

Fig. 1.1.7. Absorption of γ-rays in lead. The 'total' curve is obtained by adding the μ for the 3 important processes. (From W. Heitler, *The Quantum Theory of Radiation*, 3rd Ed., Clarendon Press, Oxford, 1954.)

1.1.3 DETECTORS FOR NUCLEAR PARTICLES

The survey of interaction between particles and matter would help us in understanding features of detectors for nuclear particles. It will be impossible to describe all the different types of detectors in this small section and so, we will stick to some widely and currently used instruments. Ionisation produced by charged particles is the basis for detecting many nuclear particles. In gases, one electron-ion pair is formed for each 30 eV of energy lost by the charged particle. The α-particles and protons, lose energy rapidly by ionisation, and so such particles lose all their energy in the detector. On the other hand, electrons and photons (γ-rays) lose only a fraction of their original energy in a gas-filled detector. Because of its high penetrating power, the γ-ray is particularly difficult to detect.

(i) Proportional Counter

A schematic sketch of the proportional counter is shown in Fig. 1.1.8. It is a metal chamber filled with a gas and having a thin wire (diameter ~ 0.1 mm) axially along the centre. This wire is made anode, by connecting it to a power supply as shown in the figure. A voltage of a few hundred volts which does not cause a discharge is applied between the wire anode and the metal case, which acts as the cathode. Consider now the entry of an ionising particle into the chamber through the thin mica "end window". Electrons produced are attracted toward the central wire anode. The electric field in the vicinity of the fine wire is very large compared to the other regions in the chamber and as a result, an electron near the wire acquires enough energy between two successive collisions with the gas atoms to enable it to ionise gas atoms. This produces additional ion pairs (electrons and positive ions). This process is called *gas amplification* and the number of a ions increases by a factor ~10^4.

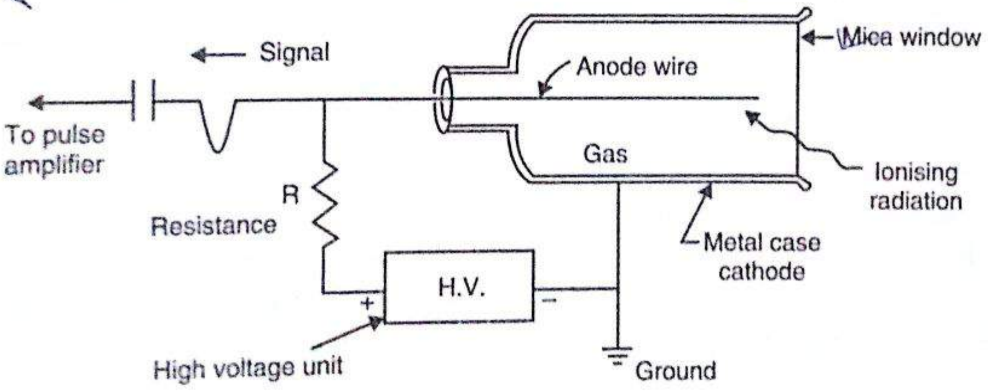

Fig. 1.1.8. 'End window' type proportional counter.

The important fact is that the output pulse of the current is *proportional* to the number of initial ion pairs produced by the ionising particle entering the chamber. That is, the output signal is proportional to the energy of the incident particle. Because of the IR drop across the resistance, the current pulse produces a voltage pulse, which is amplified and recorded.

When a γ-photon enters the chamber, the ionisation occurs mainly due to the emission of electrons from the counter walls. Due to the large penetrating power of gamma rays a γ-ray photon is less likely to produce direct ionisation of gas atoms.

output signal ∝ energy of incident particle

Usually the gas used is a pure noble gas, because electrons then remain free and can be rapidly collected. For counting fast neutrons, a gas containing hydrogen can be used. Due to elastic collisions, protons are produced and can be detected. When slow neutrons are to be counted, the counter can be filled with the gas BF_3. The following reaction takes place:

ost Neutron → H_2 gas

ow Neutron → BF_3

$${}^{1}_{0}n + {}^{10}_{5}B \rightarrow {}^{7}_{3}Li + {}^{4}_{2}He \qquad \text{...(1.I.3)}$$

The ${}^{7}_{3}Li$ and ${}^{4}_{2}He$ atoms move very rapidly and so their electrons are stripped off as they pass through the gas.

(ii) The Geiger Counter - T.Y. Book

The construction of the Geiger Counter is similar to that of the proportional counter (see Fig. 1.I.8). However, the voltage applied to the Geiger Counter is large enough, so that even a single ion pair produced by a single incident particle can produce an electric discharge. Usually, a voltage of about 1000 volts or so for a typical pressure of about 100 mm of mercury is enough to trigger off a discharge when an incident particle enters the Geiger Counter. The important thing is that the electric pulse produced in this discharge is the *same, whatever the energy of the incident particle.*

The anode wire is surrounded by the slow moving positive ion sheath, which reduces the electric field, making the discharge stop within a few microseconds (10^{-6}s). As the positive ion sheath moves away from the anode wire towards the tube's wall (cathode), the value of the electric field rises to permit another electric discharge due to production of electrons when the positive ions hit the wall of the tube. This results in a continuous electric discharge and the tube is not ready to receive another incident particle. *Therefore, some mechanism must be devised to terminate the discharge after each event (Quenching of the counter).*

The simplest method for achieving this is to make the resistor R very large (~10^6 ohms). For a large current (at the time of discharge), this resistance has a large voltage drop (IR drop) which makes the potential difference between the anode and cathode *fall off* to such an extent that the *discharge in the counter cannot be maintained.* However, this has the effect of prolonging the time before the counter can become ready to accept another pulse. This time interval is called the dead time and is of the order of 200 μ sec.

The monoatomic argon, which is transparent to ultraviolet light, is usually used in the Geiger Counters at a pressure of about 100 mm of mercury. It is possible to make these counters self-quenching by mixing argon with a polyatomic molecule such as alcohol. Typically, a Geiger Counter contains about 10 per cent alcohol and 90 per cent argon. This has the effect of ultraviolet photons from the argon getting absorbed by the alcohol so that they do not reach the cathode. Now, as the positive ions move toward the cathode, they collide with alcohol molecules resulting in the transfer of an electron from the alcohol molecule to the argon, neutralising it. The alcohol molecules, upon arrival at the cathode, dissociate rather than eject electrons so that the discharge gets quenched. Such self-quenching by organic molecules results in the dissociation of molecules and after about 10^9 discharges, these molecules are used up necessiating refilling

Electric pulse is independant of the particle's Energy.

of the Geiger Counter. It is possible to use halogen molecules for quenching, their advantage being their tendency to recombine after dissociation.

In conclusion, one can say that the Geiger Counter is a very sensitive device for detecting charged particles and it produces a large pulse requiring no amplification. It suffers from the disadvantages of being quite slow, being incapable of providing information about the type of particle which may have produced a count and its lack of information about the energy of the particle counted.

(iii) Scintillation Counter

One of the early methods used for the detection and counting of α-particles was to make them strike a zinc sulphide screen and then observe the scintillations on the screen through a lens acting as a magnifier. The modern scintillation counter uses a scintillating crystal. Light from the crystal is incident on a photosensitive surface called the photo cathode of a photomultiplier tube. Photoelectrons produced at this photocathode are directed by an appropriate accelerating voltage to the first dynode (anode), where a single accelerated photoelectron can knock out "secondary" electrons. This dynode is the cathode relative to another dynode where more secondary electrons are liberated. This process continues through several stages (about 10 to 14) until the burst of

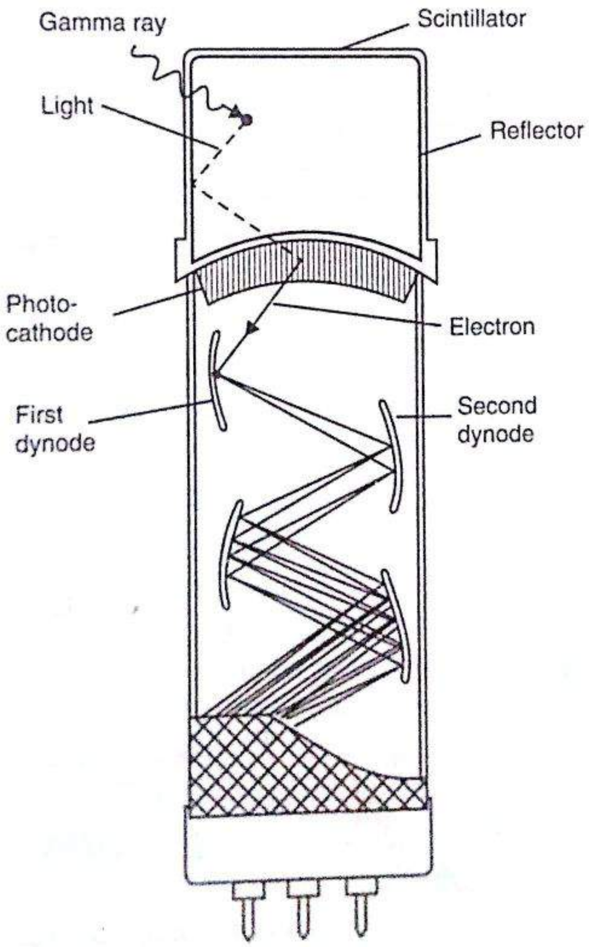

Fig. 1.1.9. Scintillator put on a photomultiplier tube. An overall multiplying factor of up to 10^9 can be achieved.

electrons becomes large enough to constitute an electric pulse that can be further amplified by an electronic amplifier. Pulses from this amplifier are then electronically counted. By this technique individual radiation particles of very low energy can also be counted. Figure 1.I.9 shows a scintillator mounted on a photomultiplier tube. The most important property of such an assembly is that the electric pulses produced are *proportional to the energy* of the incident γ-rays. Thus it is possible not only to detect the γ-rays but to measure their energy as well. A specialised computer like device called a multichannel analyser can sort out the output-electric pulses according to their magnitudes and record the number of pulses of each magnitude entering the instrument. The resulting data constitutes an energy spectrum of the γ-rays penetrating the scintillator crystal.

A typical γ-ray spectrum obtained with ^{137}Cs source is shown in Fig. 1.I.10.

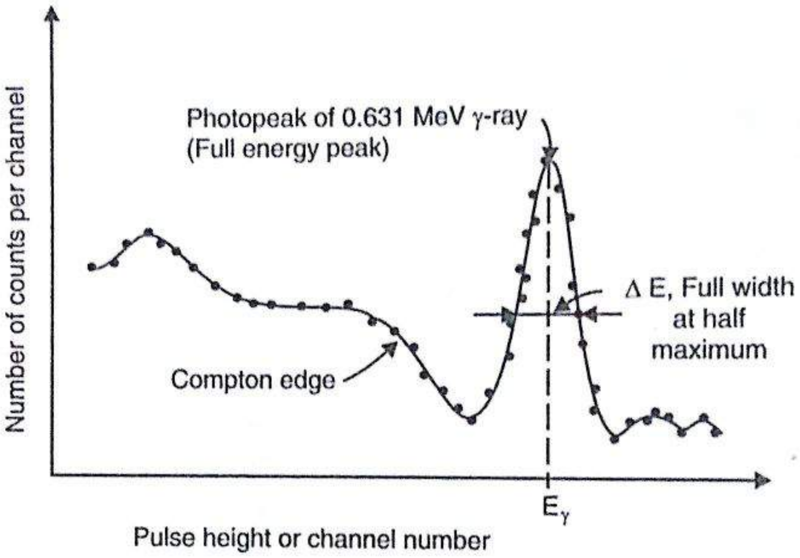

Fig. 1.I.10. γ-ray spectrum of ^{137}Cs. The single photoelectric peak of 0.631 MeV γ-ray follows the Compton edge.

γ-ray being energetic photons (uncharged) have to be indirectly detected. As seen in the previous section, γ-rays interact with matter mainly in three ways: the photoelectric effect, the Compton effect and the production of the positron-electron pair. For γ-ray having an energy of up to 2 MeV, the first two processes are the most important, *but it is the photoelectric effect which is actually utilised.* This is because when a γ-ray produces a photoelectron, the photoelectron has an energy which is essentially the same as the absorbed γ-ray energy. In the photoelectric effect, the γ-ray loses all its energy. Thus all γ-ray of one energy will produce in a scintillating crystal, photoelectrons having the same energy. The amount of light produced in the crystal being proportional to this energy, the electrical pulse obtained from the photomultiplier will also be proportional to the γ-ray energy.

Two types of scintillators are widely used: sodium iodide and plastic. *Sodium iodide* crystals are usually doped with a small amount of thallium and denoted by NaI(Tl). The Tl atoms act as luminescence centres. NaI(Tl) crystals are dense enough to have good efficiency of γ-ray detection but the decay of each pulse is slow (~ 0.25 μ sec) compared to plastic which has a decay time of ~ 10^{-9} sec. However, the γ-ray collection efficiency of plastic is low and so they are mainly used for the detection of charged particles like electrons.

Look at Fig. 1.I.10. The Compton electrons may have any value from zero up to the maximum, which is about 0.22 MeV less than the γ-ray energy (in the energy range of 0.5 MeV to 5 MeV). The Compton electrons are spread out more or less continuously under the photopeak and form a 'background'. The *Compton 'edge'* representing the maximum energy Compton electrons, can be clearly seen in Fig. 1.I.10. The pair production effect is useful for detecting higher energy γ-ray.

A scintillation counter coupled with a multichannel analyser constitutes a γ-ray spectrometer. Such a γ-ray spectrometer must be calibrated using γ-ray of known energy. The width of the full energy peak at half height is called *full width at half maximum, FWHM.* It depends on the number of light photons produced by the incident γ-ray photon. Typically $\Delta E/E_\gamma$ is of the order of 20 per cent at $E_\gamma = 100$ keV and 6 to 8 per cent at $E_\gamma = 1$ MeV (for the NaI detector).

$$\frac{\Delta E}{E_\gamma} = \text{energy resolution.}$$

In many cases, a resolution of about 10 per cent is sufficient. However, in some cases γ-ray energies are so close that a scintillation counter is unable to separate them. One has to then use a semiconductor detector.

(iv) Solid State or Semiconductor Detectors

Before discussing the semiconductor detector, it will be of interest to compare a gamma ray spectrum as seen by a semiconductor detector and by a scintillation detector. Figure 1.I.11 shows the γ-ray spectrum of ^{60}Co (cobalt-60) observed by a germanium detector and a scintillation detector.

The tremendous improvement in energy resolution provided by the solid state, Lithium Drifted Germanium (Ge(Li)) detector has brought these detectors to the forefront since 1960 and in many areas, they have completely replaced scintillation counters.

A solid state detector, like an ionisation chamber, collects and measures the charge liberated by incident radiation. However, it has *two* great advantages over an ionisation chamber using a gas: (*i*) Because of the greater density of solids.

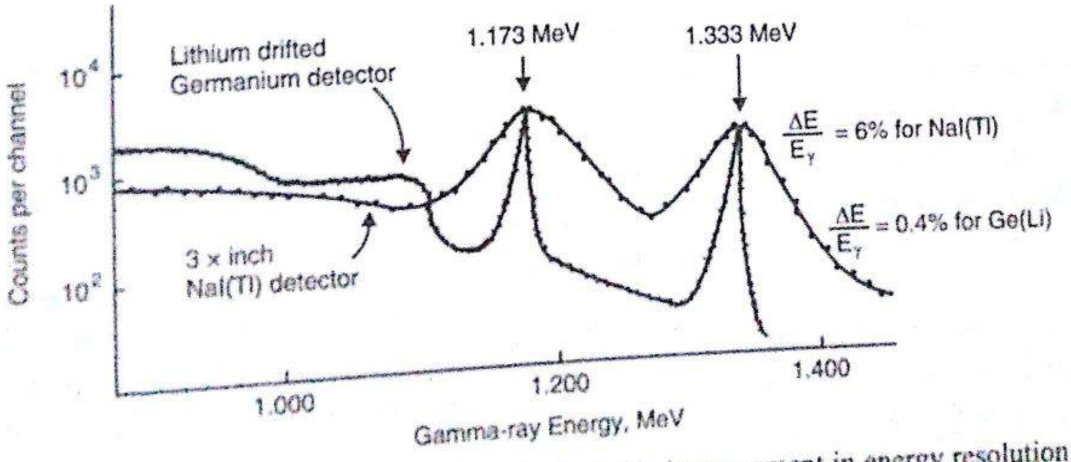

Fig. 1.I.11. Gamma ray spectrum of ^{60}Co. Note the fantastic improvement in energy resolution provided by Ge(Li), (Lithium drifted Germanium detector) compared to NaI(Tl) scintillation detector.

compared to gases they have much greater stopping power for incident radiation. This implies that even for penetrating radiation like γ-ray, a solid state detector can be used. (*ii*) The energy required for the production of an ion pair in solids is much lower than in gases. Let this energy be W. $W = 42$ eV for helium, 22 eV for xenon and 34 eV for air. On the other hand, $W = 2.9$ eV for germanium and 3.5 eV for silicon. The energies are low for these solids because ionisation does not occur from an atomic level to the continuum, but from the valence band to the conduction band. Lower values of W imply higher energy resolution, as is clear from Fig. 1.I.11.

A semiconductor detector is actually a *reverse biased p-n junction.* It is schematically shown in Fig. 1.I.12.

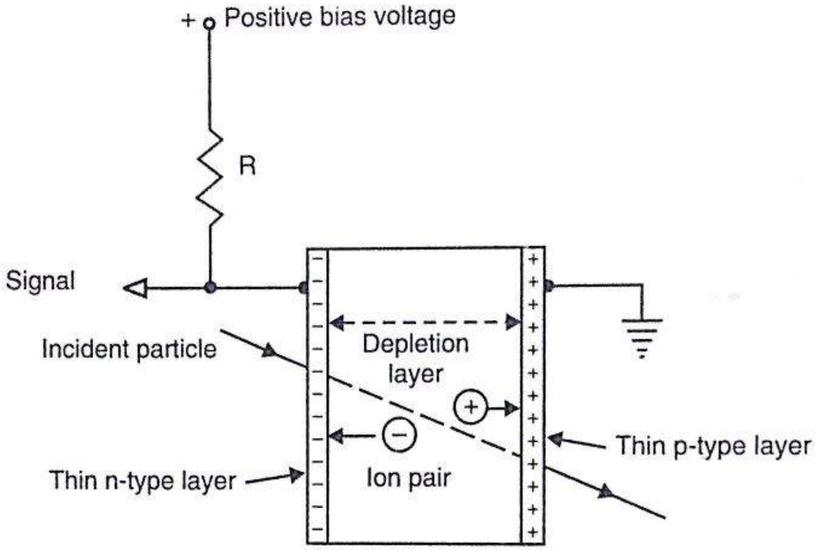

Fig. 1.I.12. An ideal semiconductor detector, showing fully depleted region and thin heavily doped surface layers of opposite types.

When ionising radiation enters the depletion layer which is free from any charges, it produces hole-electron pairs. Because of the smaller value of W compared to gases we have many more ions produced, and hence the statistical fluctuation in the number of ions is much less, resulting in highly improved resolution.

With very pure semiconductor materials, depletion layers of only about 1 mm are attainable. This thickness is enough to stop an α-particle or a proton, but not to stop a γ-ray photon. It was for this reason that an ingenious technique known as lithium drifting was developed.

Usually lithium is diffused into the surface of p-type germanium. The device is then heated (~ 200° C) to increase the mobility of lithium atoms and a reverse bias is applied. Positive lithium ions then *drift* into the depletion layer and *compensate the negative impurities* in the p-type region. Thus, this drift of Li-ions produces a very pure semiconductor region (with no charge carrier) between the n and p-type regions. Depletion layers of several centimetres (7 cm or more) have been produced in this manner, making the detector extremely useful for γ-ray detection as well.

Figure 1.I.13 shows the γ-ray spectrum of 7.5 h ^{171}Er using a 20 cm^3 Ge(Li) detector. The energy resolution is ~0.4 per cent at 1 MeV. Ge(Li)-detectors having volumes up to 100 cm^3

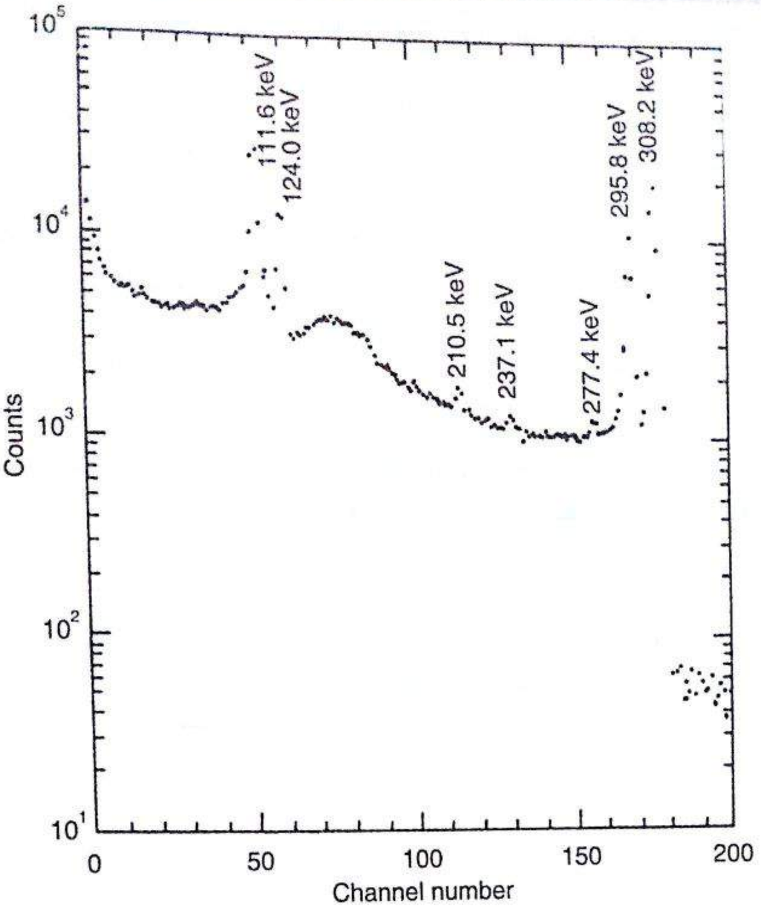

Fig. 1.I.13. γ-ray spectrum of 7.5 h ^{171}Er using a 20 cm^3 Lthium Drifted Germanium, Ge(Li) detector. (S.B. Patel et al., *Phys*., *Rev. C*. Vol. 14 No. 5, 1976.)

have been routinely built. These are particularly useful in high energy physics. Germanium, because of its higher density as compared to silicon, is more suitable for γ-ray detection. However, it has disadvantage: It must be cooled since some hole-electron pairs can be produced by as little as 0.66 eV and at room temperature thermal energies are sufficient to produce such pairs. Ge(Li) detectors are thus thermally connected with a copper finger, the tip of which is always kept dipped into liquid nitrogen.

(v) Compton Suppressed Germanium Detectors

Two recent developments have taken the field of γ-ray spectroscopy by storm. The first is the development of intrinsic germanium detectors made from ultra pure germanium. Large enough depletion layers can be obtained without lithium drifting. Further a compact liquid nitrogen devar arrangement makes it possible to use many detectors together for multiple coincidence work.

The second is the use of anti-Compton shields on the germanium detectors. This makes even the weakest γ-lines to stand out in the γ-spectrum.

These developments have revolutionised our tools for nuclear spectroscopy. Let us therefore look at this new γ-ray detector in some detail.

The primary criterion for a γ-ray detector is that every γ-ray that strikes the detector should result in a voltage pulse, proportional to the original γ-ray energy. Technically, one says that a detector must have a good response function. Unfortunately, a germanium detector does not satisfy this requirement quite well. It has the atomic number $Z = 32$, which is relatively low. Germanium is also moderately dense and it interacts with γ-rays mainly by Compton scattering, for γ-rays in the energy range of about 1 MeV. With about a 20 cm^3 Ge-detector, a 1 MeV γ-rays has an absorption probability of about 3/4. This implies that 1/4 of such γ-rays do not interact at all with the detector. Further, out of those γ-rays which interact with the Ge-detector, only about 15 to 20 per cent give rise to useful full-energy peaks (photo-peaks). This is evident in Fig. 1.I.11. If the area under the γ-rays spectrum is measured, it gives the ratio:

$$\frac{\text{Area under photo-peak}}{\text{Total area}} = \frac{P}{T} \cong 15 - 20\%$$

Thus about 80 to 85 per cent events in the Ge-detector do not correspond to full γ-ray energy, implying a poor response function. Consequently, these majority events (80–85 per cent) form unwanted garbage. This is the story of the γ-ray *singles spectrum.* Often one wants to determine a sequence of γ-rays and so a coincidence measurement has to be performed (see Sec. 1.I.6). Coincidence measurement involving 2 γ-rays is called a doubles coincidence measurement. One involving 3 γ-rays is called a triples coincidence measurement. At least 2 detectors are required for a doubles experiment, 3 for a triples experiment and so on. Consider a double coincidence measurement. Clearly, now 15 to 20 per cent events in each detector give useful full-energy events. Thus, in a doubles coincidence measurement, only 2 to 4 per cent of the total events obtained in the two detectors are good peak-peak values. This implies that the remaining 96 to 98 per cent events are unwanted garbage. This is a horrifying and very undesirable situation.

What is the way out of such a situation? Clearly the small peak to total (P/T) ratio is due to the fact that the Ge-detector interacts with γ-rays primarily by Compton scattering in the energy range of interest. About 80 per cent events are Compton events. Is it possible to take away these Compton events from the γ-rays spectrum? This will increase the (P/T) ratio. The solution is: put Compton-suppression shields around the Ge-detectors.

Figure 1.I.14 shows the outline of a Compton-suppression shield on a Ge-detector. The figure shows a γ-rays photon interacting with the Ge-detector.

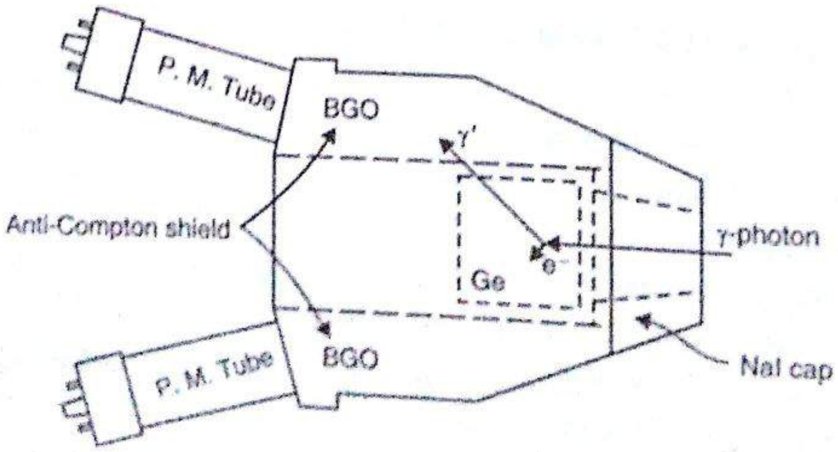

Fig. 1.I.14. Outline of the anti-Compton shield surrounding a Ge-detector. The sequence of events is discussed in the text.

The Compton scattered γ-photon, labelled γ′, is lost if there is no shield surrounding the Ge-crystal. If this shield is made from a scintillator which is sufficiently dense to stop γ′, then the output of the photomultiplier tube gives a signal. This signal is essentially due to the Compton events originating in the Ge-detector. By putting this pulse produced by the scintillator shield in anti-coincidence with the Ge-detector signal pulse it is possible to reject the Compton events produced in the Ge-detector. (See Sec. 1.1.6 to get an idea of about how to get a coincidence signal and an anti-coincidence signal.) This is the reason why the shield is called an anti-Compton or Compton-suppression shield. The scintillator used for such a shield has to be dense enough to stop the Compton scattered γ-rays. Further, its light output should be sufficiently good.

NaI anti-Compton shields were successfully tried first. Large 20 × 25 cm NaI shields were placed on 6 Ge-detecters at Daresbury, University of Manchester. [P.J. Twin *et al.*, Nucl. Phys. A 409, 343 (1983)]. This gave a markedly improved (P/T) ratio: more than 3 times the case without shielding. At Berkeley, shields of bismuth germanate (BGO) were successfully tried for the first time. This material has the chemical formula $Bi_4\ Ge_3\ O_{12}$. Its density is 7.13 gm/cm^2. In comparison, the density of NaI is only 3.67 gm/cm^3. The average atomic number Z for BGO too is higher than NaI. Consequently, this material (BGO) has a γ-ray absorption length 2.5 times smaller than NaI. This means more compact shields, so that more Compton-suppressed detectors can be placed near the source of γ-rays, usually the target kept in the path of an

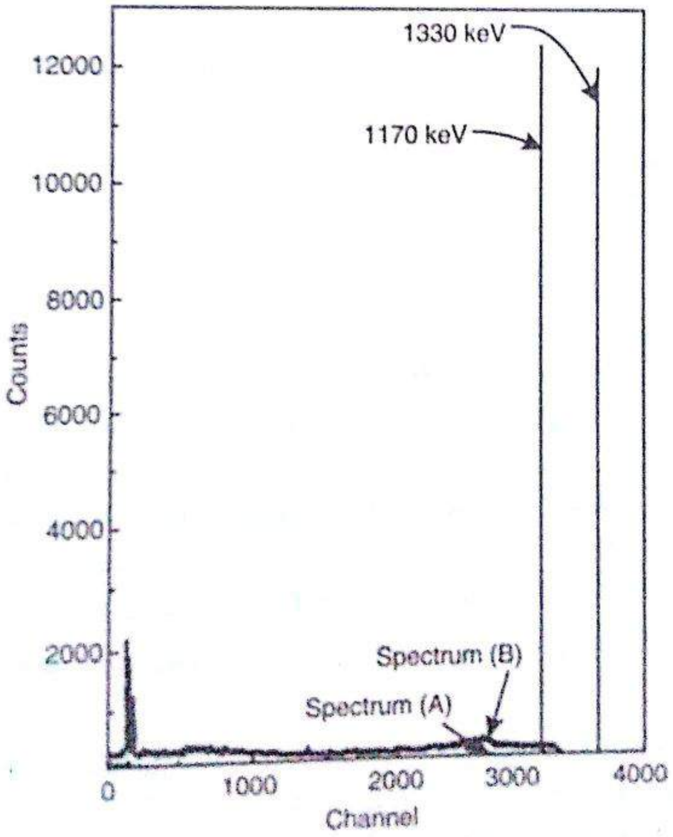

Fig. 1.1.15. ^{60}Co γ-spectrum taken with Compton-suppressed Ge (A) and an unsuppressed Ge (B). The data is without NaI cap in front of the detector. (R.M. Diamond – the Berkeley high resolution ball.)

accelerator beam. Figure 1.1.14 is the outline of the Berkeley BGO Compton-suppression shiel showing a 5 × 5 cm Ge-detector inside. It is actually made of six coaxially mounted BGO section The figure shows only two of the six photomultiplier tubes on the back surface. It also shows NaI cap on the front, tapering portion. This NaI cap is added to suppress the ~180° Compton scattered γ-rays. These γ-rays (~180°) correspond to Compton edges just below the full-energ photo-peaks and so must be removed from the spectrum; otherwise these Compton edges appea precisely where we are interested in having a clean, low-background region in the γ-ray spectrum Figure 1.I.15 shows two γ-rays spectra of ^{60}Co taken with the Berkeley Ge-detector; one (A with a Compton-suppressed (BGO-shielded) Ge and the other (B) with an unsuppressed G detector. Notice that in spectrum (A), the Compton 'hump' is almost not there. The *P*/*T* rati now improves drastically. For spectrum (A) it is,

$$\frac{P}{T} \cong 50 - 60\%$$

For spectrum (B) it is ~ 15–20 per cent. The addition of NaI caps (see Fig. 1.I.14) almos wipes out any remaining Compton edge. The response function of a germanium detector ca thus be seen as drastically improved.

The compactness of BGO shields has made if possible to pack as many as 21 Compton-suppressed detectors at a distance of about 14 cm from the target in the system in operation a Berkeley.

Let us briefly discuss the tremendous advantage of having such an array of Compton-suppressed Ge-detectors. It enables us to greatly improve the resolution of the detector—not single detector but the system as a whole. Today Ge-detectors give the highest resolution possibl about 2 keV at 1 MeV. Of course, with a single detector we cannot have more resolution. T understand this and the effect of more than one Ge-detectors, let us define resolution as th reciprocal of the number of resolvable points. Consider a range of energy 0–1 MeV and assum for the purpose of discussion, a constant resolution of 2 keV. We thus have 500 resolvable point Two γ-rays falling on the same point cannot be resolved. However, in nuclear spectroscopy, w are usually not interested in single γ-rays but members of a γ-ray cascade; e.g., members of rotational band discussed in Chapter 7. If two detectors are used, we can make use of th coincidence relationships between the two γ-rays (which cannot be resolved by a single detector with the other members of their individual cascades. This is shown in Fig. 1.I.16. It is muc less probable that the two pairs of γ-rays coincide than the original two (singles) γ-rays.

For two detectors in coincidence we have a two-dimensional array of points as shown i Fig. 1.I.16, bottom portion.

Notice that the 500 resolvable points of the single detector have now become 500^2 points i the two-dimensional array of two coincident detectors.

Coincidences of a still higher order yield more effective resolution for coincident cascad of γ-rays by greatly increasing the number of possible resolvable points. For instance, a trip coincidence would give us 500^3 possible resolvable points. So there should be as man Ge-detectors as possible close to the target.

With plain Ge-detectors, as remarked earlier, 96 to 98 per cent of the total events are unwanted garbage in a doubles coincidence measurement. With Compton-suppressed Ge-detectors, we have seen that peak to total (*P*/*T*) ratio of over 50 per cent is obtained. In a doubles measurement therefore 50 per cent of 50 per cent *i.e.*, 25 per cent of events are good peak-peak values. The Table 1.I.1 by R.M. Diamond (LBL preprint — 202241, Sept., 1985) shows the advantage of using Ge-detectors, it is possible to establish γ-cascades right up to a spin ~ 50 ħ, by

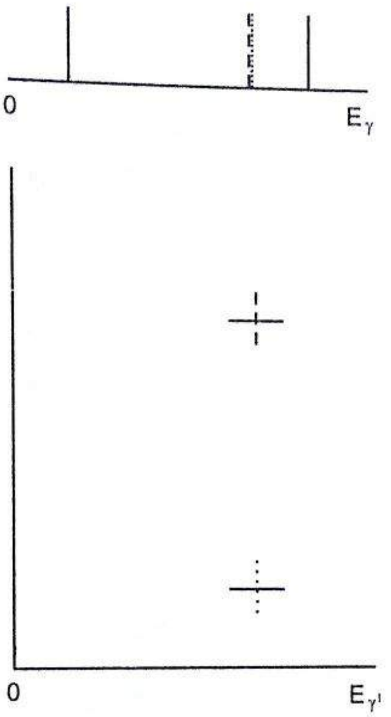

Fig. 1.I.16. The top portion shows how a single detector cannot resolve two γ-rays; they overlap. The bottom portion shows how they can be resolved in the doubles spectrum by their different cascading partners.

TABLE 1.1

Type (order) of coincidences	*Singles* Ge^1	*Doubles* Ge^2	*Triples* Ge^3	*Quadruples* Ge^4
Unsuppressed Ge Peak/Total	20%	4%	0.8%	0.16%
Compton-suppressed Ge Peak/Total	50%	25%	13%	6%
Improvement factor	2.5	6	16	39

Notice that for unsuppressed Ge-detectors full-energy triple coincidences are only 0.8 per cent of the total events, making them unusable. On the other hand, the use of Compton-suppressed Ge-detector gives 13 per cent useable triples. Even quadruple coincidences can be used. Using such an array of Compton-suppressed Ge-detectors, it is possible to establish

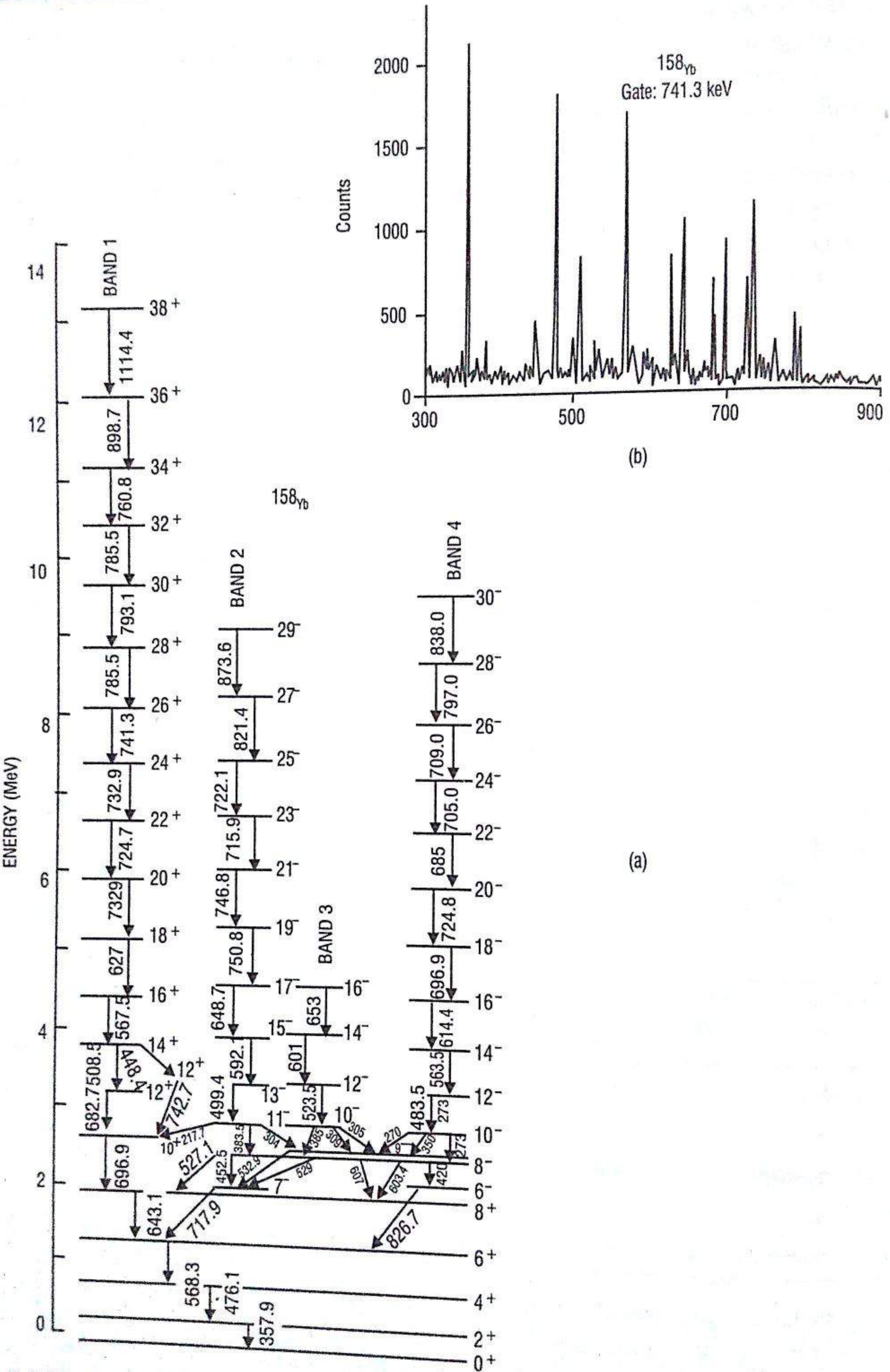
158Yb
Gate: 741.3 keV
Counts
2000
1500
1000
500
0
300
500
700
900
(b)
158Yb
(a)
ENERGY (MeV)
0
2
4
6
8
10
12
14
BAND 1
BAND 2
BAND 3
BAND 4
38+
36+
34+
32+
30+
28+
26+
24+
22+
20+
18+
16+
14+
12+
12+
10+
8+
6+
4+
2+
0+
1114.4
898.7
760.8
785.5
793.1
785.5
741.3
732.9
724.7
7329
627
567.5
508.5
448.
682.7
742.7
696.9
643.1
568.3
476.1
357.9
217.7
527.1
717.9
29⁻
27⁻
25⁻
23⁻
21⁻
19⁻
17⁻
15⁻
13⁻
11⁻
7⁻
873.6
821.4
722.1
715.9
746.8
750.8
648.7
592.1
499.4
452.5
383.5
532.9
304
16⁻
14⁻
12⁻
10⁻
653
601
523.5
385
309
305
529
601
30⁻
28⁻
26⁻
24⁻
22⁻
20⁻
18⁻
16⁻
14⁻
12⁻
10⁻
8⁻
6⁻
838.0
797.0
709.0
705.0
685
724.8
696.9
614.4
563.5
483.5
273
270
350
273
420
603.4
826.7

Fig. 1.I.17. (*a*) Level scheme of ^{158}Yb using the Berkeley array of 21 Compton-suppressed Ge-detectors. (*b*) Coincidence spectrum in ^{158}Yb.

γ-cascades right up to a spin ~ 50ℏ, by detecting γ-rays weakest in intensity. Multiple transitions (of the same energy) can be unambiguously placed in the energy level scheme by higher-order coincidence work. Further, nuclear spectroscopic studies at high spin are possible. In particular, this enables us to study how nuclei carry angular momentum and what are the changes that take place in shape and collective motion with the increase in spin.

Thus a new and exciting approach to nuclear structure studies opens up with the advent of Compton-suppressed Ge-detector arrays. Figure 1.I.17 (a) shows the level scheme of ^{158}Yb studied by using the Berkeley array. Notice that a level with spin 38ℏ is reached. Also, many γ-transitions are multiple. Figure 1.I.17 (b) shows a typical coincidence spectrum in ^{158}Yb. The Compton edges are practically absent.

[Ref: S.B. Patel, *et al., Phy. Rev. Lett.*, Vol. 57, 1 (1986)].

(vi) Cloud and Bubble Chambers

Without doubt these are the most dramatic radiation detectors. The basic principle of their operation is the same: a cloud chamber contains a super-cooled vapour while a bubble chamber contains a superheated liquid. *These detectors enable you to actually 'see' the path of the charged particle and the events taking place along this path.* A simple expansion cloud chamber is sketched in Fig. 1.I.18. It consists of an air tight chamber having a large glass window, so that it can be illuminated and the events can be seen or photographed. The chamber contains saturated vapour of a liquid, usually water, with a little alcohol and the radioactive source. One wall of the chamber is a movable piston.

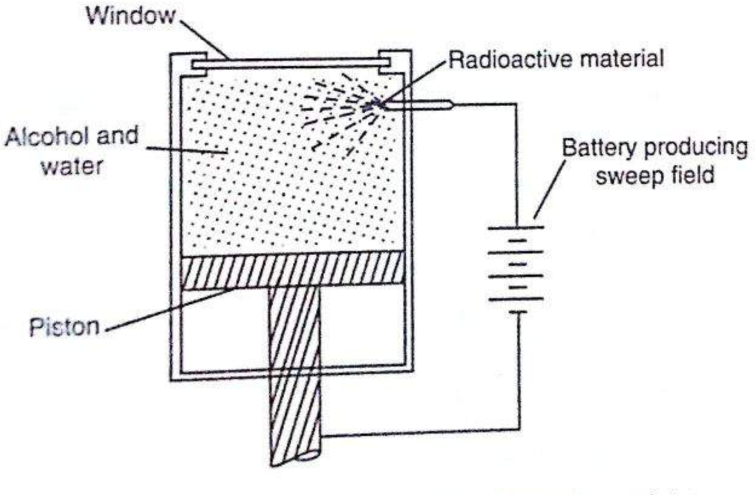

Fig. 1.I.18. Expansion cloud chamber (schematic).

If the volume of the chamber is suddenly increased by moving the piston, the adiabatic expansion results in cooling and consequent supersaturation of vapour. If there are ions within the chamber, these provide nuclei for condensation. A small electric field of few volts is provided within the cloud chamber to 'sweep out' any stray ions which are not of interest (sweep field). Clearly the chamber is sensitive for an incident charged particle, just before the piston expansion, and so the ions produced will not have enough time to get swept away and the droplets formed due to condensation will make positions of ions along the path of the particle visible. However, such a picture gets quickly spoilt as the droplets move due to gravity and gas turbulence. They also evaporate. If the piston is then returned to its original position, it takes about a minute or so for the chamber to get ready for another expansion. By applying a magnetic field B to the chamber, the curved tracks of the incident particles can be photographed and studied. This enables one to measure the radius of curvature r and from this the velocity or energy of the incident charged particle can be computed by using the relation,

$$\frac{mv^2}{r} = qvB \quad \text{or} \quad mv = qBr \qquad \ldots(1.1.4)$$

The thickness of the track is characteristic of the particle. Alpha tracks can be easily distinguished from those made by electrons. On an average an α-particle under atmospheric pressure produces about 50,000 ion pairs per cm in air. On the other hand, β-particles produce only 50 ion pairs per cm. Since both α-and β-particles lose energy by giving up about 34 eV per ion pair produced, α-tracks are *short and thick,* while β-tracks are *long and thin.* To the practised eye, cloud chamber tracks due to different charged particles are as different as the tracks left by different animals on wet sand. The study of cloud chamber pictures has been very rewarding and it practically enables us to 'see' reaction on an atomic scale.

When it is required to detect very *high-energy* particles, such as cosmic rays or those produced by accelerators, a *bubble chamber* is more advantageous since it is filled with a dense liquid instead of a gas. It was invented in 1952 by Glaser. In Glaser's own words: "A bubble chamber is a vessel filled with a transparent liquid which is so highly superheated that an ionising particle moving through it starts violent boiling by initiating the growth of a string of bubbles along its path."

To understand the principle of a bubble chamber consider the bottle of a carbonated soft drink like "Thums Up". Prior to the opening of the bottle, the CO_2 gas over the drink and that dissolved in it are in equilibrium. When the bottle is opened, the pressure gets reduced and the solution of the gas in the liquid is supersaturated. From this unstable condition, bubbling results and we have the familiar effervescence. By adding some salt one can get a very large effervescence. Why is it so? Clearly the bubbles form most readily on discontinuities provided by the specks of salt, so that most of the CO_2 gas effervesces almost at once (giving rise to much frothing). In much the same manner, when ions are produced in a bubble chamber, they act as nuclei for the formation of small bubbles.

In a bubble chamber, a superheated liquid is at a temperature and pressure lower than the equilibrium vapour pressure. This creates an unstable condition and the passage of a single charged particle initiates bubble formation. The superheated condition is thus achieved. The liquid in the chamber is first kept at the equilibrium pressure and then the pressure, like in the case of the cloud chamber, is suddenly lowered by rapidly moving a piston. A few milli-seconds after the chamber has become sensitive, the process is reversed and the chamber pressure is brought back to its equilibrium value. The time during which the chamber is sensitive is synchronised with the arrival time of the pulse of high-energy particles from an accelerator. An electronic photoflash is used to illuminate the bubbles and stereoscopic photographs are recorded. Figure 1.1.19 shows a typical bubble chamber.

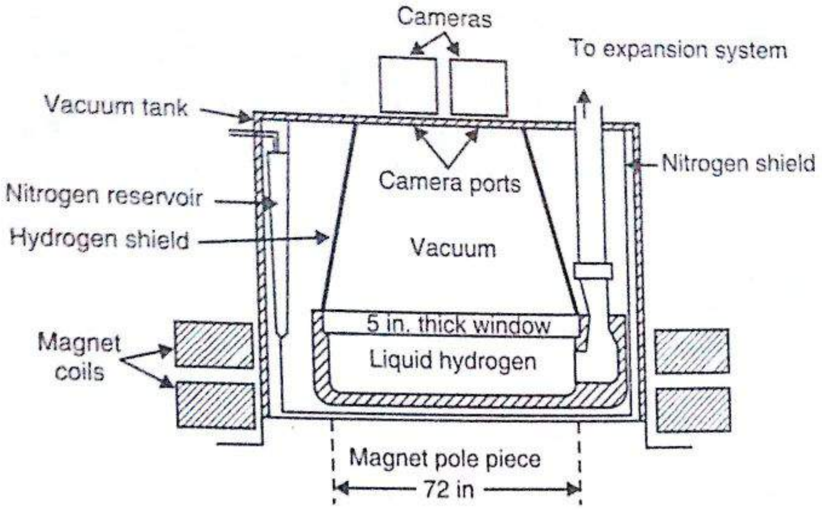
Cameras
To expansion system
Vacuum tank
Nitrogen shield
Camera ports
Nitrogen reservoir
Hydrogen shield
Vacuum
5 in. thick window
Magnet coils
Liquid hydrogen
Magnet pole piece
72 in

Fig. 1.I.19. A typical bubble chamber.

Glaser's first chamber contained only a few cm^3 of liquid. The modern bubble chambers are huge and very expensive. The superheated liquid is often hydrogen at –245°C. Sometimes xenon at –20°C or helium or deuterium is used. Extreme care has to be taken since hydrogen becomes explosive when it comes in contact with oxygen. However, hydrogen has the advantage of having the chamber function as proton target. The 12-feet hydrogen bubble chamber of the Argonne National Laboratory, USA, contains 20,000 litres of hydrogen. A superconducting magnet produces a field of about 18 kg in the chamber of volume 25 m^3. Because of the high density of liquid (compared to gas) a bubble chamber is indispensible in the study of high-energy particles. The existing bubble chambers produce about 35 million photographs per year and the process of data evaluation is a complex one employing computers. In 1970, the Argonne Laboratory bubble chamber recorded the first neutrino interaction in pure hydrogen. Figure 1.I.20 schematically shows this remarkable event.

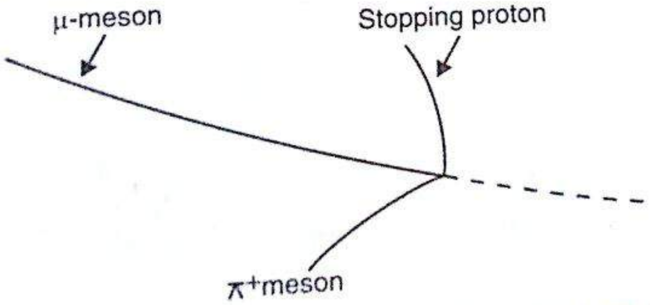
μ-meson
Stopping proton
π+meson

Fig. 1.I.20. Neutrino interaction in the hydrogen bubble chamber. A neutrino enters from right and interacts with the proton of hydrogen atom to yield a π^+, a proton and a μ^-.

(vii) Spark Chamber

The spark chamber is based on the simple fact that if the voltage across two metal plates separated by a distance of a few centimetres is increased beyond a certain value, a breakdown in the form of sparking occurs. The spark chamber consists of a series of thin parallel plates spaced a few millimetres apart as shown in Fig. 1.I.21.

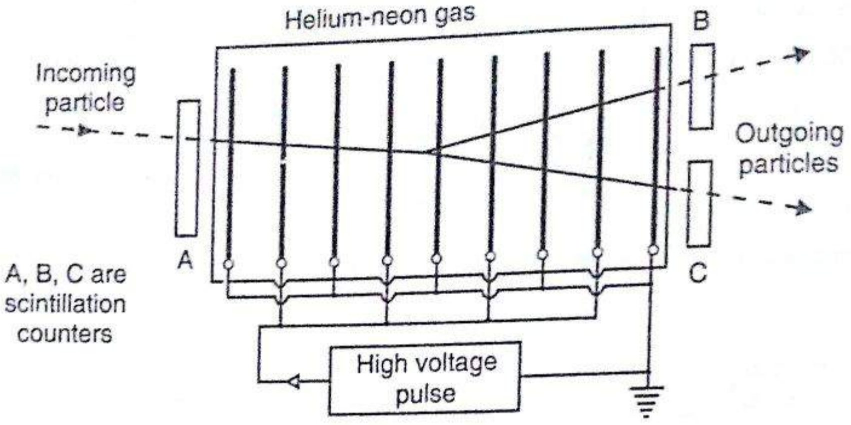

Fig. 1.I.21. Spark chamber arrangement.

The first, third, fifth and all other odd-number plates are grounded and the second, fourth, sixth and all even-number plates are connected to a high—voltage source. (A small "clearing" voltage is always operative.) The high voltage is almost-but not quite—sufficient to produce a discharge between the adjacent plates. A 'trail' of ionisation is produced by an incident charged particle. If the voltage (in a pulse form) is applied in a fraction of a micro-second during which electrons in this 'trail' remain free (before becoming attached to molecules in the gas) a small localised spark discharge between each pair of plates will occur along the particle's path. A photograph will then reveal the trajectory of the incident particle and then collision events or deflections in a magnetic field can be observed similar to the bubble chamber. The voltage pulse is quickly removed and the ions are swept by the small field, so that the chamber is ready for the next pulse. The chief advantage of a spark chamber over a bubble chamber is that it can be made sensitive for a very short time ($\sim 10^{-6}$ secs or so). This is because the ions remain between the plates for a few μ sec, and so the pulse (high) voltage can be applied after passage of the particle. A spark chamber can thus be *triggered.*

In Fig. 1.I.21, there is one incoming particle giving rise to two charged product particles. Three scintillation counters *A, B* and *C* detect the three charged particles. If the particles pass through these three counters, an electronic LOGIC circuit can be made to trigger (activate) the high-voltage supply (10–20 kV). It is possible to apply this pulse within a time interval of less than 50 nano secs (1 ns = 10^{-9} s), so that the resulting sparks can be photographically recorded. The track of this particular incoming particle is recorded and there is not much possibility of some *background* particle triggering off the spark track. In this way, rare events and interactions can be studied without the confusing or misleading background of unimportant events.

1.I.4 PARTICLE ACCELERATORS

Nuclear detectors and accelerators are to a nuclear physicist what a microscope is to a biologist and a telescope is to an astronomer. Let us first understand the need to have accelerators for doing nuclear physics.

Need for an Accelerator of Charged Particles

(*a*) To create a new particle or state of mass *m,* we need at least an energy $E = mc^2$. For a state of mass approximately equal to a proton, for example, we need at least an energy of about 1000 MeV.

(*b*) High energies are also necessary for studying the structure of nuclear systems. Let us see how.

The reduced de Broglie wavelength of a particle with momentum p is given by:

$$\bar{\lambda} = \frac{\lambda}{2\pi} = \frac{\hbar}{p} \qquad \text{...(1.I.5)}$$

where

$$\hbar = \frac{h}{2\pi}, h \text{ being Planck's constant.}$$

$$= 6.582 \times 10^{-22} \text{ MeV-sec.} \qquad \text{...(1.I.6)}$$

We know from optics that to see the structure in detail of an object with linear dimensions *d,* we must use a wavelength comparable to or smaller than *d.*

i.e.,

$$\lambda \leq d \qquad \text{...(1.I.7)}$$

For this wavelength, the momentum p required must then be,

$$p \geq \frac{\hbar}{d} \qquad \text{...(1.I.8)}$$

It is clear that to see the details of very small objects like nuclear particles, high momenta and thus high energies are needed. For $d = 10^{-15}$ m = 1 fm, and protons as probe, it is easy to calculate the kinetic energy required to see linear dimensions of 1 fm is about 20 MeV. Obviously, we do not have naturally produced beams of particles with such energies; they must be produced artificially.

Today we have accelerators producing beams of charged particles with energies ranging from a few MeV to giant machines giving a few hundred GeV (1 MeV = 10^6 eV, 1 GeV = 10^9 eV). Intensities can be as high as 10^{16} particles per sec. The beams can be concentrated on targets of only a few mm^2 in area. The particles that are most often used as *projectiles* are protons and electrons.

Let us now consider in brief the principles of some widely used accelerators.

(i) Van de Graaff Generator

This electrostatic generator was first built by Van de Graaff in 1931. In this generator, a charge Q is transported to one terminal of a huge condenser C. This results in a voltage

$$V = \frac{Q}{C},$$

which is used to accelerate the ions. Figure 1.I.22 shows the main features of a Van de Graaff accelerator. A voltage of 30 kV is used to spray positive charges on an insulating belt made of rubber, silk, linen or paper. This belt is motor-driven to carry the charge continuously to the dome-shaped terminal, where it is removed. To spray and collect charges, sharp spray-points, called *corona points* and *collector points* respectively, are used. Positive ions are produced in ion source. These are usually protons, deuterons, α-particles. They are accelerated in the evacuated accelerating

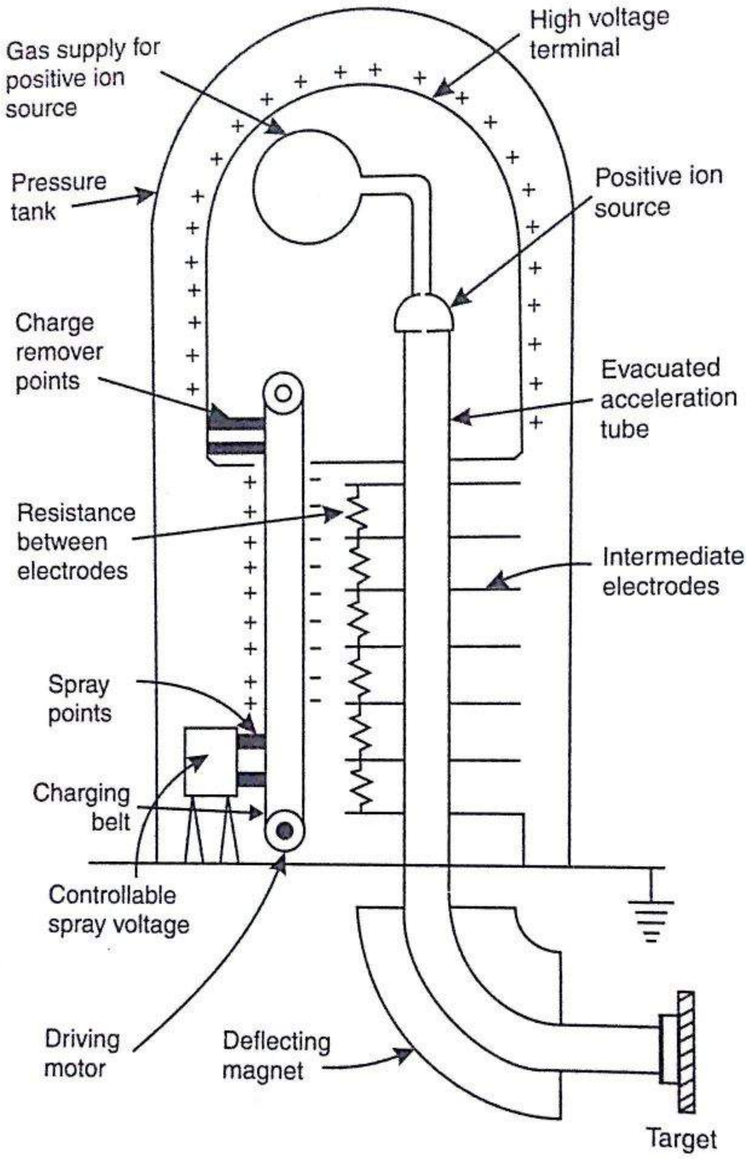
Gas supply for positive ion source
High voltage terminal
Pressure tank
Positive ion source
Charge remover points
Evacuated acceleration tube
Resistance between electrodes
Intermediate electrodes
Spray points
Charging belt
Controllable spray voltage
Driving motor
Deflecting magnet
Target

Fig. 1.I.22. Schematic diagram of a Van de Graaff accelerator.

tube. When this system is placed in air, voltages of up to a few MeV can be reached, beyond which the insulation provided by air breaks down. If the system is placed in a pressure tank filled with an inert gas like nitrogen and carbon dioxide (~ 5 per cent) at pressure 15 atm., voltages up to 12 MV and current, up to about 100 μ amperes can be obtained. (At higher pressures, air can withstand stronger electric fields before breakdown occurs.)

The Tandem Van de Graaff accelerator is an ingenious modification of the Van de Graaff generator. Here two insulating columns are used back-to-back in one pressure tank, so that the particles are accelerated to energies twice the energies given by the conventional Van de Graaff machine.

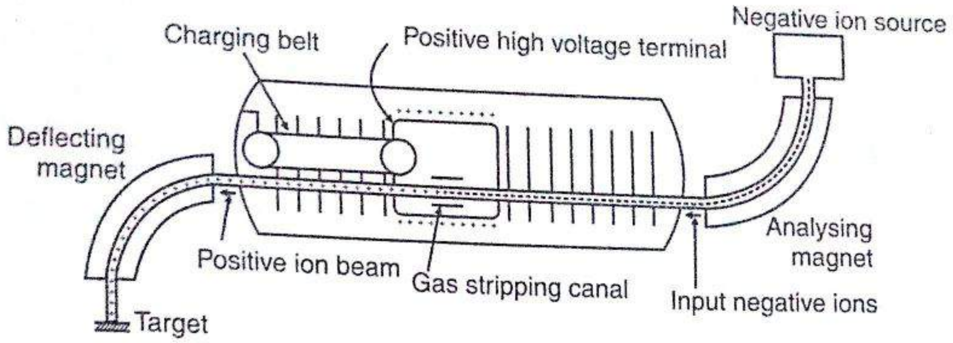
Charging belt
Positive high voltage terminal
Negative ion source
Deflecting magnet
Analysing magnet
Positive ion beam
Gas stripping canal
Input negative ions
Target

Fig. 1.I.23. Tandem Van de Graaff accelerator.

Figure 1.I.23 schematically shows the Tandem Van de Graaff accelerator. Note that the terminal (high, positive voltage) is in the middle of a long pressure tank and the ion source producing negative ions like H^- is at one end. These negative ions get accelerated towards the central positive terminal, where they enter a gas-containing canal, called *stripping canal.* Here the negative ions are stripped of their electrons and become positive ions. The positive ions are repelled from the positive terminal and go on gaining energy as they go to the grounded region to hit the target. The total energy gain is therefore twice that of a single-stage Van de Graaff machine. About 30 MeV protons can be obtained by Tandem Van de Graaff generator.

(ii) The Cyclotron

It is another commonly employed machine for producing high-energy particles, first developed by E.O. Lawrence and M.S. Livingston in 1931. Figure 1.I.24 schematically shows the path of a charged particle in a cyclotron.

A short hollow, cylinder is divided into two 'dees'—D_1 and D_2 resembling the letter D. These dees are placed between the poles of a large electromagnet (Poles of ~5 ft diameter), so that the magnetic field is parallel to the axis of the cylinder. (Of course, the dees have to be kept in a vacuum chamber, which in turn is to be kept between the magnetic poles.) An ion source is kept at the centre between the dees (usually giving protons). The two dees—D_1 and D_2 are connected to the terminals of a high-frequency oscillating (A.C.) circuit. This changes the charge on each dee several million times per second. When D_1 is negative, protons are attracted towards it. Inside D_1, the magnetic field B makes each proton travel in a circle of radius r, given by:

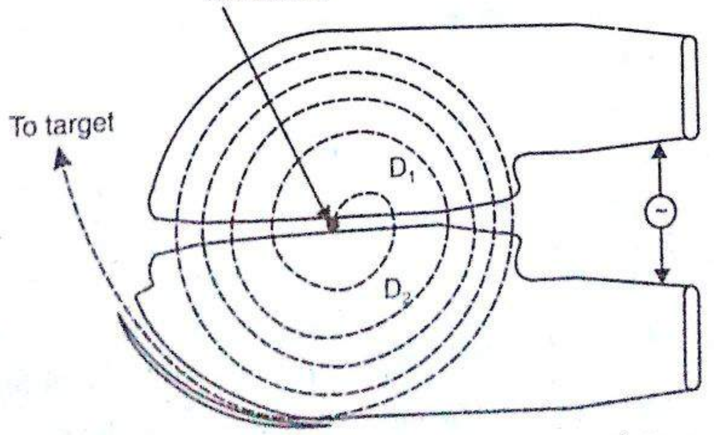
Ion source
To target
D1
D2

Fig. 1.1.24. Path of a charged particle in a cyclotron.

$$\frac{Mv^2}{r} = Bqv \qquad \ldots(1.I.9)$$

where M and q are mass and charge of the proton. Once inside the dee, the protons (or any other charged particles) are in an *electric field-free zone* and as a result, move with constant speed. After travelling one semicircle, the proton comes to the edge of D_1. If we now adjust the frequency of the oscillator is such a way that by the time the proton comes to the edge of D_1, the potential difference between D_1 and D_2 changes direction so as to make D_2 negative and D_1 positive. The proton will then get attracted to D_2 and its speed will increase due to the acceleration. Once inside D_2, the proton is in a field-free zone again and it will now move in a circular path at constant speed (higher than the previous constant speed in D_1). The radius of the path in D_2 will be larger. After traversing a semicircle in D_2, the proton will come at the edge of D_2, where, if the direction of the electric field changes, it will receive additional energy. The proton will continue travelling in semicircles of increasing radii every time it goes from D_1 to D_2 and from D_2 to D_1.

The important fact is that the time required by the proton to travel a semicircle (within the dee) is *independent of the radius of the circle.*

Let us verify this. If t is the time required to travel a distance πr (semicircle) with speed v,

$$t = \frac{\pi r}{v}$$

From Eq. 1.I.9,

$$v = \frac{Bqr}{M}$$

$$t = \frac{\pi r}{\frac{Bqr}{M}} = \frac{\pi M}{Bq} \qquad \ldots(1.I.10)$$

Thus by *adjusting the magnetic field B, t can be made the same as that required to change the potentials of D_1 and D_2.*

Protons gain tremendous energy after traversing through several rotations. When they come near the circumference of the 'dees', an auxiliary electric field is used to deflect them from the circular path to eventually reach a target.

The voltage between D_1 and D_2 is usually 100,000 volts. When a particle emerges from the cyclotron, due to successive accelerations it acquires an energy of tens of MeV. Thus a comparatively low voltage is used to get high-energy particles. The upper limit of energy for a proton is about 22 MeV. This is because, Eq. 1.I.9 is non-relativistic and as the speed of the particle increases its mass increases too. This disturbs the cyclotron operation—the speed does not increase at the proper rate so as to remain in phase with the oscillations.

To get some idea of how large the frequency might be, let us calculate it, for proton and a magnetic field of 1 Wb/m² or 10,000 gauss.

$$\text{Frequency } f = \frac{\omega}{2\pi} = \frac{v}{2\pi r} = \frac{Bq}{2\pi M} \qquad \text{(from Eq. 1.I.10)}$$

$$= \frac{1\ \text{Wb/m}^2 \times 1.6\times 10^{-19}\ \text{coul.}}{2\times 3.14\times 1.67\times 10^{-27}\ \text{kg}} = 1.52\times 10^{7}\ \frac{\text{cycles}}{\text{sec}}$$

$$= 15.2\ \frac{\text{megacycles}}{\text{sec}} \qquad \text{or} \qquad 15.2\ \text{MHz}$$

In other words, a radiofrequency source is required.

(iii) Synchrotron

The cyclotron Eqs. 1.I.9 and 1.I.10 are non-relativistic. As the mass of the particle increases, B also should be increased to satisfy Eq. 1.I.10. For non-relativistic velocities, K.E. of particles in a cyclotron is,

$$\text{K.E.} = \frac{1}{2} Mv^2 = \frac{1}{2} \frac{B^2 r^2 q^2}{M} = Vq \qquad \text{...(1.I.11)}$$

where, V is the effective potential difference through which the particles have been accelerated.

$$V = \frac{1}{2} B^2 r^2 \frac{q}{M} \qquad \text{...(1.I.12)}$$

It is clear from Eq. 1.I.12 that the energy increases as the square of both B and r. As the mass increases for a fixed B and q, the required frequency goes down and as a result, the particles in a fixed frequency machine go 'out of step' with the accelerating voltage.

Figure 1.I.25 illustrates another important requirement for the cyclotron if the particles are to be kept together in a beam. The magnetic field must be shaped so that if a particle moves vertically away from a central plane, it experiences a *restoring force.* To accomplish this, the magnetic force field should get weaker as the radius increases. This is shown by curved lines of force in Fig. 1.I.25. The force experienced by the particles above and below the central plane is also indicated.

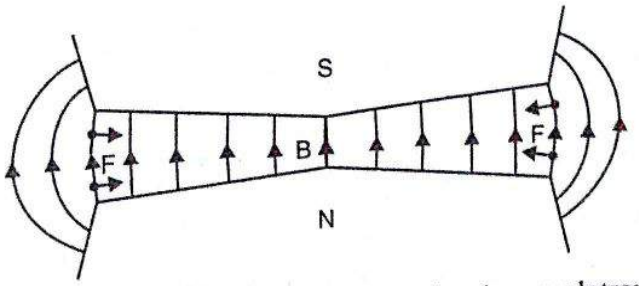

Fig. 1.I.25. This magnetic field produces vertical focussing in a cyclotron. The particles move in a plane perpendicular to $\vec{B}$.

Thus the vertical focusing requirement implies that the field must decrease with the radius, which is just the opposite of the variation required to compensate for a relativistic increase in mass. It is obvious from Eq. 1.I.9 that as M, increases, the frequency $\omega\,(\equiv v/r)$ can remain constant only if B increases to keep the ratio of B to M constant. It turns out that this approach conflicts with the focusing conditions of the beam. Relativity sets a limit to the maximum energy that can be obtained using a cyclotron, which for protons is about 22 MeV.

To reach higher energies, Veksler and independently, McMillan suggested an ingenious technique in 1945 which uses the principle of *phase stability*. Let us understand this principle somewhat qualitatively as a full picture is beyond the scope of this book.

Phase Stability and Phase Oscillations

Consider a particle circulating in an orbit through a constant magnetic field and crossing a gap (between the dees) with an applied alternating electric field. Let us assume that the velocity of the particle is such as to make it cross the gap when the electric field is zero. The particle will then circulate in this orbit at a constant velocity. The energy, frequency and radius of this orbit are referred to as *synchronous* and the particle is called synchronous particle.

Suppose now that another particle arrives at the gap a little earlier (at time t_1) than a synchronous particle. This is shown in Fig. 1.I.26. This particle will clearly gain energy in crossing the gap. Because of this gain in energy, its angular frequency will decrease ($\omega = Bq/M$ and so an increase in M implies a decrease in ω) and the particle will next cross the gap at a time t_2, which is closer to the moment the synchronous particle crosses the gap. This process continues and each time the particle comes a little closer in phase to the synchronous particle (t_2, t_3, etc.). When it crosses the gap in phase with the synchronous particle, there is no electric field. However, the energy of the particle by now is higher than the synchronous particle and so after some turns, it enters the decelerating part of the cycle. In this part, the particle loses energy and hence its angular frequency ω increases. It is back in phase with the synchronous particle. Thus the phase energy and radius of the orbit of a particle oscillate around the equilibrium situation of a synchronous particle.

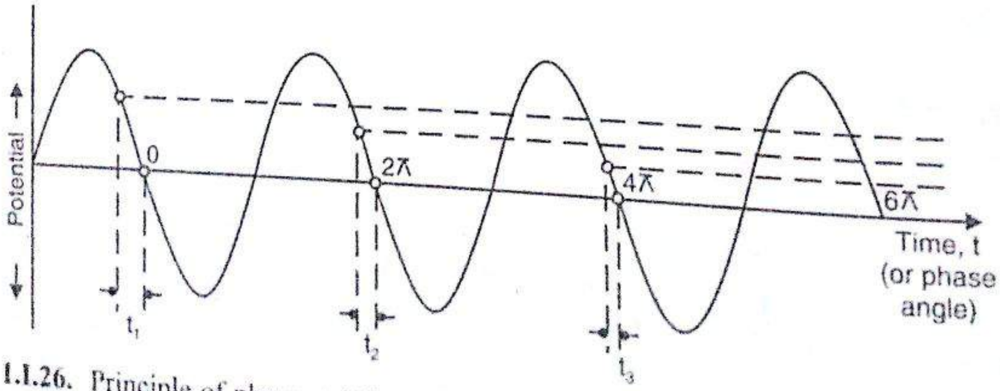

Fig. 1.I.26. Principle of phase stability. O corresponds to the synchronous particle.

A group of particles therefore can be carried out to the maximum possible radius in a series of phase stable, synchronous orbits, by starting with a frequency $\omega_0 = Bq/m_0$ and then slowly decreasing the frequency. Note that the smaller ω is made, the larger becomes the radius of the phase stable orbit. In other words, by keeping the magnetic field constant and slowly decreasing the frequency of the accelerating field, the radius of the orbit would increase along with the energy of the bunch of particles. This is the principle of the *synchrocyclotron*. We can also increase the magnetic field very slowly, keeping the frequency constant. In this case the momentum (and so energy) of the bunch of particles increases as the radius oscillates slightly around the equilibrium value. This is the principle of the *synchrotron*. In each case, the energy oscillates around the equilibrium value (corresponding to the synchronous orbit), which slowly increases with time.

The advantage of synchrotron over synchrocyclotron is obvious. The synchrotron is a constant radius machine. The ions move in an evacuated ring to which a magnetic field is applied to keep the charged particle in an orbit of proper radius. Figure 1.I.27 shows the essential features of a synchrotron. For the sake of simplicity only a few of the repetitive elements are shown.

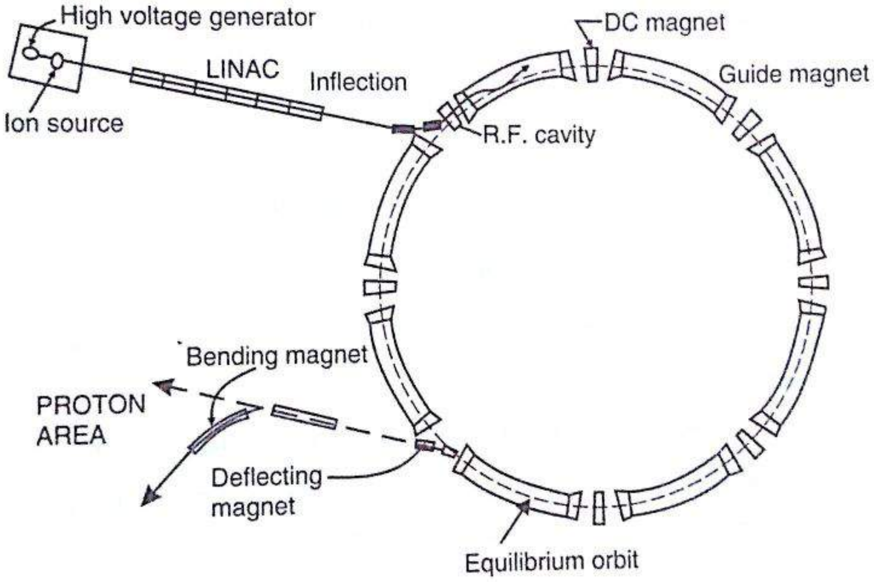

Fig. 1.I.27. Features of a proton synchrotron.

(iv) The Betatron

The betatron is an electron accelerator which uses the principle of electromagnetic induction as the accelerating force. Electron moving in a circular annular vacuum chamber under a guiding magnetic field are accelerated by a magnetic flux time varying linking the electron's orbit. The first successful machine was built by D.W. Kerst in 1940. In the betatron, the rate of increase of the flux linking the electron's orbit is very slow compared to the circulation frequency. The electrons are accelerated continuously during the beginning of the rising magnetic field (see Fig. 1.I.29). To ensure that the electrons are held on a fixed orbit of radius r_0, a certain relation between the flux density at the orbit B_0 and the total flux linking the whole orbit must be satisfied. This relation is easily derived.

For an electron of linear momentum p moving on a circular orbit of radius r_0. we have,

$$p = B_0 r_0 e \quad \text{and} \quad \frac{dp}{dt} = r_0 e \frac{dB_0}{dt} \qquad \ldots(1.I.13)$$

The electromotive force accelerating the electrons is, $d\phi/dt$ where ϕ is the total magnetic flux linked with each orbit.

The effective electric field E, accelerating an electron is given by

$$E \times 2\pi r_0 = \frac{d\phi}{dt} \qquad \ldots(1.I.14)$$

The effective electric force acting on an electron is eE and

$$eE = \frac{dp}{dt} \qquad \ldots(1.I.15)$$

Combining Eqs. 1.I.13, 1.I.14 and 1.I.15, we obtain,

$$\frac{d\phi}{dt} = 2\pi r_0^2 \frac{dB_0}{dt} \qquad \ldots(1.I.16)$$

Integrating Eq. 1.I.16, we obtain the required flux condition,

$$\Delta\phi = 2\pi r_0^2 \Delta B_0 \qquad \ldots(1.I.17)$$

This condition must be satisfied during the entire acceleration period if the electrons are to be kept on a constant radius r_0.

An estimate of the final energy in the acceleration period can be made as follows:

Suppose the electrons are accelerated during one quarter cycle of the flux (time interval $\pi/2\omega$) $\phi = \phi_0 \sin \omega$ linking the orbit, the average energy gained per orbit during this quarter period is

$$e\frac{d\bar{\phi}}{dt} = e\omega\phi_0 \int_0^{\pi/2\omega} \frac{\cos \omega t \, dt}{\pi/2\omega} = e\omega\,\phi_0 \frac{2}{\pi} \qquad \ldots(1.I.18)$$

During most of their journey the accelerated electrons have a speed close to that of light. However, Eq. 1.I.16 holds for relativistic energies as well as in the non-relativistic range because the law of force as written in Eqs. 1.I.13 and 1.I.15 satisfies the requirements of special relativity with the mass now referring to the relativistic mass m_v of the electron:

$$m_v = \frac{m_0}{\sqrt{1 - \dfrac{v^2}{c^2}}}$$

The total distance travelled during the time $\pi/2\omega$ is nearly $c\pi/2\omega$ and each electron makes

$$\frac{c\pi}{2\omega}\Big/ 2\pi r_0 = \frac{c}{4\omega r_0} \text{ revolutions}$$

The final kinetic energy T of an electron is the average energy gained per revolution multiplied by the number of revolutions; hence

$$T = \frac{ec\,\phi_0}{2\pi r_0} \qquad \ldots(1.I.19)$$

For an orbit of radius 100 cms and peak flux ϕ_0 of 1.5 webers, T is approximately 100 MeV. The final energy T as given by in Eq. 1.I.19 is independent of the angular frequency ω of the changing flux. The value of ω should not be too small, otherwise the time of acceleration is increased and the loss of energy by radiation (ignored in the derivation of Eq. 1.I.19) increases.

As is known, the radial acceleration of the electrons in their orbit results in electromagnetic radiation. The rate of radiation as given by classical electrodynamics is

$$u = \frac{4\pi e^2}{3r}\left(\frac{\omega}{m_0 c^2}\right)^4 \beta^3$$

where $\beta = v/c$

Substituting the fundamental constants and expressing w, the electron energy in electron volts,

$$u = 4.22 \times 10^{-24}\,\frac{(\omega/e)^4}{r^2}\,\text{eV/sec} \qquad \ldots(1.I.20)$$

But one revolution takes $2\pi r/c$ sec and therefore $u = 8.85 \times 10^{-32}\left(\frac{\omega/e}{r}\right)^4$ eV/revolution.

The radiated energy for a 100 MeV electron on a 100 cm orbit radius is 8.8 eV/revolution. The total energy loss during the acceleration cycle can be obtained by integrating Eq. 1.I.20 over the acceleration cycle. If we consider a frequency cycle of 180 cps, the total acceleration time is 0.0014 sec, and consequently, the total energy loss for a 100 MeV electron is 0.59 MeV. Thus about 0.6 per cent of the electron energy is lost in the form of radiation. This energy is radiated in a continuous spectrum that has a maximum for frequencies near

$$V_{\max} = \frac{3}{2}\left(\frac{E}{m_0 c^2}\right)^3 \frac{\omega_0}{2\pi}$$

which for the case considered occurs in the visible region, the corresponding light of which has been observed.

A schematic drawing of the vertical cross-section of a typical betatron magnet and vacuum chamber is shown in Fig. 1.I.28.

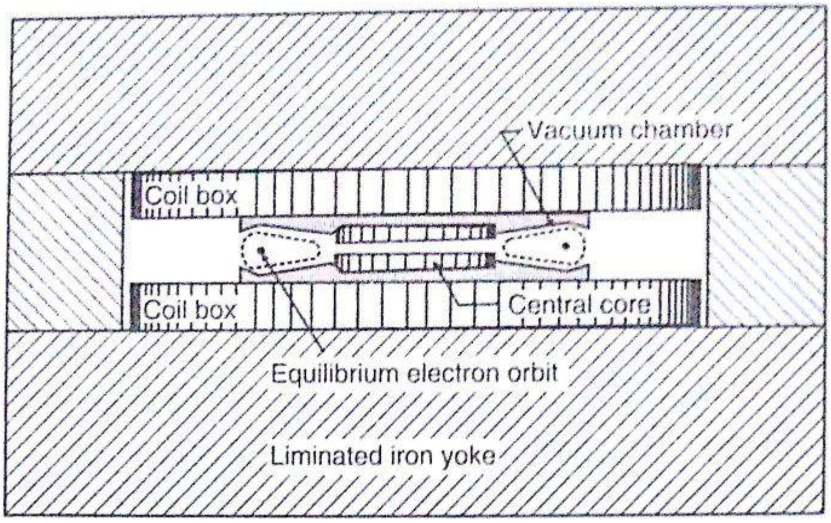

Fig. 1.I.28.

The field is shaped so that the flux condition of Eq. 1.I.17 is always satisfied. The annular vacuum chamber is made of glass, coated on the inside with a thin layer of silver to prevent the accumulation of surface charges. However, the silver film has a low conductivity, so that induced eddy currents, which set up disturbing magnetic fields, are kept at low values. Electrons are injected into the equilibrium orbit of 20 to 50 kV from a pulsed electron gun, when the changing field has the correct value to guide them on to an orbit of radius r_0. The electrons, however, must move sufficiently inwards to avoid hitting the back of the electron gun after the first and subsequent revolutions. Beam extraction is possible but it is difficult to achieve a high extraction efficiency. The high-energy electrons are often used to produce high-energy photons by allowing the circulating beam to strike the target. At the desired instant, the electrons are deflected on to the X-ray target by passing a current pulse through a set of coils close to the vacuum chamber.

As seen above, radiation losses strongly limit the maximum energies to which the electrons can be accelerated. This loss becomes appreciable at energies of about 100 MeV. For energies higher than this, special arrangements are needed to compensate for the loss. For a 300 MeV electron, the loss is estimated at about 13 per cent. One of the largest betatron built so far is the 300 MeV machine at the University of Illinois. Figure 1.I.29 shows the typical acceleration cycle in a betatron.

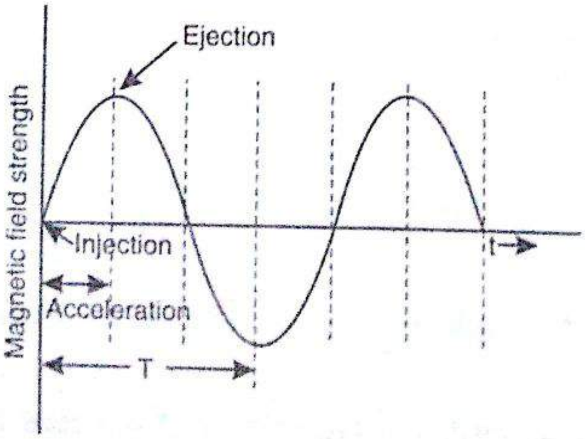

Fig. 1.I.29. The acceleration cycle in a betatron.

1.I.5 BETA RAY SPECTROMETER

The velocity of β-particles can be measured by making them travel across a magnetic field and noting down the deflection produced. One type of instrument is called semicircular focussing or/180° *magnetic spectrograph*. It is sketched in Fig. 1.I.30.

When a charged particle of charge q moves across a magnetic field of induction B, it describes a circular path of radius ρ given by:

$$Bqv = \frac{mv^2}{\rho} \qquad \ldots(1.I.21)$$

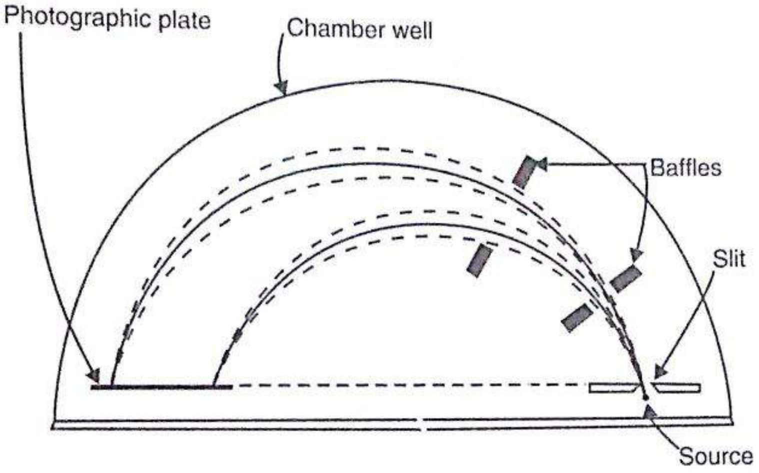

Fig. 1.I.30. Schematic diagram of a 180° magnetic spectrograph.

where m and v are the mass and velocity of the particle.

This equation can be written for velocity v.

$$v = \frac{q}{m} B\rho \qquad \ldots(1.I.22)$$

Thus the velocity v can be determined if (q/m) and $B\rho$ are experimentally known. In a 180° magnetic spectrograph, a magnetic field of known strength acting in a direction perpendicular to the plane of the diagram bends the charged particles through an angle of 180°. Note that this instrument can be used to find the velocity of charged particles like α-particles also. The baffles reduce the scattering of charged particles. Particles having the same velocity move in semicircular paths of the same radius and are detected by a photographic plate or counters. Figure 1.I.30 shows two groups of α-particles with different velocities. For electrons, a field of about 1 kg is strong enough while for α-particles one needs a field of about 10 kg.

In the older instruments, the magnetic field was uniform. In recent designs, however, the focussing of the particles is made better by using a 'shaped' or inhomogeneous field. For example, in an iron yoke double-focussing spectrometer of the type designed by Swartholm and Siegbahn (Ark Mat. Astra Fys. 33 *A* 21 (1946)), the focussing takes place under the condition that the magnetic field decreases as $1/\sqrt{\rho}$ in the neighbourhood of the central path $\rho = \rho_0$ after the electrons move through an angle $\pi\sqrt{2}$. With such a machine, a momentum resolution of about 0.1 per cent can be obtained. The electron conversion lines shown in Fig. 1.I.33 are obtained by using such a machine. More recently, iron-free spectrometers of much higher resolution have been developed.

Let us now see how kinetic energy of electrons can be estimated by measuring the $B\rho$ value in Eq. 1.I.22. It should be remembered that electrons are *always relativistic*. The fundamental relativistic relations are:

$$m = \frac{m_0}{\left(1 - v^2/c^2\right)^{1/2}}$$

$$p = mv$$

and

$$\left(E_{\text{total}}\right)^2 = \left(mc^2\right)^2 = p^2c^2 + m_0^2c^4 \qquad \dots(1.I.23)$$

Putting

$$W = \frac{mc^2}{m_0c^2} \quad \text{and} \quad n = \frac{p}{m_0c},$$

we get a very useful relation,

$$W^2 = n^2 + 1 \qquad \dots(1.I.24)$$

Clearly for electrons,

$$n = B\rho\frac{e}{m_0c^2} = \frac{B\rho}{1704} \qquad \dots(1.I.25)$$

(When we put $\dfrac{e/c}{m_0} = 1.7589 \times 10^7$ emu/g)

In Eq. 1.I.25, $B\rho$ is in gauss cm. We have made use of the gaussian system here because usually in experiments, $B\rho$ is obtained in gauss-cm.

The connection between the kinetic energy E_k in MeV and $B\rho$ is given by

$$W^2 = \left(\frac{E_k}{0.511} + 1\right)^2 \qquad \dots(1.I.26)$$

where 0.511 MeV = m_0c^2 = rest energy of electron in MeV.

Proof of this Eq. 1.I.26 is left as an exercise to the student. Combining Eqs. 1.I.25 and 1.I.26, we have, from Eq. 1.I.24.

$$\left(\frac{E_k}{0.511} + 1\right)^2 = \left(\frac{B\rho}{1704}\right)^2 + 1 \qquad \dots(1.I.27)$$

This is a very general relationship between an electron of any kinetic energy E_k expressed in MeV and $B\rho$ expressed in gauss-cm. To become familiar with the use of this equation the student is advised to see illustrative Example 4.6 in Chapter 4 and also the Problems 4.20 and 4.21 in that chapter.

1.I.6 BRIEF ACCOUNT OF COUNTER ELECTRONICS: LOGIC

Electronics is extensively used with particle detectors. In fact, it has almost become an integral part of the detecting device. A detailed discussion of nuclear electronics, as it is called, is beyond the scope of this book, though useful references are given at the end of the book. However, to appreciate the role played by electronics in nuclear experiments, let us consider the extensively used scintillation detector and circuitry associated with it. This is shown in Fig. 1.I.31 for a single detector.

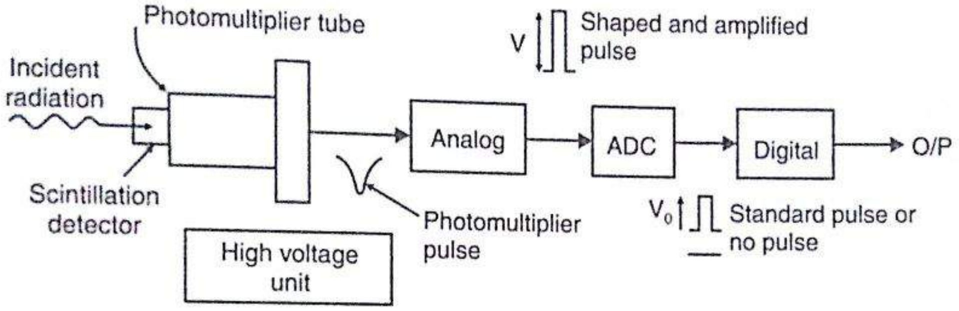

Fig. 1.I.31.

A regulated power supply provides the voltage for the photomultiplier tube. The analog part shapes and amplifies the pulse given by the photomultiplier when incident radiation is 'detected' by the scintillation detector like NaI (T1). This is shown in the Fig. 1.I.31. The height V of the analog output pulse is proportional to the size of the original pulse given by the photomultiplier. The ADC part is the *analog to digital converter,* which transforms the information into a digital form. For example, the ADC can act as a discriminator, when it is set to accept only those pulses between say V_0 and $V_0 + \Delta V$. In other words, we have a 'window' for accepting a pulse. If a pulse comes into this window, the ADC gives an output which is a standard pulse, otherwise there is no output pulse. It is possible to have an ADC unit called a *multichannel analyser* which can at once look at the entire output pulse by having windows corresponding to different pulse heights. If there are 512 windows, we speak of a 512 channel analyser. A 4000-channel analyser is a common sight in a nuclear physics laboratory. The digital part works with a standard pulse. It is usually a scalar which records the events. For example, for every 10 input pulses, one output pulse may be given. The single ADC unit shown in Fig. 1.I.31 is obviously called a single-channel analyser. For data processing, scalars and registers can be used. In a multichannel analyser as seen above, all analogy pulses are digitised and the data processing becomes involved—scalars and registers will not do, as they become unwieldy. In a multichannel analyser, the digital information is stored in a two-dimensional memory. A digital signal corresponding to a given pulse height is then *stored* in some part of the memory, which can be 'read out' on an oscilloscope or on a magnetic tape. An online computer is clearly a very advantageous data processing system.

Coincidence and Anti-Coincidence Work

The technique of coincidence spectrum was first used by Rossi in the studies pertaining to the cosmic rays. It is an indispensable tool in nuclear spectroscopy.

Figure 1.I.32, three excited states of a nucleus, 1, 2 and 3 are shown. The γ-rays γ_1 and γ_2 are emitted successively. Is it possible to correlate them as a sequence by an experiment? Two scintillation detectors D_1 and D_2 are arranged to detect the two γ-rays as shown in Fig. 1.I.32.

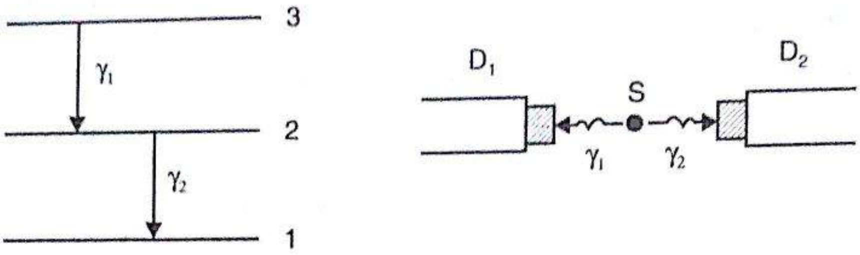
3
γ_1
2
γ_2
1
D_1
D_2
S
γ_1
γ_2

Fig. 1.I.32. Arrangement for double coincidence work to establish the sequence $\gamma_1 \to \gamma_2$.

The sequence $\gamma_1 \to \gamma_2$ can be established by detecting the simultaneous arrival of pulses produced by these γ-rays. The Rossi coincidence circuit using two triode valves is sketched in Fig. 1.I.33(*a*).

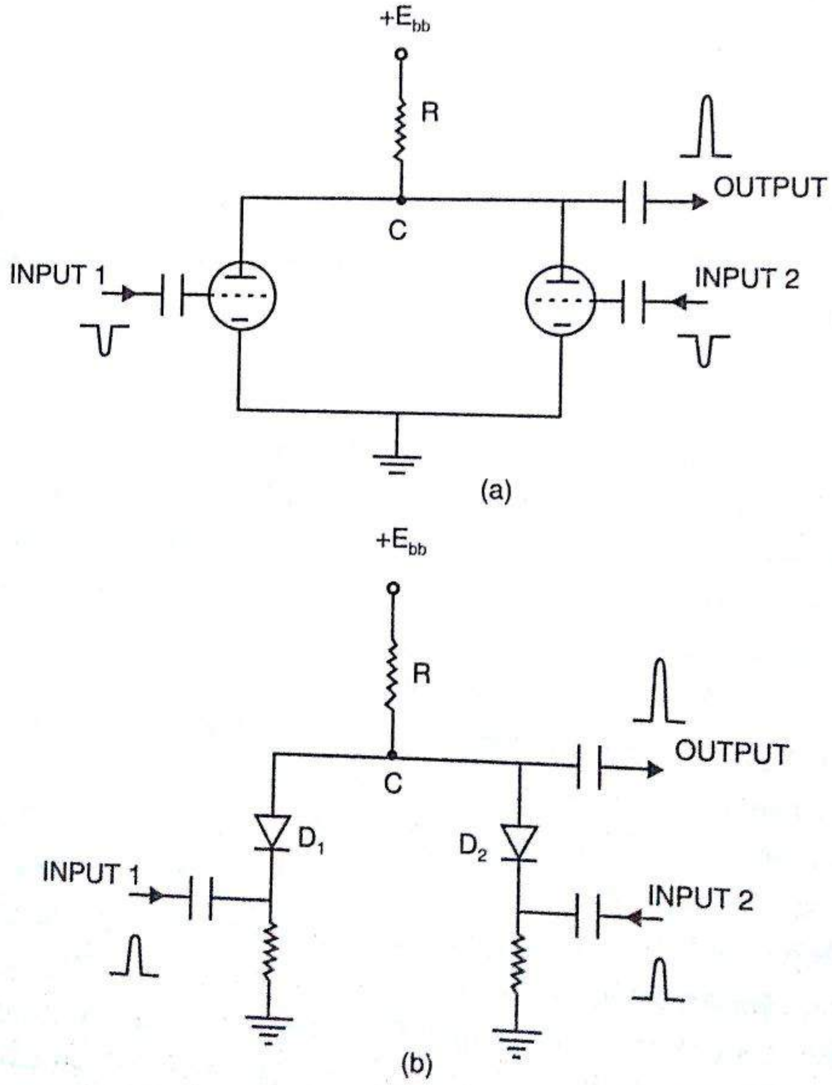
$+E_{bb}$
R
OUTPUT
C
INPUT 1
INPUT 2
(a)
$+E_{bb}$
R
OUTPUT
C
D_1
D_2
INPUT 1
INPUT 2
(b)

Fig. 1.I.33. (*a*) Rossi coincidence circuit using triodes.
(*b*) A coincidence circuit using diodes D_1 and D_2.

The voltage drop is equal to $2iR$, in the absence of an input. An input pulse of either tube would reduce the voltage drop across R by iR. The simultaneous arrival of both the input pulses would change the voltage at C by $2iR$ and a positive pulse would then appear. Usually a coincidence circuit is followed by a discriminator, so that the smaller output pulse arising out of the arrival of only one pulse can be rejected. In part B of the figure, a coincidence circuit using diodes D_1 and D_2 is shown. When the output pulse from a coincidence circuit is rejected by a logic element from the data, the process is called taking anti-coincidences. In our discussion on germanium detectors, we have seen how it is possible to remove Compton edges from a γ-ray spectrum by using an anti-Compton shield. The output pulse given by such a shield is due to the Compton events in the Ge-detector. To remove these Compton events from the γ-ray spectrum, the output of anti-Compton shield is put in anti-coincidence with the output of the Ge-detector.

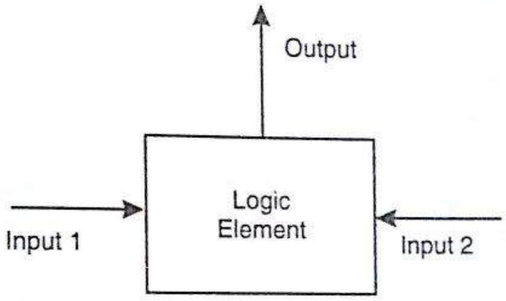

Fig. 1.I.34. Action of basic logic elements.

In nuclear spectroscopy, four basic logic elements are very useful. They are: AND, OR, NAND and NOR. Input and output pulses are of standard size. Figure 1.I.34 illustrates the use of these logic elements. An AND element produces no output, unless both the input pulses arrive simultaneously. OR produces an output pulse if one or more input pulses arrive. NAND (NOT AND) and NOR (NOT OR) are the logical complements. NAND gives an output pulse, whenever an AND does not. NOR gives an output pulse whenever an OR does not. Thus in general, AND logic elements serve as coincidence circuits. Figure 1.I.33 gives two examples of electronic circuits with which the logic element AND can be realised in practice. NAND and NOR provide anti-coincidence signals.

PART–II: MATHEMATICAL TOOLS

MINIMUM WAVE MECHANICS FOR AN INTRODUCTION TO NUCLEAR PHYSICS

1.II.1 INTRODUCTION

Let us make a distinction between wave mechanical (or quantum) systems and classical systems. Planck's constant h, has dimensions of 'action' $[ML^2T^{-1}]$. Note that the dimensions of the following quantities are the same as h.

$$\text{(Length)} \times \text{(Momentum)}$$

$$\text{(Time)} \times \text{(Energy)}.$$

and

When we say that 'small' systems are wave mechanical and 'large' systems are classical, the 'size' of a system must be judged by comparing it with the typical action, h. For example, in a deuteron (nucleus), the typical 'action' is the product of potential range a (which is of the order of distance of separation between the proton and neutron in the deuteron) and the relative momentum p of the particles.

Now, $a \sim 1.5 \times 10^{-15}$ m

and $p \sim 130$ MeV/c $= 6.9 \times 10^{-20}$ mks units.

giving product of the order of 10^{-34} Js, which is close to h. Thus we see that a nucleus is a wave mechanical system, and we cannot progress very far in our discussion without using wave mechanical concepts. Most students must have been exposed to an introductory course in wave mechanics as a part of modern physics study. However, to make this book self-sufficient, we quickly review elementary wave mechanics, which is all that is needed for this book. Of course, a student is expected to be familiar with Schrödinger's time independent matter wave equation and Max Born's interpretation of the wave function.

1.II.2 PARTICLE IN A ONE-DIMENSIONAL INFINITE SQUARE WELL

To begin with, it is interesting to consider the simple case of a one-dimensional infinite square well. The particle in such a well is bound within the region $|x| \leq L$ as shown in Fig. 1.II.1.

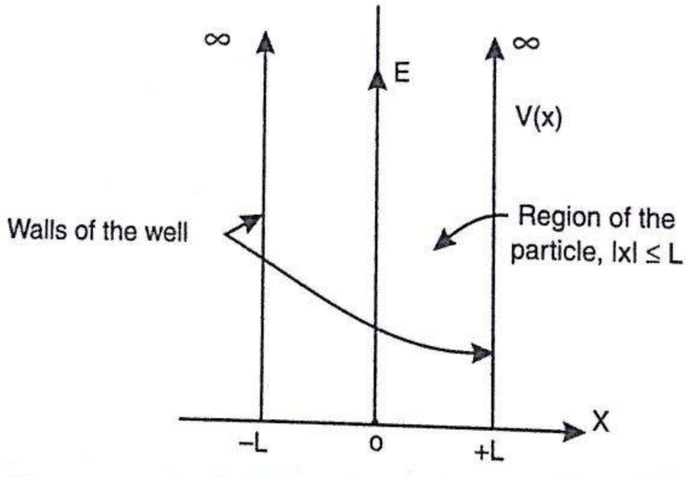

Fig. 1.II.1. One-dimensional infinite square well.

This type of potential is certainly not a realistic potential, as compared to, say, the Coulomb potential experienced by an electron bound in a hydrogen atom. In spite of this crudity, it is amazing to see how a discrete energy spectrum results for the possible energy states of a particle in such an infinite square well.

Clearly,

$$V(x) = 0, \; |x| \leq L$$

and

$$V(x) = \infty, \; |x| \geq L \qquad \text{...(1.II.1)}$$

Classically, the particle inside such a well can take any energy and it bounces to and fro due to elastic collisions with the walls.

For $| x | \leq L$, the Shrodinger's time independent equation can be written as:

$$\frac{\hbar^2 \partial^2}{2m\partial x^2} u_n(x) = E_n u_n(x) \qquad \text{...(1.II.2)}$$

Since $V \to \infty \; | x | \geq L$, we must impose the condition,

$$u_n(x) = 0 \text{ for } | x | \geq L \qquad \text{...(1.II.3)}$$

Now putting Eq. 1.II.2 in the form

$$\left(\frac{\partial^2}{\partial x^2} + K_n^2\right) u_n(x) = 0 \qquad \text{...(1.II.4)}$$

where,

$$K_n^2 = \frac{2mE_n}{\hbar^2} \qquad \text{...(1.II.5)}$$

The solutions satisfying the boundary condition at $x = L$ are,

$$u_{2n}(x) = A \sin K_{2n}\, x$$

where

$$LK_{2n} = 2n(\pi/2),\ n = 1, 2, \ldots \qquad \text{...(1.II.6)}$$

and

$$u_{2n+1}(x) = B \cos K_{2n+1}\, x$$

where

$$LK_{2n+1} = (2n + 1)(\pi/2),\ n = 0, 1, 2, \ldots \qquad \text{...(1.II.7)}$$

Combining Eqs. 1.II.6 and 1.II.7

$$K_n = \left(\frac{\pi}{2L}\right) n, \quad n = 1, 2 \ldots$$

$\therefore$ By Eq. 1.II.5, the possible energy levels are,

$$E_n = \frac{\hbar^2}{2m}\left(\frac{\pi^2}{4L^2}\right) n^2 \qquad \text{...(1.II.8)}$$

where $n = 1, 2, 3, \ldots$

The integer n, called the quantum number, is used as a subscript on E to indicate the discrete character of energy. The first three energy levels are shown in Fig. 1.II.2. This result for the infinite square well shows a very important feature of wave mechanical solutions. When a particle is in a bounded system, there are discrete energy levels. If Eq. 1.II.8 is compared with the Bohr energies for hydrogen,

$$E = \frac{\hbar^2}{2m}\frac{1}{a_0^2}\frac{1}{n^2}$$

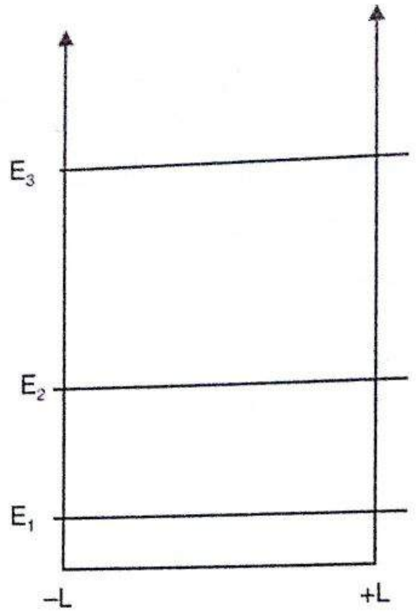

Fig. 1.II.2. Discrete energy states for the infinite square well.

(a_0 is the Bohr radius for ground state), the similarity is obvious. The difference in sign is because for hydrogen, the levels are measured from the top of the potential well downward. For our square well, levels are measured from the bottom (upward).

1.II.3 ONE-DIMENSIONAL POTENTIAL STEP

If a particle of total energy E is incident from left, the situation is wave mechanically very interesting and would lead us to one of the most important wave mechanical effects in nuclear physics, which is barrier penetration or the tunnelling effect. For simplicity of calculation, we take a square step approximation as shown in Fig. 1.II.3.

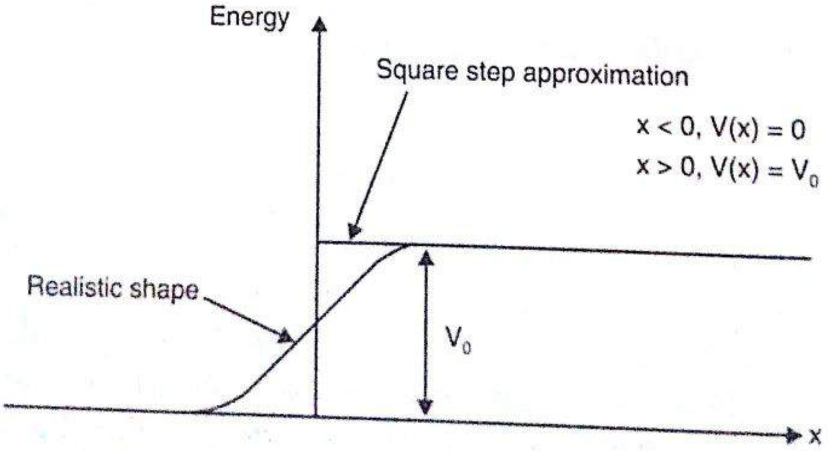

Fig. 1.II.3. A one-dimensional square step.

Classically, for $E < V_0$, the particle has insufficient energy to cross the step and thus gets *reflected*. Also for $E > V_0$ the particle has sufficient energy to surmount the step and there is *total transmission*.

Let us now see what happens wave mechanically. Schrödinger's time independent equation for this problem is,

$$\left(-\frac{\hbar^2}{2m}\frac{\partial^2}{\partial x^2}+V(x)\right)u(x)=Eu(x)$$

where for $x<0,\ V(x)=0$

and $x>0,\ V(x)=V_0$ ...(1.II.9)

The wave function $u(x)$ must be finite everywhere. Also, at the discontinuity $x=0$, both $u(x)$ and $u'(x)$ are continuous. Let us apply these boundary conditions to the two cases; particle energy $E>V_0$ and $E<V_0$ and find the solutions to Eq. 1.II.9.

For $E>V_0$, let us define,

$$k_0^2=\frac{2mE}{\hbar^2}$$

and

$$k_1^2=\frac{2m(E-V_0)}{\hbar^2} \qquad \text{...(1.II.10)}$$

Equation 1.II.9 now becomes,

$$\left(\frac{\partial^2}{\partial x^2}+k_0^2\right)u_L(x)=0 \quad \text{for } x<0$$

and

$$\left(\frac{\partial^2}{\partial x^2}+k_1^2\right)u_R(x)=0 \quad \text{for } x>0 \qquad \text{...(1.II.11)}$$

where $u_L(x)$ is the wave function at the left of the origin $x=0$ and $u_R(x)$ is the wave function at the right of the origin $x=0$.

The solutions to Eq. 1.II.11 are

$$u_L(x)=\underset{\text{(incident)}}{e^{ik_0x}}+\underset{\text{(reflected)}}{Ae^{-ik_0x}}$$

and,

$$u_R(x)=\underset{\text{(transmitted)}}{Be^{ik_1x}} \qquad \text{...(1.II.12)}$$

Here the coefficient of the incident wave is taken as one and coefficients A and B determine the reflected and transmitted intensities. To find A and B, we use the boundary conditions stated before.

$u(x)$ is continuous at $x=0$ and $u'(x)$ is continuous at $x=0$. This gives (from Eq. 1.II.12):

$$1+A=B$$

and

$$k_0(1-A)=k_1B \qquad \text{...(1.II.13)}$$

solving
$$A = \frac{k_0 - k_1}{k_0 + k_1} \quad \text{and} \quad B = \frac{2k_0}{k_0 + k_1} \qquad \text{...(1.II.14)}$$

Notice that energy E does not take discrete values, and so the system can have any energy similar as in the classical case. However, the motion of the particle is now different from the classical conclusion, where for $E > V_0$ there is total transmission.

Now the relative probability of finding the particle at some $x < 0$ corresponding to a reflection is:

$$\begin{aligned} P(x) &= |u_L(x)|^2 \\ &= |e^{ik_0x} + Ae^{-ik_0x}|^2 \\ &= \left(e^{ik_0x} + Ae^{-ik_0x}\right)\left(e^{-ik_0x} + Ae^{ik_0x}\right) \\ &= 1 + |A|^2 + 2A\cos 2k_0x \qquad \text{...(1.II.15)} \end{aligned}$$

The cosine term in this equation is oscillating and its average can be taken as 0. Thus we have:

$$P(x) = 1 + |A|^2$$

The terms on the right can be interpreted as relative intensities of the incident and reflected beams. Thus we come across an important feature of wave mechanics: that even though $E > V_0$, since $|A|^2 \neq 0$, there is a *finite reflection probability*. The classical limit is obtained for, $E \gg V_0$, as from Eq. 1.II.10 $k_0 \sim k_1$ and so Eq. 1.II.14 gives, $A \sim 0$ and $B \sim 1$ corresponding to total transmission.

Now consider the second important case, that of $E < V_0$. Classically, this corresponds to total reflection of the particle by the potential step. Let us find the wave mechanical predictions.

The situation for $x < 0$ is the same as before and so we have

$$u_L(x) = e^{ik_0x} + Ae^{-ik_0x} \quad \text{as solution}$$

for the left of the origin.

For the solotion $u_R(x)$ to the right of the origin we now define,

$$k_2^2 = \frac{2m}{\hbar^2}(V_0 - E) \qquad \text{...(1.II.16)}$$

The Schrödinger equation for the right of the origin is then:

$$\left(\frac{\partial^2}{\partial x^2} - k_2^2\right)u_R(x) = 0 \qquad \text{...(1.II.17)}$$

(for $x > 0$)

The solution is a combination of $e^{\pm k_2 x}$ and we have:

$$u_R(x) = C\, e^{-k_2 x} + D\, e^{+k_2 x}$$

Clearly $D = 0$, otherwise as $x \to \infty$, $u_R(x)$ would not remain finite.

$\therefore$

$$u_R(x) = C\, e^{-k_2 x} \qquad \ldots(1.\text{II}.18)$$

As before, using continuity conditions at $x = 0$,

$$1 + A = C$$

and

$$ik_0(1 - A) = -k_2 C \qquad \ldots(1.\text{II}.19)$$

giving,

$$A = \frac{k_0 - ik_2}{k_0 + ik_2}$$

$$C = \frac{2k_0}{k_0 + ik_2} \qquad \ldots(1.\text{II}.20)$$

Again there are no discrete values for particle energy E. As in the classical case, we have total reflection of the particle as

$$|A|^2 = 1.$$

The essential difference in wave mechanical consideration is that, for the region $x > 0$ corresponding to transmission, the relative probability of finding the particle is finite, $P(x)_R$ given by

$$\begin{aligned} P(x)_R &= |u_R(x)|^2 \\ &= |Ce^{-k_2 x}|^2 \\ &= \frac{4k_0^2}{k_0^2 + k_2^2} e^{-2k_2 x} \qquad \ldots(1.\text{II}.21) \end{aligned}$$

from Eq. 1.II.20.

Thus wave mechanically, it is possible to find the particle in the classically forbidden region (for $E < V_0$) $x > 0$. In nuclear physics, one always encounters the potential step in the form of a *barrier*. A typical example is that of a *Coulomb barrier*. To understand the phenomenon of α-emission, fission process, etc. one must treat the Coulomb barrier wave mechanically. A rectangular top barrier though a rather crude approximation of a realistic barrier can be handled wave mechanically in a very simple way and shows a number of important features. Figure 1.II.4 shows just such a potential barrier, of thickness b (one-dimensional).

If we project a particle with an energy $E < V_0$ on this barrier, then from the foregoing discussion it should be clear that the particle has a finite probability to overcome this barrier ('leak' through the barrier or 'tunnel' through this barrier) and then move to the right as a free

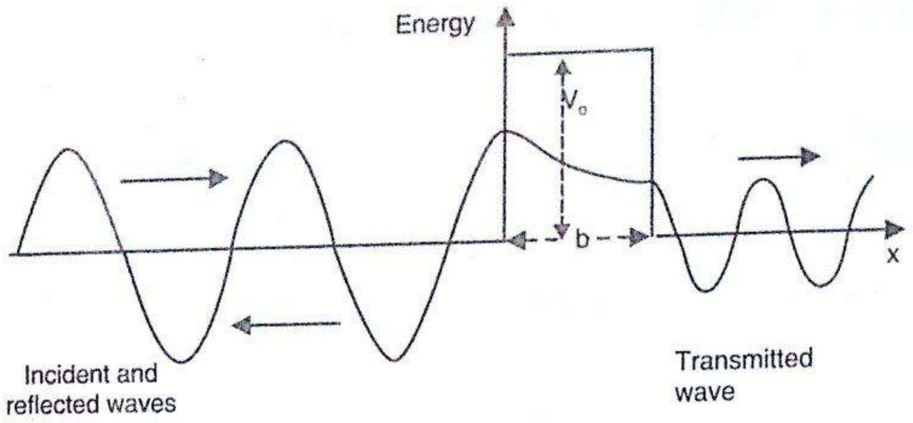

Fig. 1.II.4. A rectangular top potential barrier of height V_0 and breadth b (reflection from the right edge is neglected).

particle. From Eq. 1.II.21, the relative probability of finding the particle at $x = b$ and at $x = 0$ is,

$$P_{\text{relative}} = e^{-2k_2 b}$$

$$= e^{\left[-2\left(\frac{2m}{\hbar^2}\right)^{1/2}(V_0 - E)^{1/2} b\right]} \qquad \text{...(1.II.22)}$$

(from Eq. 1.II.16)

In this simple treatment, we have assumed that the barrier is thick enough to neglect the reflection from the right edge.

For a realistic barrier not having a rectangular shape,

$$P_{\text{relative}} = e^{-2\int_0^b k_2 dx} \qquad \text{...(1.II.23)}$$

We will see in Chapters 4 and 5 that it is possible to wave mechanically calculate half-life of radioactive nuclides using basically Eq. 1.II.22.

1.II.4 PARITY

It will be an advantage to consider potentials which are symmetrical with respect to a reflection of the coordinates about the origin. As before, we will take the one-dimensional system for convenience. Thus, we consider potentials which satisfy,

$$V(x) = V(-x) \qquad \text{...(1.II.24)}$$

This symmetrical property of the potential makes us expect that the physical results should also be unaffected by such a transformation. We may, particularly, expect that the probability of finding a particle between a certain range of coordinates is not affected by such a transformation (of coordinate reflection).

$$|u(x)|^2 = |u(-x)|^2 \qquad \text{...(1.II.25)}$$

That is,

The requirement of Eq. 1.II.25 is satisfied when,

$$u(x) = +u(-x) \qquad \text{even parity} \qquad \ldots(1.\text{II}.26)$$

or

$$u(x) = -u(-x) \qquad \text{odd parity} \qquad \ldots(1.\text{II}.27)$$

Wave functions satisfying Eq. 1.II.26 are known as *even parity* wave functions and those satisfying Eq. 1.II.27 are known as *odd parity* wave functions. *Even parity* is also called *positive parity,* and *odd parity* is also called *negative parity.*

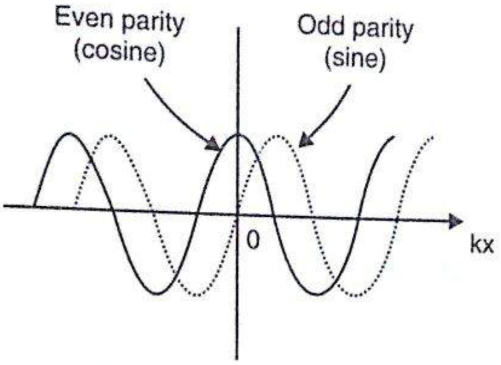

Fig. 1.II.5. Even and odd parity functions.

cos kx → symmetrical about the origin. sin kx → symmetrical about the origin.

Figure 1.II.5 shows examples of even parity and odd parity wave functions. Cos kx wave functions satisfy the condition cos kx = cos $(-kx)$ and so, correspond to even or positive parity. On the other hand, sin kx = –sin $(-kx)$; corresponding to odd or negative parity. From Fig. 1.II.5, notice that cos kx functions are symmetric about the origin and sin kx are antisymmetric about the origin. The student should check that if one takes $u(x) = A \sin kx + B \cos kx$, Eq. 1.II.25 is not satisfied and so a wave function, which is a sum of functions of opposite parity, is not an acceptable function.

If there is more than one solution, and a particular solution does not have a definite parity, then from $u(x)$ and $u(-x)$, it is always possible to construct solutions.

$$u_{\text{even}}(x) = \frac{1}{2}[u(x) + u(-x)]$$

$$u_{\text{odd}}(x) = \frac{1}{2}[u(x) - u(-x)] \qquad \ldots(1.\text{II}.28)$$

Each of these has definite parity. Thus, one can always construct symmetric or antisymmetric solutions.

1.II.4A PARTICLE IN A ONE-DIMENSIONAL SQUARE POTENTIAL WELL

The idea of parity developed in the last section can be now exploited to understand bound states of a particle in a one-dimensional square well. Clearly, such a potential is symmetric with respect to a reflection of the x-coordinate about the origin (see Fig. 1.II.6).

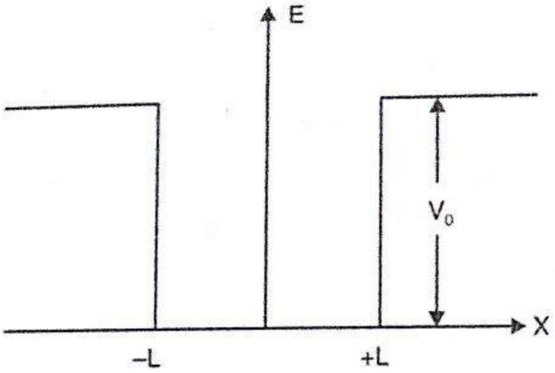

Fig. 1.II.6. One dimensional square potential well.

For $\quad |x| \leq L, \quad V(x) = 0$

and $\quad |x| > L, \quad V(x) = V_0 \qquad \ldots(1.II.29)$

The physically interesting cases is:

$$E < V_0$$

where, as before, E is the particle energy. This condition implies that the particle is confined by the potential in the region $| x | \leq L$. In Sec. 1.II.2, we have considered the limiting case, $V(x) \rightarrow \infty$.

For $| x | \leq L$, Schrödinger's time independent equation is obviously identical with the first part of Eq. 1.II.11; viz;

$$\left(\frac{\partial^2}{\partial x^2} + k_0^2\right) u_{in}(x) = 0$$

where we have denoted u_L as u_{in} to signify that this wave function belongs to the "inside" of the potential well. As before,

$$k_0^2 = \frac{2mE}{\hbar^2}$$

For $| x | > L$, i.e. outside the well the wave equation is identical with Eq. 1.II.17; viz;

$$\left(\frac{\partial^2}{\partial x^2} + k_2^2\right) u_{\text{out}}(x) = 0$$

where u_{out} is the wave function "outside" the well and is same as u_R in Eq. 1.II.17. As given in Eq. 1.II.16,

$$k_2^2 = \frac{2m(V_0 - E)}{\hbar^2}$$

To take advantage of the knowledge of even or odd (symmetric or antisymmetric) eigen functions, instead of writing the solutions to the above equations in the exponential form, we will write them as sine (odd)-or cosine (even) for "inside" the potential well.

$$u_{\text{in}}(x) = \cos k_0\, x \text{ or } \sin k_0\, x \qquad \ldots(1.II.30)$$

For the "outside" region, we have two parts, one on the right side "out" region and the other on the left side "out" region. Let us denote them by, $u_{\text{out}}^{R}(x)$ and $u_{\text{out}}^{L}(x)$ respectively.

Clearly,

$$u_{\text{out}}^{R}(x) = Ce^{-k_2 x} \qquad \text{as in Eq. 1.II.18.}$$

The parity requirements give:

$$u_{\text{out}}^{L}(x) = \pm Ce^{-k_2|x|}$$

We thus have two sets of solutions. Those with positive parity (symmetric function) form one set:

$$u_{\text{in}}(x) = \cos k_0 x$$

$$u_{\text{out}}^{R}(x) = Ce^{-k_2 x}$$

and

$$u_{\text{out}}^{L}(x) = Ce^{-k_2|x|} \qquad \text{...(1.II.31)}$$

The second set corresponds to negative parity (anti-symmetric functions)

$$u_{\text{in}}(x) = \sin k_0 x$$

$$u_{\text{out}}^{R}(x) = C^{1}e^{-k_2 x}$$

and

$$u_{\text{out}}^{L}(x) = -C'e^{-k_2|x|} \qquad \text{...(1.II.32)}$$

For each solution, we can now put the continuity conditions for u and u' at $|x| = L$.

$\therefore$ For even (positive parity) solutions,

$$\cos k_0 L = Ce^{-k_2 L}$$

and

$$k_0 \sin k_0 L = k_2 Ce^{-k_2 L} \qquad \text{...(1.II.33)}$$

These equations can be satisfied only if,

$$k_0 \tan k_0 L = k_2 \qquad \text{...(1.II.34)}$$

Similarly, for odd (negative parity) solutions, continuity conditions for u and u at $|x| = L$ give:

$$k_0 \cot k_0 L = -k_2 \qquad \text{...(1.II.35)}$$

Substituting for k_0 and k_2, clearly Eqs. 1.II.34 and 1.II.35 are satisfied only for certain *discrete* values of energy E_n. To find these values of energy E_n that the particle can take one can solve Eqs. 1.II.34 and 1.II.35 graphically. This is shown in Fig. 1.II.7.

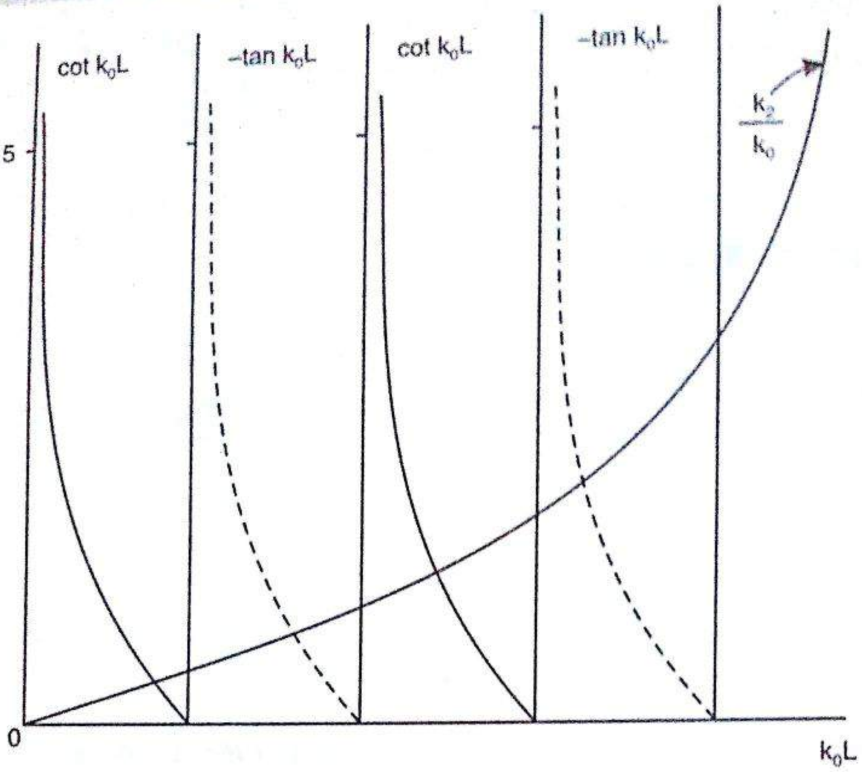

Fig. 1.II.7. Continuity conditions at the boundary of a one-dimensional square well are satisfied by discrete values of energy E_n. The points of intersection give these values.

Figure 1.II.8 shows the typical shape of wave functions of the first three energy levels.

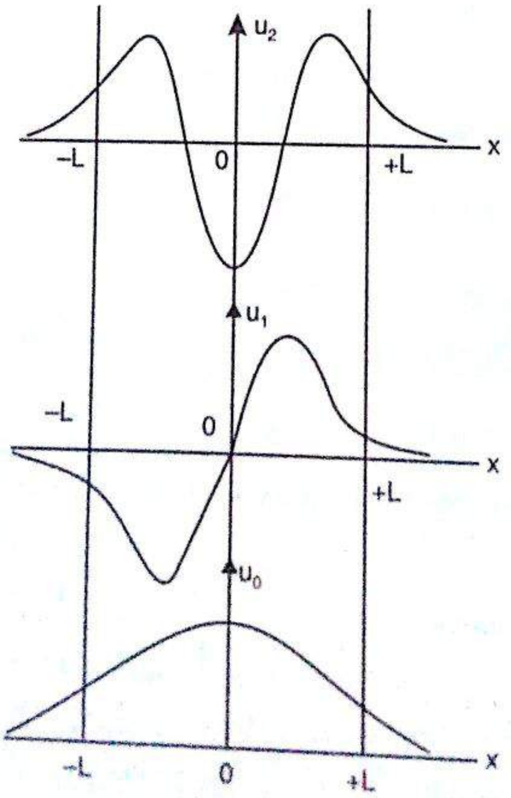

Fig. 1.II.8. Shape of wave functions for the first three states. Notice the parity and the number of nodes.

The ground state function $u_0(x)$ is symmetrical about the origin and has no nodes. Clearly, it is an even state (positive parity). The next state $u_1(x)$ is an odd state (negative parity). It has a single node at the origin. The state $u_2(x)$ has two nodes and is an even state. Thus, in general, the n^{th} state has parity $(-1)^n$, with n nodes.

Notice also the penetration of the wave functions in the classically forbidden regions.

1.II.5 HARMONIC OSCILLATOR—PARABOLIC POTENTIAL WELL

Classically, the harmonic oscillator is a particle moving under the action of a restoring force:

$$F = -m\omega^2 x$$

The potential is related to the force by

$$F = -\frac{\partial V}{\partial x}$$

This gives the potential energy of the harmonic oscillator.

Figure 1.II.9 shows this potential. We thus have a parabolic potential well. Wave mechanical results with such a potential well are interesting. In Chapter 7, when we discuss the shell model of a nucleus it will be clear how a square well potential and a parabolic potential are very useful in calculating the shell structure of nuclei.

Schrödinger's equation for the harmonic oscillator potential is (one-dimensional well)

$$\left(-\frac{\hbar^2}{2m}\frac{d^2}{dx^2} + \frac{1}{2}m\omega^2 x^2\right)U_n(x) = E_n U_n(x) \qquad \text{...(1.II.36)}$$

We shall not solve this equation, but write down the energy eigenvalues.

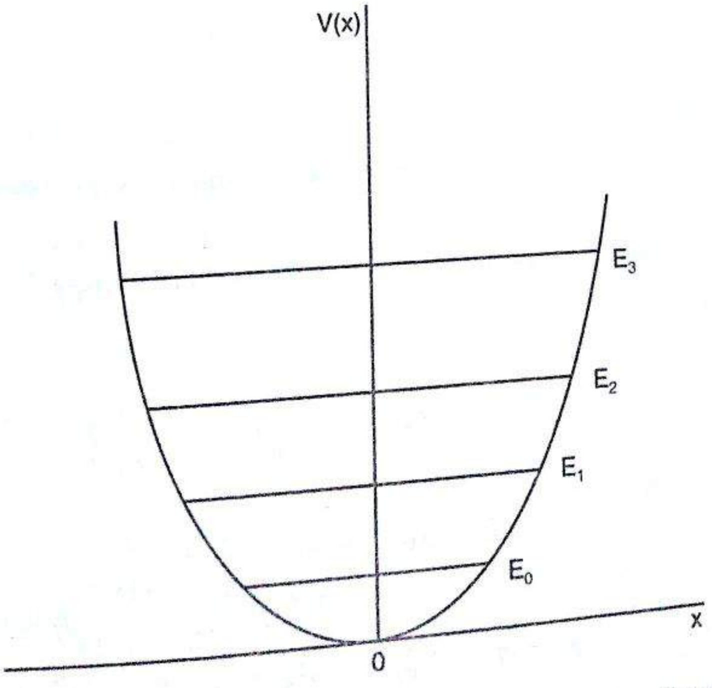

Fig. 1.II.9. Parabolic harmonic oscillator potential well (One-dimensional).

A discrete set of energies is obtained:

$$E_n = \left(n + \frac{1}{2}\right)\hbar\omega, \; n = 0, 1, 2, 3, \ldots \qquad \text{...(1.II.37)}$$

These discrete energy states are also shown in Fig. 1.II.9.

1.II.6 ANGULAR MOMENTUM OPERATOR AND ITS EIGENVALUES

It is of advantage to consider the angular momentum operator and its eigenvalues, before taking Coulomb potential in hydrogen atom. Spherical polar coordinates are found to be convenient. They are related to cartesian coordinates by equations:

$$x = r \sin\theta \cos\phi, \; y = \sin\theta \sin\phi \text{ and } z = r \cos\theta \qquad \text{...(1.II.38)}$$

This can be clearly seen from Fig. 1.II.10.

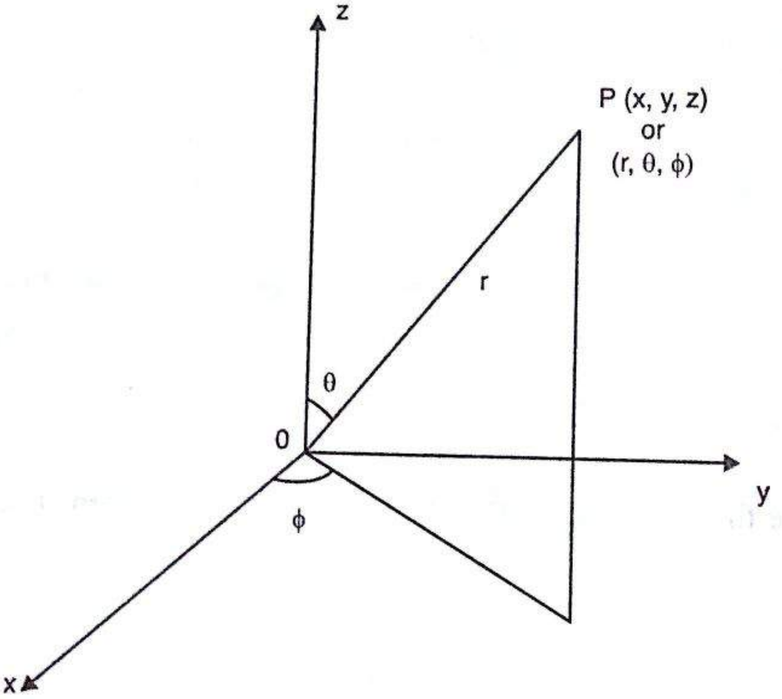

Fig. 1.II.10. The point *P* specified by (x, y, z) and (r, θ, ϕ) coordinates.

The components of angular moment $\vec{L} = \vec{r} \times \vec{p}$ in Schrödinger's operator form can be expressed as: $(\phi + 2n\pi)$

$$\hat{\mathbf{l}}_x = \hat{\mathbf{y}}\hat{\mathbf{p}}_\mathbf{z} - \hat{\mathbf{z}}\hat{\mathbf{p}}_\mathbf{y} \rightarrow -i\hbar\left(y\frac{\partial}{\partial z} - z\frac{\partial}{\partial y}\right)$$

$$\hat{\mathbf{l}}_y = \hat{\mathbf{z}}\hat{\mathbf{p}}_\mathbf{x} - \hat{\mathbf{x}}\hat{\mathbf{p}}_\mathbf{z} \rightarrow -i\hbar\left(z\frac{\partial}{\partial x} - x\frac{\partial}{\partial z}\right)$$

$$\hat{\mathbf{l}}_z = \hat{\mathbf{x}}\hat{\mathbf{p}}_\mathbf{y} - \hat{\mathbf{y}}\hat{\mathbf{p}}_\mathbf{x} \rightarrow -i\hbar\left(x\frac{\partial}{\partial y} - y\frac{\partial}{\partial x}\right) \qquad \text{...(1.II.39)}$$

When expressed in spherical polar coordinates by using,

$$\frac{\partial}{\partial z}=\frac{\partial r}{\partial z}\cdot\frac{\partial}{\partial r}+\frac{\partial\theta}{\partial z}\cdot\frac{\partial}{\partial\theta}+\frac{\partial\phi}{\partial z}\cdot\frac{\partial}{\partial\phi}$$

we get,

$$\hat{\mathbf{l}}_x=i\hbar\left(\sin\phi\frac{\partial}{\partial\theta}+\cot\theta\cos\phi\frac{\partial}{\partial\phi}\right)$$

$$\hat{\mathbf{l}}_y=i\hbar\left(-\cos\phi\frac{\partial}{\partial\theta}+\cot\theta\sin\phi\frac{\partial}{\partial\phi}\right)$$

and

$$\hat{\mathbf{l}}_z=-i\hbar\left(\frac{\partial}{\partial\phi}\right) \qquad \ldots(1.\text{II}.40)$$

The possible eigenvalues of $\hat{\mathbf{l}}_z$ can be at once determined

$$\hat{\mathbf{l}}_z u_m(\phi)=\hbar m u_m(\phi) \qquad \ldots(1.\text{II}.41)$$

where $\hbar\, m$ are the eigenvalues.

The solution to this equation can be obtained by noting that ($\phi + 2n\pi$) for any integral n denotes the same position and so, u_m (ϕ) is periodic in 2π. The solution of

$$-i\hbar\frac{\partial}{\partial\phi}u_m(\phi)-\hbar m u_m(\phi) \qquad \ldots(1.\text{II}.42)$$

$$\text{is } u_m(\phi)=\exp(im\phi) \qquad \ldots(1.\text{II}.43)$$

where

$$m=0,\pm1,\pm2,\ldots$$

This quantum number m fixes the orientation of angular momentum vector with respect to certain fixed z-axis. Figure 4.I.7 in Chapter 4 shows this.

Let us now consider the total angular momentum operator and its eigenvalues. It is constructed by putting

$$\hat{\mathbf{l}}^2=\hat{\mathbf{l}}_x{}^2+\hat{\mathbf{l}}_y{}^2+\hat{\mathbf{l}}_z{}^2$$

$$=-\hbar^2\left[\frac{1}{\sin\theta}\frac{\partial}{\partial\theta}\left(\sin\theta\frac{\partial}{\partial\theta}\right)+\frac{1}{\sin^2\theta}\frac{\partial^2}{\partial\phi^2}\right] \qquad \ldots(1.\text{II}.44)$$

It can be checked that the commutator,

$$\left[\hat{\mathbf{l}}^2,\hat{\mathbf{l}}_z\right]=0.$$

This implies that it is possible to find *exact values* of total angular momentum and its z-component, i.e., simultaneous eigen functions $Y_{\beta m}(\theta,\phi)$ exist for these operators, $\hat{\mathbf{l}}^2$ and $\hat{\mathbf{l}}_z$.

$$\hat{\mathbf{l}}_z Y_{\beta m}(\theta,\phi) = \hbar m Y_{\beta m}(\theta,\phi)$$

and

$$\hat{\mathbf{l}}^2 Y_{\beta m}(\theta,\phi) = \hbar_\beta^2 Y_{\beta m}(\theta,\phi) \qquad \text{...(1.II.45)}$$

Since $\hat{\mathbf{l}}_z$ depends only on ϕ we can write, function

$$Y_{\beta m}(\theta,\phi) = P_{\beta m}(\theta) e^{im\phi}$$

Using Associated Legendre Polynomials, it is possible to show that,

$$\hbar^2\beta = \hbar^2 l(l+1), \quad l = 0, 1, 2, \ldots \qquad \text{...(1.II.46)}$$

where

$$l \geq |m|$$

i.e. the eigenvalues of the angular momentum operator are $l(l+1)$. l is called the angular momentum quantum number.

Coulomb Potential, Hydrogen Atom

The Schrodinger equation for a particle of mass m in a potential $V(r)$ in 3-dimension is:

$$\left[\frac{-\hbar^2}{2m}\nabla^2 + V(r)\right] u(r,\theta,\phi) = E_n u(r,\theta,\phi) \qquad \text{...(1.II.47)}$$

In spherical polar coordinates this becomes:

$$\left[-\frac{-\hbar^2}{2m}\left\{\frac{1}{r^2}\frac{\partial}{\partial r}\left\{r^2\frac{\partial}{\partial r}\right\} + \frac{1}{r^2}\frac{1}{\sin\theta}\frac{\partial}{\partial\theta}\left\{\sin\theta\frac{\partial}{\partial\theta}\right\} + \frac{1}{r^2\sin^2\theta}\frac{\partial^2}{\partial\phi^2}\right\}\right.$$

$$\left. + V(r)\right] u(r,\theta,\phi) = E_n u(r,\theta,\phi) \qquad \text{...(1.II.48)}$$

As seen from our discussion before, the dependence on (θ, ϕ) is the same as that of the total angular momentum operator, $\hat{\mathbf{l}}^2$. Therefore, Eq. 1.II.48 can be written as:

$$\left[\frac{-\hbar^2}{2m}\frac{1}{r^2}\frac{\partial}{\partial r}\left\{r^2\frac{\partial}{\partial r}\right\} + \frac{\hat{\mathbf{l}}^2(\theta,\phi)}{2mr^2} + V(r)\right] u(r,\theta,\phi) = E_n u(r,\theta,\phi) \qquad \text{...(1.II.49)}$$

Now the Coulomb potential for hydrogen atom is:

$$V(r) = -\frac{e^2}{r}$$

and so Eq. 1.II.49 becomes:

$$\left[\frac{-\hbar^2}{2m}\frac{1}{r^2}\frac{\partial}{\partial r}\left\{r^2\frac{\partial}{\partial r}\right\} + \frac{l(l+1)\hbar^2}{2mr^2} - \frac{e^2}{r}\right] . u(r) = E_n u(r)$$

This equation can be solved by a laborious process. The conclusion being very important, we state it below. We get a discrete energy spectrum,

$$E_n = -\frac{me^4}{2\hbar^2}\frac{1}{n^2} \qquad \text{...(1.II.50)}$$

This is the formula for Bohr levels of hydrogen. n is the principal quantum number and it has to satisfy the condition $n > l$.

n can take integral values; 1, 2, 3, ...

$l = 0, 1, 2, ... (n - 1)$

and $m = 0, \pm1, \pm2, ... \pm l$, in all $(2l + 1)$ values.

These quantum numbers combined with Pauli's exclusion principle can account for the periodic classification of elements. Notice that the three degrees of freedom (r, θ, ϕ) can be equivalently specified by the quantum numbers, n, l and m.

1.II.7 THE TOTAL ANGULAR MOMENTUM VECTOR $\vec{J}$

Let us now consider the case of an orbiting electron. It has an orbital angular momentum $\vec{L}$ and the spin angular momentum $\vec{S}$. These two angular momenta together give a total angular momentum vector, $\vec{J}$.

Thus we have,

$$\vec{J} = \vec{L} + \vec{S} \qquad \text{...(1.II.51)}$$

Note that $\vec{J}$ is the *vector sum* of $\vec{L}$ and $\vec{S}$.

The magnitudes of these 3 vectors are given by the following relations:

$$L = |\vec{L}| = \sqrt{l(l+1)}\,\hbar$$

$$S = |\vec{S}| = \sqrt{s(s+1)}\,\hbar$$

and

$$J = |\vec{J}| = \sqrt{j(j+1)}\,\hbar \qquad \text{...(1.II.52)}$$

Since s can take only one value of 1/2, we have

$$S = \sqrt{\frac{1}{2}\left(\frac{1}{2}+1\right)}\,\hbar = \sqrt{\frac{3}{2}}\,\hbar \qquad \text{...(1.II.53)}$$

In Eq. 1.II.52,

l is the orbital quantum number.

s is the spin quantum number.

and j is the total angular momentum quantum number.

Figure 1.II.11 shows the coupling of vectors $\vec{L}$ and $\vec{S}$ resulting into $\vec{J}$. There are tw possibilities, parallel and anti-parallel alignments. (Remember that according to wave mechanic perfect alignment is not possible.) Thus, in terms of the quantum numbers, we have the followin two values of j:

$$j = l + \frac{1}{2}$$

and

$$j = l - \frac{1}{2} \qquad \ldots(1.\text{II}.54$$

For example, in the case of a p-electron, $l = 1$, $s = 1/2$ and so $j = 3/2$ or $1/2$.

and so,
$$L = \sqrt{2}\,\hbar,\ S = \frac{\sqrt{3}}{2}\hbar \text{ and } J = \frac{\sqrt{15}}{2}\hbar \text{ or } \frac{\sqrt{3}}{2}\hbar.$$

What is the angle θ between the vectors $\vec{L}$ and $\vec{S}$? (see Fig. 1.II.11). Clearly, since both $\vec{L}$ and $\vec{S}$ are quantized, θ can take only certain definite values.

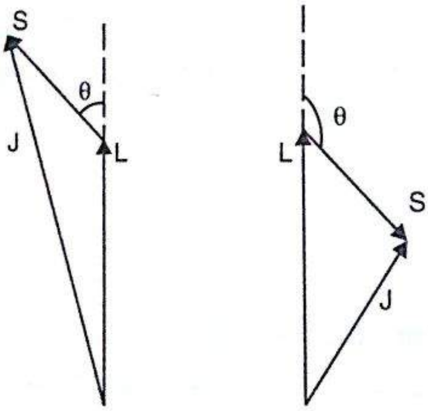

Fig. 1.II.11. Parallel and anti-parallel addition of $\vec{L}$ and $\vec{S}$ to form the vector $\vec{J}$.

Applying the cosine law to Fig. 1.II.11, we have

$$J^2 = L^2 + S^2 + 2LS\cos\theta \qquad \ldots(1.\text{II}.55)$$

i.e.
$$\cos\theta = \frac{j(j+1) - l(l+1) - s(s+1)}{2\sqrt{l(l+1)}\sqrt{s(s+1)}}$$

Equation 1.II.55 can be also written as

$$(\vec{L}\,.\,\vec{S}) = \frac{J^2 - L^2 - S^2}{2}$$

$$= \frac{\hbar^2}{2}[j(j+1) - l(l+1) - s(s+1)] \qquad \ldots(1.\text{II}.56)$$

This coupling of vectors $\vec{L}$ and $\vec{S}$ will be very useful in our discussion of the shell model of the nucleus in Chapter 7.

EXERCISES

1. Give an account of interaction between particles and matter. How do you explain the existence of range for a beam of heavy charged particles?
2. Calculate the thickness of lead sheet required to reduce to one half the intensity of 1 MeV gamma-rays. The absorption coefficient of lead for 1 MeV γ-rays is 0.75 cm^{-1}.
3. From the Geiger rule Eq. 1.I.1 obtain a relation between the range and energy of a heavy charged particle. For α-particles, the relation between range R in air expressed in cm and kinetic energy K_α in MeV is given by

$$R = 0.31 K_\alpha^{3/2}$$

Calculate the range of 8 MeV α-particle in air. Express this range in terms of kgm^{-2}.

4. Calculate the thickness of an aluminium plate required to stop 12 MeV protons incident normal to the plate. The density of aluminium is 2700 kg m^{-3}.
5. A beam of γ-rays consists of equal numbers of 1 MeV and 3 MeV photons. The beam passes through 0.01 m of lead. Calculate the ratio of 1 MeV to the 3 MeV component.
   (*Hint:* Use Fig. 1.I.7)
6. An α-particle is stopped in an ionisation chamber in which it produces 2×10^5 ion pairs. Production of one ion pair results into α-particle losing 35 eV of energy. Calculate the
7. For α-particles, the relation between the range R_s in a substance with mass number A and the range R in air (both expressed in cm) is

$$R_s = 0.56 R A^{1/3} \text{ mg/cm}^2.$$

Both R_s and R refer to α-particles of the same energy. Can you explain how this relation is obtained?

From the relation given above and the one given in Prob. 3, determine the range of an α-particle in lead, ^{208}Pb., if its energy in known to correspond to a range of 10 cm in air.

8. Give an account of interaction of photons with matter. Which is the effect used to detect γ-rays and measure their energy in a scintillation detector like the NaI crystal? Discuss a γ-rays spectrum taken with a NaI detector. How is the energy resolution defined and measured?
9. Describe how a Ge (Li) detector tremendously improves the resolution of a γ-ray spectrometer.
10. Why are accelerators required in Nuclear Physics? Describe the Tandem Van de Graaff machine.
11. A radioactive source put inside a cloud chamber emits 6 MeV α-particles. What magnetic field should be applied so that the radius of curvature of the path of the α-particles is 20 cm?
12. A radioactive source put inside a cloud chamber emits 1.8 MeV electrons. What magnetic field should be applied so that the radius of curvature of the path of the electrons is 50 cm?
13. Describe the working of a cyclotron. What are its typical voltage and frequency? What is the maximum energy obtainable with protons?
14. Protons are accelerated in a 100 cm cyclotron. The oscillator frequency is 10 megacycles. Calculate the magnetic field needed and the maximum energy that can be given to the protons.
15. What are phase stability and phase oscillations? Describe how the principle of phase stability is used in a synchrotron.
16. Describe the working of a betatron. How will you estimate the loss of electron energy due to radiation? Calculate the de Broglie wavelength of a 200 MeV electron.
17. Taking help from a book on modern physics, obtain Schrödinger's time independent wave equation. Discuss Born's interpretation of the wave function. What are expectation values of observables?

18. Why do we say that a nucleus is a wave mechanical system? Explain.
19. For the infinite potential well problem (Sec. 1.II.2), obtain eigen functions and sketch the plots of $|\psi|^2$ against x. How do these graphs look when the value of the quantum number n increases? What conclusions can you draw regarding probability distribution?
20. Using a square potential step, explain the wave mechanical phenomenon of barrier penetration or tunnelling. Calculate the transmission probability. On what factors does it depend? What is the role of uncertainty principle in the phenomenon of "tunneling"?
21. It is unacceptable to have a wave function that is a sum of functions of opposite parities. Explain. Which of the following functions would be acceptable on the grounds of parity:

    (*i*) $\psi_1(x) = A \sin(3k\ x) + B \cos(5k\ x)$

    (*ii*) $\psi_2(x) = A \sin(3k\ x) + B \sin(5k\ x)$?

    Explain your answer.
22. Calculate the possible values of $\vec{L} \cdot \vec{S}$ for $L = 1$ and $S = 1/2$ and $L = 2$ and $S = 1/2$.
23. Calculate the possible values of J for $L = 3$ and $S = 1/2$.

2

Radioactivity

"Physicists always publish their results completely. If our discovery has a commercial future, that is an accident from which we must not profit. And if radium is to be used in the treatment of disease, it seems to me impossible for us to take advantage of that."

—*Marie (Sklodowska) Curie*

2.1 INTRODUCTION

Knowledge concerning atomic nuclei began as early as 1896 with the discovery of radioactivity.

In 1895, Roentgen discovered the X-rays. The French scientist Becquerel got interested in Roentgen's work. Becquerel was seized of the fact that the production of X-rays was always accompanied by fluorescence from the material of the X-ray tube (glass). He thought that X-rays existed whenever there was fluorescence. To investigate this problem, Becquerel took uranium sulphate, which fluoresces under the action of sunlight. He found that fluorescent uranium sulphate did give out rays, which could affect a photographic plate even when wrapped in thick black paper. Becquerel argued that the fluorescent salt had given rise to X-rays, which had penetrated the black paper and affected the photographic plate.

But he soon saw that he was mistaken. During one such experiment the sky happened to be overcast and the uranium salt was hardly fluorescent. On developing the photographic plate, Becquerel was surprised to see a dark spot on it, as before. He had obviously stumbled on some new kind of rays (1896) which could penetrate the thick wrapper and affect the photographic plate. It was soon established that any salt of uranium emits Becquerel rays. Unlike the X-rays, which appear in an X-ray tube only under special conditions, the Becquerel rays are emitted in a spontaneous manner.

Is uranium the only substance emitting Becquerel rays? Marie Curie found that pitchblende, the ore from which uranium is extracted, emits Becquerel rays with a much stronger intensity than what its uranium content would. After a long and laborious process of chemical separation, Marie Curie and her husband Pierre Curie discovered two new elements, polonium and radium, which emitted Becquerel rays.

They gave the name 'radioactive' to all substances capable of emitting, Becquerel rays and the phenomenon itself came to be known as 'radioactivity'.

The discovery of radium was a great event, as it was found to be about a million times more radioactive than uranium. This power of radium radiation made it possible to study radioactivity systematically.

2.2 PROPERTIES OF RADIOACTIVE RAYS

(*i*) By a calorimetric experiment, Curie estimated that one *gm* of radium liberates 140 calories in one hour. Though small, this energy is released continuously over a very long period of time.

(*ii*) Radioactive rays ionize the surrounding air and affect photographic plates.

(*iii*) Radioactive rays act differently on different cells and tissues. Cells that multiply rapidly are most readily destroyed by these rays. This outstanding discovery made radium an invaluable aid to physicians to fight tumours, particularly cancerous growths.

(*iv*) Fluorescence is produced in substances like zinc sulphide, barium platinocynide, etc. By adding minute quantities of radium to, say, zinc sulphide, we can get a compound that is continuously luminous in the dark. This can be used to produce luminous watch dials, gun sights and instrument pointers (coating) for those instruments which are required to be read in the dark.

(*v*) Rutherford found that a beam of radioactive rays from radium sample splits into three components in a strong magnetic or electric field. See Fig. 2.1.

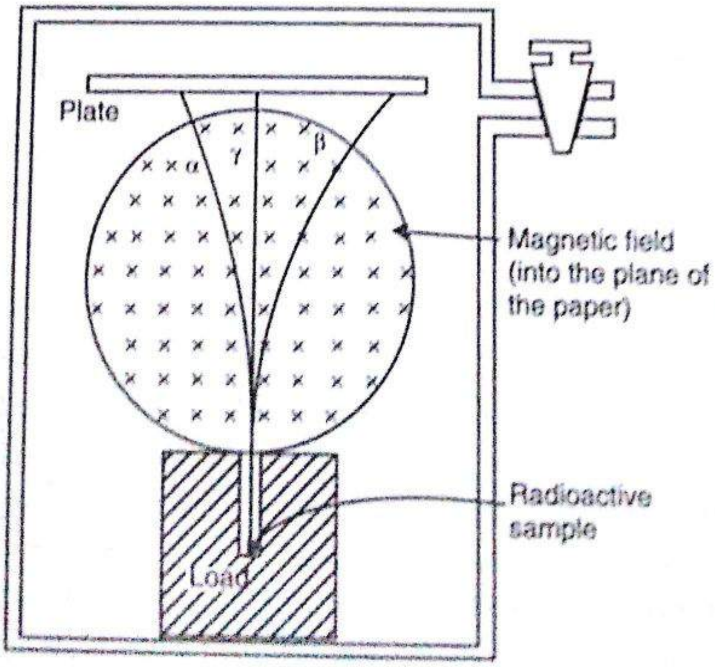

Fig. 2.1. Deflection of α, β, γ rays by a magnetic field.

(*a*) *The α-rays* (particles) are the nuclei of helium atoms. This identification was made by Rutherford and Royds in 1909. By the spectroscopic method, they found traces of helium in an originally pure sample of radon gas, which is an alpha emitter. When an electric discharge was passed through a tube containing pure radon gas, initially only characteristic radon lines appeared.

After a day Rutherford found that, Radon lines became somewhat weaker and new lines started appearing. These new lines were identified with helium spectrum. As the days passed, the radon spectrum began weakening while the helium lines grew brighter. Thus, for the first time, people 'saw' decay of an element (radon) and 'birth' of a new element, helium. Such a transformation in which a parent element gives rise to a new element—called the daughter product—by emitting radioactive rays is called a radioactive transformation. For the above example of radon, we can write the radioactive transformation equation as:

$$ {}^{222}_{86}\mathrm{Rn} \rightarrow {}^{4}_{2}\mathrm{He} + {}^{218}_{84}\mathrm{Po} \qquad \ldots(2.1) $$

Parent element → α-particle + daughter product

Notice that during a radioactive transformation, the mass number and total charge is conserved.

Equation 2.1 is an example of nuclear reaction.

Clearly, radioactivity is a nuclear phenomenon. In other words, the radioactive rays come out of the atomic nucleus.

A few examples of alpha decay are,

$$ {}^{238}_{92}\mathrm{U} \rightarrow {}^{4}_{2}\mathrm{He} + {}^{234}_{90}\mathrm{Th} \qquad \ldots(2.2) $$

$$ {}^{226}_{88}\mathrm{Ra} \rightarrow {}^{4}_{2}\mathrm{He} + {}^{222}_{86}\mathrm{Rn} \qquad \ldots(2.3) $$

$$ {}^{218}_{84}\mathrm{Po} \rightarrow {}^{4}_{2}\mathrm{He} + {}^{214}_{82}\mathrm{Pb} \qquad \ldots(2.4) $$

Alpha rays can be stopped by a thin sheet of paper. On the other hand, they cause intense ionization in air. Most α-particles are emitted with velocities between $\sim 1.5 \times 10^7$ m/s and $\sim 2.2 \times 10^7$ m/s. Any group of α-particles emitted from the same type of nuclei always has a definite velocity and hence a definite energy.

The alpha particles cover a definite distance in a given material, practically without any loss of intensity and then suddenly in a small distance are absorbed completely. The definite distance they travel within a given material is called their range in that material. For example, α-particles from radium $\left({}^{226}_{88}\mathrm{Ra}\right)$ have a range in air equal to 3.4 cm. at 0° C and 76 cm. of pressure. We will look at these aspects in chapter 4, where we will see how range is related to energy (See Chapter 1 also) and how one can theoretically account for alpha decay.

(*b*) *The* β *rays* are identical with electrons. A β-particle therefore has a mass (1/1836) mass of a proton.

A few examples of β decay are:

$$ {}^{234}_{90}\mathrm{Th} \rightarrow {}^{234}_{91}\mathrm{Pa} + {}^{0}_{-1}e \qquad \ldots(2. $$

$$ {}^{210}_{83}\mathrm{Bi} \rightarrow {}^{210}_{84}\mathrm{Po} + {}^{0}_{-1}e \qquad \ldots(2. $$

$$ {}^{14}_{6}\mathrm{C} \rightarrow {}^{14}_{7}\mathrm{N} + {}^{0}_{-1}e \qquad \ldots(2. $$

Notice that the mass number and charge are conserved and the daughter product move one place up in the periodic table, as loss of a negative charge by a nucleus would imply gai of a positive charge. Beta rays cause much less ionization in air, but are ~100 times mor penetrating than α-rays. They can penetrate a sheet of aluminium a few mm thick.

The velocities of β-particles emitted from various nucleii range up to 0.99c, where $c = 3 \times 10^8$ m/s, is the velocity of light. A particular β-active element emits β-particles with energies varying between zero and a certain maximum. This maximum energy is called the end-point energy. We shall study a number of interesting aspects of β-rays in Chapter IV.

(*c*) *The* γ*-rays* are part of the electromagnetic spectrum. They have wavelengths smaller than those usually associated with the X-rays. Thus, usually γ-ray photons (energy of a photon $E = hf = hc/\lambda$) are more energetic than the X-ray photons and are even more penetrating than the X-rays. (They are ~100 times more penetrating than β-rays.) The wavelength of γ-ray photons ranges between ~1.7×10^{-8} cm and ~4×10^{-6} cm.

The ionization due to γ-rays is a photoelectric effect. Owing to their large energies, the γ-ray photons can dislodge electrons not only from outer orbits (valence orbits on conduction bands) of the atoms but also from the inner orbits. Besides this photoelectric effect, γ-rays lose energy by (*i*) Compton scattering, in which the γ-photon collides with an electron and gets scattered with a shift in wavelength $[\Delta\lambda = h/m_0c\,(1 - \cos\alpha)]$, and (*ii*) pair production in which a γ-photon is converted into a pair consisting of an electron and a positron. For this, the energy of the γ-ray has to be >1.02 MeV.

We will study γ-rays and γ-decay in some detail in Chapter 4.

2.3 THE LAW OF RADIOACTIVE DECAY

When a nucleus disintegrates by emitting a particle (α or β) or a gamma ray, or by capturing an electron from the atomic shell (*K*-capture), the process is called radioactive decay. This decay is spontaneous.

By using a Geiger Counter (see Chapter 1), it is possible to study how radioactive decay depends on time.

Let us take a radioactive sample containing N_0 nuclei at time $t = 0$, i.e., at the beginning. We wish to calculate the number N of these nuclei left after time t.

The number of nuclei of a given radioactive sample disintegrating per second is called the activity of that sample.

$$\therefore \quad \frac{dN}{dt} = \text{Rate of decrease of nuclei with time}$$

$$= \text{Activity at time } t. \qquad \ldots(2.8)$$

Experimentally, it is found that the activity at any instant of time t is directly proportional to the number N of parent type nuclei present at that time.

$$\therefore \qquad -\frac{dN}{dt} \propto N$$

or

$$-\frac{dN}{dt} = \lambda N \qquad \ldots(2.9)$$

where $\lambda > 0$, is the proportionality constant.

The negative sign indicates that N decreases as t increases.

For unit time, from Eq. 2.9, we get,

$$\lambda = \left(-\frac{dN}{N}\right) \qquad \ldots(2.10)$$

i.e., λ is fractional change in N per sec. and we see that λ is not a mere proportionality constant, but it gives us the probability of decay per unit interval of time. Hence λ is called the probability constant, the decay constant or the disintegration constant.

Notice that dN is the number of parent nuclei that decay between times t and $t + dt$, and that we have taken N as a continuous variable. We will come back to this in Sec. 2.4.

From Eq. 2.9, by integration we get,

$$\int_{N_0}^{N} \frac{dN}{N} = -\int_{0}^{t} \lambda \, dt$$

or

$$N = N_0 e^{-\lambda t} \qquad \ldots(2.11)$$

Here, N_0 = Number or radioactive nuclei at $t = 0$.

Thus we see that the law of radioactive decay is exponential in character. Figure 2.2 depicts a typical experimental decay curve for radon.

Notice that only half the amount of radon present initially remains after 3.83 days; only one-fourth of it remains after 7.66 days and only one-eighth remains after 15.32 days.

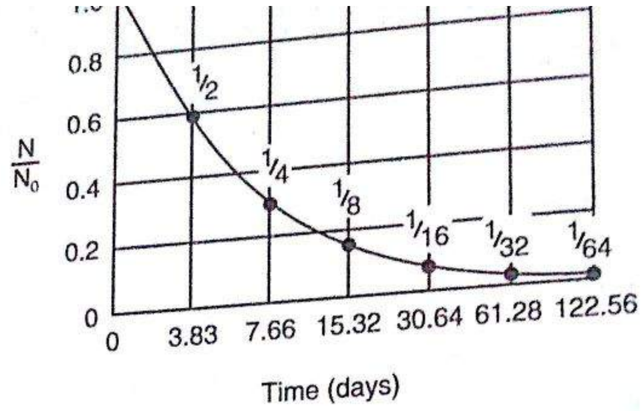

Fig. 2.2. Decay curve for radon, $\left({}^{222}_{88}\text{Rn}\right)$.

The plot shows that in a fixed time interval (say, 3.83 days for radon) a fixed fraction (1/2 for radon) of the amount of radioactive substance at the beginning of the interval decays. This fraction is independent of the amount of radioactive substance or whether you have a freshly prepared sample or not and instead depends only on the interval of time. This is a characteristic of the exponential nature of the law of radioactive decay.

The decay constant λ is a characteristic of radioactive substance and it depends in no way on the amount of the substance present.

Half Life (*T*): It is convenient to define a time interval during which half of a given sample of radioactive substance decays. This interval is called the half life or half value period of that substance, denoted by *T*.

$$\frac{N}{N_0} = \frac{1}{2} = e^{-\lambda T}$$

$$\therefore \qquad e^{\lambda T} = 2$$

$$\text{or} \qquad \lambda T = \log_e 2 = 0.693$$

$$\therefore \qquad \boxed{T = \frac{0.693}{\lambda}} \qquad \ldots(2.12)$$

Mean Life (τ): Individual radioactive atoms may have life spans between zero and infinity. Hence it is meaningful to talk about the average or mean life τ, defined as,

$$\tau = \frac{\text{Total life time of all nuclei in a given sample}}{\text{Total number of nuclei in that sample}} = \frac{1}{\lambda} \qquad \ldots(2.13)$$

To evaluate Eq. 2.13, see Fig. 2.3.

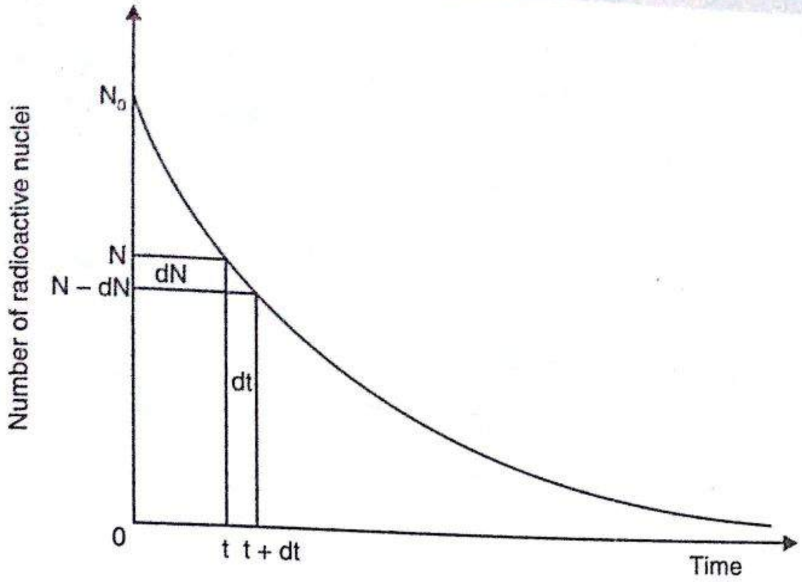

Fig. 2.3. Curve shows how *dN* number of nuclei decay in time *dt*.

From the curve, one can see that each of the *dN* number of radioactive nuclei has lived a life of *t* seconds, i.e., the total life span of *dN* nuclei is $(dN \cdot t)$ seconds.

$\therefore$ We can put Eq. 2.13 as,

$$\tau = \frac{\int_{N_0}^{0} t\,dN}{\int_{N_0}^{0} dN}$$

$$= \frac{-N_0\lambda \int_{0}^{\infty} te^{-\lambda t}\,dt}{-N_0}, \qquad \because \quad dN = -\lambda\, N\, dt = -\lambda\, N_0 e^{-\lambda t} dt$$

$$= \lambda \int_{0}^{\infty} te^{-\lambda t}\, dt,$$

which on integration by parts becomes,

$$\tau = \lambda \cdot \frac{1}{\lambda^2} = \frac{1}{\lambda} \qquad \ldots(2.14)$$

From Fig. 2.2,

T of radon = 3.83 days

i.e. in n half lives, $1/2^n$ of the original sample survives.

Also, $\qquad \because \qquad T = \dfrac{0.693}{\lambda}$

$\therefore$ λ of radon = $\lambda_{Rn} = 2.1 \times 10^{-6}\ \text{sec}^{-1}$.

ILLUSTRATIVE EXAMPLE

Example 2.1: According to measurements by Rutherford and Geiger, one gram of radium emits in one second 3.7×10^{10} alpha particles. Estimate the half life of radium.

Solution: The decay constant of radium is,

$$\lambda_{Ra} = \frac{3.7 \times 10^{10}}{2.7 \times 10^{21}} \text{ sec}^{-1} \qquad \text{see Eq. 2.10}$$

where 2.7×10^{21} = Number of radium atoms in one gram of radium.

($\because$ There are 6.02×10^{23} atoms [Avogadro's number] in one gm-atom of radium-226)

$$\therefore \qquad \lambda_{Ra} = 1.37 \times 10^{-11} \text{ sec}^{-1}$$

$$\therefore \text{ Half life, } T_{Ra} = \frac{0.693}{\lambda_{Ra}} \cong 5 \times 10^{10} \text{ sec} \cong 1600 \text{ yrs.}$$

Unit of Activity $= \frac{dN}{dt} = \lambda N$

The most commonly used unit is the curie. It was originally based on the rate of decay of a gram of radium. Experiments have yielded the result that there are-about 3.7×10^{10} disintegrations per second per gram of radium. This number is taken as a standard and is called the curie. Thus by definition,

$$\text{One curie} = 1 \text{ Ci} = 3.7 \times 10^{10} \frac{\text{disintegrations}}{\text{sec}} \qquad \ldots(2.15)$$

This is applicable to all types of nuclear disintegrations.

A Curie of activity is a very strong source of radiation.

Thus, one has

$$1 \text{ millicurie} = 1\text{m Ci} = 10^{-3} \text{ Ci}$$

and

$$1 \text{ microcurie} = 1\mu \text{ Ci} = 10^{-6} \text{ Ci.}$$

Sometimes one uses another unit for activity, called the rutherford.

$$1 \text{ rutherford} = 1 \text{ rd} = 10^{6} \frac{\text{disintegrations}}{\text{sec.}} \qquad \ldots(2.16)$$

$$1 \text{ mrd} = 10^{-3} \text{ rd}$$

$$1 \mu\text{rd} = 10^{-6} \text{ rd}$$

From Eq. 2.8,

$$\text{Activity} = \left|\frac{dN}{dt}\right| = \lambda N = \frac{0.693}{T} N$$

Notice that a very short-lived substance gives rise to large activity, even if it is present in minute quantities.

ILLUSTRATIVE EXAMPLE

Example 2.2: Calculate the activity of (*i*) One gram of radium ${}^{226}_{88}\text{Ra}$, whose half life is 1622 years and (*ii*) 3 × 10^{-9} kg of active gold, ${}^{200}_{79}\text{Au}$, whose half life is 48 mins.

Solution:

(*i*) $$N = 1\,\text{gm}\left(\frac{1\,\text{gm-mole}}{226\text{gm}}\right)\left(6.03 \times 10^{23}\,\frac{\text{atoms}}{\text{gm-mole}}\right)$$

$$= 2.66 \times 10^{21}\ \text{atoms}$$

$$\text{and}\ \lambda = \frac{0.693}{T}$$

$$= \frac{0.693}{1622 \times 365 \times 24 \times 60 \times 60}\,\text{sec}^{-1} = 1.355 \times 10^{-11}\,\text{sec}^{-1}$$

$$\therefore\ \underline{\text{Activity} = \lambda N} = 3.604 \times 10^{10}\,\frac{\text{disintegrations}}{\text{sec}}$$

$$= 0.974\ \text{Ci}$$

$$\sim 1\text{Ci}$$

(*ii*) $$N = \left(3 \times 10^{-6}\,\text{gm}\right)\left(\frac{1\,\text{gm-mole}}{200\,\text{gm}}\right)\left(6.03 \times 10^{23}\,\frac{\text{atoms}}{\text{gm-mole}}\right)$$

$$= 9.04 \times 10^{15}\ \text{atoms.}$$

$$\text{and}\ \lambda = \frac{0.693}{T}$$

$$= \frac{0.693}{48 \times 60}\,\text{sec}^{-1}$$

$$= 2.406 \times 10^{-4}\,\text{sec}^{-1}$$

$$\text{Activity} = \lambda N = 2.18 \times 10^{12}\,\frac{\text{disintegrations}}{\text{sec}}$$

$$= 58.9\text{Ci}$$

Notice that in (*ii*) the quantity of active substance is only about a millionth compared t that in (*i*), though the activity in (*ii*) is ~60 times that in (*i*).

2.4 STATISTICAL NATURE OF RADIOACTIVITY

In the previous section we have treated N, the number of radioactive nuclei present at time t, as a continuous variable. We are justified in doing this as long as N is very large compared to dN, the number of nuclei decayine between times t and $t + dt$. This is usually the case, as even in a minute quantity of radioactive material we have a very large number of nuclei, e.g., in one microgram of radium, there are still 2.7×10^{15} radium nuclei.

IMP

Actually N varies discontinuously and the smallest value of dN is one, corresponding to decay of a single nucleus. Thus we see that, the law of radioactive decay is valid only for a sample of radioactive material which is sufficiently large to enable us to treat dN as a differential. The concepts of half life and mean life become meaningless when you have a sample containing only a few nuclei. For example, if you are given say, 100 active nuclei on a sample holder, and the half life of the material is one hour, then it does not mean that you will be left with 50 nuclei after one hour! As the number of nuclei in the sample is increased—though we cannot say which nuclei will decay at a given instant—we can say that about half of them will decay after one half life.

Basically therefore, the radioactivity phenomenon is statistical in nature. We cannot say which radioactive nucleus will decay at a given instant of time, though we can predict what portion of the given sample will decay in an interval of time, provided the given sample is sufficiently large. This is characteristic of all quantum mechanical phenomena, e.g., emission of light when atoms de-excite.

It is possible to obtain the law of radioactive decay purely on the basis of statistical arguments, as follows.

Assume that disintegration of a nucleus depends only on the law of chance and the probability P for a nucleus to decay is the same for all nuclei of its kind. Further, P is independent of the age or past history of a nucleus.

∴ P depends only on time interval and for short intervals, it is proportional to the interval, i.e.,

$$P = \lambda \, \Delta t \qquad \ldots(2.17)$$

The probability Q_1, that a nucleus will not decay during the time interval Δt, is:

$$Q_1 = 1 - P = 1 - \lambda \, \Delta t$$

The probability Q_2, that a nucleus will not decay during time $2\Delta t$, is:

$$Q_2 = (1 - P)\,(1 - P) = (1 - \lambda\Delta t)^2$$

In general, the probability Q_n, that a nucleus survives n such intervals, is:

$$Q_n = (1 - \lambda\Delta t)^n \qquad \ldots(2.18)$$

Consider a finite time interval t, made up of n intervals of Δt, i.e.

$$\Delta t = t/n$$

Notice that in (*ii*) the quantity of active substance is only about a

that in (*i*), though the activity in (*ii*) is ~60 times that in (*i*).

2.4 STATISTICAL NATURE OF RADIOACTIVITY

In the previous section we have treated N, the number of radioactive nuclei present at time t, as a continuous variable. We are justified in doing this as long as N is very large compared to dN, the number of nuclei decayine between times t and $t + dt$. This is usually the case, as even in a minute quantity of radioactive material we have a very large number of nuclei, e.g., in one microgram of radium, there are still 2.7×10^{15} radium nuclei.

IMP

Actually N varies discontinuously and the smallest value of dN is one, corresponding to decay of a single nucleus. Thus we see that, the law of radioactive decay is valid only for a sample of radioactive material which is sufficiently large to enable us to treat dN as a differential. The concepts of half life and mean life become meaningless when you have a sample containing only a few nuclei. For example, if you are given say, 100 active nuclei on a sample holder, and the half life of the material is one hour, then it does not mean that you will be left with 50 nuclei after one hour! As the number of nuclei in the sample is increased—though we cannot say which nuclei will decay at a given instant—we can say that about half of them will decay after one half life.

Basically therefore, the radioactivity phenomenon is statistical in nature. We cannot say which radioactive nucleus will decay at a given instant of time, though we can predict what portion of the given sample will decay in an interval of time, provided the given sample is sufficiently large. This is characteristic of all quantum mechanical phenomena, e.g., emission of light when atoms de-excite.

It is possible to obtain the law of radioactive decay purely on the basis of statistical arguments, as follows.

Assume that disintegration of a nucleus depends only on the law of chance and the probability P for a nucleus to decay is the same for all nuclei of its kind. Further, P is independent of the age or past history of a nucleus.

∴ P depends only on time interval and for short intervals, it is proportional to the interval, i.e.,

$$P = \lambda\,\Delta t \qquad \ldots(2.17)$$

The probability Q_1, that a nucleus will not decay during the time interval Δt, is:

$$Q_1 = 1 - P = 1 - \lambda\,\Delta t$$

The probability Q_2, that a nucleus will not decay during time $2\Delta t$, is:

$$Q_2 = (1 - P)\,(1 - P) = (1 - \lambda\Delta t)^2$$

In general, the probability Q_n, that a nucleus survives n such intervals, is:

$$Q_n = (1 - \lambda\Delta t)^n \qquad \ldots(2.18)$$

Consider a finite time interval t, made up of n intervals of Δt, i.e.

$$\Delta t = t/n$$

$$Q_n = (1 - \lambda t/n)^n$$

But the limit of this quantity Q_n, as $n \to \infty$ is N/N_0, the surviving fraction after time t.

Now
$$Q_n = 1 - n\frac{\lambda t}{n} + \frac{n(n-1)}{2!}\frac{\lambda^2 t^2}{n^2} - \frac{n(n-1)(n-2)}{3!}\frac{\lambda^3 t^3}{n^3} + \ldots$$

$$= 1 - \lambda t + \left(1 - \frac{1}{n}\right)\frac{\lambda^2 t^2}{2!} - \left(1 - \frac{1}{n}\right)\left(1 - \frac{2}{n}\right)\frac{\lambda^3 t^3}{3!} + \ldots$$

$$\therefore \lim_{n\to\infty} Q_n = \frac{N}{N_0} = 1 - \lambda t + \frac{\lambda^2 t^2}{2!} - \frac{\lambda^3 t^3}{3!} + \ldots$$

$$= e^{-\lambda t}$$

giving the law of radioactive decay,

$$N = N_0 e^{-\lambda t}.$$

2.5 THE STATISTICAL ERRORS OF NUCLEAR PHYSICS

Using a detector like the Geiger Counter (see Chapter 1), it is possible to count the radioactive particles. From the preceding section, we know that the time t necessary for the observation of any finite number of counts N is subject to statistical fluctuations, giving rise to an error in the observed counting rate, $n = N/t$.

This is fundamental to the phenomenon of radioactivity and not a property of the instrument. We shall show below that the number of counts observed in a given time obeys a Poisson distribution.

Let the probability that N particles are observed in time t be P_N. Suppose that the interval t is divided into n equal intervals so small that the probability of emission of two particles within an interval is negligible.

∴ The probability of the emission of one particle in a given interval is, N/n, where N is the average number.

The purpose of this section is to treat the fluctuations or differences between the actual number of decaying nuclei N and the average number $\bar{N}$, sometimes denoted by $\langle N \rangle$.

The probability of emission of N particles in the first N intervals and none in the remaining $(n - N)$ intervals is:

$$\left(\frac{\bar{N}}{n}\right)^N \left(1 - \frac{\bar{N}}{n}\right)^{n-N} \qquad \ldots (2.19)$$

This is only one possible way of obtaining N particles in the total time t. The first particle could have been in any one of the n intervals, the second one in any one of the remaining $(n - 1)$ and so on, so that finally N^{th} in any of the remaining $(n + 1 - N)$. The N^{th} particle can choose any one of the intervals between the one it occupies and all the $n - N$ unoccupied intervals. Thus the number of ways of distributing the N particles in the n intervals is:

$$n(n-1)(n-2)\ldots\ldots(n-N+1).$$

However, all of these ways are not independent, since the particles may be interchanged without influencing the result. Therefore, the number of essentially different ways

$$= \frac{n(n-1)(n-2)\ldots\ldots(n-N+1)}{\text{Number of ways of interchanging particles}}$$

Any one of the N particles can be chosen as the first, any one of the remaining $(N-1)$ as the second and so on.

∴ Number of ways of interchanging particles = $N!$

Hence, probability of obtaining N counts is,

$$P_N = \frac{n(n-1)(n-2)\ldots\ldots(n-N+1)}{N!}\left(\frac{\bar{N}}{n}\right)^N\left(1-\frac{\bar{N}}{n}\right)^{n-N} \qquad \ldots(2.20)$$

This is the binomial distribution law.

When $n \to \infty$, Eq. (2.20) becomes

$$P_N = \frac{n^N}{N!}\left(\frac{\bar{N}}{n}\right)^N e^{-\bar{N}}$$

$$= \frac{\bar{N}^N e^{-\bar{N}}}{N!} \qquad \ldots(2.21)$$

This is the famous Poisson distribution formula. It is illustrated in Fig. 2.4.

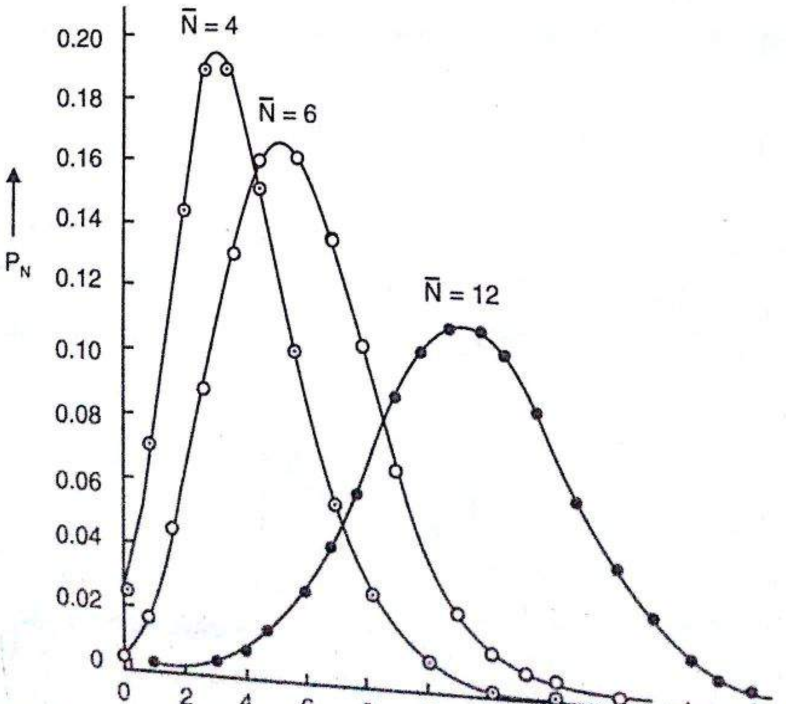

Fig. 2.4. *Poisson's Series.* Notice that as N becomes larger, the curve becomes more symmetrical about the maximum.

Strictly speaking, Eq. 2.21 is valid for only integral values of N. However, a continuous curve of P_N against N plotted through the points given by this formula yields a curve with an asymmetrical maximum for small values of N. As N becomes large the curve becomes symmetrical about the maximum and it can be shown analytically that the Poisson distribution approaches a Gauss error curve.

Then,

$$P_N = \frac{1}{\sqrt{2\pi\bar{N}}} e^{-\left(\frac{(N-\bar{N})^2}{2\bar{N}}\right)} \qquad \ldots(2.22)$$

which is the Gauss law. Proof of this is left to the reader (see Prob. 2.18).

∴ If on an average N counts are observed in given time t, the standard deviation in the number of counts,

$$S = \sqrt{\bar{N}} \qquad \ldots(2.23)$$

$$\left(\because \text{the precision index } h = \frac{1}{\sqrt{2\bar{N}}} \text{ and } S = \frac{\sqrt{2}}{h}\right)$$

Usually a single reading N is taken, which is assumed to be close enough to $\bar{N}$. Thus standard deviation,

$$S = \sqrt{N}$$

To appreciate this, let us take an example from laboratory data.

ILLUSTRATIVE EXAMPLE

Example 2.3: A cesium ($^{137}_{55}\text{Cs}$) sample was counted using a Geiger counter and the number of beta particles emitted in 1 min. was recorded in 10 intervals, each of 1 min. duration. The data is shown in the table below. The first column shows the observed counts, the second one shows the difference between average number of counts and particular 1 min. count.

Show that the standard deviation of a single measurement is in satisfactory agreement with that given by

$$S = \sqrt{\bar{N}}$$

N	$N - \bar{N}$	$(N - \bar{N})^2$
28792	13	169
28640	–139	19321
28510	–269	72361

Contd...

28680	-99	9801
28840	61	3721
28823	44	1936
28780	1	1
28975	196	38416
29010	231	53361
28740	-39	1521
		Σ 190807
$\bar{N} = 28779$		

Solution: Average counts for one min. interval = 28779. Since there are 9 intervals, standard deviation of a single measurement

$$= \left(\frac{190807}{9}\right)^{\frac{1}{2}}$$

$$\cong 150$$

Now, we know that,

$$S = \sqrt{\bar{N}} = (28779)^{\frac{1}{2}} \cong 169, \text{ in good agreement.}$$

2.6 RADIOACTIVE GROWTH AND DECAY

Let us consider decay of the type,

$$A \rightarrow B \rightarrow C \ \text{(stable)}$$

Our aim is to find out the abundance of substance B if A decays to B and B decays to C.

Let N_A be the number of nuclei of A type at any instant. Assume that originally only A type was present and the initial number of nuclei of A type be N_0.

Let N_B be the number of nuclei of B type at the same instant t. At $t = 0$, the initial number is zero.

B is formed as a result of decay of A.

Therefore, the number of nuclei entering the B category is,

$$-\frac{dN_A}{dt} = \lambda_A N_A$$

where λ_A is decay constant of A type.

The number of nuclei leaving the B category is,

$$= \lambda_B N_B$$

where λ_B is decay constant of B type.

$\therefore$ The net change in number of nuclei (per sec) of the *B* category is,

$$\lambda_A N_A - \lambda_B N_B = \frac{dN_B}{dt} \qquad \ldots(2.24)$$

Now, $$N_A = N_0 e^{-\lambda_A t}$$

$$\therefore \qquad \frac{dN_B}{dt} = \lambda_A N_0 e^{-\lambda_A t} - \lambda_B N_B$$

Multiplying by the integrating factor, $e^{\lambda_B t} dt$

$$e^{\lambda_B t} dN_B = \lambda_A N_0 e^{(\lambda_B - \lambda_A)t} dt - \lambda_B N_B e^{\lambda_B t} dt \qquad \ldots(2.25)$$

L.H.S. can be now integrated by parts.

$$\int e^{\lambda_B t} dN_B = e^{\lambda_B t} N_B - \int \lambda_B N_B e^{\lambda_B t} dt \qquad \ldots(2.26)$$

Integrating Eq. 2.25, and substituting Eq. 2.26, we get,

$$e^{\lambda_B t} N_B = \frac{\lambda_A}{\lambda_B - \lambda_A} N_0 e^{(\lambda_B - \lambda_A)t} + C$$

$$\because \qquad N_B = 0, t = 0,$$

$$C = -\left(\frac{\lambda_A N_0}{\lambda_B - \lambda_A}\right)$$

$$\therefore \qquad N_B = \frac{N_0 \lambda_A}{\lambda_B - \lambda_A}\left(e^{-\lambda_A t} - e^{-\lambda_B t}\right) \qquad \ldots(2.27)$$

Which is the desired result, giving the number of nuclei of *B* type present at any time *t*.

The decay of *A* type and growth and decay of *B* type is shown in Fig. 2.5.

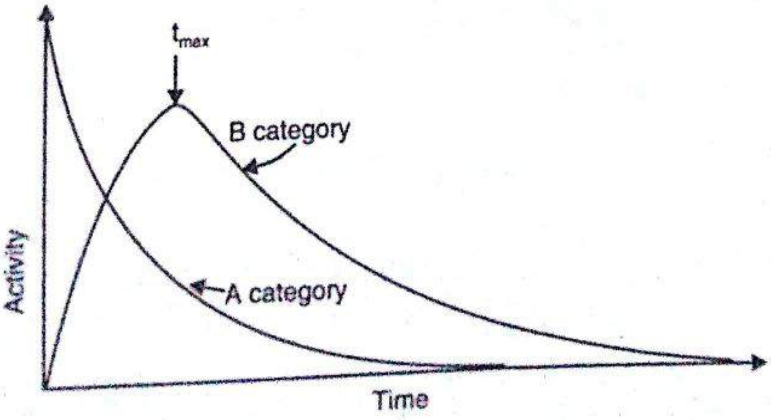

Fig. 2.5. Decay and growth of radioactivity.

ILLUSTRATIVE EXAMPLE

Example 2.4: Show that if there are initially N_0 radioactive nuclei of the parent present, the time at which the number of radioactive daughter nuclei is maximum is:

$$\boxed{t_{\max} = \frac{\log(\lambda_B/\lambda_A)}{\lambda_B - \lambda_A}} \qquad A \rightarrow B \rightarrow C$$

Solution: Figure 2.5 indicates how the daughter reaches the maximum activity.

We know that,

$$N_B = \frac{N_0\lambda_A}{\lambda_B - \lambda_A}\left(e^{-\lambda_A t} - e^{-\lambda_B t}\right)$$

For N_B to be maximum,

$$\frac{dN_B}{dt} = 0 = \frac{N_0\lambda_A}{\lambda_B - \lambda_A}\left[-\lambda_A e^{-\lambda_A t_{\max}} + \lambda_B e^{-\lambda_B t_{\max}}\right]$$

$$\therefore \qquad t_{\max} = \frac{\log(\lambda_B/\lambda_A)}{\lambda_B - \lambda_A}$$

2.7 IDEAL EQUILIBRIUM

From Eq. 2.24, at $t_{\max}$ we have

$$\lambda_A N_A = \lambda_B N_B \qquad \ldots(2.28)$$

since

$$\frac{dN_B}{dt} = 0$$

Thus at time $t_{\max}$, (and only at $t_{\max}$), the activity of parent and activity of accumulated daughter are equal.

At $t_{\max}$ (as considered in the illustrative example above), we have:

$$\lambda_A N_A = \lambda_A N_0 e^{-\lambda_A t_{\max}}$$

$$= \lambda_A N_0 e^{-\lambda_A \frac{\log\left(\frac{\lambda_B}{\lambda_A}\right)}{\lambda_B - \lambda_A}}$$

$$= \lambda_A N_0 \left(\frac{\lambda_A}{\lambda_B}\right) e^{\frac{\lambda_A}{\lambda_B - \lambda_A}}$$

$$= \lambda_A N_0 \left(\frac{T_B}{T_A}\right) e^{\frac{T_B}{T_A - T_B}} \qquad \ldots(2.29)$$

When the activities of parent and daughter are, equal, the situation is called *ideal equilibrium*. Note that this situation exists only at the moment when, time = t_{max}.

Look at Fig. 2.5 where dN_B/dt is positive between times, $t = 0$ and $t = t_{max}$. This implies that parent activity in this time range always exceeds daughter activity. Conversely between times $t = t_{max}$ and $t = \infty$, dN_B/dt is negative, implying that the daughter activity exceeds the activity of its parent.

2.8 TRANSIENT EQUILIBRIUM AND SECULAR EQUILIBRIUM

Consider, the daughter shorter-lived than the parent.

i.e $$T_A > T_B.$$

From Eq. 2.27 the activity of *B* type is,

$$\lambda_B N_B = N_0 \lambda_A \frac{\lambda_B}{\lambda_B - \lambda_A}\left(e^{-\lambda_A t} - e^{-\lambda_B t}\right)$$

Since $$\lambda_A N_A = \lambda_A N_0 e^{-\lambda_A t},$$

$$\lambda_B N_B = (\lambda_A N_A)\frac{\lambda_B}{\lambda_B - \lambda_A}\left(1 - e^{-(\lambda_B - \lambda_A)t}\right) \quad \text{...(2.30)}$$

or $$\frac{\lambda_B N_B}{\lambda_A N_A} = \frac{T_A}{T_A - T_B}\left(1 - e^{-[(T_A - T_B)/T_A]\lambda_B t}\right) \quad \text{...(2.31)}$$

For large *t*, Eq. 2.31 becomes,

$$\frac{\lambda_B N_B}{\lambda_A N_A} = \frac{T_A}{T_A - T_B} \quad \text{...(2.32)}$$

When the ratio, $\frac{T_A}{T_A - T_B}$ is greater than one, from Eq. 2.31, it is clear that for large *t*,

Equation 2.32 should hold. Since we have $T_A > T_B$ such is the case. When the Eq. 2.32 holds, we say that *transient equilibrium* exists between parent and the daughter. Note that according to Eq. 2.32 the ratio of daughter and parent activities is constant.

A prominent example of transient equilibrium is the following decay:

$$^{228}_{88}\text{Ra} \xrightarrow[T_A = 6.7\text{ yrs}]{\beta^-} {}^{228}_{89}\text{Ac} \xrightarrow[T = 6\text{ hours}]{\beta^-} {}^{228}_{90}\text{Th} \xrightarrow[T_B = 1.9\text{ yrs}]{\alpha} {}^{224}_{88}\text{Ra}$$

$^{228}_{89}\text{Ac}$ has half life of ~6 hours and promptly decays into $^{228}_{90}\text{Th}$.

Thus we can ignore the presence of ^{228}Ac as an intermediate product. From Eq. 2.32; the activity ratio corresponding to equilibrium is,

$$\frac{\lambda_B N_B}{\lambda_A N_A} = \frac{\text{Activity of } ^{228}\text{Th}}{\text{Activity of } ^{228}\text{Ra}}$$

$$= \frac{T_A}{T_A - T_B}$$

$$= \frac{6.7}{6.7 - 1.9}$$

$$= 1.39 \qquad \ldots(2.33)$$

i.e., it is >1.

Thus it is an example of transient equilibrium. Figure 2.6 shows decay of ^{228}Ra and growth of ^{228}Th.

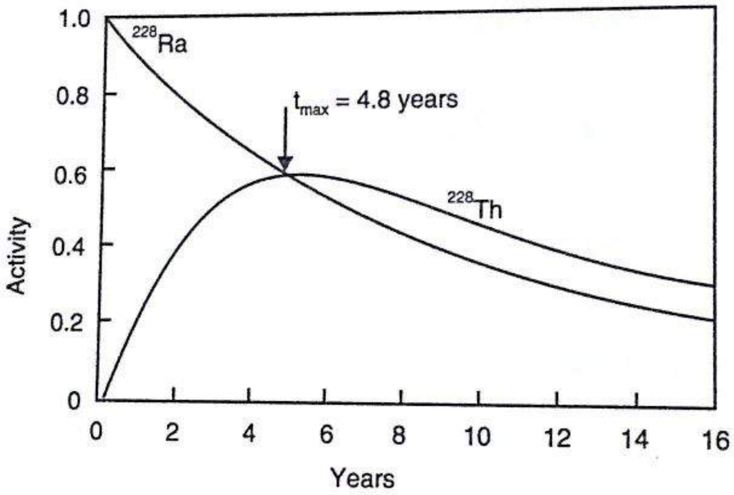

Fig. 2.6. Transient equilibrium between ^{228}Ra parent and ^{228}Th daughter. Initially, the source is pure ^{228}Ra.

Verify that t_{max} = 4.8 yrs (see Example 2.4).

Notice from the Fig. 2.6 that at larger values of time, the activity of the daughter approaches its transient equilibrium value of 1.39 times the remaining parent activity (as given by Eq. 2.33).

If the daughter is *longer-lived* than the parent, i.e., if $T_A < T_B$, from Eq. 2.31 it can be seen that, the ratio $\frac{\lambda_B N_B}{\lambda_A N_A}$ continuously increases as time t increases.

In other words, after sufficient time, the activity of the daughter becomes independent of the residual activity of the parent, and there can be no equilibrium between them. This is indicated in Fig. 2.7 for the case of

$$^{210}_{83}\text{Bi} \xrightarrow[T_A = 5.1 \text{ days}]{\beta} {}^{210}_{84}\text{Po} \xrightarrow[T_B = 138.4 \text{ days}]{\alpha} {}^{206}_{82}\text{Pb}$$

Let us now consider the important case of the daughter being much shorter-lived than parent.

Here, $\lambda_A \ll \lambda_B \qquad (T_A \gg T_B)$

and Eq. 2.30 becomes

$$\lambda_B N_B = \lambda_A N_A \left(1 - e^{-\lambda_B t}\right) \qquad \ldots(2.34)$$

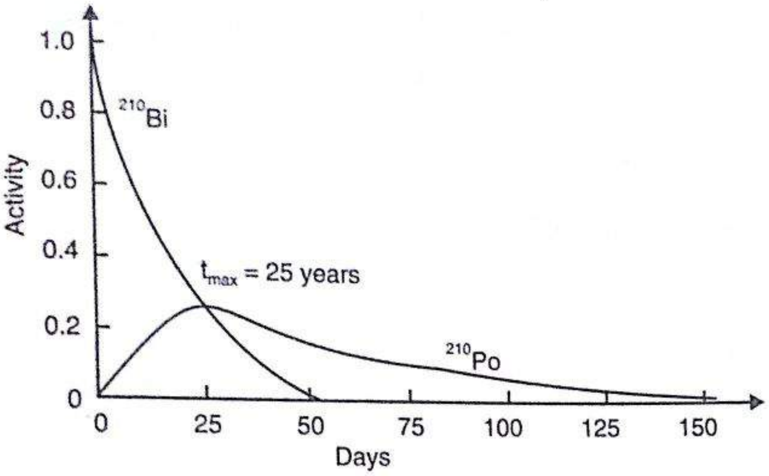

Fig. 2.7. There is no equilibrium between ^{210}Bi (5.1 *d*) and ^{210}Po (138.4 *d*).

that is the daughter activity is controlled only by its own decay constant.

It can be at once seen that for,

$$t \gg T_B,$$

the exponential,

$$e^{-\lambda_B t} = e^{-\frac{0.693}{T_B} t}$$

$$\cong 0$$

and so

$$\lambda_B N_B = \lambda_A N_A \qquad \ldots(2.35)$$

It should be kept in mind that Eq. 2.35 is valid only if $T_A \gg T_B$ and $t \gg T_B$.

Thus in these cases, the daughter activity equals the parent activity and the equilibrium is called *secular equilibrium.*

For a very long-lived parent, on physical grounds, the result given by Eq. 2.35 is expected. In this case, the activity of the parent can be taken as almost constant and so the rate of production of the daughter too is constant. As the daughter quantity grows (accumulates), its rate of decay increases and finally catches up, after sufficient time, with the rate of its production. When the two rates become equal, we say that the daughter is in secular equilibrium with the parent, and,

$$\lambda_B N_B = \lambda_A N$$

$$\frac{\lambda_B}{\lambda_A} = \frac{T_A}{T_B} = \frac{N_A}{N_B} \qquad \ldots(2.36)$$

giving,

Therefore in the case of secular equilibrium, the ratio of the number of parent nuclei and daughter nuclei is constant, and is equal to the ratio of their half lives.

This explains why the percentage of radium contained in uranium was always experimentally found to be the same—an average of one gram of radium per 3.2 tons of pure uranium.

From Eq. 2.36

$$\frac{N_{\text{Ra}}}{N_U} = \frac{T_{\text{Ra}}}{T_U} = \frac{1620\text{yrs.}}{4.5\times10^9\text{ yrs.}} (T_U \gg T_{\text{Ra}})$$

$$= 3.6\times10^{-7}$$

giving the experimentally observed ratio of 1 gm to 3.2 tons. Actually, radium is not the immediate daughter of uranium and we have to consider a radioactive series. (We will see this in the next section.) However, uranium has the longest half life in the series and hence all other products which are successively formed (except the end-product) are in secular equilibrium with uranium and their per cent content in a given sample of uranium is constant, equal to the ratio of their half lives as given by Eq. 2.36.

Another example of secular equilibrium, (which is not a part of a naturally occurring radioactive series) is,

$$^{90}_{38}\text{Sr} \xrightarrow[28\text{ yrs.}]{\beta^-} {}^{90}_{39}\text{Y} \xrightarrow[64.8\text{ hrs.}]{\beta^-} {}^{90}_{40}\text{Zr(stable)}.$$

If we start with a freshly prepared sample of pure ^{90}Sr, the number of ^{90}Y nuclei at first increases as per Eq. 2.34, then almost reaches the saturation value, and from then on slowly decreases with the half life of ^{90}Sr.

2.9 RADIOACTIVE SERIES

Each series is formed by successive daughter products, all ultimately derived from a single parent. Radioactive nuclei found in nature are said to exhibit natural radioactivity. There are now a few thousand radioactive isotopes which have been produced in the laboratory, mostly by neutron bombardment. These are said to exhibit artificial radioactivity. Compared to this, the number of naturally occurring radioactive nuclides is quite small, about 70.

When naturally occurring radioactive isotopes were studied, scientists found that they could be divided into four series (isotopes between $Z = 81$ and $Z = 92$).

The reason that there are exactly four series is a consequence of the fact that alpha decay reduces the mass number of nucleus by 4.

Therefore, the nuclei whose mass numbers are all given by

$$A = 4n. \qquad \ldots(2.37)$$

where n is an integer, can decay in descending order of mass number.

Radioactive nuclides whose mass numbers obey Eq. 2.37 are members of the $4n$ series.

The four series of naturally occurring nuclides are:

Mass Number	*Series*	*Parent*	*T of parent*
$A = 4n$	Thorium Series	${}^{232}_{90}\text{Th}$	1.39×10^{10} yrs.
$A = 4n + 1$	Neptunium Series	${}^{237}_{93}\text{Np}$	2.25×10^{6} yrs.
$A = 4n + 2$	Uranium Series	${}^{238}_{92}\text{U}$	4.51×10^{9} yrs.
$A = 4n + 3$	Actinium Series	${}^{235}_{92}\text{Ac}$	7.07×10^{8} yrs.

The members of each of these series can decay into one another (in the same series) in descending order of mass number.

The table gives the half lives of parent nuclide in each of the four series, which is very large, except for the parent of the neptunium series. For ${}^{237}_{93}\text{Np}$, half life is, $T = 2.25 \times 10^6$ yrs., which is quite short compared to the estimated age of earth which is about $\sim 10^{10}$ yrs. (see the following section). Thus, the members of this series are not found in nature today. However, they have been produced in the laboratory by neutron bombardment of other heavy nuclei. Note that the origin of this series can be traced back to Americium and Plutonium.

This process of chain of alpha and beta decays that leads from parent to stable end-point product in each series is shown in Figs. 2.8, 2.9, 2.10 and 2.11.

Branching: A given type of nuclei will normally decay by one particular mode, say by emission of β-particles. But many cases have been found in which a smaller percentage of nuclei will decay by a different mode such as α emission. This phenomenon is known as branching. For example, 99.96 per cent of nuclei of ${}^{214}_{83}\text{Bi}$ undergo β decay (see Fig. 2.10) to form ${}^{214}\text{Po}$; whereas 0.04 per cent of nuclei undergo alpha decay to form ${}^{210}\text{Tl}$ (Thulium).

Let us denote the probability of α emission by one nucleus, in time dt, $\lambda_\alpha dt$ and that of β emission by $\lambda_\beta dt$.

Then the total probability of decay of a nucleus in time dt by either α or β emission is:

$$(\lambda_\alpha + \lambda_\beta)dt$$

Hence the activity is:

$$\frac{dN}{dt} = -(\lambda_\alpha + \lambda_\beta)N. \qquad \ldots(2.38)$$

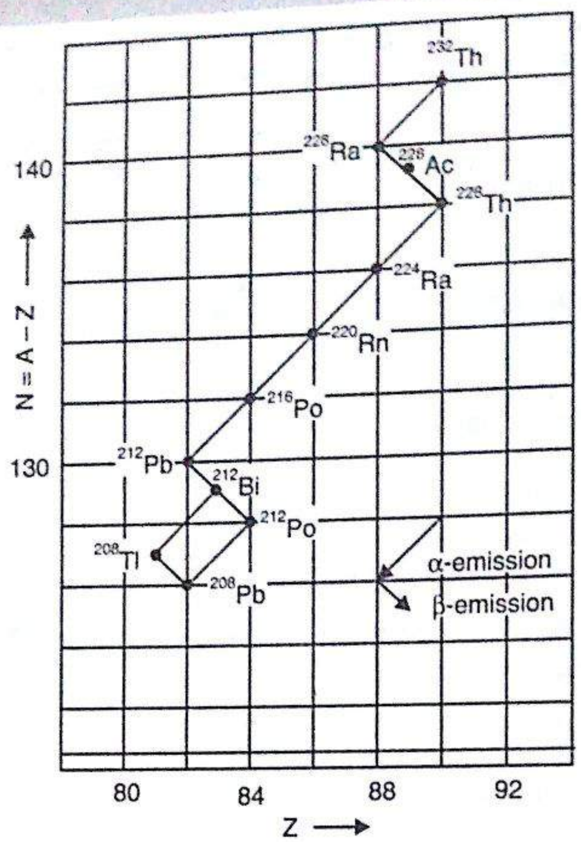

Fig. 2.8. $A = 4n$, thorium series. End product (stable) is ^{208}Pb. Notice the branching where ^{212}Bi may decay by α and then β emission or in the opposite order.

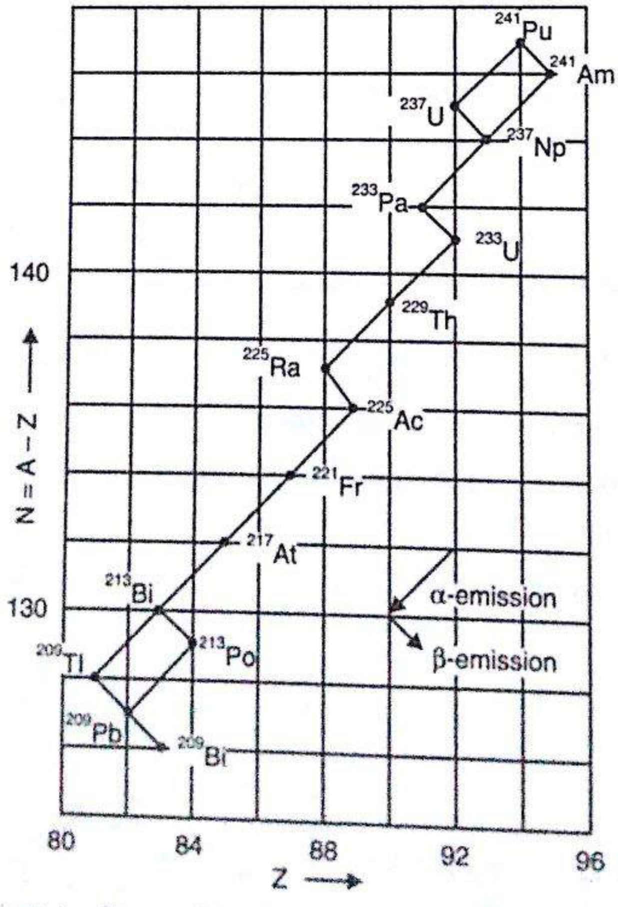

Fig. 2.9. $A = 4n + 1$, neptunium series. End product (stable) is ^{209}Bi. ^{213}Bi may decay by α emission followed by β emission or in the reverse order.

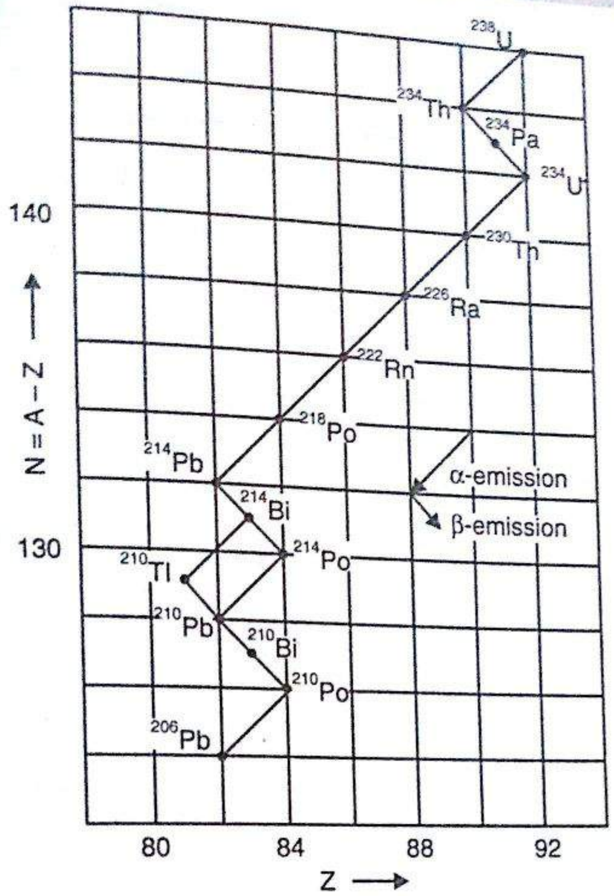
^{238}U
^{234}Th
^{234}Pa
^{234}U
140
^{230}Th
^{226}Ra
^{222}Rn
N = A − Z →
^{218}Po
^{214}Pb
α-emission
^{214}Bi
β-emission
130
^{210}Tl
^{214}Po
^{210}Pb
^{210}Bi
^{210}Po
^{206}Pb
80
84
88
92
Z →

Fig. 2.10. $A = 4n + 2$, uranium series. Stable end product is ^{206}Pb. Again notice branching.

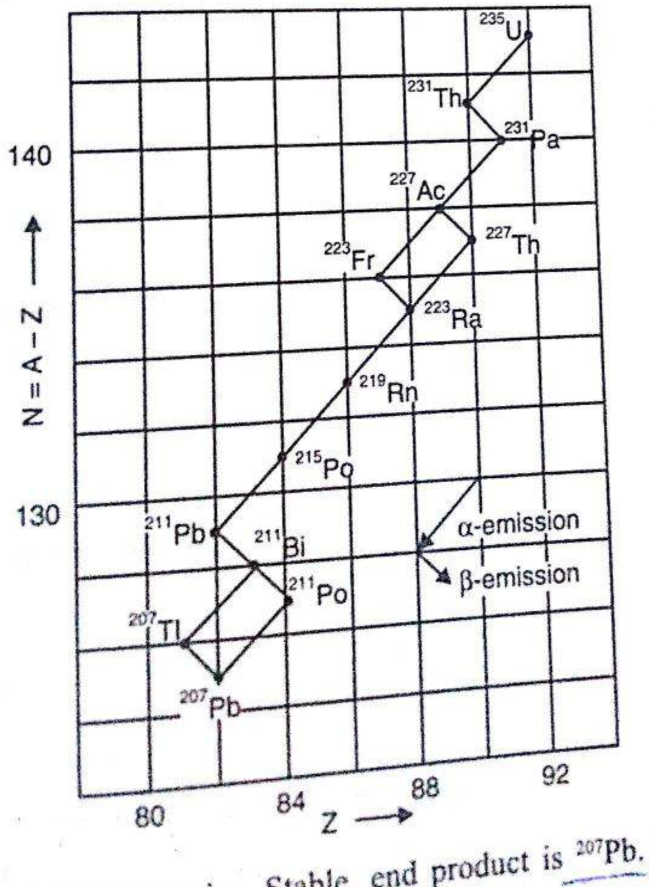
^{235}U
^{231}Th
^{231}Pa
140
^{227}Ac
^{227}Th
^{223}Fr
^{223}Ra
N = A − Z →
^{219}Rn
^{215}Po
130
α-emission
^{211}Pb
^{211}Bi
β-emission
^{211}Po
^{207}Tl
^{207}Pb
80
84
88
92
Z →

Fig. 2.11. $A = 4n + 3$, actinium series. Stable, end product is ^{207}Pb. Note the branching at ^{227}Ac and ^{211}Bi.

giving mean life,

$$\tau = \frac{1}{\lambda_\alpha + \lambda_\beta} \qquad \ldots(2.39)$$

The ratio

$$\boxed{\frac{\lambda_\alpha}{\lambda_\beta} = \text{branching ratio.}}$$

From Eq. 2.39 it follows that,

$$\frac{1}{\tau} = \frac{1}{\tau_\alpha} + \frac{1}{\tau_\beta} \qquad \ldots(2.40)$$

ILLUSTRATIVE EXAMPLE

Example 2.5: One is often required to deal with a situation where a radioactive substance, initially absent, is formed at a constant rate. For example, using particle accelerators (see Chapter 1), it is possible to artificially produce radioactive nuclei. Assume that a particular type of nucleus with decay constant λ is produced at a steady rate of P nuclei per second. Find the number of nuclei $N(t)$ present t seconds after the production starts.

Solution: Rate of formation of nuclei = P

Rate of decay of nuclei = λN at time t.

$$\therefore \qquad \frac{dN}{dt} = P - \lambda N.$$

We know that at time $t = 0$, $N = 0$

$\therefore$ Multiply by integrating factor $e^{\lambda t}\, dt$,

$$e^{\lambda t}\, dN = Pe^{\lambda t}\, dt - \lambda\, N e^{\lambda t}\, dt.$$

Integrating $e^{\lambda t}\, dN$ by parts and R.H.S. in a straightforward way

$$Ne^{\lambda t} - \int N\lambda e^{\lambda t}\, dt = \frac{P}{\lambda} e^{\lambda t} - \int N\lambda e^{\lambda t}\, dt + C$$

$$C = -\frac{P}{\lambda}, \quad \because \text{at } t = 0, N = 0$$

$$\therefore \qquad Ne^{\lambda t} = \frac{P}{\lambda}(e^{\lambda t} - 1)$$

or

$$N = \frac{P}{\lambda}(1 - e^{-\lambda t})$$

which is the required result.

2.10 RADIOACTIVE ISOTOPES OF LIGHTER ELEMENTS

Though the lowest atomic number among the naturally occurring radioactive series is found to be 81, radioactive isotopes of lower atomic numbers have also been found in nature. Most of these isotopes have very long half lives and very low abundances, so that the activity of samples is extremely small. Continuous and extensive testing of nuclear weapons has added new radioactive isotopes to the atmosphere. ^{90}Sr is an example of this nuclear pollution. It is a serious hazard as half life of ^{90}Sr is 27.7 years. Some of the prominent radioactive isotopes, mainly of the lighter elements, are given in Table 2.1.

TABLE 2.1

Atomic number Z	*Element*	*Mass number* A	*Type of radioactivity*	*Half life T in years*
1	Hydrogen	3	Beta	12.26
6	Carbon	14	Beta	5730
19	Potassium	40	Beta	1.3×10^9
38	Strontium	90	Beta	27.7
57	Lanthanum	138	Beta	1.1×10^{11}
60	Neodymium	144	Alpha	2.4×10^{15}
62	Samarium	147	Alpha	1.06×10^{11}
72	Hafnium	174	Alpha	2×10^{15}
78	Platinum	190	Alpha	6×10^{11}
82	Lead	204	Alpha	1.4×10^{17}

The nuclei of ^{14}C are being constantly produced by cosmic ray neutron bombardment of ^{14}N. Hence its activity is continuously replenished.

2.11 ARTIFICIAL RADIOACTIVITY

Rutherford was the first man to accomplish, in 1919, the artificial transmutation of one element into another. His apparatus is schematically represented by Fig. 2.12.

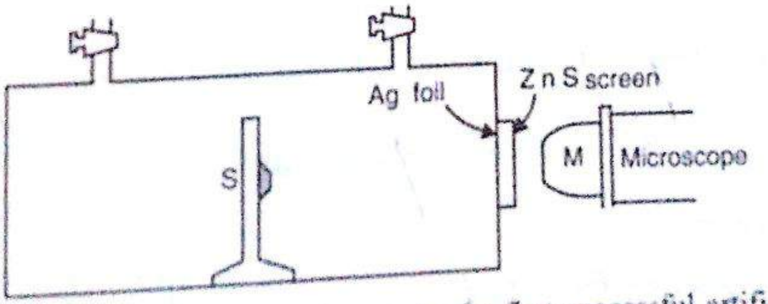

Fig. 2.12. Apparatus used by Rutherford to study the first successful artificial disintegration of nuclei.

The chamber was filled with nitrogen and alpha particles from ^{212}Po source (*S* in Fig. 2.12) were made to bombard the nuclei of nitrogen. A sheet of silver foil thick enough to absorb α-particles was placed over an opening in the chamber. The screen made from ZnS was placed outside this opening and a microscope *M* could observe the scintillations produced on this screen. (Zinc sulphide is fluorescent under radioactive rays.) Scintillations were observed when the chamber was filled with nitrogen. Rutherford concluded that the scintillations were produced by particles which were ejected from nitrogen nuclei as a result of α-bombardment. Later these particles were identified as protons (by the magnetic deflection method) having a range of ~ 50 cm in air.

The reaction can be written as:

$$ {}^{14}_{7}\mathrm{N} + {}^{4}_{2}\mathrm{He} \rightarrow {}^{17}_{8}\mathrm{O} + {}^{1}_{1}\mathrm{H} $$

After the discovery of the neutron in 1932 by Chadwick, it became possible to see that many of the induced nuclear transformations are radioactive. Today we have a few thousand radioactive species that have been made in the laboratory, by using accelerators.

The decay theories are the same for these artificially produced radioactive substances as the same laws that govern natural radioactivity hold.

In 1934, M. and Mme. Curie-Joliot were bombarding light element by α-particles and these studies led to important observations. They found that the bombarded substances continued to emit radiation even after the source of α-particles had been removed. Magnetic deflection experiments showed that the radiations consisted of positrons (positron is the anti-particle of the electron, having a +ve charge of the same magnitude as that of the electron).

The half life *T* of the positron emitters was measured. Curie-Joliot explained this phenomenon by suggesting the following nuclear process:

Step I: Bombardment of ^{10}B by α-particles giving a neutron and a residual nucleus rich in protons.

$$ {}^{10}_{5}\mathrm{B} + {}^{4}_{2}\mathrm{He} \rightarrow \underbrace{\left({}^{14}_{7}\mathrm{N}\right)^{*}}_{\substack{\text{Compound}\\ \text{nucleus}\\ \text{(See Chapter 4)}}} \rightarrow {}^{13}_{7}\mathrm{N} + {}^{1}_{0}n $$

Step II: Proton rich residual nucleus decays by positron emission.

$$ {}^{13}_{7}\mathrm{N} \rightarrow {}^{13}_{6}\mathrm{C} + \beta^{+} + \text{neutrino.} $$

Half life $T = 9.96$ min.

Another reaction studied by Curie-Joliot:

$$ {}^{27}_{13}\mathrm{Al} + {}^{4}_{2}\mathrm{He} \rightarrow \left({}^{31}_{15}\mathrm{P}\right)^{*} \rightarrow {}^{30}_{15}\mathrm{P} + {}^{1}_{0}n $$

and then, $${}^{30}_{15}\text{P} \rightarrow {}^{30}_{14}\text{Si} + \beta^{+} + \text{neutrino.}$$

Half life $T = 2.5$ mins.

After the pioneering work by Curie-Joliot in the study of artificial radioactivity, a massive programme to produce artificially radioactive isotopes was launched by various laboratories all over the world using particle accelerators, nuclear reactors (as neutron source) to bombard elements by different projectiles. A study of these reactions and the artificial radioactivity produced has enabled us to experimentally understand the structure of over a thousand isotopes of different elements. In this sense, in nuclear physics today, we know much more about nuclear energy levels and their properties experimentally than what we know of nuclear matter theoretically.

Some more examples of artificial radioactivity are given below:

(*i*) $${}^{11}_{5}\text{B} + {}^{4}_{2}\text{He} \rightarrow \left({}^{15}_{7}\text{N}\right)^{*} \rightarrow {}^{14}_{6}\text{C} + {}^{1}_{1}\text{H}$$

followed by $${}^{14}_{6}\text{C} \rightarrow {}^{14}_{7}\text{N} + \beta^{-} + \text{anti-neutrino.}\, T = 5730 \text{ yrs.}$$

(*ii*) $${}^{34}_{17}\text{Cl} \rightarrow {}^{34}_{16}\text{S} + \beta^{+} + \text{neutrino.}\, T = 32 \text{ mins.}$$

(*iii*) $${}^{7}_{3}\text{Li} + {}^{4}_{2}\text{He} \rightarrow \left({}^{11}_{5}\text{B}\right)^{*} \rightarrow {}^{11}_{5}\text{B} + \gamma(\gamma-\text{rays}).$$

(*iv*) $${}^{2}_{1}\text{H} + {}^{2}_{1}\text{H} \rightarrow \left({}^{4}_{2}\text{He}\right)^{*} \rightarrow {}^{3}_{1}\text{H} + {}^{1}_{1}\text{H}$$

followed by, $${}^{3}_{1}\text{H} \rightarrow {}^{3}_{2}\text{He} + \beta^{-} + \text{anti-neutrino.}\, T = 12.26 \text{ hrs.}$$

(*v*) $${}^{27}_{13}\text{Al} + {}^{1}_{0}n \rightarrow \left({}^{28}_{13}\text{Al}\right)^{*} \rightarrow {}^{24}_{11}\text{Na} + {}^{4}_{2}\text{H}$$

followed by, $${}^{24}_{11}\text{Na} \rightarrow {}^{24}_{12}\text{Mg} + \beta^{-} + \text{anti-neutrino.}\, T = 15 \text{ hrs.}$$

(*vi*) $${}^{14}_{7}\text{N} + n \rightarrow \left({}^{15}_{7}\text{N}\right)^{*} \rightarrow {}^{14}_{6}\text{C} + {}^{1}_{1}\text{H}$$

followed by, $${}^{14}_{6}\text{C} \rightarrow {}^{14}_{7}\text{N} + \beta^{-} + \text{anti-neutrino.}$$

A systematic study of energetics of nuclear reactions is undertaken in Chapter 3. As can be noticed, most of the artificially produced radioactive isotopes have small half lives. This can be a valuable aid in the identification of an element by chemical, analysis, e.g., Curie-Joliot, in their boron reaction made a target of

BN (Boron nitride)

This they irradiated with α-particles for several minutes and then heated it with NaOH (caustic soda).

The chemical reaction was:

$$BN + 3NaOH \rightarrow Na_2\,BO_3 + NH_3 \uparrow$$

They found that the gaseous NH_3 (ammonia) was the only radioactive chemical product. This clearly indicated that the nitrogen $\left({}^{13}_{7}N\right)$ was the radioactive element produced in this experiment. The short half lives also enable a quick identification, as half lives are characteristic of the emitting nuclei.

2.12 DETERMINATION OF THE AGE OF THE EARTH

Radioactivity is the best clock we can employ to estimate the absolute age of the earth, as it is totally unaffected by environmental change or natural upheavals like earthquakes, storms etc. The determination of geological ages is done very often by the so-called lead methods. It involves the following nuclear processes:

$${}^{238}_{92}U \rightarrow \text{ emission of 8 } \alpha\text{-particles} \rightarrow {}^{206}_{82}Pb$$

$${}^{235}_{92}U \rightarrow \text{ emission of 7 } \alpha\text{-particles} \rightarrow {}^{207}_{82}Pb$$

$${}^{232}_{90}Th \rightarrow \text{ emission of 6 } \alpha\text{-particles} \rightarrow {}^{208}_{82}Pb$$

To illustrate how an estimate of time can be made, consider the ${}^{238}_{92}U$ series. The stable end-product is ${}^{206}_{82}Pb$, and so we can take $\lambda_{Pb} = 0$. The half life of ^{238}U is 4.5×10^9 years. Hence after sufficient time, (say, a billion years) the only elements present in any appreciable amount will be uranium and lead. This is because, all elements in the uranium series will be in secular equilibrium with the parent ^{238}U and only ^{206}Pb will not be in equilibrium, and hence quantity of Pb will continuously go on increasing while uranium will continuously get depleted. This is indicated in Fig. 2.13 which depicts the flow of water from a reservoir into a collector, through a chain of other tanks in between. The diameters of the connecting pipes determine the 'probability' of decay (rate of flow). The situation is analogous with decay of a radioactive series, finally ending in a stable product.

Therefore it is possible for us to apply Eq. 2.27 not only to the first and second elements ($A \rightarrow B$) but also to the first and last. (^{238}U and ^{206}Pb in the case referred).

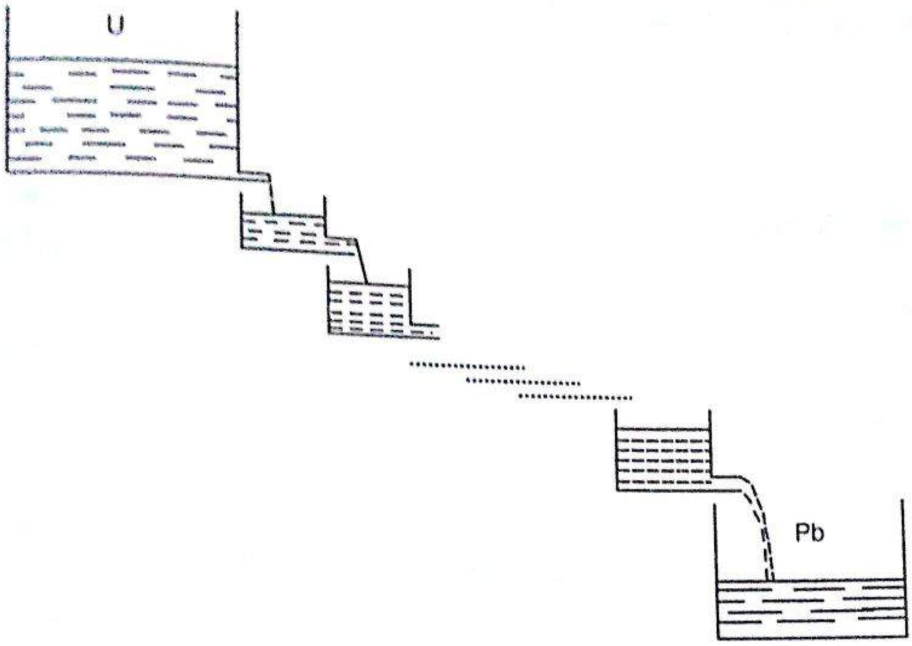

Fig. 2.13. Water flow analogy to illustrate depletion of U and accumulation of Pb. Note that Pb cannot be in equilibrium with U. All other members of the series are, and so they are present in minute and fixed amounts.

Equation 2.27 is:

$$N_B = \frac{N_0 \lambda_A}{\lambda_\beta - \lambda_A}\left(e^{-\lambda_A t} - e^{-\lambda_B t}\right)$$

For our case,

$$\lambda_A = \lambda_U$$

$$\lambda_B = \lambda_{\text{Pb}} = 0 \quad \text{as Pb is stable.}$$

$$N_B = N_{\text{Pb}}$$

$$N_0 = N_v$$

$\therefore$

$$N_{\text{Pb}} = -N_v\left(e^{-\lambda_U t} - 1\right)$$

$$= N_v\left(1 - e^{-\lambda_U t}\right) \qquad \text{...(2.41)}$$

^{238}U ore always contains ^{206}Pb, which can be assumed to be of radioactive origin (^{206}Pb is the end-product).

∴ Present number of Pb atoms + Present number of U atoms

= Number of U atoms originally present.

i.e.,

$$N_{Pb} + N_U = N_v \qquad \text{...(2.42)}$$

Eqs. 2.41 and 2.42 can be solved simultaneously to give:

$$t = \frac{1}{\lambda_U} \log\left(\frac{N_{Pb} + N_U}{N_U}\right) \qquad \text{...(2.43)}$$

Thus by spectro-chemically analysing a sample and knowing its uranium and lead content, it is possible to estimate the age of that sample. Of course, the most important factor is to ensure that no helium or uranium has escaped the rock sample during its lifetime.

The oldest surface rocks have been found to have an age of about 3×10^9 years.

When the same method is applied to determine the age of meteorites, it is found that oldest of these are about 4.5×10^9 years. This corresponds to the age of the earth and is different from the segregation of surface rocks.

Another method may be mentioned. It consists of using the $^{206}Pb/^{207}Pb$ isotopic ratio of radiogenic lead.

Using Eq. 2.41 it is easy to see that

$$\frac{^{206}\text{Pb}}{^{207}\text{Pb}} = \frac{^{238}\text{U}(1 - e^{-\lambda_U t})}{^{235}\text{U}(1 - e^{-\lambda'_U t})} \qquad \text{...(2.44)}$$

where $\qquad \lambda_U = \lambda \text{ of } {}^{238}\text{U}$

and $\qquad \lambda'_U = \lambda \text{ of } {}^{235}\text{U}.$

From Eq. 2.44, t can be evaluated.

The main disadvantage of this method is that radon which forms in the decay of ^{238}U has a half life of 3.82 days and being gaseous, might escape from the system.

Thus for this method or the first method, the rock samples have to be taken from massive pitchblende, deeply buried. In such a case, the gas would get trapped in rock cavities and radon (T = 3.82 days) cannot be expected to diffuse very far from the dense rocks.

2.13 CARBON DATING—ARCHAEOLOGICAL TIME SCALE

Cosmic rays continuously form $^{14}_{6}C$ in atmosphere. The nuclear reaction is

$$^{1}_{0}n + {}^{14}_{7}\text{N} \rightarrow {}^{14}_{6}\text{C} + {}^{1}_{1}\text{H}$$

$^{14}_{6}C$ is a neutron-rich (6 protons and 8 neutrons) isotope of carbon, which is β^- active.

$$^{14}_{6}C \rightarrow {}^{14}_{6}N + \beta^- + \text{antineutrino.}$$

Half life of $^{14}_{6}C$ is 5730 years.

Thus $^{14}_{6}C$ would not have been present in the atmosphere, had it not been continuously replenished. ^{14}C gets combined with hydrogen and oxygen and eventually finds its way into all organic matter. Since ^{14}C has a half life of 5730 years it is an ideal radioactive isotope for studying the age of civilisations and is extensively used in archaeology and anthropology.

When an animal or plant dies, its intake of carbon stops and from that moment decay of ^{14}C is the only process that continues. Coal and petroleum are organic in nature, but they are so old that there is no trace of ^{14}C in them. This has been established by experiments. In a young animal or tree, ^{14}C activity is same as atmospheric carbon which is about 15 disintegrations per gm per min.

By carefully measuring the ^{14}C activity of a fossil or dead tree, it is possible to estimate its age. This is shown in the problem given below.

ILLUSTRATIVE EXAMPLE

Example 2.6: In an archaeological expedition, charcoal from an ancient fire-pit was excavated. The absolute activity of ^{14}C This sample showed a ^{14}C activity of 11.3 counts per gm per min. in a living tree is independent of species and it is ~15.3 counts per gm per min. Estimate the age of the charcoal sample.

Solution: We have,

$$11.3 = 15.3e^{-\lambda t}$$

Is it λ? or what?

$$\frac{dN}{dt} = \lambda e^{-\lambda t}$$

where
$$\lambda = \frac{0.693}{T} = \frac{0.693}{5730 \text{ years.}}$$

Didn't get

Thus
$$1.354 = e^{\lambda t} = e^{0.000121t} \text{ where } t \text{ is in year}$$

$$t = \text{age of charcoal sample in years}$$

$$= \frac{\log_e 1.354}{0.000121} \text{ years}$$

$$= 2504.65 \text{ years.}$$

EXERCISES

1. Calculate the weight 1Ci of,

   (*i*) $^{238}_{92}\text{U}, T = 4.5 \times 10^{9}$ yrs.

   (*ii*) $^{234}_{92}\text{U}, T = 2.48 \times 10^{5}$ yrs.

   (*iii*) $^{212}_{82}\text{Pb}, T = 10.6$ hrs.

   (*iv*) $^{212}_{84}\text{Po}, T = 3.04 \times 10^{-7}$ sec.

2. Calculate the volume of 1 Ci of radon $\left(^{222}_{86}\text{Rn}\right)$ at N.T.P. (at 0° C and 760 mm of Hg pressure). Half life of radon = 3.82 days.

3. Sixty hours after a sample of beta emitter $^{24}_{11}\text{Na}$ has been prepared, only 6.25% of it remains undecayed. What is the half life of this isotope?

4. The mass of one millicurie (mCi) of $^{214}_{82}\text{Pb}$ is 3×10^{-14} kg. Find the half life of this isotope. Also calculate the mean life.

5. Radium has a half life of ~1600 yrs. The earth's age is ~4×10^{9} yrs. Thus one expects the amount of radium present to be negligibly small. But still Mme Curie was able to extract radium from uranium ore. Explain.

6. The nucleus of $^{238}_{92}\text{U}$ decays into a stable isotope of some element through successive emissions of 8 alpha particles and 6 beta particles. Identify the stable element, and give its Z and A values.

7. If a radioactive element disintegrates over a time equal to its average life τ, what fraction of the original amount remains?

8. The activity of a sample of $^{55}_{24}\text{Cr}$ is measured at the end of 5min. intervals. The following activities are measured in millicuries: 19.2, 7.13, 2.65, 0.99 and 0.37. Plot log (activity) against time and determine the half life from the graph.

9. A mass of 4.6 gm of uranium oxide (U_3O_8) has a certain activity. What is the mass of U $(NO_3)_6$ that gives the same activity? Take uranium to be $^{238}_{92}\text{U}$.

10. Give examples to illustrate the generality of the law of exponential decay and growth.

11. Consider the decay series:

$$A \rightarrow B \rightarrow C \quad \text{(stable)}$$

Equation 2.27 gives the amount of B at time t. B decays into stable substance C. Determine how the amount of C varies with time.

12. (*i*) In a sample of 1 kg of ^{232}Th, how many decays occur per day?

    (*ii*) If all the alpha particles could escape from the given thorium and the sample were electrically insulated, how much negative charge would accumulate on the sample? (T of $^{232}\mathrm{Th} = 1.41 \times 10^{10}$ yrs.)

13. When the situation corresponds to transient equilibrium, daughter activity always exceeds the activity of the parent substance. Describe how you visualize such a situation, apart from the way it is analytically given by Eq. 2.32.

14. Express $t_{\max}$ obtained in solved Example 2.4, in terms of mean life τ and half life T of parent and daughter, A and B respectively. Is $t_{\max}$ physically acceptable for both, $T_A > T_B$ and $T_B > T_A$? Explain.

15. There are no physical cases known for which $T_A = T_B$, where as before, A is parent and B is daughter. But if you consider $T_A = T_B$, show that,

$$t_{\max} = \sqrt{\tau_A \tau_B.}$$

    (*Hint:* Put $T_A = T_B\ (1 + \delta)$ where $\delta \ll 1$).

16. ^{212}Bi decays to ^{208}Tl by α emission in 35 per cent of the disintegration and to ^{212}Po by β emission in 65 per cent of the disintegration. If the total half life is 60.6 min., find the decay constants for α and β modes of decay and also the branching ratio.

17. Radioactive isotope ^{32}P is produced by neutron bombardment of ^{31}P target in a nuclear reactor at a steady rate of 5×10^{10} nuclei per sec. If the half life of ^{32}P is 14.5 days, calculate the time required to give maximum activity of ^{32}P. (The maximum activity is sometimes referred to as saturation activity.)

18. Prove that for a Poisson distribution,

$$\sum_{n=0}^{\infty} P_n = 1$$

    What does this verify?

19. In order to measure a counting rate with an accuracy of 1 per cent, we must count at least 10,000 decays; or for an accuracy of 1 in 10^3, a measurement of 10^6 decay events is required. Discuss and explain.

20. A certain sample gives a counting rate of 140 counts per min. on a Geiger counter. The observation is continued for 21 mins. The background of the counter is 40 counts per min., which is based on an observation of 38 min. duration. Find the expected net counting rate of the sample and its probable error.

21. Isotopes of lead are produced in a uranium mineral (originally lead-free) by a radioactive decay of the isotopes ^{235}U and ^{238}U. Suppose the mineral is 6.5×10^8 years old. Calculate the isotopic ratio, $^{206}\mathrm{Pb}/^{207}\mathrm{Pb}$.

    Half lives are, $^{238}\mathrm{U} = 4.51 \times 10^9$ years

    $^{235}\mathrm{U} = 7.07 \times 10^8$ years.

22. An archaeologist finds a piece of wood in an excavated house. When this is examined by a nuclear geologist, it is found to weigh 100 gm and shows a ^{14}C activity of 650 disintegrations per min. Explain how the geologist must have obtained the age of the wood sample and estimate it yourself. Assume that (*i*) living trees show a ^{14}C activity of 15 disintegrations per gm per min. and (*ii*) T of ^{14}C is 5,730 years.

23. ^{140}La samples resulting from decay $^{140}\mathrm{Ba} \xrightarrow[300\mathrm{hr}]{\beta} {}^{140}\mathrm{La}$ are to be used in a series of experiments. Whenever the La activity reaches the maximum, La is separated from its parent, chemically, to form a sample for study. Ba continues to produce La and when the new La growth reaches a maximum value,

the second sample is separated. This procedure is continued as long as samples so obtained have an activity greater than 1 mCi at separation.

(*i*) If the initial amount of pure ^{140}Ba is 5 mCi, how many useful samples can be obtained?

(*ii*) What will be the activity of the last sample of ^{140}La at the time of separation?

24. What activity of ^{131}I is accumulated (during a 2 hr. bombardment of ^{130}Te $(d, p) \rightarrow$ ^{131}Te $\rightarrow$ ^{131}I, if the yield of ^{131}Te is 0.92 mCi per hour"?

(*T* of ^{131}I = 8 days.)

25. In a radio-active transformation, the parent element has a half life T_P which is very much greater than the half-life T_D of the daughter element. Find out the time required, in terms of T_D, to have secular equilibrium between the parent and the daughter, within, (*i*) 90%, (*ii*) 99% and (*iii*) 99.9%.

3

The Q Equation

"Don't let me catch anyone talking about the Universe in my department."

—*(Lord) Ernest Rutherford*

3.1 INTRODUCTION

A considerable part of our present knowledge of the nuclear structure comes from experiments in which a chosen nucleus is bombarded with different projectiles, such as protons, neutrons, deuterons or α-particles. When these particles come close enough to interact with the target nuclei, either elastic or inelastic scattering may take place or one or more particles which are altogether different may be knocked out of the nucleus, or the incident particle may perhaps be captured and a gamma ray emitted. When the mass number and/or atomic number of the target nuclei changes after the bombardment, we say that a *nuclear reaction* has taken place.

Typically an equation representing a nuclear reaction may be written as

$$x + X = Y + y \qquad \ldots(3.1)$$

In words this would read like: when an incident projectile x hits the target nucleus X, a nuclear reaction takes place and as a result there is a new nucleus Y and an outgoing particle y. The above reaction can also be written in short form as $X\,(x, y)\,Y$.

In 1919, Lord Rutherford found that when nitrogen is bombarded with α-particles from Polonium, protons are produced and these protons are capable of piercing 28 cm. of air. This was the first nuclear reaction to be triggered in the laboratory and to Rutherford goes the credit of breaking through the "inaccessible armour" of normal non-radioactive nuclei and producing a *transmutation*. The nuclear reaction can be put as

$$^{14}_{7}\mathrm{N}(\alpha, p)\,^{17}_{8}\mathrm{O} \qquad \ldots(3.2)$$

In 1930 Cockcroft and Walton used artificially accelerated protons and produced the following nuclear reaction,

$$ {}^{7}_{3}\text{Li} + p \rightarrow {}^{4}_{2}\text{He} + \alpha $$

or

$$ {}^{7}_{3}\text{Li}\,(p, \alpha)\, {}^{4}_{2}\text{He} \qquad \ldots(3.3) $$

Different laboratories in the world have already studied thousands of nuclear reactions and the number is continuously growing. In this chapter we will consider the case in which all of the particles may be treated non-relativistically and the target nucleus is at rest before the collision. Our interest lies in finding out when a particular nuclear reaction becomes energetically possible. This we will know by applying the laws of conservation of momentum and energy.

3.2 TYPES OF NUCLEAR REACTIONS

Nuclear reactions are classified on the basis of the projectile used, the particle detected and the residual nucleus.

(*i*) *Scattering*: In the scattering reaction, the projectile and the detected (outgoing) particle are the same. The scattering is elastic when the residual nucleus is left in the ground state. When the residual nucleus is left in an excited state, the scattering is called inelastic.

(*ii*) *Pickup reactions*: When the projectile gains nucleons from the target, the nuclear reaction is referred to as pickup reaction, e.g.

$$ {}^{16}_{8}\text{O}\left({}^{2}_{1}\text{H},\ {}^{3}_{1}\text{H}\right){}^{15}_{8}\text{O} $$

(*iii*) *Stripping reactions*: In this type, the projectile loses nucleons to the target nucleus, e.g.

$$ {}^{16}_{8}\text{O}\left({}^{4}_{2}\text{He},\ {}^{2}_{1}\text{H}\right){}^{18}_{9}\text{F} $$

In a pickup or stripping reaction it is assumed that the nucleon involved in the process enters or leaves (the shell of) the target nucleus without disturbing the other nucleons. These reactions are therefore referred to as *direct reactions*. In contrast, we have the following type of compound nuclear reactions.

(*iv*) *Compound nuclear reactions*: Here the projectile and target form a *compound nucleus* which has a typical life span of $\sim 10^{-16}$ sec. When this time is compared with a typical nuclear time, i.e., the time taken by the projectile to traverse the target nucleus ($\sim 10^{-22}$ sec.) as in the case of direct reactions, we can conclude that the decay of a compound nucleus does not depend on the way it was formed.

This situation is often described as: the compound nucleus does not "remember" how it was formed. Usually the same compound nucleus is given rise to by a number of nuclear reactions. This compound nucleus can decay in a number of ways or channels. This is illustrated by taking for example, the compound nucleus ${}^{64}_{30}\text{Zn}$ formed in an excited state $\left({}^{64}_{30}\text{Zn}\right)^*$ by two different methods and then decays as given below:

$$p + {}^{63}_{29}\text{Cu} \rightarrow \left({}^{64}_{30}\text{Zn}\right)^* \rightarrow {}^{63}_{30}\text{Zn} + {}^{1}_{0}n$$

$$\rightarrow {}^{62}_{30}\text{Zn} + {}^{1}_{0}n + {}^{1}_{0}n$$

$$\rightarrow {}^{62}_{29}\text{Cu} + {}^{1}_{0}n + p$$

or

$$\alpha + {}^{60}_{20}\text{Ni} \rightarrow \left({}^{64}_{30}\text{Zn}\right)^* \rightarrow {}^{63}_{30}\text{Zn} + {}^{1}_{0}n$$

$$\rightarrow {}^{62}_{30}\text{Zn} + {}^{1}_{0}n + {}^{1}_{0}n$$

$$\rightarrow {}^{62}_{29}\text{Cu} + {}^{1}_{0}n + p \qquad \ldots(3.4)$$

These reactions were experimentally studied by S.N. Ghoshal. [Phys. Rev. 80939 (1950)]

Figure 3.1 depicts how a compound nucleus in an excited state can have different modes of decay, giving rise to different residual nuclei and detected particles.

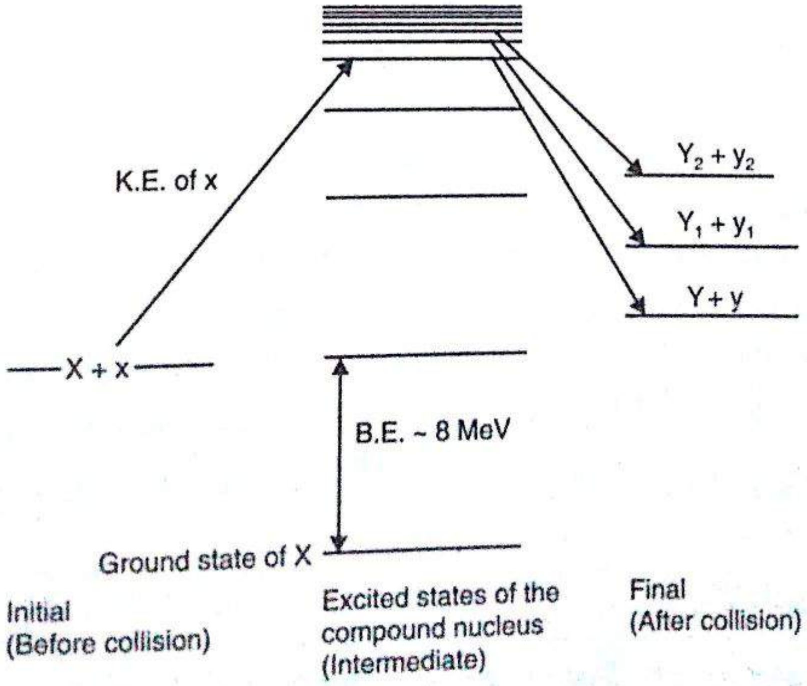
K.E. of x
Y$_2$ + y$_2$
Y$_1$ + y$_1$
Y + y
X + x
B.E. ~ 8 MeV
Ground state of X
Initial
(Before collision)
Excited states of the
compound nucleus
(Intermediate)
Final
(After collision)

Fig. 3.1. Different modes (channels) of decay of an excited compound nucleus.

The compound nucleus model has been successfully applied for targets of $A > 10$ and projectile energies up to about 15 MeV. For projectile energies between 15 MeV and 50 MeV the *direct reaction model* and the *optical model* are found to be successful. In this chapter, our main emphasis is on understanding energetics of nuclear reactions.

3.3 THE BALANCE OF MASS AND ENERGY IN NUCLEAR REACTIONS

Consider the nuclear reaction,

$$x + X \rightarrow Y + y$$

Since the total mass and energy is conserved, we have

$$(E_x + m_x c^2) + M_X c^2 = (E_Y + M_Y c^2) + (E_y + m_y c^2) \qquad \ldots(3.5)$$

Where,

E_x = kinetic energy of the projectile

$m_x c^2$ = rest energy of the projectile

and similarly E_Y and $M_Y c^2$, E_y and $m_Y c^2$ and $M_X c^2$.

The target nucleus X is assumed to be at rest.

The Q value is expressed as,

$$Q = E_Y + E_y - E_x \qquad \ldots(3.6)$$

i.e. it is the change in the total kinetic energy.

This change in the total kinetic energy in a nuclear reaction is clearly the *nuclear disintegration energy.*

From Eq. 3.5, Eq. 3.6 becomes

$$Q = E_Y + E_y - E_x$$

$$= [(M_X + m_x) - (M_Y + m_y)]c^2 \qquad \ldots(3.7)$$

Thus we see that Q is also the change in the total rest mass. We have an exoergic nuclear reaction if Q is positive. The nuclear reaction is an endoergic reaction if the Q value is negative.

From Eq. 3.7 it is clear that to determine the Q value or nuclear disintegration energy for a nuclear reaction, we must know the kinetic energies of the particles.

E_Y, the kinetic energy of the residual nucleus, is usually small and hard to measure.

In the following section, we will see how E_Y can be eliminated and how the Q equation can be set up.

3.4 THE Q EQUATION

The analytical relationship between the kinetic energy of the projectile and outgoing particle and the nuclear disintegration energy Q is called as the Q equation.

To understand the dynamics of two-body nuclear reactions in laboratory coordinate system, refer to Fig. 3.2.

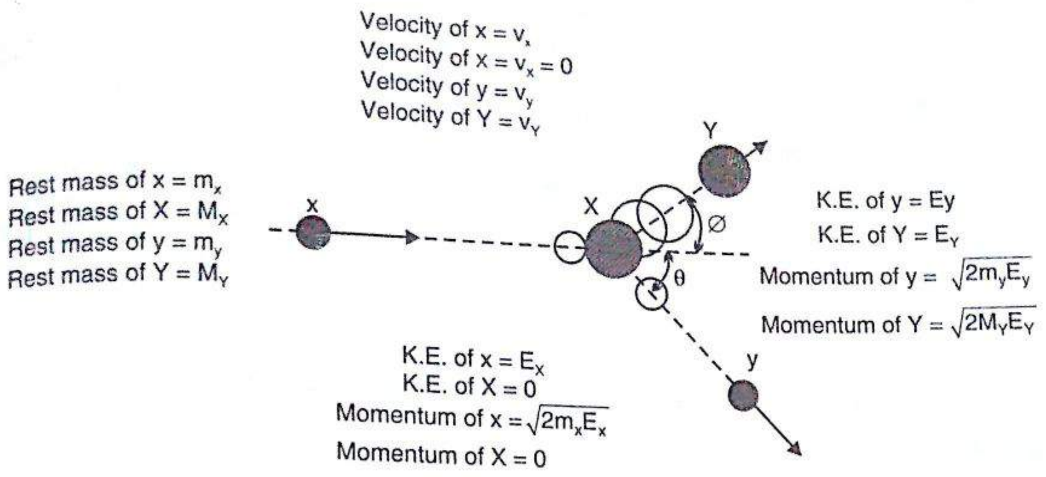
Velocity of x = v_x
Velocity of X = $v_X = 0$
Velocity of y = v_y
Velocity of Y = v_Y
Rest mass of x = m_x
Rest mass of X = M_X
Rest mass of y = m_y
Rest mass of Y = M_Y
x
X
Y
y
∅
θ
K.E. of y = Ey
K.E. of Y = E_Y
Momentum of y = $\sqrt{2m_yE_y}$
Momentum of Y = $\sqrt{2M_YE_Y}$
K.E. of x = E_x
K.E. of X = 0
Momentum of x = $\sqrt{2m_xE_x}$
Momentum of X = 0

Fig. 3.2. Two-body nuclear reaction in lab. system.

Conservation of mass-energy gives (see Section 3.3)

$$Q = E_y + E_Y - E_x$$

As remarked before, E_Y is small and hard to measure and is therefore eliminated. Conservation of linear momentum along the direction of projectile x gives,

$$\sqrt{2m_xE_x} = \sqrt{2m_yE_y}\cos\theta + \sqrt{2M_YE_Y}\cos\phi \qquad \text{...(3.8)}$$

Angles θ and ϕ are coplanar as linear momentum perpendicular to the θ plane is equal to zero. Therefore, conservation of linear momentum normal to projectile direction (in the θ, ϕ plane) gives,

$$0 = \sqrt{2M_YE_Y}\sin\phi - \sqrt{2m_yE_y}\sin\theta \qquad \text{...(3.9)}$$

From these equations E_Y and ϕ are eliminated. Squaring and adding Eqs. (3.8) and (3.9),

$$M_YE_Y = m_xE_x + m_yE_y - 2\sqrt{m_xm_yE_xE_y}\cos\theta$$

But $\qquad E_Y = Q - E_y + E_x$

$$\therefore \qquad Q = E_y - E_x + \frac{m_x}{M_y}E_x + \frac{m_y}{M_Y}E_y - \frac{2\sqrt{m_xm_yE_xE_y}}{M_Y}\cos\theta$$

$$\boxed{Q = E_y\left(1+\frac{m_y}{M_Y}\right) - E_x\left(1-\frac{m_x}{M_Y}\right) - \frac{2\sqrt{m_xm_yE_xE_y}}{M_Y}\cos\theta} \qquad \text{...(3.10)}$$

This is the standard form of the Q equation.

It is interesting to note that one can also obtain Eq. 3.10 by solving the momentum triangle and substituting for E_Y. This is indicated below:

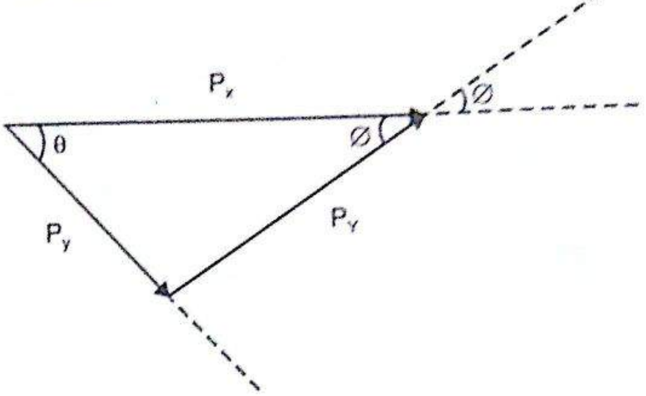

Fig. 3.3. The momentum triangle, using the notation of Fig. 3.2.

We see that

$$P_Y^2 = p_x^2 + p_y^2 - 2p_xp_y\cos\theta \qquad ...(3.11)$$

$$\therefore \qquad 2M_YE_Y = 2m_xE_x + 2m_yE_y - 2.2\sqrt{m_xE_xm_yE_y}\cos\theta$$

giving,

$$E_Y = \frac{m_x}{M_Y}E_x + \frac{m_y}{M_Y}E_y - \frac{2\sqrt{m_xm_yE_xE_y}}{M_Y}\cos\theta \qquad ...(3.12)$$

From Eq. 3.6,

$$E_Y = Q - E_y - E_x$$

Substituting this in Eq. 3.12 we get,

$$Q = E_y\left(1 + \frac{m_y}{M_Y}\right) - E_x\left(1 - \frac{m_x}{M_Y}\right) - \frac{2\sqrt{m_xm_yE_xE_y}}{M_Y}\cos\theta$$

which is the Q equation (3.10).

The kinetic energies E_x, E_y and θ are all measured in the laboratory coordinate system. Since the Q equation is based on mass-energy conservation in a nuclear reaction, it holds for all types of reactions. The exact masses can be replaced by the corresponding mass numbers, in many applications without significant error. For very accurate calculations, the neutral atomic masses are used. Let us see how we can use the isotopic masses (neutral atomic masses) to obtain Q value in alpha and beta decay reactions. For convenience, let the element symbol represent the isotopic mass. We recall that $Q = (m_x + M_X) - (m_y + M_Y)$ where the masses are the *nuclear masses,* and Q is in mass units.

(*i*) Consider the reaction

$$^{238}_{92}\text{U} \rightarrow {}^{234}_{90}\text{Th} + {}^{4}_{2}\text{He}$$

$$Q = (\mathrm{U} - 92e) - [(\mathrm{Th} - 90e) + (\mathrm{He} - 2e)]$$

where e stands for electronic mass.

i.e.,
$$Q = (\mathrm{U} - 92e) - (\mathrm{Th} + \mathrm{He} - 92e)$$
$$= [\mathrm{U} - (\mathrm{Th} + \mathrm{He})]$$

∴ Isotopic masses can be used to evaluate Q.

(ii) Consider the reaction,

$${}^{14}_{6}\mathrm{C} \rightarrow {}^{14}_{7}\mathrm{N} + {}^{0}_{-1}e + {}^{0}_{0}\overline{\nu}$$

$$Q = (\mathrm{C} - 6e) - [(\mathrm{N} - 7e) + e]$$
$$= (\mathrm{C} - 6e) - (\mathrm{N} - 6e)$$
$$= \mathrm{C} - \mathrm{N}$$

∴ Isotopic masses can be used to evaluate Q.

(iii) Consider the reaction,

$${}^{63}_{30}\mathrm{Zn} \rightarrow {}^{63}_{29}\mathrm{Cu} + {}^{0}_{+1}e + {}^{0}_{0}\nu$$

$$Q = (\mathrm{Zn} - 30e) - [(\mathrm{Cu} - 29e) + e]$$
$$= (\mathrm{Zn} - 30e) - (\mathrm{Cu} - 30e + 2e)$$
$$= \mathrm{Zn} - (\mathrm{Cu} + 2e)$$

Thus we see that the isotopic masses can be used to compute Q value in a positron decay reaction, provided two electron masses are included with that of the product particle.

3.5 SOLUTION OF THE Q EQUATION

We are often interested in E_y, the energy of the detected particle and its variation with E_x, the energy of the bombarding projectile, for a fixed Q. For this purpose, the Q equation (Eq. 3.10) can be regarded as a quadratic in $\sqrt{E_y}$. Then its general solution can be conveniently put in the form,

$$\sqrt{E_y} = v \pm \sqrt{v^2 + w} \qquad \ldots(3.13)$$

where,

$$v = \frac{\sqrt{m_x m_y E_x}}{m_y + M_Y} \cos\theta \qquad \ldots(3.14)$$

E_x has its minimum possible value at $\theta = 0$, which is the $(E_x)_{\text{thresh}}$. (see Problem 3.12).

This condition gives:

$$\frac{m_x\, m_y E_x}{(m_y + M_Y)^2} + \frac{M_Y Q + E_x(M_Y - m_x)}{m_y + M_Y} = 0$$

which gives,

$$(E_x)_{\text{thresh}} = -Q\left(\frac{m_x + M_X}{M_X}\right) \qquad \ldots(3.18)$$

In obtaining Eq. 3.18, we have made use of the fact that the value of Q/c^2 is much less than the masses of particles in a nuclear reaction, and so

$$m_y \cong m_x + M_X - M_Y \qquad \ldots(3.19)$$

Equation 3.18 can be also obtained in a straightforward way by considering M_c and V_c as mass and velocity of the compound nucleus. Then we have,

$$m_x\, v_x = M_c\, V_c$$

or

$$V_c = \frac{m_x}{M_c} v_x$$

Now, the part of kinetic energy of the projectile needed for the excitation of the compound nucleus is,

$$Q = \frac{1}{2} m_x v_x^2 - \frac{1}{2} M_c V_c^2$$

$$= \frac{1}{2} m_x v_x^2 - \frac{1}{2} M_c \left(\frac{m_x}{M_c}\right)^2 v_x^2$$

$$= \frac{1}{2} m_x v_x^2 \left(1 - \frac{m_x}{M_c}\right)$$

But

$$M_c = m_x + M_X$$

$\therefore$

$$-Q = \frac{1}{2} m_x v_x^2 \left(\frac{M_X}{m_x + M_X}\right)$$

The threshold energy is then,

$$(E_x)_{\text{thresh}} = \frac{1}{2} m_x v_x^2 = -Q\left(\frac{m_x + M_X}{M_X}\right)$$

which is Eq. 3.18.

ILLUSTRATIVE EXAMPLES

Example 3.1: Find out the unknown particles in the nuclear reactions given below:

(*i*) ${}^{6}_{3}\text{Li}(d, \alpha)X$

(*ii*) ${}^{122}_{52}\text{Te}(X, d)\,{}^{124}_{53}\text{I}$

Solution: (*i*) In a nuclear reaction, the total charge and the mass number are conserved.

We have,

$$ {}^{6}_{3}\text{Li} + {}^{2}_{1}d \rightarrow X + {}^{4}_{2}\text{He} $$

∴ X has to be put as ${}^{4}_{2}\text{X}$ i.e., it is an α-particle.

(*ii*) Here,

$$ {}^{122}_{52}\text{Te} + {}^{4}_{2}\text{X} \rightarrow {}^{2}_{1}d + {}^{124}_{53}\text{I} $$

i.e., X is an α-particle.

Example 3.2: Calculate the Q value of reaction ${}^{14}_{7}\text{N}(\alpha, p)\,{}^{17}_{8}\text{O}$ which occurred in Rutherford's α-range in nitrogen experiment.

Solution: The masses in u of neutral atoms involved in this reaction can be taken from the tables.

It may be kept in mind that,. $1u = 931.5$ MeV

$$ Q = [(m_x + M_X) - (m_y + M_Y)]c^2 $$

$$ = [4.002603u + 14.0031\,u - (1.007825u + 16.9994u)] \times \left(931.5\,\frac{\text{MeV}}{u}\right) $$

$$ = -1.418\ \text{MeV}. $$

Example 3.3: A neutron beam is incident on a stationary target of ${}^{19}\text{F}$ atoms. The reaction ${}^{19}\text{F}(n, p)\,{}^{19}\text{O}$ has a Q value of –3.9 MeV. Calculate the lowest *neutron energy* which will make this reaction possible.

Solution: We know that,

$$ (E_x)_{\text{thresh}} = -Q\left(\frac{M_X + m_x}{M_X}\right) = (3.9\ \text{MeV})\left(\frac{1+19}{19}\right) = 4.105\ \text{MeV} $$

Example 3.4: Obtain the threshold energy for the reactions,

(*i*) $^{209}_{83}\text{Bi}(p, d)\,^{208}_{83}\text{Bi}$ and

(*ii*) $^{27}_{13}\text{Al}(\alpha, p)\,^{31}_{15}\text{P}$

Solution: For (*i*), the Q value is,

$$Q = [208.980394u + 1.007825u - 207.979731u - 2.014102u] \cdot \left(931.5\,\frac{\text{MeV}}{u}\right)$$

$$= -5.23 \text{ MeV}$$

Now $$(E_x)_{\text{thresh}} = -Q\left(\frac{M_X + m_x}{M_X}\right)$$

$$= 5.23\left(\frac{209+1}{209}\right)$$

$$= 5.26 \text{ MeV}$$

For (*ii*)

$$Q = [25.986892u + 4.002603u - 30.973765u - 1.007825u] \cdot \left(931.5\frac{\text{MeV}}{u}\right)$$

$$= -2.9 \text{ MeV}$$

$$\therefore \quad (E_x)_{\text{thresh}} = 2.9\left(\frac{27+4}{27}\right) = 3.33 \text{ MeV}$$

Example 3.5: Neutrons from ^{7}Li (p, n) ^{7}Be reaction are observed at a laboratory angle $\theta = 30^\circ$. At what bombarding energy are neutrons of zero energy obtained?

Solution: First compute the Q of the reaction

$$Q = [7.016004u + 1.007825u - 7.016929u - 1.008665u] \cdot \left(931.5\frac{\text{MeV}}{u}\right)$$

$$= -1.64 \text{ MeV}$$

Now we have to find the value of E_x for which $E_y = 0$

From Eq. (3.17)

$$0 = v \pm \sqrt{v^2 + w}$$

$$\therefore \quad v^2 = v^2 + w$$

i.e.,
$$w = 0$$

$$\therefore \qquad \frac{M_Y Q + E_x(M_Y - m_x)}{M_Y + m_y} = 0$$

Giving
$$E_x = \frac{-M_Y Q}{M_Y - m_x}$$

$$= -(-1.64\,\text{MeV})\frac{7}{6}$$

$$= +1.91\,\text{MeV}.$$

Example 3.6: ${}^{52}_{25}\text{Mn}$ (6 days) decays to stable ${}^{52}_{24}\text{Cr}$ (51.9571 u) by a positron emission with maximum energy 0.58 MeV and three gamma rays in cascade; viz., 0.73 MeV, 0.94 MeV and 1.46 MeV.

(*i*) Sketch the decay scheme.

(*ii*) Calculate the mass of the neutral atom ${}^{52}\text{Mn}$.

(*iii*) Find the threshold proton bombarding energy for the reaction ${}^{52}\text{Cr}\,(p, n)\,{}^{52}\text{Mn}$.

Solution: (*i*)

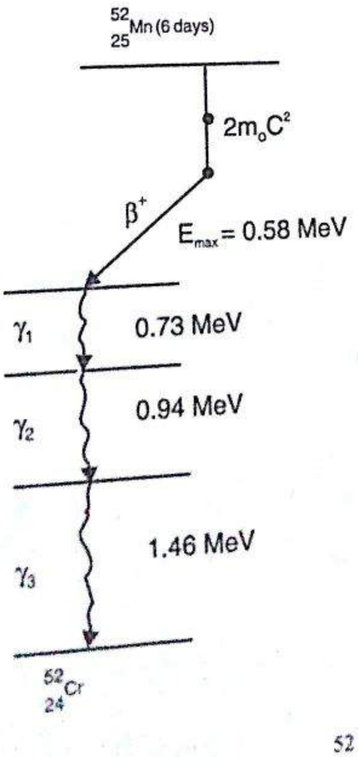
${}^{52}_{25}$Mn (6 days)
$2m_0C^2$
β^+
E_{max} = 0.58 MeV
γ_1
0.73 MeV
γ_2
0.94 MeV
γ_3
1.46 MeV
${}^{52}_{24}$Cr

Fig. 3.4. Decay scheme of ${}^{52}_{24}\text{Cr}$.

(*ii*) $${}^{X}_{25}\text{Mn} \rightarrow {}^{51.9571}_{24}\text{Cr} + \beta^{+} + Q$$

$\therefore$ $$Q = X - [(51.9571 + 2m_0)]$$ (see Sec. 3.4)

Where m_0 is rest mass of electron.

$\therefore$ $$Q = (X - 51.9571) \times 931\,\frac{\text{MeV}}{u} - 2m_0c^2$$

But Q = Nuclear disintegration energy

= (0.58 + 0.73 + 0.94 + 1.46) MeV

= 3.71 MeV

Also, $2m_0c^2 = 1.02$ MeV.

$\therefore$ $$X = 51.9648u \text{ i.e., we have } {}^{51.9648}_{25}\text{Mn}.$$

(*iii*) $$(E_x)_{\text{thresh}} = -Q\left(\frac{m_x + M_X}{M_X}\right)$$

For the reaction,

$$^{52}\text{Cr} + p \rightarrow {}^{52}\text{Mn} + n + Q$$

$$Q = [(51.9571u - 51.9648u) + (1.007825u - 1.008665u)] \times \left(931.5\,\frac{\text{MeV}}{u}\right)$$

$$= -5.44\text{MeV}.$$

$\therefore$ $$(E_x)_{\text{thresh}} = 5.44\left(\frac{53}{52}\right)\text{MeV}$$

$$= 5.54\,\text{MeV}$$

Example 3.7: In the case of an elastic collision, use the Q equation to obtain an expression for the kinetic energy of the target particle.

Solution:

$$Q = E_y\left(1 + \frac{m_y}{M_Y}\right) - E_x\left(1 - \frac{m_x}{M_Y}\right) - \frac{2\sqrt{m_x m_y E_x E_y}}{M_Y}\cos\theta$$

For an elastic collision, $Q = 0$.

$$\sqrt{E_y} = \frac{\sqrt{m_x m_y E_x}}{m_y + M_Y}\cos\theta \pm \sqrt{\frac{m_x m_y E_x}{(m_y + M_Y)^2}\cos^2\theta + \frac{M_Y Q + E_x(M_Y - m_x)}{(m_y + M_Y)}}$$

(Eqs. 3.13, 3.14, 3.15)

Putting $Q = 0$ and $m_y = M_X$, $M_Y = m_x$,

$$\sqrt{E_X} = \frac{\sqrt{m_x M_X E_x}}{m_x + M_X}\cos\theta \pm \sqrt{\frac{m_x M_X E_x}{(m_x + M_X)^2}\cos^2\theta + 0}$$

$$= \frac{2\sqrt{m_x M_X E_x}}{m_x + M_X}\cos\theta \text{ taking only positive sign.}$$

$$\therefore \quad E_x = 4E_x \frac{m_x M_X}{(m_x + M_X)^2}\cos^2\theta$$

Example 3.8: If $^{235}_{92}$U captures a thermal neutron and releases 170 MeV and if the resulting fission fragments have mass numbers 138 and 95, what is the kinetic energy of the lighter fragment?

Solution: Since the reaction is due to thermal neutrons we can consider $E_x = 0$, giving from Eq. 3.14, $v = 0$ and so, Eq. 3.13 becomes,

$$E_y = w = \frac{M_Y Q + E_x(M_Y - m_x)}{m_y + M_Y}$$

$$= \frac{M_Y}{m_y + M_Y} Q \qquad \because E_x = 0$$

$$\therefore \quad E_y = \text{K.E. of the lighter fission fragment}$$

$$= Q\frac{M_Y}{m_y + M_Y} \quad \text{and} \quad Q > 0,$$

otherwise E_y would have been imaginary.

Here $Q = 170$ MeV, since it is the nuclear disintegration energy.

$$M_Y = 138$$

and

$$m_y = 95$$

$$\therefore \quad E_y = 170 \times \frac{138}{233}\text{ MeV}$$

$$= 100.69 \text{ MeV}$$

3.6 CENTRE OF MASS FRAME IN NUCLEAR PHYSICS

Often the analysis of collision problems is much simplified by the use of a coordinate system that is moving with the centre of the mass of the colliding bodies, rather than the usual laboratory coordinate system. A nuclear physicist lives in two worlds. One is his laboratory and other is the centre of mass frame in which he studies collisions, interactions. By learning to skip nimbly from one frame to the other, he can get the best of both worlds! Let us have a look at examples of perfectly elastic nuclear collisions to appreciate the view one gets from the centre of mass frame.

(i) Proton-Proton Collisions

Figure 3.5 shows sketch of a typical photoemulsion record of *p-p* collision.

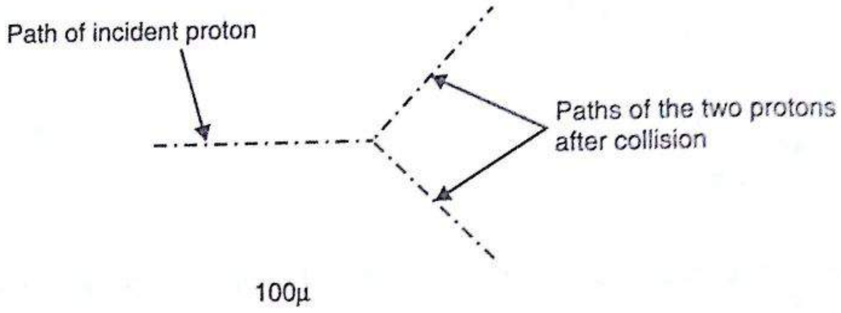

Fig. 3.5. A. *p-p* collision. Sketch of a typical photoemulsion record.

The hit proton is in the photoemulsion and can be considered to be at rest before the collision. The striking feature of Fig. 3.5 is that the paths of the two protons after collision make an angle of 90° with each other. For non-relativistic energies of incident proton, this feature is the same for all *p-p* collisions.

To understand this feature, it is profitable to look at the collision from the centre of mass frame. Let the velocity of the incident proton as observed in the laboratory be $\bar{v}$. Then the centre of mass frame has velocity $\frac{\bar{v}}{2}$. Therefore in this frame the protons approach and recede with equal and opposite velocities as shown in Fig. 3.6.

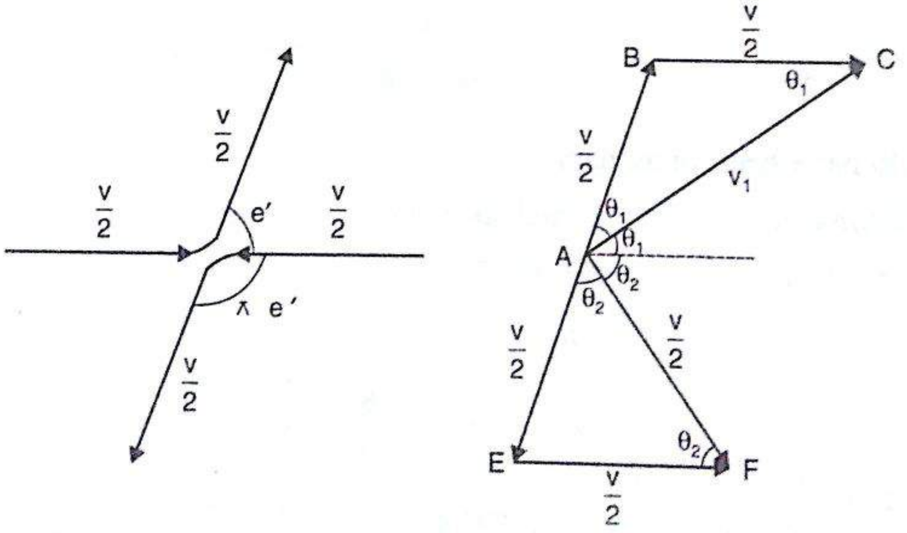

Fig. 3.6. View of *p-p* collision in the centre of mass system is shown on left. How one steps back in the lab frame is depicted on the right.

Suppose that one proton moves in the direction θ' after the collision, then the other would move in the opposite direction at an angle $(\pi - \theta')$. To get back to the laboratory frame, all that we have to do is to add the velocity $\frac{\bar{v}}{2}$ to each proton, in a direction parallel to the original direction of the motion. Now since triangles ABC and AEF are isosceles, the directions θ_1 and θ_2 of the protons as observed in the laboratory are given by,

$$\theta_1 = \frac{\theta'}{2} \quad \text{and} \quad \theta_2 = \frac{(\pi - \theta')}{2}$$

i.e.,

$$\theta_1 + \theta_2 = \frac{\pi}{2} \qquad \text{...(3.20)}$$

at once explaining the nature of Fig. 3.5.

Also lab. velocities of two protons after the collision can be easily found out.

$$v_1 = 2\left(\frac{v}{2}\right)\cos\theta_1$$

$$= v\cos\theta_1 \qquad \text{...(3.21)}$$

and

$$v_2 = 2\left(\frac{v}{2}\right)\cos\theta_2$$

$$= v\cos\theta_2$$

$$= v\sin\theta_1 \qquad \text{...(3.22)}$$

The kinetic energies are,

Initial K.E. $= \frac{1}{2}mv^2$

Final K.E. $= \frac{1}{2}mv_1^2 + \frac{1}{2}mv_2^2$

$$= \frac{1}{2}mv^2\,(\cos^2\theta_1 + \sin^2\theta_1)$$

$$= \frac{1}{2}mv^2 \qquad \text{...(3.23)}$$

The reader would appreciate the simplicity and elegance with which the *p-p* scattering dynamics is brought out in the centre of mass frame. Let us consider one more example of nuclear elastic scattering.

(ii) Neutron-Nucleus Collisions

Suppose a neutron of mass m makes an elastic collision with a nucleus of mass M. Let the initial velocity of the neutron in the laboratory frame be $\vec{u}$, while the target nucleus is stationary. Figure 3.7 shows this collision in the centre of mass frame.

The centre of mass frame has a velocity $\vec{v}$ relative to the laboratory frame, given by,

$$(m+M)\vec{v} = m\vec{u} \qquad \ldots(3.24)$$

i.e.,

$$\vec{v} = \frac{m}{m+M}\vec{u} \qquad \ldots(3.25)$$

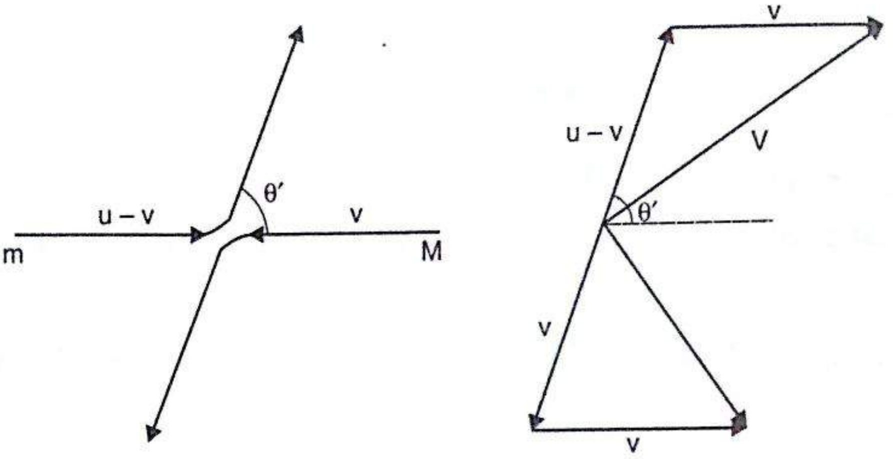

Fig. 3.7. View of neutron—nucleus collision in the centre of mass system is shown on the left. How to get back to the lab. system is shown on the right.

Let the neutron come out in direction θ′ after the collision, in the centre of mass frame. The final velocity of the neutron in the laboratory system is $\vec{V}$. as shown. $\vec{V}$, for any given θ′ can be at once calculated.

The neutrons suffer greatest energy loss, as seen in the laboratory frame, when it gets scattered backward, corresponding to θ′ = π. In this case we have,

$$\vec{V}(\pi) = \vec{v} - (\vec{u} - \vec{v})$$

$$= -(\vec{u} - 2\vec{v})$$

$$= -\vec{u}\left(1 - 2\frac{\vec{v}}{\vec{u}}\right)$$

$$= -\vec{u}\left(1 - \frac{2m}{M+m}\right) \text{ from Eq. 2.34}$$

$$= -\left(\frac{M-m}{M+m}\right)\vec{u} \qquad \ldots(3.26)$$

For θ′ = 0, the neutron loses no energy at all. Thus the neutron's kinetic energy after the collision lies between the limits,

$$(\text{K.E.})_{\text{max.}} = \frac{1}{2} m u^2$$

$$(\text{K.E.})_{\text{min.}} = \frac{1}{2} m \left(\frac{M - m}{M + m} \right) u^2 \qquad \ldots(3.27)$$

We see that, $M \cong m$ makes $(\text{K.E.})_{\text{min.}} \cong 0$.

Fission reaction releases neutrons of energy ~1 MeV. To introduce further fissions, these neutron energies have to be brought down to thermal energies ($\sim 10^{-2}$ eV). Different moderators have to be used for this purpose. From Eq. 3.27 hydrogen would have been the best moderator, but protons capture slow neutrons readily. Therefore, deuterium, carbon etc. are used as moderators.

EXERCISES

1. Complete the following nuclear reactions:

$${}^{6}_{3}\text{Li} + {}^{2}_{1}\text{H} \rightarrow {}^{7}_{4}\text{Be} + X$$

$${}^{23}_{11}\text{Na} + {}^{1}\text{H} \rightarrow {}^{20}_{10}\text{Ne} + X$$

$${}^{35}_{17}\text{Cl} + X \rightarrow {}^{32}_{16}\text{S} + {}^{4}_{2}\text{He}$$

2. A beam of deutrons is incident of ${}^{31}_{15}\text{P}$ target. Write down the nuclear reaction equations, when the emitted particle is (*i*) a proton, (*ii*) a neutron and (*iii*) an alpha particle.

3. Calculate the Q value for the reactions,

(*i*) ${}^{42}_{20}\text{Ca}\,(p, d)\,{}^{41}_{20}\text{Ca}$

(*ii*) ${}^{15}_{8}\text{O}(d, p)\,{}^{16}_{8}\text{O}$

4. Show that in a two-body elastic collision, each particle's speed will remain unchanged by the collision when measured in the centre of mass system.

5. Obtain the threshold energy for the reactions,

(*i*) ${}^{93}_{40}\text{Nb}\,(p, d)\,{}^{92}_{41}\text{Nb}$

(*ii*) ${}^{19}_{9}\text{F}\,(n, p)\,{}^{19}_{8}\text{O}$

6. The Q value of the reaction,

${}^{14}_{7}\text{N}\,(\alpha, p)\,{}^{17}_{8}\text{O}$ is -1.16 MeV.

Calculate (*i*) the threshold energy for the reaction, and (*ii*) the difference in mass between target and residual nuclei.

7. Alpha particles having a kinetic energy of 5 MeV in the lab. system, start the reaction,

$$^{9}_{4}\text{Be}\,(\alpha, n)\,^{12}_{6}\text{C}.$$

Calculate the maximum energy of the neutrons emitted in the lab. system.

8. Accelerated protons from a Van de Graaff generator are used to bombard nuclei having mass number $A \sim 20$. Assuming elastic scattering find what energies do the protons have for exit angles 45°, 90°, 135° and 179°. The incident proton energies used are, 1.0, 2.0, 4.0, 6.0, 8.0, and 10.0 MeV. (in lab. system).

9. Show that the reduction in energy ΔE of a neutron in an elastic collision with a nucleus of mass number A is given by

$$\Delta E = E\left(1 - \left(\frac{A-1}{A+1}\right)^2\right)$$

Calculate the fractional loss of energy of a neutron colliding with (*i*) a proton, (*ii*) a deuteron, (*iii*) a carbon nucleus ^{12}C and (*iv*) a beryllium nucleus. ^{7}Be.

10. The Q value of $^{18}\text{O}(p, \alpha)^{15}\text{N}$ is +3.97 MeV and that of $^{15}\text{N}(p, \alpha)^{12}\text{C}$ is +4.96 MeV. Calculate the atomic mass of ^{15}N from these reactions.

11. Calculate the Q value for the reaction

$$^{3}\text{H}(d, n)^{4}\text{He}.$$

   (*i*) Write an expression for the neutron energy for this reaction in terms of deuteron energy E_x and angle θ.

   (*ii*) In what direction will the neutron energy be smallest?

   (*iii*) If neutrons of energy between 1 MeV and 6 MeV are available, at what deuteron energy will the neutron energy be the smallest? Explain.

   (*iv*) What is the smallest possible energy for neutrons?

   (*v*) Why does this *not* occur at the smallest value of deuteron energy?

12. Consider an endoergic nuclear reaction. The smallest value of bombarding energy which induces such a reaction is called threshold energy $(E_x)_{\text{thresh}}$ (see Sec. 3.5). for that reaction. Show that E_x has its minimum possible value at $\theta = 0$, which is $(E_x)_{\text{thresh}}$.

   (*Hint:* From Eq. 3.13, write $(E_x)_\theta$ and then show that for $\theta = 0$, E_x has minimum possible value.)

13. A particle of mass M_1, kinetic energy E_1, velocity v_1, momentum p_1 is captured by a nucleus (M_2, E_2, v_2, p_2) at rest. A light particle (M_3, E_3, v_3, p_3) is ejected and the heavy particle (M_4, E_4, v_4, p_4) recoils. When the light particle is emitted at an angle of 90° with the direction of the incident particle, show that the energy E_3 is given by,

$$E_3 = \frac{E_4}{M_3 + M_4}\left(Q - \frac{M_1 - M_4}{M_4}E_1\right)$$

   (*Hint:* Use conservation of energy and momentum.)

14. When $^{11}_{5}\text{B}$ is bombarded by 200 keV protons alpha particles are emitted at right angles to the path of the incident beam. The mass of $^{8}_{4}\text{Be}$ is 8.00794 u. Calculate the energy of the alpha particles.

   (*Hint:* Use the result of problem 13.)

15. The radioactive isotope $^{37}_{18}\mathrm{A}$ can be produced by $^{37}_{17}\mathrm{Cl}\ (d, 2n)\ ^{37}_{18}\mathrm{A}$ reaction. $^{37}\mathrm{A}$ disintegrates back in to $^{37}\mathrm{Cl}$. either by emitting a very soft radiation which may be a very low energy positron or may be X rays or a possible soft γ ray, following orbital electron capture. Show that the threshold deuteron energy must be:

 (*i*) greater than 4.25 MeV if $^{37}\mathrm{A}$ emits positrons.

 (*ii*) between 3.17 and 4.25 MeV if $^{37}\mathrm{A}$ decays by electron capture only.

 (*iii*) why is the difference (4.25 – 3.17) MeV not equal to $2m_0c^2$?

16. Consider the reaction, $^{19}_{9}\mathrm{F}(\alpha, p)\,^{22}_{10}\mathrm{Ne}$ for which $Q = +1.58$ MeV. If the observed particle is chosen to be the residual nucleus $^{22}_{10}\mathrm{Ne}$, show that in the forward direction (in lab. system) it is possible to have two monoenergetic groups of $^{22}\mathrm{Ne}$ nuclei. Obtain the condition that the bombarding energy (of α-particles) must satisfy for this to happen.

17. $^{233}\mathrm{Th}$ captures a thermal neutron and releases 190 MeV. If the resulting fission fragments have mass numbers 136 and 93. what is the kinetic energy of the lighter fragment?

18. π^+ mesons at rest decay spontaneously into $\mu^+ + \nu$. The μ^+ are observed to have a kinetic energy of 4.0 MeV. If the rest mass of μ^+ is $212\ m_0$ and that of the neutrino is zero, what is the rest mass of π^+ in units of electron rest mass m_0? If kinetic energy of μ^+ is taken as 4.1 MeV, what would be m_{π^+} ?

19. Consider head-on and glancing collisions in the centre of mass coordinate system. Show that the ratio of the total kinetic energy T' in the centre of mass system and the total kinetic energy T in the laboratory system is

$$\frac{T'}{T} = \frac{m_2}{m_1 + m_2}$$

Represent a completely inelastic collision in both the centre of mass and laboratory systems. Draw neat diagrams.

4

The Nucleus

"The only laws of matter are those which our minds must fabricate and the only laws of mind are fabricated for it by matter."

—*James Clerk Maxwell*

PART–I: CONSTITUENTS OF THE NUCLEUS AND SOME OF THEIR PROPERTIES

4.I.1 INTRODUCTION

When we are about to discuss the atomic nucleus, it is worthwhile to review some of the important properties of the atom. We will emphasise the quantum mechanical properties which are also applicable to the nucleus.

To begin with it should be realized that the radius of a typical nucleus is about 10^{-14} m (10^{-12} cm) while the radius of the atom is about 10^{-10} m (10^{-8} cm). To compare these dimensions, imagine an atom so increased in size that its nucleus is a sphere of say, 6 cm in diameter; so that the corresponding atomic diameter is about 2 km!

It is now well known that the atom is composed of a massive, positively charged nucleus made up of particles called neutrons and protons. We shall describe the properties of these particles in Sec. 4.I.4. As the names imply, the proton carries a positive charge and the neutron is uncharged. They have roughly the same mass. The negatively charged electrons move around the nucleus. The orbits or *effects* of these electrons extend to about 10^{-10} m as described above.

Experimentally the negative charge on the electron is found to be exactly equal in magnitude to the charge on the proton. The mass of the electron is determined to be about 1/1836 that of the proton; the electron is much lighter than the proton or neutron. From this discussion we can conclude that the atom is electrically neutral and has a massive nucleus. From the view point of distribution of mass in the atom, the atom is made up mostly of *empty space.*

The cloud of electrons which surrounds the nucleus has been found to be arranged in layers or *shells.* The outermost, or valence electrons, are responsible for chemical properties of the atoms of various elements. The effect of the nucleus on chemical reactions is negligible. In Chapter VII, we will consider the evidence and theory of a shell model of the nucleus.

The nuclear model of the atom was first suggested by Rutherford in 1910. A schematic diagram of Rutherford's experimental set-up is shown in Fig. 4.I.1. The apparatus obviously has to be enclosed in vacuum. A beam of α-particles from radium was made to strike a thin gold foil. The scattered α-particles were detected by a fluorescent screen-telescope arrangement. Rutherford observed that many α-particles went straight through the foil or were deflected by a very small angle. However, a few α-particles were deflected through very large angles; some of them even got back scattered. This was not expected on the basis of the idea of atomic structure at that time: that the positive charge is uniformly smeared over the entire volume of the atom. Rutherford's own astonishment is reflected in his comment: "It was almost as incredible as if you fired a 15-inch shell at a piece of tissue paper and it came back and hit you."

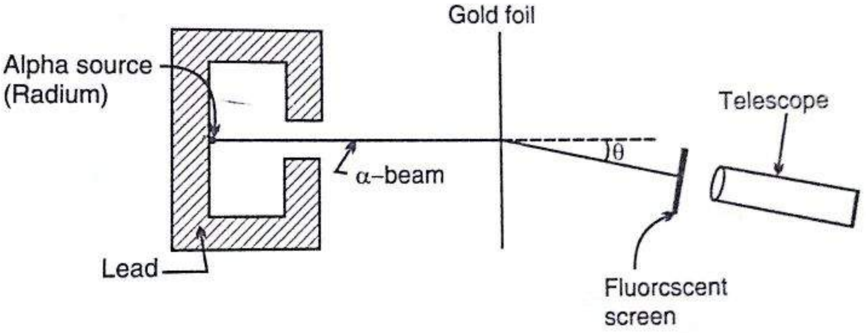

Fig. 4.I.1. Schematic diagram of the Rutherford scattering experiment.

To explain the deflections, Rutherford assumed that the positive massive part of the atom was concentrated in a very small volume at the centre of the atom. This *core*, now called the *nucleus*, is surrounded by a cloud of electrons, which makes the entire atom electrically neutral. This nuclear model of the atom accounts for the scattering of α-particles at large angles in the following way. An α-particle approaching the centre of the atom experiences an increasingly large Coulomb repulsion. Since the atom is mostly empty space, most of the α-particles do not go sufficiently close to the nucleus to get sufficiently deflected and so they pass through the foil with practically no deviation. However, an α-particle that passes close to the nucleus is subjected to a very large Coulomb repulsive force exerted by the massive positive core and is deflected at a large angle in a single encounter.

4.I.2 RUTHERFORD SCATTERING AND ESTIMATION OF THE NUCLEAR SIZE

Let us now estimate the Nuclear Radius by considering Rutherford's α-scattering experiment somewhat quantitatively, using classical ideas. Suppose the gold nucleus in the scattering experiment has a radius R. An α-particle trajectory can be specified by its *impact parameter b* as shown in Fig. 4.I.2.

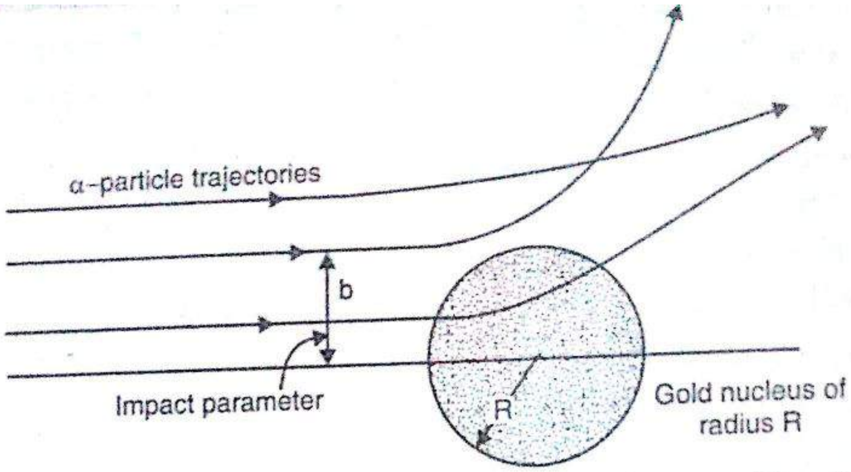

Fig. 4.I.2. Deflection of α-particle produced by a gold nucleus considered as a sphere of radius *R*. Notice how the deflection changes for the three trajectories with different impact parameters *b*. It is maximum for $b \sim R$.

Clearly, for $b > R$, due to less Coulomb repulsion, the deflection of α-particle is also less. Also when $b < R$, the α-particle goes through the nuclear positive charge distribution and so the nuclear charge above the trajectory and the one below the trajectory work in opposite directions and hence again the deflection produced in the α-particle trajectory is small. When the α-particle just grazes the nucleus (considered as a sphere of positive charge), the Coulomb repulsion becomes maximum and correspondingly for $b \sim R$, the deflection of α-particle also becomes maximum. To appreciate this qualitative discussion, let us consider a trajectory corresponding to a small deflection. As the particle approaches the gold nucleus it is slowed down by the Coulomb repulsion and is speeded up on its way out (away from the nucleus). This situation is sketched in Fig. 4.I.3.

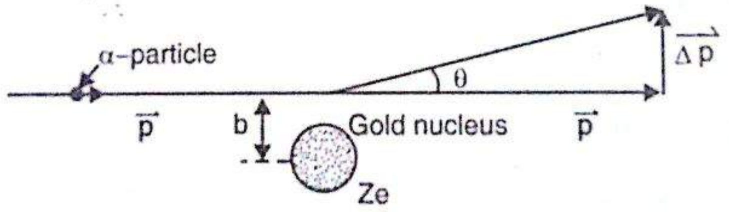

Fig. 4.I.3. Particle trajectory with impact parameter *b* and small deflection θ.

The Coulomb repulsion in the region close to the scattering gold nucleus is given by,

$$F = \frac{1}{4\pi\varepsilon_0}\frac{(2e)(Ze)}{b^2} \qquad \ldots(4.I.1)$$

where, $2e$ is α-particle charge. For gold, $Z = 79$.

This repulsive force can be approximately considered to be operating perpendicular to the incident direction, over a distance *b*. If the particle has a velocity *v*, the time during which the force operates is:

$$\Delta t = \frac{b}{v},$$

This force clearly produces a momentum Δp in a direction perpendicular to the incident direction. By Newton's law,

$$F = \frac{\Delta p}{\Delta t}$$

$$\therefore \qquad \Delta p = F\Delta t = \frac{1}{4\pi\varepsilon_0}\frac{2Ze^2}{b^2}\frac{b}{v} \qquad \ldots(4.\text{I}.2)$$

From Fig. 4.I.3 the deflection θ is,

$$\theta \sim \frac{\Delta p}{p} = \frac{1}{4\pi\varepsilon_0}\frac{2Ze^2/bv}{mv}$$

where m is the mass of α-particle.

Thus we have,

$$b = \frac{1}{4\pi\varepsilon_0}\frac{2Ze^2}{mv^2}\cdot\frac{1}{\theta} \qquad \ldots(4.\text{I}.3)$$

Equation 4.I.3 gives approximately the relation between deflections and the impact parameter.

The maximum deflections observed by Rutherford in the experiment were of the order of 1 radian. This does not mean that he did not observe larger deflections. Occasionally, he even observed deflections close to π radians. Putting $\theta = 1$ and $b = R$ (corresponding to maximum deflections) in Eq. 4.I.3,

$$R \sim \frac{1}{4\pi\varepsilon_0}\frac{2Ze^2}{mv^2} \qquad \ldots(4.\text{I}.4)$$

Putting the values $\quad Z = 79$ for gold,

$m = 6 \times 10^{-27}$ kg. for mass of α-particle

$v \sim 10^7$ m/s for speed of α-particle

and $\quad e = 1.6 \times 10^{-19}$ coulombs,

we get, $\quad R \sim 10^{-14}$ m. $\qquad \ldots(4.\text{I}.5)$

This is an extremely small distance. When compared with the atomic radius, which is $\sim 10^{-10}$ m, we see that it is smaller by a factor of 10^4.

It is easy to see that the gravitational force is completely negligible inside the nucleus, as it is inside an atom. Since a nucleus consists of protons and neutrons and since protons are positively charged, the question then arises as to how all these protons stay together in a nucleus of size given by Eq. 4.I.5? Clearly, inside the nucleus, over distances of about 10^{-14} m, there is specifically a *nuclear interaction* operating between protons and neutrons (nucleons), which is strong enough to overcome the large Coulomb repulsion between the closely-packed protons. Since the attractive force due to this nuclear interaction does not influence the extra nuclear atomic structure, i must be a *short-range force*, effective only over distances ~10^{-14} m. Obviously, this new force must depend on distance more strongly than does an inverse square force. The size of the region where this nuclear short-range force is significant (compared with the Coulomb force) can b studied with very high-energy particles obtained by using accelerators. When such particles are sent through thin foils, the analysis of the distribution of the scattering angles leads to the discovery that the radius R of the nucleus is proportional to the cube root of the mass number of the scattering nuclei; i.e.,

$$R = R_0\, A^{1/3} \qquad \ldots(4.I.6)$$

where R_0 is about 1.07×10^{-15} m.

4.I.3 MEASUREMENT OF NUCLEAR RADIUS

In the previous section we saw how an estimate of nuclear size can be made using Rutherford's α-scattering experiment. Many experimental methods exist for measuring nuclear size. Because of the important bearing that nuclear size has on our understanding of the nuclear force, in this section we will briefly and qualitatively consider one beautiful experimental method of measuring the nuclear radius, first employed by R. Hofstadter and his colleagues.

This method consists of measurement of nuclear charge distribution and assumes that charge distribution and matter distribution within nuclei are essentially the same. The charge distribution in nuclei is obtained by analysing scattering of high-energy electrons from various nuclei. The experimental arrangement is shown in Fig. 4.I.4.

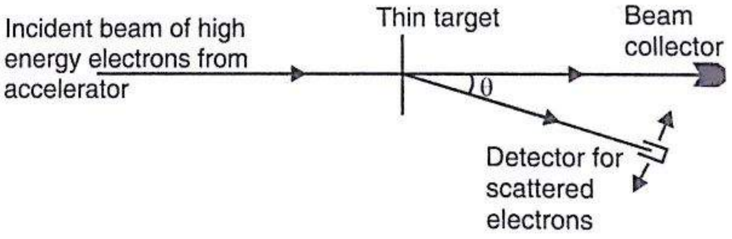
Incident beam of high energy electrons from accelerator
Thin target
Beam collector
θ
Detector for scattered electrons

Fig. 4.I.4. Experimental arrangement for nuclear radius measurement.

Electrons are chosen as bombarding particles because their interaction with the nucleus, the familiar electro-magnetic interaction, is so well-known. As shown in Fig. 4.I.4, the elastically scattered electrons are observed by a detector as a function of angle.

It is easy to see that the de Broglie wavelength of 200 MeV electrons is about 10^{-14} m (use the relation, $\lambda = h/p$) which is the size of a nucleus. Thus to get information about nuclear charge distribution, the incident electron beam energy has to be of the order of 200 MeV. The assumption that nuclear charge is uniformly spread over a spherical volume and not a point charge leads one to expect diffraction effects. Portions of electron waves incident on different parts of the nucleus will be scattered in a particular direction, with phase differences resulting in constructive or destructive interference at some angle. Figure 4.I.5(a) is taken from the work of Hofstadter and his collaborators and shows the angular distribution of elastically scattered

200 MeV electrons from nuclei assumed to have spherical uniform charge distribution [having uniform density up to radius r, as shown in Fig. 4.I.5(b)]. The actual nuclear charge distribution is not exactly given by a step function, but is shown by the dotted line.

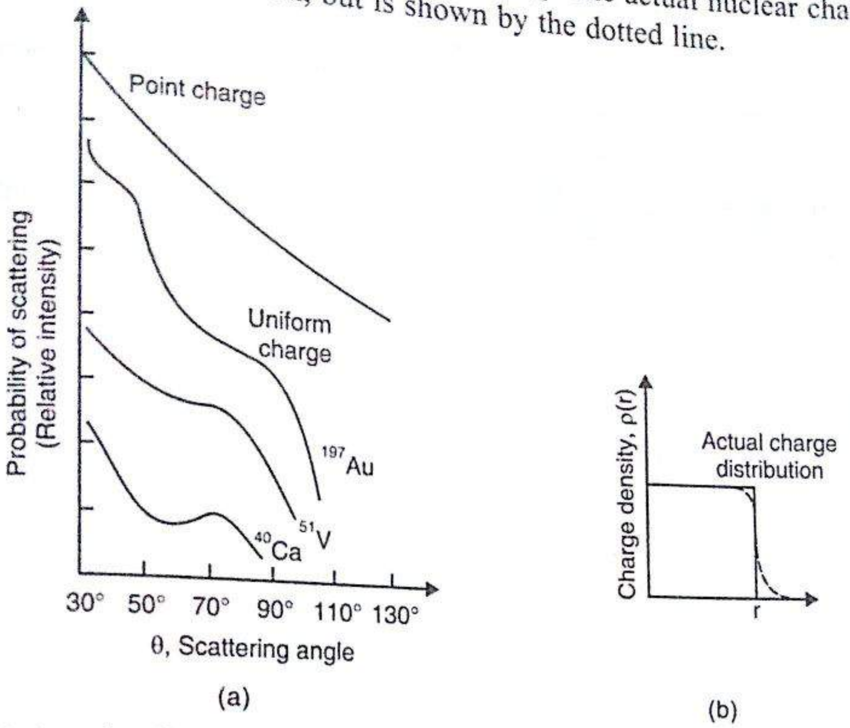

(a) (b)

Fig. 4.I.5. (*a*) Angular distribution (experimental) of scattered electrons from three types of nuclei. For comparison, curve for point charge assumption is also shown.
(*b*) Step function showing uniform charge distribution.

One can clearly see in Fig. 4.I.5(a) that experiments do show diffraction maxima and minima as expected from a uniform charge distribution. For comparison, the expected result (which is not obtained experimentally) from a point charge assumption is also shown in Fig. 4.I.5(a). For theoretical calculations Hofstadter and his colleagues assumed a charge density of the form,

$$\rho(r) = \frac{\rho_0}{1 + e^{(r-R)/b}} \qquad \ldots(4.I.7)$$

where, ρ_0 is density at the nuclear centre, R is the radius at which ρ falls to $\frac{\rho_0}{2}$ and b measures how rapidly ρ falls to zero at the nuclear surface.

Clearly, the distribution given by Eq. 4.I.7 has the property that for $R \gg b$, ρ is close to ρ_0, until $(R - r)$ is a few times b, at which point ρ decrease to very small values in a distance determined by b, but not by R. This charge distribution was found to conveniently fit the experimental data involving many nuclei if one takes,

$$\rho_0 \sim 1.65 \times 10^{44} \, \frac{\text{nucleons}}{\text{m}^3}$$

$$a \sim 0.55 \text{ fermi}$$

$$R \sim 1.07 A^{1/3} \text{ Fermi} \qquad \ldots(4.I.8)$$

and

where

$$1 \text{ Fermi} = 1F = 10^{-15} \text{m}.$$

By varying the values of R and b, a charge distribution could be obtained which would give the observed angular distribution shown in Fig. 4.I.5 (a).

Figure 4.I.5 (c), shows that the charge density is essentially same for all nuclei (except for the lightest nuclei like H and He) decreasing slowly for increasing A. As given in Eq. 4.I.8 the general relationship,

$$R = R_0 A^{1/3} \qquad \ldots(4.I.9)$$

is found to exist.

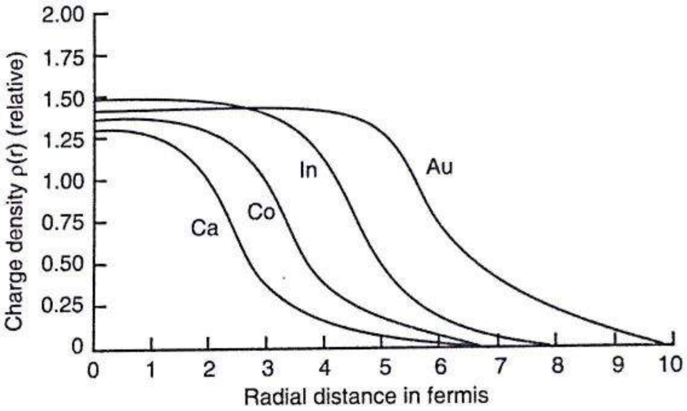

Fig. 4.I.5. (*c*) Nuclear charge distribution found in some nuclei using high-energy electrons as probes.

There are other methods of obtaining the nuclear radius. Another important method probes the extent of the nuclear force rather than the nuclear charge. We get the same general relationship, $R = R_0 A^{1/3}$. In Chapter 8, we will see some features of this approach. Equations 4.I.8 and 4.I.9 are extensively used in the following chapters, particularly on nuclear models. Having become familiar with the size of the nucleus, let us now look at its constituents.

4.I.4 CONSTITUENTS OF THE NUCLEUS AND THEIR PROPERTIES

As mentioned in the introduction, neutrons and protons are nuclear constituents. Using Heisenberg's uncertainty principle, it is interesting to see why electrons cannot be within a nucleus.

Let the uncertainty in the position of the electron, Δx be of the order of nuclear size. 10^{-14} m. This will permit the electron to remain inside the nucleus. We can now calculate Δp the uncertainty in electron's momentum, using the uncertainty principle,

$$\Delta x \cdot \Delta p \sim h \qquad \ldots(4.I.10)$$

$$\therefore \qquad \Delta p = \frac{h}{\Delta x} = \frac{6.62 \times 10^{-34} \text{Js}}{10^{-14} \text{m}} = 6.62 \times 10^{-20} \text{kg ms}^{-1}.$$

Now it is reasonable to assume that the momentum p must be at least equal to Δp, the uncertainty in momentum. Then using the relativistic relation between the total energy E_T and momentum p.

$$E_T^2 = p^2c^2 + m_0^2c^4 \qquad \text{...(4.I.11)}$$

where, m_0 is the rest mass of electron, we have,

$$E_T^2 = (6.62 \times 10^{-20})^2 \times (3 \times 10^8)^2 + m_0^2c^4$$

Note that we have put $p = \Delta p$.

Now converting the energy units from joules to MeV and remembering that for electron the rest energy $m_0c^2 = 0.511$ MeV, we have:

$$E_T^2 = 15{,}406 + (0.511)^2$$

giving

$$E_T = 124 \text{ MeV}.$$

This is a very large energy for the electrons to have, as it is known that electrons emitted in β-decay process from the nucleus have energies of the order of a few MeV. Therefore it is quite reasonable to conclude that electrons as such cannot exist in the nucleus. When they are emitted in the radioactive decay (β-decay) they must be created at the time of emission. It is useful to remember that energy required to remove a nucleon (either a proton or a neutron) from the nucleus is of the order of 10 MeV. (see Chapter 5).

Mass of Proton and Neutron: Students are expected to be familiar with the different mass spectrometers and the atomic mass scale based on carbon-12. One atomic mass unit (a.m.u. or simply u) is defined as 1/12 of the mass of the carbon-12 atom, whose mass is exactly taken as 12.000000000 amu. In terms of the mass unit kg, 1 a.m.u. is 1.660531×10^{-27} kg. On this scale, the proton and neutron masses are (rest masses):

Proton mass:	1.00727663 u which is equal to 1.6725×10^{-27} kg or 938.26 MeV.
Neutron mass:	1.0086654 u which is equal to 1.6748×10^{-27} kg or 939.55 MeV.

The table of neutral atomic masses of various nuclei is given at the end of the book. The discovery of neutrons being an extremely crucial factor in the progress of Nuclear Physics, we will consider it below in some detail.

Discovery of the Neutron

In Chapter 1, we have seen how heavy charged particles (α, p etc.) exhibit a range in a medium and how this range is related to the energy of the particle. By measuring the range of heavy charged particle in say, a cloud chamber, it is possible to determine the energy of the particles (see Eq. 1.1.1).

One of the classic experiments performed by Rutherford is the bombardment of lighter elements by α-particles. For example, when nitrogen was bombarded by α-particles, he could establish the following reaction.

$${}^{4}_{2}\text{He} + {}^{14}_{7}\text{N} \rightarrow {}^{1}_{1}\text{H} + {}^{17}_{8}\text{O} \qquad \text{...(4.I.12)}$$

This indeed was one of the first man-made nuclear reaction. Rutherford and Chadwick found about a dozen cases where bombardment of light element by α-particles resulted in the ejection of protons. By measuring the range of protons, their energy could be determined.

However, it was soon found that some light elements did not give out protons under α-particle bombardment. In 1930, Bothe and Becker showed that beryllium bombarded by energetic α-particles from polonium gave rise to a very *penetrating radiation* which could travel several cm of lead. They knew that γ-rays have high penetrating power and so assumed that this penetrating radiation consisted of γ-rays. Boron also, it was found, gave out a similar, highly penetrating radiation. Further in 1931-32, Mme Irene Curie-Joliot and her husband M. Joliot found that these penetrating radiations could knock out energetic protons from hydrogeneous matter like a block of paraffin wax (see Fig. 4.I.6). They thought that the assumed penetrating radiation in the form of γ-rays was knocking out protons in a manner similar to X-rays knocking out electrons in a Compton scattering experiment.

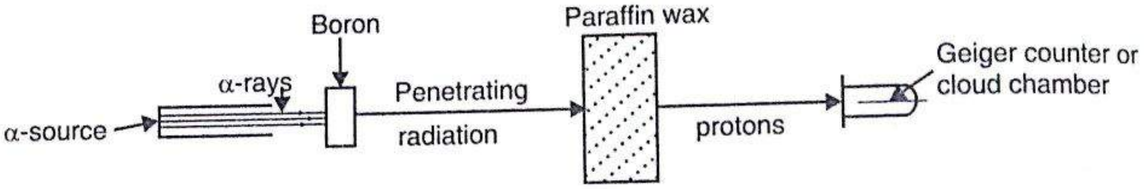

Fig. 4.I.6. Experimental arrangement to detect protons knocked out from paraffin wax.

Let us calculate the energy of the incident (assumed) γ-rays that would give the protons of observed energy. It is possible to conclude from the range-energy relationship that for protons with an observed range in air of about 26 cm, the initial speed is about 3×10^7 m/s. This corresponds to an energy of about 4.7 MeV for protons ejected out of the paraffin wax block. To compute the γ-ray energy that would give rise to 4.7 MeV protons, we proceed as follows:

The change in gamma photon wavelength $\Delta\lambda$, when it is scattered at an angle α by a proton of rest mass m_p, is given by the Compton formula:

$$\Delta\lambda = \frac{h}{m_p c}(1 - \cos\alpha) \qquad \ldots(4.I.13)$$

The largest transfer of energy (corresponding to the largest $\Delta\lambda$) from γ-photon to proton occurs at $\alpha = 180°$ corresponding to back scattering of the γ-photon. In this case, Eq. 4.I.13 becomes

$$\Delta\lambda = \frac{2h}{m_p c} \qquad \ldots(4.I.14)$$

Now if E_f is the incident γ-photon energy,

$$E_f = hf$$

and

$$dE_f = hdf$$

$$= hd\left(\frac{c}{\lambda}\right), \text{ since } f = \frac{c}{\lambda}$$

$$= \frac{-hcd\lambda}{\lambda^2} \qquad \ldots(4.I.15)$$

where dE_f gives change in γ-photon energy due to a change in wavelength, $d\lambda$. We have treated these changes as differentials as we will see that these are quite small compared to the photon energy E_f. Using Eq. 4.I.14 we can get the maximum change in photon energy as,

$$(dE_f)_{\max} = \frac{-hc}{\lambda^2}\left(\frac{2h}{m_p c}\right)$$

$$= \frac{-2(hc/\lambda)^2}{m_p c^2}$$

$$= \frac{-2(hf)^2}{m_p c^2}$$

$$= \frac{-2E_f^2}{m_p c^2} \qquad \ldots(4.I.16)$$

Clearly, the energy lost by γ-photon is the energy gained by the proton. Let the energy gained by the proton be dE_p. Thus,

$$(dE_f)_{\max} = -(dE_p) \qquad \ldots(4.I.17)$$

Now, $m_p c^2$ is clearly the rest mass energy of the knocked out proton and so,

$m_p c^2 \sim 1$ a.m.u. or about 1000 MeV.

$\therefore \quad dE_p \sim 2E_f^2$ if expressed in a.m.u.

$\sim 2E_f^2/1000$ if expressed in MeV ...(4.I.18)

As mentioned before, the observed proton energy is 4.7 MeV.

$$\therefore \qquad dE_f = 4.7 \text{ MeV} = \frac{2E_f^2}{1000} \text{ MeV} \qquad \ldots(4.I.19)$$

which gives, E_f = γ-photon energy = 47 MeV

This calculation shows that in order to knock out protons of 4.7 MeV energy, the incident γ-photons in a favourable back scattering situation must have an energy of about 47 MeV. This energy is unusually high for γ-rays to have. Further the same penetrating radiation (from boron) was found to eject nitrogen nuclei from nitrogenous compounds. The energy of these nitrogen nuclei from range measurements was found to be about 1.2 MeV. If one again assumes the incident penetrating radiation as γ-rays, a similar calculation gives the energy of the incident photons as about 95 MeV, which is greater still and does not agree with the earlier value of 47 MeV given by Eq. 4.I.19.

In Chapter 3, we have seen how one can apply the law of conservation of mass energy to nuclear reactions. Let us apply this law to this α bombardment of boron reaction giving rise to an assumed γ-photon and ${}^{15}_{7}\text{N}$ nucleus:

$$ {}^{4}_{2}\text{He} + {}^{11}_{5}\text{B} \rightarrow {}^{15}_{7}\text{N} + \gamma \text{ photon.} \qquad \ldots(4.\text{I}.20)$$

The isotopic masses were known fairly accurately by 1932. The energy of a particle is its rest energy plus kinetic energy.

Thus, the mass energy of L.H.S. of Eq. 4.I.20 is,

(4.00106 + 0.00565) a.m.u. + 11.00825 a.m.u. = 15.01496 a.m.u.

i.e., a total of 15.01496 a.m.u. mass energy goes in the reaction given by Eq. 4.I.20. Here we have assumed that the ${}^{11}\text{B}$ target nuclei are at rest.

The rest mass-energy of ${}^{15}_{7}\text{N}$ on the R.H.S. of Eq. 4.I.20 is about 14.999 a.m.u. Assuming that all the kinetic energy of the product is taken by the γ-ray we have the γ-ray energy as,

$$(15.015 - 14.999) \text{ a.m.u.} = 0.016 \text{ a.m.u.}$$

or

$$(0.016 \times 931) \text{ MeV} = 14.9 \text{ MeV.}$$

In other words, the energy of the assumed γ-rays on the basis of mass-energy conservation is found to be far less than 47 MeV or 95 MeV calculated before. This situation is paradoxical and confusing. Chadwick in 1932 obtained and analyzed the data, given above in the light of Rutherford's earlier idea that there was a neutral particle. Chadwick's calculation gave proof of the existence of such a particle. He proposed that the penetrating radiation emitted on the bombardment of boron with α-particles was *not gamma rays* but a beam of neutral particles called *neutrons*. Chadwick proposed the following nuclear reactions:

$$ {}^{4}_{2}\text{He} + {}^{11}_{5}\text{B} \rightarrow {}^{14}_{7}\text{N} + {}^{1}_{0}n \qquad \ldots(4.\text{I}.21)$$

Since a neutron does not have any charge, it can have great penetrating power. Chadwick made the important assumption that the mass of the neutron is almost the same as that of the proton. From elementary mechanics one knows that the kinetic energy transfer in an elastic collision between two particles of mass m_1 and m_2 is complete when $m_1 = m_2$

If E_{k_1} is the incident K.E. of particle with mass m_1 and E'_{k2} is K.E. (after collision) of mass m_2 then it is easy to see that

$$E'_{k_2} = \frac{4m_1 m_2}{(m_1 + m_2)^2} E_{k_1} \qquad \ldots(4.I.22)$$

Clearly for $m_1 \sim m_2$ $E'_{k_2} = E_{k_1}$, implying complete transfer of kinetic energy after the elastic collision. Following Chadwick, let us now apply Eq. 4.I.22 to collisions (treated as elastic collisions) between (*i*) the assumed neutrons and protons in the paraffin wax block and (*ii*) the neutrons and nitrogen nuclei. The reaction giving rise to neutrons is assumed to be Eq. 4.I.21.

In Eq. 4.I.22, let m_1 = mass of the neutron

m_2 = mass of the proton

~ 1 a.m.u.

and E'_{k_2} = K.E. of the ejected proton

= 4.7 MeV.

$$\therefore \quad 4.7 = \frac{4m_1}{(m_1 + 1)^2} E_{k_1} \qquad \ldots(4.I.23)$$

On the other hand, if in Eq. 4.I.22 we let,

m_1 = mass of the neutron

m_2 = mass of the nitrogen nucleus

~ 14 a.m.u.

and E'_{k_2} = K.E. of the ejected nitrogen nucleus

= 1.2 MeV,

$$\text{We have} \quad 1.2 = \frac{4m_1 \times 14}{(m_1 + 14)^2} E_{k_1} \qquad \ldots(4.I.24)$$

By simultaneously solving Eqs. 4.I.23 and 4.I.24, we get,

$m_1 \sim 1.02$ a.m.u.

and $E_{k_1} \sim 4.7$ MeV

Though we have not taken the exact masses in the above calculations, it becomes clear that by proposing the penetrating radiation to be a beam of neutral particles, neutrons, Chadwick could show that a single reasonable energy of a neutron satisfactorily accounted for observed recoil energies of a proton and a nitrogen nucleus. There is no need for the paradoxical gamma ray hypothesis which gives two different energies, 47 MeV and 95 MeV, for the observed recoil energy of a proton and a nitrogen nucleus. Further, the mass of the neutron turns out to be almost the same as that of the proton. The nuclear reaction given by Eq. 4.I.21 was analyzed by Chadwick to get a good estimate of the neutron mass. The mass energy equation corresponding to Eq. 4.I.21 can be put as:

$$\begin{aligned} &{}^{4}_{2}\text{He (rest energy)} + \left(\text{K.E. of } {}^{4}_{2}\text{He}\right) + {}^{11}_{5}\text{B (rest energy)} \\ &= {}^{14}_{7}\text{N (rest energy)} + \left(\text{K.E. of } {}^{14}_{7}\text{N}\right) + \left(\text{K.E. of } {}^{1}_{0}n\right) + {}^{1}_{0}n\text{ (rest energy)} \end{aligned} \qquad \text{...(4.I.25)}$$

Expressing energies in a.m.u.

$$4.00106 + 0.00565 + 11.00825 = 14.0042 + 0.00061 + {}^{1}_{0}n \text{ (rest energy)} + 0.0035$$

The mass values were taken by Chadwick from Aston's mass spectroscopic work.

The K.E. of the α-particle and the neutron were measured by range measurement of α-particles and knocked out protons respectively. The K.E. of the nitrogen nucleus was estimated by applying the law of conservation of momentum.

Solving the above equation for neutron mass, Chadwick obtained the value 1.0067 a.m.u. This value is remarkably close to the modern value:

Rest mass of neutron = 1.008665 a.m.u. ...(4.I.26)

A free neutron was found to decay by beta activity of a half life of 12 min. (1950).

4.I.5 NUCLEAR SPIN, MOMENTS AND STATISTICS

In the last section we saw how electrons cannot be within a nucleus and the constituents of nuclei are protons and neutrons. In this section, we will take a look at some important quantum mechanical properties of nuclei.

From elementary mechanics, we know that the angular momentum of an isolated system is conserved. The nucleus being an isolated system (net external torque equal to zero), its angular momentum is a constant quantity. This situation is analogous to an atom. Following this analogy, if I represents the total angular momentum quantum number, then the eigen values of the square of the total angular momentum operator are $I(I + 1)$ in the units of $\hbar^2$. Expressed in eigen value equation:

$$\hat{\mathbf{I}}^2\psi_{1M} = I(I+1)\hbar^2\psi_{1M} \qquad \text{...(4.I.27)}$$

where $\hat{\mathbf{I}}^2$ is the operator belonging to the square of the total angular momentum and ψ_{1M} is common eigen function of $\hat{\mathbf{I}}^2$ and I_z, the z-component of total angular momentum. For operator $\hat{\mathbf{I}}_z$ we have,

$$\hat{\mathbf{I}}_z\psi_{1M} = m\hbar\psi_{1M} \qquad \text{...(4.I.28)}$$

Note that Eqs. 4.I.27 and 4.I.28 are satisfied by a set of common eigen functions because the commutator of $\hat{\mathbf{I}}^2$ and I_z is zero, i.e.,

$$[\hat{\mathbf{I}}^2, I_z] = 0 \qquad \text{...(4.I.29)}$$

Clearly, Eq. 4.I.27 states that the magnitude of the total angular momentum is quantized and is restricted to values,

$$\text{Total angular momentum} = \sqrt{I(I+1)}\hbar \qquad \ldots(4.I.30)$$

Equation 4.I.28 states that the z-component of the angular momentum can take only values $M\hbar$. The quantum numbers I and M are integers and for a given value of I, M can take $2I + 1$ values from $-I$ to $+I$. The space quantization is expressed in a vector diagram given in Fig. 4.I.7, for $I = 5/2$.

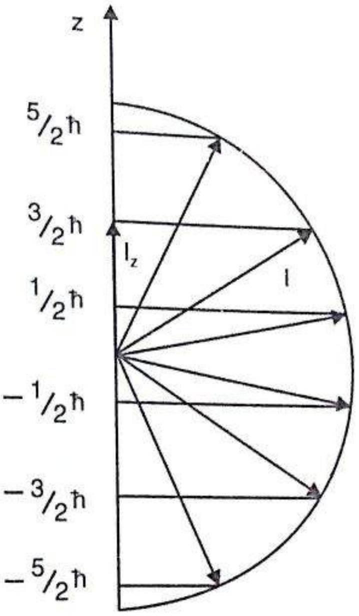

Fig. 4.I.7. Vector diagram showing possible orientations of the total angular momentum vector $\vec{I}$. The case drawn is for $I = 5/2$; the possible $(2I + 1)$ values of M being $\pm\frac{5}{2}\hbar, \pm\frac{3}{2}\hbar, \pm\frac{1}{2}\hbar$.

It should be remembered that the allowed values of I are not only integers, but also half-integers:

$$I = 0, \frac{1}{2}, 1, \frac{3}{2}, 2, \frac{5}{2}, \ldots \qquad \ldots(4.I.31)$$

Obviously the half integral values are a result of Pauli's proposal of *intrinsic spin.* The total angular momentum is the sum of orbital angular momentum and spin angular momentum. Experiments have shown that nuclei with even mass numbers A have zero or integral spins; those with odd A have half-integral spins. In particular even-even nuclei (both Z and N even) have zero spin. Spin has no analog in classical mechanics. In elementary treatment of atomic physics spin is often introduced by assuming the particle to be a fast-spinning top. However, this is not a proper idea as it turns out that for a reasonable radius of the particle, the velocity of the surface of the particle (considered as a spinning top) exceeds the velocity of light. Also, even particles like photons or neutrino which have a zero rest mass, possess an intrinsic spin. Spin is an inseparable characteristic of a particle, and its existence has to be taken as a fact.

Usually the spin operator is denoted by $\hat{S}$ and it satisfies the eigenvalue Eqs. 4.I.27 and 4.I.28. In this case, the quantum number is either half-integral or integral depending on the type of particles. The quantum number M describes the orientations of the particle in space with respect to some chosen z-axis. Clearly there are $(2S + 1)$ orientations.

The famous Stern and Gerlach experiment and hyperfine atomic spectroscopy are used to determine atomic angular momenta. For nuclear particles, if we can determine the number of possible orientations in space, the spin S can be found out because there are $2S + 1$ possible orientations. Let us now consider the electromagnetic moments associated with nuclei and nucleons.

Figure 4.I.8 shows the *magnetic dipole moment* μ associated with a current loop of area A and carrying a current i. From an elementary course in electricity and magnetism it is well known that,

$$\mu = iA \qquad \ldots(4.I.32)$$

Now for an electron moving in a circular orbit of radius r with a period T

$$i = \frac{e}{T} = \frac{e}{2\pi r / v}$$

and

$$A = \pi r^2$$

∴

$$\mu = \frac{ev}{2\pi r} \times \pi r^2 = \frac{e}{2} vr$$

i.e.,

$$\mu = \frac{e}{2m} mvr = \frac{e}{2m} L \qquad \ldots(4.I.33)$$

where L is the angular momentum.

Though Eq. 4.I.33 has been obtained in a very simple-minded way it tells us an important fact that the angular momentum L gives rise to a magnetic dipole moment μ for a charged particle.

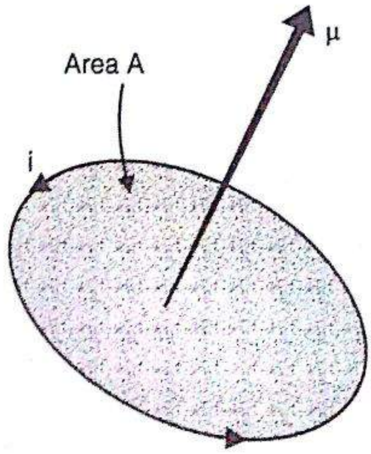

Fig. 4.I.8. Magnetic dipole moment given rise to by a circular current loop, of area A.

Equation 4.I.33 can be generalised as,

$$\mu = \frac{e}{2m} Lg \qquad \ldots(4.I.34)$$

where g is a factor called the gyromagnetic ratio or g-factor. For a nucleus, Eq. 4.I.34 can be put as,

$$\mu = \frac{e}{2m} Ig \qquad \ldots(4.I.35)$$

Usually e is defined as positive and the sign of the magnetic dipole moment μ is given by the sign of the *g-factor*. I, the total nuclear angular momentum has the units of $\hbar$ and so $I/\hbar$ is dimensionless. Eq. 4.I.35 can be written as,

$$\mu = g\mu_0 \frac{I}{\hbar}$$

where

$$\mu_0 = \frac{e\hbar}{2m} \qquad \ldots(4.I.36)$$

The constant μ_0 is called a *magneton* and it is taken as the unit to measure magnetic moments. In atomic physics m is the electron mass m_e and we call the unit, the *Bohr magneton* μ_β:

$$\mu_\beta = \frac{e\hbar}{2m_e} = 0.927 \times 10^{-23} \text{ joule/weber/m}^2 \qquad \ldots(4.I.37)$$

For nuclei, we express the magnetic moments in terms of *nuclear magnetons* μ_N, defined as,

$$\mu_N = \frac{e\hbar}{2m_p} = \frac{\mu_\beta}{1836} = 5.05 \times 10^{-27} \text{ joule/weber/m}^2 \qquad \ldots(4.I.38)$$

where m_p the proton mass is 1836 times the mass of the electron. Clearly, the nuclear magneton is about 2000 times smaller than the Bohr magneton. Determination of the g-factor is an important experimental problem as g-factor measures the deviation of an actual magnetic moment from the simple value $e\hbar/2m$. The g-factor has been measured for many particles and nuclear states and these measurements are a critical challenge to any theory of the nucleus.

Let us consider the Zeeman splitting of a nuclear level of energy E_0 when a magnetic field B is applied. The particle magnetic moment μ interacts with the magnetic field B, the interaction energy being, $-\vec{\mu} \cdot \vec{B}$ (see Chapter 7 for the shell model of nucleus). Thus the Hamiltonian H in the Schrödinger equation

$$H\psi = E\psi$$

is of the form

$$H = H_0 + H^1$$

$$= H_0 - \vec{\mu} \cdot \vec{B}$$

From Eq. 4.I.36 this becomes,

$$H = H_0 - g\frac{\mu_0}{\hbar}\vec{I} \cdot \vec{B} \qquad \ldots(4.I.39)$$

Clearly, the spin-independent Hamiltonian H_0 corresponds to an energy E_0 given by,

$$H_0\psi = E_0\psi$$

If the z-axis is conveniently chosen as the direction of magnetic field B, then

$$\vec{I} \,.\, \vec{B} = IB\cos\theta$$

$$= (I\cos\theta)B$$

$$= I_z B$$

From Eq. 4.I.28 the eigen values of I_z are $M\hbar$ and so when operator H of Eq. 4.I.39 operates on ψ we get eigen values E,

$$E = E_0 - g\mu_0\, MB \qquad \ldots(4.I.40)$$

The quantum number M takes values $(2I + 1)$ from $-I$ to $+ I$. Figure 4.I.9 shows the Zeeman energy splitting for a spin $I = 3/2$.

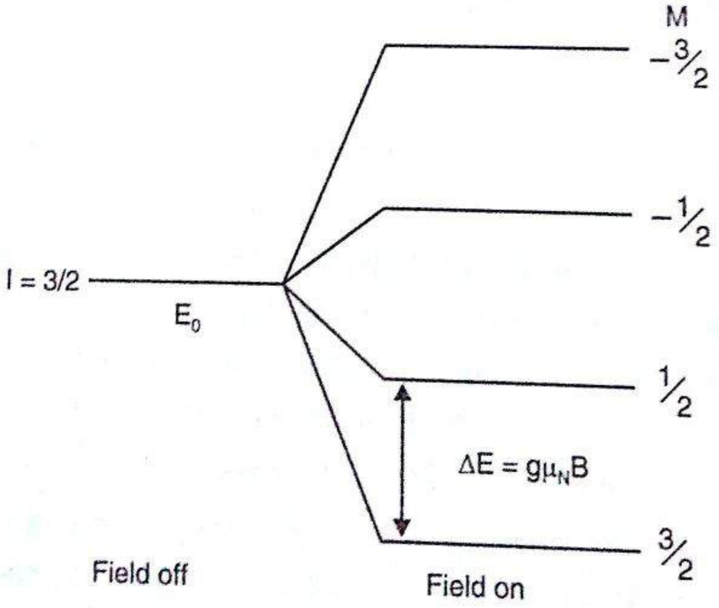

Fig. 4.I.9. Zeeman splitting of a nucleus in an external magnetic field B, for the case of nuclear spin 3/2. The splitting $\Delta E = g\mu_N B$.

To find out the g-factor, experimentally the splitting $\Delta E = g\mu_N B$ is determined. As we are considering a nuclear Zeeman effect, μ_0 is replaced by the nuclear magneton μ_N If now B is known, g can be obtained. From Eq. 4.I.36,

$$\mu = g\mu_N \frac{I}{\hbar}$$

Thus to determine the dipole moment μ, g and I have to be known. The total number of Zeeman levels being $(2I + 1)$, in principle I can be found.

The actual measured values of the nuclear magnetic moments are broadly between $-3\mu_N$ and $+10\mu_N$, the positive sign implying that μ is parallel to the spin and the negative sign gives their directions anti-parallel. In Chapter 10 we will see how proton magnetic moment was measured using the NMR technique. The magnetic moment of a proton is,

$$\mu_{\text{proton}} = +2.79276\mu_N \qquad \text{...(4.I.41)}$$

This is an unexpected value and quite different from the expected value of about one nuclear magneton. This indicates that the proton has a non-uniform charge distribution.

Similarly, one expects the neutron magnetic moment to be zero as the neutron has no charge. However, the measured value of the neutron magnetic moment is,

$$\mu_{\text{neutron}} = -1.191315\mu_N \qquad \text{...(4.I.42)}$$

This indicates that the neutron also has a non-uniform charge distribution and the direction of the magnetic moment is opposite to that of its intrinsic spin angular momentum vector. In Chapter 8, we will study nuclear force and get to know nuclear force field particles—π-mesons. The π-mesons may have either sign of electric charge and are constantly exchanged between nuclear particles. Figure 4.I.10 illustrates how a neutral particle like the neutron contributes to a non-zero orbital magnetic moment.

Apart from the Stern-Gerlach atomic beam and Zeeman effect studies (hyperfine structure) other methods of measurement of μ include the NMR, and the Perturbed Angular Correlation technique. Recently it has been possible to use a high power intense beam of Laser light tuned to resonance with some hyperfine transition. This induces nuclear orientation (Laser induced nuclear orientation—LINO) and causes anisotropic emission of the nuclear radiation. Measuring this anisotropy, it is possible to obtain the hyperfine structure and measure the moments of nuclear states. Some of these techniques are beyond the scope of this book. However the NMR technique being very versatile, sensitive and well established, it will be taken up in some detail in Chapter 10.

In a course in electromagnetism, it is usually shown that any distribution of electric charge produces an electric potential V at a distance R in the Z direction. This potential V can be expanded as:

$$V = \frac{1}{4\pi\varepsilon_0}\left[\frac{1}{R}\int \rho\, dV + \frac{1}{R^2}\int \rho z\, dV + \frac{1}{R^3}\int \rho(3z^2 - r^2)\, dV + \ldots\ldots\right] \qquad \text{...(4.I.43)}$$

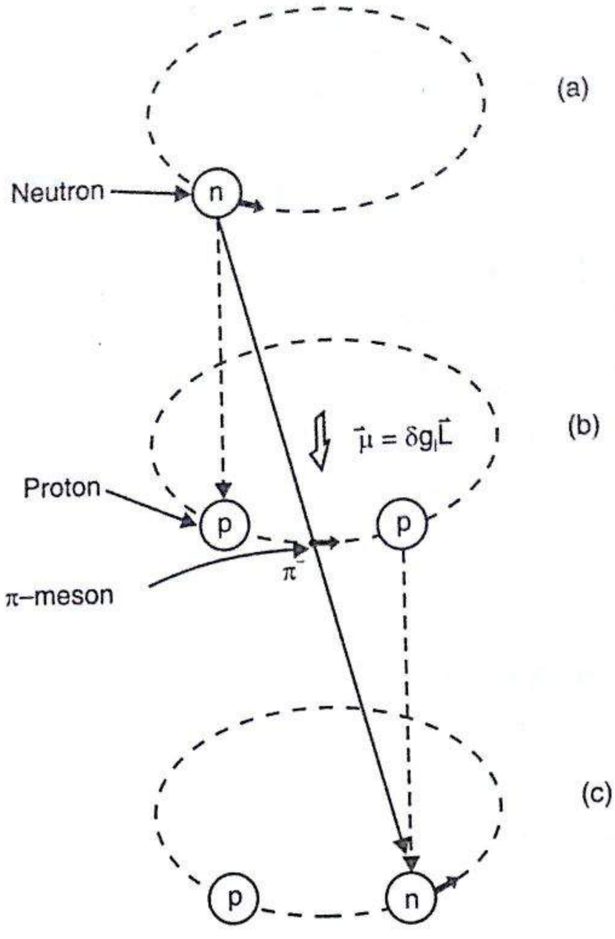

Fig. 4.I.10. Illustration of mesonic exchange that gives rise to neutron magnetic moment.

(*a*) *Initial state:* The neutron itself produces no orbital moment.

(*b*) *Intermediate state:* π^- (negative *pi* meson) contributes to negative orbital moment.

(*c*) *Final state:* π^- is absorbed by a core proton.

where, ρ is the charge density. The integration is performed over the region containing the electric charge. This is a rapidly convergent series and as R increases, only the first two or three terms become important. The first term is the net charge and for very large R,is the only important term. The integral in the second term is called the *dipole moment* and that in the third term is called the *quadrupole moment.* It turns out that a nucleus must have a zero electric dipole moment and so the lowest order contribution to V due to a point charge arises from the quadrupole moment. Two examples of non-zero electric quadrupole moments are shown in Fig. 4.I.11.

The four-charge (quadrupole) system in the left part of Fig. 4.I.11 has net charge and dipole moment zero and so the entire electric field is produced by the electric quadrupole moment. An ellipsoidal charge distribution shown on the right corresponds to a highly deformed nucleus.

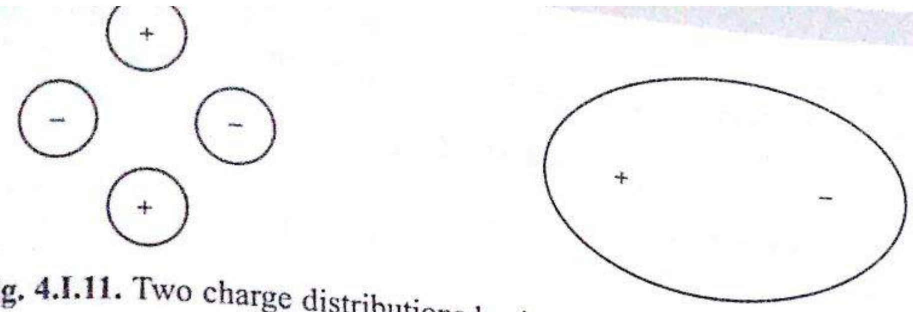

Fig. 4.I.11. Two charge distributions having an electric quadrupole moment.

It has a quadrupole moment; however, its dipole moment is zero. The charge density at point $\vec{r}=(x, y, z)$ is given by $Ze\,\rho(r)$ where Ze is nuclear charge. The quadrupole moment Q as defined by Eq. 4.I.43 is:

$$
\begin{aligned}
Q &= Z\int (3z^2 - r^2)\,\rho(\vec{r})\,d^3r \\
&= Z\int r^2 (3\cos^2\theta - 1)\,\rho(\vec{r})\,d^3r \qquad \text{...(4.I.44)}
\end{aligned}
$$

For a spherically symmetric $\rho(\vec{r})$, the quadrupole moment vanishes.

For a prolate nucleus, the charge is concentrated along the z-axis and so Q is positive. Q is negative for an oblate nucleus (Fig. 4.I.12). From Eq. 4.I.44, it is clear that Q has dimensions of area and is given in m^2 or barns (10^{-24} cm^2) or F^2 (fermi^2). In an external inhomogeneous electric field, a nucleus with quadrupole moment acquires an energy that depends on the

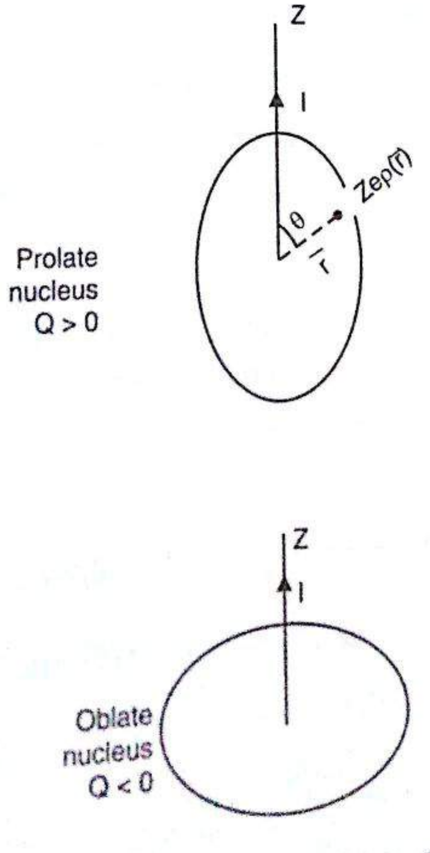

Fig. 4.I.12. For prolate nucleus $Q > 0$. For oblate nucleus $Q < 0$ Spins point in Z-direction which is the symmetry axis.

orientation of the nucleus with respect to the field gradient. Experimentally, this interaction enabl us to determine Q. As an example, the deuteron quadrupole moment is,

$$Q_{\text{deuteron}} = 0.282 \text{ fm}^2 \qquad \ldots(4.I.45)$$

This result has important implications as regards to our understanding of nuclear forces and we will consider this aspect in Chapter 8.

Another aspect of quadrupole moment measurement is that it makes it possible to determin nuclear *deformation.* The quadrupole moment is related to the nuclear deformation paramete δ by the relation,

$$Q = \frac{4}{5} Z R_0^2 \delta \left(1 + \frac{1}{2}\delta + \ldots\ldots\right) \qquad \ldots(4.I.46)$$

where Z is the atomic number and R_0 is the mean nuclear radius.

Knowledge of nuclear deformation is important for studying collective behaviour of nuclear particles (see Chapter 7).

In Chapter 1 Part II, we have considered symmetric and antisymmetric wave functions. Since nuclear particles like protons are identical, the probability distribution $|\psi|^2$ remains unchanged by an exchange of particle co-ordinates. If x_1 are the general co-ordinates of one particle (which may include spin) and x_2 are the general co-ordinates for the other then we have,

$$|\psi(x_1, x_2)|^2 = |\psi(x_2, x_1)|^2 \qquad \ldots(4.I.47$$

giving

$$\psi(x_1, x_2) = \pm\,\psi(x_2, x_1) \qquad \ldots(4.I.48$$

The sign we choose depends on the type of particle we are considering. For electrons, proton etc. we must choose the negative sign, and the eigen function for the two electrons is ant symmetric for an exchange of co-ordinates. Such particles are said to satisfy Fermi-Dira statistics and are called fermions. On the other hand, for photons, one must choose the positi sign so that the eigen function of two photons is symmetric for an exchange of co-ordinate Photons are said to satisfy Bose-Einstein statistics and are called bosons.

For two electrons, the antisymmetric state function is,

$$\psi(x_1, x_2) = \sqrt{\frac{1}{2}}[\psi_\alpha(x_1)\psi_\beta(x_2) - \psi_\beta(x_1)\psi_\alpha(x_2)] \qquad \ldots(4.I.4$$

Now if two electrons are in the same quantum state, the R.H.S. of Eq. 4.I.49 vanishes a the state function becomes equal to zero. Thus $\psi_\alpha \neq \psi_\beta$ (where α and β indicate quant states) and no two electrons can be in the same quantum state. This is Pauli's exclusion princi for particles with half-integral spins. Pauli was the first person to realize this important connect between spin and symmetry of wave function on exchange of co-ordinates. The following ta summarizes the spin-symmetry relationship:

Spin I	*Particles*	*Wave function on exchange of co-ordinates*
Integer	Bosons	Symmetric
Half-integer	Fermions	Antisymmetric

PART–II: ALPHA RAYS: SPECTRA AND DECAY

4.II.1 RANGE OF α-PARTICLES

In Chapter 2 pertaining to radioactivity, we have become familiar with the α-particle. Usually the α-particles emitted by radioactive substances have kinetic energies between 5 and 10 MeV corresponding to velocities of the order of 10^7 m/s. We have also seen that α-particles exhibit a definite *range* when they traverse a material medium (see Chapter 1). In Sec. 4.I.4 as well as in Chapter 1, the relation between the range and energy is brought out. Figure 4.II.1 shows the range of α-particles emitted by ^{214}Po. Notice that towards the end of the range, the ionization increases. This is because there, the α-particles move slowly and so have more time to interact with surrounding atoms and molecules, thereby increasing the number of ion pairs produced. The straggling is due to the long-range α-particles given by ^{214}Po. The existence of long range α-particles is discussed at the end of this section.

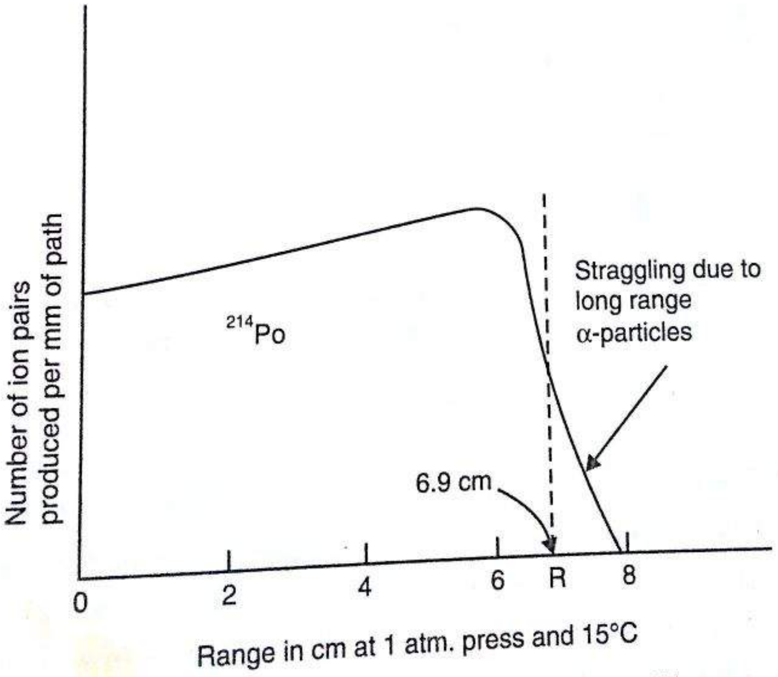

Fig. 4.II.1. Range of α-particles in air from ^{214}Po.

This range of about 6.9 cm. corresponds to an energy of 7.68 MeV. The range-energy relationship is given by *Geiger rule*, Eq. 1.I.1, $\boxed{V_0^3 = C^1 R.}$ Figure 1.I.4 shows ranges of α-particles and protons in air at 15°C and, 76 cm. Hg pressure (also see Fig. 1.I.3). The constant C^1 is numerically equal to $C^1 = 9.6 \times 10^{-28}$, when range R is expressed in cm. and speed V_0 is in cm/s.

V = velo. of charged particle

There is one more important, empirical relation between the range of an alpha particle and the decay constant $\lambda\left(=\frac{1}{\tau}\right)$ of the α-emitter.

$$\boxed{\log R = A\log\lambda + B} \qquad \text{...(4.II.1)}$$

where the constant A has almost the same value for all the three radioactive series (see Chapter 2 for radioactive series) and B is a constant with a different value for each series. This relationship is known as the *Geiger-Nuttall law* and is plotted for the three radioactive series in Fig. 4.II.2.

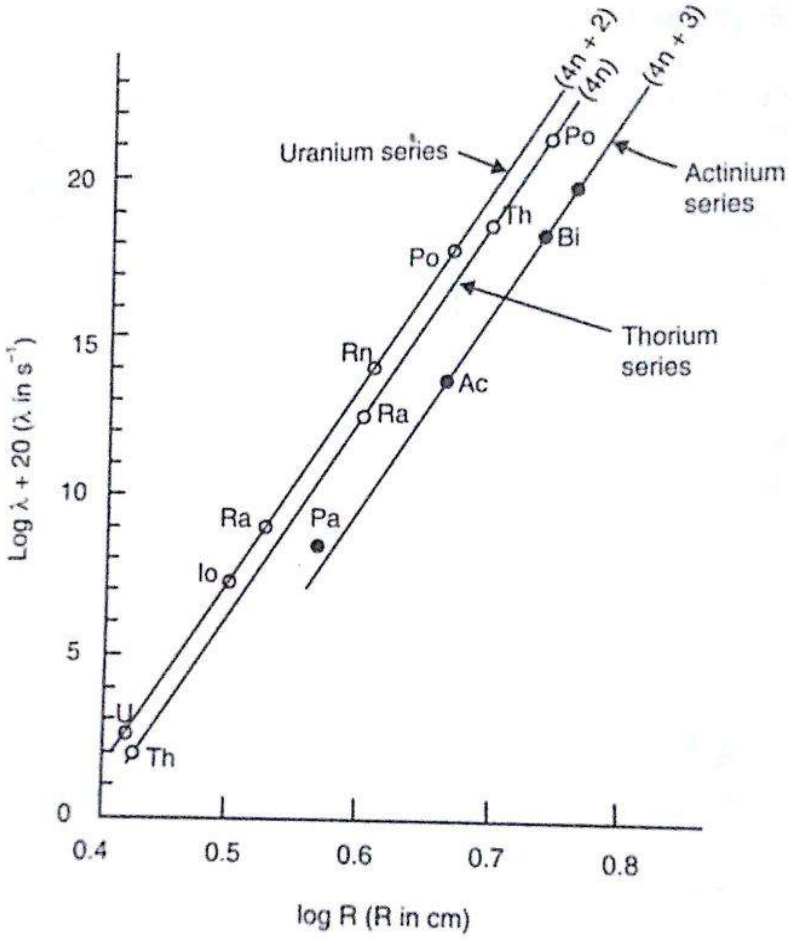

Fig. 4.II.2. The Geiger-Nuttall law for α-emitters in the three radioactive series.

The Geiger-Nuttall law acquired prominence because it enabled physicists to estimate half lives of α-emitters which could not be easily determined by experimental measurements. Further any acceptable theory of α-emission must be able to predict this law. To become more familiar with the concept of α-particle range and its relationship with energy, students are advised to carefully go through Sec. 1.2 of Chapter 1.

The α-Spectrum and Fine Structure

Till now we have implied that every α-emitter has only one associated α-energy. This is experimentally true for many α-emitters where one finds that the velocity spectrum of the α-particle from these isotopes is always a *sharp line spectrum*. This is to be expected since the emission of an α-particle is a result of *energy transition* between *two definite nuclear energy states;* the initial state is that of the parent nucleus and the final state is that of the daughter nucleus.

However, some α-emitters exhibit a fine structure in the line spectrum. For example, ${}^{214}_{84}\text{Po}$ decays to ${}^{210}_{82}\text{Pb}$ by emitting 4 groups of α-particles having ranges in air 6.91 cm, 7.79 cm, 9.04 cm and 11.51 cm. These ranges correspond to energies, 7.68 MeV, 8.28 MeV, 9.07 MeV and 10.51 MeV respectively. Another example is the decay of ${}^{228}_{90}\text{Th}$.

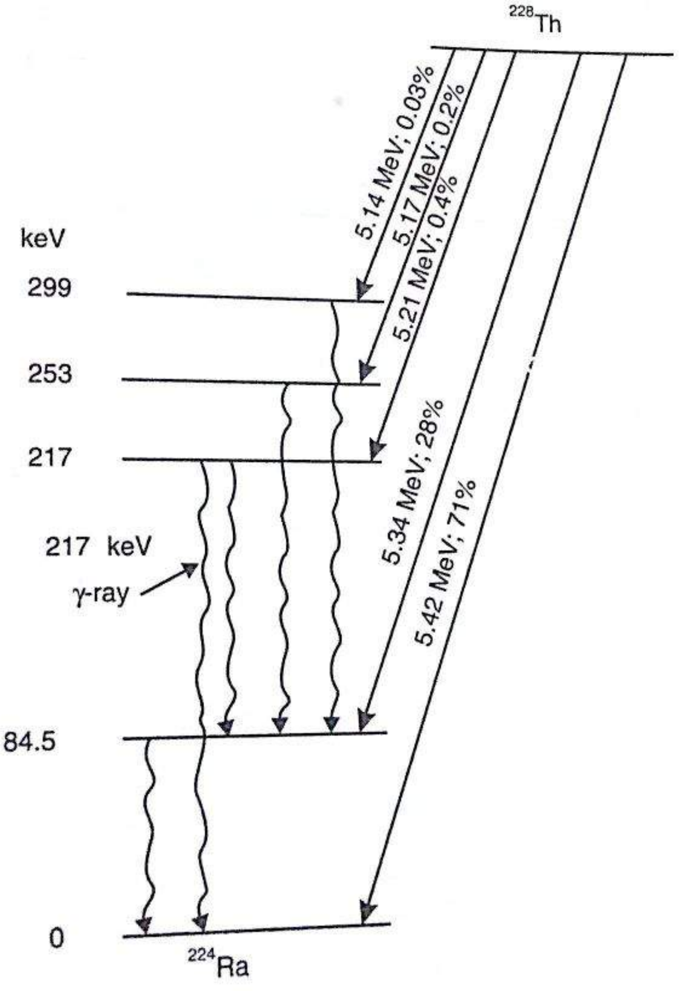

Fig. 4.II.3. Five groups of α-particles, indicated by slanting lines, emitted by ^{228}Th. Percentages are the intensities of α-rays.

$${}^{228}_{90}\text{Th} \rightarrow {}^{224}_{88}\text{Ra} + \alpha$$

Figure 4.II.3 shows this decay schematically.

There are five groups of α-particles with different energies. Out of these, four groups of α-particles leave the daughter nuclei in the excited state. The fifth group of 5.42 MeV α-rays takes one to the ground state of the daughter nuclei. Note that the excited states of nuclei reach the ground state by emitting γ-rays, shown by vertical wavy lines. Thus the fine structure of the α-spectrum tells us about the *energy levels* in the daughter nuclei. We emphasize that the existence of these different α-energy groups and γ-rays proves the existence of *discrete nuclear energy states*. One of the important problems of nuclear physics is to determine the energy levels (excited states) of nuclei and the transitions that take place in the process of de-excitation of these levels. These results are compared with theoretical predictions and often form critical tests for theory. These types of studies come under the heading of *nuclear spectroscopy*. Nuclear spectroscopists are able to establish *genetic relationships* between different nuclear transitions by using the "coincidence technique". A simple coincidence unit is described in Chapter 1. For ^{228}Th, for example, 5.34 MeV α-rays are found to be in coincidence with 84.5 KeV γ-rays. Similarly γ-γ coincidences are observed. These studies can uniquely fix decay schemes of nuclei and Fig. 4.II.3 is in fact obtained by such nuclear spectroscopic work.

Long Range α-Particles

If the parent α-emitter emits α-particles when it is in an excited state, then we get long-range α-particles. This is because the energy of excitation becomes available to the α-particles as they reach the ground state of daughter nuclei. Figure 4.II.4 illustrates the emission of long-range α-particles from $^{212}_{84}$Po. This α-emitter is known to have a type of fine structure in which there are a few α-particles with much greater energies than those of the main group. It has a very short half-life of ~10^{-6} sec. The main group has an energy of about 8.95 MeV. In addition, there are two groups of energies 9.67 MeV and 10.75 MeV. The intensities of these groups are, however, very small (about 100 in 10^6 of the main group).

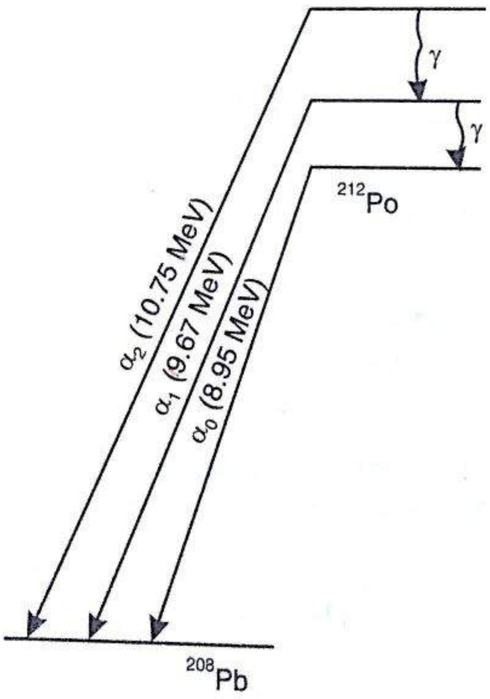

Fig. 4.II.4. Long range α-particles emitted by ^{212}Po.

In Fig. 4.II.4, α_0 is the normal α group corresponding to transition between ground states of ^{212}Po and ^{208}Pb. The other groups α_1 and α_2 originate from the excited states of the parent

^{208}Po and go directly to the ground state of daughter ^{208}Pb. Thus, nuclear spectroscopic studies of long-range α-emitters provide information about nuclear energy levels of the parent.

4.II.2 DISINTEGRATION ENERGY OF SPONTANEOUS α-DECAY

In Chapter 3, we have become familiar with the Q-value of nuclear reactions and the Q-equation. Using those ideas, let us estimate the α-particle disintegration energy. This will tell us the condition under which a nucleus will decay by α-emission. Typically an α-decay can be written as,

$$ {}^{A}_{Z}\mathrm{X} \rightarrow {}^{A-4}_{Z-2}\mathrm{Y} + {}^{4}_{2}\mathrm{He} + Q_\alpha \qquad \ldots(4.\mathrm{II}.2)$$

i.e.,

$$\text{parent} \rightarrow \text{daughter} + \alpha + Q_\alpha$$

The quantity Q_α is the total energy released in this α-decay process and is called *disintegration energy.* Suppose the mass of the daughter is M_d and that of the α-particle is m_α. When an α-particle is emitted with velocity v_α, the residual daughter nucleus will recoil with velocity V_d such that,

$$M_d V_d = m_\alpha v_\alpha \text{ by conservation of momentum,}$$

Now

$$Q_\alpha = (\text{Final K.E.}) - (\text{Initial K.E.})$$

$$= \left(\frac{1}{2}M_d V_d^2 + \frac{1}{2}m_\alpha v_\alpha^2\right) - 0, \quad \because \text{ K.E. of the parent nucleus is 0.}$$

$$= \frac{1}{2}M_d\left(\frac{m_\alpha v_\alpha}{M_d}\right)^2 + \frac{1}{2}m_\alpha v_\alpha^2$$

$$= \frac{1}{2}m_\alpha v_\alpha^2\left(\frac{m_\alpha}{M_d} + 1\right)$$

K_α = K.E. of α-particle

Putting $\frac{1}{2}m_\alpha v_\alpha^2 = K_\alpha$, we have,

$$\rightarrow \quad \boxed{Q_\alpha = K_\alpha\left(\frac{m_\alpha}{M_d} + 1\right)}$$

It is quite reasonable to replace the ratio of masses with the ratio of the mass numbers.

$\therefore \quad \dfrac{m_\alpha}{M_d} \sim \dfrac{4}{A-4}$, A is mass number of parent nucleus.

$\therefore \quad$ The disintegration energy becomes,

$$\boxed{Q_\alpha = \frac{A}{A-4}K_\alpha} \qquad \ldots(4.\mathrm{II}.3)$$

Since usually A is large, and so $Q_\alpha \sim K_\alpha$, i.e., the α-particle carries away most of the disintegration energy.

ILLUSTRATIVE EXAMPLES

Example 4.II.1: $^{212}_{83}\mathrm{Bi}$ decays with a half life of 60.5 min. by emitting 5 groups of α-particles with energy, 6.08 MeV, 6.04 MeV, 5.76 MeV, 5.62 MeV and 5.60 MeV. Calculate the α disintegration energies. What is the daughter nucleus? Sketch its level scheme.

Solution: From Eq. 4.II.3,

$$Q_\alpha = \frac{A}{A-4} K_\alpha$$

ood

Thus
$$Q_{\alpha_1} = \left(\frac{212}{208}\right) 6.08\,\text{MeV} = 6.20\,\text{MeV}$$

$$Q_{\alpha_2} = \left(\frac{212}{208}\right) 6.04\,\text{MeV} = 6.16\,\text{MeV}$$

$$Q_{\alpha_3} = \left(\frac{212}{208}\right) 5.76\,\text{MeV} = 5.87\,\text{MeV}$$

$$Q_{\alpha_4} = \left(\frac{212}{208}\right) 5.62\,\text{MeV} = 5.73\,\text{MeV}$$

$$Q_{\alpha_5} = \left(\frac{212}{208}\right) 5.60\,\text{MeV} = 5.71\,\text{MeV}$$

The daughter nucleus is $^{208}_{81}\mathrm{Tl}$.

Energy levels (excited states) of $^{208}_{81}\mathrm{Tl}$ which are fed by the α-ray groups are drawn in the Fig. 4.II.5.

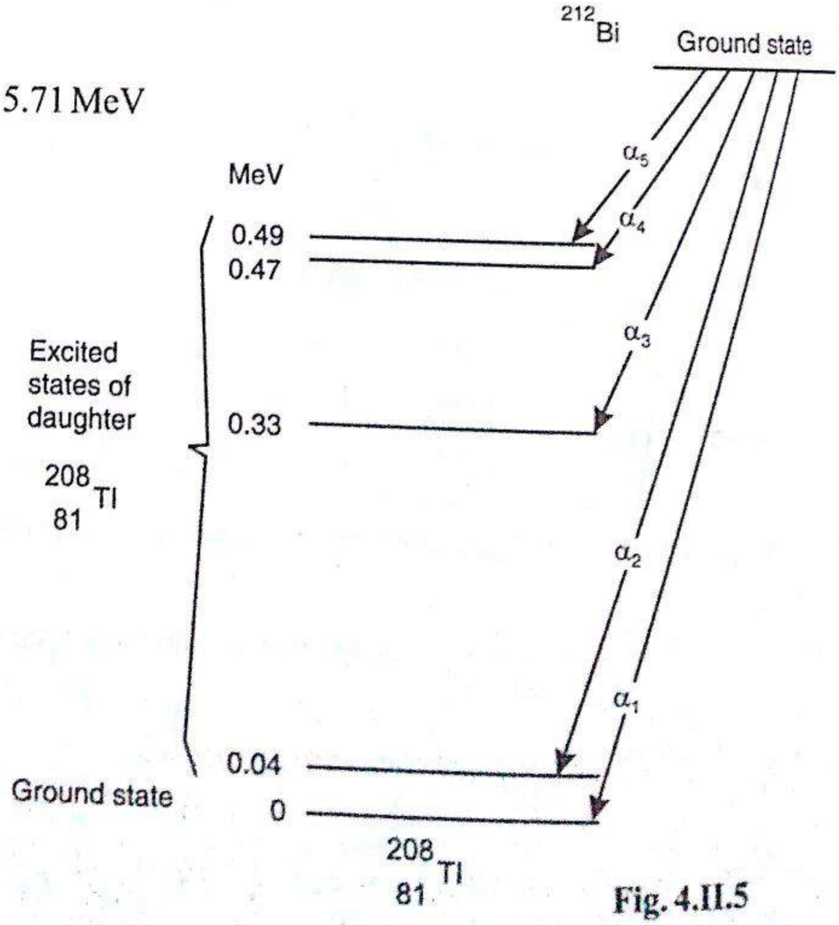
^{212}Bi
Ground state
α5
α4
α3
α2
α1
MeV
0.49
0.47
0.33
0.04
0
Excited states of daughter
$^{208}_{81}$Tl
Ground state
$^{208}_{81}$Tl

Fig. 4.II.5

Example 4.II.2: Show that ${}^{236}_{94}\text{Pu}$ is unstable against α-decay (use mass values given at the end).

Solution: The reaction is:

$$ {}^{236}_{94}\text{Pu} \rightarrow {}^{232}_{92}\text{U} + {}^{4}_{2}\text{He} + Q $$

$$ \therefore \quad Q = (236.04607u - 232.03717u - 4.00260u)\left(931.5\,\frac{\text{MeV}}{u}\right) = 5.87\ \text{MeV} $$

$\therefore$ Q being positive, ${}^{236}\text{Pu}$ will decay by α-emission.

4.II.3 ALPHA DECAY PARADOX—BARRIER PENETRATION

The facts of α-particle emission presented a difficult theoretical problem which is brought out clearly when the spontaneous emission of α-particles by a nucleus is compared with the scattering of α-particles by the same nucleus. Consider the case of emission and scattering of α-particles by ${}^{238}\text{U}$ nucleus. The ${}^{238}\text{U}$ nucleus emits an α-particle by the following reaction:

$$ {}^{238}_{92}\text{U} \rightarrow {}^{234}_{90}\text{Th} + {}^{4}_{2}\text{He} + Q_\alpha \qquad \ldots(4.\text{II}.4) $$

where Q_α is the α-disintegration energy.

The kinetic energy of α-particle $K_\alpha(\sim Q_\alpha)$ was found by range measurement to be 4.20 MeV.

i.e.
$$ K_\alpha \sim Q_\alpha = 4.20\ \text{MeV}. $$

Thus a 4.20 MeV α-particle is able to come out of the uranium nucleus.

On the other hand it was found that α-particles from ${}^{212}\text{Po}$ having Kinetic Energies of the order of 9 MeV get scattered and there is no absorption of α-particles by ${}^{238}\text{U}$ nuclei. In other words, α-particles from ${}^{212}\text{Po}$ with $K_\alpha \sim$ 9MeV are unable to penetrate close enough to the ${}^{238}\text{U}$ nucleus to show departures from the Coulomb law, while α-particles with $K_\alpha \sim$ 4.20 MeV are able to come out of the ${}^{238}\text{U}$ nuclei. Clearly the 9 MeV α-particle is unable to cross the repulsive Coulomb *potential barrier* to enter ${}^{238}\text{U}$ nucleus, while the 4.2 MeV α-particle emitted by ${}^{238}\text{U}$, is able to cross its own potential barrier. This paradoxical situation is illustrated in Fig. 4.II.6. The paradox is that energetic α-particles from ${}^{212}\text{Po}$ are unable to cross the potential barrier, while the lower energy α-particles from ${}^{238}\text{U}$ succeed in doing so. Let us look at Fig. 4.II.6 carefully.

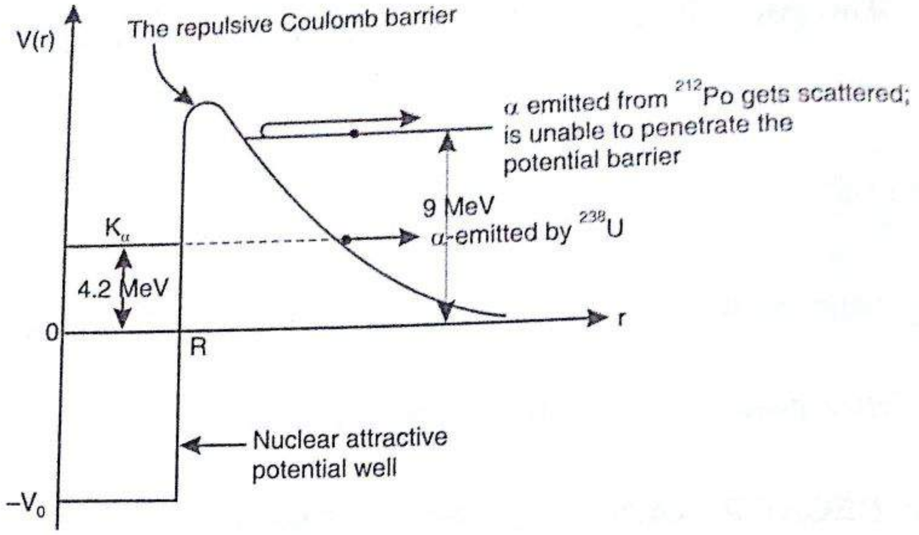
V(r)
The repulsive Coulomb barrier
α emitted from ²¹²Po gets scattered; is unable to penetrate the potential barrier
9 MeV
α-emitted by ²³⁸U
K_α
4.2 MeV
0
R
r
Nuclear attractive potential well
−V₀

Fig. 4.II.6. Potential well and Coulomb potential barrier of a nucleus (schematic).

The rising portion indicates increasing Coulomb repulsion as r is decreased, and ^{212}Po—α-particle approaches the ^{238}U nucleus. Close to the nucleus, the shape of the potential energy $V(r)$ curve is not definitely known, but the Coulomb potential must break down and be replaced by an attractive nuclear potential. This may be represented by a constant attractive potential $-V_0$ over a distance R, the effective nuclear radius. Such a potential is spoken of as a potential well of depth V_0 and range R. For ^{238}U, V_0 is about 40 MeV. (The diagram in Fig. 4.II.6 is schematic and not to scale).

The maximum value of the potential energy corresponds to the value of the kinetic energy an α-particle must have, according to the classical mechanics to get into the nucleus from *outside* or to escape from *inside* the nucleus. This maximum value must be certainly greater than 9 MeV, since α-particles from ^{212}Po are scattered by ^{238}U nucleus and are unable to enter it. The ^{238}U nucleus as remarked earlier emits an α-particle with $K_\alpha \sim 4.20$ MeV and classically it is impossible to understand how the α-particle contained within the ^{238}U nucleus can surmount a potential barrier at least about twice as high as its total energy.

In 1928, George Gamow and, independently, R. Gurney and E. Condon applied wave mechanics to the problem of α-decay and were able to successfully resolve the α-decay paradox.

In Chapter 1, Sec. 1.II.3, we have considered the wave mechanical probability of tunnelling through a rectangular barrier of height V_0 and breadth b (see also Fig. 1.II.4). Equation 1.II.22 gives the relative probability of finding the particle at $x = b$ and at $x = 0$. We rewrite that equation for discussion, with respect to the α-particle.

The relative probability of tunnelling through the rectangular barrier is,

$$P_{\text{relative}} = e^{-2k_2 b} = \exp\left[-2\left(\frac{2m}{\hbar^2}\right)^{1/2}(V_0 - E)^{1/2} b\right] \qquad \ldots(4.II.5)$$

where,
E = kinetic energy of the α-particle ~ Q_α
V_0 = height of the potential barrier
b = width of the potential barrier
m = m_α, mass of the α-particle.

For a realistic barrier like a Coulomb barrier,

$$P_{\text{relative}} = e^{-2\int_0^b k_2 dx} \qquad \ldots(4.\text{II}.6)$$

For the Coulomb barrier, Fig. 1.II.4 would look like Fig. 4.II.7.

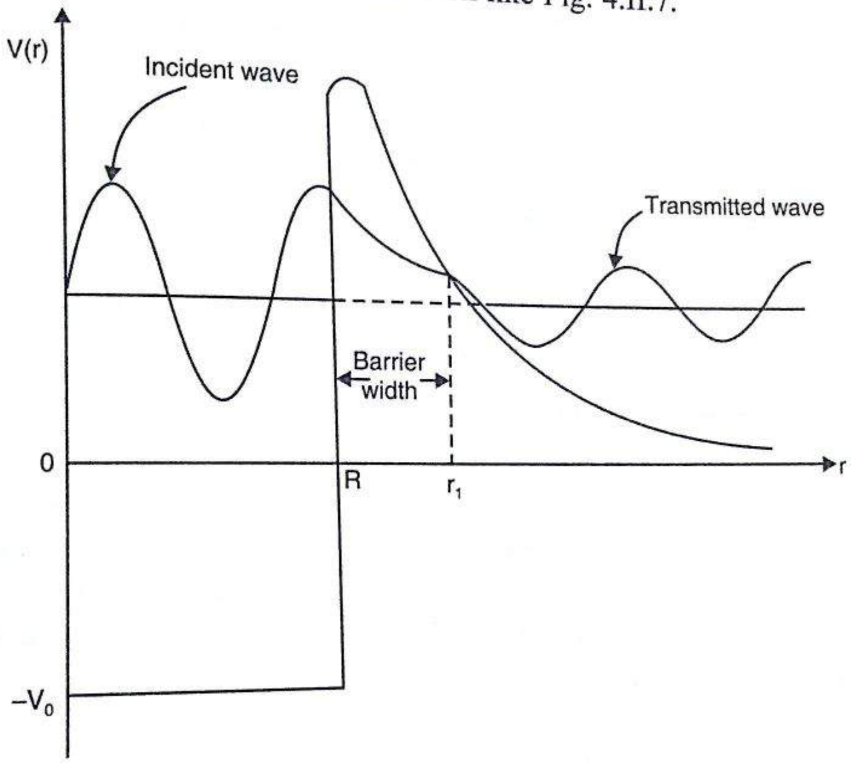

Fig. 4.II.7. Wave mechanical barrier penetration or tunnelling.

Equation 4.II.5 is evaluated to get a number for P_{relative}. $V_0 \sim \dfrac{1}{4\pi\varepsilon_0}\dfrac{2Ze^2}{R}$. Value of R is taken from Eq. 4.I.8. This gives maximum of potential about 28 MeV. Equation 4.II.6, for a (realistic) Coulomb barrier can be put as,

$$P_{\text{relative}} = e^{-2\int_0^b k_2 dx} = \exp\left[-2\left(\frac{m_\alpha}{\hbar^2}\right)^{1/2}\int_R^{r_1}\left(\frac{Ze^2}{4\pi\,\varepsilon_0 R} - E\right)dr\right] \qquad \ldots(4.\text{II}.7)$$

where $\qquad V_0 = \dfrac{Ze^2}{4\pi\varepsilon_0 R}.$

Here the limits for integration are between $r = R$ and the value of $r = r_1$ for which the integrand becomes zero (see Fig. 4.II.7).

Introducing a new variable,

$$y = \frac{E}{V_0}$$

and

$$f(y) = \left[\cos^{-1}\sqrt{y} - \sqrt{y(1-Y)}\right] \qquad \text{...(4.II.8)}$$

the above integral can be evaluated to give,

$$P_{\text{relative}} = e^{[-\beta f(y)]} \qquad \text{...(4.II.9)}$$

where

$$\beta = \frac{4(2Ze^2)}{\hbar v}$$

v being the velocity of the α-particle after emission.

$$v = \sqrt{\frac{2E}{m_\alpha}} \qquad \text{...(4.II.10)}$$

Since $E = 4.2$ MeV and $V_0 \sim 28$ MeV,

$$y = 0.15$$

$$f(y) \sim 0.83 \qquad \text{...(4.II.11)}$$

and

$$\beta \sim 114$$

Putting these values in Eq. 4.II.9,

$$P_{\text{relative}} \sim e^{-93}$$

If a more rigorous calculation is made by not using the square well approximation, then we get,

$$P_{\text{relative}} \sim e^{-87} \sim 2 \times 10^{-38} \qquad \text{...(4.II.12)}$$

This means that when an α-particle makes 10^{38} attempts to come out of the ^{238}U nucleus it succeeds only twice! From this value of P_{relative} for α-particles, we can now make an order of magnitude calculation to estimate half-life of parent; viz. ^{238}U.

Let us first find out how many attempts an α-particle makes to come out of the uranium nucleus in one second.

Nuclear diameter ~ 10^{-14}m.

α-particle velocity ~ 3×10^6 m/s.

$\therefore$ Number of collisions made by an α-particle against the nuclear wall in 1 sec.

$$\sim \frac{3\times10^{6}\,\mathrm{m}}{10^{-14}\,\mathrm{m}} = 3\times10^{20}$$

When this number is multiplied by the tunnelling success probability given by Eq. 4.II.12, we get the decay probability λ_U for uranium - 238.

i.e.
$$\lambda_U \sim (3\times10^{20})\,(2\times10^{-38})$$

$$= 6\times10^{-18}\ \mathrm{sec}^{-1} \qquad \ldots(4.II.13)$$

Thus the half-life of ^{238}U is estimated to be,

$$T_U = \frac{0.693}{\lambda_U} \sim 1.2\times10^{17}\ \mathrm{sec} \sim 4\times10^{9}\ \mathrm{years} \qquad \ldots(4.II.14)$$

In spite of the crudeness of this quick calculation, it is remarkable that the half-life of ^{238}U predicted by the wave mechanical barrier penetration (tunnelling) calculation agrees quite well with the experimentally observed value of 4.4 × 10^9 yrs.

One of the most striking features of α-decay is that for a variation of nuclear charge Z from 84 to 92 and of α-energy E from 4.2 MeV to 9 MeV, the half-lives of α-emitters vary from 10^{10}years (e.g. $^{232}_{90}\mathrm{Th}$) to 10^{-6} sec. (e.g. $^{212}_{84}\mathrm{Po}$). This is indeed an extremely rapid change by a factor of nearly 10^{24} or so. Clearly the large value of the exponent in Eq. 4.II.12 makes the value of (P_{relative}) extremely sensitive to any change in the exponent, i.e., to variations in Z and E. If one changes, the exponent in Eq. 4.II.12 only by 5 per cent, P_{relative} changes by a factor,

$$e^{4.35} \sim 100$$

i.e., the half-life also changes by that factor.

A 10% change makes P_{relative} to change by a factor, $e^{8.7} \sim 6000$.

A 20% change makes P_{relative} to change by a factor,

$$e^{17.4} \sim 3.6\times10^{7}$$

Thus, on the basis of the wave mechanical barrier penetration calculations, the observed large variation in half-lives of α-emitters for a small change in Z and E values can be satisfactorily understood. Students are advised to inspect the half-lives of α-emitters occurring in the radioactive series (Chapter 2).

The Geiger-Nuttall law which holds approximately for α-emitters in the radioactive series can also be well understood on the basis of the above discussion. Equation 4.II.1 expresses the law in this form:

$$\log R = A \log\lambda + B$$

Expressed in an exponential form, the above equation will look like:

$$\lambda = (\text{constant})e^{(-G)} \qquad \ldots(4.\text{II}.15)$$

where the factor G would depend on the α-particle range R and so it would depend on α energy E. Now clearly, Eq. 4.II.15 which expresses the Geiger Nuttall law in exponential form, is identical with to Eq. 4.II.13 obtained by using wave mechanics. For comparison, Eq. 4.II.13 is explicitly written as:

$$\lambda_U \sim (\text{constant})(2 \times 10^{-38})$$

$$= (\text{constant})e^{-87} \qquad \ldots(4.\text{II}.16)$$

Of course, Eq. 4.II.16 is for the special case of ^{238}U. The general form of equation giving λ of any α-emitter will be similar to Eq. 4.II.16. The exponent is determined by the energy of α-particle, in a way given by Eq. 4.II.17. Thus the α-decay theory is able to account for the Geiger-Nuttall law.

PART–III: BETA RAYS: SPECTRA AND DECAY

4.III.1 INTRODUCTION

In Chapter 2, we became familiar with nuclear transformations accompanied by the emission of electrons. Some nuclei emit positrons. Also, sometimes the nucleus captures one of the orbital electrons, mostly from the shell closest to it, the K-shell. All three of these processes are closely related and are known as *beta decay*. In this part, you will encounter several examples of these three beta decay processes. For beta decay there is no change in mass number, i.e., $\Delta A = 0$. In Chapter 3, which pertains to the Q-equation, we have considered the energetics of β-decay and the mass-energy condition that makes Q positive, thereby making β-decay energetically possible. Students are advised to go through Chapter 3 carefully to appreciate energetics of β-decay. (It is interesting to note that though K-capture is energetically more favourable than the positron emission, it also depends on overlap of the nuclear wave function with the K-electron wave function). Characteristic X-rays are emitted following a K-capture or L, M etc. capture. This is obviously due to the atomic re-adjustment because of a vacancy in K or any other shell. If a nucleus of atomic number Z captures one of its own orbital electrons, the X-rays emitted are characteristic of element (Daughter) with atomic number $Z - 1$. K-capture (or L, M-capture) may be detected by observing these X-rays.

In Part I of this chapter, we saw a good reason why electrons cannot be within a nucleus and it must be formed at the time of its emission by the β-decay process. A simple β-ray spectrometer was discussed in Chapter 1 Part I, when we introduced some prominent tools required for nuclear physics. Unlike the line spectrum of α-rays studied in Part II of this chapter, the spectrum of β-rays happens to be *continuous*. This continuous nature of the β-ray energy spectrum gave rise to serious difficulties in understanding β-decay. The chief problem is that

Just like the α-decay, β-decay also is an energy transition between two definite energy states as shown in Fig. 4.III.1. The beta emitter parent nucleus $^{A}_{Z}X$ emits a β-particle to form the daughter nucleus $^{A}_{Z+1}Y$. Thus monoenergetic β-rays (forming a line spectrum) are expected. However, the spectrum observed is continuous, implying that electrons emitted in β-decay process do not have the same kinetic energy. Let us now look at this continuous spectrum of β-rays closely.

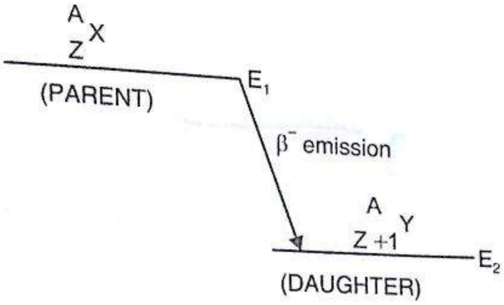

Fig. 4.III.1. β-decay is transition between two definite energy states.

4.III.2 CONTINUOUS β-RAY SPECTRUM—DIFFICULTIES IN UNDERSTANDING IT

Figure 4.III.2(a) shows the distribution of energy among beta particles emitted by $^{210}_{83}\text{Bi}$. In Part (b) of the same figure, this is shown for positrons emitted by ^{64}Cu.

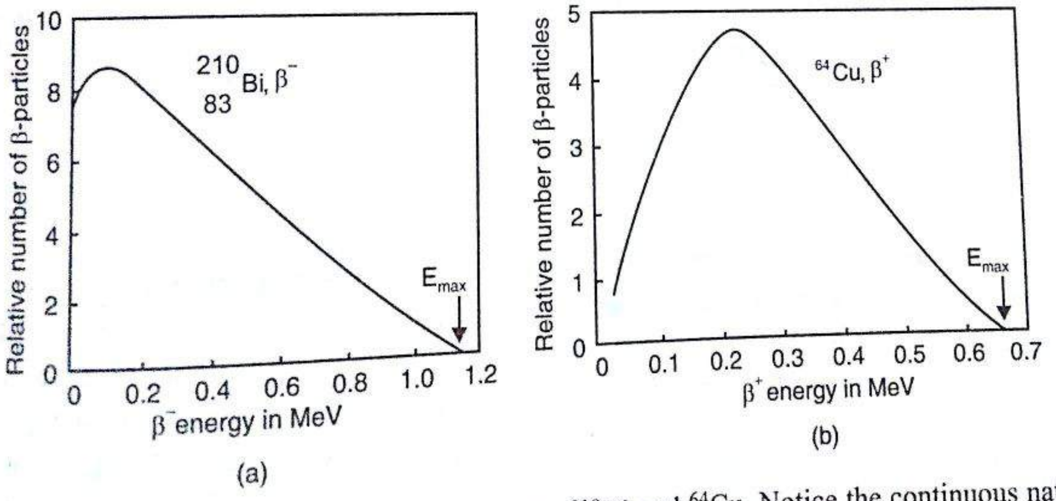

(a)

(b)

Fig. 4.III.2. Energy spectrum of β rays from ^{210}Bi and ^{64}Cu. Notice the continuous nature of the spectra and the end-point energy E_{max}.

As remarked in the introduction, this continuous nature of the β-ray spectrum is unexpected, since β-transition connects two states of definite energy. Most of the electrons (corresponding to peaks of curves in Fig. 4.III.2) are emitted with only about 1/3 rd the maximum energy E_{max}. What happens to the missing (about 2/3 rd of E_{max}) energy? This missing energy must be accounted for to uphold the principle of conservation of energy. One of the hypotheses suggested for this purpose was that the missing energy in the β-spectrum was carried away by a gamma ray. However, careful observation with sensitive calorimeters did not reveal any energy, apart from that given by the continuous beta spectrum. In the calorimetric experiments, the experimentalists measured the energy released in β-decay by its heating effect. They assumed that all the particles involved in the β-disintegration are stopped by the calorimeter. We will see soon that this assumption is not correct. For β^- emitter, ^{210}Bi, an energy of 0.34 MeV/disintegration was found, which agrees very well with the average energy of the β-ray spectrum of ^{210}Bi (see Fig. 4.III.2). However, this does not agree at all with the maximum energy, $E_{max} = 1.17$ MeV.

From Fig. 4.III.2 it should be clear that the continuous β-spectrum has a *definite upper energy limit*, E_{max}. This energy E_{max}, called the *end-point energy* is found to be the total energy available for disintegration by β-decay process. For the two cases shown in Fig. 4.III.2 it is found out that the mass-energy of the nuclear reactions is *exactly balanced* if we make the Q-value *equal* to E_{max}, the upper limit of kinetic energy of the β particles. The nuclear reactions are,

$${}^{210}_{83}\mathrm{Bi} = {}^{210}_{84}\mathrm{Po} + {}^{0}_{-1}e + Q$$

and

$${}^{64}_{29}\mathrm{Cu} = {}^{64}_{28}\mathrm{Ni} + {}^{0}_{+1}e + Q \qquad \ldots(4.\mathrm{III}.1)$$

To balance mass-energy of these reactions, Q has to be made equal to E_{max}. Students should check this out for themselves.

Another serious difficulty presented by the continuous nature of the β-ray spectrum is that it appears to violate not only the principle of conservation of energy but also the principle of conservation of angular momentum. This is well brought out by the case of tritium which is a β-emitter. The nuclear reaction is,

$${}^{3}_{1}\mathrm{H} \rightarrow {}^{3}_{2}\mathrm{He} + {}^{0}_{-1}e \qquad \ldots(4.\mathrm{III}.2)$$

Clearly the charge and mass number are conserved. However, angular momentum of ^{3}H is 1/2 and that of ^{3}He + e is 0 or 1 from their spins since both ^{3}He and e are fermions and the sum of their spins is either 0 or 1. In addition to this ^{3}He + e may have an integral angular momentum because of a possible orbital motion. Thus, the angular momentum of L.H.S. is half-integral while that of the R.H.S. is integral and the law of conservation of angular momentum seems to be in question. Further ^{3}H is a fermion and the system (^{3}He + e) is a boson.

All these difficulties were overcome by the introduction of the *neutrino hypothesis*.

4.III.3 PAULI'S NEUTRINO HYPOTHESIS

Pauli postulated the existence of a new particle, *neutrino*, as early as in 1930. According to Pauli: an additional particle called a *neutrino*, denoted by υ, is emitted in the process of β-decay. This undetected particle (it took about 26 years for conclusive, direct experimental evidence to detect the neutrino) according to Pauli, carries away an amount of energy equal to the difference between the observed energy for a particular β-particle and the maximum energy $E_{\max}$ of the continuous, β-spectrum. The principle of conservation of energy is thus upheld (see Fig. 4.III.3). To satisfy the principle of conservation of angular momentum, and of charge and rules of nuclear statistics, the neutrino must be assigned the following properties:

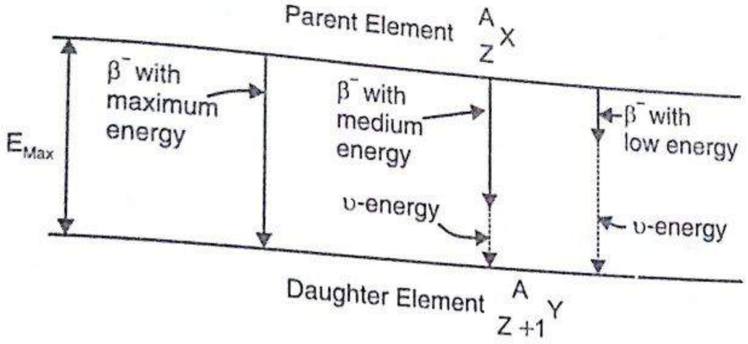
Parent Element $^{A}_{Z}X$
E_{Max}
β^- with maximum energy
β^- with medium energy
β^- with low energy
υ-energy
υ-energy
Daughter Element $^{A}_{Z+1}Y$

Fig. 4.III.3. Schematic diagram showing the sharing of the total disintegration energy between the β-particle and the neutrino.

(*i*) It must have *zero charge*, because in a β decay process the charge is conserved without the neutrino. Also if neutrino is charged it would produce ionization which certainly could have been detected. Zero charge in turn implies negligible magnetic moment.

(*ii*) It must have *zero* or *almost zero mass*. The mass-energy balance of β-decay processes like those given by the reactions in Eqs. 4.III.1 and 4.III.2 shows that the neutrino rest mass is negligible. The student can compute the rest mass of υ by the energy balance. This gives the neutrino rest mass of a few hundred eV. Soon we will see that in all probability, the υ rest mass is zero. The argument leading to this result is based on the concept of *helicity* of neutrino which we will take up a little later.

(*iii*) It must have a *spin* of 1/2; this will satisfy the law of conservation of angular momentum in β-decay process, e.g., the transformation given by Eq. 4.III.2. In this case, giving the neutrino a spin 1/2, makes both the L.H.S. and the R.H.S. sides of Eq. 4.III.2 have half-integral angular momentum. Further, the neutrino must be a *fermion* so that nuclear statistical requirements are fulfilled, e.g., in the case of Eq. 4.III.2 both L.H.S. and R.H.S. are fermion systems.

All these properties are assigned to the neutrino in order to preserve important conservation laws in β-decay process. We know that the *anti-particle* of the electron is the positron. Similarly, a neutrino υ has an anti-particle called an *anti-neutrino,* $\bar{\upsilon}$. An anti-neutrino has zero mass, zero charge and a spin of 1/2. Is it possible to distinguish between υ and $\bar{\upsilon}$, since both of them have the same properties? Experiments show that the neutrino exhibits a "handedness" similar to a screw. A neutrino υ has its spin S_υ always *anti-parallel* to its momentum p_υ while spin $S_{\bar{\upsilon}}$ of an anti-neutrino $\bar{\upsilon}$ is always *parallel* to its momentum $p_{\bar{\upsilon}}$. In other words, υ is a *left-handed* particle while $\bar{\upsilon}$ is a *right-handed* particle.

Figure 4.III.4 schematically shows this handedness of υ and $\bar{\upsilon}$.

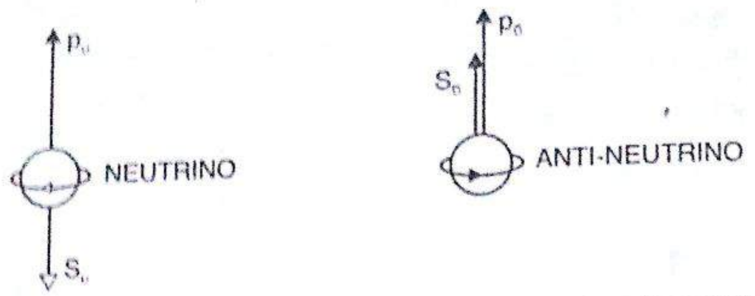

(a) For υ, s_υ is antiparallel to p_υ (b) For $\bar{\upsilon}$, $s_{\bar{\upsilon}}$ is antiparallel to $p_{\bar{\upsilon}}$

Fig. 4.III.4. Handedness in neutrino and anti-neutrino.

To describe this handedness in the neutrino, the idea of *helicity* is used. Helicity is defined as,

$$H = \frac{\vec{p} \cdot \vec{s}}{|\vec{p}||\vec{s}|} \qquad \ldots(4.\text{III}.3)$$

where, $\vec{p}$ is the momentum and $\vec{s}$ is the spin of the particle. In terms of helicity H, it can be at once seen that,

$$H = -1 \text{ for a neutrino and}$$

$$H = +1 \text{ for an anti-neutrino} \qquad \ldots(4.\text{III}.4)$$

The *fixed* value of helicity for υ and $\bar{\upsilon}$ has been confirmed by experiments. This clearly shows that υ and $\bar{\upsilon}$ are two different particles. We will discuss a couple of experiments related to this a little later.

The fixed helicity of the neutrino and the anti-neutrino has an interesting implication—*they move with the velocity of light c.* Otherwise, a υ will have opposite helicity in a frame of reference moving faster or slower compared to the velocity of the υ. (Remember that a clockwise or right-handed sense as viewed from the front becomes an anti-clockwise or left-handed sense when viewed from the back.) Thus we conclude that it is not possible to overtake υ or $\bar{\upsilon}$ by a faster moving frame and so these particles move with velocity c. Further, since υ and $\bar{\upsilon}$ move with velocity c they must have a rest mass exactly equal to zero.

By definition, the neutrino (υ) is the particle emitted in β^+ decay and the, anti-neutrino ($\bar{\upsilon}$) is the particle emitted in β^- decay. Incorporating the neutrino hypothesis we may write the equations for beta decay as,

$$_{Z}^{A}\text{X} \rightarrow {}_{Z+1}^{A}\text{Y} + {}_{-1}^{0}e + \bar{\upsilon} \qquad \text{for } \beta^- \text{ decay,}$$

$$_{Z}^{A}\text{X} \rightarrow {}_{Z-1}^{A}\text{Y} + {}_{+1}^{0}e + \upsilon \qquad \text{for } \beta^+ \text{ decay} \qquad \ldots(4.\text{III}.5)$$

and $${}^{A}_{Z}\mathrm{X} + {}^{0}_{-1}e \rightarrow {}^{A}_{Z-1}\mathrm{Y} + \upsilon \qquad \text{for electron capture.}$$

Thus the correct nuclear reactions corresponding to the β-decay given in Eqs. 4.III.1 and 4.III.2 are:

$${}^{210}_{83}\mathrm{Bi} = {}^{210}_{84}\mathrm{Po} + {}^{0}_{-1}e + \overline{\upsilon}$$

$${}^{64}_{29}\mathrm{Cu} = {}^{64}_{28}\mathrm{Ni} + {}^{0}_{+1}e + \upsilon$$

and $${}^{3}_{1}\mathrm{H} = {}^{3}_{2}\mathrm{He} + {}^{0}_{-1}e + \overline{\upsilon}$$

A simple and interesting example of β-decay is the disintegration of the free neutron with a half-life of about 12 minutes. In Part I of this chapter, we have noted that the neutron is slightly heavier than the proton. This extra mass gives the energy required for β-decay of neutron. The decay process can be represented as

$${}^{1}_{0}n \rightarrow {}^{1}_{1}p + {}^{0}_{-1}e + \overline{\upsilon}$$

Clearly, charge, mass number and spin (also statistics) are all conserved. The mass difference between n and p is about 1.3 MeV. Thus, subtracting the electron rest mass, 0.511 MeV, we have about 0.8 MeV left. This energy of 0.8 MeV is available for sharing between the electron and the anti-neutrino.

Fermi proposed the following basic nuclear transformations which lead to the beta decay process,

$${}^{1}_{0}n \rightarrow {}^{1}_{1}p + {}^{0}_{-1}e + \overline{\upsilon} \qquad \text{for } \beta^{-} = \text{decay}$$

$${}^{1}_{1}p \rightarrow {}^{1}_{0}n + {}^{0}_{+1}e + \upsilon \qquad \text{for } \beta^{+} = \text{decay} \qquad \ldots(4.\mathrm{III}.6)$$

and $${}^{1}_{1}p + {}^{0}_{-1}e \rightarrow {}^{1}_{0}n + \upsilon \qquad \text{for electron capture.}$$

Let us now look at the features of Fermi's theory of beta decay. An excellent and rigorous version will be found, for example, in the book by E. Segre, Nuclei and Particles.

4.III.4 FERMI'S THEORY OF BETA DECAY

One of the persons who took Pauli's neutrino hypothesis very seriously was Enrico Fermi (1934). He was successful in showing that by incorporating the neutrino in β-decay process, it is possible to quantitatively study it and make predictions. We will consider a much simplified version of the Fermi theory.

Fermi postulated that the electron and the neutrino are *created* at the time of β-particle emission. This is similar to the situation where a photon is created at the time of atomic or nuclear de-excitation.

The starting point of Fermi's theory of β-decay is the assumption that the interaction responsible for β-decay process is *weak*, so that the perturbation theory of quantum mechanics can be used. An introductory text in quantum mechanics (for example, the book by L. Schiff) gives the expression for transition rate between an initial state i and final state f, brought about by the Hamiltonian responsible for the decay. For β-decay, if we call the interaction Hamiltonian H_w, then in Dirac notation the transition probability dW_{fi} is given by

$$dw_{fi} = \frac{2\pi}{\hbar}|\langle f|H_w|i\rangle|^2\rho(E) \qquad \ldots(4.\text{III}.7)$$

Fermi called Eq. 4.III.7 the Golden Rule. The derivation of this equation will not be given here; it can be found in any book on quantum mechanics. The factor $\rho(E)$ is called the *density of states factor*. It gives the number of available final states per unit energy. Clearly,

$$\rho(E) = \frac{dN}{dE} \qquad \ldots(4.\text{III}.8)$$

where N is the number of states of particles involved in the decay that can be put in a given volume and E is the total energy of the particles.

Using Eq. 4.III.7 it is possible to consider the transitions with electron energies between E_e and $E_e + dE_e$. It is found that the density of final states, $\rho(E)$, completely determines the form of the β-spectrum, as for most of the β-transitions $|\langle f|H_w|i\rangle|$ can be treated as constant, being independent of energy of the electrons emitted. $|\langle f|H_w|i\rangle|$ is called the *matrix element* (it gives an energy times volume) of β-decay and its computation involves nuclear wave functions of the initial and final states. This represents the difficult part of Fermi's theory. However, fortunately, $\rho(E)$ completely determines the form of the β-spectrum. So let us first evaluate it for β-decay.

Computation of ρ(E)

Let us first consider a one-dimensional case. A particle moves along x-axis with momentum p_x, if we plot x against p_x we get an $x - p_x$ plot, usually called *phase space*. In this one-dimensional phase space, the position and momentum of the particle is determined *simultaneously*. Clearly such a representation gives different pictures from the viewpoint of classical and quantum mechanics. According to classical mechanics, x and p_x can be simultaneously measured to any accuracy, and so in the phase space, a point represents the state of a particle. On the other hand, quantum mechanics limits this accuracy due to the Heisenberg's uncertainty relation $\Delta x \cdot \Delta p_x \geq h$. This implies that a particle in phase space has to be represented by a *cell* and not by a point. Figure 4.III.5 depicts this. The measurement may determine the shape of the cell, but the volume is always the same. It is h.

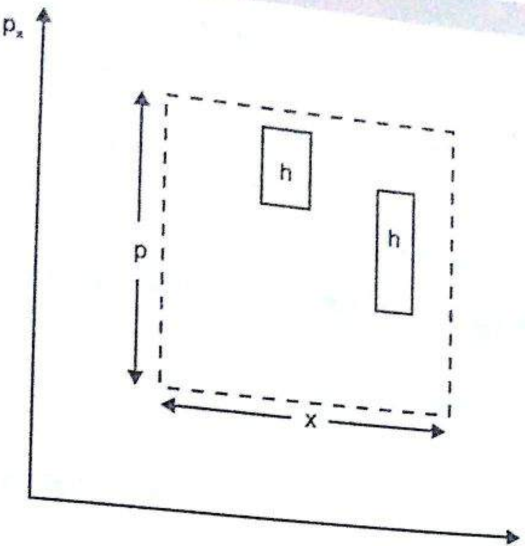

Fig. 4.III.5. One-dimensional phase space in quantum mechanics. A state is described by a cell of volume *h*.

From this figure, it should be evident that the maximum number of cells that can be put in a volume *px* is given by,

$$N = \frac{px}{h} = \frac{px}{2\pi\hbar} \qquad \ldots(4.III.9)$$

N consequently represents the *number of states* in the volume *px* in phase space. In three-dimensional terms, Eq. 4.III.9 becomes,

$$N_1 = \frac{1}{(2\pi\hbar)^3}\int d^3x d^3p$$

In this equation, the number of states have been put N_1 and not N, to indicate that N_1 is the number of states for *one particle.*

It is convenient to confine the particle in a unit volume so that

$$\int d^3x = 1$$

$$\therefore \qquad N_1 = \frac{1}{(2\pi\hbar)^3}\int d^3p \qquad \ldots(4.III.10)$$

Using Eq. 4.III.8, we can compute the density of states factor for one particle,

$$\begin{aligned}\rho_1(E) &= \frac{dN_1}{dE} \\ &= \frac{1}{(2\pi\hbar)^3}\frac{d}{dE}\int d^3p \\ &= \frac{1}{(2\pi\hbar)^3}\frac{d}{dE}\int p^2 dp d\Omega \qquad \ldots(4.III.11)\end{aligned}$$

where $d\Omega$. is the solid angle element corresponding to the emitted particle.

From the relativistic relation, $E^2 = p^2c^2 + m_0^2c^4$.

$$\frac{d}{dE} = \frac{E}{pc^2}\frac{d}{dp}$$

Remembering that differentiation and integration are inverse operations, Eq. 4.III.11 becomes,

$$\rho_1(E) = \frac{1}{(2\pi\hbar)^3}\frac{pE}{c^2}\int d\Omega$$

For all momentum directions, when the transition to all final states is considered, $\int d\Omega = 4\pi$ and so, the density of states factor for one particle becomes,

$$\rho_1(E) = \frac{1}{2\pi^2\hbar^3}\frac{pE}{c^2} \qquad \ldots(4.\text{III}.12)$$

The beta decay problem involves three particles. For Example,

$$n \rightarrow p + e^- + \overline{\upsilon}$$

The initial state *i* corresponds to the neutron. In the final state we have three particles; viz. a proton, an electron and an anti-neutrino. Therefore we must extend Eq. 4.III.12 to three particles. This is a straightforward task. For three particles, the momenta of two particles can change independently. However, the conservation of momentum *fixes the momentum of the third particle*. That is if $\vec{p}_1$ and $\vec{p}_2$ are the momenta of two particles, then $\vec{p}_3$ the momentum of the third particle gets fixed by the relation $\vec{p}_1 + \vec{p}_2 + \vec{p}_3 = 0$, in their centre of mass system.

The number of states that can be crammed in a unit volume in phase space, for 3 particles can be put as (see Eq. 4.III.10):

$$N_3 = \frac{1}{(2\pi\hbar)^6}\int d^3p_1 \int d^3p_2 \qquad \ldots(4.\text{III}.13)$$

Therefore, the density of the final states, is;

$$\rho_3(E) = \frac{dN_3}{dE}$$

$$= \frac{1}{(2\pi\hbar)^6}\frac{d}{dE}\int d^3p_1 \int d^3p_2 \qquad \ldots(4.\text{III}.14)$$

The subscript 3 is put in Eqs. 4.III.13 and 4.III.14 to denote that we are dealing with three particles in the final states.

Let us now choose particle 1 to be the electron and particle 2 to be the anti-neutrino. The third particle in the final state is the recoiling nucleus which is much more massive than either the electron or the anti-neutrino. In Sec. 4.III.5 it will be seen that the energy taken away by the recoiling nucleus is negligible and so we can assume that the total energy of disintegration is shared by the electron and the anti-neutrino.

Equation 4.III.14 for the β-decay problem can be written as:

$$\rho(E)=\frac{1}{(2\pi\hbar)^6}\frac{d}{dE_{\max}}\int d^3p_e\int d^3p_{\bar{\upsilon}} \qquad \ldots(4.\text{III}.15)$$

where p_e is electron momentum $p_{\bar{\upsilon}}$ is anti-neutrino momentum and $E_{\max}$ = Total energy of disintegration.

Note that $E_{\max}$ being the total energy of β disintegration, it is incorporated in Eq. 4.III.15. The object is to know how the integral changes when the total energy (which is $E_{\max}$) is varied. Equation 4.III.15 can be put as (see Eq. 4.III.11 for one particle):

$$\rho(E)=\frac{1}{(2\pi\hbar)^6}\frac{d}{dE_{\max}}\int p_e^2dp_ed\Omega_ep_{\bar{\upsilon}}^2dp_{\bar{\upsilon}}^2d\Omega_{\bar{\upsilon}} \qquad \ldots(4.\text{III}.16)$$

$d\Omega_e$ is the solid angle element in which the electron having a momentum between p_e and p_e+dp_e is emitted. Similarly $d\Omega_{\bar{\upsilon}}$ is the solid angle element corresponding to the anti-neutrino.

How to evaluate ρ(*E*) from Eq. 4.III.16? Look at the continuous spectra shown in Fig. 4.III.2. What is plotted on the *y*-axis is the number of β-particles emitted between energy range, E_e and E_e+dE_e. Therefore to calculate ρ(E), E_e (and so also p_e) is kept constant. This implies that the terms concerning the electron in Eq. 4.III.16 remain unaffected by the differentiation w.r.t. the total energy $E_{\max}$.

Equation 4.III.16 then becomes,

$$\rho(E)=\frac{1}{(2\pi\hbar)^6}p_e^2dp_ep_{\bar{\upsilon}}^2\frac{dp_{\bar{\upsilon}}}{dE_{\max}}\int d\Omega_e\int d\Omega_{\bar{\upsilon}} \qquad \ldots(4.\text{III}.17)$$

As mentioned before, neglecting the recoil energy of the daughter, we can put, to a good approximation,

$$E_{\max}=E_e+E_{\bar{\upsilon}} \qquad \ldots(4.\text{III}.18)$$

If we assume that the rest mass of neutrino is zero then,

$$E_{\bar{\upsilon}}=cp_{\bar{\upsilon}}$$

Treating E_e constant, from Eq. 4.III.18,

$$\frac{dp_{\bar{\upsilon}}}{dE_{\max}}=\frac{1}{c}\frac{dE_{\bar{\upsilon}}}{dE_{\max}}=\frac{1}{c}\frac{d(E_{\max}-E_e)}{dE_{\max}}=\frac{1}{c}$$

Substituting in Eq. 4.III.17, the density of states factor for β-decay becomes:

$$\rho(E)=\frac{1}{(2\pi\hbar)^{6}\cdot c}\,p_e^2 p_{\bar{\upsilon}}^2 dp_e \int d\Omega_e \int d\Omega_{\bar{\upsilon}}$$

Putting $\rho_{\bar{\upsilon}}^2=\frac{E_{\bar{\upsilon}}^2}{c^2}=\frac{(E_{\max}-E_e)^2}{c^2}$, we get

$$\rho(E)=\frac{1}{(2\pi\hbar)^{6}c^{3}}\,p_e^2(E_{\max}-E_e)^2\,dp_e \int d\Omega_e \int d\Omega_{\bar{\upsilon}} \qquad \ldots(4.\text{III}.19)$$

Note that in deriving Eq. 4.III.19, we have considered a transition in which an electron with a momentum between p_e and $p_e + dp_e$ is emitted. Let us put this density of states factor in Eq. 4.III.7 to get the transition probability dw_{fi} for a transition between an initial state i and final state f.

$$dw_{fi}=\frac{2\pi}{\hbar}|\langle f|H_w|i\rangle|^2\rho(E)$$

$$=\frac{2\pi}{(2\pi\hbar)^6\hbar c^3}|\langle f|H_w|i\rangle|^2 p_e^2(E_{\max}-E_e)^2\,dp_e\int d\Omega_e\int d\Omega_{\bar{\upsilon}}$$

If we put $|\langle f|H_w|i\rangle|^2$ as the average value of the matrix element when it is averaged over the angle between the electron and the anti-neutrino, then we can put $d\Omega_e=4\pi$ and $d\Omega_{\bar{\upsilon}}=4\pi$. The above equation thus becomes,

$$dw_{fi}=\frac{32\pi^3}{64\pi^6\hbar^7c^3}|\langle f|H_w|i\rangle|^2 p_e^2(E_{\max}-E_e)^2\,dp_e$$

$$=\frac{1}{2\pi^2\hbar^7c^3}|\langle f|H_w|i\rangle|^2 p_e^2(E_{\max}-E_e)^2\,dp_e \qquad \ldots(4.\text{III}.20)$$

Equation 4.III.20 gives us the transition rate for an electron emitted in the momentum range p_e and $p_e + dp_e$. However, we have not yet taken into account an important fact which would affect the energy of the emitted β-particle. The β-particle must experience the Coulomb force after emission. The nucleus with charge Ze will accelerate positrons and retard electrons. This implies that we shall have more electrons of low energy and more positrons of high energy than predicted by Eq. 4.III.20. This will get reflected in the β-spectrum. Fermi computed this *Coulomb correction*. This has to be incorporated in Eq. 4.III.20. We may write

$$dw_{fi}=\frac{1}{2\pi^3\hbar^7c^3}|\langle f|H_W|i\rangle|^2 F(Z,E_e)p_e^2(E_{\max}-E_e)^2\,dp_e \qquad \ldots(4.\text{III}.21)$$

The function $F(Z, E_e)$ is called the Fermi function. Its sign changes, depending on whether it is applied for electrons or positrons. Tables of the Fermi function have been prepared.

Figure 4.III.6 shows the variation of Fermi functions F with atomic number Z and electron energy E_e [From Hine, Nucleonics, 3.32 (1948)].

Here Z is taken negative for positron emitters and positive for electron emitters.

Notice in Fig. 4.III.6 that low-energy electrons are more favoured in comparison to positrons. For $Z = 0$, $F(Z, E_e) = 1$. Calculations have been done to include the *screening effect* of the orbital electrons in the Fermi function [e.g., Longmire and Brown, Phys; Rev., 75, 264 (1949)].

How does one test Eq. 4.III.21 experimentally? For this purpose, it is most convenient (and so, common) to put Eq. 4.III.21 in the following form:

$$\left[\frac{dw_{fi}}{Fp_e^2 dp_e}\right]^{1/2} = \text{constant.} (|\langle f | H_w | i \rangle|^2)^{1/2} (E_{\max} - E_e) \qquad \ldots(4.III.22)$$

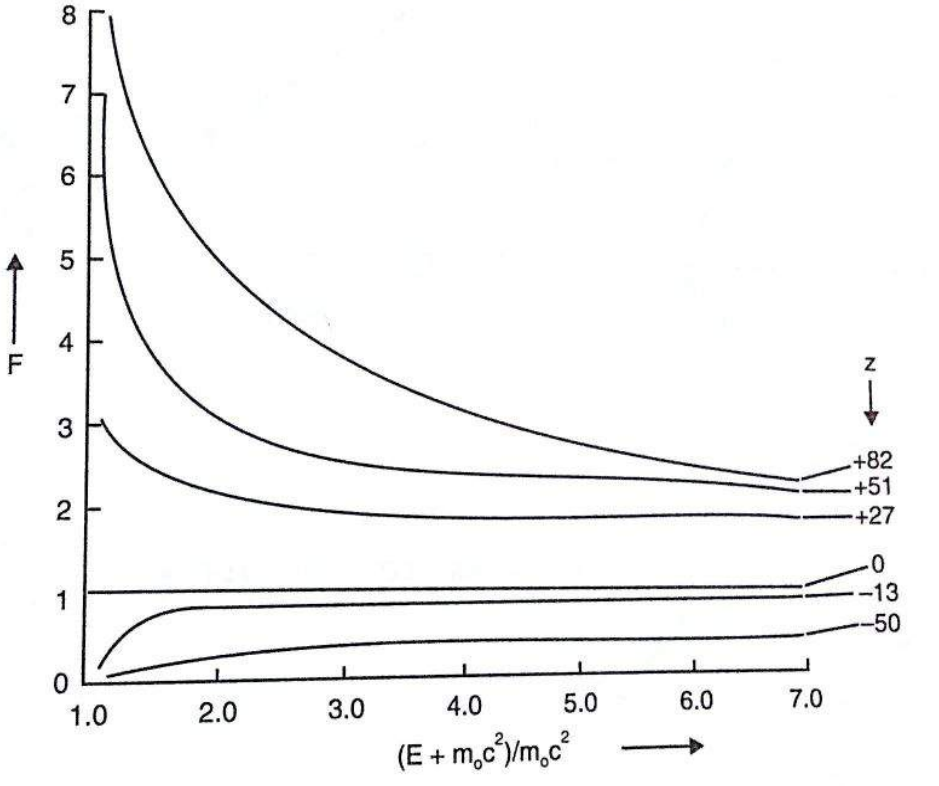

Fig. 4.III.26. Dependence of the Fermi function F on Z and E_{e^+}

The L.H.S. of this equation is determined experimentally and it is plotted against the measured electron energy E_e. Such a graph is expected to give a straight line, (it is $y = mx$ type) provided the matrix element does not depend on electron momentum. Intuitively we would expect the matrix element to be momentum independent for most of the β-decays because if it were to change from decay to decay then to understand the interaction responsible for beta decay would be a formidable task. The energy operator H_W in the matrix element should be applicable universally to all beta decays.

The function on the L.H.S. of Eq. 4.III.22 is called the Kurie function K.

$$K = \left(\frac{dw_{fi}}{Fp_e^2 dp_e}\right)^{1/2} \qquad \ldots(4.III.23)$$

When K is plotted against E_e we get what is called a *Kurie plot* or *Fermi plot*. Experimentally the transition rate dw_{fi} is the number of β-particles per energy interval. A Geiger counter may be employed to detect and count the number of β-particles. The energy or momentum interval may be determined by a magnetic spectrograph (see Section 1.5). The Kurie plot is found to be a straight line over a wide energy range. Figure 4.III.7 shows three Kurie plots: (*i*) for the neutron decay ($F = 1$, since $Z = 0$), (*ii*) ^{3}H decay, and (*iii*) ^{60}Co decay. Notice how the curve changes slightly when neutrino mass is not assumed to be zero. Experimental data of this type puts an upper limit of about 200 eV on the neutrino mass. Recent experiments have lowered this limit to 46 eV. [Review of Particle Properties by the Particle Data Group, Physics Lett. 170B (April 1986)].

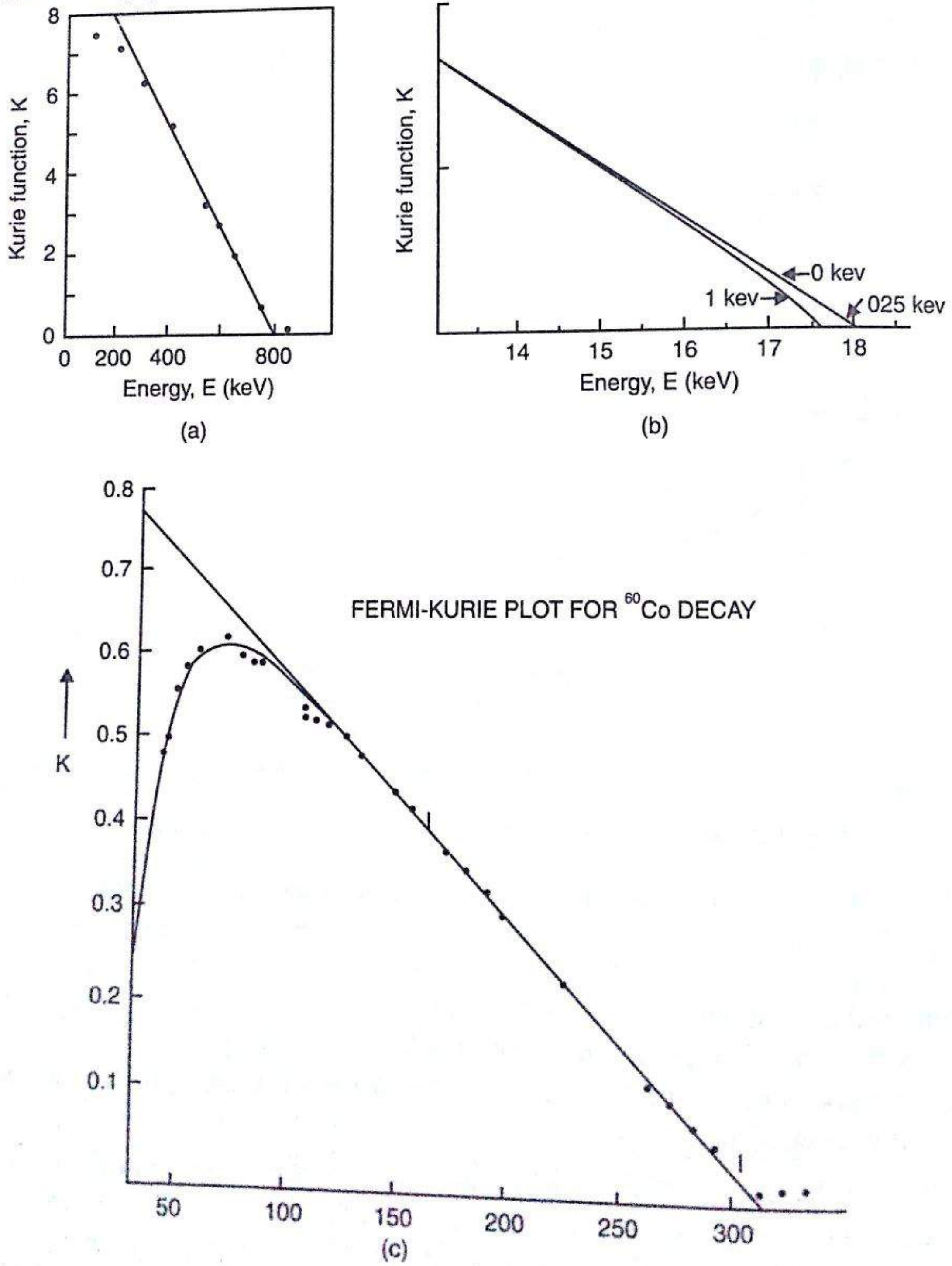

(a)

(b)

(c)

Fig. 4.III.7. (*a*) Kurie plot for the neutron decay, (*b*) Kurie plot for ^{3}H, (*c*) Kurie plot for ^{60}Co.

As predicted by the Fermi theory (Eq. 4.III.22) the Kurie plots are straight lines and the intercept on energy axis gives the end-point energy, $E_{\max}$. Thus, the Fermi theory is quantitatively able to account for the form of the β-spectra. Notice that for low-energy electrons, the points in Figs. 4.III.7 (*a*) and (*b*) do not lie on the line. This deviation is due to the window thickness of the β-counter (a Geiger tube) which is about 5mg/cm² and enough to absorb the low energy electrons. Part (*b*) of the same figure shows the change in the Kurie plot with a non-zero rest mass for the neutrino. Experimental data leading to the Kurie plot enable us to put an upper limit on the neutrino rest mass.

As remarked earlier, the matrix element in the Fermi theory (Eq. 4.III.22) being momentum-independent (for most β-decay) does not influence the shape of the β-spectrum. This shape is mainly due to the phase space consideration which leads to the Kurie plot. The β-spectrum shape thus cannot give us information about the interaction which brings about β-decay. It is possible to get an idea about the strength of this interaction by considering the life times of β-emitters.

Life Times of β-Decay and Strength of the Interaction Matrix Element

The total transition probability w can be obtained by integrating Eq. 4.III.21 over the momentum. The matrix element being momentum-independent, we have,

$$w = \int_0^{p_{\max}} dw_{fi}$$

$$= \frac{1}{2\pi^3 \hbar^7 c^3} |\langle f | H_w | i \rangle|^2 \int_0^{p_{\max}} F(Z, E_e) p_e^2 (E_{\max} - E_e)^2 \, dp_e \qquad \ldots(4.III.24)$$

The total transition rate w is related to the mean life of a beta emitter by the familiar relation,

$$w = \frac{1}{\tau} \quad \text{(see Eq. 2.14)}$$

The mean life τ is measured experimentally. Thus, an idea of the magnitude of the matrix element can be had by evaluating the integral in Eq. 4.III.24. It is very easy to evaluate this integral for small Z and large energies so that $F\ (Z\ .\ E_e) \sim 1$ (see Fig. 4.III.6) and $E_{\max} \sim cp_{\max}$. Under these assumptions:

$$\int_0^{p_{\max}} p_e^2 (E_{\max} - E_e)^2 \, dp_e = (\text{constant})\, E_{\max}^5 \qquad \ldots(4.III.25)$$

The R.H.S. is a function of $E_{\max}$. It is possible to evaluate the integral in Eq. 4.III.24 accurately and in general we can put,

$$\int_0^{p_{\max}} F(Z, E_e) p_e^2 (E_{\max} - E_e)^2 \, dp_e = m_e^5 c^7 f \qquad \ldots(4.III.26)$$

where m_e = mass of the electron. The factor $m_e^5c^7$ is put to make the function f dimensionless. As seen in Eq. 4.III.25, the function f is of E_{max}. Putting Eq. 4.III.26 in Eq. 4.III.25, we have

$$w = \frac{1}{\tau} = \frac{m_e^5 c^7 f}{2\pi^3 \hbar^7 c^3} |\langle f | H_w | i \rangle|^2$$

which gives

$$|\langle f | H_w | i \rangle|^2 = \frac{2\pi^3}{f\tau} \frac{\hbar^7}{m_e^5 c^4} \quad \text{...(4.III.27)}$$

Clearly, from Eq. 4.III.26, an estimate of the matrix element responsible for the β-decay can be made if we know the product ($f \cdot \tau$). The mean life τ is experimentally measured. The function f is calculated.

It is more common to use $ft_{1/2}$ · $f\tau$ is called *comparative life time* and $ft_{1/2}$ is called *comparative half-life*. If the matrix element is the same for all β-emitters, then it implies that they will all have the same $f\tau$ value. This is the reason why $f\tau$ is called the comparative life time; it compares the matrix elements of β-emitters. Actually a wide variation in $f\tau$ values is observed: from about 10^3 to 10^{20} sec. As remarked at the beginning of this section, the value of the matrix element depends on the wave functions of the nuclear particles involved in the beta decay, for the initial state i and final state f, and the interaction operator H_w. Such tremendous variation in $f\tau$ values one can hope to understand only if the interaction is universal for β-decay, and does not change from decay to decay. The observed large changes in $f\tau$ values must then come from the nuclear wave functions that enter the calculation of the matrix element. Fermi was able to show that this is indeed the case. In general, the most fundamental β-decays (those corresponding to low Z) give rise to the largest matrix elements and therefore, the smallest $f\tau$ values. For example, the decay $n \rightarrow p + e^- + \overline{\upsilon}$ which has a half-life of about 11 minutes and E_{max} = 0.782 MeV, gives rise to $ft_{1/2}$ = 1100 sec. Let us estimate the matrix element corresponding to this "fundamental decay". We rewrite Eq. 4.III.27 as:

$$|\langle f | H_w | i \rangle|^2 = \frac{2\pi^3}{f\tau} \frac{\hbar^7}{m_e^5 c^4}$$

$$f\tau = \frac{ft_{1/2}}{\log_e^2} = \frac{1100}{0.693} = 1587 \text{ sec.}$$

Substituting this value of $f\tau$ and taking square root,

$$|\langle f | H_w | i \rangle| = 2.7 \times 10^{-4} \text{ MeV. fm}^3 \quad \text{...(4.III.28)}$$

As remarked at the beginning, the matrix element gives an energy times volume. The volume of the proton, which is the product of the decay can be estimated from Eq. 4.I.6. It is about

1 fm³. Thus, the interaction energy responsible for the β-decay process, which is distributed over the proton volume, is of the order of,

$$H_w \sim 2\times10^{-4}\,\text{MeV} \qquad \ldots(4.\text{III}.29)$$

This is the reason why β-decay is called as the *weak interaction* and we are quite correct in using the perturbation theory in quantum mechanics to calculate the transition rate (Fermi's Golden Rule). The energy associated with the mass of the proton is ~10^3 MeV. This is due to the nuclear interaction termed strong interaction.

The weak interaction is smaller by factor of about 10^7.

Selection Rules for β-Decay

For the purpose of discussion let us denote the matrix element by M. Since M determines the transition probability, it fixes the order of the transition. The nuclear wave function (plane wave), $e^{i\vec{k}\cdot\vec{r}}$ can be expanded to give higher terms.

$$e^{i\vec{k}\cdot\vec{r}} = 1 + i\vec{k}\cdot\vec{r} + \frac{(\vec{k}\cdot\vec{r})^2}{2} + \ldots \qquad \ldots(4.\text{III}.30)$$

Thus, it can be seen that M can be expressed as a series of terms, which if they do not vanish, become progressively smaller. Only the first non-vanishing term is important. From Eq. 4.III.30, clearly the first term is unity and is independent of energy. This term leads to what are called *allowed transitions*.

For certain transitions, the initial and final nuclear wave functions are such that the first term of the M-expansion is zero. These are called *first forbidden* transitions. For these, the second term in M-expansion is used in Eq. 4.III.21. The square of this term is of the order of 10^{-2} and so the transition probability is smaller by that amount. This in turn implies a correspondingly longer half-life. If the first and second terms both vanish in the M-expansion, then we have to use the third term, which is still smaller. This is a *second forbidden* transition. It turns out that for all the forbidden transitions, dependence of M on electron kinetic energy E_e is governed by assumption regarding the type of interaction. The β-decay theory then predicts that the shapes of all allowed spectra should be the same and shapes of forbidden spectra should differ according to the order of forbiddenness and the type of assumed interaction.

The rules connecting the characteristics of the transition in terms of change in angular momentum and parity, with the transition order, are called *selection rules*. Their origin is the incorporation of the laws of conservation of angular momentum and parity into the β-decay theory, and is governed by the nature of interaction. In Sec. 4.III.6 we will see that in β-decay, parity is not conserved. By comparing the experimentally determined order of a β-transition with what is theoretically expected it is possible to know about the type of interaction giving rise to the β-decay. There are *two* selection rules in practice. Since electrons and anti-neutrinos are emitted without orbital angular momentum, they will not carry any angular momentum if they are emitted with anti-parallel spins. On the other hand, they will carry a total angular momentum 1 if they are emitted with parallel spins. For the first case, the spin of the nucleus *does not* *change* in β-decay and we have the selection rule:

$$\Delta I = 0 \quad (F \text{ selection rule}) \qquad \ldots(4.\text{III}.31)$$

This is called the Fermi selection rule.

In the second case, the vector difference between the initial and final angular momentum of the nucleus must be 1 and so we have the selection rule;

$$\Delta I = \pm 1 \text{ or } 0, \text{ but no } 0 \rightarrow 0 \qquad \ldots(4.\text{III}.32)$$

(GT — selection rule)

This selection rule is due to Gamow and Teller. Experiments show that both types of selection rules are operative. For example, the transition

$n \rightarrow p + e^- + \bar{\upsilon}$ is allowed by both selection rules.

As mentioned earlier, it is possible to find the order of a spectrum by evaluating the comparative life times. The following table shows this for some nuclei:

	Nucleus	*Half-life T s*	E_{max} (*MeV*)	*Comparative life time* ($f\tau$)
Allowed transitions	^{51}Mn	2760	1.99	11.3×10^4
	^{62}Cu	630	2.60	8.4×10^4
	^{69}Zn	3420	1.00	4.3×10^4
	^{73}As	1.8×10^5	0.597	5.7×10^4
First forbidden transitions	^{51}Ti	6.2×10^6	0.37	1.3×10^6
	^{80}Br	1080	2.00	0.3×10^6
	^{131}I	6.9×10^5	0.59	3.9×10^6
Second forbidden transitions	^{56}Co	6.2×10^6	1.36	0.6×10^8
	^{90}Y	2.2×10^5	2.60	1.8×10^8
	^{198}Au	2.3×10^5	0.82	0.1×10^8

4.III.5 THE DETECTION OF NEUTRINO

The zero charge and the zero rest mass make the neutrino the most difficult particle to detect. It is clear from Eq. 4.III.6 that beta decay is a three-body problem. (In contrast, α-decay is a two body problem). Conservation of momentum therefore demands that after emission of a β-particle and neutrino, the daughter nucleus *recoils* in a direction *not exactly opposite* to the emitted β-particle. If this recoil of the daughter can be detected, then it would form an indirect evidence of neutrino existence. Figure 4.III.7 indicates this recoil of the daughter and the momentum triangle for the β-particle, the daughter nucleus and the neutrino.

An estimate of the recoil energy can be made for the daughter nucleus. If the neutrino carries all the energy in the β-decay then its momentum is:

$$P_{\upsilon(\max)} = \frac{E_{\upsilon(\max)}}{c}$$

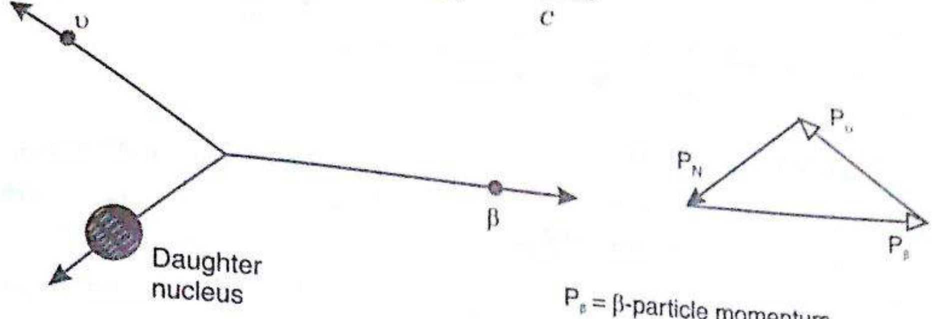
υ
β
Daughter nucleus
P_υ
P_N
P_β
P_β = β-particle momentum
P_υ = neutrino momentum
P_N = daughter nucleus momentum

Fig. 4.III.8. Recoil of the daughter nucleus after β-emission. The momentum triangle is shown at the right.

where $E_{\upsilon(\max)}$ will correspond to end-point energy of the β-spectrum. For a light nucleus like ^{14}O which β-decays by the process, $^{14}_{8}O \rightarrow {}^{14}N + \beta^+ + \upsilon$ the end-point energy is $E_{\max} = E_{\upsilon(\max)} = 1.812$ MeV.

$$\therefore \qquad p_{\upsilon(\max)} = \frac{1.812\ \text{MeV}}{c} = p_N \quad \text{by momentum conservation.}$$

where p_N = daughter nucleus momentum.

Clearly this momentum corresponds to daughter recoil energy, $E_N = \frac{p_N^2}{2M}$, where M = mass of daughter ^{14}N.

$$\therefore \qquad E_N = \frac{(1.812\ \text{MeV})^2/c^2}{(26087.73\ \text{MeV})^2/c^2, (M \text{ taken from tables, gives at the end}).}$$

$$= 0.000125\ \text{MeV or } 125\ \text{eV.}$$

Thus, we see that even for a very favourable case of a light nucleus the recoil energy is only about 125 eV. This makes experimental measurements on daughter recoil extremely difficult.

The recoil experiments have been performed with several β-emitters. Some of them are *n*, ^{6}He, ^{7}Be, ^{19}Ne, ^{35}A. In ^{6}He, for example, the nuclear recoil has been observed in a low-pressure cloud chamber. A cloud chamber photograph reveals that the daughter nucleus recoils in a direction not opposite to the path of the emitted β-particle. This clearly demonstrates that the β-decay is a three-body problem and gives indirect proof of the existence of the neutrino. These measurements require difficult techniques involving the further acceleration of the recoil daughter nucleus in an external magnetic field.

We will now consider direct experimental evidence demonstrating the existence of the neutrino. An experiment of this type would indeed be very difficult as the neutrino, being chargeless and massless, interacts extremely weakly with matter. In fact, calculations show that a neutrino with an energy of a few MeV can travel a distance of 100 light years in a chamber containing liquid hydrogen without any interaction! In spite of these difficulties, an experiment performed in 1953 gave conclusive evidence about the neutrino.

Cowan and Reines Experiment

Cowan and Reines were the first to observe the direct interaction of free neutrino in 1953. Because of the importance of the experiment they repeated their experiment with better equipment in 1957. As seen earlier, Pauli postulated the neutrino to satisfy the various conservation laws. Thus, verification of these laws does not give us independent proof of the existence of neutrino. The Cowan and Reines experiment tells us more about the neutrino than what the conservation laws do and so provides us with direct, independent proof of the existence of the neutrino. The basic idea behind the experiment is as follows:

From Eq. 4.III.6, we know that:

$${}^{1}_{0}n \rightarrow {}^{1}_{1}p + {}^{0}_{-1}e + \overline{\upsilon}$$

This reaction may be inverted by bombarding protons with anti-neutrinos. The inverse reaction is:

$$\overline{\upsilon} + {}^{1}_{1}p \rightarrow {}^{1}_{0}n + {}^{0}_{+1}e \qquad \ldots(4.\text{III}.33)$$

i.e., when protons are bombarded with anti-neutrinos it is expected that they emit positrons to become neutrons. Cowan and Reines utilized the large flux of antineutrons existing in the neighbourhood of a nuclear reactor to observe this reaction (Eq. 4.III.33). In Chapter 6 we will consider neutron induced fission and nuclear reactors. There you will learn that the fission fragments are *neutron rich* and so *highly beta active*. This intense beta activity of the fission fragments gives rise to a large flux of anti-neutrinos of the order of 10^{13} /cm^2/sec in the neighbourhood of reactors. Thus, even though neutrinos interact extremely weakly with matter, because of the very large flux of anti-neutrinos near a nuclear reactor there is a possibility of observing the reaction given by Eq. 4.III.33. Cowan and Reines observed this reaction using the experimental arrangement described below.

Figure 4.III.9 shows schematically the experimental arrangement. The protons for the reaction are provided by water in a large plastic tank. About 200 litres of water was stored in this tank.

I and II are liquid scintillation detectors (In the form of tanks). Each tank contained about 400 litres of liquid scintillator solution.

Cadmium has a large cross-section (probability) of capturing thermal neutrons (very slow, having energy of ~eV). In Chapter 6, we will learn how this property of Cd is used in reactors to control the fission chain reaction. CdCl$_2$ was dissolved in water to provide Cd nuclei for neutron detection. Two large tanks of liquid scintillator

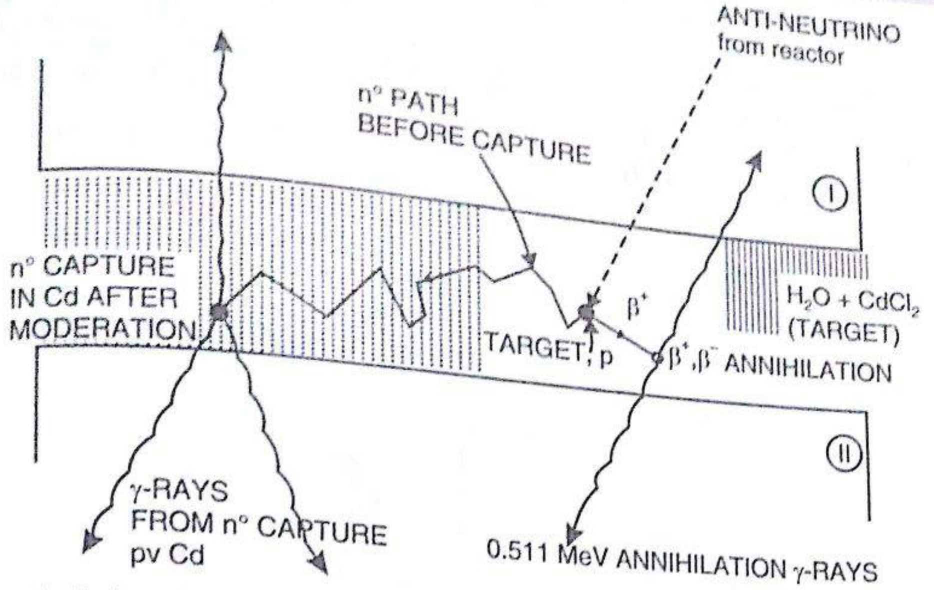

I and II are liquid scintillation detector tanks each containing about 400 litres of liquid scintillator solution.

Fig. 4.III.9. Cowan and Reines neutrino detection experiment—schematic diagram of arrangement

are placed on two sides of the water tank. To establish the reaction given by Eq. 4.III.33, the following sequence of events must be identified.

(i) An anti-neutrino from the reactor interacts with a proton in the water tank. This interaction produces a neutron and a positron according to reaction given by Eq. 4.III.33.

(ii) The positron comes to rest quickly and it is well known from a course on modern physics (see Chapter 1) that it annihilates with an electron, resulting in two gamma rays emitted in opposite directions. Each of these γ-rays carries an energy equal to the electron rest mass 0.511 MeV. These γ-rays can be detected by the liquid scintillators marked I and II. Of course, a large number of photomultiplier tubes are required to collect the light emitted by the scintillator. Cowan and Reines observed this annihilation radiation which follows very quickly (in an interval of time ~10^{-9} s) the emission of positron.

(iii) The neutron as indicated in Fig. 4.III.9 diffuses in the water (with dissolved $CdCl_2$) and after many collisions with protons slows down to thermal energies to eventually get captured by a Cd nucleus. This capture of the neutron takes place much later than the emission of annihilation γ-rays. The time gap is ~10^{-5}s. This capture results in the emission of γ-rays by the (*n*, γ) reaction. Usually three gamma rays are emitted and there is a good chance of detecting one γ-ray in the upper detector I and one γ-ray in the lower detector II. On an average the neutron requires about 6 microseconds to be captured. Cowan and Reines succeeded in establishing the characteristic sequence of events outlined above (*i*, *ii* and *iii*). They delayed the annihilation pulse so that it could be displayed at the beginning of the oscilloscope trace. A delay of about 30 μs was required. An electronic circuit was *gated* for about 20 μs so that it was able to accept a *neutron pulse* (triggered by capture γ-rays).

The oscilloscope display was photographed each time the sequence of annihilation γ-ray pulse neutron pulse was displayed. Figure 4.III.10 shows this acceptable sequence of events, every time the oscilloscope was triggered. Cowan and Reines were able to record about 30 events per hour. To check their result they used water without any cadmium in it and found that the neutron pulses due to capture γ-rays disappeared. Also when the nuclear reactor was shut down they found that the events mentioned above could not be observed. The observed sequence of events is sufficiently characteristic to establish the interaction,

$$\bar{\upsilon} + {}^{1}_{1}p \rightarrow {}^{1}_{0}n + {}^{0}_{+1}e$$

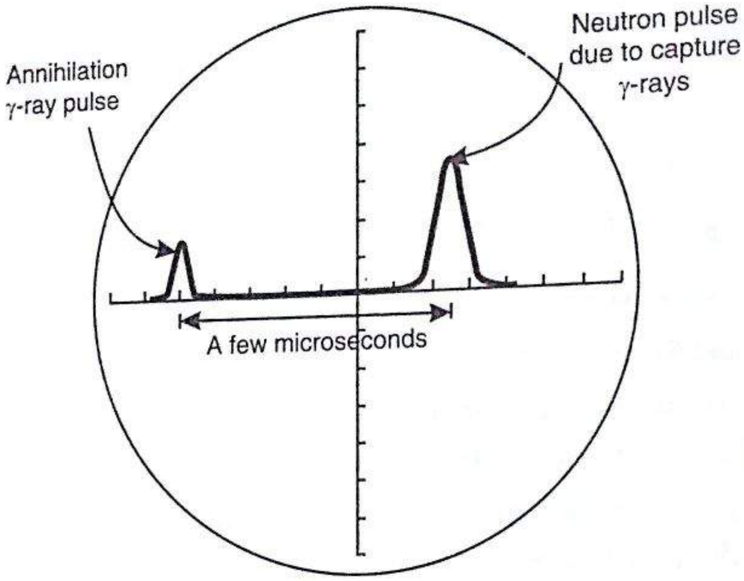

Fig. 4.III .10. Triggered pulses due to positron annihilation and neutron capture. This sequence establishes direct neutrino interaction given by Eq. 4.III.33.

Thus, Cowan and Reines experiment proved beyond doubt the existence of the neutrino.

Earlier, we have mentioned the fixed helicity for υ and $\bar{\upsilon}$. Apart from this argument, it has been shown by experiments that υ is different from $\bar{\upsilon}$. Physically the emission of a neutrino has the *same consequence* as the absorption of an anti-neutrino (υ and $\bar{\upsilon}$ are a particle-antiparticle pair). Davies in 1955 considered the reaction

$$\bar{\upsilon} + {}^{37}_{17}\mathrm{Cl} \rightarrow {}^{37}_{18}\mathrm{A} + {}^{0}_{-1}e \qquad \ldots(4.\mathrm{III}.34)$$

if υ and $\bar{\upsilon}$ are identical then the reaction given by Eq. 4.III.34 is the inverse of

$${}^{37}_{17}\mathrm{Cl} \rightarrow {}^{37}_{18}\mathrm{A} + {}^{0}_{-1}e + \bar{\upsilon} \qquad \ldots(4.\mathrm{III}.35)$$

Thus, if ^{37}Cl is bombarded with antineutrinos we should get ^{37}A. Davies showed that ^{37}A is not produced and so concluded that υ and $\bar{\upsilon}$ are different particles.

Having discussed some experiments with the neutrino, let us now conclude this part of Chapter 4 by outlining an important property of weak interactions: non-conservation of parity.

4.III.6 PARITY NON-CONSERVATION IN BETA DECAY

Chapter 1, Sec. 1.II.4 we studied the concept of parity. We say that the parity is conserved if the probability of finding a particle between a certain range of coordinates is not affected by a ansformation of the type of coordinate reflection. We may define a parity operator *P*. For the odd parity wave function, a change in sign on reflection gives,

$$\psi(x, y, z) = -\psi(-x, -y, -z)$$

so that

$$P = -1 \qquad \ldots(4.\text{III}.36)$$

For even parity wave function on reflection we have,

$$\psi(x, y, z) = \psi(-x, -y, -z)$$

so that

$$P = +1 \qquad \ldots(4.\text{III}.37)$$

The parity of a system of particles is given by the product of the parities of the individual particles. As late as 1956 it was assumed that parity was conserved in all nuclear interactions. In other words, physicists thought the mirror image of an object or process was indistinguishable from the object or process itself. Lee and Yang in 1957 questioned the conservation of parity in beta decay.

To appreciate this, let us consider the mirror image of a neutrino. Let the neutrino travel toward a mirror with momentum $\vec{p}_\upsilon$. We have learnt that its spin $\vec{s}_\upsilon$ is oppositely directed to $\vec{p}_\upsilon$. This is shown in Fig. 4.III.10. Clearly the mirror image of this neutrino is a different particle—the anti-neutrino—because in the mirror image the vectors $\vec{s}_\upsilon$ and $\vec{p}_\upsilon$ are in the same directions (see also Fig. 4.III.5). Hence, the motion of a neutrino given by the mirror image is not a possible motion for it, as it refers to a different particle viz., an antineutrino. This is termed as non-conservation of parity by the neutrino.

Let us now discuss the non-conservation of parity in a different way. On reflection through the origin, the three coordinates (*x*, *y*, *z*) of a physical quantity become (–*x*, –*y*, –*z*) i.e., they *change in sign*. For example, the components of momentum vector $\vec{p}, (p_x, p_y, p_z)$ become on reflection, $(-p_x, -p_y, -p_z)$.

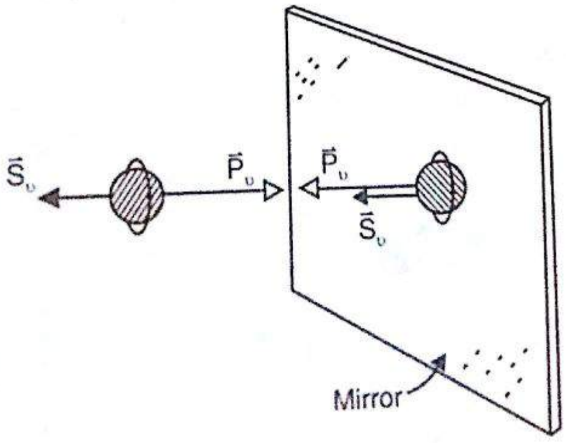

Fig. 4.III.11. Non-conservation of parity by the neutrino. The mirror image of a υ is an $\bar{\upsilon}$.

Vectors of this type are called polar vectors

Consider now the angular momentum vector,

$$\vec{L} = \vec{r} \times \vec{p}$$

the z - component is, $L_z = xp_y - yp_x$. The other components can be put in a similar way. Clearly, in this case on reflection both $\vec{r}$ and $\vec{p}$ change sign and so the components of $\vec{L}$ remain same on reflection; there is *no change of sign.* A vector like angular momentum vector $\vec{L}$ is called an *axial vector* or *a pseudovector.* It should be realized that vectors and pseudovectors behave similarly for translations or rotations of a coordinate system. However, on reflection (or inversion of coordinate system), their behaviour is different, as seen above. Some other examples of pseudovectors are: torque, magnetic field, spin etc.

Now, if one takes a scalar product of two polar or axial vectors we get a scalar that remains invariant under reflection of the coordinate system. On the other hand, the scalar product of a polar vector and an axial vector gives us a number that changes sign on reflection of coordinates. These numbers are referred to as *pseudoscalars.* Thus, if in an experiment one gets a number which is a pseudoscalar we can conclude that mirror reflection of the experimental process can be distinguished from the process itself. In other words, parity is not conserved during the experimental process. *Observation of pseudoscalar quantity therefore signifies non-conservation of parity.*

In 1956, Lee and Yang pointed out that no experiment on β-decay was performed to test observation of a pseudoscalar quantity. Wu and fellow workers in 1957 carried out an experiment specifically designed to detect a pseudoscalar in β-decay. They polarized (oriented) the nuclei of beta emitter ^{60}Co by cooling in a magnetic field. The process of adiabatic demagnetization was used to reach a temperature as low as ~ 0.01 °K. They found that emission of beta particles in the transformation ${}^{60}_{27}\mathrm{Co} \rightarrow {}^{60}_{28}\mathrm{Ni} + {}^{0}_{-1}e + \bar{\upsilon}$ is *preferentially* opposite to the spin direction. In other words a pseudoscalar of the form $\vec{v} \cdot \vec{I}$, where $\vec{v}$ is the β-velocity and $\vec{I}$ is the nuclear spin was found to exist. This experiment conclusively proved the non-conservation of parity. The detailed discussion of this experiment is beyond the scope of this book.

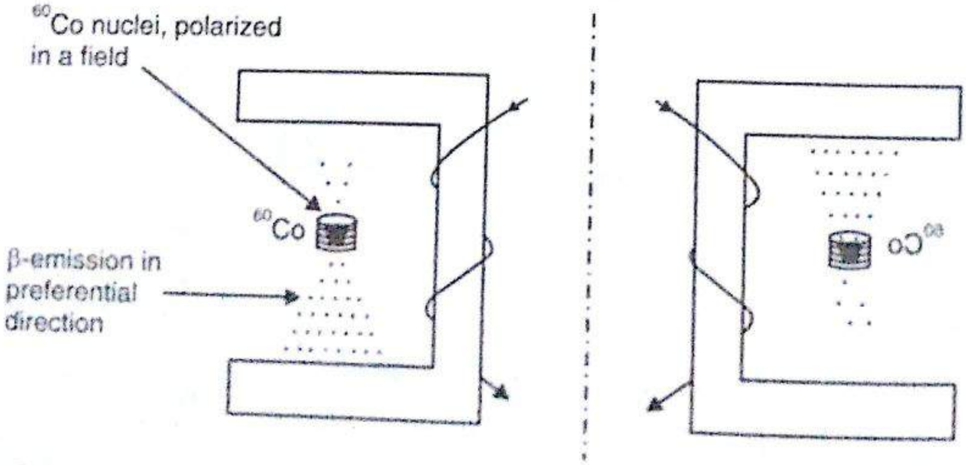
^{60}Co nuclei, polarized in a field
^{60}Co
β-emission in preferential direction

Fig. 4.III.12. Schematic diagram depicting result of the ^{60}Co experiment. The mirror symmetry is clearly seen to be broken here.

However, its result is schematically depicted in Fig. 4.III.12. ^{60}Co nuclei which are polarized in an external magnetic field were found to emit β-rays preferentially in one direction as indicated in left side of Fig. 4.III.12. On reversing the field the direction of preferential emission of β-particles was found to have changed, contrary to the expection that mirror image of the phenomenon is also a possible physical reality. This is shown on the right of Fig. 4.III.12. Clearly the mirror symmetry is broken here and the experiment leads to non-conservation of parity in β-decay.

An example which may elucidate the point made in this discussion can be described. This may help to appreciate the significance of results shown in Fig. 4.III.12. Suppose you were holding a ball in your *right hand* and allowed it to fall. Obviously the ball would fall on the floor. In the mirror it would be the *left hand* which drops the ball. The image ball would also drop on the floor. Here the mirror image corresponds to reality. However, if you had a special ball discovered by some one, which falls down whenever it is dropped from right hand, but goes up when dropped from the left hand then the mirror symmetry would be broken, like the one in Fig. 4.III.12. This is because the mirror image of this special ball falling down from the right hand would be a ball also falling down from the left hand, a situation contradicting the reality.

This is what Wu and fellow workers found in their historic experiment on ^{60}Co polarized nuclei. We will conclude this part by considering two illustrative examples.

ILLUSTRATIVE EXAMPLES

Example 4.III.1: Calculate the energy of γ-rays emitted in the β-decay of ^{28}Al. (Given E_{max} = 2.86 MeV).

Solution: Since γ-rays are emitted during β-decay $^{28}\text{Al} \rightarrow {}^{28}\text{Si}$, the β-transformation must be leading to an excited state of a daughter nuclei, ^{28}Si. This is shown in Fig. 4.III.13.

The neutral atomic masses of the parent and daughter are:

$$^{28}\text{Al} \rightarrow 27.981908\,\text{a.m.u.}$$

and

$$^{28}\text{Si} \rightarrow 27.976929\,\text{a.m.u.}$$

∴

$$Q = (27.981908 - 27.976929)\,\text{a.m.u.}$$

$$= (4.979 \times 10^{-3}) \times 931.5\ \text{MeV}$$

$$= 4.638\ \text{MeV} \sim 4.64\ \text{MeV}.$$

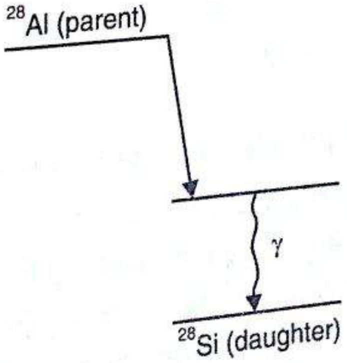

Fig. 4.III.13

However, the end-point energy,

$$E_{\text{max}} = 2.86 \text{ MeV}$$

∴ the γ-ray energy = 1.78 MeV.

Example 4.III.2: Find the energy of a neutrino in the following *K*-capture reaction.

$$^{131}_{55}\text{Cs} + {}^{0}_{-1}e \rightarrow {}^{131}_{54}\text{Xe} + \upsilon$$

The total energy released in this process is 355 keV and the binding energy of the *K*-electron in ^{131}Xe is 35 keV. Further the daughter nucleus is formed directly in the ground state.

Solution: Clearly in this process electrons of definite energy corresponding to *K* shell of ^{131}Xe are captured by ^{131}Cs nuclei and so all the emitted neutrinos will carry same energy.

$$\begin{aligned}\text{Energy of a neutrino} &= 355 \text{ keV} - 35 \text{ keV}\\ &= 320 \text{ keV or } 0.32 \text{ MeV.}\end{aligned}$$

PART–IV: INTRODUCTION OF GAMMA EMISSION

4.IV.1 INTRODUCTION

We have seen earlier that when a nucleus is in an excited state, γ-rays are emitted and the nucleus is eventually brought to the ground state. Usually when a nucleus decays by α-emission or β-emission, it is left in an excited state. If it is energetically impossible for this nucleus to emit another particle, or if the decay by emission of another particle is slow, then the nucleus decays by electromagnetic interaction. Let E_i be the energy of an excited state of a nucleus. When there is a transition to a lower state (or ground state) of energy E_f, we have the release of energy

$$\Delta E = E_i - E_f \qquad \text{...(4.IV.1)}$$

This energy ΔE is emitted by one of the following three electromagnetic interactions:

(*i*) γ-ray emission

(*ii*) internal conversion or

(*iii*) internal pair production.

The last process of internal pair production occurs much less frequently than others.

To create an electron-positron pair, ΔE must be at least 1.02 MeV. The gamma emission and internal conversion are much more frequent and in fact, they are the competing processes by which an excited nucleus may get rid of the energy ΔE to come to lower state. Let us now consider these two processes — (*i*) and (*ii*) — in some detail.

4.IV.2 γ-RAY EMISSION—SELECTION RULES

Look at Fig. 4.II.3. Obviously, the gamma-ray spectra would correspond to discrete energies. Or, in other words, a γ-ray spectrum consists of sharp lines. This spectrum can be accurately studied by using, for example, a NaI (T1) scintillation detector mounted on a photomultiplier tube and a pulse height analyzer. Or, when energy resolution is important, one can use a solid-state Ge detector. These γ-ray detectors are discussed in Chapter 1, Part I. In that chapter, Fig. 1.I.10 shows a γ-spectrum of ^{137}Cs using a NaI (Tl) detector and Fig. 1.I.11 shows a γ-spectrum of ^{60}Co by using a Ge (Li) detector.

If we neglect the small recoil energy of the γ-emitter nucleus, the energy of the γ-ray is given by

$$hf = \Delta E = E_i - E_f \qquad \ldots(4.\text{IV}.2)$$

where f is the frequency of the γ-photon.

Though many aspects of the γ-emission can be understood on the basis of Maxwell's electrodynamics, one must use quantum mechanics to understand the finer aspects. This treatment is beyond the scope of this book. A lucid treatment of γ-emission may be found for example in the book, Theoretical Nuclear Physics by Blatt and Weisskopf—John Wiley (1952).

Now, if the spin of the initial state of the nucleus is $\vec{I}_i$ and that of the final state is $\vec{I}_f$ then, $\vec{L}$, the angular momentum carried off by the γ-photon is:

$$\vec{L} = \vec{I}_i - \vec{I}_f = \Delta\vec{I} \qquad \ldots(4.\text{IV}.3)$$

In other words we have,

$$|I_i - I_f| \le L \le |I_i + I_f| \qquad \ldots(4.\text{IV}.4)$$

We have the following selection rules for γ-decay.

(*i*) the γ-photon must carry away at least one unit of angular momentum, and

(*ii*) in γ-decay, parity is always conserved.

In this discussion, $\Delta\vec{I}$ represents the vector change in angular momentum which must be distinguished from the change in the magnitude of the angular momentum $\Delta I = |I_i \pm I_f|$. It is $\Delta\vec{I}$ that is conserved during a γ-emission, though ΔI is what is easily obtained if spins of the initial and final states are known. To appreciate this, let us consider a case in which the nuclear spin changes from 4 to 2 during a transition. Clearly ΔI is simply the scalar difference 2. However $|\Delta\vec{I}|$ can have values 2, 3, 4, 5, or 6 since any integral value from 4 – 2 to 4 + 2 is possible.

Obviously $\Delta\vec{I}$ for a γ-transition cannot be zero, because the intrinsic spin of the photon is one.

Multipolarity in γ-transitions

The γ-emission can be classified according to a *multipole order*. One has dipole, quadrupole, octopole and still higher order transitions. For any order, the transitions can be either *electric* or *magnetic* type. The origin of these terms is pointed out a little later. For the present, let us consider the properties of these terms:

(*i*) Multipole order of a transition is said to 2^L.

(*ii*) If $|\Delta\vec{I}| = |\vec{L}| = 1$, the multipole order is 2 and we have what is called a *dipole transition*.

(*iii*) If $|\vec{L}| = 2$, the multipole order is 4 and we have a *quadrupole transition*, and so on.

(*iv*) The parity change for the nucleus determines the nature of the multipole transition. For example, if $|\vec{L}| = 2$ we have an electric quadrupole transition if the nuclear parity does not change and a magnetic quadrupole transition if it does.

If π_i denotes the parity of the initial state of the nucleus and π_f denotes the parity of the final state then the two selection rules for the γ-transition can be rewritten in this form:

$$|I_i - I_f| \le |L \le| I_i + I_f| \qquad \text{...(4.IV.5)}$$

and

$$\pi = \pi_i \, \pi_f$$

where π is the parity of the emitted radiation.

Further, γ-transitions are classified as electric 2^L pole and magnetic 2^L pole according as

$\pi = (-)^L$ for electric 2^L pole radiation

$\pi = (-)^{L+1}$ for magnetic 2^L pole radiation ...(4.IV.6)

$\Delta\vec{I}(=\vec{L})$ or parity change are not directly observable, and so by detecting the γ-rays from a radioactive source we cannot say what is the kind of transition is involved. However, a measurable quantity—the mean life of the excited state that gives rise to the γ-transition—depends on L. This dependence is given by a general expression for the γ-emission rate. (Stated without proof),

$$T(L) = \frac{1}{\tau} = \frac{8\pi(L+1)}{\hbar L[(2L+1)!!]^2}\left(\frac{\Delta E}{\hbar c}\right)^{2L+1} B(L) \qquad \text{...(4.IV.7)}$$

where, $T(L)$ = transition probability (sec^{-1})

τ = Mean life of the excited state, a quantity which can be measured.

$L = |\vec{L}|$ gives multipole order

ΔE = transition energy

$(2L + 1)!! = 1 \times 3 \times 5 \times \ldots \times (2L + 1)$

and $B(L)$ = reduced transition probability

$$= |\langle \psi' | O_{EM}^{L} | \psi \rangle|^2$$

where ψ, ψ' are wave functions of initial and final states of the nucleus and O_{EM}^{L} is the electric or magnetic multipole operator.

The most frequently encountered transitions are magnetic dipole and electric quadrupole, written as $M1$ and $E2$ respectively.

Apart from the life times of nuclear-excited states, other experimentally measured quantities which are related to L and parity (and therefore which can fix multipole order of the transition) are *internal conversion coefficient* and *angular correlation* between γ-rays emitted in succession by a nucleus. In the next section, we will become familiar with the internal conversion process.

Let us now look at the origin of the multipole order. Equation 4.I.43 gives the electric potential produced by a charge distribution at a distance R in the z-direction.

$$V = \frac{1}{4\pi\varepsilon_0}\left[\frac{1}{R}\int \rho dV + \frac{1}{R^2}\int \rho z dV + \frac{1}{R^3}\int \rho(3z^2 - r^2)dV + \ldots\right]$$

where, ρ is the charge density.

In Part I of this chapter, we considered the dipole moment and quadrupole moment of this charge distribution. A single charge at the origin is a simple monopole. It turns out that the dipole term (second term on R.H.S.) vanishes for charge distributions that have a mirror symmetry about a plane through the origin and perpendicular to the chosen z-axis. Nuclei satisfy this condition and so, generally speaking, nuclear electric dipole moments are zero or extremely small. This, in turn, implies that nuclear electric dipole moments are not at all common. This is in contrast to large atomic electric dipole moments associated with polarized atoms. For the liquid drop model studied in Chapter 5, the electric dipole moments are always zero. On the other hand, nuclear electric quadrupole moments are quite common and, as seen in Part I of this chapter, give us an idea of nuclear deformation. Nuclear quadrupole moments are discussed in some detail in Chapter 7.

4.IV.3 INTERNAL CONVERSION

We have mentioned earlier that the process of internal conversion is an alternative to γ-decay. Let us consider this process in some detail.

Internal conversion is a process which enables an excited nuclear state to come down to some lower state without the emission of a γ-photon. The energy ΔE involved in this nuclear transition gets transferred *directly* to a bound electron of the atom. Such an electron gets knocked out of the atom. Electrons like this are called *conversion electrons* and the process is called *internal conversion.* A quantum mechanical treatment of internal conversion is beyond the scope of this text. However, it is interesting to note that wave mechanically, an atomic electron spends part of its time *inside a nucleus*. This probability is highest for the K-shell electrons which are closest to the nucleus. For such a case, the nucleus may de-excite not by γ-emission but by giving the excitation energy ΔE directly to a K-shell electron. Internal conversion is also possible (though less, as compared to the K-shell) for higher atomic shells, L, M etc.

Clearly the kinetic energy of the converted electron K_e is,

$$K_e = \Delta E - B_e \qquad \ldots(4.\text{IV}.8)$$

where B_e is the atomic binding energy of the electron, and $\Delta E = E_i - E_f$ = Nuclear excitation energy between initial state i (higher) and final state f (lower).

In Part III of this chapter we have studied the continuous β-spectrum. Usually these continuous β-spectra are superimposed by discrete lines due to conversion electrons. Figure 4.IV.1 shows two internal conversion lines from ^{137}Cs. The continuous β-distribution is also shown.

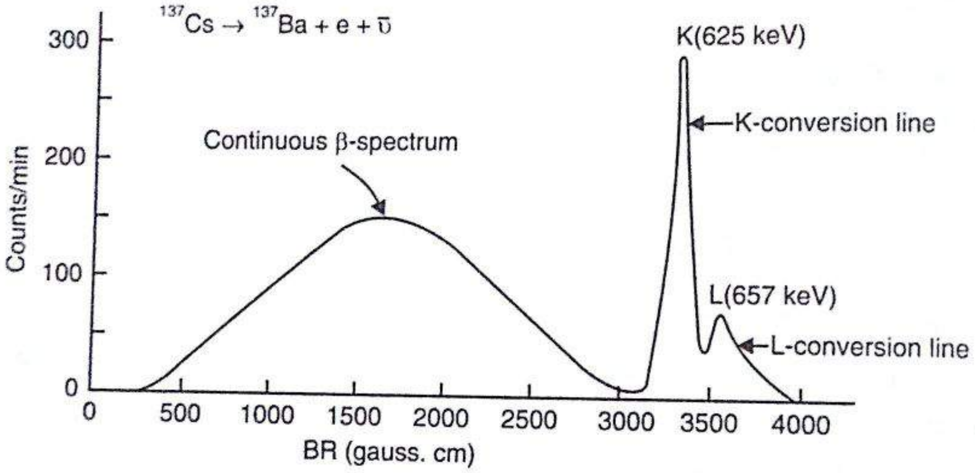

Fig. 4.IV.1. Continuous β-spectrum of ^{137}Cs, showing K and L internal conversion lines.

Actually the L-conversion line is due to L_I, L_{II}, L_{III} etc. subshells. Figure 4.IV.2 shows the conversion spectrum of ^{165}Ho, 94.6 keV transition. This spectrum was taken by a double focussing β-ray spectrometer with a momentum resolution of ~0.1%. The L-subshell conversion lines can be clearly seen.

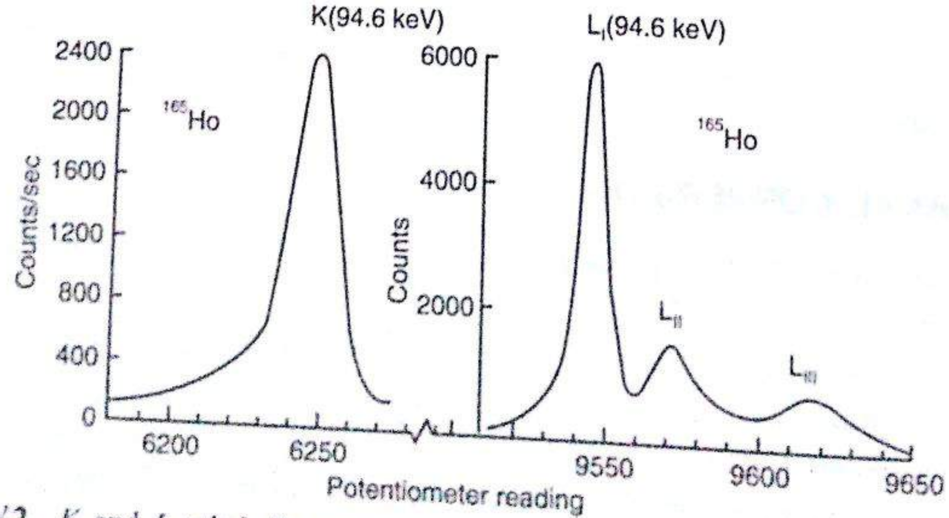

Fig. 4.IV.2. K and L-subshell conversion spectrum of the 94.7 keV transition in ^{165}Ho (S.B. Patel and K.P. Gopinathan in Int. Conf. on γ-ray transition probabilities, New Delhi, 1974).

It was wrongly believed that the internal conversion process is like the photoelectric effect; a γ-photon emitted by a nucleus is absorbed by the orbital electron which is then emitted as in the photoelectric effect. The simplest situation which disproves this is a transition between two states having spin equal to zero. A $0 \to 0$ transition ($\Delta I = 0$) is forbidden for all multipole orders and so γ-emission by the nucleus is completely forbidden. However $0 \to 0$ transition readily found to proceed by internal conversion. The experiment was performed on 0.7 MeV level of ^{72}Ge. This is a $0 \to 0$ transition and it was found that conversion electrons can be detected, but there is a complete absence of γ-ray emission.

If a given radioactive source emits N_γ γ-rays and N_e conversion electrons during the same interval of time then the *conversion coefficient* α is defined as

$$\alpha = \frac{N_e}{N_\gamma} \qquad \text{...(4.IV.9)}$$

For K-conversion electrons, we talk about α_K.

For L-conversion electrons we talk about α_L and so on.

The value of α is found to depend on transition energy, multipole character of transition and the atomic number Z.

The values of α can be experimentally determined by measuring the intensities of γ-lines and corresponding conversion electron lines. The most extensive calculations of conversion coefficients have been performed by Hager and Seltzer [Nucl. Data A 4 (1968)]. Using experimental electron binding energies, they have calculated conversion coefficients for $Z = 30$ to $Z = 103$. The experimental value of conversion coefficient when compared with the theoretical value gives information about the multipolarity of a transition and the extent of *multipole mixing*. For example, in the case of K and L subshell internal conversion studies of the 94.6 keV transition in ^{165}Ho (see Fig. 4.IV.2) the experimental ratio of $L_I / L_{II} / L_{III}$ was found to be 100/15.7/8.5. This result when compared with theoretical values gave the multipolarity of the 94.6 keV transition in ^{165}Ho as (M1 + E2, 3.1%) i.e. this is a magnetic dipole transition with electric quadrupole admixture to the extent of 3.1%.

ILLUSTRATIVE EXAMPLES

Example 4.IV.1: ^{203}Tl atoms resulting from β-decay of ^{203}Hg atoms emit 4 groups of conversion electrons with kinetic energies of 266.3, 264.2, 263.6 and 193.3 keV. To what shell of Tl atom, K, L_I, L_{II}, L_{III} does each group correspond? The electron binding energies in the shells are 87.7, 15.4, 14.8 and 12.7 keV respectively. Calculate the energies of γ-quanta concurrent with that decay.

Solution: We know that,

$$K_e = \Delta E - B_e, \qquad \text{(Eq. 4.IV.8)}$$

Clearly the maximum kinetic energy group corresponds to L_{III} conversion electrons as they are least tightly bound.

$$266.3 \text{ keV} = \Delta E - 12.7 \text{ keV}$$

∴

$$\therefore \qquad \Delta E = 279 \text{ keV}$$

Similarly,

$$264.2 \text{ keV} = \Delta E - 14.8 \text{ keV}$$

$$263.6 \text{ keV} = \Delta E - 15.4 \text{ keV}$$

and 193.3 keV = ΔE – 87.7 keV for the K-shell

For all these, ΔE = 279 keV

Thus, the γ-energy concurrent with the β decay is 279 keV.

Example 4.IV.2: The β decay of ^{141}Ce leads to ^{141}Pr. The daughter nuclei (^{141}Pr) are found to have been left in an excited state. They reach the ground state by emission of γ-rays or conversion electrons. Determine the excitation energy of a ^{141}Pr nucleus, if for the conversion of K-electrons, $B\rho$ = 1135 gauss-cm and the binding energy of the K-electrons is equal to 42 keV.

Solution: We know that,

$$K_e = \Delta E - B_e$$

B_e = binding energy of K-electron = 42 keV

Thus to find ΔE, the excitation energy of a ^{141}Pr nucleus, we must know K_e the kinetic energy of the K-conversion electrons. While discussing a magnetic β-ray spectrometer in Chapter 1, we have seen that $B\rho$ value is a measure of electron momentum. Also usually $B\rho$ value is measured in gauss-cm. Electrons being always relativistic, from Eq. 1.I.27 we have the relation between the kinetic energy of electrons in MeV and the $B\rho$ value in gauss-cm. We rewrite this equation for our use:

$$\left(\frac{K_e}{0.511}+1\right)^2 = \left(\frac{B\rho}{1704}\right)^2 + 1$$

$$= \left(\frac{1135}{1704}\right)^2 + 1$$

$$= 1.444$$

$\therefore \quad K_e$ = 0.103 MeV = 103 keV = kinetic energy of the K – conversion electrons.

$\therefore \quad \Delta E$ = 103 keV + 42 keV = 145 keV

= Excitation energy of a ^{141}Pr nucleus.

4.IV.4 NUCLEAR ISOMERISM

In the early study of radioactive isotopes it was common to assign a separate isotope to a particular half-life. Thus if two half-lives were observed in a given sample, it was assumed that they were due to two different isotopes, each decaying with a particular half-life. For example, consider the decay:

$$^{234}_{90}\text{Th} \rightarrow {}^{234}_{91}\text{Pa} + {}^{0}_{-1}e + \bar{\upsilon}$$

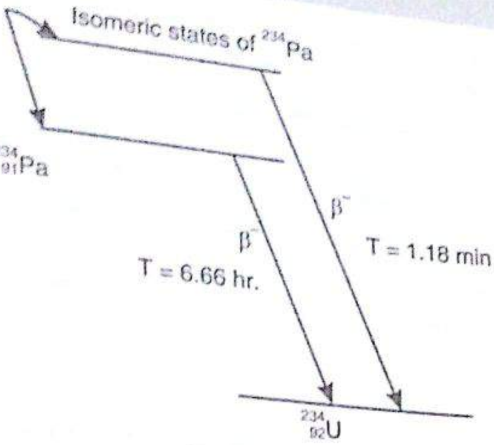

Fig. 4.IV.3.

$^{234}_{91}$Pa (protactinium) was found to decay by emission of β-particles of *two different half-lives*, one of 1.18 min. and the other of 6.66 hr. People assumed at that time that these two half-lives were due to two different isotopes. In 1921 Hahn showed that these two half-lives of β-decay are due to *two different energy states* (excited) of the *same nucleus*. Such long-lived excited states of the same nucleus are called *isomeric states* or *nuclear isomers*. Some times they are referred to as *metastable states*, and denoted by ^{234m}Pa in our case as shown in Fig. 4.IV.3. In 1936 Weizsacher pointed out that γ-decay of levels whose excitation energy ΔE is small should be *delayed* by an easily measurable amount if the angular momentum change ΔI is large. The so-called islands of isomerism are shown in Chapter 7 on shell model. The half-lives of isomers are found to vary from a fraction of a second to several months. By definition, the isomeric state is one whose half-life is measurably long. Thus today, when we can measure half-lives of the order of picoseconds (1ps = 10^{-12} s) accurately we have hundreds of candidates in the form of nuclear excited states which can be labelled as isomeric states.

Nuclear isomers have both the same mass number and atomic number. Their separation is a challenge to the radiochemist. Further, development of experimental techniques using scintillation counters and coincidence circuits has enabled physicists to measure with accuracy, half-lives of nuclear excited states to the order of picoseconds.

EXERCISES

1. Explain why α-particles exhibit a definite range in matter.
   Using the data from Chapter 2 about the three radioactive series plot log λ against log R for the 3 series.
   Determine the constants A and B of the Geiger-Nuttal law for these series.
2. The α-emitter ^{212}Po emits α-particles with kinetic energy 10.54 MeV. Calculate (*i*) the α disintegration energy Q_α and (*ii*) the energy of the recoil nucleus.
3. Show that $^{238}_{92}U$ is unstable and will decay by α-emission (use masses given at the end of the book).
4. A radioactive isotope with atomic number A emits two groups of α-particles with kinetic energies $K_{\alpha 1}$ and $K_{\alpha 2}$. Show that the energy of the emitted γ-ray is

$$E_\gamma = \frac{A}{A-4}(K_{\alpha 1} - K_{\alpha 2})$$

5. ${}^{240}_{94}\text{Pu}$ decays by emission of two groups of α-particles with kinetic energies $K_{\alpha 1} = 5.17$ MeV and $K_{\alpha 2} = 5.12$ MeV. Calculate the energy of the accompanying γ-ray.

6. The α-particles emitted in the α-decay of ${}^{214}_{84}\text{Po}$ have an energy of 7.68 MeV. Assuming that the α-particles have the same kinetic energy inside the ${}^{214}\text{Po}$ nucleus, determine the number of collisions per second that the α-particles makes with the walls of the nucleus.

7. Determine the energies of the α-particle and the daughter nucleus in the decay

   (*i*) ${}^{144}_{60}\text{Nd} \rightarrow {}^{140}_{58}\text{Ce} + \alpha$ (*ii*) ${}^{213}_{84}\text{Po} \rightarrow {}^{209}_{89}\text{Pb} + \alpha$

8. ${}^{226}\text{Th}$ decays from the ground state by emitting four groups of α-particles with energies: 6.33, 6.23, 6.10 and 6.03 MeV. Draw a diagram showing energy levels of the daughter nucleus.

9. ${}^{212}\text{Po}$ decays by emitting four groups of α-particles. The main α-group has an energy of 8.780 MeV. The other 3 α-groups are long-range α-particles, with energies 9.492, 10.422 and 10.543 MeV. It is known that the daughter nuclei are produced in the ground state. Draw an energy-level diagram for the parent ${}^{212}\text{Po}$.

10. If A_p, A_d are mass numbers and B_p, B_d are total binding energies of the parent and the daughter respectively then show that a nucleus will decay by α-emission only if

$$4(7A_d - B_d) > (B_p A_p - B_d A_d).$$

Assume α-particle binding energy ~28 MeV.

11. Assume nuclear radius to be $R = 1.3 \times A^{1/3}$ fermi. Calculate the minimum energy required by an α-particle, from entirely classical view-point, to overcome the Coulomb barrier of a ${}^{210}_{84}\text{Po}$ nucleus.

12. ${}^{64}\text{Cu}$ nucleus decays by β^-, β^+ and electron capture with a half-life of about 13 hrs. Write down the nuclear reactions for these three processes and identify the daughter elements in each case.

13. Consider the following K-capture reaction

$${}^{37}_{18}\text{Ar} + {}^{0}_{-1}e \rightarrow {}^{37}_{17}\text{Cl} + \upsilon\,.$$

The total disintegration energy in this process is 0.82 MeV. Calculate recoil energy and velocity of the Cl nucleus. Assume neutrino rest mass to be zero.

14. Determine the maximum possible speed of the daughter nucleus in a β decay of ${}^{6}_{2}\text{He}$ nucleus which is initially at rest.

15. Compute the radius of curvature of the path of a 1 MeV beta particle in a constant magnetic induction of 0.1 tesla (= 1 KG.) (This will give you an idea about the size of a beta ray spectrometer.)

16. For a particular neutron decay, the neutrino carries off no energy. If the neutron was at rest before the decay, calculate the kinetic energies of the proton and the emitted β-particle.

17. Consider K-capture in ${}^{120}_{50}\text{Sn}$. The Q-value is 2.0 MeV. Calculate the fraction of the energy Q that is carried away by the neutrino.

18. Calculate the maximum momentum for electrons emitted by ${}^{10}\text{Be}$ nuclei. Assume that the daughter nuclei are produced directly in the ground state.

19. Consider the following decay leading directly to the ground state of daughter

$$^{11}_{6}\mathrm{C} \rightarrow {}^{11}_{5}\mathrm{B} + {}^{0}_{+1}e + \upsilon.$$

Calculate the maximum kinetic energy of the positrons and the corresponding kinetic energy of the daughter nucleus.

20. An isomer ^{109m}Ag comes to ground state by either emitting a 87 keV γ-ray or a *K*-conversion electron with $B\rho = 860$ gauss-cm. Calculate the binding energy of the *K*-electron.

21. ^{177}In beta decay leads to ^{117}Sn nuclei in excited state, which come to the ground state by emitting two consecutive γ-rays. This process is competed by the emission of two groups of *K*-conversion electrons corresponding to $B\rho$ values, 3050 and 1300 gauss-cm. The binding energy for *K*-electrons is 29 keV. Calculate the energy of the two γ-rays emitted.

5

The Liquid Drop Model of a Nucleus

> "God does not care about our mathematical difficulties. He integrates empirically."
>
> —*Albert Einstein*

> "In some sort of crude sense which no vulgarity, no humour, no overstatement can quite extinguish, the physicists have known sin; and this is a knowledge they cannot lose."
>
> —*J. Robert Oppenheimer*

5.1 INTRODUCTION

We shall discuss an extremely simple model of a nucleus, which in spite of its simplicity is able to account for a number of salient features of nuclear behaviour. Weizsacher in 1935 recognized the experimental evidence which suggested that in some ways, a nucleus resembles a drop of a liquid. In 1939, Bohr and Wheeler employed a liquid drop model of the nucleus in their theory of nuclear fission.

In the last chapter (Chapter 4, Part I) we have seen that a nucleus consists of neutrons and protons. A convenient way of depicting nuclear information is to plot the neutron number against the proton number for various stable nuclides. This was first done by Segre and hence is called the Segre chart. It is shown in Fig. 5.1. Notice that a curve drawn through the points representing stable nuclei shows that its path goes away from the line $N/Z = 1$ for low Z toward the direction of a higher number of neutrons as one takes heavier elements. For A = 238 $N/Z = 1.6$. As we shall see later in some detail, this trend is ascribed to an increase in Coulomb repulsion among protons with increase in Z. To counteract this, heavy nuclei tend to be made up of more neutrons than protons.

The curve depicted in Fig. 5.1 for stable nuclides is often referred to as the stability curve The isotopes lying 'above and below' this curve are radioactive. They decay in such a way that finally they reach a stable product lying on the curve. This is displayed by Fig. 5.2, whic is a schematic representation of Fig. 5.1.

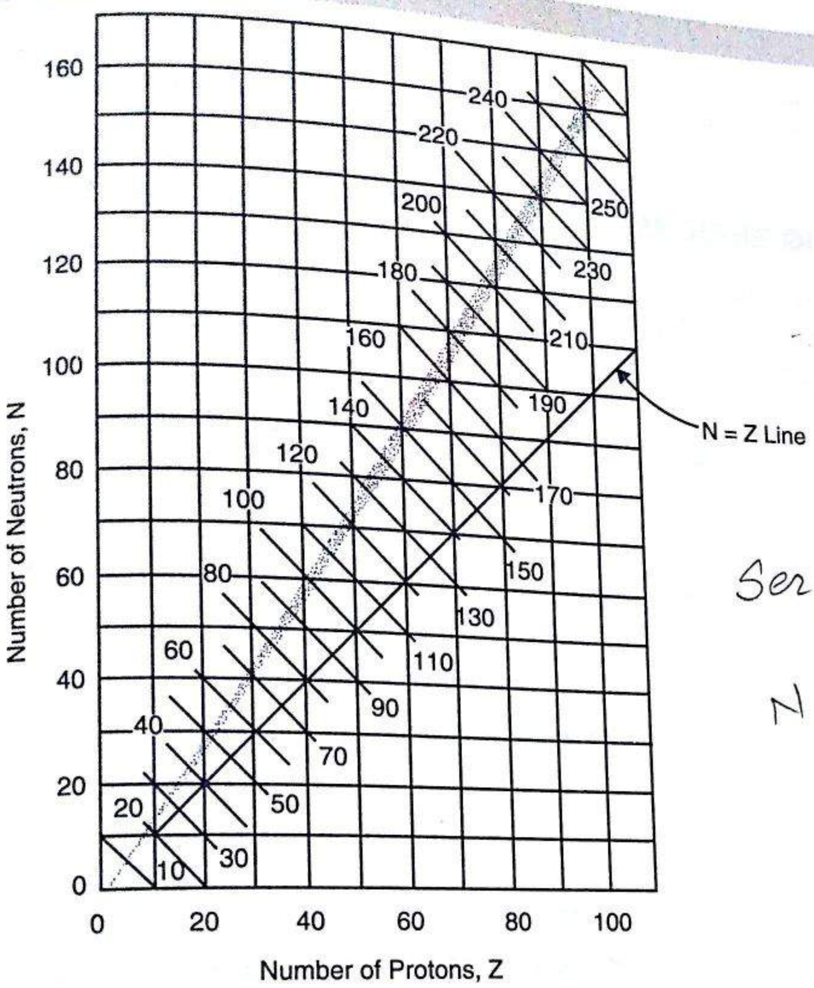

Fig. 5.1. Segre chart of stable nuclides.

Serge chart

N v/s Z

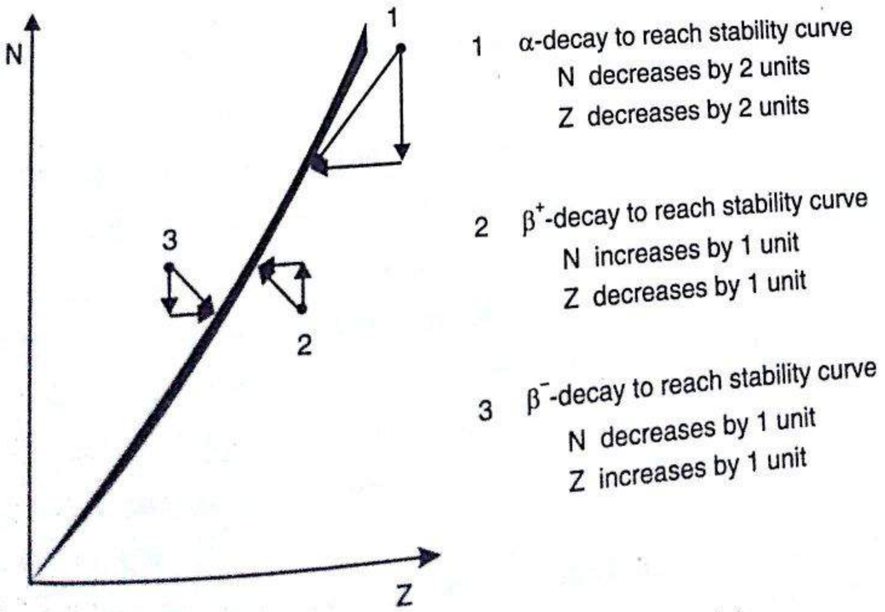
N
Z
1
2
3
1 α-decay to reach stability curve
N decreases by 2 units
Z decreases by 2 units
2 β⁺-decay to reach stability curve
N increases by 1 unit
Z decreases by 1 unit
3 β⁻-decay to reach stability curve
N decreases by 1 unit
Z increases by 1 unit

Fig. 5.2. $N \rightarrow Z$, stability curve (schematic).

In the course of our discussion on the liquid drop model of a nucleus, we shall see how it can account for the stability curve. To begin with, let us become familiar with the binding energies of nuclei.

5.2 BINDING ENERGIES OF NUCLEI: PLOT OF *B/A* AGAINST *A*

When nuclear masses are measured, it is found that they are less than the sum of the masses of the neutrons and protons of which they are composed. This is in agreement with Einstein's relativity theory, according to which the mass of a system bound by an energy B is less than the mass of its constituents by B/c^2.

For a nucleus of mass M containing Z protons and N neutrons, the binding energy B is defined as,

$$B = (ZM_p + NM_n - M)c^2 \quad \text{...(5.1)}$$

where M_p is the mass of free proton and M_n is the mass of free neutron.

Physically we recognize binding energy B of a nucleus as the energy required to break it up into free neutrons and protons.

On an average, binding energy per nucleon is found to be approximately:

$$\frac{B}{A} \sim 8 \text{ MeV} \quad \text{...(5.2)}$$

Here as usual $A = Z + N$ = mass number.

From Eq. 5.1, B can be obtained in MeV, when masses are expressed in atomic mass units (u), remembering,

$$1u = 931.5 \text{ MeV}$$

Equation 5.1 holds for any bound system. For example, an electron bound in a hydrogen atom. Here also the mass of the bound system (H atom) is less than the sum of the masses of its constituents (proton + electron) by B/c^2.

However, in the case of hydrogen atom we know that B = 13.6 eV, while the mass of hydrogen atom is about $\sim 1u \sim 10^9$ eV.

We see that the change in mass is only about 1 part in 10^8, which is extremely small.

For nuclei, from Eq. 5.2, we see that the change in mass is about 1 per cent, which is appreciable and readily measurable.

Figure 5.3 indicates the way in which the binding energy per nucleon, B/A varies as a function of the mass number A. Notice that it reaches a peak (maximum) for $A \sim 60$, then gradually decreases. This gradual decrease in B/A implies that it approximately remains constant.

A number of interesting conclusions can be drawn by noting the features of B/A against A plot.

(*i*) Approximately $B/A \sim$ constant. In other words, B/A appears to be approximately independent of the overall size of a nucleus. (B/A does not depend on A). As we shall see in the following section, this characteristic of the curve of B/A against A enables us to draw an analogy between a nucleus and a liquid drop.

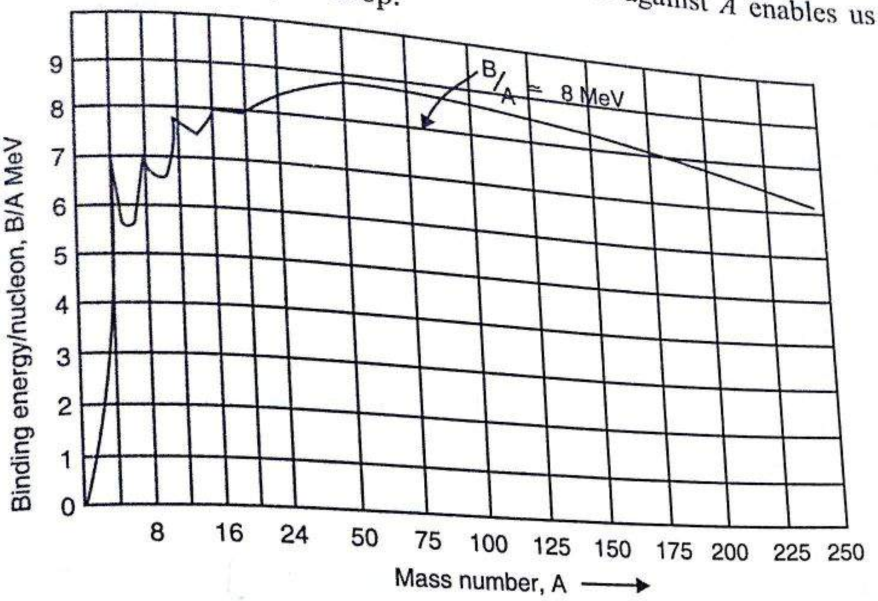

Fig. 5.3. B/A against A plot.

(*ii*) B/A falls off at small values of A. This is because very light nuclei have a larger fraction of their nucleons residing on the surface rather than inside. This reduces the B/A value as a surface nucleon is surrounded by fewer nucleons compared to a nucleon residing in the interior and consequently is not so strongly bound. The situation described here is similar to what one finds for a liquid drop. In the case of a liquid drop too, the surface molecules are bound less tightly compared to molecules which are in the interior of the drop, since full binding is reached only when a molecule is surrounded completely by other molecules. This situation is depicted in Fig. 5.4.

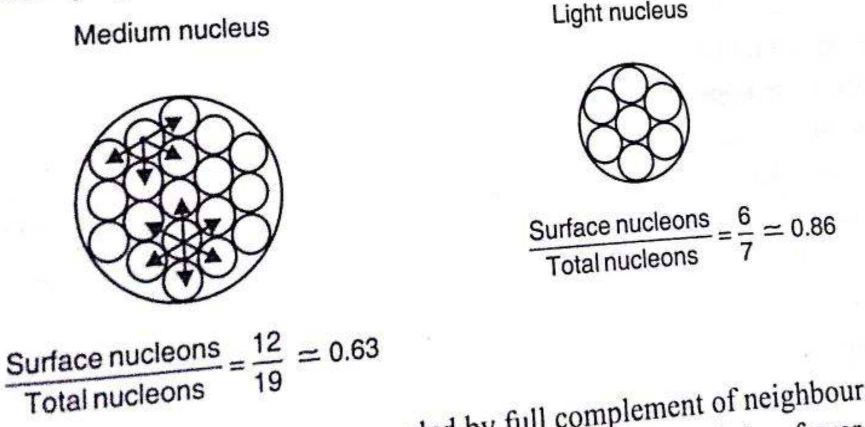
Medium nucleus
Light nucleus
Surface nucleons / Total nucleons = 6/7 ≃ 0.86
Surface nucleons / Total nucleons = 12/19 ≃ 0.63

Fig. 5.4. Nucleon in the interior is surrounded by full complement of neighbours and hence is more strongly bound than a nucleon on the surface which has fewer neighbours.

(*iii*) B/A falls off at large values of A. This is clearly a Coulomb effect. Between every pair of protons, there is a Coulomb repulsion which increases as Z^2. Notice that for naturally occurring nuclei, Z^2 increases faster than A and so the Coulomb effect cannot be adequately compensated by an increase in A.

(*iv*) B/A against A plot is peaked around $A \sim 60$. This enables us to draw extremely important conclusions which are practically useful.

Binding energy can be increased by either breaking a heavy nucleus into parts or fusing light nuclei together. From Eq. 5.1, it is easy to see that when the binding energy is increased, energy in other forms can be released, since a decrease in M corresponds to conversion of mass into energy.

These considerations highlight the importance of fission and fusion reactions, which are basic in the production of nuclear energy.

(*v*) The peak of this plot corresponds to Fe. This explains for the large abundance of Fe in nature.

(*vi*) The plot indicates that binding becomes strong for a grouping of four particles.

This unit is the alpha particle (2 neutrons + 2 protons). The peaks in Fig. 5.3 at mass numbers 4, 8, 12, 16, 20 and 24 are clear evidence of this effect. This effect is due to a pairing force which exists between pairs of neutrons and pairs of protons. We shall consider this point when we discuss nuclear forces in Chapter 8.

(*vii*) On closer inspection, it is found that the B/A against A plot shows discontinuities at neutron or proton number values, 2, 4, 8, 20, 50, 82 and 126. At these values of neutron or proton numbers, the binding energy is found to be unusually large. Large binding energy means high stability. This high stability is reflected in high abundance of isotopes with these proton numbers and isotones (same number of neutrons) with these neutron numbers.

In Chapter 7 we shall see how this led physicists to propose a shell model for the nucleus, similar to that which has been so successful in explaining the chemical properties of atoms.

5.3 WEIZSACHER'S SEMI-EMPIRICAL MASS FORMULA

We devoted the last section to defining nuclear binding energy and qualitatively understanding the features of B/A against A plot. In fact, we can do much better as nuclear masses are experimentally very accurately known and hence the binding energy B too is very accurately known. Using a semi-empirical approach (an approach based on experimental results) Weizsacher in 1935 showed that it is possible to achieve a quantitative and more basic understanding of binding energies of nuclei. He developed a mass formula, which has many practical applications. In particular, it is able to predict stability against beta decay for members of an isobaric family (same A, but different Z). In 1937, Bohr and Wheeler developed a theory for nuclear fission by considering the analogy between a nucleus and a liquid drop. Using Weizsacher's semi-empirical mass formula, they were able to calculate stability limit against spontaneous fission.

We shall now consider the steps which lead to this mass formula. Notice how an approximate comparison of a nucleus with a drop of liquid is fruitful. A liquid drop has volume energy and surface energy. The various contributions to the binding energy of a nucleus are discussed below:

1. Volume Energy Term, B_v

When a liquid drop evaporates completely, the energy required for this evaporation is the product of the latent heat of vaporization and the mass of the drop.

This heat energy is utilized to overcome all the bonds of molecules in the liquid drop, i.e., it is equal to the binding energy of the liquid drop, B.

∴ For a liquid drop,

$$B = LM_mA \qquad \text{...(5.3)}$$

where,

L = Latent heat of liquid.
M_m = Mass of each molecule,
A = Number of molecules.

From Eq. 5.3 we see that, B/A = constant, i.e., B/A is independent of A, the total number of molecules in the liquid drop. (We have already seen, in the last section, that for nuclei, B/A ~ constant). Physically, for a liquid drop, this is to be expected, since each liquid molecule interacts only with its neighbours and the number of neighbours surrounding a molecule is independent of the overall size of the liquid drop, i.e., B/A is independent of A. This is an important characteristic of any system (whether a liquid drop or a nucleus which is an assembledge of nucleons) in which range of interactions among constituent particles is much smaller than the dimensions of the system. Later, in Chapter 8, we shall see how nuclear force is a short range one. For nuclei, therefore, by analogy with a liquid drop we expect a volume term in the expression of binding energy, viz.,

$$\text{Volume term } B_v = a_vA \qquad \text{...(5.4)}$$

where a_v is a constant called volume coefficient and a_v corresponds to LM_m for a liquid drop (see Eq. 5.3). Since $V \propto A$ we can consider B_v is vol^m energy.

2. Surface Energy Term, B_s

In the discussion of volume energy term, B_v, we had assumed that the size of the liquid drop is so large that practically all molecules are fully surrounded by neighbours, with which they interact. This is not true for those molecules that find themselves at the surface, since they are not surrounded by neighbours from all sides. (see Fig. 5.4). Consequently these surface molecules are not bound as tightly as the molecules which are in the interior of liquid drop. For light nuclei, the fraction of nucleons on the surface is quite large and hence there is a sharp drop in B/A (Section 5.2). Therefore we see that the surface energy term, B_s, is proportional to the surface area of the nucleus, i.e.,

$$-B_s \propto 4\pi R^2 \qquad \text{...(5.5)}$$

where R is the nuclear radius.

The negative sign indicates that B_s reduces the total binding energy. From Chapter 4, we know that,

$$R = 1.07A^{1/3} \text{ fermi} \qquad \text{...(5.6)}$$

$$1 \text{ Fermi} = 1F = 10^{-15}\text{m} \qquad \text{...(5.7)}$$

where,

$$-B_s = a_s \cdot A^{2/3} \qquad \text{...(5.8)}$$

where a_s is called the surface coefficient.

A *rough estimate* can be made of the values of coefficients a_v in Eq. 5.4 and a_s in Eq. 5.8. The space available to a single nucleon in the nucleus is

$$\frac{\frac{4}{3}\pi R^3}{A}$$

Now imagine a nuclear surface region of thickness t,

$$t = \sqrt[3]{\frac{\frac{4}{3}\pi R^3}{A}}$$

Then the surface region must contain approximately,

$$\frac{4\pi R^2 t}{\frac{4}{3}\pi R^3 / A} = 3\sqrt[3]{\frac{4}{3}\pi A^{2/3}}$$

$$= 4.8A^{2/3} \text{ nucleons.}$$

These nucleons are not attracted from all sides and approximately about (1/4th) space of a surface nucleon would have no neighbours. This enables us to have a quick estimate of B_s.

$$-B_s = \left(\frac{1}{4}\right) a_v 4.8A^{2/3}$$

$$= 1.2a_v A^{2/3} \qquad \ldots(5.9)$$

Comparing with Eq. 5.8, we see that,

$$a_s \sim 1.2a_v$$

i.e.

$$a_s \sim a_v \qquad \ldots(5.10)$$

This estimate is in good agreement with the values of the coefficients determined from the experimental data.

3. Coulomb Energy Term, B_c

This term represents electrical repulsion of the protons and is like B_s, a negative term in the expression of nuclear binding energy. The amount of work done against Coulomb repulsion to assemble a nucleus is numerically B_c. To calculate this work done, let us assume that a nucleus is a uniformly charged sphere with a constant charge density ρ up to the radius R. For $r > R$, there is no charge.

Then,

$$\rho = \frac{Ze}{\frac{4}{3}\pi R^3} \qquad \ldots(5.11)$$

Consider a thin spherical shell of this charge of radius r. Using Coulomb's law, we can ulate the work dW required to bring this shell up to its radius r.

$$dW = \frac{1}{4\pi\varepsilon_0 r}\left[\frac{4}{3}\pi r^3\rho \times 4\pi r^2\, dr\rho\right] \qquad \ldots(5.12)$$

∴ B_c can be estimated by integrating this between $r = 0$ and $r = R$. Thus, integrating Eq. 5.12 between $r = 0$ and $r = R$ and substituting for ρ from Eq. 5.11, total work done in assembling a nucleus.

$$W = B_c = \frac{3/5Z^2e^2}{4\pi\varepsilon_0 R} \qquad \ldots(5.13)$$

owever, when we have only one proton as a nucleus,

$$(B_c)_{\text{proton}} = \frac{3/5e^2}{4\pi\varepsilon_0 R} \qquad \ldots(5.14)$$

or such a nucleus of only one proton, no work is done against the Coulomb repulsion in bling the nucleus.

ur basic Eq. 5.1 is based on the assumption that protons already exist and so, in our omb energy term of nuclear binding energy, we cannot include such terms as given by .14, which consider the assembling of single protons. There are Z such terms as there are tons. Therefore, the true Coulomb energy term is given by:

Didn't get

$$-B_c = \left[\frac{3/5Z^2e^2}{4\pi\varepsilon_0 R} - Z\left(\frac{3/5e^2}{4\pi\varepsilon_0 R}\right)\right]$$

$$= \frac{3/5Z(Z-1)e^2}{4\pi\varepsilon_0 R} \qquad \ldots(5.15)$$

he negative sign again indicates the disruptive nature of this term.

quation 5.15 may now be written in the form,

$$-B_c = \frac{3}{5}m_ec^2\,\frac{e^2}{4\pi\varepsilon_0 m_ec^2}\,\frac{Z(Z-1)}{(1.3)A^{1/3}F}$$

$$= a_c\,\frac{Z(Z-1)}{A^{1/3}} \qquad \ldots(5.16)$$

e know that,

$$m_ec^2 = 0.511 \text{ MeV}$$

Consider a thin spherical shell of this charge of radius r. Using Coulomb's law, we can calculate the work dW required to bring this shell up to its radius r:

$$dW = \frac{1}{4\pi\varepsilon_0 r}\left[\frac{4}{3}\pi r^3 \rho \times 4\pi r^2 \, dr\rho\right] \qquad \ldots(5.12)$$

$\therefore$ B_c can be estimated by integrating this between $r = 0$ and $r = R$. Thus, integrating Eq. 5.12 between $r = 0$ and $r = R$ and substituting for ρ from Eq. 5.11, total work done in assembling a nucleus.

$$W = B_c = \frac{3/5 Z^2 e^2}{4\pi\varepsilon_0 R} \qquad \ldots(5.13)$$

However, when we have only one proton as a nucleus,

$$(B_c)_{\text{proton}} = \frac{3/5 e^2}{4\pi\varepsilon_0 R} \qquad \ldots(5.14)$$

For such a nucleus of only one proton, no work is done against the Coulomb repulsion in assembling the nucleus.

Our basic Eq. 5.1 is based on the assumption that protons already exist and so, in our Coulomb energy term of nuclear binding energy, we cannot include such terms as given by Eq. 5.14, which consider the assembling of single protons. There are Z such terms as there are Z protons. Therefore, the true Coulomb energy term is given by:

Didnt get

$$-B_c = \left[\frac{3/5 Z^2 e^2}{4\pi\varepsilon_0 R} - Z\left(\frac{3/5 e^2}{4\pi\varepsilon_0 R}\right)\right]$$

$$= \frac{3/5 Z(Z-1)e^2}{4\pi\varepsilon_0 R} \qquad \ldots(5.15)$$

The negative sign again indicates the disruptive nature of this term.

Equation 5.15 may now be written in the form,

$$-B_c = \frac{3}{5} m_e c^2 \frac{e^2}{4\pi\varepsilon_0 m_e c^2} \frac{Z(Z-1)}{(1.3)A^{1/3} F}$$

$$= a_c \frac{Z(Z-1)}{A^{1/3}} \qquad \ldots(5.16)$$

We know that,

$$m_e c^2 = 0.511 \text{ MeV}$$

$$\text{Electron radius} = \frac{e^2}{4\pi\varepsilon_0 m_e c^2}$$

$$= \frac{8.99\times10^9\times(1.6\times10^{-19})^2}{(9.11\times10^{-31})(3\times10^8)^2}$$

$$= 2.8\times10^{-15}\,\text{m.}$$

$$\therefore \qquad -B_c \sim (0.60\,\text{MeV})\,Z\,(Z-1)\,A^{-1/3} \qquad \ldots(5.17)$$

Thus we see that the Coulomb coefficient has a value,

$$a_c = 0.60\ \text{MeV} \qquad \ldots(5.18)$$

4. The Asymmetry Energy Term, B_a

This is a term which depends on the neutron excess, $(N-Z)$, and decreases the nuclear binding energy. We shall see that this term is proportional to

$$\rightarrow \quad \frac{(N-Z)^2}{A}.$$

Consider a medium or heavy nucleus, of mass number A. The mass of such a nucleus can be written as (see Eq. 5.1):

$$M = ZM_p + NM_n - B = ZM_p + (A-Z)M_n - B \qquad \ldots(5.19)$$

Here M and B are measured in the same mass units.

This equation can be rewritten by substituting the different terms which binding energy B is made up of. Thus using Eqs. 5.4, 5.8 and 5.16, Eq. 5.19 becomes:

$$M = AM_n - Z(M_n - M_p) - a_v A + a_s\,A^{2/3} + a_c\frac{Z(Z-1)}{A^{1/3}} \qquad \ldots(5.20)$$

Equation 5.20 has two Z dependent terms, which are opposite in sign. Thus we see that, for a given A by differentiating Eq. 5.20 w.r.t. Z and setting $dM/dZ = 0$, we can find a value of Z for which M is a minimum. This minimum value of M will of course be expected to correspond to the maximum stability at that value of Z.

Putting $A = 216$, Eq. 5.20 gives a minimum M and hence greatest stability for $Z = 3$, which is absurd!

Hence, some important term in the binding energy is still not accounted for. The sign of this term has to be such as to increase Z for a given A, i.e., it must produce a deficit in the nuclear binding energy.

Looking back, one can see that so far in our preoccupation with comparison between a nucleus and a liquid drop we have neglected the quantization of energy states of the individual nucleons in the nucleus and the application of the Pauli exclusion principle.

Look at Fig. 5.5. If we put Z protons and N neutrons into a nucleus, the lowest Z energy levels get filled up first. By Pauli's exclusion principle, the excess neutrons, $(N - Z)$ must go into previously unoccupied quantum states, since the first Z quantum states are already filled up with protons and neutrons.

Thus, these $(N - Z)$ excess neutrons are occupying higher energy quantum states and are consequently less tightly bound, than the first $2Z$ nucleons which occupy the deepest lying energy levels.

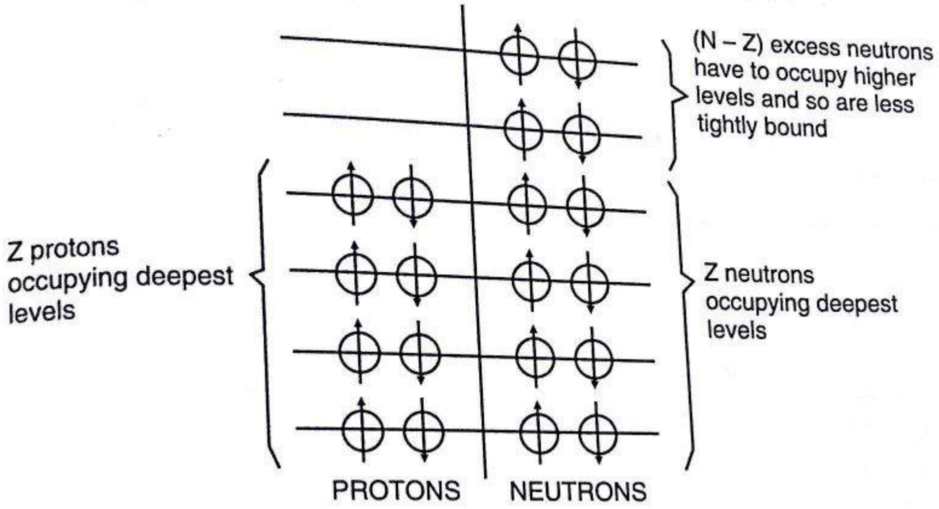
(N – Z) excess neutrons have to occupy higher levels and so are less tightly bound
Z protons occupying deepest levels
Z neutrons occupying deepest levels
PROTONS
NEUTRONS

Fig. 5.5. Application of Pauli's principle to nucleon energy quantum states (schematic).

The neutron asymmetry therefore gives rise to a disruptive term in nuclear binding energy expression, called the asymmetry energy, B_a.

To get the form of B_a in a simple way, we note that the number of excess neutrons is $N - Z$ and the neutron excess per nucleon is,

$$\frac{(N-Z)}{A}$$

Since the total number of excess neutrons is $(N - Z)$, the total deficit in nuclear binding energy is proportional to the product of these, i.e.,

$$-B_a = a_a \frac{(N-Z)^2}{A}$$

$$-B_a = a_a \frac{(A-2Z)^2}{A} \qquad \ldots(5.21)$$

or

where a_a is called the asymmetry coefficient and is evaluated empirically.

$$a_a \sim 19.8 \text{ MeV} \qquad \ldots(5.22)$$

Using this value of a_a and putting $dM/dZ = 0$, it can now be seen that for $A = 216$, M is minimum for $Z \sim 80$, which is quite reasonable. Thus, by incorporating a purely quantum mechanical effect in the binding energy, one can go much beyond the liquid drop analogy.

5. The Pairing Energy Term, B_p

Till now, all our energy terms have involved a smooth variation of B whenever proton number Z or neutron number N are changed. In the last section (Fig. 5.3) we have seen that B/A against A plot shows several links and there is evidence for favoured pairing. (Also, whenever Z or N becomes equal to 2, 4, 8, 20, 50, 82 and 126 the corresponding nuclides have large binding energies.) This fact does not appear in a liquid drop model because we have omitted the intrinsic spin of the nucleons and the shell effects. This omission is partly corrected by adding a pairing energy term B_p to the nuclear binding energy. It is interesting to look at the following data (in Tables) for stable nuclei classified in four possible groups.

TABLE 5.1: Classification or Stable Nuclides

A	Z	N	*Number of stable nuclei*
Even	Even	Even	165
Odd	Even	Odd	55
Odd	Odd	Even	50
Even	Odd	Odd	4

Table 5.1 brings out the Odd-Even effect. Obviously, Even-Even nuclei are the most abundant and hence the most stable. Odd-Odd nuclei are the least stable. Odd-Even nuclei have an intermediate stability. This pairing effect can be incorporated by putting

$$-B_p = a_p A^{-3/4} \qquad \ldots(5.23)$$

Equation 5.23 was empirically determined by Fermi.

TABLE 5.2

A	Z	a_p
Even	Even	–33.5 MeV
Odd		0
Even	Odd	+33.5 MeV

Table 5.2 gives values of a_p for Even-Even and Odd-Odd cases.

To account for the closed shells, one may add one more energy term. Actually the liquid drop model does not take cognisance of the shell structure. Therefore, normally the extra binding energy which is about 1 to 2 MeV for the nuclei of closed shells is not represented in the semi-empirical mass formula.

Finally, incorporating all the terms from (1) to (5) in equation for nuclear mass (Eqs. 5.1 and 5.20) we have:

$$M(Z, A) = AM_n - Z(M_n - M_p) - B$$

$$= AM_n - Z(M_n - M_p) - a_v A + a_s A^{2/3} + a_c \frac{Z(Z-1)}{A^{1/3}} + a_a \frac{(A-2Z)^2}{A} + a_p A^{-3/4} \qquad \ldots(5.24)$$

This is known as Weizsacher's semi-empirical mass formula.

Figure 5.6 neatly summarizes the effect of different energy terms in deciding B/A.

The five empirical coefficients are to be evaluated by using accurate information about binding energies of nuclei which, in turn, are obtained by knowing the nuclear masses accurately. Thus, we see that once these five coefficients are determined from five nuclear masses, they can be used to predict hundreds of other masses and reactions. In other words, by using some empirical data it is possible to predict a large amount of nuclear behaviour. This is the reason why Eq. 5.24 is called the *semi-empirical mass formula*.

Typically, the values of the empirical coefficients are:

$$\begin{aligned}
a_v &= 14 \text{ MeV} \\
a_s &= 13 \text{ MeV} \\
a_c &= 0.60 \text{ MeV} \\
a_a &= 19 \text{ MeV} \\
a_p &= -33.5 \text{ MeV for Even-Even nuclei} \\
&= 0 \text{ for Even-Odd} \\
&= +33.5 \text{ MeV for Odd-Odd nuclei}
\end{aligned} \qquad \text{...(5.25)}$$

Equation 5.24 is a quadratic in Z and so for each value of A, there is some particular value of Z for which M is minimum. A family of different nuclides for which the mass number A is the same is called a family of *isobars* or an *isobaric family*. The Z value which corresponds to minimum mass M gives the most stable member of this particular isobaric family.

Good

Let us now take a second look at Figs. 5.1 and 5.2. The line through the stable nuclei is referred to as the stability curve or the line of beta stability. From the discussion in the previous paragraph, it can be seen that the approximate equation of this line of beta stability could be obtained by putting the following condition on Eq. 5.24.

in N v/s Z graph

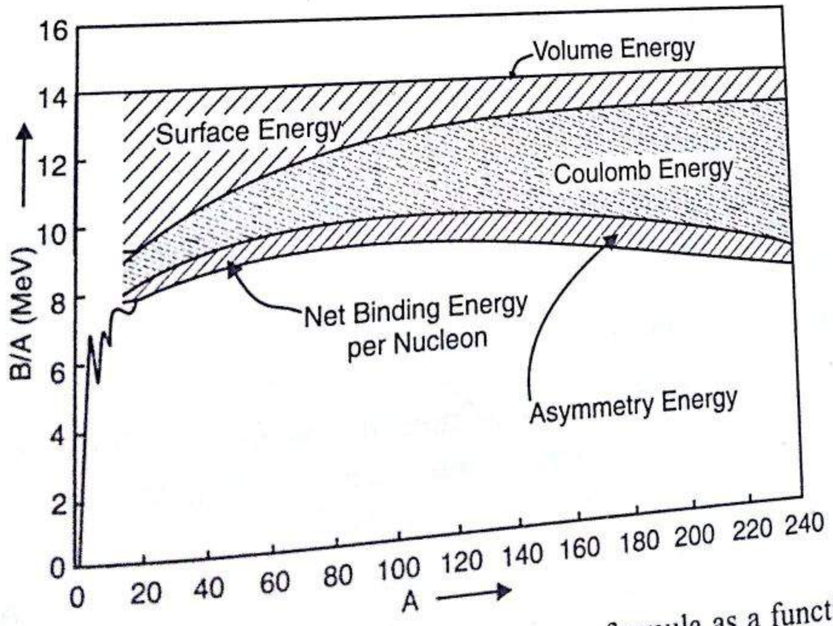

Fig. 5.6. Schematic representation of the terms in the mass formula as a function of A (Pairing energy is neglected). Notice how for higher A, increase in the Coulomb energy and decrease in the surface energy together produce the maximum B/A at $A \sim 60$.

$$\left[\frac{\partial M}{\partial Z}\right]_{A=\text{const}} = 0 \qquad \text{...(5.26)}$$

It can be seen from Figs. 5.1 and 5.2 that this line follows $N = Z$ for light nuclei, but then deviates from it as the increasing Coulomb term causes stable nuclides to have more neutrons than protons, giving rise to an increasing asymmetry energy term. In Fig. 5.2, it is indicated .how nuclei lying above this line decay either by β^+ or by electron capture and those below the line decay by β^-.

5.4 MASS PARABOLAS: PREDICTION OF STABILITY AGAINST β-DECAY FOR MEMBERS OF AN ISOBARIC FAMILY

Equation 5.24 giving the mass formula can be rewritten as:

$$M(Z,A) = A(M_n - a_v) + a_s\, A^{2/3} + Z\left[(M_p - M_n) - \frac{a_c}{A^{1/3}} - a_a.4)\right]$$

$$+ Z^2\left[\frac{a_c}{A^{1/3}} + \frac{4a_a}{A}\right] + a_a A \pm E_p$$

$$= \alpha A + \beta Z + \gamma Z^2 \pm \delta \qquad \text{...(5.27)}$$

where,

$$\alpha = M_n - \left(a_v - a_a - \frac{a_s}{A^{1/3}}\right) \qquad \text{...(5.28)}$$

$$\beta = -4a_a - (M_n - M_p) \qquad \text{...(5.29)}$$

$$\gamma = \left(\frac{4a_a}{A} + \frac{a_c}{A^{1/3}}\right) \qquad \text{...(5.30)}$$

and $\pm\delta$ = pairing energy

$= +\,\delta$ for odd Z odd N

$= 0$ for odd Z even N

$= 0$ for even Z odd N

$= -\,\delta$ for even Z even N ...(5.31)

When A is constant, Eq. 5.27 is the equation of a *parabola.* Thus, we expect plots of M against Z to be parabolic in shape with a *minimum* corresponding to that value of Z which gives the (hypothetical) 'most stable' isobar in an isobaric family.

For Odd A nuclei, $\delta = 0$ and thus there is only one parabola, implying that there is only one stable nucleus. For *even A* there can be up to three stable nuclei, because double beta decays have not been observed in nature. This is explained in detail below by taking a few families of isobars.

Odd A nuclei: Consider the isobaric family for $A = 91$. The parabolic relationship between the masses $M(Z, A)$ of the members of this family, as given by Eq. 5.27 is shown in Fig. 5.7 where ${}^{91}_{40}Zr$ can be seen to be the stable isobar. Other isobars whose binding energies are less than that of the stable one lie on the two arms of the mass parabola. Their masses are greater than that of the stable isobar and hence they decay by the emission β^- or β^+ or by K-capture as shown in Fig. 5.7.

From Eq. 5.27,

$$\left(\frac{\partial M}{\partial Z}\right)_{A=\text{const.}} = \beta + 2\gamma Z_0 = 0 \qquad \ldots(5.32)$$

giving Z_0 = nuclear charge of the "most stable" isobar

$$= \frac{-\beta}{2\gamma} \qquad \ldots(5.33)$$

For odd A ($\delta = 0$), the mass $M(Z_0, A)$ of the 'most stable' isobar is given by (using Eq. 5.33):

$$\begin{aligned} M(Z_0, A) &= \alpha A - 2\gamma Z_0 Z_0 + \gamma Z_0^2 \\ &= \alpha A - \gamma Z_0^2 \qquad \ldots(5.34) \end{aligned}$$

and so, the difference in masses for odd A is:

$$M(Z, A) - M(Z_0, A) = \beta Z + \gamma Z^2 + \gamma Z_0^2 = -2\gamma Z_0 Z + \gamma Z^2 + \gamma Z_0^2 = \gamma(Z - Z_0)^2 \qquad \ldots(5.35)$$

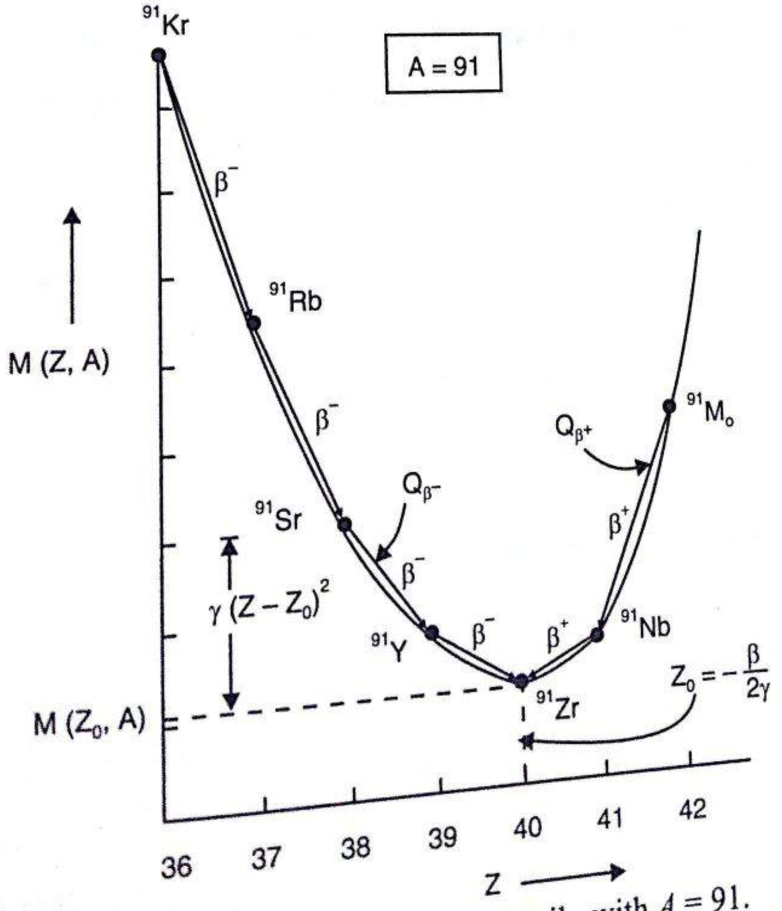

Fig. 5.7. Mass parabola for isobaric family with $A = 91$.

This gives the parabolic mass relationship for Odd-*A* isobars with vertex at $[Z_0, M(Z_0, A)]$ as shown in Fig. 5.7.

By making use of Eqs. 5.28 and 5.30 it is possible to estimate the values of $M(Z_0, A)$ and $M(Z, A) - M(Z_0, A)$. These values are marked in Fig. 5.7.

Consider now the *transitions between* isobars (Odd *A*).

For β^- decay, the energy release, which is the Q value (see Chapter 3) is given by,

$$Q_{\beta^-} = M(Z,A) - M(Z+1, A)$$

$$= \gamma\left[(Z - Z_0)^2 - (Z + 1 - Z_0)^2\right] \qquad \text{from Eq. 5.35}$$

$$= 2\gamma\left(Z_0 - Z - \frac{1}{2}\right) \qquad \ldots(5.36)$$

In a similar way,

$$Q_{\beta^+} = 2\gamma\left(Z - Z_0 - \frac{1}{2}\right) \qquad \ldots(5.37)$$

Typical Q_{β^-} and Q_{β^+} are also shown in Fig. 5.7.

ILLUSTRATIVE EXAMPLE

Example 5.1: For the family of isobars with $A = 91$, estimate (*i*) nuclear charge of the most stable isobar, (*ii*) the energy release Q_{β^-} and Q_{β^+}, for transitions leading to Z_0.

Solution: (*i*) From Eq. 5.33,

$$Z_0 = \frac{-\beta}{2\gamma}$$

From Eq. 5.29, $\beta = -4a_a - (M_n - M_p)$

$$\sim(76 + 0.8) \text{ MeV}$$

$$\sim 77 \text{ MeV}$$

and Eq. 5.30, $\gamma = 0.96$ MeV for $A = 91$.

∴ Nuclear charge for the most stable isobar,

$$Z_0 = \frac{-\beta}{2\gamma} = \frac{77}{0.96 \times 2} = 40.104$$

(From Fig. 5.6, this Z_0 corresponds to ${}^{91}_{40}\text{Zr}$ and one see that this estimate based on liquid drop model is excellent.)

(*ii*) From Eq. 5.36,

$$Q_{\beta^-} = 1.92\left(40 - 39 - \frac{1}{2}\right)\text{MeV}$$
$$= 0.96\ \text{MeV}$$

and

$$Q_{\beta^+} = 1.92\left(40 - 40 - \frac{1}{2}\right)$$
$$= 0.96\ \text{MeV}.$$

Even A isobars: Here the pairing term $\delta \neq 0$ and since both odd-odd and even-even nuclei are included, we have two parabolas, displaced in binding energy by 2δ. For example in Fig. 5.8 the parabolic relationship between the masses $M(Z, A)$ of the members of the isobaric family, $A = 104$, as given by Eq. 5.27 is shown.

Energetically possible decays are shown in the figure. Notice that ${}^{104}_{44}\text{Ru}$ cannot β^- decay to ${}^{104}_{45}\text{Rh}$ as the mass of ${}^{104}\text{Rh}$ is greater than the mass of ${}^{104}\text{Ru}$. We see that ${}^{104}\text{Pd}$ is stable, having least mass in the family. Mass of ${}^{104}\text{Ru}$ is greater than the mass of ${}^{104}\text{Pd}$, but this decay is again forbidden as mass of the intermediate nucleus ${}^{104}\text{Rh}$ is greater than the mass of ${}^{104}\text{Ru}$.

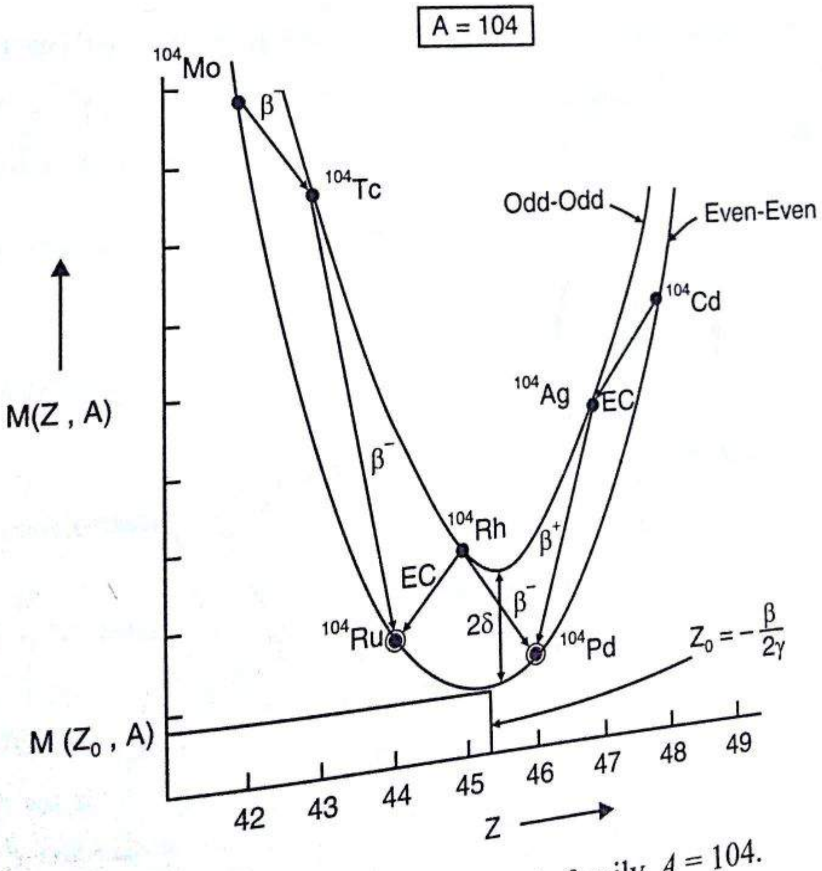
A = 104
104Mo
β⁻
104Tc
Odd-Odd
Even-Even
104Cd
104Ag
EC
M(Z , A)
β⁻
104Rh
β⁺
EC
β⁻
104Ru
2δ
104Pd
Z₀ = −β/2γ
M (Z₀ , A)
42
43
44
45
46
47
48
49
Z

Fig. 5.8. Mass parabolas for isobaric family, $A = 104$.

However, if ^{104}Ru decays into ^{104}Rh in a time

$$\Delta t = \frac{\hbar}{\Delta E} \qquad \ldots(5.38)$$

then the violation of conservation of energy by an amount ΔE, is consistent with Heisenberg's uncertainty principle, and provided, ^{104}Rh decays to ^{104}Pd within this time, a double beta decay, leading ^{104}Ru to ^{104}Pd is possible. Typically this Δt called nuclear time, is:

$$\Delta t \sim 10^{-22} \text{ sec} \qquad \ldots(5.39)$$

and generally the time required for normal beta decay is many seconds, so that the probability for a decay taking place in 10^{-22} sec is extremely small and consequently not yet observed experimentally. In other words, nuclear processes in which two protons simultaneously become two neutrons or two neutrons become two protons (double beta decay) have not yet been experimentally observed. This is the reason why for even A nuclides there can be one, two or three stable nuclei. In Figs. 5.9 and 5.10, mass parabolas are drawn for A = 136 and A = 200.

Notice that there are three stable nuclides for A = 136 isobaric family and there is only one stable nuclide for A = 200 isobaric family.

From Figs. 5.8 to 5.10, it can be seen that the Odd-Odd nuclei lie on the upper curve and are therefore unstable with respect to those on the lower curve, with the result that no stable Odd-Odd nuclei should exist. The only exceptions to this rule are extremely light nuclei e.g., isobaric family with $A = 14$. ${}^{14}_{6}\text{C}$, ${}^{14}_{7}\text{N}$, and ${}^{14}_{8}\text{O}$ are members of this family. We know that only ${}^{14}_{7}\text{N}$ is the stable member as $^{14}\text{C} \xrightarrow{\beta^-} {}^{14}\text{N}$ and $^{14}\text{O} \xrightarrow{\beta^+} {}^{14}\text{N}$. However ${}^{14}_{7}\text{N}$ nuclide lies on the Odd-Odd parabola (upper curve). This again emphasises the fact that light nuclei should not be treated on the basis of a liquid drop model as they have too few nucleons to be treated as a liquid drop.

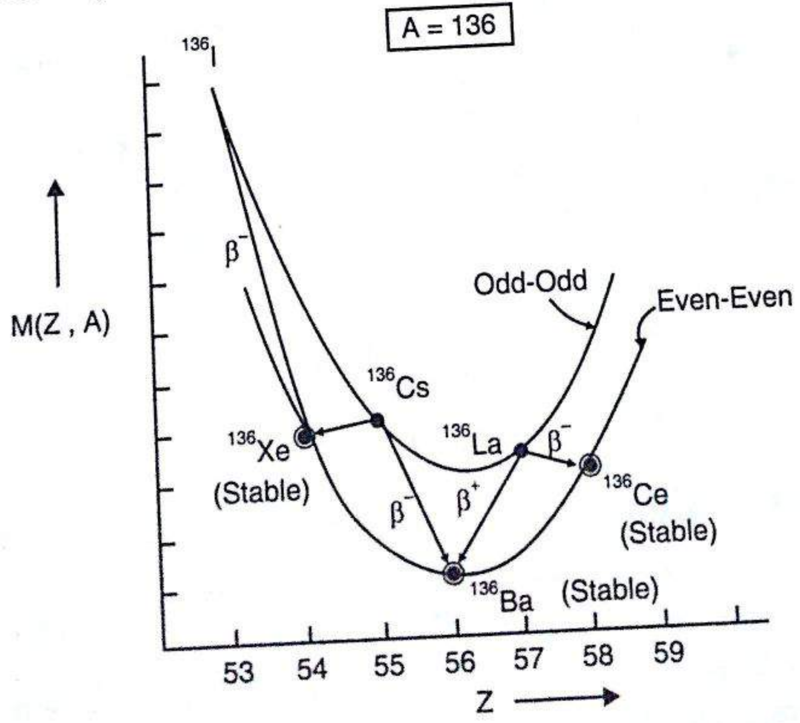

Fig. 5.9.

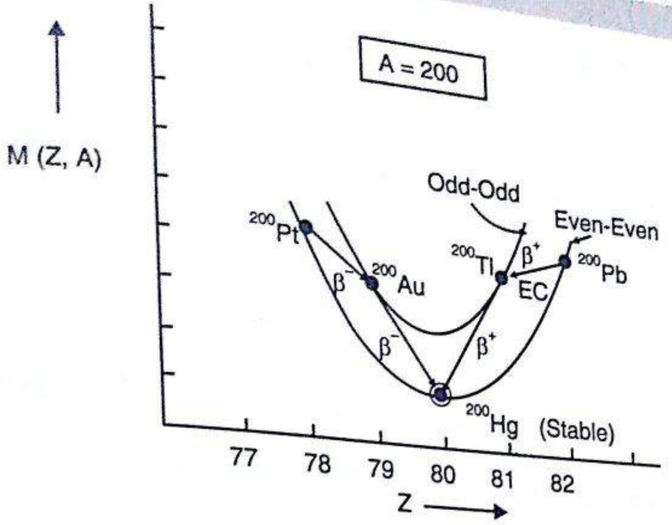

Fig. 5.10.

For Even A isobars, like for Odd A isobars, we can at once find:

(*i*) Z_0, the nuclear charge of the hypothetical 'most stable' nuclide (Eq. 5.33)

(*ii*) $M(Z_0, A)$ (See Eq. 5.34)

(*iii*) $M(Z, A) - M(Z_0, A)$ (See Eq. 5.35) and

(*iv*) Q_β (see Eqs. 5.36 and 5.37).

However, in this case we have to remember to take the $\pm\,\delta$ term in Eq. 5.27 as $\delta \neq 0$.

These calculations are left as an exercise to the students (see Problems 5.11).

We conclude this section by pointing to the fact that Weizsacher's semi-empirical mass formula agrees with the experimental values to more than one per cent for $A > 20$. Also the difference in binding energies of nuclei (for nearly same A) is given correctly up to 0.1 per cent.

This fact highlights the accuracy of predictions of the liquid drop model, inspite of its great simplicity.

ILLUSTRATIVE EXAMPLE

Example 5.2: (*i*) For "mirror" nuclei which have N and Z differing by one unit, determine the mass difference. Consider A to be odd.

(*ii*) The masses of $^{15}_{7}\mathrm{N}$ and $^{15}_{8}\mathrm{O}$ are 15.000108u and 15.003070u respectively.

Using this data, determine the Coulomb coefficient a_c in the semi-empirical mass formula.

Solution: (*i*) Mirror nuclei to be considered have the same odd value of A but the values of N and Z are interchanged such that they differ by one unit.

The $(A - 2Z)$ value in the asymmetry term in mass formula can be written as,

$A - 2Z = N + Z - 2Z = N - Z$. so that,

if N and Z differ by one unit,

$$N - Z = \pm 1$$

$$\therefore \quad M_{z+1} - M_z = (M_p - M_n)[(Z+1) - Z] + \frac{a_c}{A^{1/3}}[(Z+1)^2 - Z^2]$$

$$= M_p - M_n + a_c\frac{(2Z+1)}{A^{1/3}}$$

$$= M_p - M_n + a_c A^{2/3}, \because A = 2Z + 1 \text{ for these mirror nuclei.}$$

(*ii*) For the given mirror nuclei, using the above equation,

$$(2.962 \times 10^{-3})u = (-0.000844) + a_c(15)^{2/3}$$

$$\therefore \quad a_c = \frac{3.542}{6.08}\text{ MeV}$$

$$= 0.58 \text{ MeV}$$

5.5 STABILITY LIMITS AGAINST SPONTANEOUS FISSION

The success of the semi-empirical mass formula encouraged Bohr and Wheeler in 1938 to take the idea of the liquid drop model a little further and suggest an explanation for the important process of nuclear *fission.* The outcome was a satisfactory account of fission energetics.

Energy Available per Fission

We have seen that B/A against A plot shows a maximum at $A \sim 60$, and that in heavier nuclei (say $A > 100$) the total binding energy of A nucleons can be increased by dividing the original nucleus in two smaller nuclei. Such a process is called nuclear fission.

Consider $^{238}_{92}\text{U}$ nucleus divided into two nuclei with

$$A = \frac{238}{2}$$

The B/A value increases from ~7.6 MeV to ~ 8.5 MeV, i.e., 0.9 MeV per nucleon.

$\therefore$ For a division of ^{238}U nucleus the total increase in binding energy is,

$$(0.9 \text{ MeV}) \times (238) = 214 \text{ MeV}.$$

Such a fission for $A > 85$ is seen to be energetically advantageous. However, such a spontaneous fission is opposed by a Coulomb potential barrier, which is shown in Fig. 5.11. For simplicity, let us consider a '*symmetric fission*,' in which a nucleus (Z, A) breaks into two equal halves $(Z/2, A/2)$.

Energetics of 'Symmetric Fission'

The energy released in a symmetric fission is:

$$Q = M(Z, A) - 2M(Z/2, A/2) \qquad \ldots(5.40)$$

From the semi-empirical mass formula, binding energy for a nucleus (Z, A) is:

$$B(Z, A) = a_v A - a_s A^{2/3} - a_c \frac{Z(Z-1)}{A^{1/3}} - a_a \frac{(A-2Z)^2}{A} - a_p A^{-3/4} \qquad \ldots(5.41)$$

and binding energy for two fission fragments (Z/2, A/2) is:

$$2B(Z/2, A/2) = a_v A - 2a_s \left(\frac{A}{2}\right)^{2/3} - 2a_c \frac{\frac{Z}{2}\left(\frac{Z}{2}-1\right)}{\left(\frac{A}{2}\right)^{2/3}} - 2a_a \frac{(A/2-Z)^2}{A/2} - 2a_p \left(\frac{A}{2}\right)^{-3/4} \qquad \ldots(5.42)$$

Giving $Q = a_s A^{2/3}(1 - 2^{1/3}) + a_c \frac{Z(Z-1)}{A^{1/3}}\left(1 - \frac{1}{2^{2/3}}\right) +$ pairing energy difference.

The difference in pairing energy is small and thus can be neglected as an approximation.

$$\therefore \qquad Q = A^{2/3}\left(-0.260 a_s + 0.370 \frac{Z(Z-1)}{A} a_c\right) \qquad \ldots(5.43)$$

Using the values of a_s and a_c from Eq. 5.25

$$Q \sim A^{2/3}\left(-3.38\,\text{MeV} + 0.22\,\text{MeV}\,\frac{Z(Z-1)}{A}\right) \qquad \ldots(5.44)$$

From this we see that Q becomes > 0 for

$$\frac{Z^2}{A} \geq \frac{3.38}{0.22} \sim 15 \qquad \ldots(5.45)$$

Thus for all nuclei having $Z > 35$, $A > 80$, fission is possible and would release energy.

For the symmetric fission of $^{238}_{92}\text{U}$,

$$Q = (238)^{2/3}\left(-3.38 + 0.22 \frac{92(92-1)}{238}\right)\text{MeV} \qquad \ldots(5.46)$$

$$= 38.4(4.36)\,\text{MeV} \sim 170\,\text{MeV}.$$

This is somewhat less than the 214 MeV estimated from the change in B/A, since the B/A alues correspond to stable nuclides. The two fission fragments (Z/2, A/2) will have large neutron xcess and hence would be unstable.

Looking at Eqs. 5.45 and 5.46, we can ask why heavy nuclei do not all spontaneously undergo fission. To understand this, one has to realize that the surface area is considerably increased when one large liquid drop breaks into two small liquid drops. In the case of ^{238}U, about 6 MeV are required to overcome the surface forces and separate the two small liquid drops before the energy Q is released. This situation is described below in terms of a potential barrier through which the fission fragments have to pass. The quantum mechanical probability for such a barrier penetration is calculated in the next section. Because of the large masses involved, this probability is extremely small and for ^{238}U, we get a half-life of ~10^{16} yrs. for decay by spontaneous fission.

Equation 5.46 can be written as:

$$Q = -3.38(238)^{2/3} + 0.22\frac{92(92-1)}{(238)^{1/3}}$$

$$\sim (-130 + 300)\text{MeV}$$

$$= 170 \text{ MeV} \qquad \ldots(5.47)$$

We at once see that the energy release Q is positive because of a large decrease in the Coulomb energy, ~300 MeV, which dominates over a change in the opposite direction ~ –130 MeV due to increase in the surface area because of fission. The Coulomb energy and the surface energy together control the energetics of nuclear fission.

Let us now consider the potential barrier opposing spontaneous fission.

Potential Barrier for Fission

Figure 5.11 shows how the mutual potential energy of two fission fragments changes when they approach each other from a large distance and finally coalesce to form a ^{238}U nucleus. For simplicity, symmetric fission is considered.

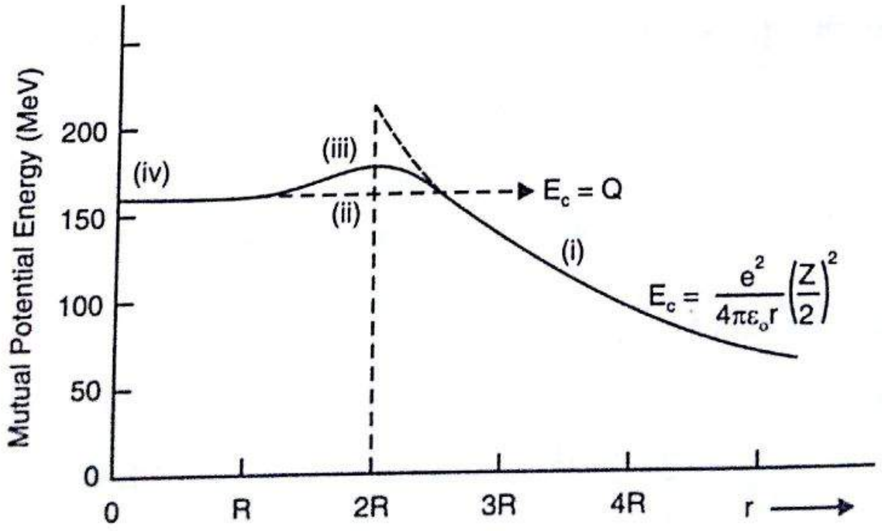

Fig. 5.11. Potential barrier opposing spontaneous fission for ^{238}U Stages (*i*) to (*iv*) indicate fission in the reversed order.

For $r > R$, the radii of fission fragments, the mutual potential energy is simply the Coulomb energy

i.e.,
$$E_c = \frac{1}{4\pi\varepsilon_0}\frac{e^2}{r}\left(\frac{Z}{2}\right)^2 \qquad \ldots(5.48)$$

When $r \sim 2R$, the two particles are just touching and nuclear attractive forces become operative, implying that mutual potential energy is < Coulomb value. This indicated by (*ii*) and (*iii*) Fig. 5.11.

If there were no attractive forces, the Coulomb energy at $r = 2R$, where the two articles just touch, would be:

$$E_c = \frac{1}{4\pi\varepsilon_0}\frac{e^2(Z/2)^2}{2R}$$

i.e.
$$E_c = \frac{1}{4\pi\varepsilon_0}\frac{e^2(Z/2)^2}{2R_0(A/2)^{1/3}}$$

$$= \frac{2^{1/3}e^2Z^2}{4\pi\varepsilon_0 8R_0A^{1/3}} \qquad \ldots(5.49)$$

But the Coulomb coefficient a_c (from Eq. 5.15) is

$$a_c \sim \frac{3}{5} - \frac{1}{4\pi\varepsilon_0}\frac{e^2}{R_0}$$

$$E_c = \frac{2^{1/3}}{8}\left(\frac{5}{3}a_c\right)\frac{Z^2}{A^{1/3}}$$

$$= 0.262a_c\frac{Z^2}{A^{1/3}} \qquad \ldots(5.50)$$

$$\sim 210 \text{ MeV for } ^{238}\text{U}$$

This value is shown in Fig. 5.11 as extrapolated curve at $r = 2R$ when the two spheres $Z/2$, $A/2$) just touch.

In reality, because of the nuclear attractive forces the Coulomb energy at position (*ii*) in ig. 5.11 is equal to:

$$Q \sim 170\,\text{MeV}.$$

As the two particles come closer, the nuclear attractive forces become stronger, the two ragments finally coalesce to form a single (Z, A) nucleus. The energy of symmetric fission for his nucleus as shown at position (*iv*) in Fig. 5.11 can be seen to be *below* the barrier height.

Actually for ^{238}U, gamma-rays of energy ~6 MeV are able to induce fission reaction. This γ, f) reaction is called photofission for which the threshold energy is ~6 MeV. Therefore, we conclude that the barrier is only about 6 MeV above Q, the dissociation energy for spontaneous fission of ^{238}U. This is the reason why for all practical purpose ^{238}U is stable against decay by spontaneous fission (half-life $T \sim 10^{16}$ yrs).

Stability Limits

We can approximately estimate Z and A values of a heavy nucleus which is unstable against spontaneous fission by demanding that Q for symmetric fission is as large as the Coulomb energy E_c for two spheres, ($Z/2$, $A/2$) in contact. A nucleus will be unstable if

$$Q \geq E_c \qquad \ldots(5.51)$$

Substituting for Q and E_c from Eqs. 5.43 and 5.50,

$$A^{2/3}\left(-0.260a_s + 0.370a_c \frac{Z(Z-1)}{A}\right) \geq 0.262a_c \frac{Z^2}{A^{1/3}}$$

putting $Z(Z-1) \sim Z^2$, we get

$$\left(-0.260a_s\, A^{2/3} + 0.370a_c \frac{Z^2}{A^{1/3}}\right) \geq 0.262a_c \frac{Z^2}{A^{1/3}} \qquad \ldots(5.52)$$

i.e.,

$$\frac{Z^2}{A} \geq 2.4\frac{a_s}{a_c} = 52 \qquad \ldots(5.53)$$

giving stability limit against spontaneous symmetric fission.

The value of $\frac{Z^2}{A}$ obtained is an upper limiting value as we have omitted here the possibility of spontaneous fission by quantum mechanical barrier penetration. Though small, this probability is finite, as we will see in the next section. Notice how the parameter $\frac{Z^2}{A}$, which decides stability against spontaneous fission, is solely governed by Coulomb energy, which is proportional to $\frac{Z^2}{A^{1/3}}$ and surface energy, which is proportional to $A^{2/3}$.

The limit given by Eq. 5.53 is found to be too high, as we find that in nature elements having $\frac{Z^2}{A}$ values around 44 or so are unstable against spontaneous fission. This is primarily because it is not accurately known how the potential barrier behaves around $r = 2R$ and less. A much better estimate of the critical value of $\frac{Z^2}{A}$ can be obtained, as shown by Bohr and Wheeler, by considering oscillations of a liquid drop (incompressible) under the joint action of surface forces and Coulomb forces.

How oscillations of this type will result into a division of a drop is indicated in Fig. 5.12.

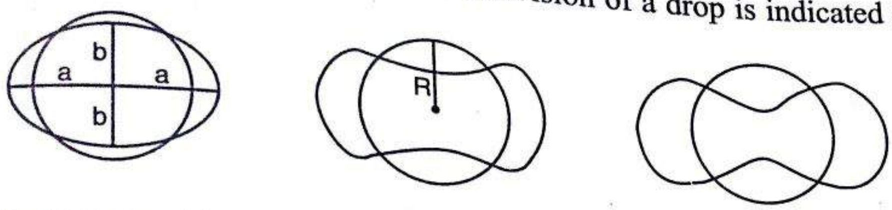

Fig. 5.12. Nucleus considered as an incompressible liquid drop. Notice how the surface changes finally lead to 'fission' of the drop.

As the drop is considered incompressible, the volume of the sphere of radius R is same as volume of the ellipsoid of semi major axis a and semi minor axis b.

$$\frac{4}{3}\pi R^3 = \frac{4}{3}\pi a b^2$$

If ε devotes the eccentricity ($\varepsilon = 0$ for sphere),

$$a = R(1+\varepsilon) \quad \text{and} \quad b = \frac{R}{(1+\varepsilon)^{1/2}}$$

surface energy of ellipsoid is,

$$B_s = (\text{Area of ellipsoid}) \times \text{surface tension}$$

$$= 4\pi R^2\left(1+\frac{2}{5}\varepsilon^2+\ldots\right)\times \text{surface tension}$$

$$= a_s A^{2/3}\left(1+\frac{2}{5}\varepsilon^2+\ldots\right) \qquad \ldots(5.54)$$

The coulomb energy of ellipsoid is,

$$B_c \sim \frac{3}{5}\cdot\frac{1}{4\pi\varepsilon_0}\frac{e^2Z^2}{R}\left(1-\frac{1}{5}\varepsilon^2+\ldots\right)$$

$$= a_c\frac{Z^2}{A^{1/3}}\left(1-\frac{1}{5}\varepsilon^2+\ldots\right) \qquad \ldots(5.55)$$

Clearly in the ellipsoidal form, the Coulomb energy is less compared to the spherical form, e charges are comparatively farther apart. On the other hand, the ellipsoidal form has a r surface energy term compared to the spherical form because of the large surface area.

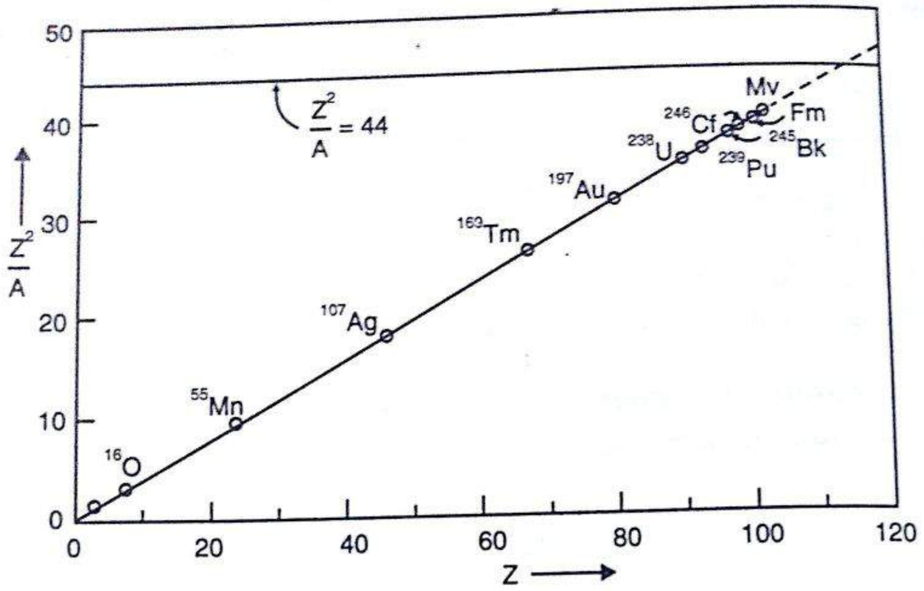

Fig. 5.13. A plot of fission parameter $\frac{Z^2}{A}$ against Z. The limiting value $\frac{Z^2}{A} = 44$, obtained from the liquid drop model is shown.

From Eqs. 5.54 and 5.55, taking only terms in ε^2, the stability condition against spontaneous fission becomes:

$$a_c \frac{Z^2}{A^{1/3}}\left(\frac{1}{5}\varepsilon^2\right) \ge a_s\, A^{2/3}\left(\frac{2}{5}\varepsilon^2\right) \qquad \ldots(5.56)$$

i.e.,

$$\frac{Z^2}{A} \ge 2\frac{a_s}{a_c} = 44 \qquad \ldots(5.57)$$

Equation 5.57 gives a much more experimentally realistic stability limit against spontaneous fission.

Figure 5.13 shows a plot of $\frac{Z^2}{A}$ against Z. $\frac{Z^2}{A}$ is often called the fission parameter or critical parameter because it governs the stability limit against spontaneous fission. It can be seen that spontaneous fission does not become a major mode of decay right up to Z ~ 110.

5.6 BARRIER PENETRATION—DECAY PROBABILITIES FOR SPONTANEOUS FISSION

In the last section, we studied features of the potential barrier which opposes spontaneous fission. Since the threshold energy for photofission of $^{238}_{92}$U is ~6 MeV, we observed that this barrier is bout 6 MeV above Q, the dissociation energy for spontaneous fission of ^{238}U. Equation 5.45 says that for all nuclei with $A > 80$, spontaneous fission is possible and would release energy. However, because of the potential barrier, the fission decay process is extremely slow. This is the reason why nuclei with $A > 80$, exist at all in nature.

Let us calculate decay probabilities for spontaneous fission, using wave mechanics. From Chapter 1 (Eq. 1.II.22), we know that the barrier penetration (probability) is given by:

$P \sim e^{-2kb}$ for a rectangular barrier of thickness b.

$$\ldots(5.58)$$

where

$$k = \frac{1}{\hbar[2M(V - E_0)]^{1/2}} \qquad \ldots(5.59)$$

For a non-rectangular barrier, k is a function of x and so,

$$P = e^{-2\int_0^b k\,dx} \qquad \ldots(5.60)$$

Recall that V = height of the potential barrier.

E_0 = disintegration energy.

M = Mass of the particle.

We have seen that (Eq. 1.II.22, Chapter 1):

$$P = \exp\left[-2\sqrt{\frac{2M}{\hbar^2}}\int\left(\frac{\left(\frac{Ze}{2}\right)^2}{4\pi\varepsilon_0 r} - F\right)^{1/2} dr\right]$$

For ${}^{238}_{92}\text{U}$ symmetric fission, the product of charges of the two fission fragments is:

$$46 \times 46 = 2{,}116.$$

(Compare this for alpha decay, 2 × 90 = 180)

Also mass M involved for fission is very large as compared to say, the alpha particle.

These factors reduce the barrier penetration probability P, which is sensitive to the shape f the barrier. For ^{238}U, decay rates are correctly predicted for a rectangular barrier of width ~ fermi and height ~6 MeV (schematically shown in Fig. 5.14).

It is found that:

$$P \sim e^{-102} \sim 10^{-44} \qquad \ldots(5.61)$$

(Compare again with alpha decay, Chapter 4, $P \sim e^{-81} \sim 10^{-38}$).

It is seen that the fission decay rate for $^{238}_{92}\text{U}$ is $\sim 10^6$ times slower than alpha decay.

In the Fig. 5.15, we will see that in some transuranium elements, fission decay is faster than alpha decay.

This discussion is, of course, pertaining to decay rates of spontaneous fission, and not, for example, *neutron induced fission,* which will be taken up in the next chapter.

For ^{238}U, the fission decay rate is about $\sim 10^6$ times slower than the alpha decay rate, as remarked earlier, and so the half-life of $^{238}_{92}\text{U}$ against decay by spontaneous fission is $\sim 10^{16}$ years. (Recall that T for α decay for $^{238}\text{U} \sim 10^9$ years.)

Figure 5.15 shows the half-life plot for spontaneous fission against fission parameter $\frac{Z^2}{A}$. As can be seen from the figure, the spontaneous fission mode of decay is negligible in ^{232}Th and ^{238}U, but for ^{254}Cf, ^{254}Fm and ^{256}Fm, it becomes the main decay channel.

Figure 5.14 shows a fission barrier. Actually fission fragments are quite complicated compared to nucleons, α-particles etc. Being neutron-rich they are unstable and can take non-spherical shapes, undergo oscillations and are generally in highly excited states. Consequently, the shape of barrier is much more complex than the one shown in Fig. 5.14. Careful experiments reveal that the fission barrier has two maxima, with a dip in between. However, a detailed discussion of this 'double hump' is beyond the scope of this book.

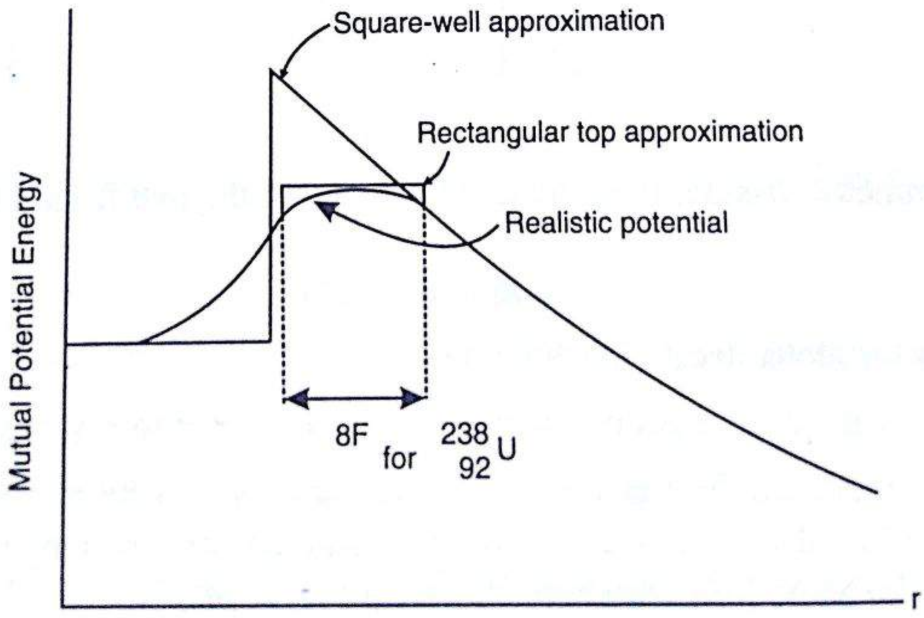
Square-well approximation
Rectangular top approximation
Realistic potential
Mutual Potential Energy
8F for $^{238}_{92}\text{U}$
r

Fig. 5.14. Diagram shows how a more realistic potential is better represented by a rectangular top approximation than a square-well approximation.

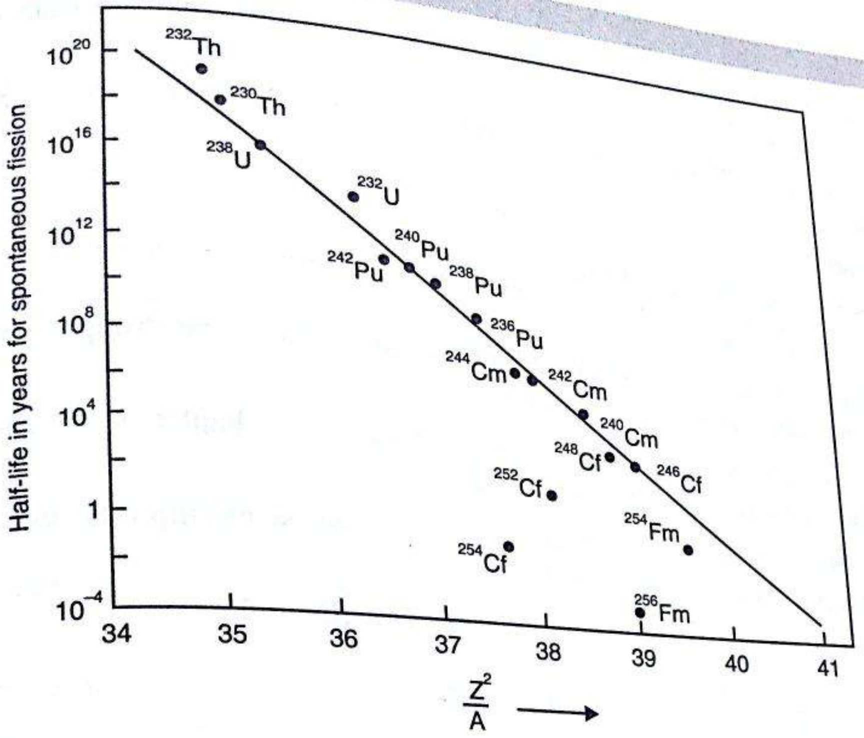

Fig. 5.15. Plot shows half-lives for spontaneous fission for Even Z, Even *N* nuclides against fission parameter $\frac{Z^2}{A}$. Notice that for heavy nuclides, as $\frac{Z^2}{A}$ increases, fission becomes an important mode of decay.

5.7 NUCLEON EMISSION

When a nucleus decays by either neutron or proton emission, the process is called nucleon emission. We have seen that *B/A* for stable nuclides is –8 MeV and so, nucleon emission is energetically possible only when the nuclear excitation energy is more than 8 MeV. However, in light nuclei, *B/A* is much less and so nucleon emission is possible for smaller nuclear excitation energies, e.g., the binding energy of a deuteron $\left({}^{2}_{1}\text{H}\right)$ is ~2.2 MeV. Another important example is ^{5}He, which decays by neutron emission, and as a result, there are no stable nuclei for $A = 5$.

It is also possible for groups of nucleons to come out of a nucleus. In Chapter 3 we saw that when a nucleus is bombarded by an energetic projectile, a variety of light nuclei can get emitted. We also saw that the bombardment of a nucleus by an energetic particle releases a variety of energetic particles. If a deuteron is emitted the excitation energy must be at least the sum of excitation energies of a proton and a neutron minus the binding energy of a deuteron.

i.e., Excitation energy $= (2 \times 8 - 2.2)$ MeV

$$\sim 14 \text{MeV}$$

which is much higher than the excitation energy required for the emission of a single nucleon.

In Chapter 4, we saw that the binding energy of an alpha-particle (^{4}He nucleus) is very large and is about –28 MeV.

Therefore, we can make a similar estimate about the excitation energy required by a nucleus for α-emission.

It can be seen that,

$$\text{excitation energy} = (4 \times 8 - 28)\ \text{MeV}$$
$$= 4\ \text{MeV}.$$

This is relatively a very small value and the reason for this is the strong binding of α-particle, ^{4}He being a closed shell (see also Chapter 7).

Thus, α-emission is a frequently occurring process. In Chapter 4, we saw that in heavy nuclei, α-emission is more favoured, energetically.

Estimate for nucleon separation energy: An accurate, semi-empirical estimate of nucleon separation energy, S_N, can be made as follows:

$$S_N = B(A) - B(A-1)$$
$$= \frac{dB}{dA}$$

This can be expressed in a more advantageous form amenable for direct calculation, by considering

$$\frac{d(B/A)}{dA} = \frac{1}{A}\frac{dB}{dA} - B \cdot \frac{1}{A^2}$$

$$\therefore \qquad S_N = \frac{dB}{dA}$$

$$= A\frac{d(B/A)}{dA} + \frac{B}{A} \qquad \text{...(5.62)}$$

Equation 5.62 can be evaluated directly by measuring the slope of the B/A against A curve (see Fig. 5.3).

ILLUSTRATIVE EXAMPLE

Example 5.3: For $A = 150$ and 220, values for $\frac{d(B/A)}{dA}$ are about – 1/125 and – 1/110 and values for B/A are 8.3 MeV and 7.7 MeV. Calculate nucleon separation energies for these two nuclides

Solution: Using Eq. 5.62, we see that,

$$S_N = 150\left(-\frac{1}{125}\right) + 8.3\ \text{MeV}$$
$$= 7.1\text{MeV for } A = 150$$

$$S_N = 200\left(-\frac{1}{110}\right) + 7.7 \text{ MeV}$$

$$= 5.7 \text{ MeV for } A = 220.$$

Quantum-mechanically, by considering a Coulomb barrier and an angular momentum barrier, it is possible to calculate nucleon emission probabilities for different nuclides. This does not fall within the scope of this book. However, a list of books is given for further reading.

For $S_{1/2}$ protons, only the Coulomb barrier is present and the proton emission probability is given by:

$$P \sim \exp\left[-2\sqrt{\frac{2M}{\hbar^2}} \int \left(\frac{Ze^2}{4\pi\varepsilon_0 r} - E_0\right)^{1/2} dr\right] \quad \text{...(5.63)}$$

The range of integration is between $r = R_0$ and the value of the radius where the integrand becomes zero.

For a medium mass nucleus, $P \sim 10^{-3}$ for $E_0 = 4$ MeV (E_0 = proton energy) and $P \sim 10^{-13}$ for $E_0 \sim 1$ MeV.

Compare Eq. 5.63 with Eq. 5.60 for fission decay.

EXERCISES

(Neutral atomic masses are given in appendix)

1. Calculate the binding energy of ^{4}He nucleus (α-particle).
2. Calculate the binding energies of the following nuclei:
   (*i*) ^{2}H (*ii*) ^{65}Cu (*iii*) ^{127}I (*iv*) ^{195}Pt (*v*) ^{238}U (*vi*) ^{245}Bk.
3. Calculate the binding energy per nucleon for:
   (*i*) ^{55}Mn (*ii*) ^{98}Mo (*iii*) ^{197}Au (*iv*) ^{234}Th
4. Find out the minimum energies required to remove a neutron from $^{91}_{40}$Zr, $^{92}_{40}$Zr and $^{93}_{40}$Zr.

   Take mass data from the table given in the appendix.

   $\left(\textit{Hint}: {}^{91}_{40}\text{Zr} + E = {}^{92}_{40}\text{Zr} + n\right)$

   Compare these values. Can you account for the difference?
5. Obtain the neutron separation energy for $^{92}_{40}$Zr by making use of Fig. 5.3 and Eq. 5.62. How does this value compare with that in Ex. 4?
6. Using Eq. 5.47, compute and plot the fission energy release as a function of the parent nuclide mass number.

7. Calculate the surface energy and Coulomb energy for a ${}^{236}_{92}U$ nucleus.

8. For the mirror nuclei, ${}^{23}_{11}Na$ and ${}^{23}_{12}Mg$, calculate Coulomb coefficient a_c (use masses from table).

   (*Hint:* See Illustrative Example 5.2)

   Hence estimate r_0.

9. Using the liquid drop model, find the most stable isobar for (*i*) $A = 25$ (*ii*) $A = 75$.

10. Mass spectrometer values are often reported in terms of "packing fractions" defined as,

$$P = \frac{M - A}{A}$$

   in which $M - A$ is called the "mass defect".

   Compute the mass defects and packing fractions for (*i*) ${}^{7}Li$ (*ii*) ${}^{98}Mo$ (*ii*) ${}^{238}U$ and (*iv*) ${}^{4}He$. Obtain the expected mass of ${}^{98}Mo$ using Weizsacher's semi-empirical mass formula. How does it compare with the mass spectrometer result?

11. For the isobaric family, $A = 200$ (see Fig. 5.10), obtain

    (*i*) Z_0, the nuclear charge of the 'most stable' isobar

    (*ii*) Mass, $M(Z_0, A)$

    (*iii*) $M(Z, A) - M(Z_0, A)$ and

    (*iv*) $Q_{\beta^\pm}$, the energy release for $\beta^\pm$ decay.

12. For the isobaric family with $A = 39$, estimate nuclear charge Z_0 of the most stable isobar.

13. Applying the semi-empirical mass formula to isobaric pairs (${}^{123}Sb - {}^{123}Te$); (${}^{207}T1 - {}^{207}Pb$) and (${}^{171}Tm - {}^{171}Yb$), what type of β activities do you expect?

    Also calculate Q_β, beta disintegration energy.

14. Considering symmetric fission, calculate the energy released by fission when the parent nuclide is:

    (*i*) ${}^{100}_{42}Mb$ (*ii*) ${}^{120}_{52}Te$ (*iii*) ${}^{170}_{70}Yb$ and (*iv*) ${}^{200}_{80}Hg$

15. Show that the binding energy per nucleon can be represented by:

$$\frac{B}{A} = a_v - \frac{a_s}{A^{1/3}} - a_c \frac{Z(Z-1)}{A^{4/3}} - a_a\left(1 - \frac{2Z}{A}\right)^2 \pm \frac{\delta}{A}.$$

16. What are the basic assumptions for a liquid drop model of a nucleus? Discuss the limitations of th liquid drop model.

6

Nuclear Energy

"No power (energy) is costlier than no power."

—*Homi J. Bhabha*

"Whatever Nature has in store for mankind, unpleasant as it may be, men must accept, for ignorance is never better than knowledge."

—*Enrico Fermi*

6.1 INTRODUCTION

In the last chapter we saw how in 1938, Bohr and Wheeler obtained the stability condition against spontaneous symmetric fission, $\frac{Z^2}{A} \geq 44$, by using a liquid drop model of the nucleus. We also discussed the features of the potential barrier opposing the fission process.

Actually, the laboratory evidence for fission dates back to 1934, when Fermi and his fellow workers were trying to produce elements with $Z > 92$ by bombarding uranium with neutrons. They found beta activity in the product after such a bombardment. Since the normal uranium decays by α-activity, Fermi and his fellow researchers concluded that the products of the reaction were transuranium elements. (Recall that β-decay increases Z by one.) Many chemists entered the field to check Fermi's hypothesis. One of them, Noddack, succeeded in precipitating the β-activities by adding a manganese salt to a solution of uranium salt that had been bombarded with neutrons. The manganese was precipitated as MnO_2. Noddack suggested that since many elements lighter than uranium were precipitated with MnO_2, it was possible that the bombarded uranium nuclei had been split into nuclei of elements with a lower atomic number. Her suggestio was apparently ignored and the search for transuranium elements was continued.

In Dec., 1938, Hahn and Strassmann found, after a series of very careful chemical experiments, that one of the radioactive elements formed by the bombardment of uranium with neutrons was an isotope of barium, $Z = 56$. ${}_{56}$Ba decays by β emission into an isotope of Lanthanum, ${}_{57}$La. They were able to find traces of ${}_{57}$La also. This clearly suggested that the beta activities were not due to any transuranium elements but were due to radioactive isotopes of elements having a lower atomic number than uranium, thus confirming Noddack's idea. Hahn and Strassman, therefore, concluded that when uranium is bombarded with neutrons, uranium nucleus splits into two medium atomic mass nuclei. Since one frangment is the nucleus of barium, the other must be the Krypton nucleus, $Z = 36$. This type of disintegration in which a heavy nucleus splits up into two medium mass nuclei (of comparable masses) is called nuclear fission. Hahn and Strassman are thus credited with the observation of the first "neutron induced fission".

In the last chapter, we took into account, the liquid drop model treatment of symmetric, spontaneous fission and saw that a large amount of energy released. In this chapter, we will take up *neutron induced fission* for study. The liquid drop model is quite helpful in this study too. The consideration of neutron induced fission will lead us to the ways of harnessing nuclear energy for practical purposes—a study of nuclear reactors.

6.2 NEUTRON INDUCED FISSION

It is possible to accelerate fission by means of neutron-capture. However, all heavy nuclei do not undergo fission when bombarded by slow, thermal neutrons ($E_n \sim 10^{-2}$ eV). Weizsacher's mass formula helps us to understand, for example, why ${}^{235}_{92}\text{U}$, an isotope of uranium with only 0.7% abundance, will undergo fission if it captures a neutron, whereas ${}^{238}_{92}\text{U}$ will not.

From the *B*/*A* against *A* curve, we know that the binding energy per nucleon in the uranium region is about 7 MeV, which is almost equal to the height of the potential barrier opposing fission. Now when a neutron is added to the nucleus of ${}^{235}_{92}\text{U}$, we get ${}^{236}_{92}\text{U}$, i.e., an Even-Even nuclide. The pairing term in mass formula for uranium is about 0.6 MeV $(\sim a_p A^{-3/4} = 0.58\,\text{MeV})$. Thus, we see that thermal neutron capture in ^{235}U (which produces ^{236}U) results in a total energy release of 7.6 MeV and since to cross the potential barrier, only about 7 MeV are spontaneously required, ^{235}U can undergo fission by neutron-capture.

On the other hand, ${}^{238}_{92}\text{U}$ nucleus, after neutron-capture becomes a ${}^{239}_{92}\text{U}$ nucleus, which is an Even-Odd nuclide. Due to the absence of the pairing term for ^{239}U, the fission barrier cannot be crossed. This effect of the pairing term, though small, decides whether thermal neutrons will induce fission or not. Figure 6.1 depicts the influence of the pairing energy on the energy released by neutron-capture in ^{235}U and ^{238}U nuclides.

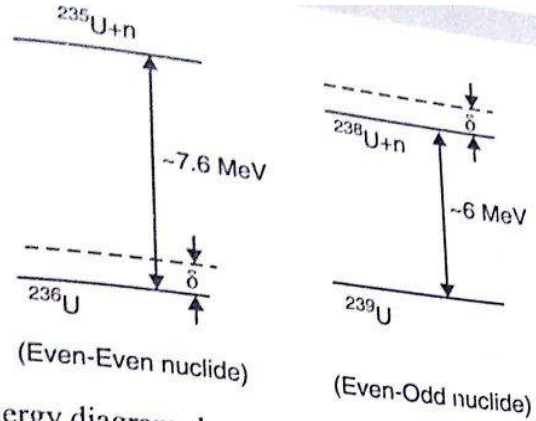

Fig. 6.1. Schematic energy diagram showing effect of the pairing energy term in the mass formula when nuclei of ^{235}U and ^{238}U capture a thermal neutron.

Thus we see that if the height of the fission barrier is lower by even ~1 MeV, the 99.3% abundant isotope ^{238}U would be fissionable under thermal neutrons!

The isotopes ^{233}U and ^{239}Pu behave exactly like ^{235}U as they too are Even-Odd and become Even-Even after slow neutron-capture. Similarly, $^{232}_{90}Th$ would behave like $^{238}_{92}U$, being an Even-Even isotope.

In the language of reaction crosssections, (see Appendix) crosssections for fission by thermal neutrons for $^{235}_{92}U$ and $^{239}_{94}Pu$ are 577 barns and 742 barns, respectively (1 barn = 10^{-24} cm^2).

For $^{238}_{92}U$, neutrons must have an energy of ~ 0.5 MeV, before the crosssection for fission becomes ~ 0.1 barn. If the neutron energy is lower, the potential barrier strongly depresses the crosssection (for ^{238}U) and it is negligible. Thus it should be remembered that for ^{238}U, even though $Q > 0$, the fission crosssection is practically zero.

This was experimentally confirmed by Nier and his fellow workers. Using a mass spectrometer, they separated small quantities of the uranium isotopes ^{235}U and ^{238}U and then subjected them to irradiation by thermal neutrons. They observed that (*i*) there was almost no fission in ^{238}U and (*ii*) there were a large number of fissions for the ^{235}U sample.

In the last chapter we considered symmetric fission in the frame work of liquid drop model treatment for reasons of simplicity. Actually, experiments show that asymmetric fission is far more probable. From the liquid drop model view-point, the isotope distribution of the fission products is quite surprising.

6.3 ASYMMETRICAL FISSION—MASS YIELD

Fission is unsymmetrical, showing that the liquid drop model requires refinements. Figure 6.2 shows a schematic representation of nuclear fission.

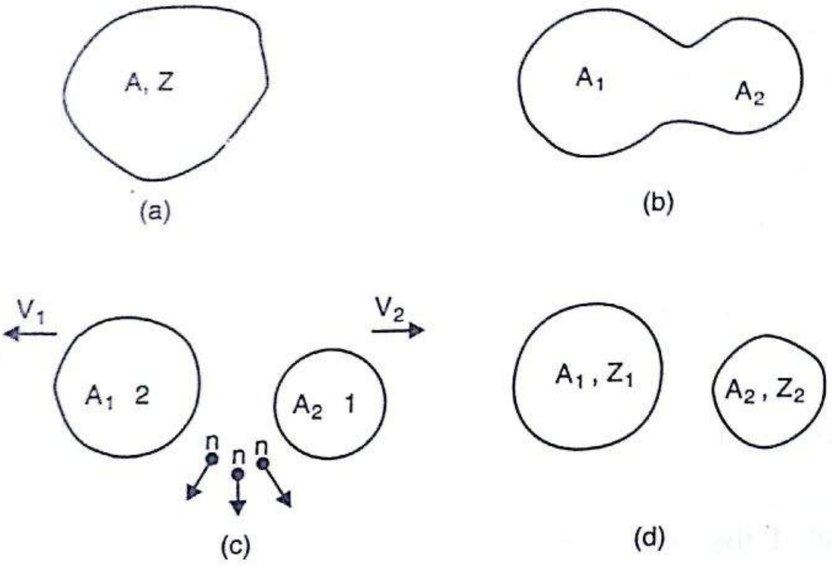
A, Z
(a)
A₁
A₂
(b)
V₁
V₂
A₁ 2
A₂ 1
n
n
n
(c)
A₁, Z₁
A₂, Z₂
(d)

Fig. 6.2. Asymmetrical Nuclear Fission (schematic)

- (*a*) Parent nucleus, considered as a liquid drop.
- (*b*) State before fission.
- (*c*) Neutron rich fission fragments in highly excited states.
- (*d*) Motion of fission fragments and release of prompt neutrons.

The fission results in two massive fission fragments, having equal and opposite momenta. This has been seen in a cloud chamber photograph, which shows two tracks for the two massive fission fragments travelling in almost opposite directions. These fission fragments are neutron-rich, they have too many neutrons to be stable. This is shown in Fig. 6.3. Each fragment may emit one or two neutrons in a period of less than 10^{-15} sec. On an average, about three neutrons are emitted per fission of uranium. These neutrons are called 'prompt' neutrons, shown in Fig. 6.2. Thus, for example, in a fission of ^{235}U nucleus we may consider the nuclear reaction as:

$$ {}^{235}_{92}\mathrm{U} + {}^{1}_{0}n \rightarrow \underset{\text{Compound nucleus}}{\left[{}^{236}_{92}\mathrm{U}\right]^{*}} \rightarrow {}^{143}_{56}\mathrm{Ba} + {}^{90}_{36}\mathrm{Kr} + \underset{\text{'Prompt' neutrons}}{3\,{}^{1}_{0}n} \qquad \ldots(6.1) $$

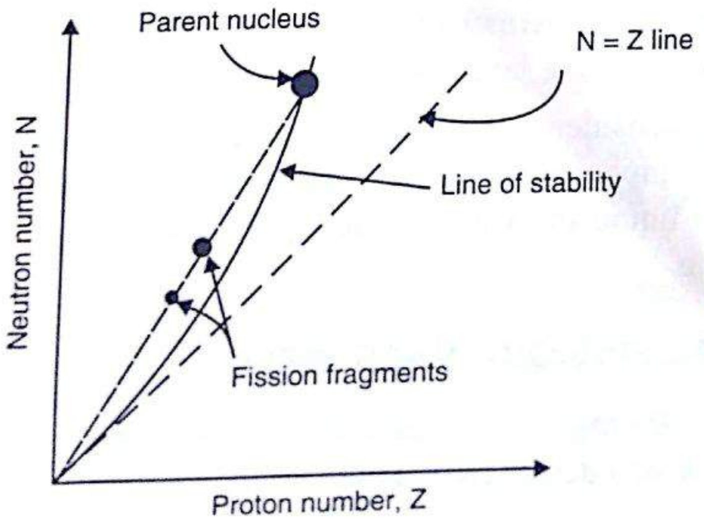
Parent nucleus
N = Z line
Line of stability
Neutron number, N
Fission fragments
Proton number, Z

Fig. 6.3. Diagram showing how fission fragments are neutron-rich.

The stable isotope of barium with maximum A is ^{138}Ba. Similarly, the stable isotope of Krypton with maximum A is ^{86}Kr.

Thus, we conclude that these fission fragments must exhibit much beta-activity to get rid of their excess neutrons. Experimentally, this is confirmed by the following beta decay observations:

$$
\begin{aligned}
{}^{143}_{56}Ba &\rightarrow {}^{143}_{57}La + \overline{\beta} + \overline{\upsilon}\\
&\rightarrow {}^{143}_{58}Ce + \overline{\beta} + \overline{\upsilon}\\
&\rightarrow {}^{143}_{59}Pr + \overline{\beta} + \overline{\upsilon}\\
&\rightarrow \underset{\text{(stable)}}{{}^{143}_{60}Nd} + \overline{\beta} + \overline{\upsilon}
\end{aligned}
\qquad \ldots(6.2)
$$

and

$$
\begin{aligned}
{}^{90}_{36}Kr &\rightarrow {}^{90}_{37}Rb + \overline{\beta} + \overline{\upsilon}\\
&\rightarrow {}^{90}_{38}Sr + \overline{\beta} + \overline{\upsilon}\\
&\rightarrow {}^{90}_{39}Y + \overline{\beta} + \overline{\upsilon}\\
&\rightarrow \underset{\text{(stable)}}{{}^{90}_{40}Zr} + \overline{\beta} + \overline{\upsilon}
\end{aligned}
\qquad \ldots(6.3)
$$

Equation 6.1 gives only one of the many ways in which a nucleus of ^{235}U undergoes fission. It is found that there are more than 30 modes of fission, in each of which a different pair of nuclei (fission fragments) is formed. Equations. 6.2 and 6.3 are examples of a *fission chain*. There are about 60 such chains known experimentally.

The fission yield $Y(A)$ is defined as:

$$Y(A) = \frac{\text{Number of nuclei of mass number } A\text{, formed in fission}}{\text{Total number of fissions}} \times 100\% \qquad \ldots(6.4)$$

$$= \frac{N_A}{N_0} \times 100\%$$

When this percentage of fission yield is plotted against mass number A for fission chains of ^{235}U, we get a mass distribution of fission fragments, as shown in Fig. 6.4.

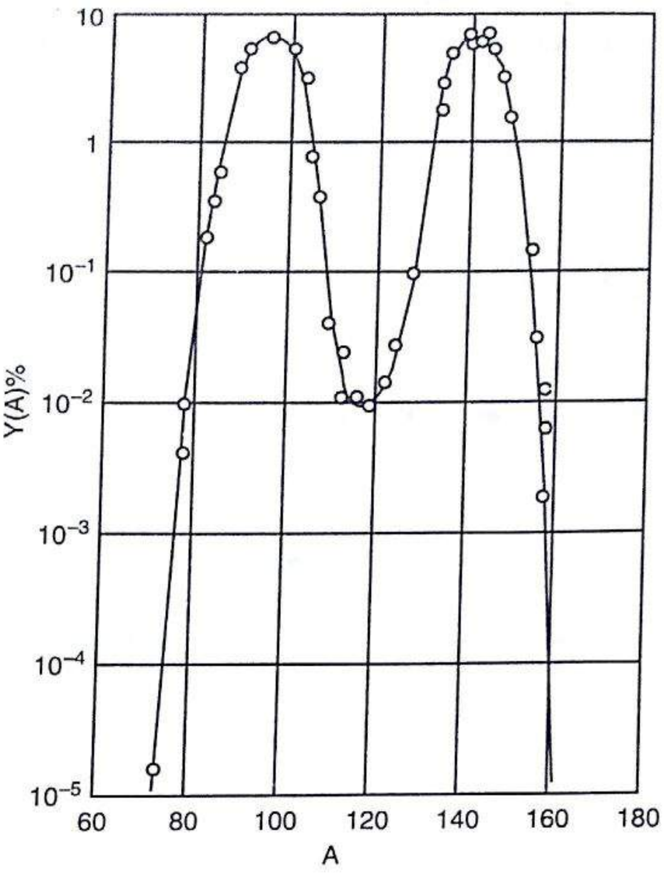

Fig. 6.4. Mass distribution of fission fragments for different fission chains of $^{235}_{92}$U.

It is clear from Fig. 6.4 that the most probable values for the mass numbers of the two fission fragments are about 95 and 139. Notice that the yield is minimum for $A \sim 117$, which corresponds to symmetrical fission (equal masses).

This just cannot be understood on the basis of a liquid drop model of nucleus. The asymmetrical mass distribution of the fission fragments involves the shell structure of nuclei, as expressed in the existence of magic numbers.

Notice that for $A \sim 95$ and 139 (peaks in Fig. 6.4) the corresponding atomic numbers are, $Z \sim 42$ and 57.

On the other hand, for $A \sim 117$ (minimum yield in Fig. 6.4) the corresponding Z value is $Z \sim 50$, which corresponds to a magic number (see Chapter 7, the shell model of a nucleus). $Z \sim 50$ is a magic number and so its nuclear binding is strong, corresponding to a filled nucleonic shell. Hence, the fission yield must be minimum. We, therefore, see that for uranium, asymmetrical fission is more probable.

6.4 EMISSION OF DELAYED NEUTRONS BY FISSION FRAGMENTS

In addition to the 'prompt' neutrons, the process of fission also gives rise to the emission of what are called delayed neutrons. As seen in the last section, fission fragments beta decay since they neutron-rich. Neutron emission would occur if in the process of beta decay, the product nucleus re left in an excited state with an energy more than the binding energy of a neutron in that cleus. However, this neutron emission follows the beta decay of the preceding nucleus, and so neutron activity of a sample will have the same apparent half-life as the beta activity of the

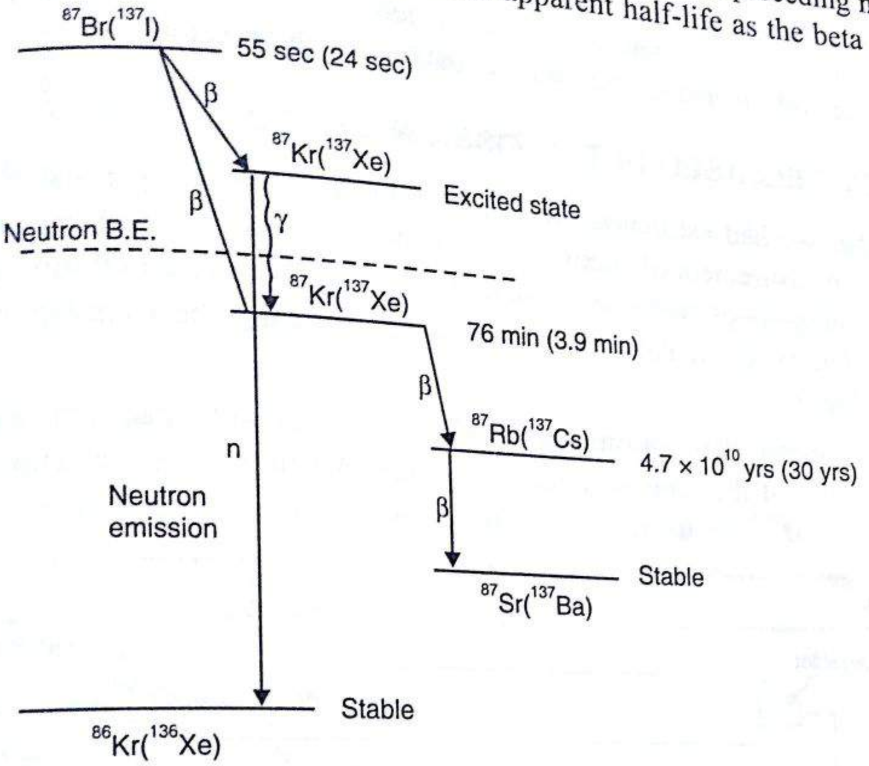
^{87}Br(^{137}I)
55 sec (24 sec)
β
^{87}Kr(^{137}Xe)
Excited state
β
γ
Neutron B.E.
^{87}Kr(^{137}Xe)
76 min (3.9 min)
β
^{87}Rb(^{137}Cs)
4.7 × 10^{10} yrs (30 yrs)
n
Neutron emission
β
Stable
^{87}Sr(^{137}Ba)
Stable
^{86}Kr(^{136}Xe)

Fig. 6.5. Emission of delayed neutrons.

arent nuclide. This type of neutron emission is called *delayed neutron emission* and the neutrons mitted are called *delayed neutrons*. Figure 6.5 shows the nuclear decay scheme for fission agments ^{87}Br and ^{137}I for delayed neutrons by A.H. Snell and his co-workers.

Since the delayed neutrons play an important part in maintaining a chain reaction, they have een intensively studied, particularly for ^{235}U fission. The results are shown in Table 6.1.

TABLE 6.1: Delayed Neutrons for ^{235}U Fission

Half-life (sec)	*Neutron energy (keV)*	*Yield, relative to total neutron emission (%)*
55.00	250	0.025
24.00	560	0.166
4.51	430	0.213
1.52	620	0.241
0.43	420	0.085
0.05	–	0.025
Total Yield		0.754

It can be seen from the Table 6.1 that the total yield (relative to total neutron emission) of delayed neutrons is close to 1% with half-lives of the order of seconds. Though the number of delayed neutrons is quite small, they are a great advantage because of their delays, as reflected in the "apparent" half-lives of several seconds. In a nuclear reactor, these delayed neutrons prevent very rapid changes in neutron density, when the condition of the operation is close to critical. This effectively increases the "time constant" of the reactor.

6.5 ENERGY RELEASED IN THE FISSION OF ^{235}U

In the last chapter, we had estimated the energy released in a symmetrical fission of uranium nucleus. Accurate measurement of energies of fission fragments was made by Leachman in 1952. He measured the velocities of the fission fragments from thermal neutron fission of ^{235}U, by a time-of-flight method. The experimental arrangement is schematically shown in Fig. 6.6 and the results are displayed by Fig. 6.7.

The fissionable material is put on a thin nickel foil and placed near one end of the time-of-flight tube. The length of the tube is about 3.5 metres. A scintillation detector is placed at each end, pulses are amplified and then fed to an oscilloscope. Slow neutrons from a nuclear reactor induce fission. When fission occurs, one fission fragment travels about ~1 cm and produces a pulse while the other fission fragment travels about ~3.5 m and produces a pulse. The oscilloscope is used to determine the time interval between these pulses. Figure 6.7 shows the distribution of velocities of the fission fragments for ^{235}U. From the values of the velocities, the total kinetic energy of the fission fragments works out to be ~ 166 MeV. Table 6.2 gives the complete energy distribution when a ^{235}U nucleus undergoes fission by a thermal neutron.

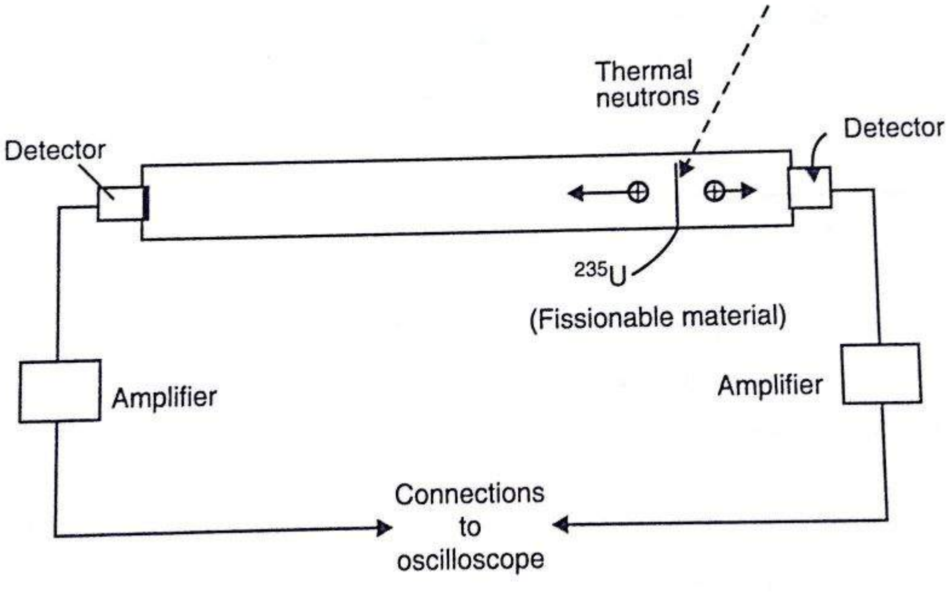

Fig. 6.6. Apparatus (schematic) used to measure velocities of fission fragments by a time-of-flight method.

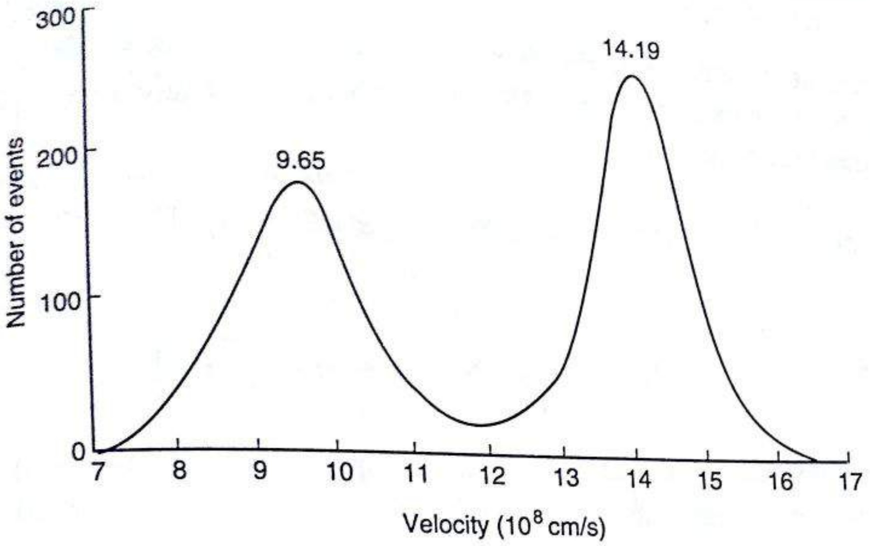

Fig. 6.7. Velocity distribution of fission fragments of ^{235}U.

TABLE 6.2: Energy Liberated by a Fission of ^{235}U Nucleus

Distribution of energy	*Energy, MeV*
Kinetic Energy of Fission Fragments	166
Total Kinetic energy of fission neutrons (2.5 neutrons per fission carry ~2 MeV each)	5
Gamma rays emitted in fission	7
Gamma rays, beta rays, neutrons emitted in the decay of fission fragments	21
Total Energy per fission	199

6.6 FISSION OF LIGHTER NUCLEI

In 1951, Batzel and Seaborg bombarded ^{63}Cu by high energy protons from a cyclotron and looked for ^{38}Cl as one of the products. ^{38}Cl shows beta activity with a half-life ~37 mins. When proton energy crossed ~60 MeV, they detected ^{38}Cl. With increasing bombarding energy, the crosssection for ^{38}Cl production increased. One way in which ^{38}Cl could be produced is the reaction:

$$^{63}\text{Cu} + p \rightarrow {}^{38}\text{Cl} + {}^{25}\text{Al} + n \qquad \ldots(6.5)$$

Another fission product of ^{63}Cu investigated by Batzel and Seaborg was ^{24}Na, which gets formed in the fission reaction,

$$^{63}\text{Cu} + p \rightarrow {}^{24}\text{Na} + {}^{39}\text{K} + n \qquad \ldots(6.6)$$

The proton energy threshold for this reaction is ~50 MeV.

ILLUSTRATIVE EXAMPLE

Example 6.1: Spallation reaction is the name given to a nuclear reaction in which several light particles are emitted. For example, when ^{63}Cu is bombarded by energetic protons, the following spallation reactions may take place:

$$^{63}\text{Cu} + p \rightarrow {}^{38}\text{Cl} + p + n + 6\left({}^{4}_{2}\text{He}\right) \quad \ldots(i)$$

or

$$^{63}\text{Cu} + p \rightarrow {}^{24}\text{Na} + p + 3n + 9\left({}^{4}_{2}\text{He}\right) \quad \ldots(ii)$$

Calculate thresholds for the above reactions and compare them with thresholds given for fission reactions, given by Eqs. 6.5 and 6.6. Given for (*i*) $Q = -108$ MeV and for (*ii*) $Q = -167$ MeV.

Solution: (*i*) $Q = -108$ MeV

Now $$E_{\text{threshold}} = -Q\left(\frac{M_i + m_i}{M_i}\right) \quad \text{(see Chapter 3)}$$

$$= (-108)\left(\frac{64}{63}\right)$$

$$\sim 110 \text{ MeV}$$

by putting $M_i \sim 63$ and $m_i \sim 1$.

(*ii*) $Q = -167$ MeV

$$\therefore \quad E_{\text{threshold}} = (-167)\left(\frac{64}{63}\right)$$

$$\sim 170 \text{ MeV}$$

Thus we see that these spallation reaction thresholds are much higher than the fission reaction thresholds (Eqs. 6.5 and 6.6).

The important conclusion that we can draw from these values of spallation reaction thresholds is that since ^{38}Cl and ^{24}Na nuclei are formed at proton energies less than the spallation threshold, ^{63}Cu nuclei are *fissionable.*

6.7 FISSION CHAIN REACTION

We have seen that the energy released per fission of ^{235}U by thermal neutrons is ~200 MeV pe 235 atomic mass units, i.e., 200 MeV / 235 *u* per *u*.

This energy is about $\sim 16 \times 10^{9} \dfrac{\text{kcal}}{\text{kg}}$.

When this is compared with energy obtained by burning 1 kg of coal, which is ~7200 kcal, e can see the enormous amount of energy released by the process of nuclear fission. Figure .8 graphically illustrates the quantities of different types of fuel, which can supply the same mount of energy.

Can this tremendous energy liberated by the nuclear fission process be tapped? The answer this question depends on whether we can produce a *fission chain reaction* in the laboratory. When a neutron is captured by say a ^{235}U nucleus, there is a good chance of it inducing fission f that nucleus. In the process about 2.5 neutrons (fast, each having an energy ~2 MeV)

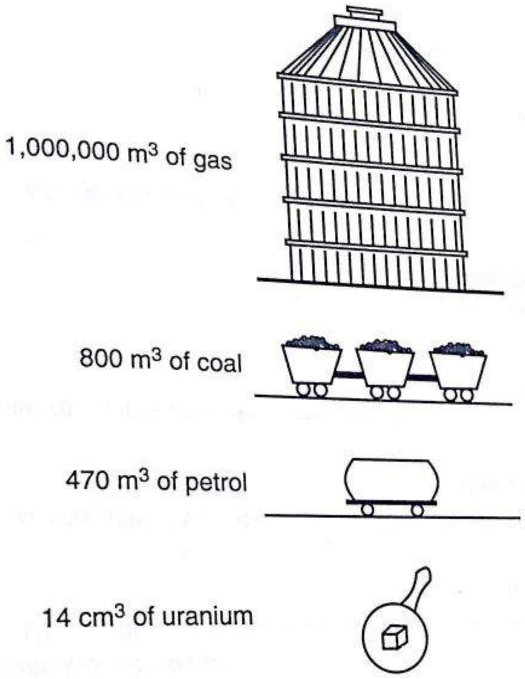

Fig. 6.8. Volumes of different fuels that produce the same amount of energy (heat).

re released. If even one of them slows down and attains thermal energy, it can induce further ssion and the game can continue. *A chain reaction which is just able to sustain itself, occurs for each neutron, on an average, one successor is produced.*

The achievement of a chain reaction with uranium depends on a favourable balance among e following four competing processes:

(*i*) Fission of uranium nuclei with the emission of more neutrons than are captured.

(*ii*) Non-fission capture of neutrons by uranium nuclei.

(*iii*) Non-fission capture of neutrons by materials other than uranium nuclei, e.g., moderator nuclei, structural material, etc.

(*iv*) Escape of neutrons without being captured at all.

It should be realised that to sustain a chain reaction would have been an easy matter if all e 2.5 prompt neutrons released in one fission could have been used to produce further fissions. t this is not so, as neutrons are lost for the purpose of a chain reaction in many ways. If the loss of neutrons by processes (*ii*), (*iii*) and (*iv*) is less than the surplus produced by (*i*) then the chain reaction is possible; otherwise it cannot be sustained.

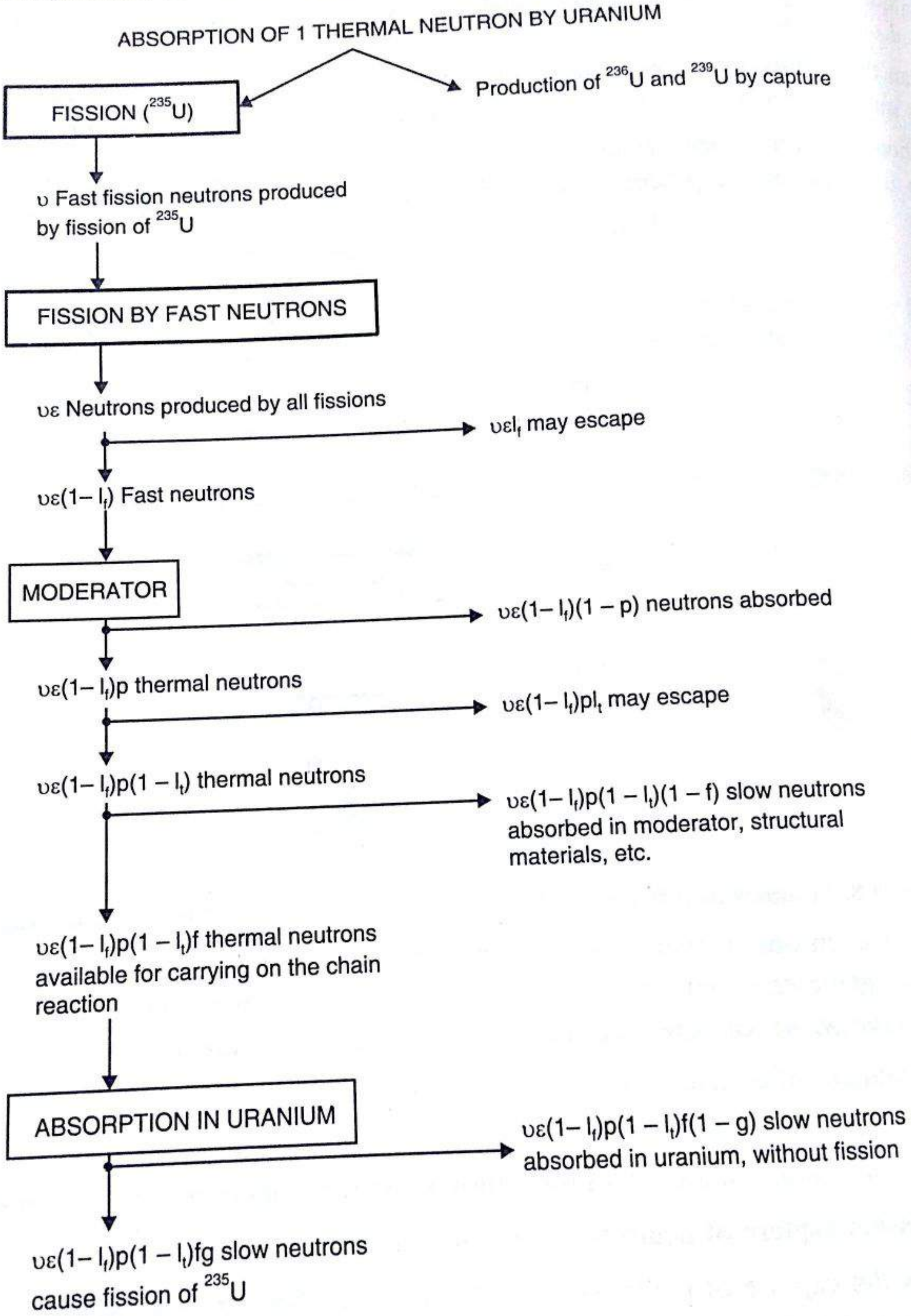
ABSORPTION OF 1 THERMAL NEUTRON BY URANIUM
FISSION (^{235}U)
Production of ^{236}U and ^{239}U by capture
υ Fast fission neutrons produced by fission of ^{235}U
FISSION BY FAST NEUTRONS
$\upsilon\varepsilon$ Neutrons produced by all fissions
$\upsilon\varepsilon l_f$ may escape
$\upsilon\varepsilon(1-l_f)$ Fast neutrons
MODERATOR
$\upsilon\varepsilon(1-l_f)(1-p)$ neutrons absorbed
$\upsilon\varepsilon(1-l_f)p$ thermal neutrons
$\upsilon\varepsilon(1-l_f)pl_t$ may escape
$\upsilon\varepsilon(1-l_f)p(1-l_t)$ thermal neutrons
$\upsilon\varepsilon(1-l_f)p(1-l_t)(1-f)$ slow neutrons absorbed in moderator, structural materials, etc.
$\upsilon\varepsilon(1-l_f)p(1-l_t)f$ thermal neutrons available for carrying on the chain reaction
ABSORPTION IN URANIUM
$\upsilon\varepsilon(1-l_f)p(1-l_t)f(1-g)$ slow neutrons absorbed in uranium, without fission
$\upsilon\varepsilon(1-l_f)p(1-l_t)fg$ slow neutrons cause fission of ^{235}U

Fig. 6.9. The neutron cycle in a fission chain reaction.

6.8 NEUTRON CYCLE IN A THERMAL NUCLEAR REACTOR

An assembly of nuclear fuel and moderator which is able to sustain a chain reaction is ca nuclear reactor. An arrangement to control the chain reaction, so that it does not become dive is an integral part of a nuclear reactor. Figure 6.9 presents a schematic account of what happens to the neutrons in the course of a fission chain reaction in a homogeneous nuclear reactor. A homogeneous nuclear reactor is one in which the fuel is homogeneously mixed with a moderating material used to slow down neutrons to thermal energies. The fuel may be, for example, a mixture of the uranium isotopes ^{235}U and ^{238}U, and the moderator may be for example heavy water, D_2O or graphite, C.

Let us consider the neutron cycle in a fission chain reaction with reference to Fig. 6.9. υ fast neutrons are produced due to thermal neutron fission of a ^{235}U nucleus. Some of them can cause further fission of uranium nuclei. Such additional fission depends on whether the fission neutrons can collide with uranium nuclei before colliding with moderator nuclei. A small fraction of neutrons can cause fission and this results in some additional neutrons. The total number of fast neutrons thus becomes $\upsilon\varepsilon$, where ε is called as the *fast fission factor*. ε is close to 1, since the crosssections for uranium fission by fast neutrons are very small usually $\varepsilon \sim 1.03$. This effect which is ~3% is important for neutron balance in a chain reaction.

These $\upsilon\varepsilon$ fast neutrons diffuse in the assembly and most of them are slowed down by the collision with moderator nuclei. A fraction l_f of neutrons escapes before being slowed down. The remaining $\upsilon\varepsilon\,(1 - l_f)$ fast neutrons are slowed down by the moderator, but during the slowing down process some of the neutrons may be captured by ^{238}U to form ^{239}U, which then β-decays.

$$\left({}^{239}_{92}\mathrm{U}\right)^{*} \xrightarrow{\beta^-} {}^{239}_{93}\mathrm{Np} \xrightarrow{\beta^-} {}^{239}_{94}\mathrm{Pu} \qquad \ldots(6.7)$$

This neutron capture reaction, ${}^{238}_{92}\mathrm{U} + n \rightarrow \left({}^{239}_{92}\mathrm{U}\right)^{*}$ is a resonance reaction. Whenever neutron energy corresponds to one of the energy states of the excited compound nucleus $\left({}^{239}_{92}\mathrm{U}\right)^{*}$, it gets readily absorbed. Therefore, of the $\upsilon\varepsilon\,(1 - l_f)$ fast neutrons which start the slowing down process a fraction $\upsilon\varepsilon\,(1 - l_f)p$ escapes resonance capture by ^{238}U. The remaining fraction $\upsilon\varepsilon\,(1 - l_f)(1 - p)$ is captured and goes to form ${}^{239}_{94}\mathrm{Pu}$ as per Eq. 6.7. The quantity p is called the *resonance escape probability*. Although we lost some neutrons by absorption in ^{238}U, we can derive solace from the fact that they go to form ^{239}Pu, for which, as we have seen, the crosssection of thermal neutron fission is very high.

Thus we have $\upsilon\varepsilon\,(1 - l_f)\,p$ neutrons, which have escaped resonance absorption in ^{238}U, reduced to thermal energies (~0.025 eV) by collisions with the moderator nuclei. Of these a fraction l_t may escape the system. The remaining thermal neutrons are $\upsilon\varepsilon\,(1 - l_f)p(1 - l_t)$. Not all these neutrons are available for carrying on a chain reaction. If a fraction f is absorbed in uranium, the fraction $(1 - f)$ is absorbed in materials other than uranium, such as the moderator, structural materials, etc. and these neutrons are lost. Therefore, the number of thermal neutrons still available for carrying on the chain reaction is:

$$\upsilon\varepsilon(1-l_f)p(1-l_t)f$$

The quantity f is called thermal utilisation factor. Again, not all the neutrons absorbed in uranium cause fission of ^{235}U nuclei. Some of the neutrons are absorbed by ^{235}U to form ^{236}U. The fraction of thermal neutrons absorbed in uranium that produces fission of ^{235}U is;

$\dfrac{\sigma_f(U)}{\sigma_a(U)}$, where $\sigma_f(U) =$ Fission cross section of ^{235}U

and $\sigma_a(U) =$ Absorption cross section of ^{235}U to form ^{236}U.

For ^{235}U, (thermal neutrons)

$$\frac{\sigma_f}{\sigma_a} \sim 0.84 \qquad \text{...(6.8)}$$

$\therefore$ $\sigma_f \sim 576$ barns and $\sigma_a \sim 680$ barn.

$$(\sigma_a = \sigma_f + \sigma_{\text{capture}})$$

Let us define a factor k such that

$k =$ Number of second generation fissions in ^{235}U per fission of ^{235}U by a first generation neutron

$$= \frac{\text{Number of neutrons in the } (n+1)^{\text{th}} \text{ generation}}{\text{Number of neutrons in the } n^{\text{th}} \text{ generation}} \qquad \text{...(6.9)}$$

Then we have:

$$k = \upsilon\varepsilon(1-l_f)p(1-l_t)f\,\frac{\sigma_f(U)}{\sigma_a(U)} \qquad \text{...(6.10)}$$

k is called as the *reproduction factor* or *multiplication factor.*

Now, $$\upsilon\frac{\sigma_f(U)}{\sigma_a(U)} = \eta \qquad \text{...(6.11)}$$

= Number of fast fission neutrons produced per thermal neutron absorbed in uranium (to produce fission).

$$k = \eta\varepsilon p f(1-l_f)(1-l_t) \qquad \text{...(6.12)}$$

Equation 6.12 gives k corresponding to an assembly of finite size. It can be seen that,

$k = 1$ corresponds to a chain reaction operating in a *steady state*. The size of the assembly for $k = 1$, is referred to as the *critical size.*

$k < 1$ no chain reaction is possible. This is called the *sub-critical size.*

$k > 1$ corresponds to a chain reaction in which the number of neutrons in a given generation is more than that in the previous generation, i.e., fissions increase from cycle to cycle and we get a *divergent chain reaction*. This is known as the *super-critical size.*

The first step in the theory and design of a nuclear reactor is to calculate the value of multiplication factor k for an infinitely large assembly. As there can be no leakage of neutrons, Eq. 6.12 reduces to,

$$k_\infty = \eta \varepsilon p f \qquad \text{...(6.13)}$$

Equation 6.13 is the so-called *four-factor formula.*

TABLE 6.3: Cross Sections for Thermal Neutrons (in barns)

Element	σ_{abs}	$\sigma_{fission}$	$\sigma_{capture}$	$\sigma_{scattering}$
^{1}H	0.33	—	—	20.4
^{2}H(D)	0.46×10^{-3}	—	—	7
^{12}C	4×10^{-3}	—	—	4.8
^{232}Th	7.6	~ 0	7.3	—
^{233}U	581	527	54	—
^{235}U	680	576	104	—
^{238}U	2.8	~ 0	2.7	—

[Notice that ^{1}H, σ_{abs} is appreciable and hence it cannot be very useful as a moderator. Compare this with ^{2}H and ^{12}C. ($\sigma_{abs} = \sigma_{fission} + \sigma_{capture}$)]

k_∞ is the multiplication factor for an infinitely extended nuclear reactor.

Note that,

$$k = (1 - l_f)(1 - l_t)k_\infty \qquad \text{...(6.14)}$$

From Eq. 6.8, for pure ^{235}U (see Table 6.3)

$$\eta = \upsilon \frac{\sigma_f}{\sigma_a} \sim 2.5 \times 0.8 \sim 2.1 \qquad \text{...(6.15)}$$

Thus we see that η is somewhat smaller than υ.

For natural uranium one finds:

$$\eta \sim 1.3 \qquad \text{...(6.16)}$$

It is worth mentioning here that for pure ^{235}U, $\eta > 1.3$ *for all neutron energies.* It is this at makes a nuclear bomb possible.

We will see in the next section that p, the resonance escape probability, is greatly increased a heterogenous arrangement of the uranium fuel in the moderator.

The thermal utilisation factor f depends strongly on the ratio of number of atoms of fuel and moderator. For example in a homogenous reactor using natural uranium as fuel and carbon as moderator,

$$f = \frac{N_U \sigma_{ab}(U)}{N_U \sigma_{ab}(U) + N_C \sigma_{ab}(C)} \quad \ldots(6.17)$$

where $N_U \rightarrow$ uranium atoms and $N_C \rightarrow$ carbon atoms.

Table 6.4 shows numerical values for constants p, f and k_∞ for different ratios N_C/N_U. For this calculation Table 6.3 is used.

TABLE 6.4

N_C/N_U	p	f	k_∞
0	0	1	0
100	0.50	0.96	0.64
400	0.72	0.85	0.82 (nearly Max)
1000	0.88	0.69	0.80
∞	1	0	0

Note in Table 6.4 that for pure uranium, the resonance escape probability $p \sim 0$, since for the compound nucleus of ^{239}U, between 6 eV and 70 eV, there is a rather high capture probability for neutron. Thus, slowing down neutrons with a moderator is a very fortunate step that increases p. Also note how k_∞ reaches a maximum value of 0.82. This certainly is not sufficient to sustain a chain reaction.

It is found that by using heavy water as a moderator, $k_\infty \sim 1.15$, for a homogenous reactor using natural uranium and it is possible to sustain a chain reaction. *Most favourable values* of k_∞ for homogeneous mixtures of natural uranium for different moderators are given in Table 6.5.

TABLE 6.5

Moderator	*Molecules of moderator* / *Atoms of uranium*	p	f	k_∞
H_2O	2.43	0.755	0.828	0.838
D_2O (heavy water)	167	0.910	0.955	1.145
C	452	0.757	0.837	0.849

From Table 6.5, one can see that with natural uranium as the fuel, a homogenous reactor can be operated *only with heavy water as moderator*. If other moderators are used then the fuel must be *enriched* in ^{235}U.

We conclude this discussion by emphasising, that of the four factors—

(*i*) η depends on nuclear properties of the fuel.

(*ii*) ε depends on nuclear properties of the fuel, as well as its size and shape.

(*iii*) p and f depend on nuclear properties of the fuel, moderator and as we will see, also on the way all these materials are arranged.

The basic design problem is to find the optimum amount of (see Table 6.4) all the materials and the way in which they can give largest value of *p.f.* For a given fuel, this arrangement gives the maximum value of k_∞.

6.9 NUCLEAR REACTORS

The design, construction and operation of a nuclear reactor are today part of a huge and expanding field of nuclear engineering. In this section, we will acquaint ourselves with the features of different types of reactors. However, the detailed calculation of critical size or critical mass of a nuclear reactor is beyond the scope of this book.

The power level at which a reactor operates is proportional to the rate of fissions, which in turn, depends on the number of neutrons in the reactor. Therefore, by controlling the number of neutrons, we can control the power level of the reactor. For this purpose, it is common to use cadmium rods or steel rods containing boron. Both cadmium and boron have high absorption crosssections for thermal neutrons. This essentially changes the value of reproduction factor k, so that the change makes it possible to operate a reactor at a constant power level. As the reactor operates, fuel is used up. To keep the power level constant, the control rods are moved out of the *reactor core* containing the fissionable material at a suitable rate. Ultimately, there would be a limit for such a compensation when all the control rods are taken out of the reactor core. On the other hand, to reduce power level, the control rods are lowered into the reactor core. By completely lowering the control rods, it is possible to shut down a reactor. The process of reactor control is invariably made automatic, and any possible human error is eliminated.

Uranium ores are found in large quantities throughout the world (0.0005% of the earth's crust). In many reactors, uranium enriched with the isotope ^{235}U is used as fuel. A number of methods are used to produce this enrichment. One of the most common methods is the gaseous diffusion through a porous barrier. Its principle is depicted in Fig. 6.10.

Like natural uranium, ^{232}Th is also found widely in the earth's crust. In fact, the earth's thorium content is ~1.5 times as much as uranium. In India, we are fortunate to have large

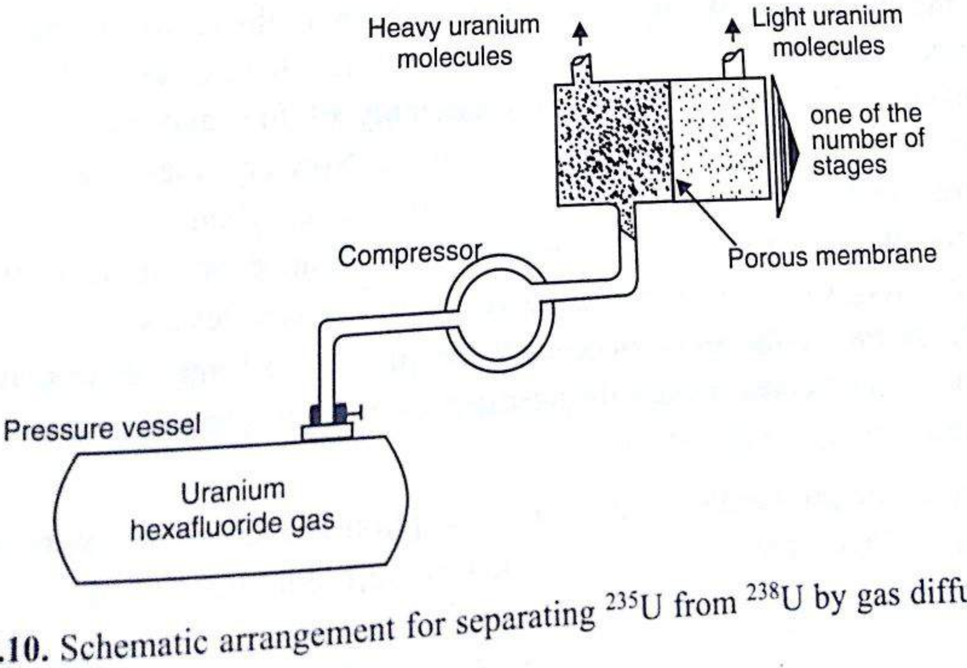

Fig. 6.10. Schematic arrangement for separating ^{235}U from ^{238}U by gas diffusion.

deposits of thorium ore—monazite sands—a phosphate compound of rare earth elements and thorium silicate. A chain reaction cannot be induced in pure ^{232}Th (like ^{238}U), but when it is irradiated by a large flux of neutrons in a nuclear reactor, we get ^{233}U which, like ^{235}U and ^{239}Pu has a large cross-section of fission by thermal neutrons (see Table 6.6).

TABLE 6.6: Cross-section for Fission by Thermal Neutrons

	^{233}U	^{235}U	^{239}Pu
$\sigma_{(\text{fission})}$ (barns)	527	576	742

To convert ^{232}Th into ^{233}U it has to be irradiated by heavy flux of neutrons in a reactor and then as ^{233}U accumulates, it can be used as nuclear fuel.

A homogenous reactor: In a homogenous reactor, the fuel and moderator are uniformly mixed. In the last section, we saw that with natural uranium as fuel, a homogenous reactor can go critical only when heavy water, D_2O, is used as the moderator. For fuel enriched with ^{235}U, ordinary water can be used as the moderator.

One of the common types of homogenous reactors consists of a solution of uranyl nitrate in water. The degree of enrichment of uranium is quite high—one part of ^{235}U to six parts of ^{238}U (For natural uranium this ratio is 1:140). The minimum critical mass of ^{235}U in this case, when a spherical container is used with its wall surrounded by a neutron reflecting material such as graphite, is about 800 gm. If the neutron-reflecting material is not used, the minimum critical mass of ^{235}U works out to ~2 kg.

The minimum critical masses for ^{233}U and ^{239}Pu, work out to about 600 gms and 500 gms respectively.

A heterogenous reactor: To produce enriched uranium is very expensive. So is the production of heavy water. In the absence of enriched uranium, the main problem for a sustained chain reaction is the small value of resonance escape probability (see Tables 6.4 and 6.5). Fermi and Szilard showed a way out of this difficulty. They proposed the use of lumps of uranium embedded in the moderator. We have seen that resonance absorption occurs when neutrons, during the course of slowing down process reach energies that correspond to the levels of the compound nucleus (^{239}U)*. In a homogenous assembly of fuel and moderator, each uranium nucleus has the same chance of capturing the neutrons. Now consider a heterogenous assembly of the fuel lumps embedded in the moderator. In this case, when uranium is present in large lumps, each uranium nucleus does not have the same chance of capturing the neutrons. The neutrons—with energies corresponding to resonant energy levels of (^{239}U)*—are mostl absorbed *on the surface only,* since once they are inside the lump of uranium, their energie do not change much, and consequently they escape resonant absorption. (Remember that uraniu is a very poor moderator of neutrons!)

In other words, the probability of neutron absorption inside the uranium lump is much l than at the surface. This effect is often described as 'self-shielding' of uranium against neut resonance-absorption.

Once out of the uranium lump, a neutron enters a zone containing moderator (uranium free one). In this region, it undergoes collisions with the moderator nuclei and its energy gets reduced onsiderably. This process enables the neutrons to skip several resonance absorption levels, before hey are confronted with the next uranium lump, where again, the resonance absorption is mostly estricted to the surface region only. To summarise this discussion, let us enlist the effects of he important invention of lumping fuel in moderator.

(*i*) It increases ε, the fast fission factor as the probability of fast neutron fission of uranium in a lump, which is moderator free, increases. $\varepsilon \sim 1.1$, an increase of 10%.

(*ii*) ^{238}U strongly resonance absorbs neutrons, and it is therefore desirable to accomplish the moderation of neutrons in a region free of uranium.

(*iii*) Resonance-absorption in uranium occurs essentially on the surface of the uranium lump and so, uranium inside a lump does not tend to lower the resonance escape probability *p*. This implies that we have large lumps in which surface layer volume is small compared to the total volume.

(*iv*) On the other hand, large volume lumps of uranium tend to lower the thermal utilisation factor because the neutron density in or near the lumps tends to be less than in the moderator, a situation which favours neutron absorption in the moderator. This is an undesirable situation.

Clearly, a compromise must be arrived at for the requirements (*iii*) and (*iv*).

ILLUSTRATIVE EXAMPLES

Example 6.2: Calculate the amount of energy available if 50 gm of ^{235}U is completely fissioned.

Solution: Energy released per fission of ^{235}U nucleus

$$= 200 \text{ MeV}$$

$$= 3.2 \times 10^{-11} \text{ watt-sec.}$$

50 gm of ^{235}U contain, $\dfrac{50}{235} \times 6.02 \times 10^{23}$ nuclei

$$= 1.28 \times 10^{23} \text{ nuclei}$$

$\therefore$ 50 gm of ^{235}U will release an amount of energy

$$= (1.28 \times 10^{23}) \times (3.2 \times 10^{-11} \text{ W.s.}) = 4.1 \times 10^{12} \text{ W.s}$$

$$= 0.5 \times 10^{2} \text{ mega watt-day}$$

Example 6.3: What is the physical meaning of the multiplication factor *k*? How many neutrons will there be in the hundredth generation if the fission process starts from 1000 neutrons and $k = 1.05$?

Solution: See Eq. 6.9

$$k = \frac{\text{Number of neutrons in the } (n+1)^{\text{th}} \text{ generation}}{\text{Number of neutrons in the } n^{\text{th}} \text{ generation}}$$

∴ Number of neutrons in the hundredth generation are,

$$\begin{aligned} N &= 1000 \times k^{(100-1)} \\ &= 1000 \times (1.05)^{99} \\ &= 1.25 \times 10^{5} \end{aligned}$$

Breeder Reactor: The fissionable materials in a reactor are ^{235}U, ^{239}Pu and ^{233}U, none of which is available naturally in large quantities. It would not be feasible to get power on a large scale from the fission of ^{235}U because only 0.7% or less of the available uranium could be used directly. Plutonium is made by the fission of ^{235}U in a reactor containing ^{238}U, a tedious and expensive process. Similarly ^{233}U, which does not occur in nature, can be made in a reactor containing ^{232}Th. Although the problem of availability and cost of nuclear fuels is a serious one, a unique and remarkable solution is possible because of one of the nuclear properties of the fission process. This property is the emission, on the average, *of more than two neutrons per fission.*

Suppose that three neutrons are emitted per fission. One of these is needed to keep the reaction going to induce fission in another fuel atom, say an atom of ^{235}U. Of the two neutrons left, one may be used to convert an atom of uranium to one of Plutonium, leaving one neutron. If this last neutron could be used to produce another atom of ^{239}Pu, one atom of ^{235}U would have been used and two atoms of ^{239}Pu would be produced, leaving a profit of one atom of fissionable material. In other words, more fissionable material would be produced than consumed. This process is called *breeding*. This example is an oversimplified one because it is inevitable that some neutrons should be lost by leakage or by non-fission absorption.

If the principle of breeding could be made to work, a reactor could make new fuel for itself and, in addition, a stockpile of fissionable material could be built up for use in new reactors.

The process of breeding fissionable material depends on two materials, one fissionable and the other fertile. ^{238}U and ^{239}Pu form one such pair and ^{232}Th and ^{233}U another pair. Consider the first pair and suppose that enough ^{239}Pu is available to achieve a chain reaction in a system which can be used to produce power. The thermal fission of ^{239}Pu yields three neutrons, so that if some of these neutrons could be absorbed in ^{238}U to form more ^{239}Pu, a breeding cycle might be achieved. In this case, ^{238}U is the fertile material because although it is not itself usefully fissionable, it can be converted into a good fissionable material. The nuclear property that determines whether the possibility of breeding exists is not the value of the number of neutrons emitted per fission, υ, but the number produced per neutron absorbed in the fuel, η, because the non-fission capture of neutron by the fuel can be large enough to interfere seriously wit breeding. For thermal neutrons η has values of about 2.1 and 1.94 for ^{235}U and ^{239}Pu, respectively This would indicate that ^{235}U fuel would yield higher production rates. In fact, since η is greate than 2, it is possible to produce more fuel than is consumed.

It is expected on theoretical grounds that the ratio of the fission cross-section to the tot absorption crosssection should be closer to unity at high neutron energies than for slow neutron and that η should be close to υ in a fast reactor. Consequently, breeding of ^{239}Pu should b possible in a fast neutron, ^{239}Pu—^{238}U system. The Experimental Breeder Reactor (EBR) h been built to study the feasibility of power production and breeding in precisely such a system

EXERCISES

1. Explain how the liquid drop model of the nucleus enables us to understand, why ^{235}U undergoes fission if it captures a thermal neutron, whereas ^{238}U does not?
2. The Q-value for fission reaction is > 0 for ^{238}U. What prevents ^{238}U from undergoing spontaneous fission?
3. How does one understand asymmetrical fission? Sketch the mass distribution of fission fragments for different fission chains of ^{235}U.
4. What are "prompt" and "delayed" neutrons? Why are there no prompt or delayed protons? Explain the important part played by the delayed neutrons in nuclear reactors.
5. Consider the fission of 1 kg of ^{235}U. Calculate the energy released in kilowatt hours. Compare this energy with energy released by burning 1 kg of coal.
6. $^{235}_{92}U$ photofissions by γ-ray of energy 6 MeV. If the fission fragments are $^{90}_{36}Kr$ and $^{142}_{56}Ba$ and 3 neutrons are given out, then calculate the total kinetic energy of the fission products.
7. Discuss the neutron cycle and possibility of a chain reaction in ^{238}U (natural). Obtain the four-factor formula and describe on what each factor depends. Explain the advantage of "lumping" in a heterogenous reactor.
8. Out of the total energy released in fission of a ^{235}U nucleus about 180 MeV can be used to produce power. If a ^{235}U nuclear reactor is continuously generating a power of 80 MW, how long will it take for 1 kg of the uranium fuel to be used up?
9. Calculate the energy released by the fission reaction given by Eqs. 6.1, 6.2 and 6.3.
10. If in Problem 8, the reactor uses 2.5 kg of fuel in 40 days, calculate the power output in MW.
11. Calculate the binding energy of thermal neutrons added to the following nuclei:

    ^{227}Th, ^{233}U, ^{235}U, ^{239}Pu, ^{238}U, ^{242}Pu.

    Which of these nuclei are fissionable under thermal neutrons?
12. If the fission process starts with 1000 neutrons and the multiplication factor $k = 1.03$, calculate the number of neutrons present in the thousandth generation.
13. A reactor with ^{235}U as fuel operates at a constant power level. Find the fraction of neutrons escaping from the core, if half of the fission neutrons are captured by uranium nuclei and impurity nuclei without causing fission.

    (*Hint:* $k = 1$)
14. Explain why a self-sustaining chain reaction cannot be obtained with ^{238}U (natural) as fuel (except with heavy water as moderator) in a homogenous assembly.

7

The Shell Model of a Nucleus

> "……two sorts of truth: trivialities, where opposites are obviously absurd, and profound truths, recognised by the fact that the opposite is also a profound truth."
>
> —*Niels Bohr*

7.1 INTRODUCTION

In Chapter 5, we discussed the curve of binding energy per nucleon (*B*/*A*) against mass numbe *A* and a passing reference was made about the fact that for nuclei, the binding energy is unusuall high if the number of neutrons or protons are equal to 2, 4, 8, 20, 50, 82 and 126. For example f

$^{140}_{58}$Ce, which contains 82 neutrons,

$$\text{B.E.} = 58M_p + 82M_n - M\left(^{140}\text{Ce}\right)$$

$$= 1172.75\ \text{MeV}$$

i.e.,

$$\frac{B}{A} = 8.377\ \text{MeV}$$

$$\sim 8.38\ \text{MeV}.$$

From the $\frac{B}{A} \to A$ graph, for $A = 140$, $\frac{B}{A} \sim 8.35\ \text{MeV}$.

Thus, we see that the B.E. of ^{140}Ce nucleus, which contains 82 neutrons, is higher by ~ compared to its neighbours, giving a discontinuity in the *B*/*A* → *A* curve.

Large binding energy means high stability. This unusual stability whenever neutron or proton number corresponds to 2, 4, 8, 20, 50, 82 and 126 is also reflected in a number of experimental facts, for example, the isotopes with these numbers of protons and isotones (same number of neutrons) with these numbers of neutrons are found to be much more numerous than other values. The numbers 2, 4, 8, 20, 50, 82 and 126 came to be known as *magic numbers* because for quite a long time, they could not be understood.

Physicists were familiar with "periodicities" existing in atoms because of the atomic shell structure. For atoms, as experiments have shown, there are marked discontinuities in the ionisation potential at regular intervals as a function of the atomic number Z. These, as is well known, occur at the noble gases and correspond to the complete filling of an electronic shell.

It was very tempting for nuclear physicists to devise a nuclear shell model similar to that which has been so successful in explaining the chemical properties of atoms. However, this task is not at all straightforward. For atoms, there is a clear-cut Coulomb force between a nucleus and electrons. On the other hand, for nuclei, there is no obvious central attractive field in which the nucleons might move. There is another grave difficulty, when one calculates the density of "nuclear matter". For a medium size nucleus, $A \sim 100$, volume V is:

$$V = \frac{4}{3}\pi(1.3A^{1/3})^3$$

$$\sim 9 \times 10^{-43}\ \text{m}^3$$

and mass $$M = 1.66 \times 10^{-25}\,\text{kg}.$$

giving nuclear density $$\rho \sim 10^{17}\ \text{kg}\,\text{m}^{-3} \qquad \ldots(7.1)$$

This is a very high value which makes it a formidable task to imagine how nucleons can move about freely in "nuclear matter" which has a density of about 10^{17} kg/m^3.

A shell structure of nucleus implies that nucleons move freely in nuclei similar to electronic motion in atoms. In other words, nucleons must largely move and behave 'independently'.

Despite the difficulties stated above, Bartlett, Guggenheimer et al. proposed an independent particle model (shell model) for the nucleus in 1933. Their approach leant heavily on the analogies of the extra-nuclear electronic structure of atoms. They assumed that each nucleon moves in an rbit characterised by a definite angular momentum and a definite energy, and that it moves ndependently of other nucleons. This assumption is certainly hard to justify in the light of the large uclear density that we have calculated. We will look at this closely in the following sections.

Following the electronic shell-filling process, Bartlett et a1. proposed closed shells of nucleons, ach shell (quantum number l = angular momentum q. no.) containing $2(2l + 1)$ neutrons or rotons. This approach was able to account for only the first three magic numbers—2, 4 and 8 orresponding to ^{16}O).

Physicists lost interest in the shell model because of its failure to explain higher magic mbers, and no significant progress was made between 1936 and 1948 in developing this model.

Perhaps this loss of interest in the shell model was more due to the spectacular success of Bohr's liquid drop model than due to its own failure. We have seen in Chapter 5, how a nucleus can be described as a collection of strongly interacting nucleons behaving in many ways like a drop of liquid. This model was quite successful in explaining nuclear fission and making predictions about the variation of nuclear mass with A and Z (Weizsacher's mass formula, Chapter 5). However, by its very nature, it was not capable of accounting for the discontinuities in binding energy at the magic numbers.

In 1948, Maria G. Mayer forcefully drew the attention of physicists to the growing and compelling experimental evidence for closed shells in nuclei at the magic numbers. The next section is devoted to the survey of this vast, conclusive experimental evidence which the liquid drop model is inherently incapable of accounting for. Attention was thus re-focussed on the independent particle model, or the shell model of a nucleus.

In 1949, Maria Mayer and, independently, Haxel, Jensen and Suess devised a nuclear shell model which was able to account for all the magic numbers with the presumption of strong spin-orbit forces for individual nucleons. The introduction of this *j-j* coupling was a very important step, which resulted in a sequence of independent particle states, matching the experimentally observed 'magic numbers'. Section 7.3 of this chapter deals with this work. We will also see how objections to the independent particle motion in nuclear matter (due to its high density) can be countered by invoking the Pauli Exclusion Principle.

Apart from accounting for the evidence of magic numbers, the shell model is quite successful in predicting, as we will see, the angular momentum of nuclei in their ground state. Its main failures are (*i*) predicting the excited states of nuclei, and (*ii*) accounting for the degree to which many nuclei are non-spherical. This implies that though the shell model represents a nucleus fairly correctly, it is still a simplified picture of the actual state of affairs.

In Sec. 7.9, we will see how it is possible to devise a *collective model* or a *unified model* of a nucleus which provides agreement with a much larger amount of experimental information. In this model, an attempt is made to combine many of the features of the liquid drop model and the shell model. Put slightly differently, this means that shell model features and the collective motions of the nucleons are considered within the same framework. The nucleus is considered to be deformable so that quantised vibrational and rotational energy levels can be formed similar to the vibrational and rotational spectra in the case of molecules.

In the next chapter, we will consider the different ideas regarding the 'nuclear force' which holds nucleons in a nucleus together. We will see that though the exact nature of the nuclear force is not known, there are some very important and useful ideas. Because of our lack of exact knowledge of the nuclear force, the various nuclear models are necessary and useful. No single model, however, is able to explain the vast experimental information that has been gathered about nuclei.

We shall conclude this introduction by stressing that when a nuclear model is able to account for some experimental facts, it is a useful scheme. There is nothing 'wrong' or 'false' about a useful model, when it is unable to account for certain experimental results, as they may be beyond its inherent capabilities. For example, the liquid drop model is totally built on the foundation that "collective" nucleon motion (strong interaction among nucleons) dominates over "individual" nucleon motion. On the other hand, we have the opposite emphasis in the shell model where nucleons are assumed to move completely independently (weak interaction among nucleons). Both these models, though resting on apparently opposite assumptions, are found to be very useful in understanding what actually goes on within the nucleus. The evidence of existence of the magic numbers is beyond the range of a liquid drop model of nucleus. On the other hand, to explain nuclear fission—perhaps the most important reaction in nuclear physics—is a formidable task for a shell model. A model of nucleus which combines features of both these models is clearly what is aimed at explaining a wide range of experimental results.

7.2 THE EVIDENCE THAT LED TO THE SHELL MODEL

(*i*) A careful study of the *B/A* against *A* curve (Fig. 7.1) revealed several kinks. These kinks correspond to a sudden increase in the value of *B/A;* the binding energy per nucleon. Figure 7.1 shows one such study between *A* = 126 and 150.

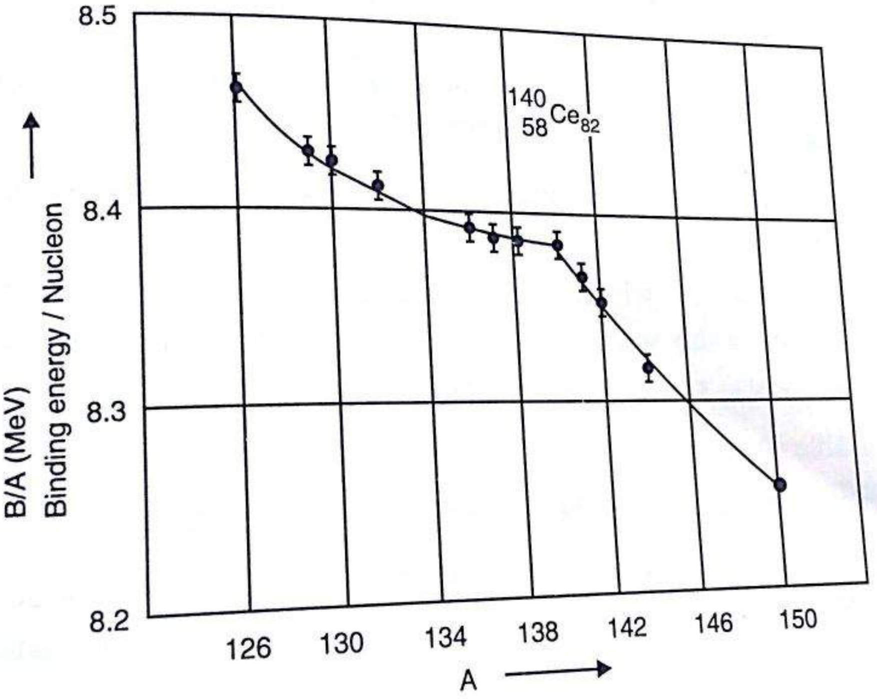

Fig. 7.1. Detail of a portion of *B/A* → *A* curve. Notice the kink at ^{140}Ce, which has 58 protons and 82 neutrons.

These kinks or discontinuities have been found to occur whenever either the neutron number or the proton number or both take the values 2, 8, 20, 50, 82 and 126. Some examples are:

$$ {}^{4}_{2}He_{2},\ {}^{16}_{8}O_{8},\ {}^{88}_{38}Sr_{50} \quad \text{and} \quad {}^{208}_{82}Pb_{82} $$

(*ii*) Stability is of course, related to *high natural abundance*. A table of relative abundances of nuclei compiled from data on the composition of the earth, the sun and the stars have been published by Brown in 1949. Pronounced peaks are found at ^{4}He, ^{16}O, ${}^{40}_{20}Ca_{20}$, ^{120}Sn, ^{140}Ce, ^{208}Pb

confirming the existence of magic numbers. Figure 7.2 shows relative abundances of the isotopes of $_{46}$Pd and $_{42}$Mo, plotted against the neutron number, N. For $_{46}$Pd isotopes, N never equals a magic number and one gets a symmetrical curve as shown in Fig. 7.2 (a). On the other hand, for $_{42}$Mo isotopes, the range of N includes a magic number, $N = 50$. This results in a striking irregularity in the curve as shown in Fig. 7.2 (b). Similar observations are made for other magic numbers too.

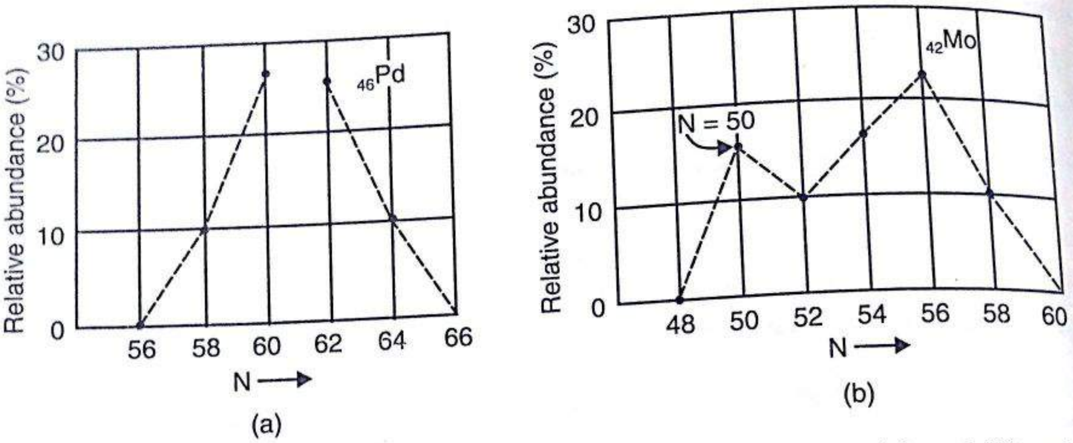

(a)

(b)

Fig. 7.2. Relative abundances of the isotopes of $_{46}$Pd and $_{42}$Mo. Compare (a) and (b) and notice the irregularity occurring at $N = 50$.

(*iii*) Relative stability of different elements is also indicated by the *number of stable isotopes* or *isotones* per element.

$_{50}$Sn has 10 stable isotopes, which is the maximum number of stable isotopes in all the elements ($Z = 50$). Compare this with $_{49}$In and $_{51}$Sb, which have only 2 stable isotopes each.

The neutron number $N = 50$ has 6 stable isotones.

$N = 82$ has 7 stable isotones.

Compare this with the average number of isotones for Even N, which is ~3.

$_{20}$Ca has 5 isotopes spread out over 8 mass numbers (Z = 20). This large spread is unusual for this region in the nuclear chart (Segre chart, see Fig. 5.1) and emphasises an exceptional stability for Z = 20.

(*iv*) ^{208}Pb has $Z = 82$ and $N = 126$, i.e., it is "doubly magic". It is the heaviest stable nucleus. The final product of three of the radioactive series (see Chapter 2) is lead, $Z = 82$, and the most abundant lead isotope is ^{208}Pb. The final product of the neptunium series is ^{209}Bi, which has $N = 126$.

In general, the doubly magic nuclei $^{4}_{2}\mathrm{He}_{2}$, $^{16}_{8}\mathrm{O}_{8}$, $^{40}_{20}\mathrm{Ca}_{20}$ and $^{208}_{82}\mathrm{Pb}_{126}$ are particularl tightly bound.

(*v*) We have described the phenomenon of Nuclear Isomerism in Chapter 4 Part IV. Wh the known long-lived isomers are plotted against proton number Z or neutron number N, we groupings just below the magic numbers. These groupings called islands of isomerism are sho in Fig. 7.3.

confirming the existence of magic numbers. Figure 7.2 shows relative abundances of the isotopes of ${}_{46}$Pd and ${}_{42}$Mo, plotted against the neutron number, N. For ${}_{46}$Pd isotopes, N never equals a magic number and one gets a symmetrical curve as shown in Fig. 7.2 (a). On the other hand, for ${}_{42}$Mo isotopes, the range of N includes a magic number, $N = 50$. This results in a striking irregularity in the curve as shown in Fig. 7.2 (b). Similar observations are made for other magic numbers too.

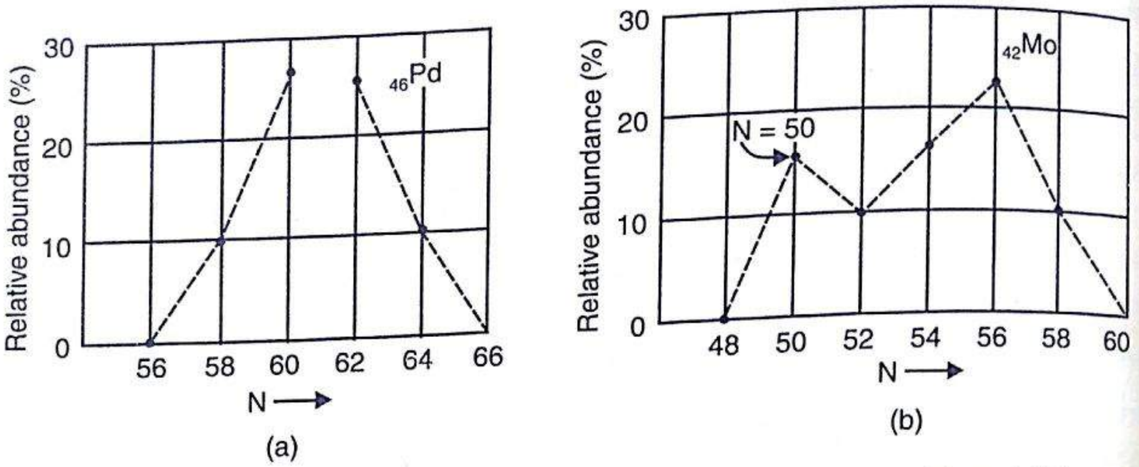

Fig. 7.2. Relative abundances of the isotopes of ${}_{46}$Pd and ${}_{42}$Mo. Compare (a) and (b) and notice the irregularity occurring at $N = 50$.

(*iii*) Relative stability of different elements is also indicated by the *number of stable isotopes* or *isotones* per element.

${}_{50}$Sn has 10 stable isotopes, which is the maximum number of stable isotopes in all the elements ($Z = 50$). Compare this with ${}_{49}$In and ${}_{51}$Sb, which have only 2 stable isotopes each.

The neutron number $N = 50$ has 6 stable isotones.

$N = 82$ has 7 stable isotones.

Compare this with the average number of isotones for Even N, which is ~3.

${}_{20}$Ca has 5 isotopes spread out over 8 mass numbers ($Z = 20$). This large spread is unusual or this region in the nuclear chart (Segre chart, see Fig. 5.1) and emphasises an exceptional tability for $Z = 20$.

(*iv*) ^{208}Pb has $Z = 82$ and $N = 126$, i.e., it is "doubly magic". It is the heaviest stable nucleus. The final product of three of the radioactive series (see Chapter 2) is lead, $Z = 82$, and the nost abundant lead isotope is ^{208}Pb. The final product of the neptunium series is ^{209}Bi, which ias $N = 126$.

In general, the doubly magic nuclei ${}^{4}_{2}\mathrm{He}_2$, ${}^{16}_{8}\mathrm{O}_8$, ${}^{40}_{20}\mathrm{Ca}_{20}$ and ${}^{208}_{82}\mathrm{Pb}_{126}$ are particularly ightly bound.

(*v*) We have described the phenomenon of Nuclear Isomerism in Chapter 4 Part IV. When he known long-lived isomers are plotted against proton number Z or neutron number N, we get roupings just below the magic numbers. These groupings called islands of isomerism are shown n Fig. 7.3.

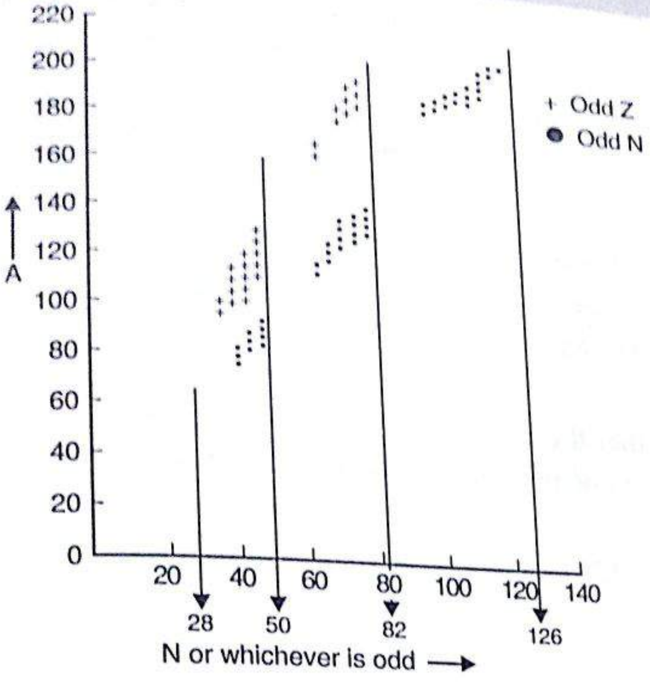

Fig. 7.3. Islands of Isomerism. Distribution of long-lived isomers in Odd A nuclei. [M. Goldhaber and J. Weneser, Ann. Rev. Nucl. Sc. 5, 1 (1955)]

In Fig. 7.3, it can be seen that there are islands of isomerism just below the magic numbers 50, 82 and 126. There is a sharp break at each of these numbers signalling a disappearance of isomerism when a shell is completely filled. Notice that isomerism does not occur again till the next shell is about half full.

(*vi*) A strikingly convincing argument for the existence of magic numbers is found when neutron-capture cross-sections for various elements are studied. Figure 7.4 shows the plot of neutron-capture cross-section against neutron number *N* of different elements, with Even *A* (thermal neutrons).

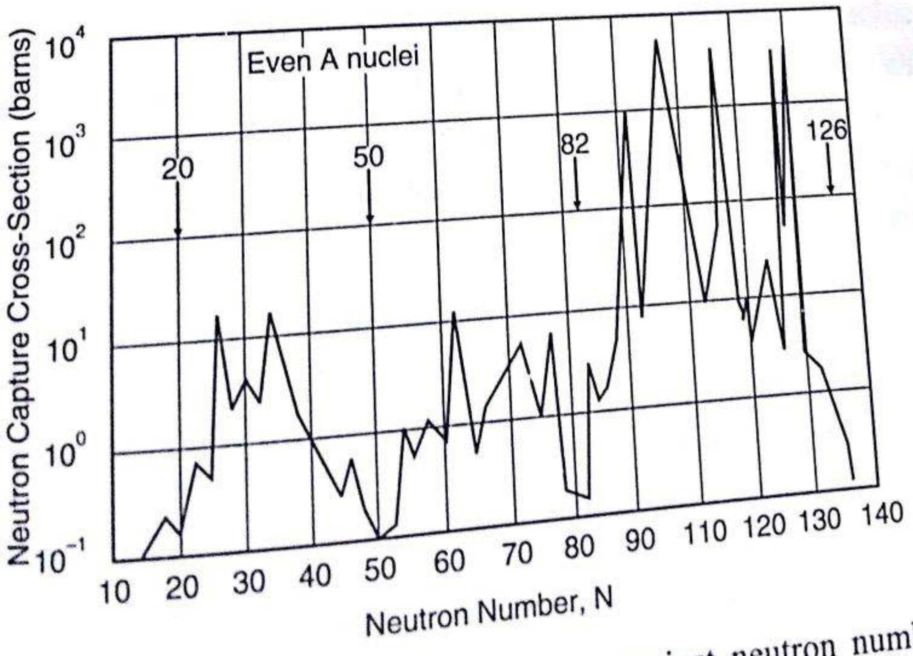

Fig. 7.4. A graph of neutron-capture cross-section against neutron number for Even A nuclides. [B. Flowers, Prog. in Nucl. Phys. 2, 235 (1952)].

As seen in Fig. 7.4, nuclei with magic numbers have very low neutron-capture cross-section. The reason for this, of course, is that at magic numbers, we have closed shells and that there is no vacancy for an additional neutron.

(*vii*) We have discussed the emission of delayed neutrons by the fission fragments, ^{87}Kr and ^{137}Xe (see Chapter 6).

The origin of this delayed neutron emission can be traced to the fact that ^{87}Kr has neutron number $N = 51$ and ^{137}Xe has $N = 83$. These values are just one unit more than the magic numbers 50 and 82 and consequently, the 51st and 83rd neutrons are bound weakly, making their emission possible.

In general, it is found that the binding energy of the last neutron added to a nucleus is quite small, corresponding to the immediate neighbourhood of nuclei having N equal to a magic number.

(*viii*) $^{212}_{84}\text{Po}\,(Z = 84, N = 128)$ emits exceptionally energetic alpha-particles (~9 MeV) with a half-life of 3×10^{-7} sec.

Notice that:

$$^{212}_{84}\text{Po} \rightarrow {}^{208}_{82}\text{Pb} + 9\text{ MeV } \alpha\text{-particles.}$$

^{208}Pb has $Z = 82$ and $N = 126$.

On the other hand, when the parent α-emitter is ^{210}Po ($Z = 84$, $N = 126$), the alpha-energies are particularly low (~6 MeV).

Similar behaviour is exhibited by β-emitters.

The results of investigations on α-decay and β-decay show that there are energy discontinuities of about two or three MeV in the neighbourhood of the magic numbers 50, 82 and 126.

(*ix*) The nuclear *electric quadrupole moment* Q_I becomes practically zero at magic numbers. Recall (Chapter 4) that the quadrupole moment vanishes for complete spherical symmetry (for Even-Even nuclei, I, the spin = 0) and so, it is not surprising that Q_I is very low for nuclides having closed shells.

Figure 7.5 shows a plot of Q_I against Z and N. For the sake of clarity, the values of Q u to ^{115}In are multiplied by 10. Dotted lines show regions in which Q_I is not firmly known. Notic that the electric quadrupole moments are very large in the rare earth region, and that the momen change in sign at the magic numbers.

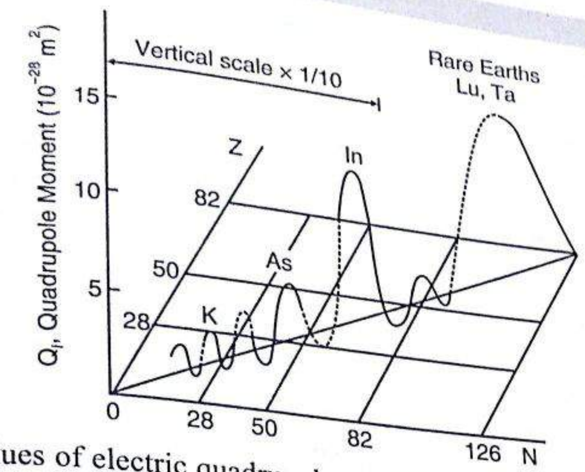

Fig. 7.5. Values of electric quadrupole moment Q_l as a function of N and Z.

7.3 MAIN ASSUMPTIONS OF THE SINGLE-PARTICLE SHELL MODEL

The single particle shell model is the simplest nuclear model obtained by applying quantum mechanics. For Odd-A nuclei, the main idea is that nuclear properties like spin, parity and moments are determined by the unpaired nucleon alone. This effectively reduces the many nucleon problem into a single-particle problem.

In contrast to the situation in atoms, the nucleus contains no massive central body that can act as a force centre. To remove this difficulty, it is assumed that each nucleon experiences a central attractive force which can be ascribed to the average effect of the remaining (A – 1) nucleons (core) in the nucleus. It is possible, as we will see to describe this central field as a short-range potential well.

In this central field, each nucleon is imagined to move in a shell, depending on its energy and angular momentum, in a manner analogous to atomic electrons. This implies that each nucleon can describe several revolutions around the force centre before being disturbed by collisions with other nucleons, i.e., the mean free path between collisions among nucleons is much larger than the nuclear diameter. The shell model, therefore, assumes the interaction among nucleons to be weak, which is a paradoxical situation since nuclear matter has a very high density ($\sim 10^{17}$ kg/m^3) and experiments show that a nucleus is almost "opaque" for any incident nucleon.

Weisskopf in 1951 invoked Pauli's Exclusion Principle to resolve this "weak interaction paradox". As the nucleons (protons and neutrons) are fermions, according to the Exclusion Principle, no two neutrons or protons can occupy identical quantum states. Thus, even though the experimentally expected strong interaction among nucleons in a nucleus is present, it is not able to show up itself, because all quantum states (low lying) into which the nucleon might get scattered after the collision are already occupied by other nucleons.

As remarked earlier in the introduction (See Sec. 7.1), Maria Mayer (and independently, Haxel, Jensen and Suess) took the important step of adding to a potential (dependent on r alone) a strong spin-orbit coupling between nucleons. What this means is that the l and s values of a nucleon combine to form total angular momentum j and these j values of different nucleons interact; giving rise to what is called a *j-j* coupling of nucleons in the nucleus. Such an approach is able theoretically to reproduce the experimentally found magic numbers, showing that the spin-orbit coupling (leading to a *j-j* coupling) is an integral part of the shell model scheme. The success of the shell model makes us go further to say that the spin-orbit coupling is vital to describe the nuclear force. We will become familiar with the concept and tentative form of the nuclear force in the next chapter. For the present, we will see how a shell model can be tailored for nuclei by simply assuming a short-range, attractive nuclear force, without going into the detail of the nature of nuclear force.

Direct evidence for the existence of a spin-orbit term in the interaction between a nucleon and a nucleus is now obtained from the polarisation effects which are observed when unpolarised beams of protons are scattered by unpolarised targets. It is beyond the scope of this book to give details of this work and the reader is recommended excellent references. (Also see next chapter)

It should be kept in mind that theoretically, the *j-j* coupling was not expected in nuclei, because of small absolute values of the nucleon magnetic moments. However, its inclusion in the shell model led to the emergence of the magic number sequence.

To appreciate the effect of the spin-orbit coupling, let us now consider the spin-orbit coupling of an electron bound in an atom. Before taking up the nuclear case, it is profitable to tread on a familiar ground.

7.4 SPIN-ORBIT COUPLING OF AN ELECTRON BOUND IN AN ATOM

The spin-orbit coupling of an electron in an atom originates from the interaction between magnetic moments associated with spin angular momentum and orbital angular momentum.

The force $\vec{F}$ acting on a charge e in an electric field $\vec{E}$ is

$$\vec{F} = -\vec{\nabla} U = e\vec{E} \qquad \ldots(7.2)$$

giving

$$\vec{E} = -\frac{1}{e}\vec{\nabla} U \qquad \ldots(7.3)$$

If the velocity of the electron is $\vec{v}$, then the induced magnetic field $\vec{B}$ at the electron site is:

$$\vec{B} = \varepsilon_0(\vec{E} \times \vec{v})$$

$$= -\frac{\varepsilon_0}{e}(\vec{\nabla} U \times \vec{v}) \text{ from (7.3)}$$

$$= \frac{\varepsilon_0}{em}(\vec{\nabla} U \times \vec{p}) \qquad \ldots(7$$

where $\vec{p} = m\vec{v} =$ momentum of the electron.

We will assume that $v << c$ (non-relativistic case).

The interaction energy between this induced magnetic field $\vec{B}$ and the magnetic moment $\vec{\mu}_s$ associated with the electron spin is:

$$W = -(\vec{\mu}_s \cdot \vec{B}) \qquad \ldots(7.5)$$

Figures 7.6 (a) and (b) show how $\vec{\mu}_s$ can be visualised and how the interaction energy W in Eq. 7.5 originates.

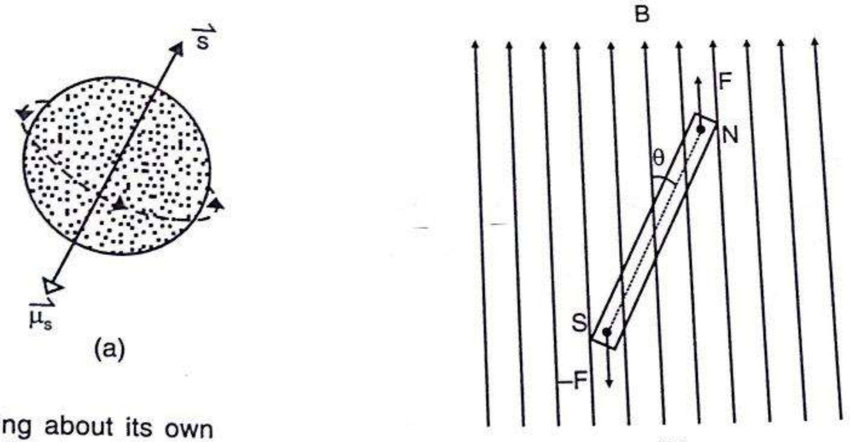

An electron spinning about its own axis may be visualised as being equivalent to a current loop, shown by a dashed curve. By applying Ampere's theorem, $\vec{\mu}_s = -g_s(\mu_e e/2m)\vec{s}$ where g_s is the g factor for spin motion.

A magnetic dipole of moment $\vec{\mu}_s$ placed in a magnetic field $\vec{B}$. It can be easily seen that the torque $\vec{\tau} = \vec{\mu}_s \times \vec{B}$ and the interaction energy $W = \int_{90^\circ}^{0} \tau de = -\vec{\mu}_s \cdot \vec{B}$

Fig. 7.6. (*a*) Dipole moment associated with the electron spin motion.
(*b*) Interaction between $\vec{\mu}_s$ and $\vec{B}$ giving rise to the interaction energy W.

In Eq. 7.5,

$$\vec{\mu}_s = -g_s \frac{\mu_0 e}{2m}\vec{s} \qquad \ldots(7.$$

where g_s = the 'g' factor (gyromagnetic ratio) associated with the spin motion (= 2 for electr

and $\vec{s}$ = the spin angular momentum, $\varepsilon_0\mu_0 = 1/c^2$

Substituting from Eqs. 7.4 and 7.6, Eq. 7.5 becomes:

$$W = -g_s \frac{\mu_0 e}{2m}\frac{\varepsilon_0}{em}\vec{s}\,.(\vec{\nabla}U \times \vec{p})$$

$$= -g_s \frac{\vec{s}\cdot(\vec{\nabla}U \times \vec{p})}{2c^2m^2} \qquad ..$$

If the potential U depends only on the distance r, then:

$$\vec{\nabla}U = \frac{dU}{dr}\frac{\vec{r}}{r}$$

The orbital angular momentum $\vec{l} = \vec{r} \times \vec{p}$

$\therefore$ Equation 7.7 becomes,

$$W = -\frac{g_s}{2c^2m^2}\frac{1}{r}\left(\frac{dU}{dr}\right)(\vec{s}\,.\,\vec{l}) \qquad \ldots(7.8)$$

From Eq. 7.8, it is at once seen how the spin-orbit coupling represented by $\vec{s} \cdot \vec{l}$ is contained in the interaction energy operator W. Eq. 7.8 becomes relativistically correct if we incorporate a factor 1/2 that is known as the Thomas correction. We will not go into the calculation leading to the Thomas correction term. Thus, the relativistically correct form of Eq. 7.8 is,

$$W = -\frac{g_s}{4c^2m^2}\frac{1}{r}\left(\frac{dU}{dr}\right)(\vec{s}\,.\,\vec{l}) \qquad \ldots(7.9)$$

When we are dealing with only a single electron, the quantum number $j = l \pm \frac{1}{2}$

For these two values of the total angular momentum quantum number j, we can get the energy contribution of the interaction energy operator W by recalling that, (see coupling of angular momenta, Chapter 1, Eq. 1.II.56)

$$(s\,.\,l)\psi = \frac{\hbar^2}{2}[j(j+1) - s(s+1) - l(l+1)]\psi$$

Thus, for $j = l + \frac{1}{2}$,

$$(s\,.\,l)\psi = \frac{\hbar^2}{2}\left[\left(l+\frac{1}{2}\right)\left(l+\frac{3}{2}\right) - \frac{1}{2}\left(\frac{3}{2}\right) - l(l+1)\right]\psi$$

$$= \frac{\hbar^2}{2}(l)\psi$$

and for $$j = l - \frac{1}{2},$$

$$(\vec{s}\,.\,\vec{l})\psi = \frac{\hbar^2}{2}[-(l+1)]\psi$$

giving the energy contribution of operator W,

$$\Delta W = \frac{\hbar^2}{8c^2m^2}\frac{g_s}{}\frac{1}{r}\left(\frac{dU}{dr}\right)\begin{cases} l \text{ for } j = l + 1/2 \\ -(l+1) \text{ for } j = l - 1/2 \end{cases}$$

$$= \alpha_0 \begin{cases} l \\ -(l+1) \end{cases} \qquad \text{...(7.10)}$$

where

$$\alpha_0 = \frac{\hbar^2 g_s}{8c^2m^2r}\left(\frac{dU}{dr}\right) \qquad \text{...(7.11)}$$

Let us discuss Eq. 7.10 in terms of the familiar spectroscopic notation:

Spectroscopic notation: s p d f g h i etc.

l: 0 1 2 3 4 5 6

For the s-term, $l = 0$, and remembering that j cannot be negative, we have only one value of ΔW corresponding to $j = l + 1/2 = 1/2$. This value,

$$\Delta W = \alpha_0 l$$

$$= 0, \text{ since } l = 0.$$

and so the s-term, with $l = 0$ is not split by the spin orbit coupling.

For the higher spectroscopic terms, we can calculate ΔW in Eq. 7.10 by putting the coulomb potential,

$$U = \frac{Ze^2}{4\pi\varepsilon_0 r} \quad \text{in Eq. (7.11)}$$

$$\therefore \quad \alpha_0 = \frac{-\hbar^2 g_s}{8c^2m^2r}\left(\frac{-Ze^2}{4\pi\varepsilon_0 r^2}\right)$$

$$= g_s \frac{e^2}{4\pi\varepsilon_0\hbar c}\frac{(\hbar c)^3}{(mc^2)^2}\frac{Z}{r^3} \qquad \text{...(7.12)}$$

This is a convenient form to estimate the magnitude of α_0. Putting the following values:

$g_s = 2$, electron spin g-factor.

$$\frac{e^2}{4\pi\varepsilon_0\hbar c} = \text{fine structure constant} \sim \frac{1}{137}$$

$$\hbar c = 197 \text{ MeV. fm.}$$

$$m_0c^2 \sim 0.511 \text{ MeV}$$

$$r \sim 0.5 \times 10^5 \text{ fm.}$$

$$Z \sim 1$$

we get an estimate of $\alpha_0 \sim 10^{-2}$eV, which corresponds to very fine splitting and so doe influence the order of filling of atomic shells.

Let us now consider the splitting of the p term for which $l = 1$, due to the spin-orbit coupl

The corresponding Schrödinger equation is,

$$(H_0 + W)\psi = E\psi$$

where

$$H_0 = -\frac{\hbar^2}{2m}\nabla^2 + U(r).$$

In Chapter 1, we have encountered the problem,

$$H_0\psi_{n,l} = E_n\,\psi_{n,l}$$

The eigen values, $E_{n,\,l}$ can be found from

$$E_{n,l} = E_n + \Delta W_l \qquad \text{...(7.1}$$

For our case of p-term ($l = 1$), Eq. 7.13 leads to the doublet splitting, (magnitude given b Eq. 7.10).

$$\Delta W_l = \alpha_0 \begin{cases} l \text{ for } j = l + 1/2 \\ -(l+1) \text{ for } j = l - 1/2 \end{cases}$$

$$\alpha_0 \begin{cases} 1 \text{ for } j = 3/2 \\ -2 \text{ for } j = 1/2 \end{cases} \qquad \text{...(7.14}$$

Figure 7.7 depicts this removal of degeneracy of the p state under the action of the spin-orbit coupling.

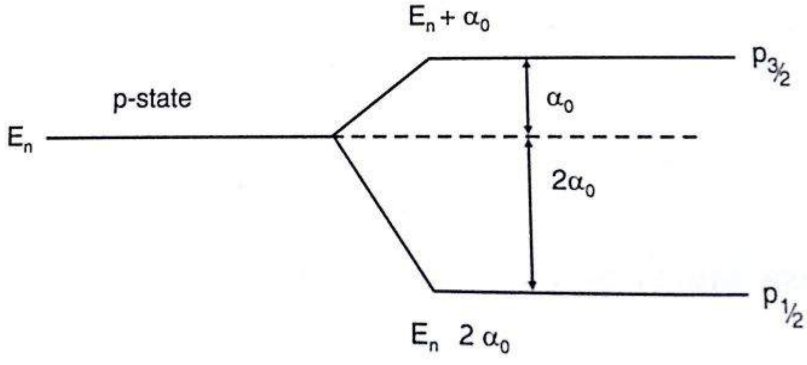

Fig. 7.7. Splitting of a p electron state under the influence of spin-orbit coupling.

The result given by Eq. 7.14 depicted in Fig. 7.7, has been experimentally verified in the study of fine structure of spectral lines for atomic spectra.

7.5 SPIN-ORBIT COUPLING IN NUCLEI, FOR A SINGLE PARTICLE SHELL MODEL

In the last section, we became familiar with the spin-orbit coupling for an electron and how it lea to splitting of various spectroscopic terms (the fine structure of spectra).

We may expect a similar effect due to motion of a nucleon inside a nucleus. A surprise awaits us here. On the basis of extremely small magnetic moments of nucleons, theoretically it was expected that the spin-orbit coupling would be negligible. On the contrary, it was found that one had not only to include a spin-orbit term of the type given by Eq. 7.9 in the Hamiltonian, but also change the sign and multiply it by a strength parameter λ to fit the experimental results. This postulated spin-orbit coupling for a nucleon is put in a form analogous to Eq. 7.9:

$$W' = -\frac{\lambda}{c^2 M}\frac{1}{r}\left(\frac{dU}{dr}\right)(\vec{s}\cdot\vec{l}) \qquad \ldots(7.15)$$

where λ is a dimensionless constant, called the *strength parameter* and M is the reduced nucleon mass.

The form of the potential U must be so chosen that by adjusting λ, results of the calculation agree with the experimental facts. M. Mayer and Haxel, Jensen and Suess independently found that a parabolic potential of a harmonic oscillator or a square well potential can be used with good results. These potentials are comparatively amenable to easy calculation and their schematic forms are shown in Fig. 7.8.

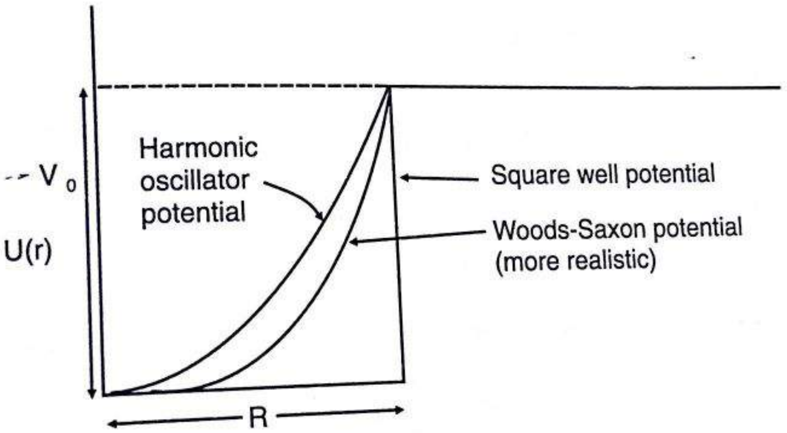

Harmonic oscillator potential
– V_0
U(r)
Square well potential
Woods-Saxon potential (more realistic)
R

Fig. 7.8. Schematic forms of different nuclear potentials.

A harmonic oscillator potential can be represented by:

$$U = -V_0 + \frac{1}{2}M\omega^2 r^2 \qquad \ldots(7.16)$$

It has two free constants, V_0 and ω.

A square well potential can be put as:

$$\begin{aligned} U &= -V_0 \text{ for } r < R \\ &= 0 \quad \text{for } r > R \end{aligned} \qquad \ldots(7.17)$$

A more realistic potential, which is intermediate between the above two potentials was first used by Woods and Saxon and is given by,

$$U = -V_0\, f(r)$$

$$f(r) = \frac{1}{1+e^{(r-c)a}} \qquad \ldots(7.18)$$

where

and a and c are adjustable constants.

For the appreciation of the results of the shell model it is enough for us to consider potentials given by Eqs. 7.16 and 7.17. Keeping with the scope of the book, we will not consider form given by Eq. 7.18, except for representation in an energy level diagram.

7.6 THE SINGLE PARTICLE SHELL MODEL—PARABOLIC POTENTIAL

Let us consider the oscillator potential given by Eq. 7.16

$$U = -V_0 + \frac{1}{2}M\omega^2 r^2$$

We know that nuclear attractive force is short range and so for $r > R$, the nuclear radius, the shell model wave function will $\rightarrow 0$.

When $r = R$, the nuclear radius, $U = 0$

i.e.

$$\frac{1}{2}M\omega^2 R^2 = V_0 \qquad \ldots(7.19)$$

We know that,

$$R = r_0\, A^{1/3},\; r_0 \sim 1.3 \text{ fm}$$

$\therefore$

$$\omega = \frac{1}{r_0}\sqrt{\frac{2V_0}{M}}\, A^{-1/3}$$

i.e.

$$\hbar\omega = \frac{\hbar c}{r_0}\sqrt{\frac{2V_0}{Mc^2}}\, A^{-1/3}$$

$$\sim 7\sqrt{\frac{V_0}{MeV}}\, A^{-1/3} \text{ MeV} \qquad \ldots(7.20)$$

Eq. 7.20 gives the relation between parameters ω and V_0 for a parabolic potential.

When the spin-orbit coupling of the form given by Eq. 7.15 is included in the Hamiltonian by arguments similar to those which led us to Eq. 7.10, we get an additional energy of:

$$\Delta W' = -\alpha' \begin{cases} l \text{ for } I = l + 1/2 \\ -(l+1) \text{ for } I = l - 1/2 \end{cases} \qquad \ldots(7.$$

where

$$\alpha' = \frac{\lambda}{2}\frac{\hbar^2}{c^2M^2}\frac{1}{r}\left(\frac{dU}{dr}\right)$$

$$= \frac{\lambda}{2}\frac{\hbar^2\omega^2}{Mc^2} \qquad \ldots($$

Compare α' with α_0 given by Eq. 7.11 and $\Delta W'$ with ΔW given by Eq. 7.10.

Notice that, there is a sign change between Eqs.7.10 and 7.21. This makes the $I = l + 1/2$ state ("parallel" orbit and spin) *deeper lying*, or more tightly bound than the $I = l - 1/2$ state, a situation compatible with experimentally observed single particle energy levels. (This is opposite of what happens for electrons.)

The strength parameter is to be so adjusted that the value of α' matches with the experimentally observed energy.

The complete energy eigen values are written as,

$$E_{n,l} = -V_0 + \hbar\omega(n + 3/2) - \alpha' \begin{cases} l \\ -(l+1) \end{cases} \qquad \ldots(7.23)$$

Compare Eq. 7.23 with Eq. 7.13.

The middle term in Eq. 7.23 represents the oscillator energy levels (see Chapter 1, Eq. 1.II.37).

In conclusion, it can be said that the spin-orbit coupling removes the degeneracy in the quantum number l and the splitting of different levels (characterised by s, p, d, f etc.) increases with l. It can become so large, for a given n, that the term with the largest value of l and $I = l + {}^1/_2$ can slide down to energies as low as those degenerate levels with quantum number $(n - 1)$.

Table 7.1 gives the sequence of the nuclear spins in the familiar spectroscopic notation, with increasing value of the quantum number n, without regard to the energy position of different terms. In order to obtain the magic numbers correctly, we count, for large l, the terms with maximum l and $I = l + 1/2$ together with the group of lower energy.

TABLE 7.1: Sequence of Nuclear Spins According to the Single-particle Shell Model

Spectroscopic term	n	l	I	*Number of states* $(2I + 1)$	*Number of nucleons in a full shell*	*Magic number*
$1s_{1/2}$	0	0	1/2	2	2	2
$1p_{3/2}$	1	1	3/2	4	6	8
$1p_{3/2}$	1	1	1/2	2		
$1d_{5/2}$	2	2	5/2	6	12	20
$1d_{3/2}$	2	2	3/2	4		
$1s_{1/2}$	2	0	1/2	2		
$1f_{7/2}$	3	3	7/2	8		28
$1f_{5/2}$	3	3	5/2	6	12	40
$2p_{3/2}$	3	1	3/2	4		
$2p_{1/2}$	3	1	1/2	2		
$1g_{9/2}$	4	4	9/2	10	10	50

Contd...

$1\ g_{7/2}$	4	4	7/2	8	32	
$2\ d_{5/2}$	4	2	5/2	6		
$2\ d_{3/2}$	4	2	3/2	4		
$3\ s_{1/2}$	4	0	1/2	2		82
$1\ h_{11/2}$	5	5	11/2	12	44	
$1\ h_{9/2}$	5	5	9/2	10		
$1\ f_{7/2}$	5	3	7/2	8		
$2\ f_{5/2}$	5	3	5/2	6		
$3\ p_{3/2}$	5	1	3/2	4		
$3\ p_{1/2}$	5	1	1/2	2		126
$1\ i_{13/2}$	6	6	13/2	14	58	
$1\ i_{11/2}$	6	6	11/2	12		
$2\ g_{9/2}$	6	4	9/2	10		
$2\ g_{7/2}$	6	4	7/2	8		
—	—	—	—	—		
—	—	—	—	—		
—	—	—	—	—		184

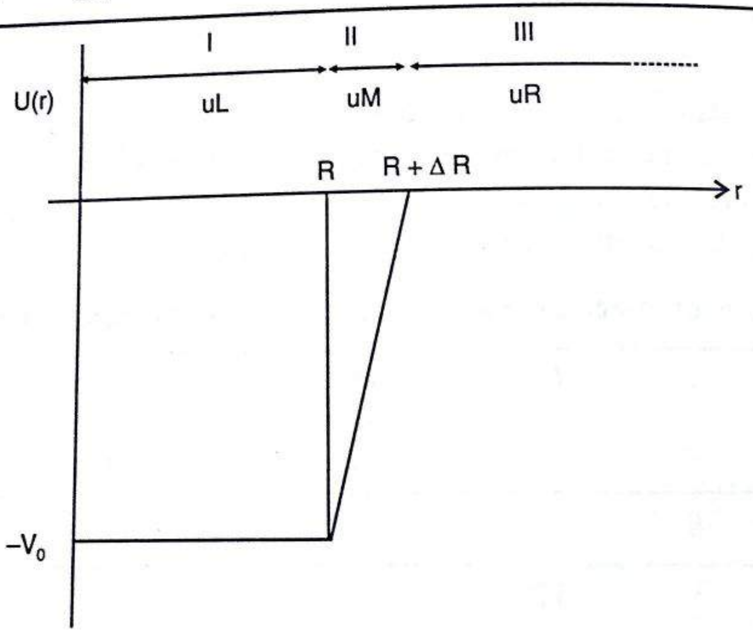

Fig. 7.9. Square well potential with a sloping wall. Continuity condition is applied to wave function $u(r)$ for $\Delta R \to 0$.

Table 7.2 gives the sequence of terms according to energy for the single-particle shell model.

TABLE 7.2

N odd	*Z odd*	*Magic number*	*N odd*	*Z odd*	*Magic number*
$1s_{1/2}$	$1s_{1/2}$	2	$2p_{3/2}$	$2p_{3/2}$	
			$1f_{5/2}$	$1f_{5/2}$	
$1p_{3/2}$	$1p_{3/2}$		$2p_{1/2}$	$2p_{1/2}$	40
$1p_{1/2}$	$1p_{1/2}$	8	$1g_{9/2}$	$1g_{9/2}$	50

Contd...

	$1d_{5/2}$				
$1d_{5/2}$	$2s_{1/2}$		$2d_{5/2}$	$1g_{7/2}$	
$2s_{1/2}$	$1d_{3/2}$	20	$1g_{7/2}$	$2d_{5/2}$	
$1d_{3/2}$			$3s_{1/2}$	$1h_{11/2}$	
	$1f_{7/2}$	28	$1h_{11/2}$	$2d_{3/2}$	
$1f_{7/2}$			$2d_{3/2}$	$3s_{1/2}$	82
			$2f_{7/2}$	$1h_{9/2}$	
			$1h_{9/2}$		
			$3p_{3/2}$		
			$2f_{5/2}$		
			$3p_{1/2}$		
			$1i_{13/2}$		
			$2g_{9/2}$		126

7.7 THE SINGLE-PARTICLE SHELL MODEL—SQUARE WELL POTENTIAL

Consider the square well potential depicted in Figs. 7.8 and 7.9 and given by Eq. 7.17.

We will briefly show how the spin-orbit coupling added to a square well potential leads to a sequence of states almost similar to the one calculated in the previous section using a parabolic potential. Some of the details will be left out for students to work out as an exercise.

The radial part of the Schrödinger's equation can be written as: (see Chapter 1, Eq. 1.II.49)

$$-\frac{\hbar^2}{2M}\left(u^{11}-\frac{l(l+1)}{r^2}u\right)+\left[U-\frac{\lambda\hbar^2}{2M^2c^2}\frac{1}{r}\left(\frac{dU}{dr}\right)\begin{Bmatrix} l \\ -(l+1)\end{Bmatrix}\right]u=Eu \qquad \ldots(7.24)$$

See Fig. 7.9.

(i) Left Region (u_L)

For $r<R, U=-V_0, \frac{dU}{dr}=0$

∴ Equation 7.24 becomes,

$$u_L^{11}+\left(\frac{2M}{\hbar^2}(V_0+E)-\frac{l(l+1)}{r^2}\right)u_L=0 \qquad \ldots(7.25)$$

(ii) Middle Region (u_M)

For $r > R$ but $<R + \Delta R$ (In the neighbourhood of nuclear surface) the term containing dU/dr is dominant (why?) and the other term in Eq. 7.24, varying slowly with r can be neglected in comparison.

∴

$$u_M^{11}+\frac{\lambda}{Mc^2}\frac{1}{r}\frac{dU}{dr}\left\{{}^{i}_{-(l+1)}\right\}u_M=0 \qquad \ldots(7.26)$$

(iii) Right Region (u_R)

For $r > R + \Delta R. U = 0$ and $\frac{dU}{dr} = 0$

and so,
$$u_R^{11} + \left(\frac{2m}{\hbar^2}(-|E|) - \frac{l(l+1)}{r^2}\right) u_R = 0 \qquad \ldots(7.27)$$

where E is put as $|E|$ since $E < 0$ for bound states.

Consider first the middle region. Integrating Eq. 7.26, between the limits, $r = R$ and $r = R + \Delta R$

$$u_M^1\,(R + \Delta R) - u_M^1(R) = -\frac{\lambda}{Mc^2}\frac{1}{R}\{^{l}_{-(l+1)}\}\, V_0 u_M(R) \qquad \ldots(7.28)$$

[We have put, $r \sim R$ and $u_M\,(r) = u_M\,(R)$]

$\because$ $u(r)$ is continuous, for $\Delta R \to 0$, we must have,

$u_L(R) = u_M(R) = u_M(R + \Delta R) = u_R(R + \Delta R)$

Also $u^1(r)$ is continuous.

$\therefore$
$$u_L^1(R) = u_M^1(R)$$

and
$$u_M^1(R + \Delta R) = u_R^1(R + \Delta R)$$

$\therefore$ Equation 7.28 becomes: $(\Delta R \to 0)$

$$\frac{1}{u_L}u_L^1(R) - \frac{1}{u_R}u_R^1(R) = \frac{\lambda}{Mc^2}\frac{V_0}{R}\begin{cases} l \text{ for } I = l + 1/2 \\ -(l+1) \text{ for } I = l - 1/2 \end{cases}$$

or
$$\left(\frac{d}{dr}(\log u_L) - \frac{d}{dr}(\log u_R)\right)_{r=R} = \frac{\lambda}{Mc^2}\frac{V_0}{R}\begin{cases} l \\ -(l+1) \end{cases} \qquad \ldots(7.29)$$

From Eq. 7.29, it can be at once seen that for $l = 0$, (since I cannot be –ve), the r.h.s. vanishes and we have the $s_{1/2}$ states in the shell model. The eigen values of energy can be obtained by solving Eqs. 7.25, 7.27 and 7.29. This is left as an exercise and can be attempted on the basis of discussion of a square well in Chapter 1.

For $l = 1$, from Eq. 7.29, the r.h.s. takes values,

$$\frac{\lambda V_0}{Mc^2 R} \text{ for } p_{3/2} \text{ state. } \left(\text{for } I = l + \frac{1}{2}\right)$$

and
$$\frac{-2\lambda V_0}{Mc^2 R} \text{ for } p_{1/2} \text{ state. } \left(\text{for } I = l - \frac{1}{2}\right)$$

and so on for $l = 2, 3, 4$ etc.

Again, we have, as in the case of parabolic potential, splitting of every state with a value of l into two states, under the action of a spin-orbit coupling. The numerical magnitude of the splitting is determined by the strength parameter λ, which is fitted to match the experimental data. In the harmonic oscillator potential, V_0 and ω are free constant. In the square well potential the values of V_0 and R (within of course, experimental limits) can be adjusted.

Figure 7.10 shows a scheme in which energy levels obtained by using both, the parabolic and the square well potential are shown. The effect of the spin-orbit coupling is shown in the middle portion of the diagram. Note that both the potentials, when taken with spin-orbit coupling, give closing of shells with magic number, a crucial experimental condition.

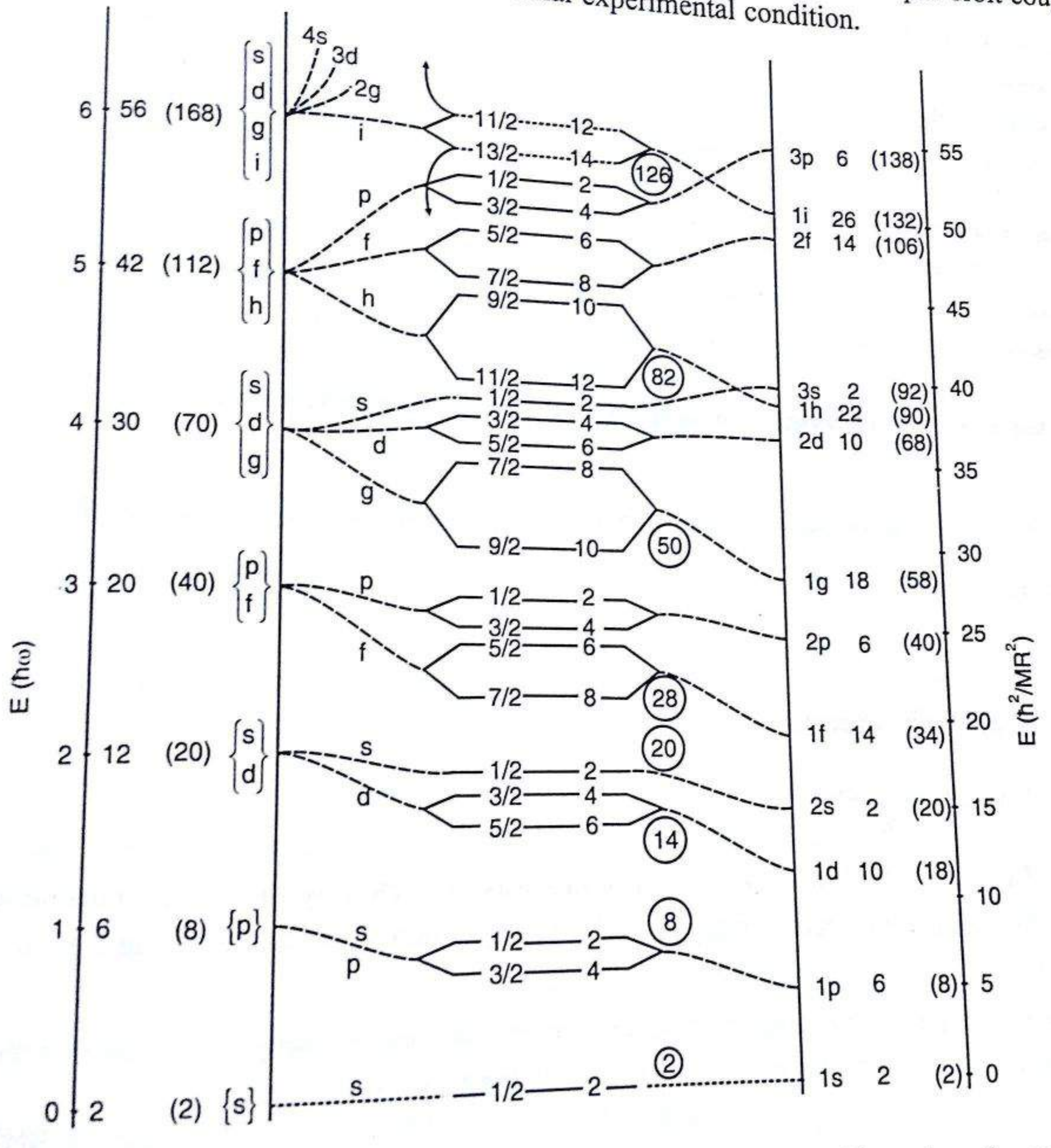
E (ħω)
6 56 (168) {s d g i}
5 42 (112) {p f h}
4 30 (70) {s d g}
3 20 (40) {p f}
2 12 (20) {s d}
1 6 (8) {p}
0 2 (2) {s}
4s
3d
2g
i
p
f
h
s
d
g
p
f
s
d
s
p
s
11/2 12
13/2 14
1/2 2
3/2 4
5/2 6
7/2 8
9/2 10
11/2 12
1/2 2
3/2 4
5/2 6
7/2 8
9/2 10
1/2 2
3/2 4
5/2 6
7/2 8
1/2 2
3/2 4
5/2 6
1/2 2
3/2 4
1/2 2
126
82
50
28
20
14
8
2
3p 6 (138)
1i 26 (132)
2f 14 (106)
3s 2 (92)
1h 22 (90)
2d 10 (68)
1g 18 (58)
2p 6 (40)
1f 14 (34)
2s 2 (20)
1d 10 (18)
1p 6 (8)
1s 2 (2)
55
50
45
40
35
30
25
20
15
10
5
0
E (ħ²/MR²)

Fig. 7.10. Nuclear energy levels given by the shell model. On the left side we have harmonic oscillator levels; at the right the square well-bound states. The effect of the spin-orbit coupling is shown in the middle, which shows the emergence of magic numbers in the sequence of nuclear levels.

Thus, this feature is not critically dependent on the exact form of the nuclear potential. The best form of nuclear potential is the intermediate between these two.

7.8 PREDICTIONS OF THE SHELL MODEL

The shell model is the first quantum mechanical model of the nucleus. Considering the oversimplified approach of the model, it is amazing to find its wide range of applicability. In fact, one of the topics substantially discussed at an advanced level course in Nuclear Physics is, "why the shell model works". Attempts are made to understand, (*i*) the free motion of nucleons (independent particles) inspite of strong forces between them (*ii*) precise form of the nuclear potential, and (*iii*) precise form and origin of the spin-orbit coupling. A discussion of these aspects, however, is beyond the scope of this book. A good reference list is provided at the end. We will now explore the applicability of the shell model in a variety of situations.

Using the results given in Tables 7.1 and 7.2, it is possible to predict spins and parities of the ground states of Even-Odd and Odd-Even nuclei. For example, in the case of ^{15}N ($Z = 7$, Odd proton number) the ground state is predicted as $p_{1/12}$ state with spin 1/2 and since for this state $l = 1$, the parity should be odd. On the other hand, in the case of ^{17}O, $Z = 8$ and the neutron number $N = 9$ (Odd). Thus according to the shell model, the ground state is predicted as a $d_{5/2}$ state with spin 5/2 and since $l = 2$ for this state the parity should be even. These predictions are in very good agreement with the experimental data, except in heavy nuclei where lot of collective motion goes on as we will see in the next section.

Consider *mirror nuclides,* ${}^{3}_{1}H$ and ${}^{3}_{2}H$. In each case, the value of spin is 1/2. For $A = 4$, there is only one known nuclide—the α-particle, ${}^{4}_{2}He$. Here $Z = 2$, $N = 2$ and the $1s_{1/2}$ is filled for both neutrons and protons. The spins of both neutrons and protons have to be anti-paralle and so $I = 0$, in agreement with the experiment.

The shell model can also be used to predict spins and parities of many of the excited state Figure 7.11 gives the energies and spin-parities of states in single-particle nuclei adjacent to th closed shell nucleus ${}^{208}_{82}Pb$.

For ^{181}Ta, one of the low-lying excited states was predicted by the single-particle shell mo as 11/2 (spin 11/2 and parity odd). Experimentally, such a state was found at an energy ~0.159 MeV.

In a single-particle shell model, the spin of the nucleus is simply the spin of the unpa nucleon, and so the magnetic moment can be obtained by using Eq. 4.36.

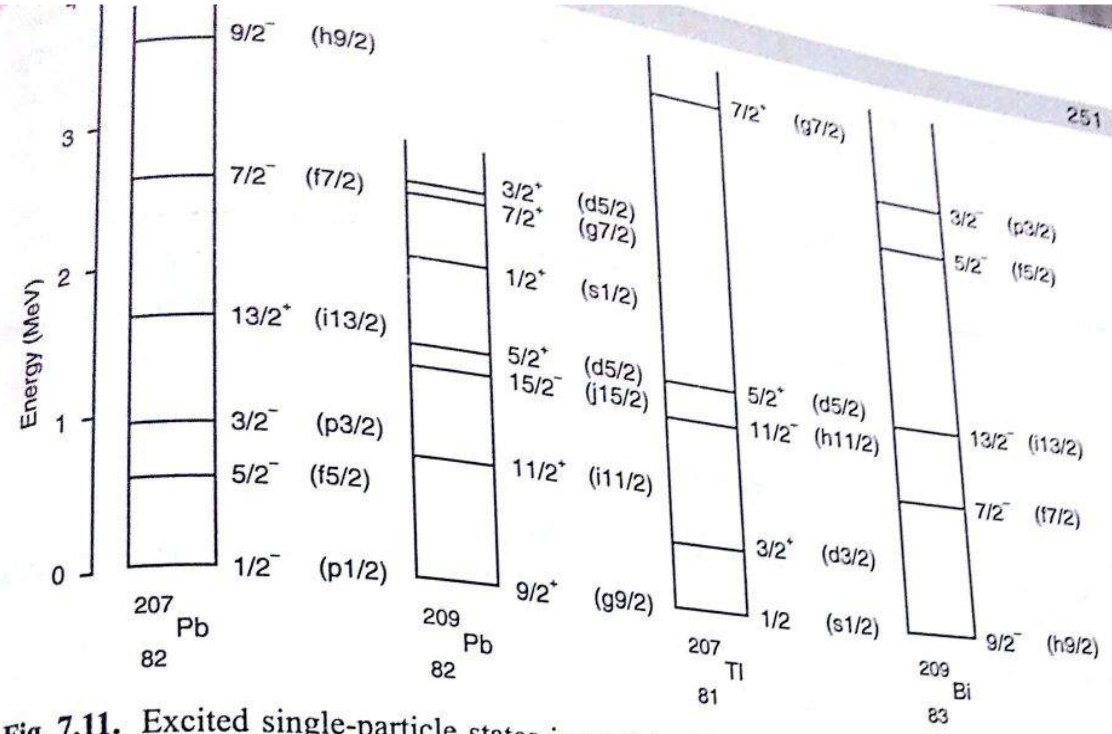
Energy (MeV)
0
1
2
3
9/2⁻ (h9/2)
7/2⁻ (f7/2)
13/2⁺ (i13/2)
3/2⁻ (p3/2)
5/2⁻ (f5/2)
1/2⁻ (p1/2)
207 Pb 82
3/2⁺ (d5/2)
7/2⁺ (g7/2)
1/2⁺ (s1/2)
5/2⁺ (d5/2)
15/2⁻ (j15/2)
11/2⁺ (i11/2)
9/2⁺ (g9/2)
209 Pb 82
7/2⁺ (g7/2)
5/2⁺ (d5/2)
11/2⁻ (h11/2)
3/2⁺ (d3/2)
1/2 (s1/2)
207 Tl 81
3/2⁻ (p3/2)
5/2⁻ (f5/2)
13/2⁻ (i13/2)
7/2⁻ (f7/2)
9/2⁻ (h9/2)
209 Bi 83

Fig. 7.11. Excited single-particle states in nuclei adjacent to the closed shell nucleus $^{208}_{82}$Pb. See the agreement with shell model prediction of sequence given in Fig. 7.10.

In Chapter 4, we saw that isomeric transitions being highly forbidden must correspond to *large spin difference* ΔI and *small energy*. Figure 7.3 shows the phenomenon of islands of isomerism, which lie just below the magic numbers. These facts are well accounted for by the shell model. Look at Fig. 7.10. For small *A*, up to 40 nucleons, the nucleonic orbits involved have $I \leq 5/2$ and there are no possibilities of large spin differences between those orbits having small energy differences. Just before the magic numbers 50, 82 and 126, there are neighbouring orbits having small energy differences and with,

$$I = 1/2, 9/2; 1/2, 11/2; 1/2, 13/2$$

Thus, the conditions here are conducive to the formation of isomers, giving rise to islands of isomerism.

The extremely low values of nuclear quadrupole moment at magic numbers corresponds to very good spherical symmetry in nuclei when shells get completely fill up (Fig. 7.5). We will look into quadrupole moments a little later.

7.9 THE COLLECTIVE MODEL OF A NUCLEUS

Let us look at some of the features of this model. In addition to the shell model features, collective motions of all nucleons are considered. This amounts to a combination of the concepts of the liquid drop model and the shell model. Consequently, the collective model is able to account for a much larger amount of experimental information. Two types of collective effects are particularly obvious: nuclear deformation leading to collective modes of excitation, viz., collective oscillations and rotations. The less obvious effects are due to centrifugal and coriolis forces.

The shell model cannot account for large quadrupole moments observed in many nuclei—a fact which implies large nuclear deformations. In Chapter 4, we defined nuclear quadrupole moment and saw that it measures the deviation of nuclear shape from a sphere. Therefore, the experimental observation of quadrupole moment implies a deformed, non-spherical nucleus. In the discussion on the shell model, it was pointed out that the quadrupole moment of nuclei corresponding to magic numbers is practically zero. The quadrupole moments for nuclei in the region between closed shells are quite large. They cannot be accounted for by a single particle shell model. Let us outline how the quadrupole moment can be estimated by the single particle model, according to which the last odd nucleon determines the electromagnetic moments. The core does not contribute to the quadrupole moment, since it is spherically symmetric. From Eq. 4.44,

$$Q = Z\int(3z^2 - r^2)\rho(\vec{r})d^3r$$

The quadrupole moment Q has dimensions of area.

If a homogeneously charged ellipsoid with charge Ze and semi-axes a and b is considered (b along z-axis), then,

$$Q = \frac{2}{5}Z(b^2 - a^2)$$

For small deviation from spherical symmetry, (see Eq. 4.46), we can talk about an average radius, $R_0 \sim \dfrac{a+b}{2}$ and $\Delta R = b - a$. Defining a deformation parameter $\delta = \dfrac{\Delta R}{R_0}$, the quadrupole moment becomes,

$$Q = \frac{4}{5}ZR_0^2\delta \qquad \text{...(7.30)}$$

It is common to introduce a reduced quadrupole moment

$$Q_{\text{reduced}} = \frac{Q}{ZR_0^2} \qquad \text{...(7.30A)}$$

For a uniformly charged ellipsoid, from Eq. 7.30A

$$Q_{\text{reduced}} = \frac{4}{5}\delta \;\; \sim\text{deformation parameter } \delta. \qquad \text{...(7.31)}$$

In wave mechanics, $\rho(\vec{r})$ the probability density in Eq. 4.44 has to be replaced by $\psi_j^*\psi_j$, where j is the spin quantum number. The nuclear spin is taken along the z-direction so that $j = m$, the magnetic quantum number.

Thus,

$$Q = Z\int\psi^*(3z^2 - r^2)\psi d^3r \qquad \text{...(7.32)}$$

To calculate Q within the framework of the single particle shell model, the wave function ψ is taken to be a single-particle wave function ψ_{nlm}. It can be for example, the wave function of a particle in a harmonic oscillator potential well. When such a wave function is put in Eq. 7.32, it can be shown that,

$$Q = -\frac{2j-1}{2(j+1)}\left\langle r^2 \right\rangle \qquad \ldots(7.33)$$

where, j = angular momentum quantum number of the single-particle $(j \neq 1/2)$.

$\left\langle r^2 \right\rangle$ = expectation value of the square of the radius of the single-particle orbit.

For a single proton, j = 3/2, 5/2, 7/2, etc. and so, for order of magnitude calculation, for higher values of j, $\frac{2j-1}{2(j+1)} \sim 1$. Also if we take, $\left\langle r^2 \right\rangle = R_0^2$, then,

$$Q \sim -R_0^2$$

or

$$Q_{\text{reduced}}\ (\text{single-particle}) = \frac{Q}{ZR_0^2}$$

$$\sim -\frac{1}{Z} \qquad \ldots(7.34)$$

Now, experimentally the measured quadrupole moment of middle of the shell nuclei like $^{175}_{71}\text{Lu}$ is

$$Q_{\text{reduced}}\left(^{175}_{71}\text{Lu}\right) = +0.25$$

On the other hand, the single-particle estimate is (from Eq. 7.34).

$$Q_{\text{reduced}}\ (\text{single}-\text{particle})\left(^{175}_{71}\text{Lu}\right) = -0.014$$

Giving

$$\frac{Q_{\text{reduced}}\ (\text{Expt.})}{Q_{\text{reduced}}\ (\text{cal. single-particle})} \sim -18$$

The single-particle estimate of quadrupole moment is not only wrong in magnitude but also wrong in sign. On the other hand, for a doubly magic plus one proton nucleus like $^{209}_{83}\text{Bi}$ (83 protons and 126 neutrons),

$$Q_{\text{reduced}}\ (\text{expt}) \sim -0.014$$

and

$$Q_{\text{reduced}}\ (\text{cal. single-particle}) \sim -\frac{1}{Z} = -0.012$$

These values are in good agreement.

Obviously the shell model is not able to explain the observed large quadrupole moments for middle of the shell nuclei. Rainwater suggested that for the nuclei like ^{175}Lu, the core is not spherical (as assumed by the shell model). It is permanently deformed by the nucleons in the outermost shell. Equation 7.31 then can give us an estimate of the deformation that produces the large quadrupole moment.

For closed shell configuration, the deforming effects of many nucleons cancel out, as orbitals are randomly oriented. When there are nucleons in the unfilled shell, the nucleus tends to adjust its surface to coincide with the density distribution of these nucleons. For sufficiently many nucleons outside the closed shells, the nucleus acquires a spheroidal equilibrium shape. This equilibrium shape is due to two opposing tendencies. On the one hand, the individual nucleons outside the closed shells forming a *core*, try to deform this core as a result of which they move in a deformed nuclear potential. On the other hand, the *pairing forces* couple two similar nucleons to make their net angular momentum zero. This second effect has the tendency to bring a state of spherical symmetry. The first effect clearly increases with more nucleons outside the closed shell core. In other words, as we go away from the closed shells the deformation of a nucleus increases, resulting into observed large quadrupole moments. Does the nuclear deformation show up itself in other experimentally observed phenomena? Yes, it is strikingly evident in the rotational and vibrational spectra of nuclei. Let us consider the rotational spectra in some detail.

Rotational Spectra

As more nucleons are added outside the closed shells, the deformation of the nucleus increases and eventually the nucleus gets permanently deformed. This implies a stability of orientation and such a nucleus in space can be described by a set of angles. This has an important consequence. In Chapter 1 (See Sec. 1.II.6), we learnt about the angular momentum operator.

The *z*-component of the orbital angular momentum operator is given by Eq. 1.II.40,

$$\hat{\mathbf{I}}_z = -i\hbar\left(\frac{\partial}{\partial\phi}\right)$$

The uncertainty relationship between the angle ϕ and corresponding angular momentu operator $\hat{\mathbf{I}}_z$ is given by,

$$\Delta\phi \cdot \Delta\hat{\mathbf{I}}_z \geq \hbar \qquad \text{...(7.3}$$

This uncertainty relationship implies that the *angular momentum cannot be restricted one value and a number of angular momentum states must exist.*

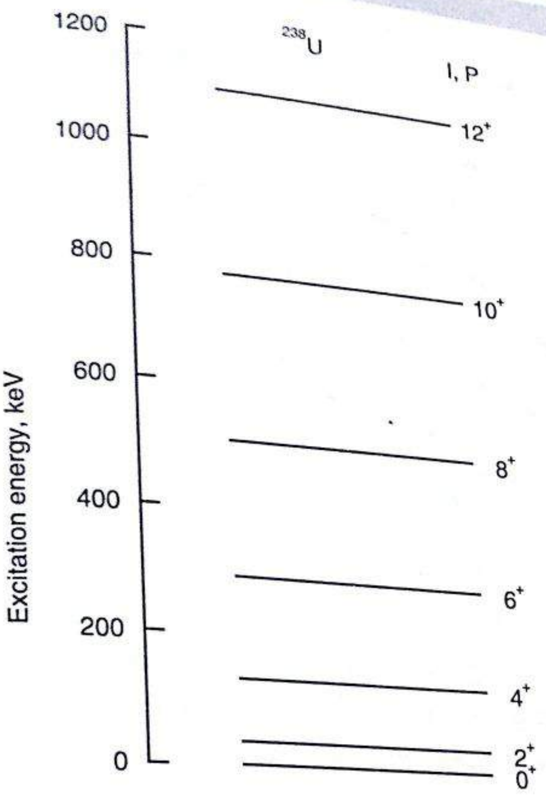

Fig. 7.12. ^{238}U-rotational spectrum.

Figure 7.12 shows an example of such angular momentum states, called *rotational states*. Notice that levels of ^{238}U show striking regularities. The *rotational spectrum* is characterised by:

(*i*) Same parity for levels.

(*ii*) Increase in angular momentum by $2\hbar$

(*iii*) Spacing between adjacent levels increases with increasing spin.

Notice that the energy of the first excited state (2^+) is less than 100 keV. ^{238}U is an even-even nucleus and so in the ground state, all the nucleons have their spins paired. In Chapter 5 we estimated the pairing energy to be of the order of 2 MeV. Thus, it should be clear that the rotational levels shown in Fig. 7.12 do not involve breaking of pairs. Then how can we understand the rotational spectrum shown in Fig. 7.12? We shall now see that it can be explained by considering the rotation of the deformed nucleus as a whole about an axis *perpendicular to the symmetry axis*. Let us first understand why we have to consider collective rotation of nuclei about an axis perpendicular to the symmetry axis.

Let z be the symmetry axis, as shown in Fig. 7.13. If we now denote (see Fig. 1.II.10) the angle about the symmetry axis z by ϕ, then for an axially symmetric nucleus, the wave function ψ must be independent of ϕ ...(7.36)

$$\therefore \quad \frac{\partial\psi}{d\phi} = 0$$

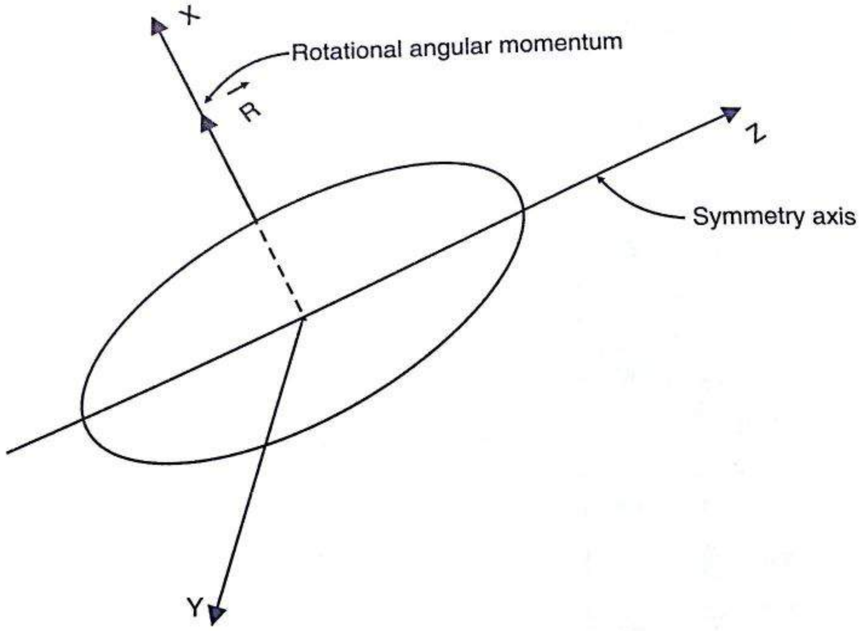

Fig. 7.13. Schematic diagram of permanently deformed, axially symmetric nucleus. It shows how the rotational angular momentum $\vec{R}$ is not along the symmetry axis. The intrinsic angular momentum is assumed to be zero, for simplicity.

Now, if $\hat{\mathbf{R}}_z$ denotes the operator for angular momentum along the symmetry axis z, then

$$\hat{\mathbf{R}}_z = -i\hbar\left(\frac{\partial}{\partial\phi}\right)$$

$$\therefore \qquad \hat{\mathbf{R}}_z\psi = -i\hbar\frac{\partial\psi}{\partial\phi} = 0 \text{ (from Eq. 7.36)}$$

Thus, axial symmetry, which implies Eq. 7.36, tells us that the component of the angular momentum along the symmetry axis is zero, ruling out collective rotation about it. However, collective rotation of deformed nucleus about any axis perpendicular to the symmetry axis is possible. This is shown by the rotational angular momentum $\vec{R}$ in Fig. 7.13. For the sake of simplicity intrinsic angular momentum of the nucleus is assumed zero. For such a "spinless" nucleus, $\vec{R}$ is the total angular momentum.

Then the rotational energy is given by,

$$H_{\text{rot}} = \frac{R^2}{2I} \qquad \ldots(7.37$$

where I is the moment of inertia about the x-axis (see Fig. 7.13).

To obtain the energy eigen values of the rotational energy operator H_{rot}, we write t Schrödinger equation,

$$H_{\text{rot}}\,\psi = E\psi$$

$$\frac{\hat{\mathbf{R}}^2}{2I}\psi = E\psi$$

(using Eq. 7.37) ...(7.38)

In Chapter 1 we saw that the operator $\hat{\mathbf{I}}^2$ has eigen values $l\,(l + 1)$ in the units of $\hbar^2$. (see Eq. 1.II.46).

Therefore, we can now write at once the eigen values of $\hat{\mathbf{R}}^2$:

$$\hat{\mathbf{R}}^2\psi = J(J+1)\hbar^2\,\psi, J = 0, 1, 2, \ldots \qquad \ldots(7.39)$$

An elementary quantum mechanics text tells that ψ is a spherical harmonic and its parity is given by $(-1)^J$. (see for example Schiff's book). Odd J gives Odd parity and Even J gives Even parity. From Fig. 7.13, it is obvious that the situation is symmetrical about x-y plane. This implies that the wave function should not change sign under reflection from the x-y plane. Thus Odd values of J, which give Odd parity are not acceptable. The allowed values of J are: 0, 2, 4, etc. From Eqs. 7.38 and 7.39, we can then write down the energy eigen values:

$$E_J = \frac{\hbar^2}{2I}J(J+1), \quad J = 0, 2, 4, \ldots \qquad \ldots(7.40)$$

Look again at the rotational spectrum of ^{238}U in Fig. 7.12. The spin assignments are in agreement with Eq. 7.40. What about energies? Let E_2 denote the energy of the first excited state. If E_2 is known then Eq. 7.40 enables us to calculate the energies of higher levels, as follows:

Since,

$$E_2 = \frac{\hbar^2}{2I}[2(2+1)] = (6)\frac{\hbar^2}{2I}$$

$$\therefore \quad E_J = \frac{\hbar^2}{2I}J(J+1)$$

$$= \frac{1}{6}J(J+1)E_2 \qquad \ldots(7.41)$$

From Fig. 7.12, it can be seen that the values of energy are in general agreement with Eq. 7.41. However, the computed values are somewhat higher than the experimental. This discripancy can be accounted for by a centrifugal stretching of the nucleus. A discussion of this is beyond the scope of this text and the reader may see for example, a paper by R.M. Diamond, F.S. Stephens and W.J. Swiatecki in Physical Rev. Letters 11,315 (1964).

I is the rotational inertia associated with the nuclear deformation. It is zero for spherical nuclei. For example, the even-even spherical nucleus ^{208}Pb has $I = 0$ and so it is not expected to show a rotational spectrum. This is confirmed by experiments. The example of ^{208}Pb cited here also shows that the nuclear matter does not rotate about the symmetry axis. The value of the rotational inertia can be experimentally obtained from the rotational spectrum. To compute this value on the basis of a model, one can consider two extreme situations. The nuclear motion may be considered as rigid, as an extreme case. For a body of mass M and radius R_0, considered spherical and rigid,

$$I_{\text{rigid}} = \frac{2}{5} M R_0^2$$

At the other extreme, we have the irrotational motion of the nucleus. If a hard-boiled egg represents a rigid nucleus then a raw egg may crudely represent the irrotational motion where the nuclear shape rotates. The rotational inertia for irrotational case is given by,

$$I_{\text{irrot}} = \frac{2}{5} M (\Delta R)^2$$

where, ΔR is the change in nuclear radius. In terms of our deformation parameter δ,

$$\delta = \frac{\Delta R}{R_0} \quad \text{(see Eq. 7.30)}$$

$$I_{\text{irrot}} = I_{\text{rigid}} \cdot \delta^2 \qquad \ldots(7.42)$$

The experimental value of I lies between these two extreme situations.

In the discussion above we had assumed a nucleus without any intrinsic angular momentum. In any text book of quantum mechanics, it is shown that a particle with spin $J < I$ cannot have an observable quadrupole moment (see Eq. 7.33). However in Fig. 7.13, we have taken a nucleus without any spin, and have shown a permanent deformation resulting into a quadrupole moment. This contradiction can be removed by noting that a nucleus can have an *intrinsic quadrupole moment* due to a permanent deformation, which gives rise to the rotational spectrum. However, the *observable* quadrupole moment is zero since for a "spinless" nucleus, we cannot talk about any particular (preferred) axis and so the quadrupole moment measurement is averaged over all directions resulting into a zero value.

Deformed Nucleus with a Spin *j*

Let us now extend the arguments made so far to a general case of a deformed nucleus of spin j. Fig. 7.14 shows this case along with the angular momentum coupling scheme.

The spin j is given rise to by the last unpaired (valence) nucleon. For simplicity, we shal assume that the valence nucleon does not affect the core, i.e., the core behaves as before (lik for a spinless deformed nucleus). The total angular momentum $\vec{J}$ is given by,

$$\vec{J} = \vec{R} + \vec{j} \qquad \ldots(7.43$$

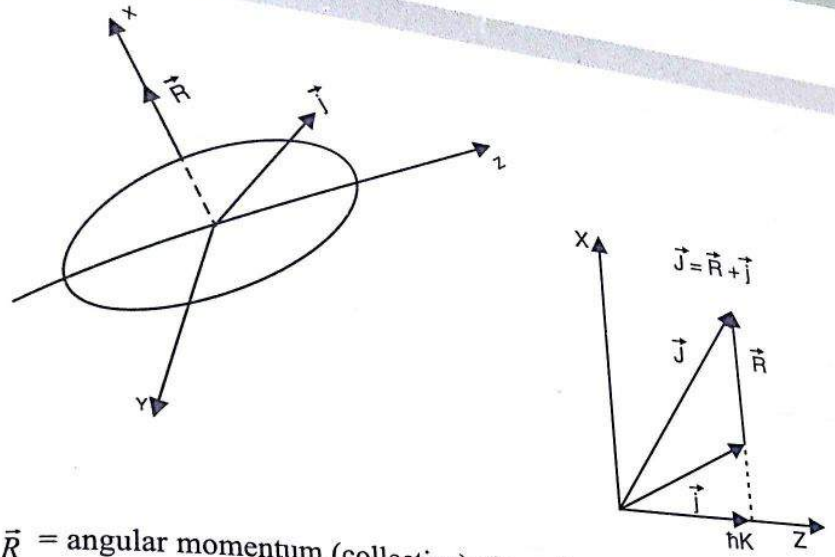

Fig. 7.14. $\vec{R}$ = angular momentum (collective) given rise to by a deformed core.
$\vec{j}$ = angular momentum of the last unpaired nucleon.
$\vec{J}$ = total nuclear angular momentum.

Notice from Fig 7.14 that $R_z = 0$, but $j_z \neq 0$. This makes $J_z \neq 0$. Now the total angular momentum $\vec{J}$ and its projection on the *z*-axis (symmetry axis), J_z are conserved. This implies that the commutator,

$$[\hat{\mathbf{J}}^2, \hat{\mathbf{J}}_z] = 0 \qquad \text{(see Eq. 1.II.44)}$$

Thus the following two eigenvalue equations are simultaneously satisfied.

$$\hat{\mathbf{J}}^2\psi = J(J+)\hbar^2\psi$$

$$\hat{\mathbf{J}}_z\psi = K\hbar\psi \qquad \text{...(7.44)}$$

where eigenvalue of $\hat{\mathbf{J}}_z$, is the projection of $\vec{J}$ on the symmetry (*z*-axis) axis. (See Fig. 7.14). Note that since $R_z = 0$,

$$\hat{\mathbf{j}}_z\psi = K\hbar\psi \qquad \text{...(7.45)}$$

The implications of the above discussion are obvious. Each state of the valence nucleon characterised by a *j*-value, will give rise to a rotational band. It would form a band-head on which the rotational states would be formed. Each band-head would be characterised by a *K*-value, which denotes the eigen value of the operators $\hat{\mathbf{J}}_z$ or $\hat{\mathbf{j}}_z$.

Figure 7.15 shows the energy level diagram for ^{239}Pu.

The observed levels fall in 3 rotational bands which are shown.

Note that 3 bands can be seen. The band-heads for these are characterised by $K = 1/2^+$, $5/2^+$ and $7/2^-$. How does one compute the energy levels of these bands? Clearly to do this, we have to put down the eigen value equation for the total energy operator, H.

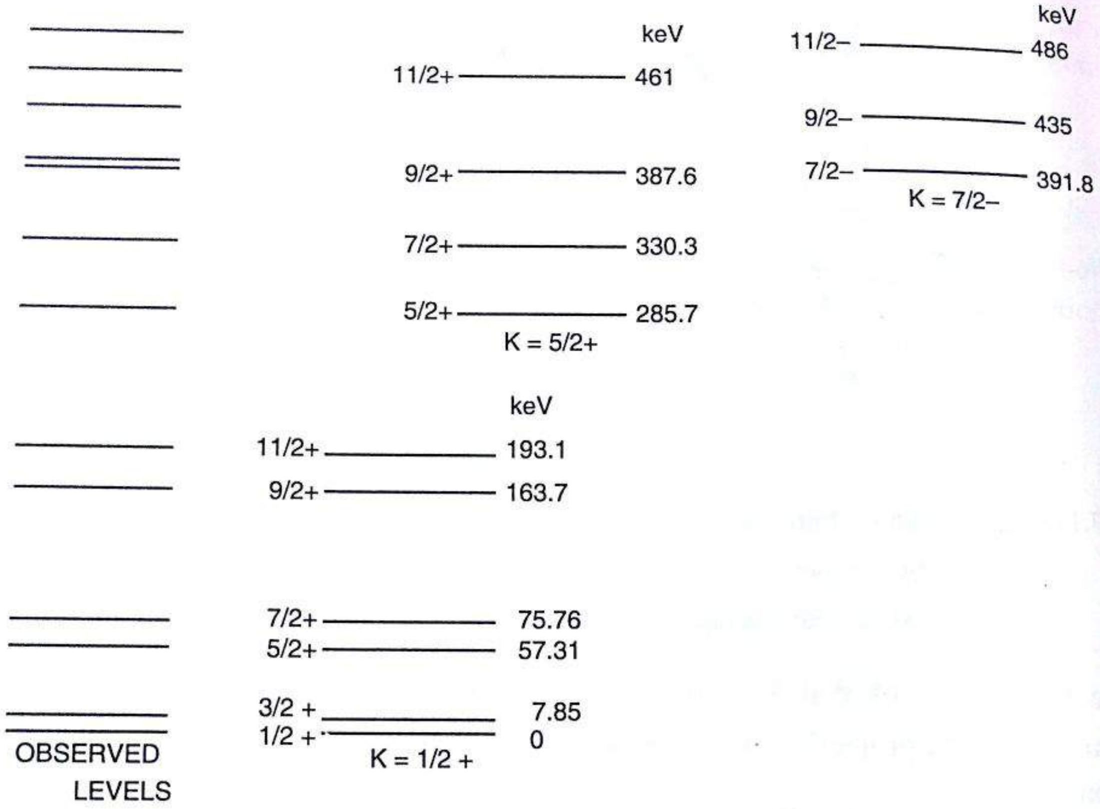
keV
11/2+ 461
9/2+ 387.6
7/2+ 330.3
5/2+ 285.7
K = 5/2+
keV
11/2– 486
9/2– 435
7/2– 391.8
K = 7/2–
keV
11/2+ 193.1
9/2+ 163.7
7/2+ 75.76
5/2+ 57.31
3/2 + 7.85
1/2 + 0
K = 1/2 +
OBSERVED
LEVELS

Fig. 7.15. Observed level scheme of ^{239}Pu.

$$H = H_{\text{rot}} + H_{\text{nucleon}}$$

$$= \frac{\hat{\mathbf{R}}^2}{2I} + H_{\text{nucleon}} \qquad \text{from Eq. 7.38}$$

where H_{nucleon} = energy of the odd nucleon with spin j. Using Eq. 7.43,

$$H = \frac{1}{2I}(\hat{\mathbf{J}} - \hat{\mathbf{j}})^2 + H_{\text{nucleon.}}$$

$$= \frac{1}{2I}(\hat{\mathbf{J}}^2 - 2\hat{\mathbf{J}}_z\hat{\mathbf{j}}_z) + \left(H_{\text{nucleon}} + \frac{1}{2I}\hat{\mathbf{j}}^2 \right) - \frac{1}{2I}(2\hat{\mathbf{J}}_x\hat{\mathbf{j}}_x + 2\hat{\mathbf{J}}_y\hat{\mathbf{j}}_y) \qquad \text{...(7.46)}$$

In obtaining the above relation we have made use of:

$$\hat{\mathbf{J}}^2 = \hat{\mathbf{J}}_x^2 + \hat{\mathbf{J}}_y^2 + \hat{\mathbf{J}}_z^2$$

$$\hat{\mathbf{j}}^2 = \hat{\mathbf{j}}_x^2 + \hat{\mathbf{j}}_y^2 + \hat{\mathbf{j}}_z^2$$

and
$$\hat{\mathbf{J}} \,.\, \mathbf{j} = \hat{\mathbf{J}}_x\hat{\mathbf{j}}_x + \hat{\mathbf{J}}_y\hat{\mathbf{j}}_y + \hat{\mathbf{J}}_z\hat{\mathbf{j}}$$

We have for the purpose of clarity grouped the terms in 3 factors in Eq. 7.46. The first factor describes the rotational energy. The second factor does not depend on the nuclear collective rotation. The third factor which looks like the coriolis force is called the coriolis term or rotation-particle coupling term. It can be neglected, except for $K = 1/2$ case. (see for example M.A. Preston, *Physics of the Nucleus*, Addison - Wesley, page 267). The second factor, which is independent of the collective nuclear rotation will give rise to an energy eigen value say, E_{nucleon}.

The energy eigen value given rise to by the first factor, $1/2I(\hat{\mathbf{J}}^2 - 2\hat{\mathbf{J}}_z\hat{\mathbf{j}}_z)$ can be at once put down by making use of Eq. 7.44. If we call it E_{Rot},

$$E_{\text{Rot}} = \frac{\hbar^2}{2I}\left[J(J+1) - 2K^2\right] \qquad \text{...(7.47)}$$

Clearly $J \geq K$.

The total energy eigen value is then,

$$\begin{aligned} E_{\text{total}} &= E_{\text{Rot}} + E_{\text{nucleon}} \\ &= \frac{\hbar^2}{2I}\left[J(J+1) - 2K^2\right] + E_{\text{nucleon}}. \end{aligned} \qquad \text{...(7.48)}$$

Equation 7.48 gives us the energy levels in a rotational band. For $K = 0$, we have the case for spinless nuclei. For $K \neq 0$, the spins of the members of a rotational band are given by, $J = K, K + 1, K + 2, \ldots$ (See Fig. 7.15).

The state with lowest spin K is called the band-head. The ratios of the energies is no longer given by Eq. 7.41. The ratio of excitation energies of the second to the first excited state is, obtained by putting $J = K + 2$ and $J = K + 1$ in Eq. 7.47 and each time subtracting the energy of the band-head state, $J = K$. This gives the following relation which can be easily verified:

$$\frac{E_{\text{total}}(J = K+2) - E_{\text{total}}(J = K)}{E_{\text{total}}(J = K+1) - E_{\text{total}}(J = K)} = 2 + \frac{1}{K+1} \qquad \text{...(7.49)}$$

Vibrational States

Having seen the collective rotational behaviour of a deformed nucleus, let us very briefly look at the collective vibrational motion of nucleons. If the frequency of the vibrational mode of the core is ω, then the corresponding energy is quantised in the units of $\hbar\omega$. (See the harmonic oscillator eigen values given in the Chapter 1). By analogy with energy quanta in vibrations of solids, these energy quanta are called *phonons*. These vibrational levels are evenly spaced; their energies are in the multiples of $\hbar\omega$.

Figure 7.16 shows vibrational levels of some even A nuclei. From this figure, it should be evident that for nuclei with 0^+ ground state, the first vibrational excited state will be 2^+ (for $l = 2$). The second is either 0^+, 2^+ or 4^+. When nuclear shape is expressed in spherical harmonics one learns that $l = 2$ deformations are first to arise. They are called quadrupole deformations.

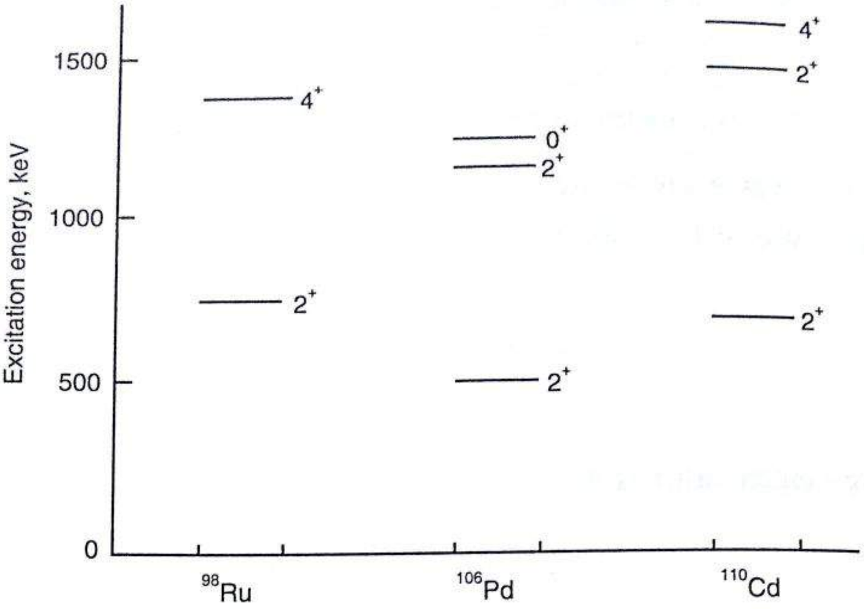

Fig. 7.16. Vibrational levels in some even A nuclei.

It is possible to separate, approximately, the intrinsic nucleonic motion relative to a deformed potential corresponding to the two types of collective motions, viz., rotational and vibrational. Observation of rotational spectra confirms this. The complete wave function can then be written down.

$$\psi = X_{\text{particle}}\phi_{\text{vibration}}D_{\text{rotation}} \qquad \ldots(7.50)$$

Such a description which attempts to combine the apparently opposite points of view, viz., intrinsic particle motion and collective motion, was successfully developed by B. Mottelson and A. Bohr. This *unified model* is lucidly described in their *Nuclear Structure Vol. II.* Such a treatment is beyond the scope of this introductory text. However, it is interesting and worthwhile to look at an important step, first taken by Nilsson.

The *Nilsson Model* describes motion of nucleons in a *deformed potential well.* It treats a deformed nucleus as consisting of independent particles moving in a deformed potential well.

The Nilsson Model

At the beginning of this chapter, we considered the single-particle shell model. We used a harmonic oscillator potential which is spherically symmetrical. To this, we added a spin-orbit term given by Eq. 7.15. The spherical shell model potential is:

$$V(r) = \frac{1}{2}m\omega^2 r^2 - \frac{\lambda}{c^2 M r}\left(\frac{dU}{dr}\right)(\vec{l}\cdot\vec{s})$$

$$= \frac{1}{2}m\omega^2 r^2 - C\vec{l}\cdot\vec{s} \qquad \ldots(7.51$$

We saw that by choosing parameters, it is possible to reproduce the experimentally observed shell closures at the magic numbers. Quantum numbers N, l and j of the nucleon are used to label the levels; they are good quantum numbers (see Table 7.1).

We have now seen that many nuclei, particularly those in the middle of the shell region, have large quadrupole moments implying large deformations. This means that nucleons do not move in a spherical potential given by Eq. 7.51, but that equation needs to be generalised. This can be done in many ways. For our purpose, let us briefly see the way it was done by Nilsson, since it is very commonly used.

The Nilsson potential describes an axially symmetrical case. The z-coordinate is taken along the symmetry axis, the z-axis. The parameter ω in the harmonic oscillator potential is taken to be ω_{II} along the z-axis and $\omega_\perp$ along the x and y axes. Since, the nuclear matter is nearly incompressible, $\omega_\perp$ and ω_{II} are related. For a quadrupole deformation, it is possible to show that:

$$\omega_{II} = \omega_0(1 - 2/3\varepsilon)$$

and

$$\omega_\perp = \omega_0(1 - 1/3\varepsilon) \qquad \ldots(7.52)$$

where ε is the deformation parameter. It is related to our deformation parameter δ (see Eq. 7.30) by:

$$\delta = \varepsilon\left(1 + \frac{1}{2}\varepsilon\right) \qquad \ldots(7.53)$$

for $\varepsilon^2 \ll 1$, the incompressibility of nuclear matter (constancy of volume) gives us the relation:

$$\omega_\perp^2\omega_{II} = \omega_0^3 \qquad \ldots(7.54)$$

Nilsson took the deformed potential of the form:

$$V\,(\text{deformed}) = \frac{1}{2}m[\omega_\perp^2(x^2 + y^2) + \omega_{II}^2 z^2] + C\vec{l}\cdot\vec{s} + Dl^2 \qquad \ldots(7.55)$$

The constant C determines the strength of the spin-orbit coupling. The term Dl^2 lowers the energy of the large angular momentum states. Both C and D are negative. Equation 7.55 shows that V (deformed) is governed by four parameters: ω_0, C, D and ε. Out of these, only ε depends chiefly on the nuclear shape. We know how quadrupole moment is related to deformation parameter δ (see Eq. 7.31) and hence on ε. Thus, ε for a particular nucleus is found by measuring the quadrupole moment Q. The other three parameters can be taken to be (for $\varepsilon^2 \ll 1$) nuclear shape-independent. They are determined from levels of spherical nuclei for which $\varepsilon = 0$. Once they (ω_0, C and D) are determined then the energy eigen values can be explored as a function of the deformation parameter ε. This is done by using a computer to solve the Schrödinger equation using the Nilsson potential. For $\varepsilon = 0$ (spherical nuclear shape) the energy levels agree to those shown in Fig. 7.10, and they can be labelled by quantum numbers, N, L and j. Figure 7.17 shows the typical *Nilsson diagrams* for small A, up to magic number 20.

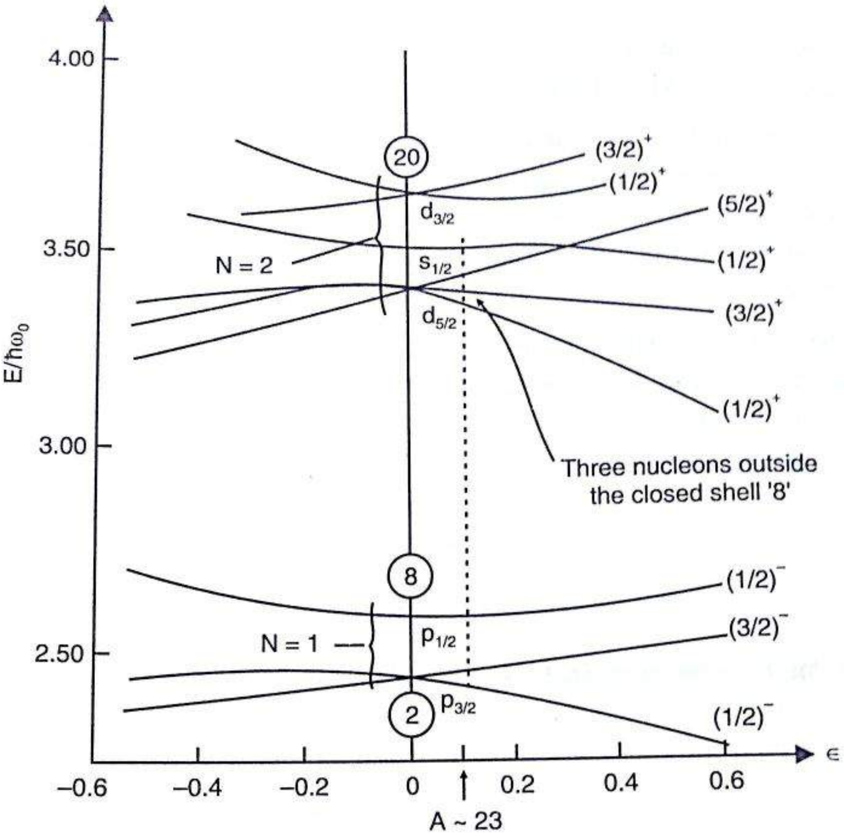

Fig. 7.17. Nilsson diagrams up to magic number 20.

To illustrate the significance of these Nilsson diagrams, consider the behaviour of say, the $d_{5/2}$ nucleon state of the second oscillator shell ($N = 2$). For a spherical potential (i.e., in the limit $\varepsilon = 0$) this state is $(2J + 1) = 6$-fold degenerate. This degeneracy is removed by the deformation, i.e., when the nucleon moves in a deformed potential (see Fig. 7.17). From the figure, it can be seen that the $d_{5/2}$ state splits up into three levels. Similarly, the $p_{3/2}$ state splits up into two levels. Generalising, a nucleon with total angular momentum j in the $\varepsilon = 0$ (spherical) case splits up into $1/2\ (2j + 1)$ levels of different energy. These levels have the K values: $j, j - 1, j - 2, ... 1/2$, i.e., in all $1/2\ (2j + 1)$ values. It should be realised that a state with a j value in the spherical potential case under deformation gets split up into $1/2\ (2j + 1)$ levels having different K values. (see again Fig. 7.14 for the origin of K). In other words, for a deformed nucleus, j (and so also l) is *not a good quantum* number. $\vec{j}$ and $\vec{l}$ are no longer conserved. In the Nilsson model, only two quantum numbers remain good: the component of total angular momentum along the symmetry axis K and the parity π, determined by the oscillator quantum number N; $\pi = (-1)^N$. A nuclear state is denoted by K^π in Fig. 7.17. Actually, Nilsson used three approximately (asymptotically) conserved numbers. But a discussion of these is of little use here (Nilsson's original paper was published in 1955 in Dan. Mat-Fys Medd. 29, No. 16).

It is interesting to see that from the viewpoint of the vector model, the total nucleon angular momentum vector $\vec{j}$ precesses rapidly about the symmetry axis (z-axis), so that its component perpendicular to the z-axis gets averaged to zero and has no effect on the energy levels

Figure 7.18 shows how a *j*-value of nucleon can give rise to various *K* values. Each *K* value determines an energy level. In all we have 1/2 (2*j* + 1), *K* values.

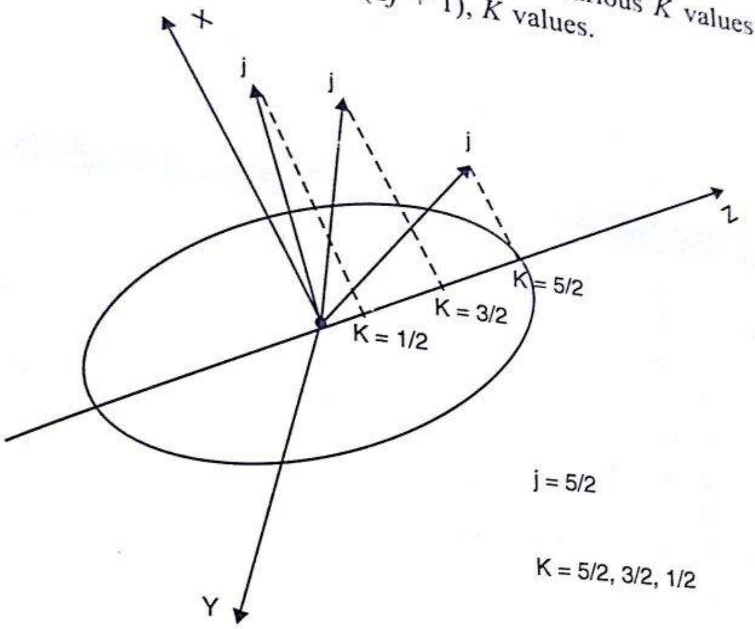

Fig. 7.18. For a deformed nucleus, the same *j*-value gives rise to 1/2 (2*j* + 1), *K* values. The total nucleon angular momentum *j* is no longer a conserved quantity. Here, the $d_{5/2}$ state is depicted.

From where does the factor 1/2 comes in 1/2 (2*j* + 1)? From Fig. 7.18, clearly, the nucleus is symmetrical about the *x*-*y* plane. This implies that the states *K* and –*K* correspond to the same energy. This two-fold degeneracy is described by the factor 1/2.

Use of Nilsson Diagrams

The measurement of the electric quadrupole moment of the nucleus gives us an estimate of the deformation parameter ε (see Eq. 7.53). For example, for ^{23}Na, Q(measured) = 14 fm^2 giving ε ~ 0.1. This nucleus has 11 protons and 12 neutrons. According to the single-particle shell model, the ground-state spin parity assignment for ^{23}Na nucleus in $(5/2)^+$. This can be seen from Table 7.1 or Fig. 7.10, for the eleventh odd proton. However, experimentally, the ground-state assignment is found to be $(3/2)^+$. Let us now see, what is the Nilsson model prediction by looking at the Nilsson diagrams in Fig. 7.17. Look along the dotted line corresponding to deformation ε ~ 0.1. The 11th proton is the 3rd one outside the closed shell with magic number 8. This leads to the prediction of $(3/2)^+$ for the ground state of ^{23}Na, in agreement with the experiment. Thus, knowing the nuclear deformation, it is possible to predict the spins and parities of the ground-states for Odd-A nuclei, using Nilsson diagrams. The results are found in excellent agreement with the experimental values. It is also possible to predict ground-state moments. Low-lying excited states can also be predicted with success. A detailed discussion on the Nilsson model can be found, for example, in the book by Preston—*Physics of the Nucleus,* Addison-Wesley.

We conclude this chapter by noting that the collective model takes into account the motion of nucleons in a deformed nuclear potential and then the shell model levels are calculated.

Because, we do not know the exact nature of the nuclear force, models discussed are useful and necessary. While discussing the shell model, the similarity of atomic and nuclear "shell behaviour" was pointed out. It is worth mentioning here that the approach of the collective model is similar to the one used in understanding the molecular spectra. In molecular spectra, the rotational, vibrational and electronic transitions are handled in a manner similar to these motions in the nucleus.

EXERCISES

1. State clearly the assumptions of the shell model of a nucleus. Obtain the sequence of the "magic numbers" using a parabolic and a square well potential.
2. What is the reason that makes the $I = l + 1/2$ state deeper-lying or more tightly bound compared to the $I = l - 1/2$ state in a nucleus?
3. Discuss the predictions of the shell model in relation to the experimental results.
4. Identify about ten rotational bands and vibrational levels in different deformed nuclei. Obtain the ratios of energy levels (Even A) from Eq. 7.29 and compare them with the experimental values.
5. Partial level scheme of ^{234}U is given below:

   10^+ .... 0.803 MeV
   8^+ .... 0.499 MeV
   6^+ .... 0.296 MeV
   4^+ .... 0.143 MeV
   2^+ .... 0.0435 MeV
   0^+ 0
   ^{234}U

   At what energy would you look for a 12^+ state?
6. What spins and parities would you predict (on the basis of the shell model) for the ground state of:

   (*i*) $^{15}_{8}O$ and (*ii*) $^{17}_{8}O$
7. For ^{17}O, the following order of levels is experimentally observed:

   Ground state ($5/2^+$): 0.871 MeV state ($1/2^+$);
   3.055 MeV state ($1/2^-$); 3.846 MeV state ($7/2^-$);
   4.553 MeV state ($3/2^-$); 5.083 MeV state ($3/2^+$);
   5.215 MeV state ($3/2^-$); 5.378 MeV state ($3/2^-$).

   Identify the shell model levels from these, giving reasons.
8. Spins and parities of the ground state are given for the following nuclei:

   $^{3}He(1/2^+)$; $^{21}Ne(3/2^+)$; $^{209}Bi(9/2^-)$.

   Justify these observed values on the basis of the shell model.

   (*Hint:* Even l has Even parity, Odd l has Odd parity).
9. Predict the shell model state of the odd nucleon in the following cases:

   (*i*) $^{63}_{29}Cu$ and (*ii*) $^{25}_{12}Mg$

   Write down the spin and parity of the ground state.

10. According to the shell model, find out the spins and parities of the following nuclei in (*a*) the ground state and (*b*) the first excited state:

(*i*) $^{17}_{9}\mathrm{F}$ and (*ii*) $^{127}_{53}\mathrm{I}$

11. Experimentally, the ground state spin of $^{23}_{11}\mathrm{Na}$ nucleus is found to be 3/2. Does it agree with the prediction of the shell model? If not, how would you account for this discrepancy?
(*Hint:* Combine angular momentum states of more than one nucleon.)

12. Draw energy level diagrams for the nuclei given below, showing the filling of the levels by neutrons and protons.

(*i*) $^{7}_{3}\mathrm{Li}$ and (*ii*) $^{41}_{20}\mathrm{Ca}$

13. The quadrupole moment measurement for the following nuclei gives the deformation parameter $\varepsilon \sim 0.10$: ^{19}F, ^{21}Ne, ^{21}Na, ^{23}Na and ^{23}Mg. The experimental ground-state assignments for these nuclei are: $(1/2)^+$, $(3/2)^+$, $(3/2)^+$, $(3/2)^+$ and $(3/2)^+$ respectively. What are the shell model and Nilsson model predictions? Which predictions agree with the experimental values?

14. For small deviations of the deformation from the ground stale deformation due to 'stretching' of a nucleus, the energies of the rotational states can be written as:

$$E_J = AJ(J + 1) + B\,[J(J + 1)]^2$$

The level scheme of $^{170}_{72}\mathrm{Hf}$ is given below:

16^+ ….. 3147.3 keV
14^+ ….. 2563.6 keV
12^+ ….. 2013.3 keV
10^+ ….. 1503.3 keV
8^+ ….. 1041.3 keV
6^+ ….. 641.1 keV
4^+ ….. 320.6 keV
2^+ ….. 100.0 keV
0^+ ….. 0

$^{170}_{72}\mathrm{Hf}$

Use the expression for E_j to fit the observed energy levels of ^{170}Hf by determining the constants *A* and *B* from the two lowest levels. Find out how well the calculated values of E_j agree with the experimental values given in the level scheme. Check right up to spin 16. Predict the energies for the 18^+, 20^+ and 22^+ levels in the rotational band.

8

Nuclear Force

"Often, it is astonishing to find that a well-established theory rests on pillars whose strength is suspect."

— *P.A.M. Dirac*

8.1 INTRODUCTION

In Chapter 5, we considered the curve of binding energy per nucleon against the mass number (*B*/*A* against *A* curve). The value of *B*/*A* is approximately constant and it is about 8 MeV/nucleon. This is about a million time higher than the binding energy of an electron in the hydrogen atom (which is 13.6 eV). In other words, the force that keeps the nucleus together is much stronger than the electrical force which keeps the atom together. Also, this nuclear force must be stronger than the electrical force between the protons since protons are bound in the nuclei.

What holds the nucleus together? Bound systems are held together by forces. The earth is bound to the sun because of the gravitational force between them. The electron in a hydrogen atom is bound to the nucleus (which is just a proton) because of the electrical force of attraction between them. These two types of forces certainly cannot account for the existence of nuclei. The gravitational attractive force between two protons is smaller by a factor of about 10^{39} than the electrical repulsive force between them. In fact, it is customary to neglect the effects of gravity when one considers atoms or nuclei. Thus, one must recognise the existence of a *third force* in nature, the *nuclear force*. Further this nuclear force must be *much stronger* than the electric force; otherwise protons cannot live in close proximity as they do inside a nucleus. This is also expected from the *B*/*A* against *A* curve. When we discussed the size of the nucleus in Chapter 4 we saw that in a Rutherford α-scattering experiment, a departure from Coulomb law was observed with light elements as targets, only with the most energetic α-particles. This clearly showed that the *effect* or *range of the nuclear force must be of the order of the* *nuclear radius*. In other words, the nuclear force is a *short-range force*. It falls off more rapidly with distance than $1/r^2$.

The nuclear force is often called the *strong interaction*, because it is the strongest of the four basic forces or interactions found in nature. Table 8.1 gives the relative strengths of the four basic interactions.

TABLE 8.1: Basic Interactions

Type of interaction	*Relative strength*	*Range*
Strong (Nuclear)	1	10^{-14} m
Electromagnetic	$\sim 10^{-2}$	∞
Weak (e.g., Beta decay)	$\sim 10^{-13}$	Almost zero
Gravitational	$\sim 10^{-39}$	∞

Obviously, the best way to obtain more information about the nuclear force is to consider a nucleus involving only *two nucleons*. Also, the scattering of nucleons by nucleons would be expected to give information about the nuclear force. The only bound system of two nucleons is the deuteron, which consists of a proton and a neutron. This system is weakly bound and it has no bound excited states and this makes it quite different from the simplest atomic bound system, that of hydrogen which has a large number of bound states experimentally known. The hydrogen atom is understood in terms of the well-known electrical force. In contrast, when we study the deuteron, we are dealing with an unfamiliar force, the nuclear force.

8.2 THE GROUND STATE OF THE DEUTERON

As remarked earlier, the only bound system of the two nucleons found in nature is the deuteron, which consists of a neutron and a proton. Four important facts are experimentally known about deuteron. They are:

(*i*) Binding energy, measured with high accuracy;

(*ii*) Size. It is measured with accuracy by considering the scattering of high-energy electrons which was discussed in Chapter 4, Part I;

(*iii*) Angular momentum, which is 1 in the units of $\hbar$. This gives rise to magnetic moment;

(*iv*) Electric quadrupole moment Q.

Any theoretical attempt to understand the deuteron and the nuclear force must be able to predict these experimental results. Let us become familiar with these results.

A straightforward method for obtaining the binding energy of the deuteron is to observe, the *smallest-energy* γ-ray required to break up the deuteron into a neutron and a proton. Using this experimentally observed *threshold energy*, one can have an idea of the deuteron binding energy.

Another direct way of obtaining the deuteron binding energy is to calculate it from the mass-spectroscopically known values of masses of the neutron, proton and deuteron. This gives a value of 2.224 MeV for the deuteron binding energy. An accurate method for obtaining the deuteron binding energy is to bombard slow neutrons on hydrogeneous matter like paraffin wax and observe the energy of the gamma rays which are given off. In this method, a proton "captures" a neutron to become a deuteron and a gamma ray emerges out. This gamma ray has an energy almost equal to the deuteron binding energy. (The difference is due to the recoil of the deuteron formed and is small.) The reaction is:

$$n + p \rightarrow d + \gamma \qquad \ldots(8.1)$$

The deuteron recoil energy is about 1.3 keV and the deuteron binding energy is found to be:

$$\longrightarrow \text{B.E. of deuteron} = 2.2256 \text{ MeV} \qquad \ldots(8.2)$$

The agreement between the values given by different methods is good. The size of the deuteron is found by studying the scattering of high energy electrons from an accelerator. This was discussed in Chapter 4; Part I. The average radius of the deuteron is found to be:

$$\longrightarrow \text{Average radius of deuteron} = 4.2 \text{ Fermi} \qquad \ldots(8.3)$$

(It is the root mean square distance (r.m.s.) between the neutron and the proton). Using the hyperfine structure studies described in Chapter 4 Part I, it is possible to measure the total angular momentum I for the deuteron. The result is:

I, Angular momentum of deuteron = 1 in units of $\hbar$. ...(8.4)

Since the spins of both, the neutron and the proton is 1/2 in the units of $\hbar$, *the deutero must be formed with the spin vectors of the neutron and the proton parallel*. The othe possibility of the two spin vectors antiparallel giving a net spin = 0 *does not lead to a boun state for the deuteron*. As remarked earlier, deuteron excited states do not exist and so th state to be studied is the *ground state* (which is the lowest-lying energy state). For the grou state, $l = 0$; it is the 1*s* state.

?

why

$$I = L + S = S = 1$$

The 1*s* state (ground state) with $S = 0$ does not give a bound state for deuteron.

The energy of the ground state of the deuteron is different if the spins of the neutron a proton are parallel than if they are antiparallel. Otherwise why should the spin parallel syst be stable and spin antiparallel not stable? The important conclusion that can be drawn from t is that *the force between a neutron and a proton is spin-dependent*. The nuclear force keep the two nucleon system bound, thus depends on whether the spins of the two nucleons parallel or antiparallel i.e., whether the total spin $S = 1$ or 0. This feature is quite different t for example, the Coulomb force which goes as $1/r^2$ and so is just a function of *r*.

8.3 MAGNETIC DIPOLE AND ELECTRIC QUADRUPOLE MOMENTS OF TH DEUTERON

In our discussion so far, we have assumed that the deuteron is in an $l = 0$ state and so we d expect any orbital angular momentum. In other words, one expects the total magnetic mome the deuteron to be the sum of the magnetic moments due to the spin motions of the neutron and the proton. Thus, we expect a value:

$$\mu\ (\text{neutron}) + \mu\ (\text{proton}) = 0.8797 \frac{e\hbar}{2M_p}$$

for the deuteron magnetic moment.

However, the experimentally obtained value of the magnetic moment of the deuteron was:

$$\text{Deuteron magnetic moment, } \mu_d = 0.8574\ \frac{e\hbar}{2M_p} \qquad \text{...(8.5)}$$

The difference is about 2.5 per cent, which is small but significant. The simplest explanation for this discrepancy is that our assumption, that the deuteron is in $l = 0$ state is *not entirely correct.* There must be some orbital momentum in the deuteron nuclear system. *This implies that the wave functions describing the deuteron are not spherically symmetric.* The spherically symmetric wave functions have only r dependence and no (θ, ϕ) dependence. This is what happens in an $l = 0$ state; the wave function is a function of r only and so, is spherically symmetric.

More experimental evidence for the lack of spherical symmetry is provided by the observation of an electric quadrupole moment for the deuteron:

$$\text{Deuteron electric quadrupole moment} = 0.282\ \text{F}^2 \qquad \text{...(8.6)}$$

This value though small (compare with the values given in the Chapter 4, Part I), is non-zero and significant. A non-zero quadrupole moment for the deuteron means that *the electric charge in the deuteron is not spherically distributed*, but it is slightly deformed in a prolate, non-spherical shape. This clearly indicates that the wave function is not the simple spherically symmetrical ($l = 0$) one, a fact in agreement with the conclusion from the value of the magnetic dipole moment.

Before we discuss the non-spherical nature of the wave function and its effects on the nature of the nuclear force, let us outline the wave mechanics of the deuteron problem assuming a square well potential.

8.4 SQUARE WELL SOLUTION FOR THE DEUTERON

Let us assume that the potential can be represented by a square well, with radius R which is of the order of the deuteron size and represents the range of the nuclear force, as shown in Fig. 8.1(a).

Actually the deuteron problem is a two-body problem. It can be reduced to a one-body problem by using the familiar centre of mass transformation of classical mechanics. We can then consider a *single particle* in a square well, where the mass of the "effective" single particle is the *reduced mass* μ given by,

$$\frac{1}{\mu} = \frac{1}{m_p} + \frac{1}{m_n} \qquad \text{...(8.7)}$$

where m_p and m_n are the proton and neutron masses respectively. Note that since $m_p \sim m_n$, the reduced mass $\mu = \dfrac{m_p \cdot m_n}{m_p + m_n}$ is approximately one half of the nucleon mass.

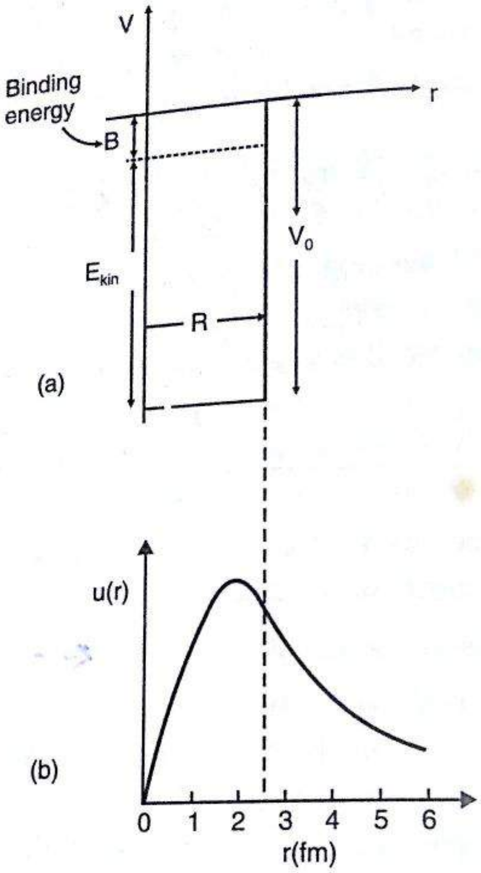

Fig. 8.1. Square well approximation for the deuteron problem.

(*a*) The square well potential. Particle with binding energy B has a kinetic energy E_{kin} where, $E_{\text{kin}} + B = V_0$

R is the range of the potential.

(*b*) The plot of the wave function $u(r)$ against r.

The mutual kinetic energy of the neutron and proton is,

$$E_{\text{kin}} = \frac{p^2}{2\mu} \qquad \text{...(8.8)}$$

An estimate of E_{kin} can be made by using the uncertainty principle. The momentum p must be equal to at least the uncertainty in it, i.e.,

$p \sim \dfrac{\hbar}{a}$ where a is the radius of the deuteron

$\therefore$

$$p \sim 100 \text{ MeV/c} \qquad \text{...(8.9)}$$

Thus from Eq. 8.8, $E_{\text{kin}} \sim 16$ MeV ...(8.10)

Figure 8.1(a) shows the relationship between the binding energy B, E_{kin} and the potential energy (negative) V_0. Note that B is the difference between attractive potential V_0 and the kinetic energy E_{kin} (which is due to the relative motion of the nucleons).

In Chapter 1, Section 1.II.4, we have considered the particle in a square potential well. For a deuteron in the ground state we have to consider $l = 0$, and so we can follow the treatment given in that section for our deuteron problem, except that we must now consider not a one-dimensional square well, but a three-dimensional square well. Schrödinger's time-independent equation for the deuteron problem is:

$$\left(\frac{\hbar^2 d^2}{2\mu dr^2} + V(r)\right)u(r) = -Bu(r) \qquad \text{...(8.11)}$$

In the case of the deuteron, the experimental knowledge of the binding energy B is taken as an input in the Schrödinger equation and an estimate of the potential V_0 is made. This is in contrast to the situation encountered in dealing with the hydrogen atom problem, where the potential is precisely known (the Coulomb potential) and what one finds are the energy eigen values of the system.

The binding energy $-B$ being the energy eigen value of the deuteron system (a neutron and proton) we have put it on the R.H.S. of Eq. 8.11. This is, as will be seen, an important experimental input, since experimentally, B is known accurately.

The boundary conditions are:

$$V(r) = 0, \qquad r > R$$

and

$$V(r) = -V_0, \quad r \le R \qquad \text{...(8.12)}$$

The student is advised to go through Sec. 1.II.4 again. For the two regions given in Eq. 8.12, the wave equation can be put as:

$$\left(\frac{\partial^2}{\partial r^2} - k_2^2\right)u(r) = 0, \quad r > R$$

where,

$$k_2^2 = \frac{2\mu B}{\hbar^2} \qquad \text{...(8.13)}$$

and

$$\left(\frac{\partial^2}{\partial r^2} + k_1^2\right)u(r) = 0, \quad r \le R$$

where,

$$k_1^2 = \frac{2\mu(V_0 - B)}{\hbar^2} \qquad \text{...(8.14)}$$

$$\sim \frac{2\mu(V_0)}{\hbar^2}$$

we have put $V_0 - B \sim V_0$ because, $V_0 \gg B$

($\because$ $E_{\text{kin}} \sim V_0 \sim 16$ MeV and $B \sim 2$ MeV).

Now, $u(r) \to 0$ as $r \to \infty$ and $1/r\, u(r)$ must be finite at the origin $r = 0$ and so the solution is:

$$u(r) = A \sin k_1 r, \quad r \le R$$

and

$$u(r) = Be^{-k_2 r}, \quad r > R \qquad \text{...(8.15)}$$

Applying continuity conditions for $u(r)$ and $u'(r)$ at $r = R$,

$$A \sin k_1 R = Be^{-k_2 R}$$

and

$$k_1 A \cos k_1 R = -k_2 B e^{-k_2 R} \qquad \text{...(8.16)}$$

$\therefore$ Taking the ratio,

$$k_1 \cot k_1 R = -k_2 \qquad \text{...(8.17)}$$

$\therefore$

$$\cot k_1 R = -\frac{k_2}{k_1} \sim -\sqrt{\frac{2\mu B/\hbar^2}{2\mu V_0/\hbar^2}} \quad \text{From Eqs. (8.13) and (8.14)}$$

$\therefore$

$$\cot k_1 R = -\left(\frac{B}{V_0}\right)^{1/2} \qquad \text{...(8.18)}$$

As argued earlier, we know that the binding energy B of the deuteron is much smaller than the depth of square well V_0, and so, from Eq. 8.18 we can approximately write:

$$\cot k_1 R \sim 0$$

$\therefore$

$$k_1 R \sim \pi/2 \qquad \text{...(8.19)}$$

The wave function is like the one that is shown in Fig. 8.1 (b). The exponential tail represents an important fact: *the deuteron is a very loosely bound structure in which the two nucleons spend a considerable amount of time outside the range of the attractive potential which binds them together.* We will come to this again a little later.

From Eq. 8.19, we can get a relation between the potential well depth V_0 and the deuteron radius R.

$$k_1^2 R^2 \sim \frac{\pi^2}{4}$$

$\therefore$

$$\frac{2\mu V_0}{\hbar^2} R^2 \sim \frac{\pi^2}{4} \quad \text{(from Eq. 8.14)}$$

$\therefore$

$$R^2 V_0 \sim \frac{\pi^2 \hbar^2}{8\mu}$$

But $\mu \sim \frac{1}{2} m_n$, where m_n = neutron mass ~ nucleon mass

$$\therefore \qquad R^2 V_0 \sim \frac{\pi^2 \hbar^2}{4 m_n} \qquad \ldots(8.20)$$

This relation between the radius of the deuteron and the depth of the potential well is a direct consequence of the experimental fact that the deuteron binding energy B is small. From Eq. 8.20, by putting in the experimentally observed value of R, one can estimate the order of the depth of the potential well, V_0. This turns out to be about 21 MeV. (In this calculation units will have to be matched between the sides of Eq. 8.20.)

The expectation value of r^2, where r is the distance between the neutron and proton, can be easily calculated. If we call it r_d,

$$r_d^2 = \langle r^2 \rangle = \int u r^2 u \, dr$$

using the wave functions given in Eq. 8.15,

$$r_d^2 = A^2 \int_0^R r^2 \sin^2 k_1 r \, dr + B^2 \int_R^\infty r^2 e^{-2k_2 r} dr \qquad \ldots(8.21)$$

The values of A and B, can be found by simultaneously solving Eq. 8.16 and using the normalisation condition,

$$A^2 \int_0^R \sin^2 k_1 r \, dr + B^2 \int_R^\infty e^{-2k_2 r} dr = 1 \qquad \ldots(8.22)$$

This gives,

$$A^2 = \frac{2k_2}{1 + k_2 R}$$

and

$$B^2 = \frac{2k_2 (\sin^2 k_1 R) e^{2k_2 R}}{1 + k_2 R} \qquad \ldots(8.23)$$

From Eq. 8.13, using the experimental value of the deuteron binding energy B and $\mu = 1/2 m_n$, we get

$$k_2 \sim 0.23 \mathrm{F}^{-1} \qquad \ldots(8.24)$$

As remarked earlier the electron scattering data gives the value of $r_d \sim 4.2$ F. When this is put in Eq. 8.21 and use is made of Eqs. 8.23 and 8.24, we get

$$R \sim 2.4 \mathrm{F} \qquad \ldots(8.25$$

and

$$k_1 \sim 0.654 \mathrm{F}^{-1}, \quad \text{for } k_1 R \sim \frac{\pi}{2}$$

Using these values from Eq. 8.14, $V_0 \sim 25$ MeV.

Thus we see that approximately, the nuclear potential responsible for the binding of the deuteron can be represented by a square well about 20–25 MeV deep and with a width $R \sim 2.4$ F (see Fig. 8.1).

The *range* of the nuclear force can be estimated in this way. Notice that it is smaller than the average radius of the deuteron (r_d), which is larger. This is an interesting fact.

From Fig. 8.1 (b), it can be seen that the wave function $u(r)$ of the deuteron falls off according to $e^{-k_2 r}$ in the region $r > R$. We may thus define the radius of the deuteron as $1/k_2$ since this is a measure of the range of values of r for which there is an appreciable probability of finding the particles. This is essentially the barrier penetration effect which we considered in Chapter 1 Part II. The probability of finding the nucleons outside the potential well (in the region $r > R$) goes as $e^{-2k_2 R}$. We know that,

$$k_2^2 = \frac{2\mu B}{\hbar^2} \qquad \text{(Eq. 8.13)}$$

$$= \frac{m_n B}{\hbar^2} \qquad \because \quad \mu = \frac{1}{2} m_n$$

$$\therefore \qquad \frac{1}{k} = \text{radius of the deuteron}$$

$$= \frac{\hbar}{(m_n B)^{1/2}} \qquad \ldots(8.26)$$

Range of the nuclear potential is,

$$R = \frac{\pi}{2} \frac{\hbar}{(m_n V_0)^{1/2}} \quad \text{(from Eq. 8.20)} \qquad \ldots(8.27)$$

$1/k$ in Eq. 8.26 can be taken to represent the average radius of the deuteron, r_d in Eq. 8.21.

The ratio:

$$\frac{(1/k)}{R} = \frac{\text{Average radius of the deuteron, } r_d}{\text{Radius of the nuclear potential well}}$$

$$= \frac{\hbar/(m_n B)^{1/2}}{\pi\hbar/2/(m_n V_0)^{1/2}}$$

$$= \frac{2}{\pi}\left(\frac{V_0}{B}\right)^{1/2} \qquad \ldots(8.28)$$

Since $V_0 \sim 25$ MeV and $B \sim 2$ MeV, this ratio is greater than one; in fact, it is probably ore than two. This is the reason why one is required to conclude that the deuteron is a loosely ound structure. The radius of the deuteron is significantly more than the radius of the nuclear otential i.e., the range of the nuclear force. The probability of any radial separation r between e neutron and proton is proportional to the square of the wave function $u(r)$. From Fig. 8.1) it is possible to make a rough estimate about the shape of the graph $u^2(r)$ against r. A mparison of the area under this curve inside the well and outside the well is a measure of e relative probability of finding the particle at $r < R$ or $r > R$. A precise calculation can be ade by using the Eqs. 8.15 and 8.23. This is left as an exercise to the student. The result is at the two nucleons spend more than 50 per cent of the time outside the range of the potential ell! The quantum mechanical effect of the barrier penetration should be appreciated in the uteron problem. The deuteron therefore has an extended structure; it is loosely bound.

Another important fact which comes out of this wave mechanical treatment of the deuteron oblem is that the depth of the potential well, which turns out to be about 25 MeV is *much ger than* the Coulomb force between the two protons separated by a distance equal to R, e range of the nuclear force. For $R \sim 2.4$ F the Coulomb force between two protons rresponds to a potential of only 0.6 MeV.

8.5 CENTRAL AND NON-CENTRAL FORCES: THE TENSOR FORCE AS AN EXAMPLE OF NON-CENTRAL FORCES

the last section, for reasons of simplicity we had assumed that the nuclear potential is *central* ., it depends only on the distance between the two nucleons. Further the ground state of the uteron was assumed to be an S - state i.e., $l = 0$ (similar to the ground state of hydrogen, having ro angular momentum). In Sec. 8.3 we learnt about the magnetic dipole moment and the electric adrupole moment of the deuteron. A non-zero quadrupole moment implies that the wave function not spherically symmetric $l = 0$ one, and so our assumption that for the deuteron $l = 0$ is not entirely rrect.

The experimental results about the magnetic dipole and electric quadrupole moments can e explained and understood by considering *admixture of l values in the wave function*. In ec. 8.2 we have seen that for the deuteron, the total angular momentum $I = 1$ and a maximum alue of spin $S = 1$. Thus the only possible values for the orbital angular momentum quantum mber l are 0, 1 and 2. We have learnt in Chapter 1 Sec. 1.II.3 on parity that, the conservation parity demands that a wave function cannot be a sum of functions of opposite parities. *Thus en and odd values of l cannot be both present in the same wave function.* The Functions even l have Even parity and those of odd l have Odd parity. Thus for the deuteron, only $l =$ can be present along with $l = 0$. The wave function (total) then can be written down as:

$$\psi = a_0\psi_{1s} + a_2\psi_{1d} \qquad \ldots(8.29)$$

Here ψ is the total wave function.

ψ_{1s} is the part corresponding to $l = 0$ state and ψ_{1d} is the part corresponding to $l = 2$ state, ich is a 1d state.

The coefficients a_0 and a_2 give the strengths of these wave function and by squaring them e can estimate, how much time the deuteron spends in state 1s and state 1d. The experimental results of the electric quadrupole moment and the magnetic dipole moment of the deuteron can be explained by taking,

$$|a_0|^2 = 0.96$$

and

$$|a_2|^2 = 0.04 \qquad \ldots(8.30)$$

imp → Our conclusion therefore is that the deuteron spends about 96 per cent of its time in an $l = 0$, 1s state and the remaining 4 per cent of its time in an $l = 2$; 1d state. For both $l = 0$ and $l = 2$ we have $S = 1$. Thus one can satisfactorily account for the observed dipole and quadrupole moments of the deuteron by considering an admixture of $l = 2$ value in to $l = 0$ value in the corresponding wave functions. What is the physical effect of changing the angular momentum of the system from $l = 0$, to $l = 2$ (for about 4 per cent of total time)? Obviously a *torque* must be considered to act. This torque is related to the potential by the relation,

torque
$$\tau = |\mathbf{r} \times \mathbf{F}| = rF_0 = -\left(\frac{\partial V}{\partial \theta}\right) \qquad \ldots(8.31)$$

We thus see that a change in the angular momentum implies that the potential V is not just a function of r as assumed previously, but it is a function of θ *also.* The force responsible for this is dependent not on r alone as in the case of a pure central force. It also depends on θ, the angle between the spin angular momentum direction and the line joining the nucleons. This force is clearly a *non-central force* and it is called the *tensor force.*

The value of the tensor force depends on the angle θ which is measured from the direction of the spin vector **S**. Therefore, the tensor force is a function of $\mathbf{S} \cdot \mathbf{r}$. The tensor force is similar to the force law for two magnets, which depends on the way they are oriented. Figures 8.2 (a) and (b) illustrates this in the case of two bar magnets.

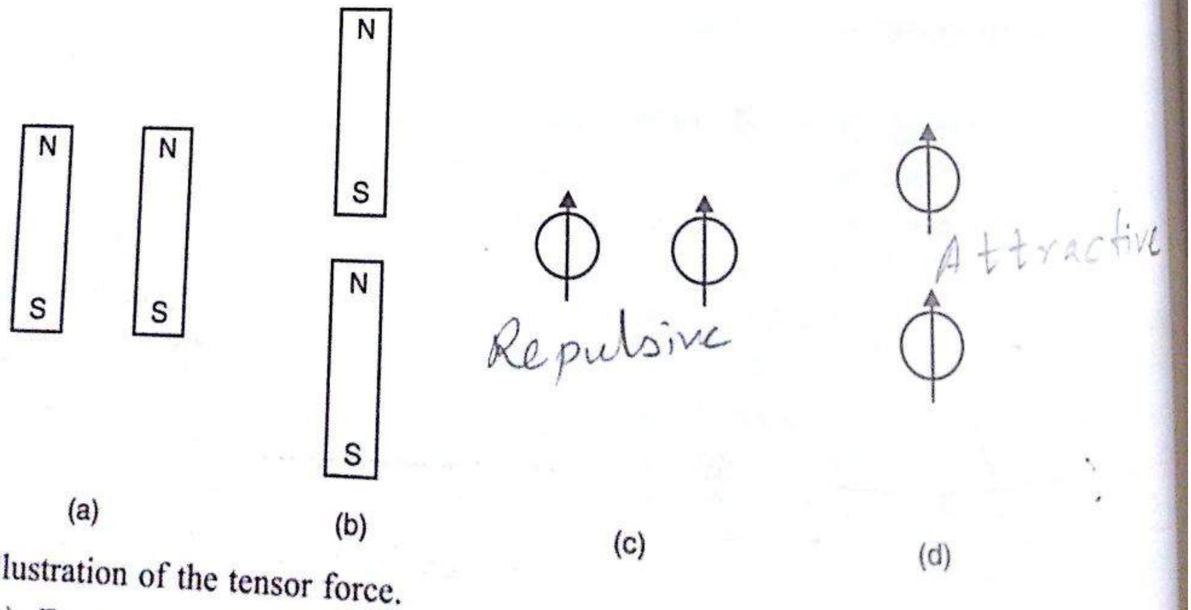

Fig. 8.2. Illustration of the tensor force.

(*a*) For two magnets kept as shown the force is repulsive.

(*b*) The force is attractive.

→ (*c*) For deuteron, the force is repulsive when the spins are parallel and perpendicular to the line joining the nucleons.

→ (*d*) When the parallel spins are also parallel to the line joining the nucleons, the force is attractive.

In part (c) and (d) of the Fig. 8.2, for the same separation of the two nucleons, it is schematically shown how tensor force can be repulsive and attractive. (Remember that there is no tensor force for $l = 0$ i.e., for 1s state, since there is perfect spherical symmetry and the force is entirely central).

If we assume that the nuclear force between nucleons is same for a pair of protons, a pair of neutrons or a pair of neutron and proton then interchanging particles reverses sign of both the distance **r** between the nucleons and their relative momentum **p**. However, the sign of the angular momentum vector $\mathbf{S} = \mathbf{r} \times \mathbf{p}$, remains unchanged because a sign change twice leaves **S** unchanged in sign. (We consider the angular momentum of the deuteron to be due to its total spin $\mathbf{S}_0$.) As a result we cannot have a term like $\mathbf{S} \cdot \mathbf{r}$ and so the tensor force must therefore be proportional to,

$(\mathbf{S} \cdot \mathbf{r})^2$ or to higher even powers of this scalar product.

The actual nuclear potential, representing the nuclear force can be written as,

$$V \text{ (nuclear)} = V_c \text{ (central)} + V_t \text{ (tensor)} \qquad \text{...(8.32)}$$

In the last section we took only the part V_c represented approximately by the square well. The additional non-central term is the tensor potential. It is found to be:

$$V_t \text{ (tensor)} = r\left[2\left(3\frac{(\mathbf{S}\,.\,\mathbf{r})^2}{r^2}\right) - \mathbf{S}\cdot\mathbf{S}\right] \qquad \text{...(8.33)}$$

The factor r^2 in the denominator of the first term makes it dimensionless. The second term is added to average over $\theta = 0$ so that there is no part due to the central potential in Eq. 8.33.

The reason why V_t is called as *tensor potential* is that, it is actually a *scalar product of two second-rank tensors*. In conclusion one can say that a *tensor force* (*a non-central force*) *is capable of explaining the deuteron quadrupole moment*.

8.6 EXCHANGE FORCES: MESON THEORY OF NUCLEAR FORCE—A QUALITATIVE DISCUSSION

In the last section we learnt about the range and strength of the nuclear force. This information was based on the experimental knowledge of the deuteron. It does not give us a theoretical picture of the nuclear force: rather it tells us about some properties of the nuclear force any theory about it ought to predict. The clue is provided by our conclusion in the last section that the nuclear force depends on whether the spin of the deuteron system is 0 or 1 and on whether the orbital momentum is even or odd. Why should the nuclear force depend on these? The answer is provided by the famous Yukawa theory of *exchange of mesons by the nucleons*. This meson exchange leads to *exchange forces*. Let us understand the basic features of Yukawa's theory.

In learning the electromagnetic interaction between two charges separated by a distance an undergraduate student is required to cope up with the idea of action at a distance. The Coulomb force seems to act at a distance even though the charged bodies are not in contact. This rather unpalatable idea of action at a distance to explain the Coulomb force is dispensed within the *electromagnetic field theory*. In this theory the electromagnetic force is transmitted by the exchange of photons. According to the quantum-mechanical theory of electromagnetic fields, each electrical charge is surrounded by a cloud of "virtual" photons which are being constantly emitted and absorbed by the charged particle. There is an exchange of virtual photons when two charged particles are brought near each other. In other words, one charged particle emits a photon and the other charged particle absorbs it. The Coulomb force is given rise to by this constant exchange of photons by the two charged particles. The field theory thus explains why the Coulomb force is not transmitted instantaneously but with a velocity, that of light.

In chemistry, the force due to exchange of electrons is commonly encountered. Take, for example, the hydrogen molecule. There is a strong binding between individual pairs of hydrogen atoms, but a third atom is not attracted to the pair. The hydrogen molecule is said to be *saturated*. The bond between the two hydrogen atoms was explained by the exchange of electrons between them. This exchange provides a covalent bond to form a molecule.

In 1935, the Japanese physicist, Hideki Yukawa, conceived the idea of treating the nuclear force originating from exchange of a particle with a *non-zero rest mass*. Yukawa postulated that each nucleon is surrounded by a *meson field*. As a result it continuously emits and absorbs particles called *mesons*. This exchange of mesons gives rise to the nuclear force. The idea that the exchange of particles gives rise to a force between two bodies can be made reasonable by considering a mechanical situation shown in Fig. 8.3. Two persons are shown standing on movable trolleys and throwing packages at each other. When one person throws a package, he acquires a net momentum in the backward direction. When the other person catches the package, he also acquires a momentum in the backward direction. If they continue to throw and catch packages, a *repulsive force* will obviously be given rise to. On the other hand, if they *pull* packages away from each other, an *attractive force* will be given rise to. Thus we see the possibility of an attractive force being produced, if nucleons interact by exchanging particles (called mesons by Yukawa). An exchange of mesons (with non-zero rest mass) leads to a constant transfer of momentum from one nucleon to the other and hence a force is exerted between them.

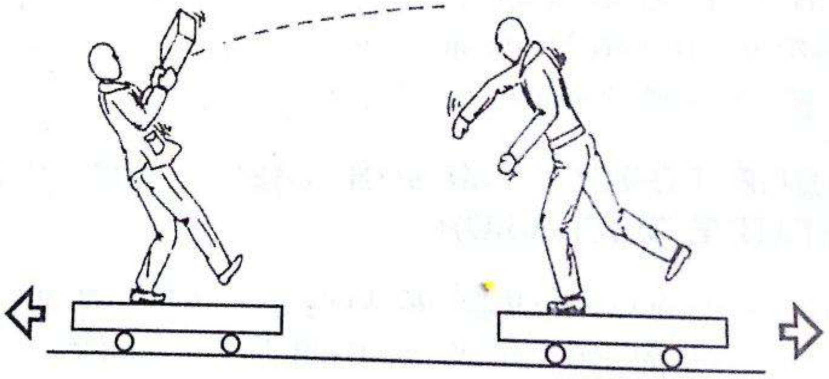

Fig. 8.3. When a mass is thrown back and forth, a repulsive force is generated between the two objects. Pulling a mass results in an attractive force.

The emission of a meson ought to reduce the mass of a nucleon. However, this is not observed. Thus the exchange of meson must take place in such a short time that the "uncertainty" in energy is consistent with the Heisenberg's uncertainty principle, $\Delta E \cdot \Delta t \sim \hbar$. This makes the detection of meson exchange not possible and so the mesons in this exchange process are referred to as virtual mesons. The approach is similar to the exchange of virtual photons giving rise to the Coulomb force in the quantum electromagnetic field theory. There a virtual photon is also undetectable because of the uncertainty principle. However, the range of the Coulomb force is infinite and the rest mass of the photon is zero. The deuteron problem studied in the last section told us that the range of the nuclear force is short, of the order of the nuclear dimensions. We will soon see, that the meson of finite rest mass would give rise to a definite, short range for the nuclear force.

Estimation of the Mass of a Meson using Heisenberg's Uncertainty Principle

If a nucleon emits a virtual meson, π of rest mass M_π, it will lose an amount of energy,

$$\Delta E = M_\pi c^2 \qquad \ldots(8.34)$$

For example, if a proton emits a meson (denoted by π^0 to bring out the electrically neutral character) of rest mass M_π, we have,

$$p \rightarrow p + \pi^0$$

Clearly, the proton mass must decrease which is not shown in careful experiments; the rest mass of proton is constant and always found, 1836 times the rest mass of an electron. This "violation" of conservation of energy can be understood if the meson is absorbed again in a short time Δt such that, $\Delta E \cdot \Delta t \sim \hbar$. The complete reaction can be written as:

$$p \rightarrow p + \pi^0 \rightarrow p \qquad \ldots(8.35)$$

Thus, emission and absorption of a particle with a rest energy $M_\pi c^2 = \Delta E$ is consistent with the uncertainty principle (and therefore consistent with the conservation of energy) if the particle encounters the same or another nucleon within a time Δt given by,

$$\Delta t \sim \frac{\hbar}{\Delta E} = \frac{\hbar}{M_\pi c^2} \qquad \ldots(8.36)$$

With what velocity does the meson travel during this interval of time, Δt? Clearly, it cannot travel with the velocity of light, otherwise its rest mass according to the special relativity will have to be zero. (This in turn will lead to an infinite range for the nuclear force which goes against the experimental facts.) On the other hand, the meson cannot travel very slowly also, as it would lead to a much shorter range (as seen below) than what is experimentally observed. If we assume that the meson travels at about one-half the speed of light then in time Δt, it can travel a distance, R given by,

$$R = \frac{1}{2} c \cdot \Delta t \qquad \ldots(8.37)$$

This value of R clearly must be of the order of the nuclear dimensions i.e., it must correspond to the experimentally observed range of the nuclear force. We can now estimate, what should be the mass of the meson to give the observed range R of the nuclear force. From Eq. 8.36 and Eq. 8.37,

$$R = \frac{1}{2}c \cdot \frac{\hbar}{M_\pi c^2}$$

$$= \frac{\hbar}{2 \times M_\pi c} \qquad \ldots(8.38)$$

From this equation, one can estimate the rest mass M_π of the meson by putting in the experimentally observed value of R. If we insert a mass of about 270 m_0 (where m_0 is the rest mass of an electron) for the meson mass M_π then,

$$R \sim \frac{\hbar}{2 \times (270 m_0)c} \sim 10^{-15}\,\text{m} = \text{one Fermi} \qquad \ldots(8.39)$$

Thus, we estimate roughly that if the nuclear force is due to the process of meson exchange then its range is of the order of a few fermis, which agrees well with the experiments. A finite short range of the order of nuclear dimensions results by putting a mass, $M_\pi \sim 270 m_0$ in Eq. 8.38. Notice that a similar calculation for the electromagnetic field (or gravitational field) gives an infinite range since the mass of the field particle, photon is zero. In Eq. 8.38 the mass equal to zero would give range infinite. $M_\pi \sim 270\, m_0 \sim 140$ MeV.

A particle of mass about 206 m_0 called a μ meson was discovered in cosmic rays, just after one year of Yukawa's prediction. For some time it was thought that this must be the Yukawa meson. However, it was shown that these mesons, called μ mesons (mu mesons) were able to penetrate very large thicknesses of matter, without interacting with nuclei. The Yukawa mesons were expected to interact strongly with nuclei. It took about 12 years when the mesons responsible for the strong nuclear interaction were discovered by physicists using high energy accelerators at Berkeley, University of California. These are the so-called π mesons (pi mesons). In fact, three different types of π mesons or pions have been found. Each nucleon is continuously emitting and absorbing pions, either by the process given in Eq. 8.35 or by one of the following processes:

$$n \rightarrow n + \pi^0;\ p \rightarrow n + \pi^+;\ \text{or}\ n \rightarrow p + \pi^- \qquad \ldots(8.40)$$

Note that two types of pions are charged, the π^+ and the π^-. One is neutral, the π^0. The following table lists some properties of the pions:

	π^+	π^0	π^-
Charge	$+e$	0	$-e$
Mass	273.2 m_0 or 139.6 MeV	264.4 m_0 or 135 MeV	273.2 m_0 or 139.6 MeV
Spin	0	0	0
Magnetic Moment	0	0	0

The pi mesons were also observed in cosmic rays. In higher part of atmosphere the cosmic rays are mostly high energy protons. When these protons interact with nuclei in atoms of atmospheric gases, π mesons are produced. Because of the zero spin, the π mesons are emitted and absorbed readily by nucleons. The law of conservation of angular momentum in Eq. 8.40 gets satisfied. On the other hand the μ-meson has spin 1/2 and so cannot be incorporated in Eq. 8.40 since the nucleons have a spin of 1/2. The π-mesons decay very rapidly and so they could not be found earlier than μ-mesons, at the sea level. The mean life of pions is about 10^{-8} s and that of the μ-mesons or muons is about 10^{-6} s. A π^+ meson tends to be repelled by a nucleus due to its charge. A π^0 meson normally decays into 2 gamma rays. A π^- meson is attracted to a nucleus and gets absorbed by it. In the process it gives up all its rest energy to the nucleus and makes it disintegrate. Such π^- induced nuclear disintegrations have been extensively observed and studied in the laboratory.

The discovery of π-meson predicted by Yukawa was a triumph of the theory and an important landmark in our quest to understand the nuclear force. Yukawa was also able to write an approximate expression for the potential energy of interaction between two nucleons:

$$V = -C\frac{e^{-r/R}}{r} \qquad \ldots(8.41)$$

where C is a constant, r is the internucleon distance and R is the range of force given by, say, Eq. 8.38. Equation 8.41 gives what is commonly known as the *Yukawa potential*. Figure 8.4 shows this potential.

The Yukawa potential has been found to be successful in the deuteron problem and also in understanding the low energy nucleon scattering data. One may say that it is a good approximation to the true nuclear potential. The constant C occupies a place in the Yukawa meson theory, similar to that of charge e in the electromagnetic theory. In other words, the electromagnetic potential energy $V = e\phi$ and in an

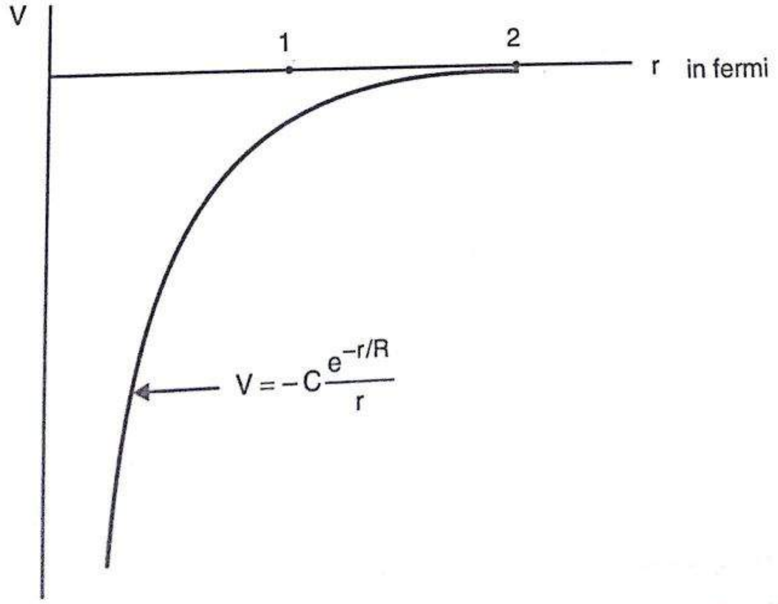

Fig. 8.4. The Yukawa potential.

analogous manner the Yukawa potential energy is, $V = \sqrt{C}\phi$. It can be shown that the meson field equation, written in a manner analogous to the electromagnetic field equation becomes,

$$\nabla^2\phi - \frac{1}{R^2}\phi = 0 \qquad \ldots(8.42)$$

This has the solution,

$$\phi = \sqrt{C}\,\frac{e^{-r/R}}{r} \qquad \ldots(8.43)$$

giving

$$V = \sqrt{C}\phi = C\frac{e^{-r/R}}{r}$$

Types of Exchange Forces

There are three types of exchange forces:

(*i*) The space exchange or Majorana force;

(*ii*) The spin exchange or Bartlett force; and

(*iii*) The space-spin exchange or Heisenberg force.

A detailed discussion of these is beyond the scope of this book. For the first type, an exchange of coordinates changes the sign of the wave function ψ if the parity is Odd and leaves ψ unchanged if the parity is Even. Whether the parity is Even or Odd is determined by the orbital momentum L. Thus if the Majorana potential is denoted by V_M after operating on ψ we have,

$$\begin{aligned} V_M &= \alpha(r)\psi \text{ for even } L \\ &= -\alpha(r)\psi \text{ for odd } L \end{aligned} \qquad \ldots(8.44)$$

Here $\alpha(r)$ is a function of r alone.

We see that the Majorana force takes care of the fact that the nuclear potential depends on whether L is Even or Odd.

For the second type, writing in a similar manner we have,

$$\begin{aligned} V_B\,\psi &= \beta(r)\psi \qquad \text{for total spin } S = 1 \\ &= -\beta(r)\psi \qquad \text{for } S = 0 \end{aligned} \qquad \ldots(8.45)$$

Note that for $S = 1$ an interchange of spins does not affect the wave function while for $S = 0$ it changes the sign of the wave function. We see that the Bartlett force explains why the nuclear potential is different for $S = 0$ and $S = 1$ i.e., nucleon spins antiparallel and parallel.

The third type, Heisenberg potential is defined as:

$$\begin{aligned} V_H\,\psi &= +\gamma(r)\psi \quad \text{for} \quad S = 1, L \text{ even} \\ & \qquad\qquad\qquad\quad\;\; S = 0, L \text{ odd} \\ &= -\gamma(r)\psi \quad \text{for} \quad S = 0, L \text{ even} \\ & \qquad\qquad\qquad\quad\;\; S = 1, L \text{ odd} \end{aligned} \qquad \ldots(8.4$$

whereas before $\gamma(r)$ is a function of r alone.

Equation 8.46 combines the effects of Eqs. 8.44 and 8.45. One usually introduces the *isobaric spin T*, sometimes called as the *i-spin* to refer to these two cases corresponding to the Heisenberg potential. We may thus put:

$$V_H \psi = +\gamma(r)\psi \qquad \text{for } T = 0$$
$$= -\gamma(r)\psi \qquad \text{for } T = 1 \qquad \ldots(8.47)$$

In addition to the three exchange forces there can be an ordinary i.e., no exchange force called the *Wigner force*. It can be written as:

$$V_W \psi = \delta(r)\psi \qquad \ldots(8.48)$$

Thus the resultant nuclear potential can be written as:

$$V = V_W + V_M + V_B + V_H \qquad \ldots(8.49\text{A})$$

The meson theory provides a physical basis to these exchange potentials. Note that all these four potentials depend only on r and so are central in character. In addition to these we must have potential due to the tensor force discussed earlier to take into account the non-central behaviour of the net nuclear potential. If we denote it by V_T, then we can put:

$$V = V_W + V_M + V_B + V_H + V_T \qquad \ldots(8.49)$$

Notice that Eq. 8.49 is general and for the deuteron, V_T will be for $S = 1$, L even and V_H for $T = 0$. All other terms will be absent.

Equation 8.49, however, does not tell the full story. Experiments show that the nuclear force is *not static*.

This makes one consider *velocity-dependent forces*. **L · S**, the spin-orbit interaction is an example of the velocity-dependent forces. Its magnitude depends upon the angle between the spin and orbital motion as well as on the magnitude of L. If $S = 0$, it becomes equal to zero. In Chapter 7 we discussed the shell model which incorporates the *j-j* coupling due to spin-orbit interaction.

In our discussion, we have deliberately avoided the nucleon-nucleon scattering. A detailed discussion and wave mechanics for this is beyond the scope of this introductory text. However, because of its importance in understanding the nuclear force, we shall qualitatively discuss the features of nucleon-nucleon scattering.

8.7 QUALITATIVE FEATURES OF NUCLEON–NUCLEON SCATTERING

Discussion of the deuteron problem was very fruitful. It told us about the range and strength of the nuclear force. It also told us about the non-central components to the nuclear force. To obtain precise information about the manner in which the nucleon separation determines the nuclear force, a study of nucleon-nucleon scattering is invaluable. The angular distribution of these scattered nucleons gives an idea about the nature of the nuclear force. Protons being easily accelerated are usually used as projectiles. The simplest experiments would be a study of protons scattered from liquid hydrogen. Using proton accelerator like a cyclotron, it is possible to have quite monoenergetic neutron beams by knocking out neutrons from a hydrogenous substance and so, *n-p* experiments are possible.

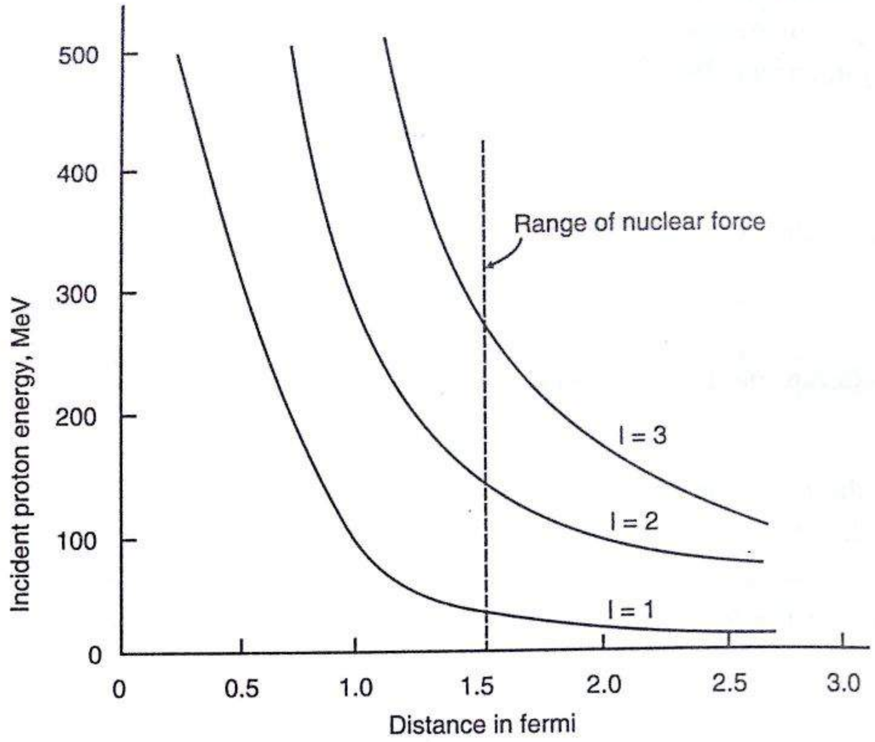

Fig. 8.5. Incident proton energies required to yield different *l*-values as a function of distance of approach.

Angular momentum *l* is a quantised quantity. This has a bearing on the nucleon scattering experiment. The minimum value of energy for scattering corresponding to $l = 1$ is less than that corresponding to $l = 2$. Figure 8.5 shows the relation between the incident energy, the distance of closest approach and the value of orbital angular momentum *l*.

A distance of about 1.5 fermis gives the range of the nuclear force; this is consistent with the deuteron results. Notice that an energy of about 40 MeV is required to get an orbital angular momentum $l = 1$. For $l = 2$ an energy more than 150 MeV is required. This makes it clear that for sufficiently low energies, the nucleon-nucleon scattering corresponds to only $l = 0$. Further for $l = 0$, the scattering distribution is isotropic (in the centre of mass system). This is referred to as the *S*-wave scattering. For higher values of *l*, the scattering distribution no longer remains isotropic and we have *P*, *D*, *E*, etc. wave scattering corresponding to $l = 1, 2, 3$, etc.

Another aspect of higher orbital angular momentum is that the de Broglie wavelength of the nucleon gets smaller. This is clearly because,

the angular momentum = $l\hbar$

$$\therefore\ mvr = l\frac{h}{2\pi} \text{ where } r \text{ is the distance of closest approach}$$

$$\therefore \qquad r = \frac{lh}{p2\pi} = \frac{lh}{\frac{h}{\lambda}\cdot 2\pi} = \frac{\lambda l}{2\pi}$$

This implies that for r, the range of the nuclear force, λ gets smaller for larger l-values.

A decrease in the de Broglie wavelength of the incident nucleon is desirable as this will enable the probe to obtain information about nuclear dimensions and in particular the details of potential at those distances. The quantum-mechanical calculations of the probability of nucleon-nucleon scattering agree well with experiments. For low energy incident nucleons, these calculations are done under the assumption of pure S-wave scattering. The conclusions of these low energy scattering experiments are:

(*i*) the neutron-proton (n-p) and the proton-proton (p-p) forces are same when one takes into account the coulomb forces in p-p experiments. This shows that the nuclear force in all probability is *charge independent*.

(*ii*) for the deuteron the state with spins antiparallel (singlet state) is not bound by a margin of only about 50 keV i.e., it is unbound by about 50 keV. This shows that the nuclear force depends on the *spin orientation* of the two nucleons.

The low-energy experiments do not give any information about the details of the nuclear potential. For this purpose one must use higher and higher incident nucleon energies. The scattering data from these high-energy experiments always contains a mixture of events corresponding to nucleon spins parallel and antiparallel. This makes it difficult to analyse data in a way to yield information about the details of the nuclear potential. In 1953, it was possible to think of experiments in which protons of known spin orientation can be made to scatter from proton targets of known spin orientations. This was possible because in that year physicists found that protons scattered by a hydrogen target were *polarised*.

In Chapter 7, we saw how the inclusion of spin-orbit interaction in the nuclear potential leads to the shell model of the nucleus; it is possible to successfully predict the magic numbers. The existence of spin-orbit interaction can be seen in scattering experiments involving *polarised* particles. To appreciate the idea and the physics that comes out, let us consider a much simplified picture: a spinless target nucleus, say ^{12}C and polarised protons as projectiles. Further let us assume that the nuclear force is attractive and so gives rise to the projectile trajectories as shown in Fig. 8.6 (a).

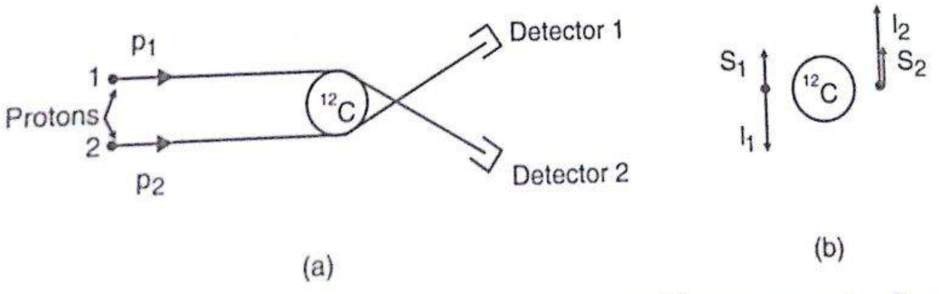

(a) (b)

Fig. 8.6. (*a*) Proton trajectories in the scattering plane. $\mathbf{p}_1$, $\mathbf{p}_2$ are linear momenta of protons 1 and 2, respectively.

(*b*) View from the detector side, in a plane perpendicular to the scattering plane. For the proton 1, $\mathbf{s}_1$ is antiparallel to $\mathbf{l}_1$ and for the proton 2, $\mathbf{s}_2$ is parallel to $\mathbf{l}_2$.

Proton 1 with initial momentum $\mathbf{p}_1$ grazes the target nucleus from the left side and due to the attractive nature of the nuclear force, gets deflected towards the detector 2. On the other hand, proton 2 with initial momentum $\mathbf{p}_2$ grazes the target nucleus from the right and gets deflected towards the detector 1. Assume that both the incoming protons are polarised with spins $\mathbf{s}_1$ and $\mathbf{s}_2$ pointing out of the page, perpendicular to the scattering plane (i.e., plane of the paper). When the protons 1 and 2 get scattered towards the detectors 2 and 1, they develope orbital momenta $\mathbf{l}_1$ and $\mathbf{l}_2$ respectively, with respect to the target nucleus (assumed spinless). Figure 8.6 (b) shows the view in a plane perpendicular to the scattering plane. The right-hand rule tells us that for proton 1, $\mathbf{l}_1$ points into the page and for proton 2, $\mathbf{l}_2$ points out of the page. Thus for the proton 1, $\mathbf{S}_1$ is antiparalled to $\mathbf{l}_1$ and for the proton 2, $\mathbf{S}_2$ is paralled to $\mathbf{l}_2$. This is depicted in Fig. 8.6 (b).

Clearly $\mathbf{l} \cdot \mathbf{s}$ has opposite signs for the two protons. This implies that, if the nuclear potential V includes a spin-orbit term then, V is larger for one proton than the other, as a result more polarised protons will get scattered to one side of the target than to the other side. Experimentally such a left-right asymmetry in scattered protons is observed; it provides the evidence for the existence of a spin-orbit force.

The familiar technique of *double scattering* widely known in optics can be used to study nucleon-nucleon scattering. The first scatterer (target I) acts as a polariser and the second one (target II) acts as an analyser. Figure 8.7 sketches such a double scattering arrangement.

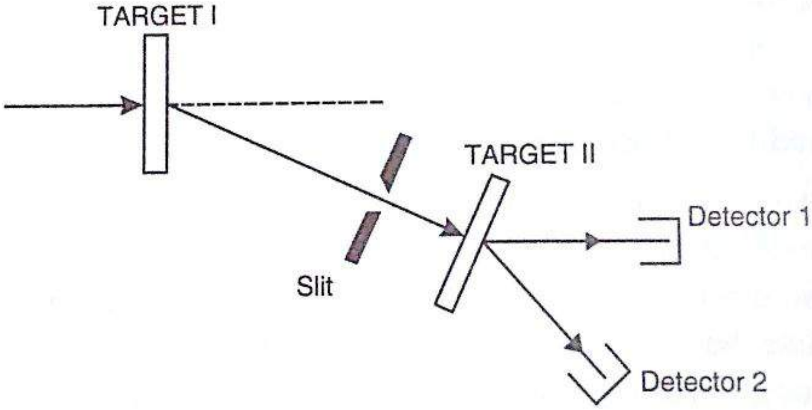

Fig. 8.7. A double scattering experiment (Schematic).

The target proton may have a spin vector going into the page, denoted by ⊗ or coming out of the page, denoted by ⊙. If the incident proton has a spin ⊙ and the target proton has a spin ⊗ then the total spin becomes equal to zero and so there is no spin-orbit force. The incident proton is then not deflected. On the other hand, if the spin of the incident proton is ⊗, the net resultant spin vector goes into the page. Now there are two possibilities, (*i*) the incident particle goes from the *right side* of the nucleus (target I) giving an orbital angular momentum out of the page, ⊙. This makes, **L** and **S** antiparallel as a result of which the force between them becomes *repulsive* (*ii*) the incident particle goes from the *left side* of the nucleus giving an orbital angular momentum into the page, ⊗. This makes **L** and **S** parallel as a result of which the force between them becomes *attractive*.

Clearly, for case (*i*) because of the repulsive force, the particle will deflect to right and for the case (*ii*) because of the attractive force, the particle will deflect to right again. *That is in both cases the spin of the incident particle is ⊗ and the particle is deflected to the right.*

For this discussion we have assumed that the target spin is into the page, ⊗. Now if the particles undergo a second scattering from target II, we expect, spin ⊗ particles will be deflected to the right and spin ⊙ particles will be deflected to the left. But since the target II as shown in Fig. 8.7 is at the right of the incident beam, only those particles with spin ⊗ will reach it. (The spin ⊙ particles get deflected to the left and so will not reach the target II). The first scattering gives as an incident beam (for the target II) for which all particles have their spin vector going into the page ⊗ i.e., a *polarised incident beam.*

Thus for target II, since all incident particles have a spin ⊗, we do not expect the detector 1 (which is at the left of the incident beam) to record any particles while the detector 2 is expected to record particles. In an actual situation, forces other than the spin-orbit forces are present and what one expects is that the detector 2 should record a much larger number of particles than the detector 1. This is what is experimentally observed and the spin-orbit force among nucleons then gets confirmed.

The observation of polarisation in the beam of scattered high energy (a few hundred MeV) protons is a *definite evidence for the existence of a spin-orbit force.*

Figure 8.8 indicates the potentials that have been found to account satisfactorily for nucleon scattering results up to about 300 MeV.

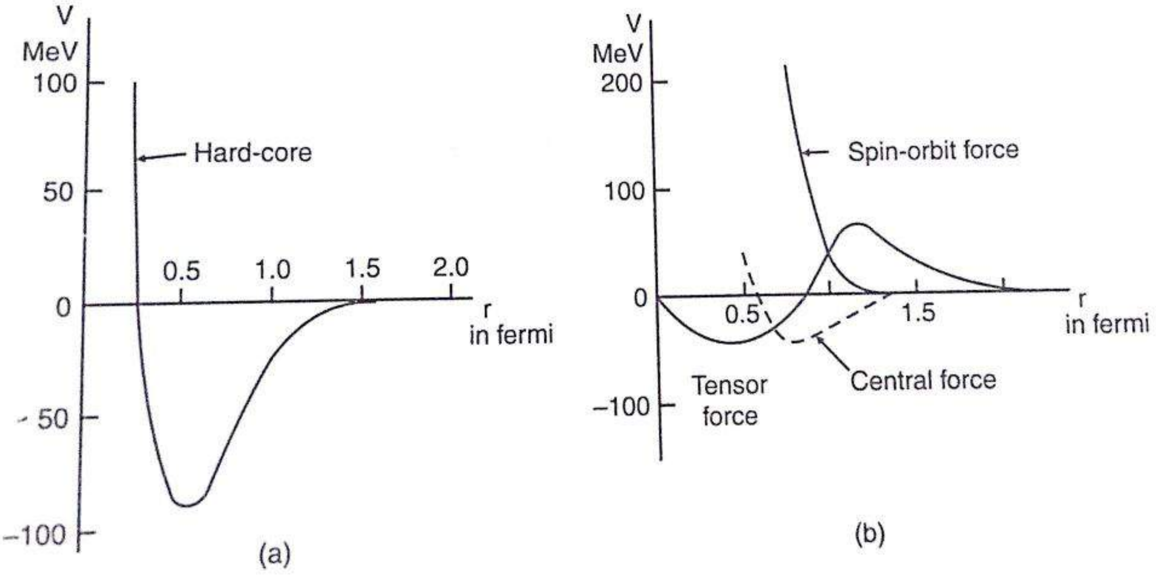

Fig. 8.8.

A striking feature of Fig. 8.8 is that the nucleon-nucleon force contains a *repulsive core.* In other words, it becomes very strongly repulsive at distances less than 0.5 fermis. For simplicity, it is referred in terms of a *hard-core*; the nuclear potential goes to infinity at some value of r. Two nucleons cannot approach one another closer than this hard-core value of r. This is to be expected, since if there were no repulsive force at the core, the nucleus would collapse to the size of the nuclear force range R. This, in turn, implies that all nuclei would have the same size, which is contrary to the experimental results. Note that in our earlier diagrams representing the nuclear potential we have ignored this repulsive hard-core since we were concerned with low energies.

We conclude this chapter by observing that nuclear potentials have been found so that they work well and reproduce the experimentally observed nuclear properties. In this sense, the problem of nuclear force appears to have been solved. However, these nuclear potentials are not unique and new sets of potentials are always found which work as well. They do not add to our knowledge of the basic nature of the nuclear force. Perhaps the farthest we have gone in our understanding of the nuclear force is Yukawa's meson exchange theory and that is now a story about 75 years old! Although a great deal has been learnt in recent years the nuclear force is, yet not fully understood.

EXERCISES

1. Summarise the important experimental properties of the deuteron. Give one method each for the determination of these properties.
2. Treat the deuteron as if it were a particle in a cubic box of side l and mass equal to the reduced mass of the proton and neutron. How far is the deuteron energy above the potential energy of interaction? Letting this to be the ground state energy of the particle in the three-dimensional box obtain l. From this, make a rough estimate of the nuclear diameter.
3. If the binding energy of the deuteron were say 16 MeV, what would be roughly the depth of the potential well, assumed square?
4. In a deuteron, show that the two nucleons spend about 50% of the time outside the range of the potential well which binds them together. Explain the basis of this result. Sketch the wave functions for the ground state.
5. What is the tensor force? Explain how this accounts for the observed quadrupole moment of the deuteron.
6. For the deuteron the maximum value of the spin $S = 0$. What are the possible values of the orbital angular momentum quantum number l? Show how the conservation of parity rules out the value $l = 1$.
7. What are the different types of exchange forces? Summarise their effects on the nuclear wave function.
8. Show how a double scattering experiment brings out the spin-orbit interaction.
9. Describe the basic ideas in Yukawa' s meson exchange theory of the nuclear force. Assuming the range the nuclear force to be of the order of the nuclear dimensions ($\sim 10^{-15}$ m), calculate the pion mass using Heisenberg's uncertainty principle.
10. A π^0 meson decays into two gamma rays. If the π^0 is at rest, what is the energy of each γ-ray?
11. Give evidence and arguments to show that,
    - (*i*) Nuclear forces are strongly attractive and have short range.
    - (*ii*) Nuclear forces show saturation.
    - (*iii*) Nuclear forces are charge independent.
    - (*iv*) Nuclear forces are velocity dependent.
    - (*v*) Nuclear forces are of exchange type.
    - (*vi*) Nuclear forces are partly non-central.
    - (*vii*) Nuclear forces are repulsive below a distance of about 0.5 F.

9

Nuclear Physics in Other Areas of Physics

"I would therefore sharpen the criterion of scientific merit by proposing that, other things being equal, that field has the most merit which contributes most heavily to, and illuminates most brightly, its neighbouring scientific disciplines."

—*Alwin M. Wienberg*

9.1 INTRODUCTION

This chapter is devoted to an introduction to some widely-known and used techniques which have originated in the study of the nucleus, but which are now more and more used in other areas of science. We certainly cannot hope to be very exhaustive in our treatment and only two relatively well-established techniques shall be considered.

9.2 THE TECHNIQUE OF NMR (NUCLEAR MAGNETIC RESONANCE)

The discovery of NMR owes a lot to the development of radar systems during World War II. Very powerful radio frequency oscillators were built for this purpose and this was responsible for the realisation of nuclear magnetic resonance (NMR). The initial discovery was made in 1946 by E.M. Purcell and his collaborators at Harvard, USA and independently, by Felix Bloch and his collaborators at Stanford, USA. This technique is now recognised as one of the most powerful techniques in Physics, Organic Chemistry and even in Biology.

The principle of NMR is discussed in a simplified form below.

Larmor Precession

While discussing the nuclear magnetic moment in Chapter 4, Part I, we came across the effect of an external magnetic field on the nucleus. The angular momentum vector *precesses* with a uniform angular frequency around the axis of the magnetic field, in a manner similar to the precession of a mechanical top in a gravitational field. This is called the *Larmor precession*. The relation expressing the frequency of precession is called the *Larmor theorem*. According to this theorem, the frequency of precession called the Larmor frequency ν_L is given by,

$$\nu_L = \frac{\omega_L}{2\pi} = \frac{1}{2\pi}\frac{d\Omega}{dt} = g\frac{e}{4\pi m}B \qquad ...(9.1)$$

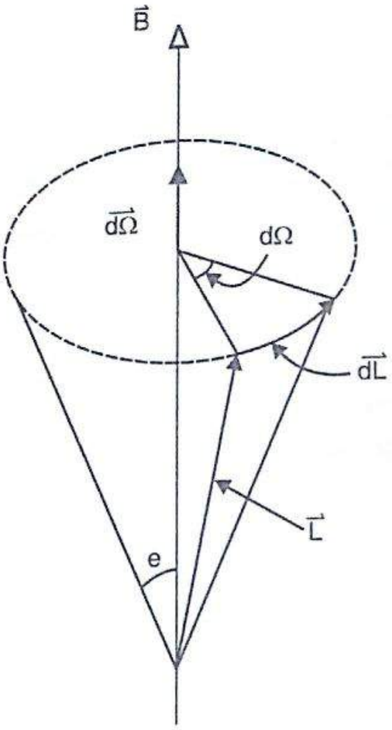

Fig. 9.1. Precession of the angular momentum vector **L** in field **B**.

Here $d\Omega$ is defined in Fig. 9.1, and g is the g-factor of the nucleus. Note that ν_L is independent of **L** and is a function of charge and mass of the particle and of the magnitude of the applied field **B**. Clearly $\nu_L = 0$ if $B = 0$ or $e = 0$. Associated with the angular momentum is a magnetic moment, which also precesses about the field direction. The magnetic field does not change the orientation of the magnetic moment with respect to the field direction. In other words, *the angle* θ *is constant.* Now if the external field has to *induce transitions* between the two orientations of protons (one parallel to the field and the other antiparallel to the field) then the angle θ has to be changed, since, the interaction energy between the magnetic moment μ and the field B is

$$\Delta E = g\,\mu_N \cdot \mathbf{B} \qquad ...(9.2)$$

where,

$$\mu_N = \frac{e\hbar}{2m_p}$$

and

$$g = \left(\frac{\mu}{\mu_N I}\right) \qquad ...(9.3)$$

μ_N = nuclear magneton,

m_p = proton mass

and I = total angular momentum.

It can be easily seen that to change θ, a magnetic field component perpendicular to B is necessary. Further this perpendicular component cannot be simply a static field, since this would only add vectorially to B and thus would merely change the axis of precession. The perpendicular component should rotate with the *same angular frequency* as the angular momentum vector in Fig. 9.1: Such a rotating field can cause θ to change, thereby changing the interaction energy given in Eq. 9.2. This, in turn, at least in principle, can give rise to transitions between different orientation states of protons in an external magnetic field. We will look at the magnitude of this interaction energy ΔE a little later. How to apply a rotating field which can change θ? From elementary mechanics, it is known that two uniform circular motions in opposite directions give rise to a linear oscillatory motion. This is shown in Fig. 9.2.

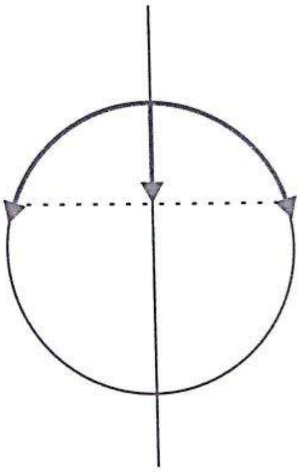

Fig. 9.2. Two circular motions in opposite directions give rise to a linear SHM.

Thus in practice, a rotating field is supplied by a *linearly oscillating field.* In this case, one of the two rotating field vectors precesses around the fixed field B, at the same rate (given by the Larmor frequency ν_L) as the magnetic moment. The other rotates in opposite direction with an apparent frequency $2\nu_L$ and so is out of phase with the magnetic moment.

Let the applied oscillating field, applied perpendicular to the external field B be given by,

$$B_{\text{applied}} = B_1 \sin \omega_L t \qquad \dots(9.4)$$

Its effect can be readily understood if the precessing vectors are viewed from a coordinate system which rotates around the fixed field B with angular frequency ω_L. The magnetic moment and one of the rotating components will be in phase with each other and will therefore appear as "constant" vectors in the new coordinate system. The magnetic moment vector will precess around the in-phase component thereby changing θ. As will soon be seen, $B >> B_1$ and so the angle θ changes only slightly during each cycle of Larmor precession. If the oscillating field is applied with a frequency other than ω_L, neither of the rotating field components will be in phase with the magnetic moment and thus there will be no net change in θ.

Let us now estimate the frequency of the applied field B_{applied}. The g-factor of the proton is experimentally found to be 5.56 (see Sec. 9.3). Therefore for protons, using Eq. 9.1 we have,

$$\nu_L = g\frac{e}{4\pi m_p}B$$

$$= 5.56\frac{eB}{4\pi m_p} \quad \ldots(9.5)$$

For

$$B = \frac{1}{10}\text{ W/m}^2$$

$$\nu_L = 4\times10^6 \text{ cycles/sec.} \quad \ldots(9.6)$$

Notice that this frequency corresponds to short radio frequencies. Thus to fulfil Eq. 9.4, one has to use a radiofrequency oscillator (*rf*-oscillator) of about this frequency. Such a frequency if applied in a direction perpendicular to the external field B, can change θ and the system becomes resonant, the Larmor frequency becoming exactly equal to the frequency of the applied *rf*-oscillator. This is referred to as the *nuclear magnetic resonance* or simply the *NMR*. To get an idea of the energy scale involved in the NMR, let us compute the energy of the nuclear reorientation transitions, $E = h\nu_L$. This is the energy absorbed or released when a proton "flips" from one orientation to other.

$$E = h\nu_L$$

$$= 6\times10^{-34}\times4\times10^6 \text{ joules}$$

$$= 2.4\times10^{-27}\text{ joules}$$

$$= 1.5\times10^{-8}\text{ eV} \quad \ldots(9.7)$$

This is an extremely small energy and tells us about the high sensitivity of the NMR technique. If we take a sample of water about 1/10 c.c. in volume it contains about 10^{22} protons. If the spin orientations of all the protons in the sample are "flipped" (i.e., changed from antiparallel to parallel position or vice versa) simultaneously, the total energy involved is,

$$E_{\text{total}} = 1.5\times10^{-8}\text{ eV}\times10^{22}$$

$$= 1.5\times10^{14}\text{ eV}$$

$$= 2.4\times10^{-5}\text{ joules}$$

This energy is also very small and corresponds to power of the order of microwatts. In this calculation, we have taken the hypothetical case of all the protons "flipped" simultaneously. Actually, the protons will interact with randomly oriented internal molecular fields, which force them to change magnetic substates. Some of them absorb,

$$\Delta E = 2\mu_p B,\ \Delta m_s = -1$$

Others give off ΔE corresponding to $\Delta m_s = +1$.

The proton being a fermion, the possible magnetic quantum numbers are +1/2 and –1/2. Also the possible values of the vector components of the magnetic moment in the direction of the main magnetic field B will be $+\mu_B$ and $-\mu_B$. This is shown in Fig. 9.3.

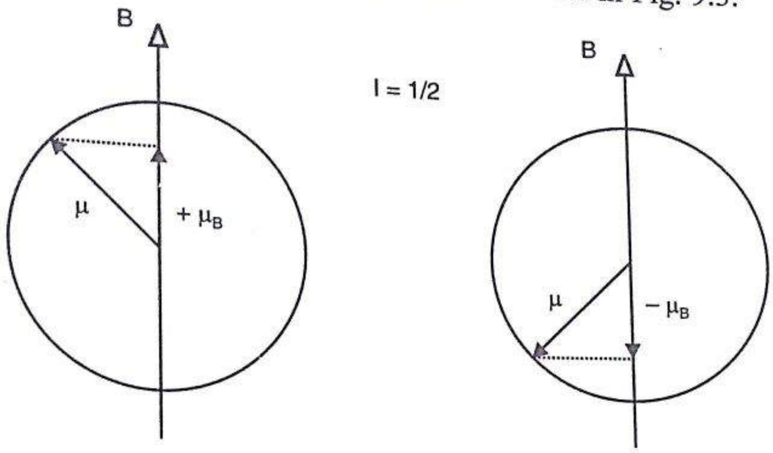

(a)

m = + 1/2

(b)

m = – 1/2

Fig. 9.3.

In the absence of a magnetic field, there is no preference for one or other of the two possible magnetic quantum numbers for protons. Thus in a large sample of protons (like the water sample of 1/10 c.c. volume discussed earlier) there are exactly equal numbers with $m = +1/2$ and $m = -1/2$. In the presence of a magnetic field, however, the protons will tend to align themselves parallel to the field and so $m = 1/2$ energy state is more favourable than $m = -1/2$. But this tendency is opposed by thermal motion. Let us calculate the equilibrium percentages of protons in each m substate by using the Boltzmann distribution law.

The equilibrium population of the two states by Boltzmann law is given by the ratio:

$$\frac{N_{-1/2}}{N_{+1/2}} = e^{-\Delta E/kT} \qquad \ldots(9.8)$$

where k is the Boltzmann constant, T is temperature in absolute degrees and

$N_{-1/2}$ = population in $m = -1/2$ state

and $N_{+1/2}$ = population in $m = +1/2$ state

Using Eq. 9.2, Eq. 9.8 becomes,

$$\frac{N_{-1/2}}{N_{+1/2}} = e^{-2/\mu_p B/kT}$$

$$\sim 1 - \frac{2\mu_p B}{kT} \qquad \ldots(9.9)$$

For $B = 0.1$ W/m^2 (1 kilo-gauss), $T \sim 300$ K the fractional difference in population works out to be $\sim 10^{-7}$. Thus in a sample of 10^{22} protons the *excess populations* in the lower energy state is only 10^{15} protons. This difference, though minute is crucial.

Applied oscillating field can induce transitions in both directions. *Any net energy absorbed by the sample from the radiofrequency field depends only on the population difference between two orientation states, $m = 1/2$ and $m = -1/2$.*

To summarise this discussion, we write down the following conclusions:

1. NMR is concerned with nuclear transitions in a magnetic field, between energy levels which are expressed by the different magnetic quantum numbers. Though protons have been considered in the above discussion, we can have NMR for different nuclei.
2. The energy transfer taking place when the nuclei are "flipped" in a magnetic field can be rendered observable by using the phenomenon of the nuclear precession. By applying an oscillating field perpendicular to the main field direction and making its frequency equal to the Larmor precessional frequency one can achieve nuclear magnetic resonance and transitions between states with different magnetic quantum numbers, which have different energies due to an applied field may be induced. Another way of achieving the resonance condition is to keep the radio frequency fixed and to adjust the main field B, which has the effect of changing the Larmor frequency, till the two frequencies become equal.
3. For any given sample of nuclei, there is a small excess population in the lower energy state. Any net energy absorbed by the sample from the applied radio frequency field depends on the population difference between the energy states.

This population difference, though minute, is crucial, since the applied radiofrequency field can *induce transitions* corresponding to absorption as well as emission (release) of energy.

In this entire discussion, a simplified picture of the NMR has been presented. We have no considered the important role of the *relaxation times* of the samples. A meaningful discussio of this aspect is beyond the scope of this text. However, a qualitative picture may be considere Consider an assembly of hydrogen nuclei, protons. We have seen that the quantum stat $m = -1/2$ being antiparallel to field B, is energetically less favourable than $m = +1/2$ state. Th if an equilibrium distribution (in which both the states have same population) is to be obtained, is necessary that energy be lost to the surroundings by the process called "nuclear relaxation"

This process is difficult for individual protons as for nuclei the probability of collisions w each other or with electrons is very small. So, instead of "relaxation", protons lose energy the nuclear precession discussed earlier. However, a group of nuclei can utilise atomic a molecular thermal motion for the purpose of relaxation. Suppose a proton is surrounded by ot protons (in H-atoms), all undergoing rapid thermal motions. These thermal motions prod random oscillatory magnetic fields which can have frequency components, equal to the Lar frequencies of the nuclei. This in turn can permit the magnetic orientation energy to be conve into thermal energy. It is found out that the rate of relaxation by this mechanism is determi by the temperature, the concentration of magnetic nuclei and the viscosity of the medium.

process can be expressed in terms of *"relaxation time"* which is defined as the *average life time of the excess nuclei in the non-relaxed state.* In other words, it is the *decay time for reaching thermal equilibrium.* Often this thermal relaxation process is slow, of the order of seconds to weeks, and so is not very effective in aiding the nuclei to get rid of excess energy to achieve thermal equilibrium. Pure water for example has a relaxation time ~3.6s. Thus to observe the NMR signal in water, this time has to be drastically reduced so that thermal equilibrium is quickly reached. Obviously, if a substance containing *unpaired electrons* is dissolved in water, then it will be effective in quick thermal relaxation. Thus, some paramagnetic ions are added to water, to help to randomise the proton spins (to reach thermal equilibrium) more rapidly. This reduces the relaxation times to about 10^{-3} sec. and so a large excess proton population is always available in the lower energy level to absorb energy from the radio frequency oscillator.

Experimental Set-up

An NMR set-up consists basically of a magnet, radiofrequency (*rf*) oscillator and a suitable *rf* detector. Figure 9.4 shows the arrangement schematically.

The magnetic field is provided by an electromagnet or permanent magnet with pole faces up to 25 cm. in diameter. The pole gap is about 3 cm. and a field of a few kilogauss (~Wb/m²). Usually a fixed-frequency *rf* oscillator is used. Thus to obtain resonance one changes the main magnetic field by modulating it with a frequency of 50 cycles per second, superimposed on it.

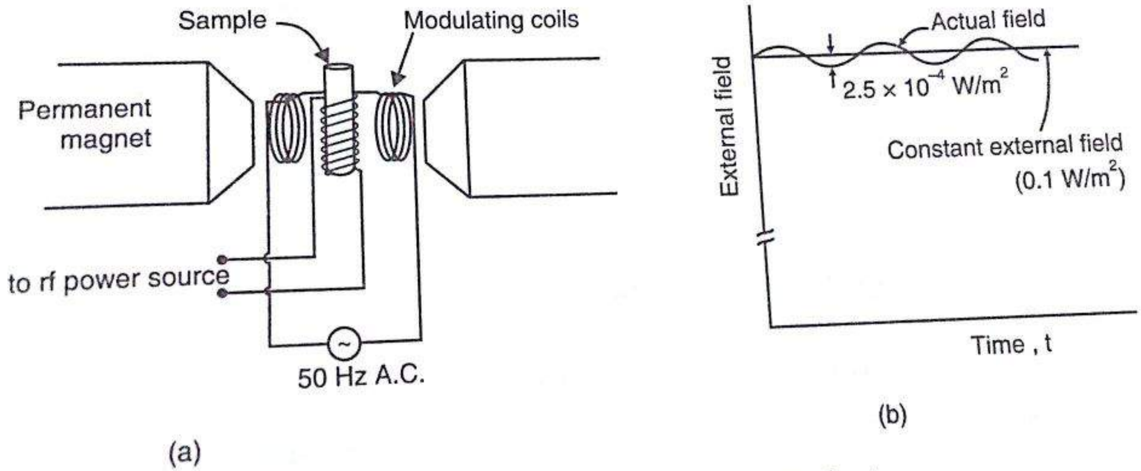

Fig. 9.4. (*a*) Schematic, NMR experimental set-up.
(*b*) Graph showing modulation of applied constant field by Helmholtz coils.

This is done by arranging two Helmholtz coils as shown in Fig. 9.4(a). The constant, large magnetic field is for the nuclear precession. The function of the modulating coil is to vary field while the *rf* frequency is held constant, so that at some value of *B* (actual) the resonance condition,

$$\nu_L = 5.56 \frac{eB_{(\text{actual})}}{4\pi m_p} \text{ is satisfied.}$$

This approach is found easier in practice, as compared to varying *rf* frequency and holding *B* constant

$$B \text{ (actual)} = B_0 + B_1 \sin \omega t$$

Typically, $$B_0 \sim 0.1 \text{ W/m}^2$$

and $$B_1 \sim 2.5 \times 10^{-4} \text{ W/m}^2$$

Figure 9.4 (b) shows the effect of modulation on the main, constant field.

The sample (say water) is placed between the pole gaps and subjected to fixed *rf* frequency. Notice that the oscillator coil is oriented with its axis perpendicular to the magnetic field produced by the main magnet. The resonant condition is most commonly observed by observing a change in the power emitted by the oscillator which supplies the radio frequency field. Alternately, a receiver coil can be put around (not shown in Fig. 9.4) the sample. The horizontal sweep of the oscilloscope is driven by the 50 cycle modulating coil signal. The vertical sweep is connected to the output of the *rf* oscillator. Figure 9.5 shows the output when the resonance condition is satisfied.

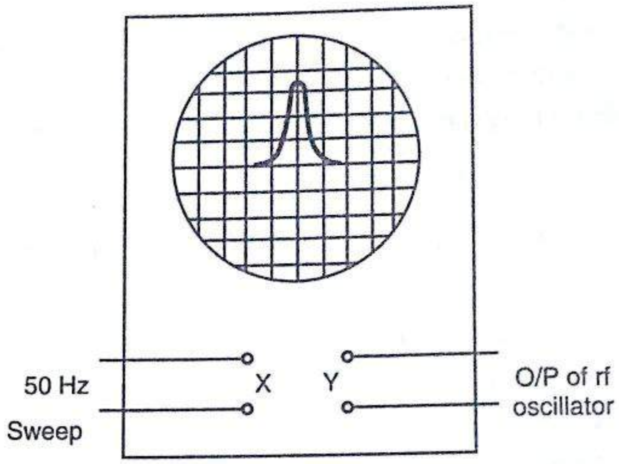

Fig. 9.5. Typical NMR signal.

9.3 SOME EXPERIMENTS WITH NMR

1. Measurement of Proton Magnetic Moment

The Larmor frequency is determined by using the NMR technique described in the previous section

$$\nu_L = g \frac{eB}{4\pi m_p} \qquad \text{(see Eq. 9.1)}$$

The measurement of B accurately poses a problem and it can be eliminated by using orbit motion of electrons in the same magnetic field. As seen in Chapter 1, the electron cyclotro frequency is,

$$\nu_c = \frac{eB}{4\pi m_e} \qquad \text{...(9.}$$

$$\frac{\nu_L}{\nu_c} = g \frac{m_p}{m_e}$$

Thus to determine the *g*-factor of the proton, it is necessary only to determine the frequencies ν_L and ν_c. Since these frequencies can be accurately determined a very precise *g*-value can be obtained. It turns out to be 5.56, a rather high value which is not fully understood. Using this value of the *g*-factor and using Eq. 9.3, one can compute the value of the proton magnetic moment. The present value is given in Chapter 4, Part I. It is roughly $2.8\mu_N$.

2. Determination of Nuclear Magnetic Moments

Let us discuss the often quoted example of ^{7}Li and ^{19}F. One can measure the magnetic moments of ^{7}Li and ^{19}F (both Odd - A nuclei) by determining ν_L using NMR technique. Aqueous solutions of these elements compounds are placed in the sample tube. Note that the spin values cannot be determined using the NMR technique. This is clearly because the NMR method gives only the change in energy for $\Delta m = +1$ or -1, which is independent of the value of *m* and thus gives no information about the spin of the nucleus. The ground state spin of ^{7}Li is known to be 3/2 and so it has four possible orientations with respect to the field direction (as shown in Fig. 9.6). ^{19}F, on the other hand has ground state spin of 1/2 and so behaves much like a free proton. The Table 9.1 gives the values of the *g*-factors measured and the calculated magnetic moments for ^{7}Li and ^{19}F. The *g*-factors are obtained by observing the resonance frequencies ν_L by the NMR technique. For comparison values for a free proton are also shown.

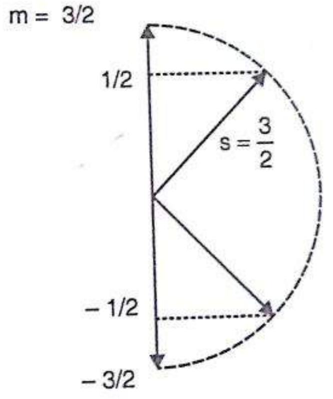

Fig. 9.6.

TABLE 9.1

Nucleus	*Spin*	*g-factor*	μ *in* μ_N
^{1}H	1/2	5.56	2.8
^{7}Li	3/2	2.16	3.2
^{19}F	1/2	5.24	2.7

Note that ^{19}F has a magnetic moment very close to that of a free proton. In contrast, the magnetic moment of ^{7}Li is significantly greater. Can one draw some conclusions about the nuclear structure of ^{7}Li and ^{19}F nuclei, which are based on this data?

For the case of ^{19}F, we can assume that its nucleus consists of an ^{18}O core and a proton. The ^{18}O core consists of 8 protons plus 10 neutrons and its resultant angular momentum is zero since all the spins and moments cancel pair-wise. Now, if the single proton outside the core is in a state having no orbital angular momentum then it is in an $S_{1/2}$ state. This implies that the magnetic moment of the ^{19}F nucleus must be entirely due to the proton in the $S_{1/2}$ state and one expects a value close to free proton magnetic moment. This is what is observed and so one can make a prediction that the structure of ^{19}F nucleus is a proton in a $S_{1/2}$ state with respect to the ^{18}O core. This is shown in Fig. 9.7. Note that the angular momentum of ^{19}F is entirely due to the spin of a proton with no orbital momentum.

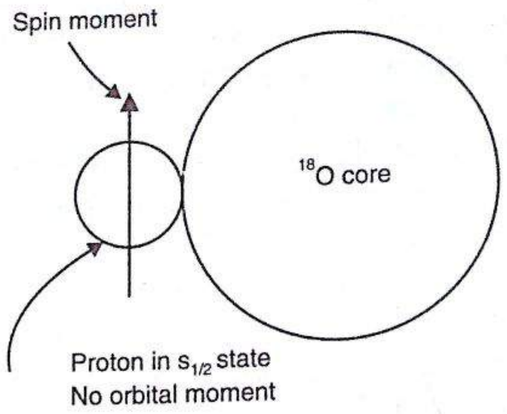

Fig. 9.7. ^{19}F nucleus.

Let us now consider the case of ^{7}Li nucleus, which has a magnetic moment considerably greater than that of a free proton. Clearly, we cannot now ascribe the magnetic moment solely to the spin of the proton, but ought to consider some orbital momentum for it. The nucleus can be assumed to consist of a ^{6}He core in which all spins get cancelled and a proton moving around the core with an orbital angular momentum $l = 1$. This corresponds to a proton in the P-state. If the proton spin and orbital angular momentum are parallel, then a magnetic moment larger than the one with free proton would result. Since this is what the experimental value of the magnetic moment of ^{7}Li suggests, we may consider the proton outside the ^{6}He core to be in a $P_{3/2}$ state as shown in Fig. 9.8. These arguments are given in some detail, because they illustrate how the data obtained by using the NMR technique can be used to make general predictions about the nuclear structure. They support the shell

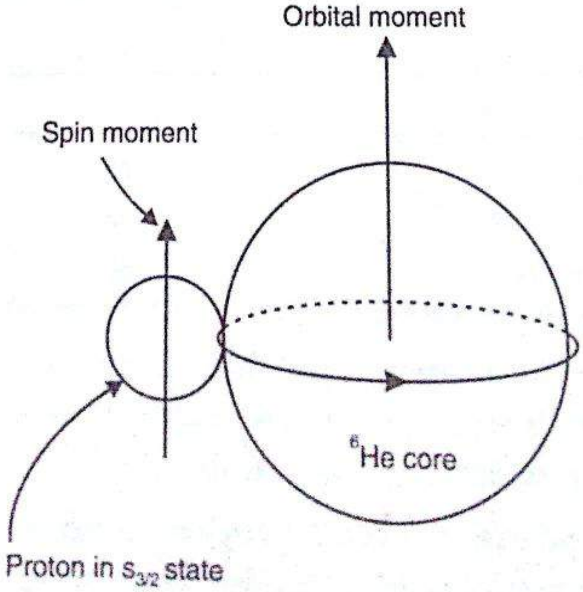

Fig. 9.8. ^{7}Li nucleus.

model of the nucleus. In odd-A nuclei, (A-1) nucleons pair off to form an even Z, even N core. The last nucleon then moves in a potential produced by this core.

3. Application in Organic Chemistry—Chemical Shift

An important application of NMR is the study of the magnetic properties of materials. A proton in a material is always surrounded by atomic electrons. This electronic structure around each proton is always somewhat diamagnetic. Thus, the precession of electrons about the field direction creates a new field B_d which opposes the external field B. We therefore have modified field, $(B - B_d)$ about which the protons precess. The observed resonance frequency gets changed and now corresponds to a field $B - B_d$. This effect is called the *chemical shift* because it is due to the electrons which determine the chemical nature of the sample and it shifts the resonance frequency from the value corresponding to the free proton.

A striking example of chemical shift is the NMR study of ethyl alcohol or ethanol. Its chemical formula is CH_3CH_2OH. Notice that the protons are distributed in such a way that they belong to three distinctly different chemical groupings, CH_3, CH_2 and OH. Figure 9.9 shows a proton NMR spectrum of ethyl alcohol at a field of about 10 KG and at *rf* frequency 40 megacycles. The areas under the peaks are nearly in the ratio 1 : 2 : 3, as would be expected because electrons in these groupings have slightly different diamagnetic properties. This breaks the usual proton resonance signal into three components. Since the OH group has only one proton, CH_2 group has two protons and CH_3 group has three protons the peaks are in the ratio 1 : 2 : 3. Note that the least chemical shift is for the OH group and maximum chemical shift is for the CH_3 group. This corresponds to the fact that the electrons in the OH structure are more tightly bond and so less diamagnetic than those in the CH_2 and CH_3 structures. The chemical shifts are directly proportional to the applied magnetic field, because the diamagnetic effect is also proportional to the magnetic field.

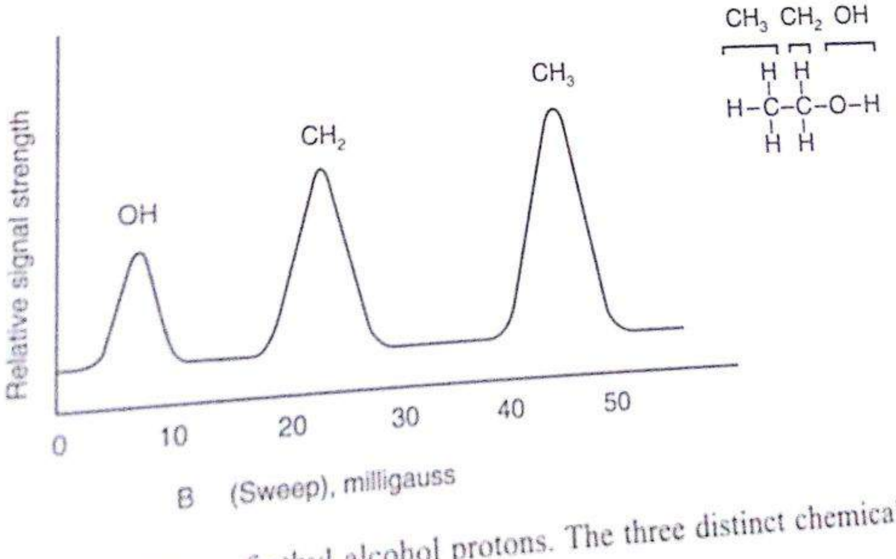

Fig. 9.9. NMR spectrum of ethyl alcohol protons. The three distinct chemical groupings for protons are shown at the right.

Measurements of chemical shifts and strengths of signals are extremely useful in determination of structures of complex organic molecules.

Figure 9.10 shows NMR spectra of the Ketol and its dehydration product.

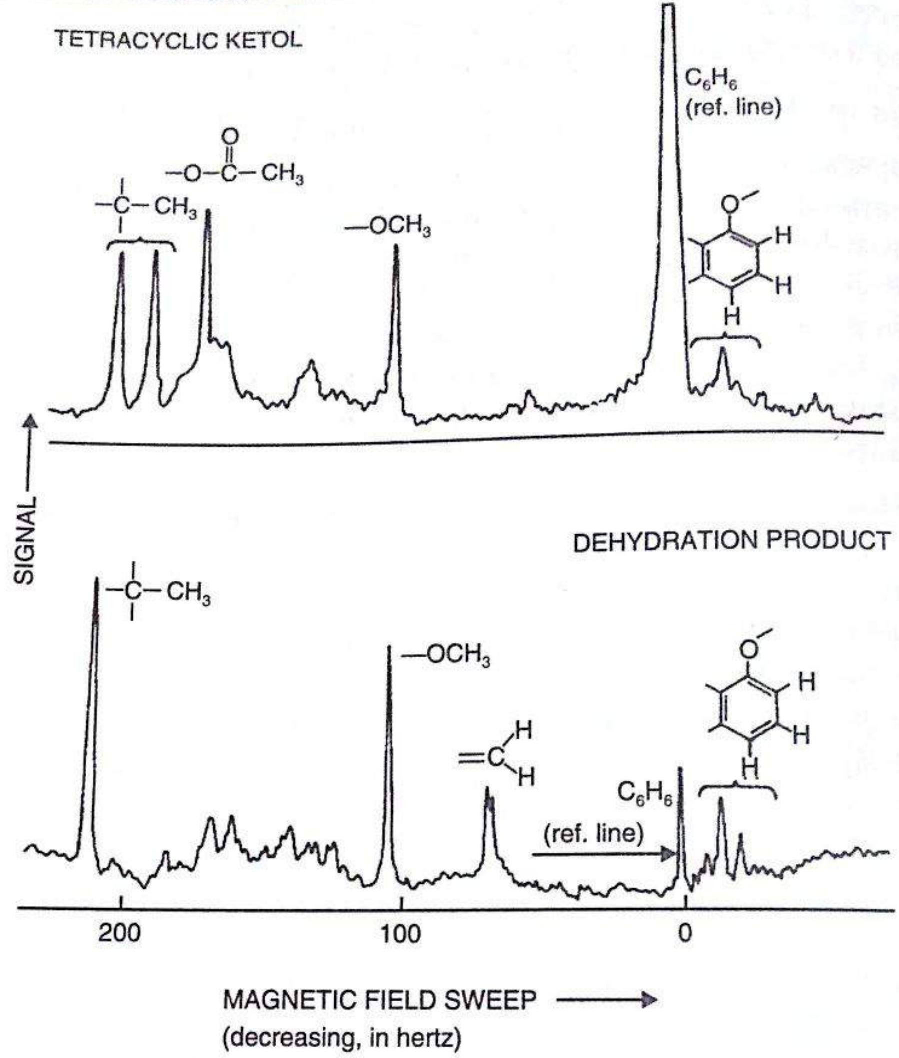

Fig. 9.10. NMR, proton resonance spectrum of tetracyclic Ketol as its acetate and a corresponding dehydration product.

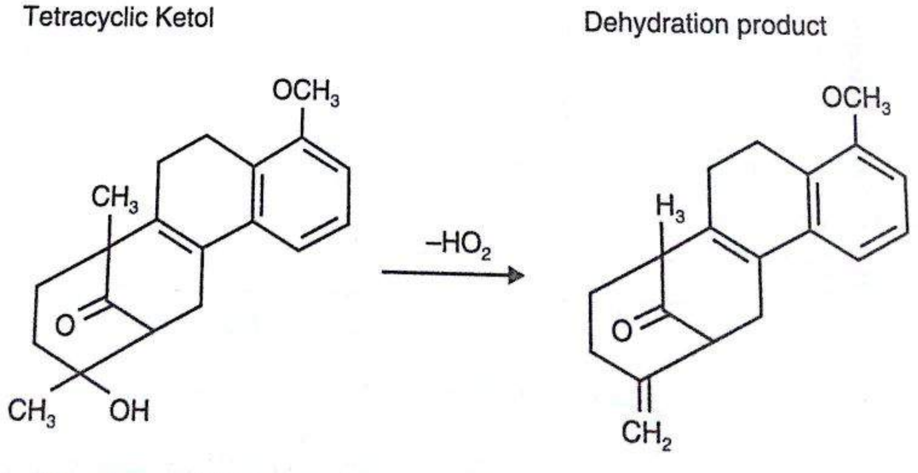
Tetracyclic Ketol
Dehydration product
OCH$_3$
CH$_3$
O
CH$_3$
OH
–HO$_2$
OCH$_3$
H$_3$
O
CH$_2$

Fig. 9.11. Structure of Ketol assigned on the basis of the NMR spectra.

There are two prominent lines in the NMR spectrum of Ketol corresponding to –C–CH group. However, one line disappears on dehydration. On the basis of the NMR spectra, it i possible to assign the structure shown in Fig. 9.11 to Ketol and its dehydrated product.

9.4 THE MÖSSBAUER EFFECT

In 1958, Rudolf L. Mössbauer was able to achieve recoilless emission and recoilless absorption of photons. This is called the *Mössbauer effect*. It provides us a technique for producing and studying gamma rays whose energies are extremely well defined. To understand and appreciate this important fact, let us consider the stable isotope of iron, ^{57}Fe which has been most often used in the Mössbauer studies. Figure 9.12 shows the decay of ^{57}Co to ^{57}Fe.

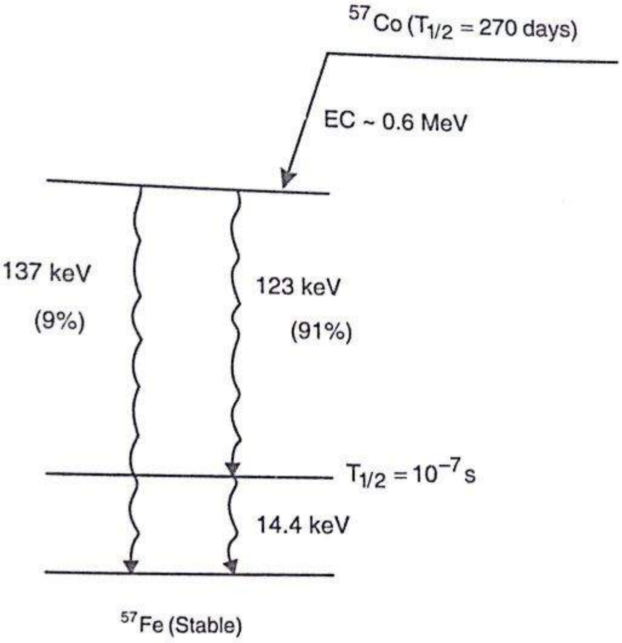

Fig. 9.12. The decay of ^{57}Co to ^{57}Fe.

^{57}Co decays to an excited state of ^{57}Fe by *K* electron capture. As seen from the Fig. 9.12, 9% of the excited ^{57}Fe nuclei go directly to the ground state by emitting a 137 keV gamma ray. The remaining 91 per cent of the transitions take place in two steps. After the emission of a 123 keV gamma ray, the nucleus goes in an intermediate excited state having a half-life of 10^{-7}s. From this state, the ^{57}Fe nucleus reaches the ground state by emitting a low energy gamma ray of energy 14.4 keV. Let us put down the factors which limit the precision of the energy value of this 14.4 keV γ-transition. Since the half-life of the excited state is known, we can use the Heisenberg's uncertainty principle to estimate the uncertainty in energy, which will be *inherent* in the γ-emission.

$$\Delta E = \frac{\hbar}{\Delta t}$$

$$= \frac{0.658 \times 10^{-15}\,\text{eV.s}}{10^{-7}\,\text{s}}$$

$$\sim 6 \times 10^{-9}\,\text{eV} \qquad \ldots(9.11)$$

Comparing this with the energy of the γ-ray, 14.4 keV, we find an uncertainty of about 4 parts in 10^{13}, an extremely small fraction. Can this γ-photon be resonance absorbed by an ^{57}Fe nucleus in the ground state? In this case, we have not yet considered the *recoiling energy* of the nucleus. Suppose that during a transition from an excited state of energy E to the ground state of energy E_0, a nucleus emits a photon of energy hf. By conservation of linear momentum,

$$\frac{hf}{c} = MV \qquad \ldots(9.12)$$

where, M is the mass and V is the recoil velocity of nucleus. In this equation $hf = 14.4$ keV which is the nominal energy of the γ-photon from ^{57}Fe. If this recoil momentum is given only to the emitting nucleus, we can at once calculate its recoil energy. For ^{57}Fe, $M \sim 10^{-25}$ kg and so the recoil velocity,

$$V \sim 80 \text{ m/s}$$

Since this recoil velocity is low enough to permit non-relativistic calculation, we can immediately proceed to estimate the *recoil energy*, E_R.

$$E_R \sim \frac{1}{2} MV^2$$

$$= 2 \times 10^{-3} \text{ eV} \qquad \ldots(9.13)$$

This nuclear recoil energy *reduces the energy of the emitted gamma ray* by the same amount. Compare this with the inherent uncertainty in the γ-ray energy given by Eq. 9.11. Note that for the case under consideration, this recoil energy is about 3 × 10^5 times *greater* than the uncertainty in the γ-ray energy calculated from Heisenberg's principle. This is what makes the resonance absorption of γ-photon formidable by a nucleus; the reduction in the γ-ray energy due to the nuclear recoil seriously affects the chance of it getting absorbed by a similar nucleus. This is in contrast with the situation on atomic level. The photon energies here are small, compared to γ-ray photon energies. For an emitted photon of energy say 1 eV, the value of E_R turns out to be of the order of 10^{-11} eV i.e., much smaller than the inherent uncertainty (For atomic transitions the mean life of an excited level may be taken to be $\sim 10^{-8}$ s. Hence resonance absorption is always possible in atomic transitions.)

There are *two ways* of achieving resonance absorption for nuclear γ-ray transitions. One is to increase the width of the levels by using *Döppler broadening* so that the recoil energy E_R becomes much less than the inherent uncertainty in the γ-ray energy. The other is to almost eliminate the energy of recoil by using solid state properties of a crystal lattice. This is what is accomplished by the Mössbauer effect.

The Döppler effect would clearly depend on the velocity of the source. P. Moon and W. Davey were able to show in 1950 that placing a source of photons on the rim of an ultracentrifuge could produce an external Döppler shift. For a rotor speed of about 800 m/s this Döppler effect increased the frequency of the emitted photons enough to compensate for the loss of energy due to recoil.

However, when a γ-ray emitting nucleus is made a part of a *crystal lattice* the situation quite different. Atom which is embedded in a crystal cannot be treated classically. Since it bound in a crystal, the atom has only *quantised vibrational energy states*. These quantised states are differently populated and the striking fact is that they are *widely separated compared to the low recoil energy* for the example of ^{57}Fe that we have discussed. At a *reduced temperature*, most of the atoms occupy the lowest energy state and effects of thermal motion become negligible. Let us now discuss the effects of embedding the ^{57}Co source in a crystal lattice. The energy of ^{57}Fe γ-ray, 14.4 keV is low enough to be insufficient to separate ^{57}Fe atom from the crystal lattice or to change its vibrational state. In this case, the recoil energy is not transferred to *one* emitting atom, but to a *group* of atoms. The whole mass of crystal—not just the recoiling particle—takes part in the recoil. This implies that the recoiling mass is extremely large and the *recoil velocity is almost zero*. Therefore for all practical purposes the uncertainty in the γ-ray energy is determined by the Heisenberg principle alone i.e., it is possible to measure γ-ray energy with an accuracy of a few parts in 10^{13} (see Eq. 9.11)!

This *recoilless emission* of γ-rays is the *Mössbauer effect*. Apart from ^{57}Fe, there are several other Mössbauer emitters like ^{61}Ni (γ of 71 keV), ^{99}Ru (γ of 89 keV), ^{129}Xe (γ of 40 keV), ^{160}Dy (γ of 84 keV), ^{191}Ir (γ of 129 keV), etc. The gamma ray energy has to be low enough so that the emitting nucleus is not freed from the crystal lattice or excited to a higher vibrational state.

A nucleus can absorb only that γ-ray photon whose energy is equal, within the limits set by the uncertainty principle, to the difference in energy between an excited state and the ground state of the nucleus. In other words, the absorbing nuclei must be identical to the emitting ones. This is what we have termed as the *resonance absorption*. Clearly, it will occur only when the emission of the γ-ray is recoilless; otherwise the γ-ray energy is reduced so much that it cannot *resonate* with a nucleus of the same kind.

Figure 9.13 illustrates schematically Mössbauer's experimental arrangement.

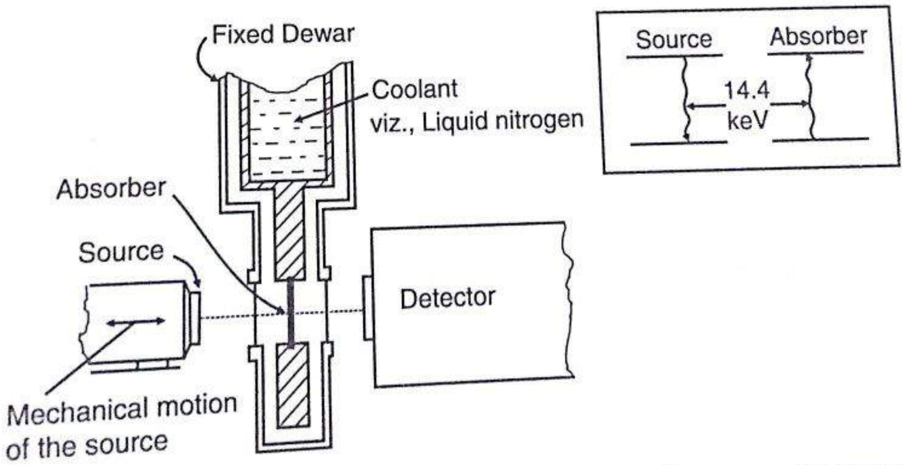

Fig. 9.13. A typical Mössbauer set-up. The frequency of the γ-ray photons emitted by the source is Doppler shifted by a vibratory mechanical motion. The source, absorber and detector are adequately shielded.

The first source used by Mössbauer was ^{191}Ir which emits photons of energy 129 keV. The source and the target (both of ^{191}Ir) were embedded in a crystal lattice and kept at a low temperature using a Dewar containing a liquid coolant like liquid nitrogen. The source can be moved toward the absorber or away from it in a stable controlled manner by mounting it on a mechanical vibrator. The detector is usually a proportional counter described in Chapter 1. By moving the source with a variable velocity, Mössbauer obtained a *resonance curve* shown in Fig. 9.14.

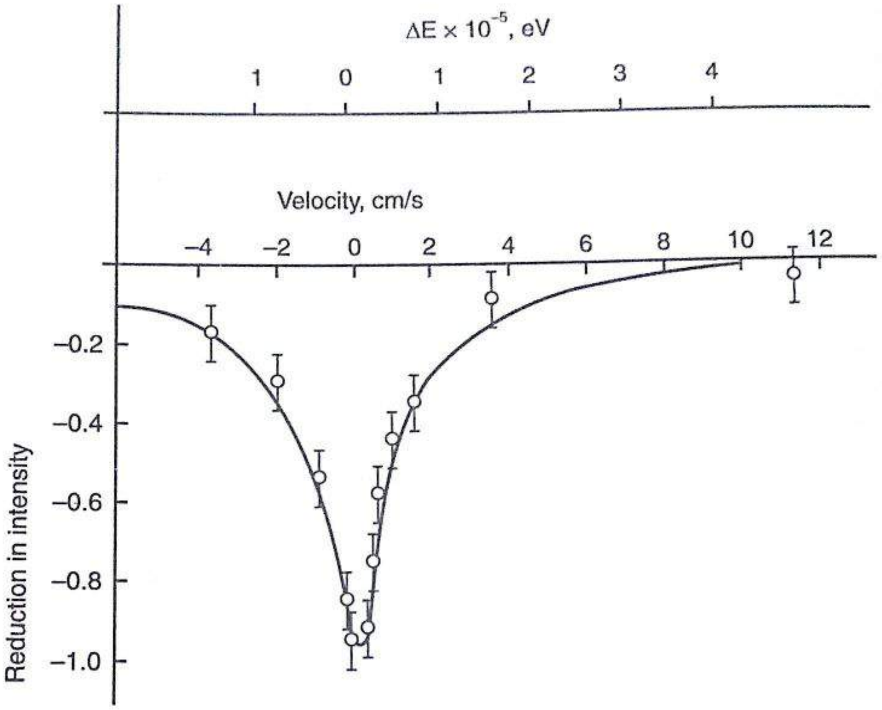

Fig. 9.14. Mössbauer absorption of 129 keV gamma ray by nuclei of ^{191}fr. The temp. was 88°K. The full width at half maximum is ~9×10^{-6} eV. (From R. Mössbauer, Naturwiss 45,538 (1958).

The rate of absorption of photons is plotted on the *Y*-axis and the source velocity is plotted on the *X*-axis. Look at the order of the source velocity. Even if the source moves very slowly, the movement affects the resonance drastically. This demonstrates that the recoil energy is zero at zero velocity and there is no need to produce any Doppler broadening as in the case of Moon's experiment.

9.5 SOME EXPERIMENTS USING MÖSSBAUER EFFECT

1. Test for the Theory of Relativity

As seen in the last section for ^{57}Fe the γ-ray energy is known with an accuracy of a few parts in 10^{13}. This is a tremendous accuracy, not equalled even by the gas lasers.

One of the phenomena predicted by the general theory of relativity is the *gravitational re* *shift*. It is the change in energy of a photon as it travels from one place to another of differen gravitational potential. If a photon of energy *E* is travelling between two points separated by distance *l* near the earth then the change in the energy of the photon is given by,

$$\Delta E = \left(\frac{E}{c^2}\right) g l \qquad \text{...(9.1}$$

where g is the acceleration due to gravity assumed constant.

Clearly the fractional change in energy, $\frac{\Delta E}{E} = \frac{gl}{c^2}$ is very minute.

This is the reason why, a terrestrial test of the theory of general relativity had to wait, till Mössbauer Effect was discovered! This change has been verified by placing an absorber about 20m above a Mössbauer emitter, and then determining the energy shift from the rate at which the source must be moved to achieve resonance absorption.

ILLUSTRATIVE EXAMPLE

Example 9.1: A gamma source is placed 20.0 m above an absorber. With what velocity should the source be displaced upward to counterbalance completely the gravitational change of the gamma energy due to the earth's gravity at the point where the absorber is located?

Solution: Using Eq. 9.14, the fractional change in energy is,

$$\frac{gl}{c^2}$$

∴ The fractional change in momentum is,

$$\frac{gl}{c} \quad (\because E = cp)$$

∴ The velocity to be given to the source to obtain resonance absorption is,

$$v = \frac{gl}{c} = \frac{9.8\text{m/s}^2 \times 20.0\text{m}}{3 \times 10^8\text{m/s}} = 6.5 \times 10^{-5}\ \text{cm/s}$$

2. Study of Hyperfine Structure

In Chapter 2, while discussing radioactivity we have seen that nuclear decay is not influenced by placing the sample in say a magnetic field. However by using a Mössbauer emitter whose radiation is detected by a Mössbauer absorber, it is possible to detect extremely small changes when nuclei are kept in different environments.

The effect of placing either the emitter or absorber in a magnetic field is to make the system go *out of resonance* due to the small changes in the nuclear energy levels. Resonance may be restored by moving the emitter very slowly (a few cm per min or so). By varying this motion in a carefully controlled manner, it is possible to *tune* the system over an extremely narrow energy range characteristic of the Mössbauer effect. Using this technique, it is possible to observe the hyperfine splitting of the nuclear energy levels.

The Mössbauer source is put into a host where its nuclear levels remain unsplit. Usually, the "host" material is a cubic crystal of a diamagnetic material and the radioactive source is put into the lattice substitutionally. The source is then Doppler-shifted (as shown in Fig. 9.13) by mounting it on a mechanical vibrator. A stationary absorber is then placed between the source and the detector. The nuclear levels in the absorber may be split by the coupling of magnetic dipole moment with the magnetic field or by the coupling of the nuclear electric quadrupole moment with the crystalline field gradient. These interactions are termed as *hyperfine interactions* or simply *hf* interactions. Thus due to the splitting of nuclear levels because of the

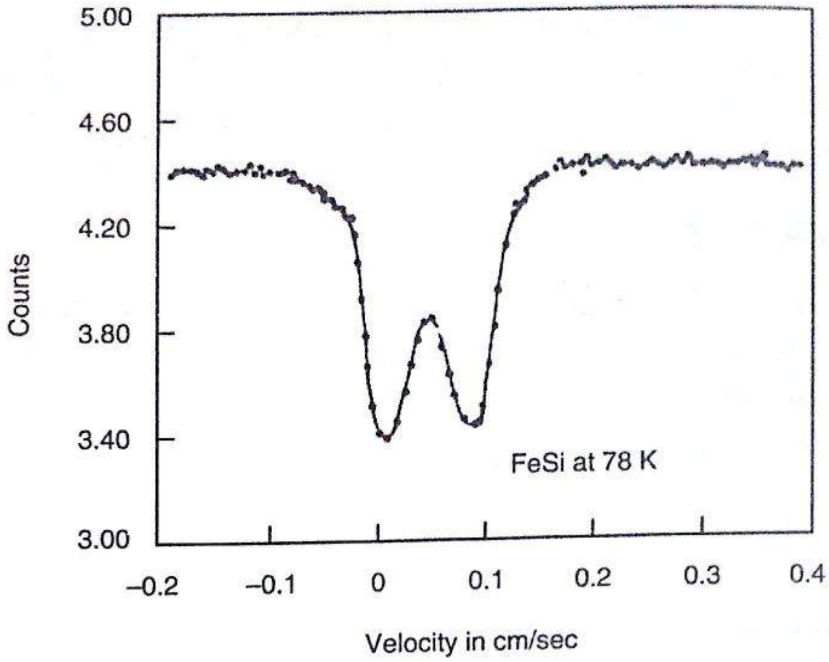

Fig. 9.15. Mössbauer spectrum of FeSi.

hf interactions, there will be a number of different energies at which resonance absorption would take place. The gamma ray intensity would drop whenever the Doppler velocity of the source brings the emitted γ-ray into resonance with an absorption energy in the absorber nuclei.

Figure 9.15 shows the Mössbauer spectrum obtained using this technique. ^{57}Co source was put in chromium and the absorber was FeSi. The two absorption lines are the result of the *quadrupole splitting* of the excited state of ^{57}Fe, which is briefly discussed below.

Figure 9.16 shows how the energy of a nucleus with quadrupole moment Q in an electric field gradient V_{zz} depends on the orientation of the spin I with respect to the direction of field gradient V_{zz}. This is *quadrupole interaction.*

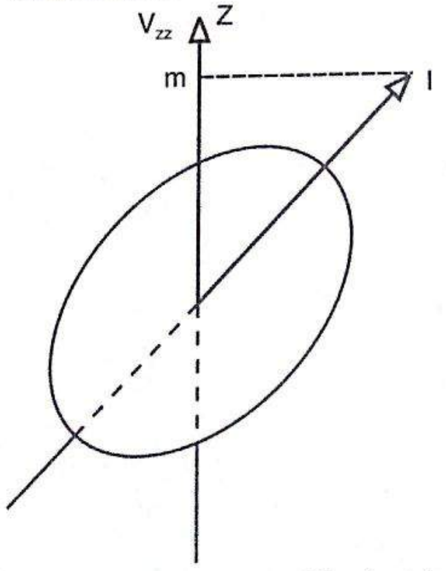

Fig. 9.16. Interaction of nuclear spin I with electric field gradient V_{zz}.

Figure 9.17 shows how in the case of ^{57}Fe the 3/2 level splits up into a *quadrupole doublet* due to the electric field gradient originating from the nuclear electric quadrupole moment.

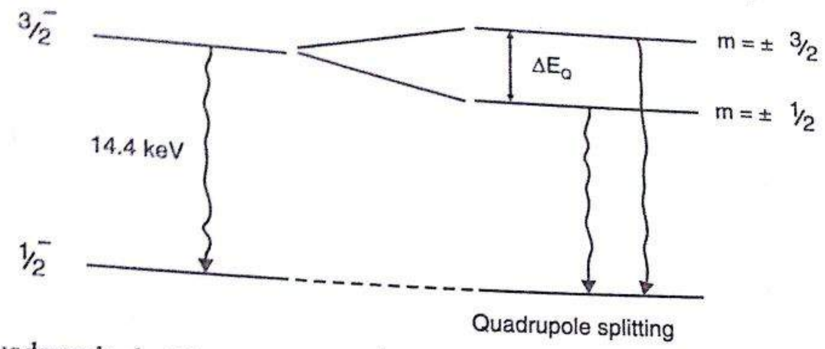

Fig. 9.17. Quadrupole doublet resulting due to the splitting of $I = 3/2$ level in ^{57}Fe due to an electric field gradient.

The energy difference between the two lines is expected to be,

$$\Delta E_Q = \frac{1}{2} eV_{zz}Q \qquad \ldots(9.15)$$

Thus knowing ΔE_Q we can obtain Q, the value of the quadrupole moment of $(3/2)^-$ state in ^{57}Fe, if the electric field gradient V_{zz} is known. For the 14.4 keV transition in ^{57}Fe, the source velocity 0.1 cm/s (see Fig. 9.17) is equivalent to 4.8×10^{-8} eV. This is the value of ΔE_Q, which the Mössbauer experiment yields. The quadrupole moment has been determined to be,

$$Q(3/2) \sim +0.28 \times 10^{-24}\,\text{cm}^2$$

Consideration of the electric field gradient (EFG), V_{zz} is chiefly due to the charges on distant ions and the electrons in incompletely filled shell of the atom itself. To obtain the EFG at the *nuclear site,* the crystal structure must be well known and also how the atom's own electrons interact with the external charge distribution must be known. It then becomes a problem of solid state and atomic physics. Mössbauer effect thus is seen to act as an important bridge between nuclear physics and atomic and solid state physics.

Magnetic Hyperfine Structure

This aspect of the *hf* interaction is due to the interaction of the nuclear magnetic dipole moment μ, with the magnetic field **B** *arising out of atom's own electrons.*

The interaction energy is,

$$\begin{aligned}\Delta E &= -\mu \cdot \mathbf{B} \\ &= -g\mu_N \mathbf{I}\cdot\mathbf{B} \qquad \ldots(9.16)\end{aligned}$$

where, μ_N is the nuclear magneton, g is the g-factor and I is the nuclear spin.

However, $\mathbf{I} \cdot \mathbf{B} = I_z B$ and eigen values of I_z are $m\hbar$ where m is the magnetic quantum number taking $(2I + 1)$ values.

Thus we have $(2I + 1)$ equally spaced levels with splitting energy $g\mu_N B$ between adjacent levels. This is shown for ^{57}Fe in Fig. 9.18.

The Mössbauer spectrum of ^{51}Fe in metallic iron is shown in Fig. 9.19.

It is interesting to note that the ^{57}Co source is inserted in non-magnetic steel (like stainless steel), while a plate of natural iron (FeF_3 in Fig. 9.19) is used as absorber. The 14.4 keV line is *not split* in the non-magnetic emitter material. On the other hand, we get the typical six finger pattern when the absorber is of natural iron. If the absorber were also stainless steel we get only a single absorption line.

ILLUSTRATIVE EXAMPLE

Example 9.2: Using the level diagram of Fig. 9.18 and the Mössbauer spectrum in ^{57}Fe absorber shown in Fig. 9.19. Find the magnetic moment of a ^{57}Fe nucleus in the excited $(3/2)^-$ state and

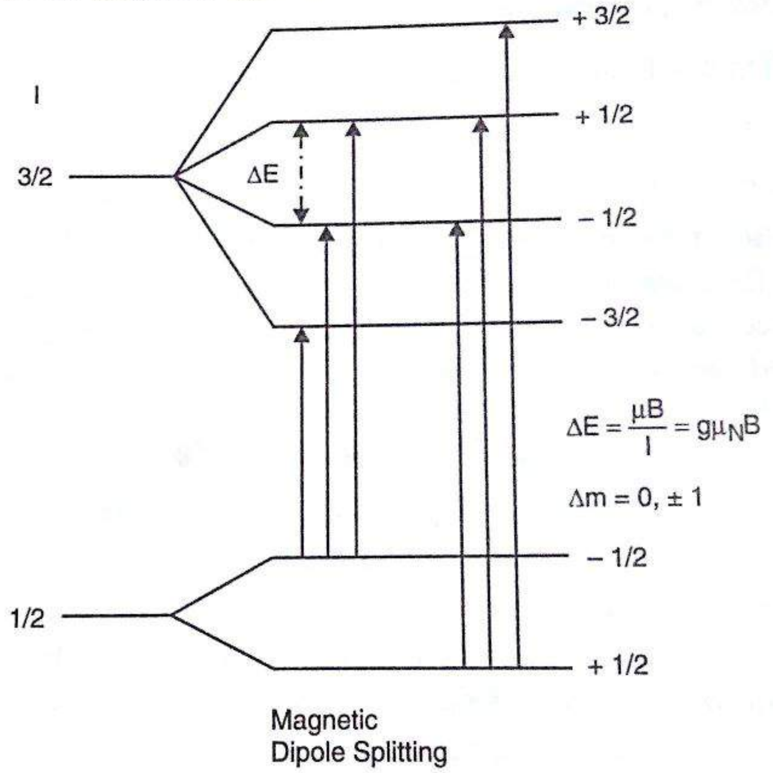

Fig. 9.18. Magnetic dipole splitting in ^{57}Fe. Splitting energy ΔE is not to the scale. There are six allowed transitions.

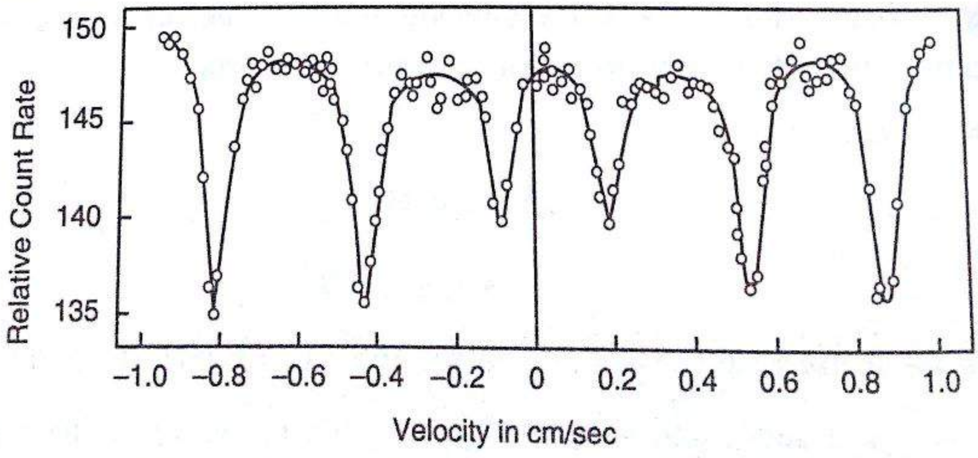

Fig. 9.19. Absorption spectrum for FeF_3 at 4 K.

the magnetic field acting on the nucleus in iron. The magnetic moment of a ^{57}Fe nucleus in the ground state $(1/2)^-$ is given: $\mu(1/2) = 0.090\mu_N$.

Solution: The splitting energy $\Delta E = \dfrac{\mu B}{I}$

The field seen by the ^{57}Fe nucleus, B in the ground or excited state is,

$$B = \Delta E \cdot I/\mu$$

For ground state, $I = 1/2$

$$\mu = 0.090\mu_N$$

We know that, $\mu_N = 4.69 \times 10^{-8}$ eV/tesla

where 1 tesla = 1 Wb/m^2

$= 10^4$ gauss

From Fig. 9.19, ΔE corresponds to a Doppler speed of about 6 mm/s. It is easy to find that for the 14.4 keV transition in ^{57}Fe a speed of 1 mm/s is equivalent to 4.8×10^{-8} eV.

$$\therefore \qquad \Delta E = 2.88 \times 10^{-7} \text{ eV}$$

$= \mu B/I$ where for ground state I and μ are known.

$$\therefore \qquad B = \frac{1/2 \times 2.88 \times 10^{-7} \text{ eV}}{0.09 \times 4.69 \times 10^{-8} \text{ eV}}$$

$$= 3.41 \times 10^1 \text{ tesla or Wb/m}^2$$

$$= 3.41 \times 10^5 \text{ gauss.}$$

Using this B, we can find the magnetic moment μ (3/2) for the excited state of ^{57}Fe nucleus.

$$\mu(3/2) = \frac{\Delta E \times 3/2}{B}$$

$$= 0.13\mu_N$$

Notice that the internal magnetic fields at the nuclear site have tremendous values—a few hundred kilogauss. Such fields cannot be produced easily in the laboratory and before the discovery of superconducting magnets it was impossible to realise such fields in the laboratory.

9.6 NATURAL FUSION—ENERGY PRODUCTION IN STARS

In Chapter 5, when we discussed the graph of binding energy per nucleon (B/A) against mass number (A) it was pointed out that fusing light elements together is energetically advantageous. This process of combining two lighter elements together is called *fusion*. The English astronomer, Eddington had shown as early as 1920 that the fusion of four hydrogen atoms into one atom of helium would release about 7 MeV/nucleon i.e., about 28 MeV in all. This work started the process of understanding the energy given by stars, in particular by the sun. Geophysical studies show that the temperature of the sun must be practically the same for at least 10^9 years. Where does the sun's energy come from? As remarked earlier, the energy released by nuclear fusion reactions is millions of times more than that released in chemical reactions. By 1939 nuclear reactions were well understood and Hans Bethe proposed a set of reactions by which hydrogen might be converted to helium in the sun. It is called the *carbon cycle* since ^{12}C acts as a catalyst. It undergoes changes but it is not used up as it again appears in the final reaction.

THE CARBON CYCLE

$$\begin{aligned}
{}^{12}_{6}C + {}^{1}_{1}H &\to {}^{13}_{7}N + Q \\
{}^{13}_{7}N &\to {}^{13}_{6}C + {}^{0}_{+1}e \\
{}^{13}_{6}C + {}^{1}_{1}H &\to {}^{14}_{7}N + Q \\
{}^{14}_{7}N + {}^{1}_{1}H &\to {}^{15}_{8}O + Q \\
{}^{15}_{8}O &\to {}^{15}_{7}N + {}^{0}_{+1}e \\
{}^{15}_{7}N + {}^{1}_{1}H &\to {}^{12}_{6}C + {}^{4}_{2}He \qquad \ldots(9.17)
\end{aligned}$$

The overall reaction can be written by adding these reactions, cancelling out nuclei appearing on both the sides and computing the total Q-value. We get,

$$4\left({}^{1}_{1}H\right) \to {}^{4}_{2}He + 2\left({}^{0}_{+1}e\right) + 24.7 \text{ MeV} \qquad \ldots(9.18)$$

The two positrons, on annihilation, give another 2 MeV of energy and so the total energy released is 26.7 MeV. This can be expressed as,

$$Q\left(4\,{}^{1}_{1}H \to {}^{4}_{2}He\right) = 26.7 \text{ MeV} \qquad \ldots(9.19)$$

Of this energy about 25 MeV heat the star, and the rest is carried off by the neutrinos.

One may ask the question: why do the 4H atoms not directly combine to give one He atom, rather than going through the cycle given by Eq. 9.17? The reason is that even at high temperatures inside stars protons do not have sufficient kinetic energy to overcome their mutual repulsion.

Can the carbon cycle be produced on the earth? For this, we will have to bombard the carbon and nitrogen nuclei with *accelerated protons*. But the temperature at the sun's centre is so great (1.4×10^7 K) that some protons at the high energy end of their Maxwellian velocity distribution are able to react leading to fusion reactions of the carbon cycle. The fraction of high energy protons is small and it may take a million years to go through this cycle. However the *total number* of protons having the capacity to produce the fusion reactions is very large to be able to account for the great amount of solar energy. Experiments show that there is enough hydrogen in the sun to maintain this carbon cycle for about 30 billion years!

As remarked earlier the temperature of the sun has remained practically unchanged for at least 10^9 years. Clearly the sun is in a state of *equilibrium*. This is due to two opposing effects. On the other hand, if the temperature of the sun were to rise, the fraction of protons participating in the carbon cycle would increase. This would heat up the sun further. On the other hand, if the temperature increases, the sun tends to expand and the concentration of the nuclei in the cycle tends to decrease. This has the effect of reducing the fusion reaction rate. These effects balance each other. Fusion on the sun is *contained* by the large gravitational field of the sun.

9.7 POSSIBILITY OF CONTROLLED FUSION

We have seen how a controlled chain reaction is possible in fission process. Thermal neutrons cause fission. For fusion, we need particles at millions of degrees kelvin. As seen in the last section, in spite of a solar core temperature of 1.4×10^7 K, the solar fusion of H into He is a slow process. The problem of producing such temperatures in the laboratory is very difficult. Which vessel will stand such temperature? The solution possibly lies in the *magnetic confinement of plasma* at about 10^8 K. Some of the possible fusion reactions which can be used are:

$$
\begin{aligned}
&{}^{2}_{1}\mathrm{H}\left({}^{2}_{1}\mathrm{H},\ {}^{1}_{1}\mathrm{H}\right){}^{3}_{1}\mathrm{H} \quad Q = 4.02\ \mathrm{MeV} \\
&{}^{3}_{1}\mathrm{H}\left({}^{1}_{1}\mathrm{H},\ \gamma\right){}^{4}_{2}\mathrm{He} \quad Q = 19.6\ \mathrm{MeV} \\
&{}^{6}_{3}\mathrm{Li}\left({}^{2}_{1}\mathrm{H},\ {}^{4}_{2}\mathrm{He}\right){}^{4}_{2}\mathrm{He} \quad Q = 22.4\ \mathrm{MeV} \\
&{}^{7}_{3}\mathrm{Li}\left({}^{1}_{1}\mathrm{H},\ {}^{4}_{2}\mathrm{He}\right){}^{4}_{2}\mathrm{He} \quad Q = 17.3\ \mathrm{MeV} \qquad \ldots(9.20)
\end{aligned}
$$

Hydrogen isotopes have been made to undergo fusion in an uncontrolled manner, in a fission bomb. This is the so-called hydrogen bomb. The fission reaction produces the high temperature needed for fusion. Once the fusion starts, it maintains the temperature to keep the process going.

A hydrogen bomb, which is a fusion bomb cannot explode until it is "ignited" i.e., the fusion reaction started by producing high temperature. Once ignited *any amount* of fusible material can be used and so there is no theoretical limit to the energy liberated.

During last few decades one of the major research programme all over the world is constructive, controlled utilisation of energy released from fusion. Clearly, it has a great advantage over the fission reactions in the fact that the fuel is cheap and plentiful, unlike ^{235}U, ^{233}U and ^{239}Pu which are expensive and difficult to produce. On the face of it, the controlled fusion appears formidable. One has not only to achieve high temperatures, but at the same time to contain the *thermonuclear reactions* at temperatures much higher than the temperatures at which materials around us evaporate.

One approach is to use particles with high velocity produced in the accelerators, rather than high temperatures. From the kinetic theory, it is well known that temperature is associated with the random motion of atoms or molecules in a gross sample. When we consider individual particle energy we can speak of its *kinetic temperature*. For example a particle with an energy 0.025 eV is said to have a kinetic temperature of 293 K. A mere 1 keV energy given to a particle corresponds to a kinetic temperature of over 1 million degrees Kelvin. Calculations show that it may be possible to maintain fusion continuously at a kinetic temperature of about 45 million degrees. This can be readily given to a particle by accelerating it through about 4000 volts.

When electrical discharge passes through a gas at such potential difference, the gas becomes completely ionised, and we get a *plasma* which is a mixture of charged particle gases. The kinetic temperature of about 100 keV in a plasma produces a pressure as high as a thousand atmosphere. The only way to contain this plasma so that it does not come in contact with the container wall and charged particles are prevented from escaping is to use strong magnetic fields. Fusion conditions have been produced in the laboratory for deuterium nuclei, though momentarily.

The problem of a controlled fusion reaction is not yet completely solved. However, because of the cheap and plentiful availability of fuel, viz. hydrogen, research on fusion is given great emphasis all over the world. The student is recommended some excellent material given at the end for further reading.

EXERCISES

1. Explain how the nuclear magnetic resonance is achieved in practice. To what characteristic energy is th NMR technique sensitive?
2. Outline the features of a NMR spectrometer. What is the purpose of the modulating field?
3. How is the technique of NMR used to:
   (*a*) Measure nuclear magnetic moments?
   (*b*) Identify the structure of chemical compounds?
4. What is Mössbauer effect? Explain how using this effect it is possible to measure photon energy w an accuracy of a few parts in 10^{13}.
5. Give the features of a Mössbauer spectrometer. Outline how it can be used to:
   (*a*) measure the gravitation red shift
   (*b*) study the *hf* interaction.
6. ^{191}Ir emits a γ-ray of energy 129 keV and goes to the ground state. Find the fractional change in en of the γ-ray photon due to the recoil of the nucleus.
7. ^{119}Sn nucleus emits a γ-ray of energy 23.8 keV and goes to the ground state. The excited state h width given by the uncertainty principle equal to 2.4×10^{-8} eV. Find out whether the resonance absor of this γ-ray by another free ^{119}Sn nucleus is possible. Assume both nuclei, initially to be at rest.

8. For the 14.4 keV transition in ^{57}Fe, show that a Doppler velocity of 1 mm/sec corresponds to an energy of 4.8×10^{-8} eV.

9. For the 93 keV transition in ^{67}Zn, calculate to what energy the Doppler velocity of 1 mm/s corresponds to.

10. What must be the relative velocity of a source and absorber consisting of free ^{129}I nuclei to observe the maximum absorption of γ-ray with an energy 27 keV?

11. Consider Illustrative Example 9.1. If the distance between the source and absorber is made 100 m, what should be source velocity to neutralise the effect of gravitational shift in γ-energy?

12. Calculate the Q values for the fusion reactions given in Eq. 9.17.

10

Elementary Particles

"If I could remember the names of all these particles, I would be a botanist."

—*Enrico Fermi*

10.1 INTRODUCTION

To understand the nature around us is the main goal of science. Man has always wondered: what are *basic, fundamental building blocks* of matter? The modern name to the fundamental building blocks of matter is *"Elementary Particles"*. The ancient Greek philosopher, Democritus believed that in nature, things were made of small basic entities and empty space. He used the word *"atom"* to denote these basic entities. Atom means an entity which is indivisible. Gradually experimental evidence for atoms emerged and around 1900 people knew that there are about 90 different types of atoms of which the matter is made up. The periodic table by Mendeleev was a triumph which established the number of elements in nature, each consisting of a particular type of atoms.

Now, we know that atoms can be divided—they are not really fundamental building blocks of matter. Electrons were discovered by Thomson in 1895, showing that an atom is not indivisible. Earlier in this book, we have studied the classic experiment of Rutherford in 1910, in which he bombarded atoms of gold by alpha particles and identified the atomic nucleus. In 1918, Rutherford discovered that nuclei are made up of protons, and in 1932, Chadwick discovered neutrons. So, at this stage there appeared to be only three elementary particles, viz. electrons, protons and neutrons.

No sooner than the establishment of this picture, experimental evidence started piling up that the story of elementary particles, in fact, was much more complicated. Several additiona particles were discovered. For example, we have already come across the neutrino propose by Pauli in 1930. Neutrinos are always emitted in, for example, beta decay, and the space i full of them, originating from nuclear reactions in stars. Another particle to be discovered aroun the same time (1932), the *"positron"* by Anderson. It has the same mass and spin of the electro but has a positive charge, $+e$. It is as elementary as its more familiar counterpart, the electro Also the well known particle, photon, which plays an important role in structure of matter, throu their role as the carrier of electromagnetic forces, has to be in same way included in our li of elementary particles. By 1960, more than 20 particles were discovered, which vied for position in the list of elementary particles! The situation become quite complex and scientist started desperately to look for ways to introduce a semblance of order in the world of elementary particles, whose number was growing every day.

Around 1965, some order began to take place in the growing list of elementary particles. Scientists started realising that most of the so called elementary particles were in fact all made up from a small number of more fundamental particles called *quarks* (Gell-Mann used this name, from the phrase "three quarks for Muster Mark" which appears in the novel *Finnegan's Wake* by James Joyce)—a name given by American physicist Murray Gell-Mann. Of all the particles, clamoring for inclusion as elementary particles, only a few are still regarded as elementary. Among these are the electron, the neutrino and the photon. None of these have till date shown any evidence to possess an internal structure. The other particles like proton and neutron appear to have been made up of two or three quarks.

It should be appreciated that elementary particles like protons, electrons etc. have a size less than 1F (1F = 10^{-15} m). The de Broglie wavelength required to study these particles, therefore, also has to be of the order of 1F or less. We have seen that the de Broglie wavelength λ is related to the momentum of the particle p, by the relation:

$$\lambda = \frac{h}{p}$$

ILLUSTRATIVE EXAMPLE

Example 10.1: Calculate the energy of a beam of electrons required to probe a distance of 10^{-15} m.

Solution: Using the relativistic relation,

$$E^2 = p^2c^2 + m_e^2c^4, \text{ where } m_e = 0.511\,\text{MeV}.$$

$$\lambda = \frac{hc}{pc}$$

$$1\text{F} = \frac{1240\ \text{MeV}\cdot\text{F}}{\sqrt{E^2 - (0.511)^2}}$$

Giving, $E \sim 1.240 \times 10^3$ MeV = 1.240 GeV

In the problem (above), $E \approx K$, the K.E. of the electrons, since the rest energy $m_ec^2 = 0.511$ MeV is negligible, compared to the total energy E. Thus, we see that the energy required to probe elementary particles is very high—in the region of GeV and above. It is due to this reason, that the field of elementary particles is often called *"high energy physics"*. The Fermilab near Chicago, for example produces protons of energies 1 TeV = 1000 GeV = 10^{12} eV. The field of high energy physics is dominated by gigantic particle accelerators.

10.2 ANTIPARTICLES AND ANTIMATTER

10.2.1 The Positron

Every particle has an antiparticle, in nature. The first antiparticle, positron, was predicted theoretically by the English physicist, Paul Dirac in 1928, when he generalised relativistically, the Schrödinger equation. Let us look briefly at the prediction, discovery and some properties of the positron. Dirac's idea was to find the form of the Schrödinger's equation that was consistent with Einstein's theory of relativity. Actually he achieved much more. He was able to show that the relativistic part of the Schrödinger's equation (the Dirac equation), was able to predict a spin $s = ½$ for the electrons. The surprise was that, the Dirac equation also predicted the existence of a second particle (along with the electron) with charge $+e$, with the same mass as that of the electron. This particle is the one, which we now call the positron. The theory predicted that if a photon with energy greater than $2m_ec^2$ undergoes a collision with a nucleus, it can disappear, producing a pair of electron and positron. This *pair production* process can be written as:

$$\gamma \text{ (photon)} + \text{nucleus} \rightarrow e^- \text{ (electron)} + e^+ \text{ (positron)} + \text{nucleus} \quad \text{...(10.1)}$$

In this equation the nucleus is required to conserve both, energy and momentum. (See problem 10.11). Inversely, if a positron meets an electron, they annihilate each other, becoming photons. American physicist Anderson verified these predictions in 1932 while studying cosmic rays, which enter the earth's atmosphere from outer space. These cosmic rays are high energy particles, mostly protons and alpha particles. A large number of secondary particles, photons, electrons and positrons are produced when these cosmic rays interact with atoms in the earth's atmosphere. Anderson was using a cloud chamber to study cosmic rays. The cloud chamber can show the tracks of charged particles in the form of condensed liquid drops. Cameras can be used to photograph these charged particles. By placing the cloud chamber in a magnetic field, the curvature of these tracks can give idea about the charge and the momentum of the particle. The mass of the particle determines the thickness of the track and with experience a skilled experimentalist can study properties like, mass, charge and momentum of particles passing through the cloud chamber. Figure 10.1 shows the tracing of such a photograph.

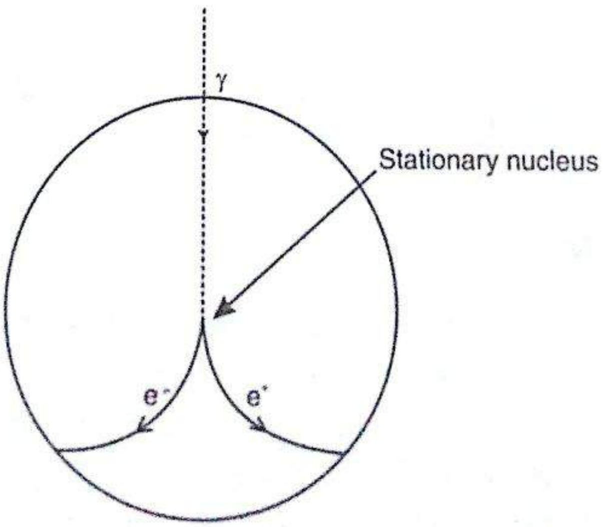

Fig. 10.1. Tracing of a cloud chamber track. The magnetic field is going into the page.

In this figure, the photon being uncharged does not produce a visible track. Also the nucleus being stationary remains invisible. However the tracks with opposite curvature belonging to the electron and positron are clearly visible. Anderson named e^+ as the positron.

The existence of *antiproton* and *antineutron* was experimentally confirmed in 1955. Like e^- and e^+, p(proton) and $\overline{p}$ (antiproton) annihilate to give photons. So also n and $\overline{n}$ and we have:

$$p + \overline{p} \rightarrow \text{photons}$$

$$n + \overline{n} \rightarrow \text{photons} \qquad \text{...(10.2)}$$

In other words, antiprotons, $\overline{p}$ have a charge $-e$. An antineutron, $\overline{n}$ has like n, zero charge, but n and $\overline{n}$, when they come together annihilate each other unlike n and n. For a process like,

$$\gamma + \text{nucleus} \rightarrow p + \overline{p} + \text{nucleus}$$

to take place, the gamma ray photon needs at least energy of $2m_pc^2 \approx 2$ GeV. Such large energy photons are rare in cosmic rays and so they have to be produced artificially in an accelerator. In 1955, Segre, Chamberlain and their collaborators at Berkeley built and used an accelerator that could accelerate protons to energies needed to produce antiprotons. These protons of about 6 GeV energy were made to hit a copper target, the protons of which (Cu target) were hit to produce p-$\overline{p}$ pairs in relation

$$p + p \rightarrow p + p + p + \overline{p} \qquad \text{...(10.3)}$$

The tracks of the annihilation process of p - $\overline{p}$ pair were recorded in photographic plates, through which the antiprotons travelled. Anderson, Segre and Chamberlain received Nobel Prize for their discoveries of e^+ and $\overline{p}$.

In Eqs. 10.2 and 10.3 the charges on both sides are balanced. Also the total number of nucleons (either neutrons or protons) remains unaltered in nuclear reactions. This can be reflected in the Eqs. 10.2 and 10.3, by defining a quantity, the *nucleon number* in the following manner. A nucleon number +1 is assigned to both proton and neutron. The antiproton and antineutron then gets assigned a nucleon number −1. On the other hand, particles like the electron and photon can be assigned a nucleon number of zero. Since the nucleon number is conserved, we have,

$$n + \overline{n} \rightarrow \text{photons} \qquad \text{...(10.4)}$$

while

$$n + n \neq \text{photons} \qquad \text{...(10.5)}$$

Also,

$$p + \overline{p} \rightarrow \text{photons} \qquad \text{...(10.6)}$$

but

$$p + p \neq \text{photons} \qquad \text{...(10.7)}$$

Soon after $\overline{p}$ and $\overline{n}$ were established, many other pairs of particle-antiparticles were also experimentally established. Every particle is found to have an antiparticle e.g. the pion, π^+ having a charge $+e$, mass 139.6 MeV/c^2, spin 0 has been found to have an antiparticle π^-, with exactly same mass and spin, but opposite charge, $-e$. It is interesting to note that in some cases particles are the same as their antiparticles, e.g., the photon which has a zero charge and zero nucleon number.

10.2.2 Antimatter

We know that the normal matter is made of electrons and nucleons. The discovery of antiparticles opens up the possibility of the existence of *antimatter* made of positrons and antinucleons. Antihelium comprising of two antiprotons and two antineutrons has been observed in the laboratory. Clearly, in the presence of normal matter, antimatter would be highly unstable since particle-antiparticle pairs would annihilate, releasing energy in terms of photons. However, antimatter would be quite stable in isolation. This raises the possibility that some distant galaxies, well separated from any galaxies with normal matter, may be made of antimatter. At present though, there is no evidence for the existence of such antimatter galaxies.

10.3 FEYNMAN DIAGRAMS

Dirac's theory, the quantum electrodynamics (QED), was later generalized by Richard Feynman, Julian Schwinger and Tomonaga and it has been very well tested by experimentalists. Feynman had a penchant for always keeping in mind a physical picture of a complex mathematical theory. In one of his brilliant exposition of quantum theory for scattering phenomenon he had interpreted the well-known Green's function, as a "propagator", which takes the scattered wave from one center of scattering to another (see e.g. Quantum Mechanics by Powell and Crassman). In another masterstroke, Feynman presented a very simple and elegant, graphical technique to describe reactions. As an example let us consider the process of two electrons approaching each other. As per the quantum theory of fields, they *exchange "virtual" photons*. These photons are called virtual because they cannot be observed directly. The virtual photons are the *carriers* or *mediators* of the electromagnetic force field (the Coulomb force). Feynman represented this exchange of a virtual photon between two electrons (or any other charged particles) by a *Feynman diagram* as shown in the Fig. 10.2.

Usually the axes in the Feynman diagram are not shown. Japanese physicist Hideki Yukaw (Nobel Prize, 1949) proposed to build a quantum field theory for the force between two nucleon in a manner analogous to that for the Coulomb force. The carrier of the electromagnetic forc is a virtual photon. What is the carrier of the much stronger nuclear force? What is the partic exchanged between nucleons to keep the strong attractive interaction between them? Yukaw proposed a new particle meson as the mediator of the nuclear force. In Greek, *meso* mea "middle". Yukawa's meson, later called a pion was finally identified in 1947 by Powell a Occhialini. Figure 10.3 depicts the Feynman diagram indicating the *pion* exchange between neutron and a proton.

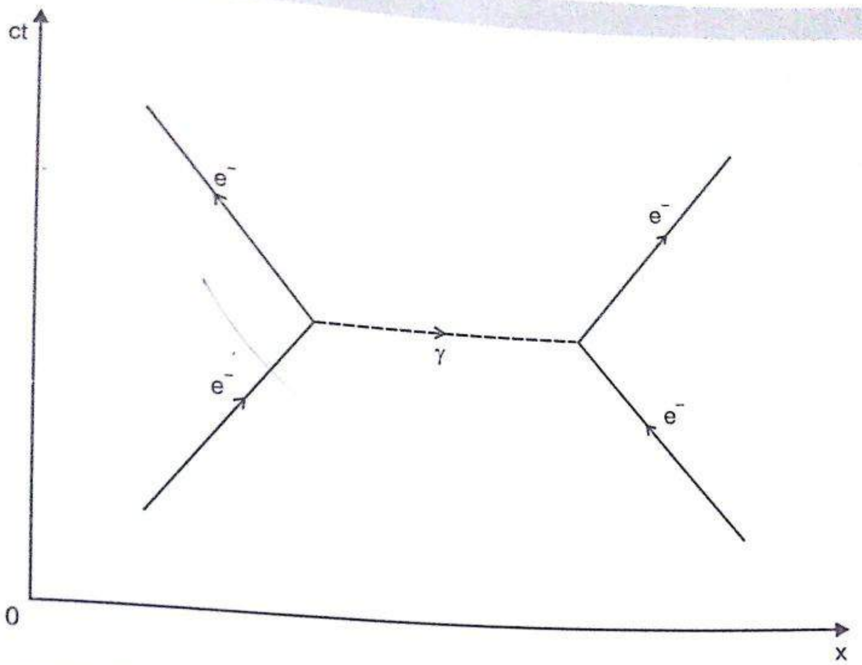

Fig. 10.2. Feynman space-time diagram, depicting emission of a photon by the electron on the left, which is then absorbed by the electron on the right. Feynman won a Nobel Prize in 1965 for his contribution to the quantum field theory.

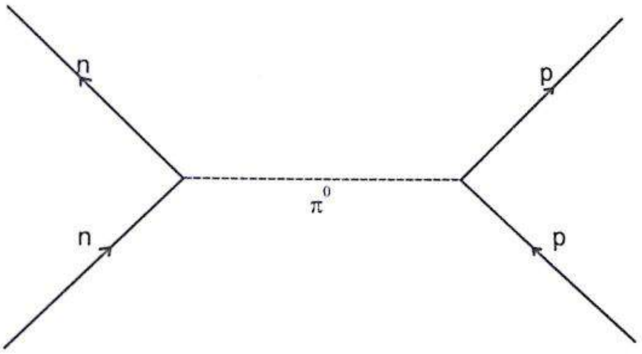

Fig. 10.3. Meson exchange between a neutron and a proton.

10.4 ESTIMATION OF PION MASS

Does the emission of a meson reduce the nucleon mass? In the laboratory, no changes in the neutron or a proton masses are observed. Clearly therefore here we are dealing with "virtual" masons, like the virtual photons in the case of Coulomb field. In other words, the exchange of mesons takes place in such a small interval of time that the "uncertainty" in the energy is allowed or consistent with the Heisenberg's uncertainty principle, $\Delta E \cdot \Delta t \sim \hbar$. The detection of the meson exchange is thus not physically possible and the mesons in this exchange process are called *virtual mesons*. The virtual photon, exchanged during an electromagnetic interaction is also undetectable due to the uncertainty principle.

Experiments show that the nuclear force is a short range force. For example, we have seen that the nuclear binding energy is approximately constant which implies that nucleons attract only those nucleons which are in their neighbourhood, within the nucleus. Clearly therefore, unlike the Coulomb force, the range of the nuclear force is short and is of the order of nuclear dimensions. Yukawa realised that the meson of finite rest mass would give rise to a short range nuclear force. Let us make an estimate of the meson mass, using the Heisenberg's uncertainty principle. If a nucleon emits a virtual meson, pion, of rest mass m_π, it will lose energy,

$$\Delta E = m_\pi c^2$$

For example, when a proton emits a meson π^0, we have,

$$p \to p + \pi^0$$

The proton mass in this process remains unchanged and this is verified in the laboratory. This "violation" of conservation of energy is alright, if it is consistent with the uncertainty principle, i.e. if the emitted π^0 meson is absorbed in an interval of time Δt, such that $\Delta E \cdot \Delta t \sim \hbar$. The complete reaction can be written as,

$$p \to p + \pi^0 \to p$$

Thus,

$$\Delta t \approx \frac{h}{2\pi \Delta E} = \frac{h}{2\pi m_\pi c^2} \qquad \text{...(10.8)}$$

Obviously, the meson cannot travel with the velocity of light, c, otherwise its rest mass as per special theory of relativity will have to be zero, like the photon in the case of electromagnetic interaction, implying an *infinite range* for the interaction. However, the range of nuclear interaction is small, of the order of a few fermis. Hence, meson cannot have zero mass. If we assume that the π^0 travels at about one-half the speed of light, then in time Δt it can travel a distance D, given by,

$$D = \frac{1}{2} c \cdot \Delta t$$

The value of D must be of the order of fermis.

$$D \sim 10^{-15}\ m$$

$$\therefore \qquad 10^{-15}\ m \sim \hbar c / 2 m_\pi c^2 \qquad \text{...(10.9)}$$

This equation gives us an estimate of the meson mass:

$$m_\pi \sim 270\ m_e, \quad m_e = \text{mass of electron}$$

$$\text{i.e. } m_\pi \sim 140\ \text{MeV/c}^2$$

A particle of mass about 106 MeV/c^2, called μ-*meson* or *muon* was discovered in cosmic rays, after about an year of Yukawa's prediction. People thought that this was Yukawa's meson. But it was observed that the μ-meson could penetrate large thickness of matter without interacting with nuclei. This was surprising, since the Yukawa mesons are expected to interact strongly with nuclei, since they are the field particles or carriers of nuclear force. It took more than a decade to discover the Yukawa mesons—called pi mesons or pions—at Berkeley using the high energy accelerator. Three types of pions have been found, which the nucleons continuously emits and absorb. Figure 10.4 shows Feynman diagrams for the emission and absorption of the π^+ and π^-, mesons.

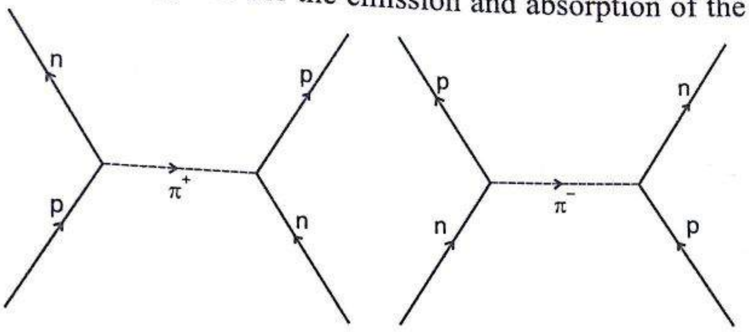

Fig. 10.4. Exchange of π^+ and π^- mesons by nucleons.

The spin of the pion is zero. The π^+ and π^- mesons have charges $+e$ and $-e$ respectively. The rest masses of π^+ and π^- (being particles-antiparticle pair) are same; 139.6 MeV/c^2 each. The mass of π^0 is 135 MeV/c^2. The π^+ and π^- mesons decay very rapidly with a mean-life of about 10^{-8} s. The π^0 decays mainly into two photons,

$$\pi^0 \rightarrow \gamma + \gamma$$

with the shorter mean-life, $\tau(\pi^0) \sim 10^{-16}$ s.

The experimental confirmation of the existence of π-mesons predicted by Yukawa was a spectacular triumph of the theory and a major landmark in our quest to understand the nucleon-nucleon interaction. Yukawa obtained the form of the potential energy of interaction between two nucleons:

$$u(r) = C\frac{e^{-r/R}}{r} \qquad \ldots(10.10)$$

where C is a constant which gives the strength of the interaction, r is the inter-nucleon distance and R is the range of the force. This equation gives the well known *Yukawa potential*, depicted in Fig. 10.5.

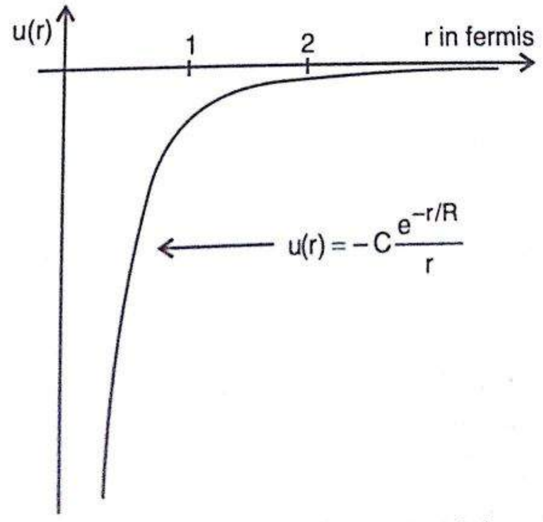

Fig. 10.5. The Yukawa potential.

10.5 THE FOUR FUNDAMENTAL FORCES OF NATURE

It was realised that the growing family of elementary particles could be grouped according to the fundamental interactions to which they belong. The two fundamental forces you are familiar with are the *electromagnetic* and *gravitational* forces. By 1935, it had become clear that in addition to these two, there are two other fundamental forces, viz. the *strong nuclear force* and the *weak force* responsible for the well known beta-decay process. The nuclear force holds nucleons in a nucleus together. On the other hand, the process of beta-decay could not be explained in terms of strong, electromagnetic or gravitational force. The typical interaction energy involved in the beta-decay process is ~10^{-4} MeV and so a "weak force" has to be responsible for the process that gives rise to the electron and neutrino in the nuclear beta-decay.

In physics, the fundamental forces are described as fundamental *"interactions"*, rather than forces. This is mainly because in quantum mechanics the force finds its expression as interaction potential energy in the Schrödinger's equation. We thus talk about, the electromagnetic, nuclear, gravitational and weak interactions. The light particles like electron and neutrino are referred to as *leptons*; the Greek word for "light" is lepton. μ-meson or muon is another example of leptons. Nucleons are subjected to strong nuclear interaction. Following the Greek word for "strong", the particles are called *hadrons*. Another example of hadrons is pion or π-meson which is mediating particle for strong interactions, proposed by Yukawa. We now know as many as six leptons and literally hundreds of hadrons. As we shall see a little later, these hadrons appear to have been built up from just six different particles called *quarks* and that these six quarks are structureless elementary particles. Table 10.1 gives the basic properties of the fundamental four interactions.

TABLE 10.1: The Four Fundamental Interactions

Interaction	*Range*	*Particles feeling the interaction*	*Relative strength*	*Exchanged particles*	*Effect of interaction*
Strong	~10^{-15} m	Hadrons Quarks	1	Mesons Gluons	Nucleons are held together, as nuclei quarks are held together as nucleons
Electromagnetic	∞	All charged particles	~10^{-12}	Photons	Holds atoms together
Weak	~10^{-17} m	Leptons	~10^{-5}	Intermediate Bosons	Responsible for β-decay
Gravitational	∞	All particles	~10^{-39}	Graviton	Formation of stars, Galaxies etc.

The relative strengths of these fundamental interactions differ by an astonishingly large facto of 10^{39}. Also the effective ranges span distances from 10^{-17} m to ∞. The gravitational interactio which is negligible on small scale, becomes dominant on a large scale. The formation of nucl is determined by the strong interaction, while atomic structures are determined by electromagnet interaction. The weak interaction ensures that nuclei with too many neutrons or protons undergo β-decays and neutron-proton ratio gets corrected, leading to stable nuclei. The exchange particles of gravitational interaction, graviton, has yet not been detected in the laboratory.

10.6 W BOSONS AND GLUONS

In Table 10.1, you must have noticed the exchange particles for strong and weak interactions; they are mesons, gluons and intermediate bosons. In 1960, Sheldon Glashow, Stevan Weinberg and Abdus Salam, predicted a particle W (for weak), which is responsible for the weak interaction. Their theory, called electroweak theory, unified the electromagnetic and weak interaction in a manner similar to the way Maxwell's theory of electromagnetism, unified electricity and magnetism together. Though it is not possible to discuss electroweak theory due to its complexity, we would like to point out that the W-particle predicted is very massive since the range of the weak interaction is very short, ~10^{-17} m. Actually, there are three particles, all bosons carrying a spin 1. These are two W's ($W^{\pm}$), each having a mass 80.4 GeV/c^2, and one Z^0 having a mass 91.2 GeV/c^2. In 1983, all these three massive bosons were discovered at CERN by C. Rubbia and his collaborators, confirming the theoretical predictions. Glashow, Weinberg and Salam received the 1979 Nobel prize and Rubbia received the 1984 Nobel prize. Feynman diagrams for the neutron and proton beta-decay are shown in the Fig. 10.6. Notice that W^- and W^+ are exchange particles carrying out the interaction.

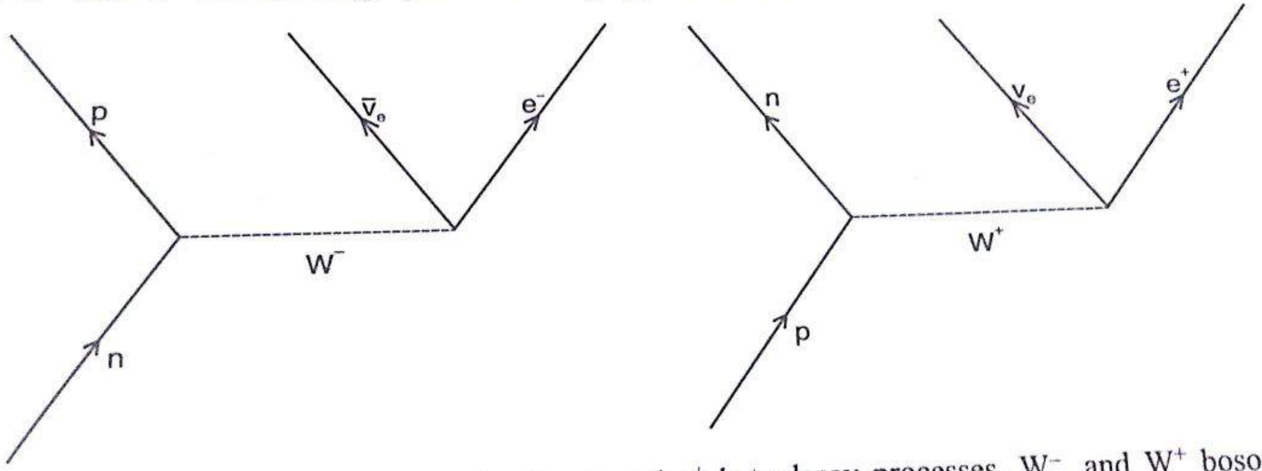

Fig. 10.6. Feynman diagrams for the e^- and e^+ beta-decay processes. W^- and W^+ bosons mediate this process and give rise to the lepton pairs e^-, $\bar{\upsilon}_e$ and e^+, υ_e.

We have seen earlier that π-meson of Yukawa (pion) is the mediating particle for the force between nucleons. Now we know more than twenty mesons that together form the strong interaction. Soon we will learn that nucleons and mesons have fine structure and are formed from even more fundamental particles called *quarks*. What is the "glue" that holds the quarks together? The exchange particle that mediates the strong interaction between the quarks is called a *gluon*; it has a spin 1 and zero mass. It is not possible to observe an isolated quark or gluon since they remain confined within the nucleons and mesons by the strong nuclear interaction. Thus, it appears that at a more fundamental level it is the gluons that are responsible for the strong force. The experimental evidence so far supports the existence of quarks and gluons though there is no direct evidence yet.

10.7 CONSERVATIONS RULES

10.7.1 Baryon Number and Lepton Number Conservation

In addition to the well known conservation laws for mass and energy, momentum, angular momentum and charge, new conservation rules have been discovered in the field of high energy physics.

Consider the hypothetical process

$$p \rightarrow e^+ + \gamma \qquad \text{...(10.11)}$$

Clearly all the known conservation laws are valid in this reaction. The fact remains however that it has never been observed. What is it, which prevents it from occurring? We have seen earlier that a nucleon can be assigned a nucleon number +1. To encompass all the hadrons, one can define a *baryon number B*, such that all *baryons* are assigned $B = 1$ and antibaryons $B = -1$. Mesons and Leptons have $B = 0$. In all the processes observed, the algebraic sum of baryon number on both the sides of the reaction is conserved. This is even when the number of particles are different on the two sides e.g.

$$\Lambda^0 \rightarrow p + \pi^-$$

or

$$\Lambda^- \rightarrow n + \pi^-$$

The baryon number is +1 on both the sides since the lambda particle, Λ^0 has $B = 1$ and for π-meson, $B = 0$. These processes are observed in the laboratory. In the hypothetical process, Eq. 10.11, the baryon number is not conserved—it violates the baryon number conservation law.

Leptons till today appear structureless and truly elementary. There are only six leptons and their six antiparticles. Earlier we have talked about the electron and muon. Each of these charged particles (e and μ) has an associated neutrino e.g. electron neutrino ν_e (and muon neutrino ν_μ). The electron and neutrinos are stable. Muon decays with half life of 2 μs,

$$\mu^- \rightarrow e^- + \nu_\mu + \bar{\nu}_e \qquad \text{...(10.12)}$$

There is another lepton, Tau (τ), and its antineutrino υ_τ which completes the lepton family. The τ is much more massive and decays into an electron, muon or even hadrons. Table 10.2 displays the six leptons and their antiparticles, with their properties. All leptons have a spin 1/2 and all the three neutrinos have been identified in the laboratory.

TABLE 10.2: The Lepton Family

Particle name and symbol	*Antiparticle*	*Mass MeV/c²*	*Mean life(s)*
Electron, e^-	e^+	0.511	Stable
Electron Neutrino, ν_e	$\bar{\nu}_e$	$< 7 \times 10^{-6}$	
Muon, μ^-	μ^+	105.7	2.2×10^{-6}
Muon Neutrino, ν_μ	$\bar{\nu}_\mu$	< 0.17	
Tau, τ	τ^+	1777	2.9×10^{-13}
Tau Neutrino, ν_τ	$\bar{\nu}_\tau$	< 18	

Neutrinos have no charge and no mass, and are very difficult to detect. Earlier we have outlined the landmark experiment by Cowan and Reins (see beta-decay) for neutrino detection — an experiment which earned them a Nobel Prize.

The processes like,

$$\nu_\mu + n \rightarrow e^- + p$$

$$\bar{\nu}_\mu + p \rightarrow e^+ + n \qquad \ldots(10.13)$$

have never been observed in the laboratory. These do not violate any of the conservation laws, including the conservation of baryon number. To understand why these reactions do not occur, lepton number, L_e and L_μ (also L_τ for the τ lepton) are introduced,

$$L_e = 1, \quad \text{for } e^-,\ \nu_e, L_\mu = 1, \quad \text{for } \mu^-, \nu_\mu \text{ and}$$

$$L_e = -1, \text{for } e^+,\ \bar{\nu}_e, L_\mu = -1, \text{for } \mu^+, \bar{\nu}_\mu$$

We then have lepton number conservation law that the algebraic sum of L_e and L_μ on each side must be conserved in any process involving leptons. Clearly, process Eq. 10.11 violates, both, the conservation of baryon number and lepton number. Also each reaction in Eq. 10.13 violates the conservation of L_e and L_μ lepton numbers and thus cannot be realized.

It is of interest to note that there are no conservation laws for number of types of mesons. Being bosons, Pauli's exclusion principle does not apply to mesons and so they can be produced in any numbers and particle reactions as long as laws of energy, momentum and electric charge conservation are obeyed.

10.7.2 Conservation of Strangeness

In 1953, Gell-Mann and Nishijima introduced a new quantum number *S*, *strangeness*. Mesons and Baryons together are called hadrons. In 1947, along with the π-meson, the K^0 (meson, 498 MeV/c²) and Λ^0(baryon, 1116 MeV/c²) were discovered in the cosmic rays. The process that was observed in the form of tracks in the cloud chamber was,

$$\pi^- + p\,(\text{strong interaction}) \rightarrow \Lambda^0 \rightarrow \pi^- + p(\text{weak interaction})$$

This is production of /

The strong interaction has a lifetime ~ 10^{-23} s. However, Λ^0 had a life time of 10^{-10} s, so that it decays via weak interaction. The interesting thing is that, the decay rate of Λ^0 is 10^{-13} of the production rate. This is the reason why the Λ particles were called 'strange' particles.

Soon another process was identified in an accelerator laboratory,

$$\pi^- + p \rightarrow K^0 + \Lambda^0 \qquad \ldots(10.14)$$

A sketch of the bubble chamber track for this process is shown in the Fig. 10.7. Note that only the decay of Λ^0 gives rise to a V-shaped track in this picture.

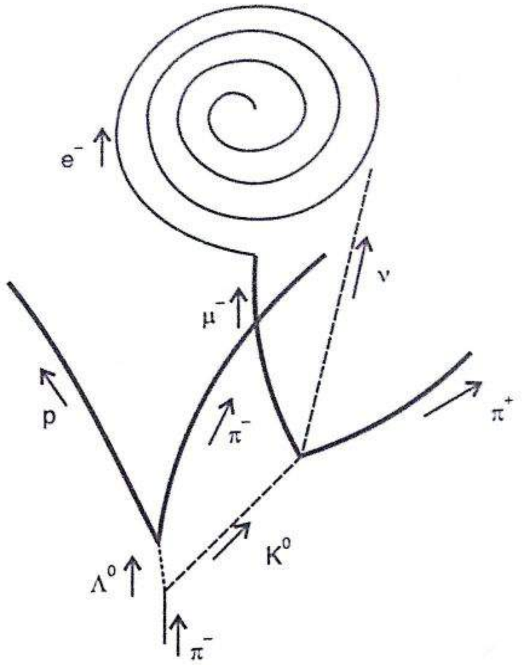

Fig. 10.7. The production and decay of the K^0 and Λ^0, when π^0 strikes a proton

Another way of producing the K and Λ is,

$$p + p \rightarrow \Lambda^0 + K^0 + p + \pi^+ \qquad \text{...(10.15)}$$

In all the cases, it is observed that these two particles (K and Λ) are produced together, *simultaneously* and so the process of their creation is called "*associated production*". In Eqs. 10.13 and 10.14, the baryon number is conserved. However, there is no restriction on their decay mode by the weak interaction. The reactions:

$$K^0 \rightarrow \pi^+ + \pi^-$$

$$\Lambda^0 \rightarrow \pi^- + p$$

belong to the weak interactions and so have, as remarked earlier, a rather long lifetime characteristic of the weak interaction. Thus, while the K^0 and Λ^0 must be produced by the strong interaction, they decay by the weak interaction! This appears strange and prompted Gell-Mann and Nishijima to introduce a new quantum number S, *strangeness*. This quantum number, S, must be conserved in strong interaction, but in weak interaction strangeness conservation could be violated.

All the particles discovered earlier had exhibited no evidence for strangeness and so were assigned a strangeness $S = 0$. K^0 was assigned $S = 1$ and Λ^0 was assigned $S = -1$. This ensured that these particles must be produced in *pairs* in order to conserve strangeness, e.g., in the processes,

$$\pi^- + p \rightarrow K^0 + \Lambda^0$$

$$S : 0 + 0 \rightarrow 1 - 1$$

and

$$p + p \rightarrow K^0 + \Lambda^0 + p + \pi^+$$

$$S: 0 + 0 \rightarrow 1 - 1 + 0 + 0$$

However in the decay process,

$$K^0 \rightarrow \pi^+ + \pi^-$$

$$S: 1 \neq 0 + 0$$

i.e. strangeness is not conserved. This implies that it must be a weak interaction process corresponding to a long decay timescale.

To sum up, therefore, conservation of strangeness quantum number holds in the strange interaction but is violated in the weak interaction. Note that assigning strangeness allows us a way of keeping track of what production and decay modes are allowed. Later we shall see that strangeness is associated with one of the six quarks.

10.7.3 Isospin and its Conservation

The neutron was discovered in 1932. By 1936 many crucial features of the strong nuclear interaction emerged. In particular, it was experimentally found in the nucleon-nucleon scattering experiments that after subtracting the effect of the Coulomb force, the hadronic force (strong interaction) was independent of the type of nucleons considered in the scattering experiments. In other words, the hadronic forces are *charge independent*. Today the experimental evidence is extensive to support this feature of the hadronic forces. The concept of isospin is a direct consequence of the charge independence of hadronic (strong) forces.

10.8 THE NUCLEON ISOSPIN

In 1932, Heisenberg treated the neutron (n) and proton (p) as two different states of one particle, the nucleon N. An *isospin space* is introduced to describe the two states of the nucleon, following the analogy with two spin states of a spin–1/2 particle. We can put orientation in isospin space *"up"* for a proton and *"down"* for a neutron. Formally, the situation is described by introducing a new quantity, *isospin* **I**. The nucleon with isospin 1/2 has 2**I** + 1 = 2 possible orientations in the isospin space. The three components of **I** are I_1, I_2 and I_3. By definition the value I_3 distinguishes between a proton and a neutron. $\mathbf{I}_3 = 1/2$ is the proton and $I_3 = -1/2$ is the neutron. Isospin space is often referred to as the charge space. The charge for the particle of the isospin I is given by:

$$q = e\left(I_3 + \frac{1}{2}\right) \qquad \ldots(10.16)$$

Putting the values of I_3 in this equation we get, as required, the charge on a proton as +e and the charge on a neutron zero.

In order to appreciate, what we have achieved by introducing isospin, we now generalize the concept of isospin for all hadrons, with its third component I_3, connected to the charge of the particle. This can be done by the linear relation of the form,

$$q = aI_3 + b \qquad \ldots(10.17)$$

Clearly with such a relationship, conservation of the electric charge *implies conservation of* I_3.

10.9 THE GELL-MANN-NISHIJIMA RELATION: ISOSPIN OF PARTICLES

By analogy with the angular momentum quantum number J, the isospin quantum number I can take $(2I + 1)$ values, 0, 1/2, 1, 3/2, 2, …… That is, I is $(2I + 1)$-fold degenerate and $(2I + 1)$ *sub-particles* all have the same mass. The electromagnetic interaction (applied magnetic field for instance) lifts the degeneracy to give rise to the Zeeman effect. In a similar manner the electromagnetic interaction in the form of the charge on the particle gives rise to isospin analog of the Zeeman effect, as depicted in the Fig. 10.8.

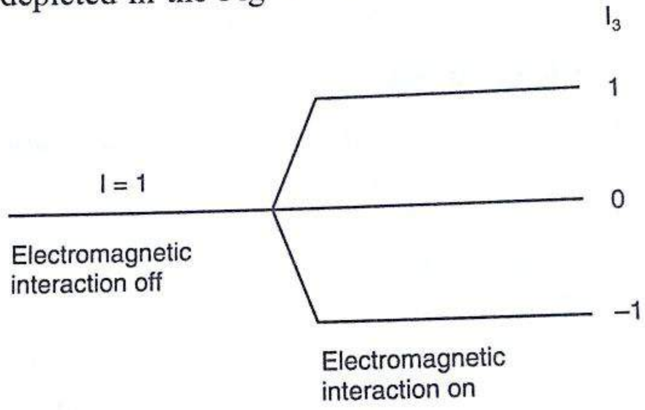
I_3
1
I = 1
0
Electromagnetic interaction off
–1
Electromagnetic interaction on

Fig. 10.8. Isospin Multiplet for $I = 1$

The electric charge of each member of this isospin multiplet is related to I_3 by Eq. 10.17. It should be appreciated that the different members of an isospin multiplet are in essence the same particle (e.g. nucleon with $I = 1/2$) appearing with different orientations in the hypothetical isospin space, in a manner similar to the various Zeeman levels which are the states of the same particle with different orientations of spin w.r.t. the applied magnetic field in the real space. The number of subparticles in an isospin multiplet, if counted, can yield the value of the isospin I.

Let us apply these considerations to the familiar pion. We know that virtual pions are exchanged by nucleons and the basic Yukawa process for this pion exchange between two nucleons is,

$$N = N' + \pi$$

This reaction should *conserve isospin*. Nucleons, we know, have isospin $I = 1/2$ and since isospins add vectorially like normal spin, the pion isospin consequently must be 0 or 1. If $I = 0$ then there should be only one pion existing. However, we know that *three* pions with mass about 140 MeV/c^2 exist and so pion isospin $I = 1$, giving rise to an isospin triplet, as shown i Fig. 10.8. The values of I_3 for pions are:

$$I_3 = +1 \text{ for } \pi^+, \text{ m} = 139.58 \text{ MeV/c}^2$$

$$I_3 = 0 \text{ for } \pi^0, \text{ m} = 134.98 \text{ MeV/c}^2$$

$$I_3 = -1 \text{ for } \pi^-, \text{ m} = 139.58 \text{ MeV/c}^2$$

The relation between the charge q and I_3, $q = aI_3 + b$, for pions becomes simply

$$q = aI_3 \qquad \text{...(10.18)}$$

Example 10.2: The kaon, (K-meson) appears in two particles and two antiparticles states. What is the isospin I assignment for the kaon?

Since the kaon appears in two particles states, like nucleon, its $I = 1/2$, which is in agreement with known facts.

Solution: The hadrons can all be characterised by a set of additive quantum numbers; the mass number A, charge q, I_3 and strangeness S. Gell-Mann and Nishijima showed that the relation between q and I_3 can be generalised to apply to strange particles as well. The constant in Eq. 10.17 is seen to be e from Eq. 10.18. To obtain the constant b, since I_3 ranges from $-I$ to $+I$, the average charge of the isospin multiplet is,

$$\langle q \rangle = b$$

$$\therefore \quad q = eI_3 + \langle q \rangle$$

It is customary to use a quantum number, the *hypercharge* Y, rather than strangeness S, defined by,

$$\boxed{Y = A + S} \qquad \text{...(10.19)}$$

where A is the mass number (baryon number).

The average charge $\langle q \rangle$ of the multiplet is related to the hypercharge Y by the relation,

$$\langle q \rangle = 1/2\, e\, Y \qquad \text{...(10.20)}$$

Therefore the generalised equation for the charge becomes,

$$\begin{aligned} q &= E\,(I_3 + 1/2\, Y) \\ &= e\,(I_3 + 1/2\, A + 1/2\, S) \qquad \text{...(10.21)} \end{aligned}$$

This equation is the well known Gell-Mann-Nishijima relation. To visualise the Gell-Mann-Nishijima relation look at the Fig. 10.9, which is a plot of the hypercharge Y against q/e.

From Fig. 10.9, it is seen that the centre of charge for the isospin multiplets shown are displaced from zero. This is verified in experiments.

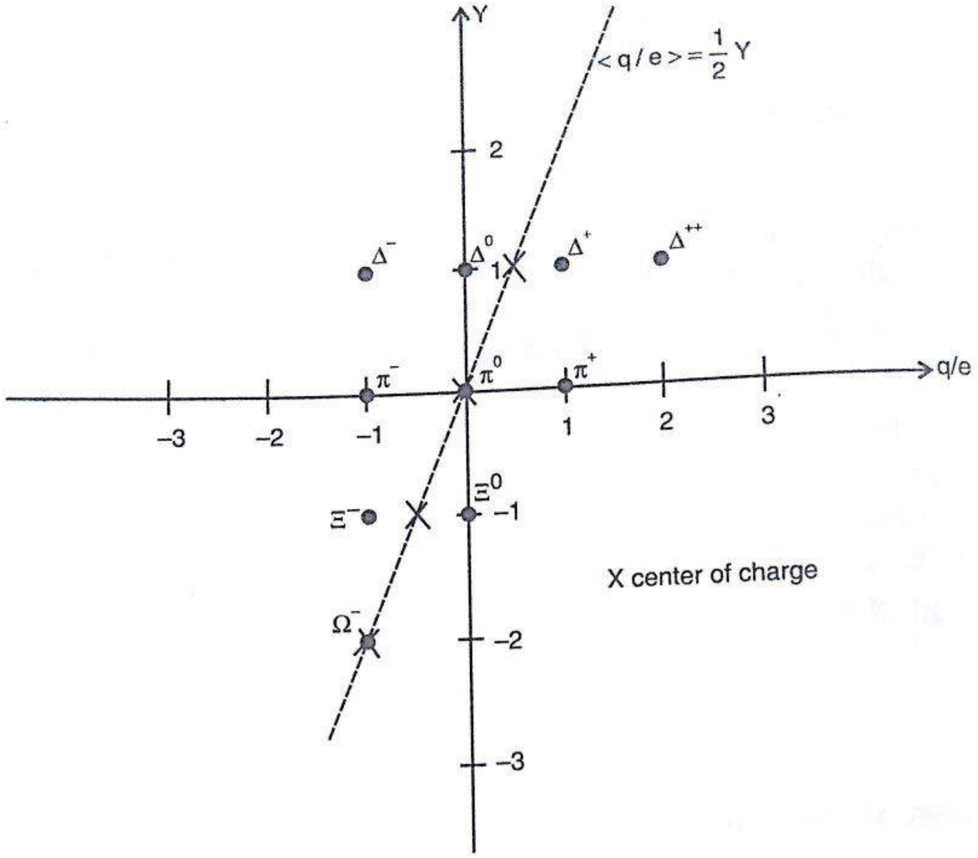

Fig. 10.9. Isospin Multiplet in a Gell-Mann-Nishijima Plot. A few multiplets are shown

10.10 THE QUARK MODEL

In 1964, Gell-Mann and independently Zweig introduced a baryonic triplet, consisting of three hypothetical particles, now known as *"quarks"*. Gell-Mann called these particles *quarks,* after James Joyce's *Finnegan's wake* where Joyce used the phrase "three quarks for Muster Mark". Zweig had called these particles *aces*, but the name "quarks" won over "aces". The quark model is able to explain many features of the elementary particles, and gives a good insight into the structure of the group of hadrons (baryons and mesons) of the elementary particle zoo. Gell-Mann and Zweig, essentially were attempting to figure out, what are simplest building blocks from which all "elementary particles" can be constructed. The quark scheme envisages that *quarks must be fermions* since with fermions as basic building blocks it is possible to construct both fermions and bosons. It is assumed that bosons (mesons) are quark-antiquark pairs. Any fermion (baryons-antibaryons), that is not one of the basic quarks, must be built from *at least* three quarks.

Originally three quarks were proposed: an up quark (u), a down quark (d) and a strange quark(s). There are 10 possible combinations of the three (uds) quarks. The strangeness conservation is related to the strange quark. Table 10.3 shows the combination of (uds) quarks.

TABLE 10.3: The Three Quark (uds) Combinations

Combination	*Charge*	*Spin*	*Baryon no.*	*Strangeness*
uuu	+2	3/2	1	0
uud	+1	1/2, 3/2	1	0
udd	0	1/2, 3/2	1	0
ddd	–1	3/2	1	0
dds	–1	1/2, 3/2	1	–1
dss	–1	1/2, 3/2	1	–2
sss	–1	3/2	1	–3
uus	+1	1/2, 3/2	1	–1
uss	0	1/2, 3/2	1	–2
uds	0	1/2, 3/2	1	–1

The properties of the *u*, *d* and *s* quarks are shown in Table 10.4.

TABLE 10.4: Properties of the u, d and s Quarks

Quark Type and symbol	*Charge, e*	*Spin*	*Baryon number, B*	*S*	*Isospin*	
					I	I_3
up (u)	+2/3	1/2	1/3	0	1/2	+1/2
down (d)	–1/3	1/2	1/3	0	1/2	–1/2
strange (s)	–1/3	1/2	1/3	–1	0	0

The *u* quark has the third component of isospin, $I_3 = +1/2$. The *d* quark has $I_3 = -1/2$. The strangeness of *u* and *d* quarks, $S = 0$, while the *s* quark has the strangeness $S = -1$.

Each baryon is made up of three quarks, which implies that the baryon number of a quark is, $B = 1/3$, and that of an antiquark is $B = -1/3$ (see Table 10.3). The Gell-Mann-Nishijima relation relates electric charge to I_3, Eq. 10.20,

$$q = e\,(I_3 + 1/2\,A + 1/2\,S) \qquad \text{mass no.} = \text{Baryon no.,}$$

$$= e\,(I_3 + 1/2\,B + 1/2\,S) \qquad \text{since } A = B$$

This implies that quarks (and antiquarks) have fractional charges. For example, for the *u* quark,

$$q = e\,(+1/2 + 1/2 \times 1/3 + 1/2 \times 0)$$

$$= +2/3\ e$$

ILLUSTRATIVE EXAMPLE

Example 10.3: Assuming Gell-Mann-Nishijima Relation obtain the quantum numbers, J, A (or B), I, I_3 and q/e for the three quarks, *u*, *d* and *s*.

Solution: Let us calculate for the up quark, *u*. We have seen that the charge on *u*, using the Gell-Mann-Nishijima Relation is, +2/3. It being a fermion, the spin $J = 1/2$. The Baryon Number as seen previously is, $B = 1/3$. The Strangeness affects only the s quark for which $S = -1$. For u and d quarks, $S = 0$. The hypercharge $Y = B + S$, for u quark $= 1/3$, which is also Y for the d quark. However for the s quark $Y = -2/3$.

Table 10.5 summarises the results:

TABLE 10.5

Type of quark	*Quantum number*						
	J	B*(or* A*)*	S	Y	I	I_3	q/e
up, u	1/2	1/3	0	1/3	1/2	1/2	2/3
down, d	1/2	1/3	0	1/3	1/2	–1/2	–1/3
strange, s	1/2	1/3	–1	–2/3	0	0	–1/3

It is interesting to note that, quarks are unique particles in nature having *fractional charges*. They are as elementary as leptons, since like leptons, quarks also have no internal structure — they are essentially point particles. Let us see how, a hadron like the proton is composed of three quarks. Consider the composition (uud), i.e. 2 up quarks and one down quark. The baryon number B for this combination is, $B = 1/3 + 1/3 + 1/3 = 1$, same as that of proton. The charge of (uud) is, $q/e = +2/3 + 2/3 - 1/3 = +1$, which is charge of proton. The spin J for (uud) is, symbolically, $\uparrow\uparrow\downarrow$, i.e. it is equal to ½, which agrees with the spin of the proton. The Strangeness for the combination (uud) is of course zero, since there is no S quark involved. The strangeness of the proton is also zero. So we see that the combination (uud) of the three quarks results into a proton. Table 10.6 gives quark composition of some of the hadrons, as per the quark model.

TABLE 10.6

Hadron	*Quark composition*	*Baryon number, B*	*Charge, e*	*Spin*	*Strangeness, S*
p	u u d	1/3 + 1/3 + 1/3 = +1	+2/3 + 2/3 – 1/3 = +1	1/2	0
n	u d d	1/3 + 1/3 + 1/3 = +1	–1/3 – 1/3 + 2/3 = 0	1/2	0
π^+	$u\bar{d}$	1/3 – 1/3 = 0	+2/3 + 1/3 = + 1	0	0
π^-	$\bar{u}\ d$	0	–2/3 – 1/3= –1	0	0
K^+	$u\bar{s}$	1/3 – 1/3 = 0	+2/3 + 1/3 = +1	0	0 + 1 = + 1
K^0	$d\bar{s}$	0	–1/3 + 1/3 = 0	0	0 + 1 = + 1
Ω^-	s s s	1/3 + 1/3 + 1/3 = +1	–1/3 – 1/3 – 1/3 = –1	3/2	–1 – 1 – 1 = –3

We have so far seen that the known hadrons could be specified by a combination of quarks and antiquarks. However based on symmetry arguments it was expected that there would be an even number of quarks and not the odd number of just three quarks. A fourth quark called the *charmed* quark (c) was proposed in 1970. The c quark gave rise to a new quantum number, charm c such that $c = +1$ for the charmed quark and $c = -1$ for its antiquark. For particles without the charmed quark, $c = 0$. Similar to the strangeness, charm is conserved in the strong and electromagnetic interactions.

In 1974, S. Ting and his collaborators and B. Richter and his collaborators discovered independently a new particle, which they named the J and ψ, respectively. This particle is now called the J/ψ (*Gipsy*) particle and it has a mass about three times the proton mass. It appears in the form of a resonance shown in the Fig. 10.10, in the process,

$$p + p \rightarrow \psi + \text{other particles}$$

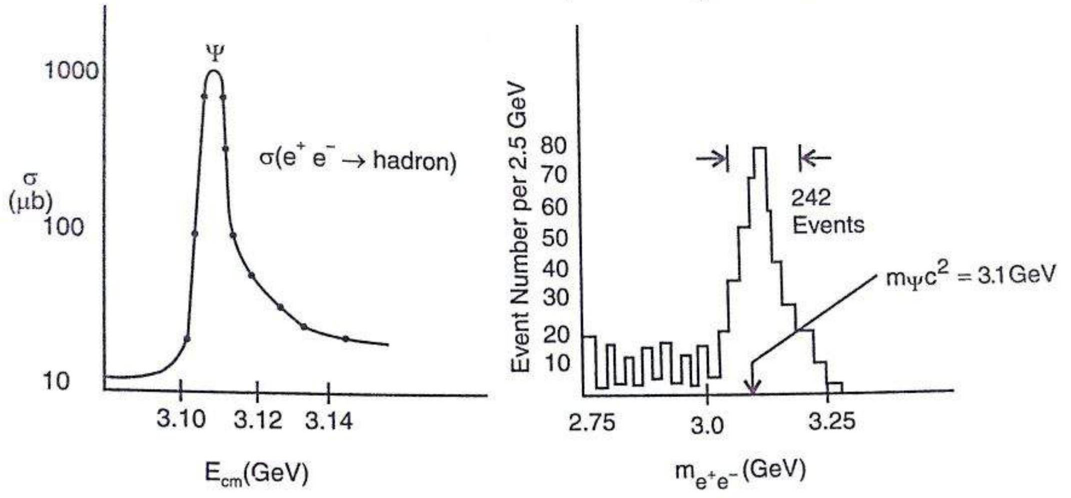

Fig. 10.10. Sketch from the figure in S.C. Ting, Science 196(1977) Resonance which lead to the discovery of the J/ψ particle

The discovery of the J/ψ particle, confirmed the existence of the fourth quark, the charmed quark c. Earlier there was a puzzling fact that the meson K^0 *never decayed* into,

$$K^0 \rightarrow \mu^+ + \mu^-$$

Because of this, in 1970, the fourth quark with a mass of two to four times that of the s quark was postulated. Such a postulate rendered the above decay *unobservable* by a reasoning, which cannot be given here due to its complexity. The discovery of the J/ψ particle therefore assumes importance as this particle could be understood as a bound state of a new quark, the c quark and its antiparticle $\overline{c}$.

$$\psi = (c\ \overline{c}) \qquad \ldots(10.22)$$

The J/ψ particle which is composed of a charm quark (c) and an anticharm quark ($\overline{c}$) forming ($c\overline{c}$) is called *charmonium*, in analogy with (e^+e^-), *positronium*. Ting and Richter shared the 1976 Noble prize for their discovery. About the J/ψ particle, Ting said: "It is just like a new species of a mankind with an expected lifetime 10,000 years". The lifetime of the J/ψ particle turned out to be more than 100 times longer than that of the ordinary hadron resonances. The long lifetime indicated that the J/ψ particle was not decaying into hadrons by the expected strong interaction. The charm quark does not exist in the ordinary hadrons. The charm quark and ordinary quarks are different in nature. It is very difficult for one to be transformed into the other. Therefore the lifetime of the J/ψ particle is very long. In 1976, the first mesons which include the charm quarks in their composition were discovered. These are the D mesons:

$$D^0 : (c\,\overline{u})$$

$$D^+ : (c\,\overline{d})$$

$$D^- : (\overline{c}\,d) \qquad \ldots(10.23)$$

10.11 THE "BEAUTY" AND "TRUTH"

A few years after the discovery of the charm quark, a fifth quark, the b or *"bottom"* was found. It is also called "beauty". In 1977, a new meson, the *upsilon* (Υ) particle was discovered and was shown to be bound state of the bottom quark b and its antiparticle $\overline{b}$:

$$\Upsilon = (b\ \overline{b})$$

The b quark is much heavier compared to the u, d, s and c quarks; its mass is $\approx$ 5 GeV/c^2. Finally in 1995 the *"top"* quark t or *"truth"* was discovered at the Fermi National Laboratory. Quantum numbers *bottomness B* and *topness T* are assigned to these quarks. Table 10.7 summarises the properties of quarks.

TABLE 10.7

Sl.No.	*Quark type*	*Mass*	*Charge*	*B(A)**	*S*	*C*	*B*	*T*
1.	Up, u	~0.003 Gev/c^2	2/3e	1/3	0	0	0	0
2.	Down, d	~0.006 GeV/c^2	–1/3e	1/3	0	0	0	0
3.	Strange, s	~0.012 GeV/c^2	–1/3e	1/3	–1	0	0	0
4.	Charm, c	~ 1.3 GeV/c^2	2/3e	1/3	0	–1	0	0
5.	Bottom, b	~ 4.25 GeV/c^2	–1/3e	1/3	0	0	–1	0
6.	Top, t	~174 GeV/c^2	2/3e	1/3	0	0	0	–1

* Here B or A stand for the baryon number.

10.12 THE GENERATIONS OF MATTER

It is interesting to notice that the discovery of six different kinds of quarks, often called as six flavours, u, d, s, c, b and t, matches very well with the six known lepton. This parallelism between quarks and leptons is very striking when it is realised that the six leptons and quarks fall naturally into three *generations*. This grouping into generations for quarks and leptons is shown in the Table 10.8.

TABLE 10.8: Leptons and quarks: The three generations of matter

Leptons	e^-	ν_e	μ^-	ν_μ	τ^-	ν_τ
Quarks	u	d	c	s	t	b
Generations	I First		II Second		III Third	

The reasoning behind these groupings into generations or families is that when a quark of one type changes to a second type, this change occurs predominantly within one generations or family. For example, a *u* quark changes to a *d* quark or vice-versa, much more readily than a *u* changes into an *s* and so on. Also it is first generation of leptons and quarks that plays an obviously important in the normal stable matter. The members of the second generations are produced in high energy accelerators and are also found in cosmic rays. It is now believed that the members of the third generation existed in the early moments of the creation of the universe and these can be created in the laboratory with very high energy accelerators. Notice that in each group, the mass increases with the generation number—the third generation has leptons and quarks having greatest mass.

10.13 THE QCD—COLOUR QUANTUM NUMBER

Need of introducin
concept of colour

All the six quarks are fermions—they all have a spin 1/2. We know that due to the exclusion principle of Pauli, no two fermions can occupy the same quantum state. Yet we have many baryons which are composed of quarks of the same types happily existing in the nature. For example the Ω^- is composed of three strange quarks (sss). This serious difficulty can be overcome by establishing a new quantum number called *colour.* The theory called quantum *chromodynamics (QCD)* is based on this idea.

Ever since the proposition of the quark model in 1964, extensive searches have been made to detect quarks as free particles. As yet there is no conclusive evidence for the existence of free quarks. However the predictions based on the quark picture have been verified experimentally and constitute indirect evidence supporting strongly the existence of quarks. A growing number of physicists now believe that free quarks cannot be observed. They assert that quarks can exist only within hadrons. This feature is called *confinement.* How are the quarks held together, when they form hadrons and mesons? They are held together by what is perceived to be the *real strong interaction*, whose propagator is the mediating particle called the *gluon.* Although, no free gluon (or glue-ball) is observed, indirect evidence has been gathered for the existence of gluons. For example, in $e^+ - e^-$ collisions, where quark-antiquark pairs are formed and the evidence shows that they decay into *three jets of particles* at very high energies. Since in this process only $q\ \overline{q}$ pairs are formed and never three quarks, one of the three jets observed must be given rise to by the gluon. Figure 10.11 depicts a sketch of the three jets of hadrons produced in the $e^+ - e^-$ collisions.

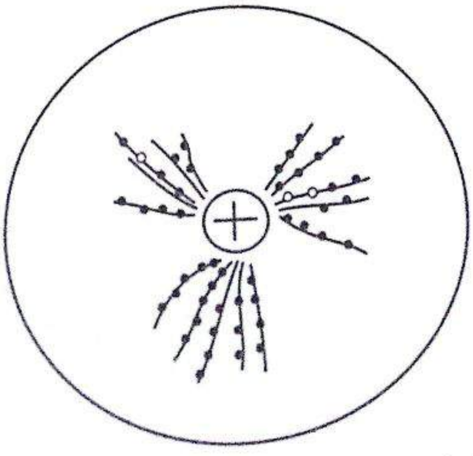

Fig. 10.11. The three jets of hadrons created by q, $\overline{q}$ and gluon in $e^+ - e^-$ collisions.

10.14 COLOURS FOR QUARKS AND GLUONS

As per the QCD, there are three colours for the quarks, defined in a manner in some ways similar to the colour triangle for visible light. These are the red (R), green (G) and bule (B). This nomenclature is for simplicity and has nothing to do with and actual colours we see visually! It is just a scheme to distinguish the properties of colour quantum number. Each of the six quarks has three colours, R, G and B. In Fig. 10.12, we show the Feynman diagram for two quark interaction. A red quark comes from the left and interacts with green quark coming from the right. They exchange a gluon, changing the green quark into a red one and the red quark into a green one.

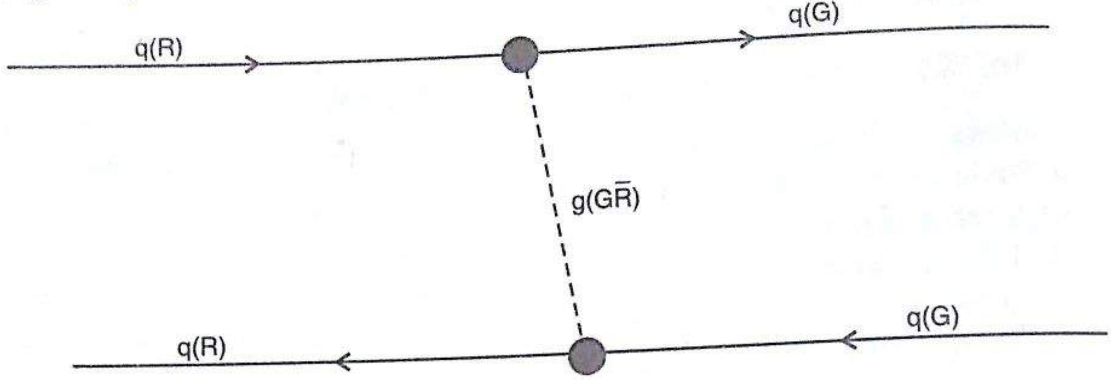

Fig. 10.12. Exchange of a gluon between red and green quarks. The colours of the quarks change.

As one looks at the role of gluons in the binding of quarks, it becomes evident that gluons must also come in colours. The colour quantum number, it turns out, is not simply a way of counting particle states allowed by the Pauli principle, but it is the basis of the binding of the quarks. The colour quantum number is related to the *true strong interaction.* In the same way as the electric charge is related to the electromagnetic interaction. Photons are exchanged between electric charges in electromagnetic interaction. The true strong interaction involves the exchange of gluons which are emitted and absorbed by the *colour charge*. Here we must distinguish between the true strong interaction (between colour charges—the quarks) from what is usually called the strong (nuclear) interaction that is observed between the hadrons. The true strong interaction (colour) is the one which binds quarks into hadrons and mesons. The meson exchange theory (e.g. Yukawa's pion exchange between nucleons) of the strong nuclear interaction is but a residual manifestation of the true strong interaction mediated by the gluon. All hadrons are *colourless*, since a colour and its anticolour cancel out giving white colour so as to say. Also all three colours or all three anticolours in combination cancel out and we get a colourless object. Quarks exchange colour when they emit or absorb a gluon. Quarks of the same colour repel, whereas, quarks of different colours attract. The strong binding of colourless protons and neutrons to form nuclei is due to the residual strong interaction between their colou charged constituents. It can be viewed as the exchange of mesons between the hadrons. Thi is similar to the residual electrical interaction which binds electrically neutral atoms to for molecules. In other words, for example, the Van der Waal's force that binds molecules is not fundamental force, but a residual interaction related to electric charge.

All leptons, photons, bosons like W and Z, do not have colour charge and so are not involv in the strong interaction.

10.15 WHY WE DO NOT SEE FREE QUARKS OR COLOUR PARTICLES?

The binding potential for quarks can be viewed as containing two terms, one proportional to $1/r$ and other to r. The $1/r$ dependence requires that the gluon, like the photon, be a massless particle. At small distances when quarks are close together, the quarks feel a weak potential and are almost free. When the quarks start to separate, the r dependent part of the potential increases very rapidly, implying that more and more gluons have appeared. Thus, the attractive force holding the quarks becomes very large and quarks just cannot succeed in becoming free.

Consider the case when a proton (or neutron) is given a lot of energy to separate out a quark. As the quark begins to leave, the gluon field that binds it would increase until, at sufficiently large distances a gluon would break up into a quark and antiquark. This new quark completes the proton (or neutron) and the antiquark combines with the escaping quark to form a meson. The two resulting particles remain colourless. Figure 10.13 depicts this sequence.

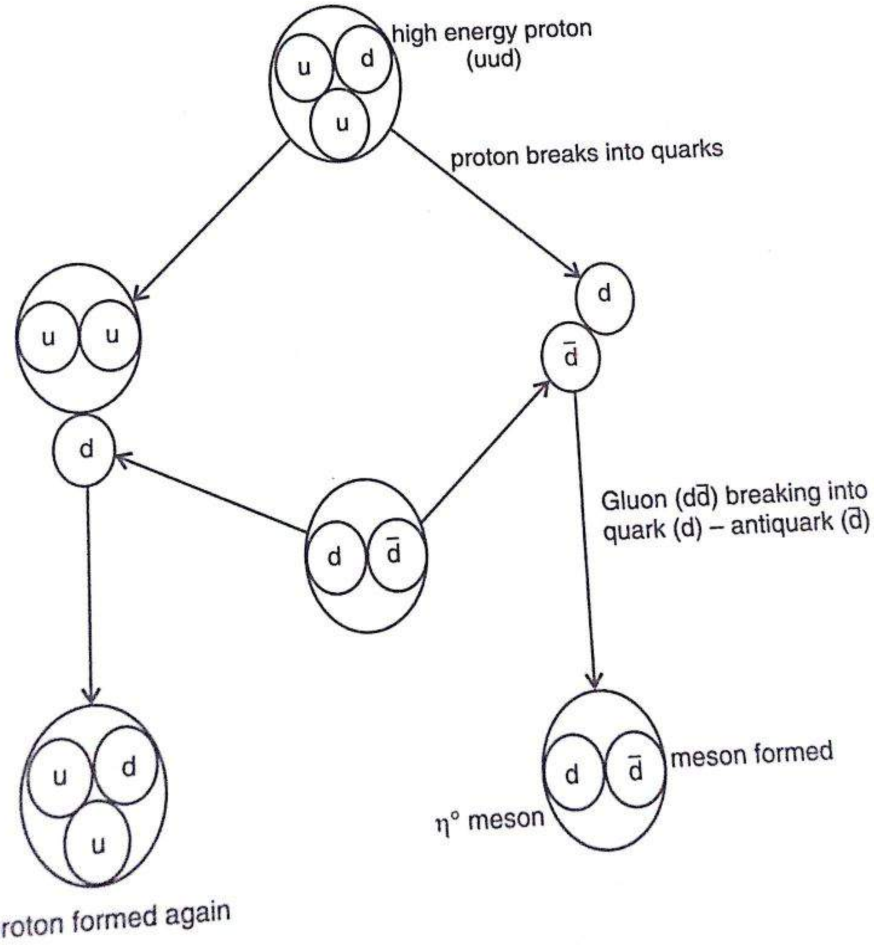
high energy proton (uud)
u
d
u
proton breaks into quarks
u
u
d
d
$\bar{d}$
d
$\bar{d}$
Gluon ($d\bar{d}$) breaking into quark (d) – antiquark ($\bar{d}$)
u
d
u
proton formed again
d
$\bar{d}$
meson formed
η° meson

Fig. 10.13. No free quark possible.

10.16 THE STANDARD MODEL: QUEST FOR THE GRAND UNIFIED THEORY (GUT)

It is the goal and dream of physicists to build a model, which can unify all the fundamen forces of nature into one theory. James Maxwell was able to unify in 1860, the electric a magnetic forces into the electromagnetic theory. As mentioned earlier, Glashow, Weinberg and Salam unified the electromagnetic and weak interaction in 1960, into the electroweak interaction.

At present the most successful and accepted theory of elementary particles is called the *Standard Model*. Basic facts on which this model rests are now experimentally well tested and established. The details of the standard model are quite complex. However the essential features and ingredients have been already presented in this chapter. In summary, there are *twelve elementary particles*—all of them *fermions* (with spin ½). Out of these twelve elementary particles six are leptons and six quarks. The matter around us consists of a *combination* of these twelve elementary particles, which exert attractive or repulsive forces on each other by exchanging the mediating particles which are referred as *gauge bosons*. The leptons and quarks can be divided into three generations. The leptons can exist independently, while the quarks exist only inside baryons and mesons. All the twelve elementary particles are subject to electroweak interactions, which are mediated by the exchange of four gauge bosons: the massless photon and the massive $W^{\pm}$ and Z^0. These have been observed directly. The six quarks are in addition subject to a truly strong force which is carried by massless gluon. The gluon has not been observed directly so far.

There are six types or *flavors* of quarks: up, down, strange, charm, bottom and top. There are three colours, red, green and blue for each flavor. A combination of coloured quarks enables us to represent and understand the internal structure of all the known hadrons.

The standard model has been spectacularly successful in particle physics. However, it is still surely not the final word. There are many questions for which it does not have answers. For example, it does not explain why the leptons and quarks have the masses which are observed. Also why do second and third generations occur and that too with particles so much heavier than the first generation? One of the major shortcomings of the standard model is that it cannot predict the particle masses. Physicists continue their search for answers to such questions, and hope and dream of a Grand Unifying Theory, unifying all the four fundamental interaction.

Summary

Elementary particles are the fundamental building blocks of matter. This study requires energies of the order of many GeV's and so the field is known as "high energy physics". Experimental observation that every particle has an antiparticle has been discussed. The exchange of virtual particles can be depicted by the Feynman diagrams. Yukawa's meson ideas lead to an understanding of the exchange nature of the nuclear force. Nature has four fundamental forces. The various conservation rules like the baryon number and lepton number conservation, strangeness conservation, isospin conservation are discussed. The quark model is discussed in some details. Six lepton and six quarks fall naturally into three generation. To understand why quarks of the same type co-exist in the nature, the theory of "quantum chromodynamics" (QCD) was formed. One can ascribe colours for quarks and gluons. Free quarks or colour particles are not seen. The standard model is currently the most successful and accepted theory of elementary particles. The quest for a Grand Unified Theory (GUT) continues.

EXERCISES

1. Using the relativistic relation between energy and momentum, calculate the energy of beam of particles of mass m, which can probe a distance of the order of 10^{-15} m.
2. Protons of total energy (relativistic) 10 GeV are produced by an accelerator. What is the minimum distance that can be probed with these protons?
3. In the problem 29.2, instead of protons if one uses electrons of 10 GeV energy, what would be the minimum distance that can be probed?
4. Consider particles of mass m, accelerated to an energy 1 TeV (= 1000 GeV). What is the minimum distance that can be probed with these particles? Calculate this distance for the case of electrons and protons. What is your conclusion?
5. Eq. 29.3 gives reaction in which the antiprotons were produced and first observed. A minimum energy of 6 GeV was required for this process. For the reactions given below, though less energy is required, the process is not possible.

   (*i*) $p + p \rightarrow p + \overline{p}$

   (*ii*) $p + p \rightarrow p + 2e^{+} + \overline{p}$

   Explain why these reactions cannot take place.
6. Estimate the range of nuclear force, assuming that the charged pion, with mass ~ 140 MeV/c^2, is the exchanged particle responsible the nuclear force.
7. Using conservation of energy and momentum show that the positron and electron cannot annihilate into one photon.
8. Consider an alpha particle having an energy of 6 MeV, inside a nucleus (~3 Fermis). Estimate the time it takes the alpha particle to cross this nucleus. What is the significance of this time?
9. What is the missing particle in the following reaction, involving elementary particles?

   (*i*) $n \rightarrow p + e^{-} + ?$

   (*ii*) $\mu^{-} \rightarrow e^{-} + ?$

   (*iii*) $\mu \rightarrow e + \nu_{\mu} + ?$

   (*iv*) $\pi^{-} + ? \rightarrow K^{0} + \Lambda^{0}$

   (*v*) $K^{-} \rightarrow \mu^{-} + ?$

   (*vi*) $\tau^{+} \rightarrow e^{+} + \nu_{e} + ?$

   (*vii*) $\tau^{+} \rightarrow \mu^{-} + \nu_{e} + ?$
10. One of the decay modes of the τ^{+} lepton is,

$$\tau^{+} \rightarrow \pi^{+} + \overline{\nu}_{\tau}$$

Only one neutrino is emitted in this process. Give reason.

11. Show that a single photon cannot spontaneously get converted into an electron-positron (e^-, e^+) pair.

    (*Hint:* This reaction cannot conserve, both, the energy and momentum)

12. The force between nucleus has a "hard core" i.e., it has a short range repulsive component, which prevents the nucleus from collapsing into a "point" nucleus. A particle, called ω meson, having a mass of 783 MeV/c^2 is believed to mediate this repulsive component of the nuclear force. Make an estimate of the range of this force, responsible for the "hard core" of a nucleus.

13. Consider the emission of a virtual pion by a nucleon N, $N \rightarrow N + \pi$ (virtual). Estimate the maximum time, $(\Delta t)_{\text{max.}}$, for which this reaction occur.

14. A proton-antiproton pair is produced, when a proton of kinetic energy K, hits a stationary proton. Assuming that the momentum of the incident proton is shared equally by the four particles that are produced in this collision, estimate the minimum value of the kinetic energy K.

15. Each of the following reaction is forbidden by conservation laws. Explain.

    (*i*) $p + p \rightarrow p + p + n$

    (*ii*) $\pi^+ + p \rightarrow p + p + \gamma$

    (*iii*) $\gamma + p \rightarrow n + \pi^0$

    (*iv*) $\pi^+ + \pi^- \rightarrow \gamma$

16. There is a speculation that the proton may be unstable, though till today proton decay has not been observed. Identify the conservation laws that get violated in the following proton decay.

    (*i*) $p \rightarrow e^+ + K^0 + \nu_e$

    (*ii*) $p \rightarrow \mu^+ + \pi^0$

    (*iii*) $p \rightarrow \pi^+ + \bar{\nu}_e$

17. Consider two stationary protons. Calculate the ratio of the gravitational and electrostatic forces between them. What is your interference from this number?

18. Give the reason why the gravitational interaction governs the motion of the planets, the sun, the stars and the galaxies, inspite of the fact that it is the weakest of all the fundamental forces.

19. An isolated electron is absolutely stable. Can you think of a reason for this perfect stability of an electron?

20. Show that the lepton number is conserved in the reactions,

    (*i*) $p \rightarrow n + e^+ + \nu_e$

    (*ii*) $\mu^+ \rightarrow e^+ + \nu_e + \bar{\nu}_\mu$

    (*iii*) $\pi^- \rightarrow \mu^- + \bar{\nu}_\mu$

    (*iv*) $\mu^- \rightarrow e^- + \bar{\nu}_e + \nu_\mu$

    (*v*) $n \rightarrow p + e^- + \bar{\nu}_e$

21. Write down the lepton number conservation law for the τ meson. Using this law complete following decay reactions for the τ meson.

    (*i*) $\tau^+ \rightarrow e^+ + ? + ?$

    (*ii*) $\tau^- \rightarrow \mu^- + ? + ?$

22. Using the law of conservation of baryon number, find out baryon numbers of neutral K and Λ-particles from the following reactions.

    $\pi^- + p \rightarrow K^0 + \Lambda^0$, where $\Lambda^0 \rightarrow \pi^- + p$.

23. Explain why quarks in a hadron should have different colours. If the spins of the quarks were either 0 or 1, what would be your conclusion as regards to their colours?

24. The quark composition of the Λ particle is (uds). What is the charge?

25. Write down the quark compositions of the particles, π^+, K^+, Ω^-, D^0 and D^-. Based on these deduce the electric charge, baryon number and strangeness for these particles.

26. What kind of particles would you expect with following quark configuration?

    (*i*) $(\bar{c}\ u)$ (*ii*) $(b\ \bar{b})$

    (*iii*) $(c\ \bar{c})$ (*iv*) $(s\ s\ s)$

    (*v*) $(\bar{d}\ u)$ (*vi*) $(u\ d\ d)$

27. Write down the interaction depicted by the Feynman diagram given below.

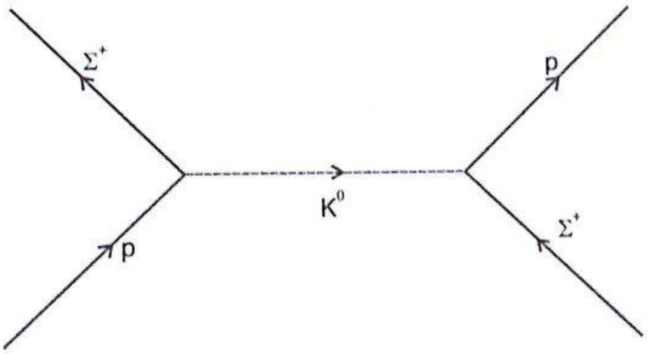

28. Draw the Feynman diagram for an interaction in which a proton and Σ^0 particle exchange a K^+.

29. Write down the following reaction in terms of the quark configurations of the hadrons involved.

    (*i*) $\pi^+ + p \rightarrow K^+ + \Sigma^+$ (*ii*) $K^+ + n \rightarrow K^0 + p$

    (*iii*) $\Sigma^- \rightarrow n + \pi^-$ (*iv*) $\Delta^0 \rightarrow \pi^- + p$

30. Isospin multiplet for the Δ particle has $\langle q/e \rangle = +1/2$. Using Gell-Mann-Nishijima relation predict how many Δ particles belong to this isospin multiplet. Write down the charges on the Δ.

Appendix I

Fundamental Constants and Conversion Factors

Values are given for both SI and cgs units with the following abbreviations:

C = coulomb, cm = centimetre, emu = electromagnetic unit, G = gauss, g = gram, Hz = hertz = cycles/sec, J = joule, K = degree Kelvin, kg = kilogram, m = metre, mol = mole, s = second, T = tesla, u = atomic mass unit ($^{12}C = 12$), V = volt, W = watt.

Fundamental Constants

Constant	*Symbol*	*Value*	*Units (SI)*	*Units (cgs)*
Speed of light	c	2.99792458	10^8 ms^{-1}	10^{10} cms^{-1}
Electron charge	e	1.6021892	10^{-19}C	10^{-20} emu
Planck's constant	h	6.626176	10^{-34} Js	10^{-27} erg s
	$h = h/2\pi$	1.0545887	10^{-34} Js	10^{-27} erg s
Avogadro's number	N_A	6.022045	10^{23} mol^{-1}	10^{23} mol^{-1}
Boltzmann constant	K	1.380662	10^{-23} JK^{-1}	10^{-16} ergk^{-1}
Unified atomic mass unit	u	1.6605655	10^{-27} kg	10^{-24} g
1/12 of $^{12}C = 1/N_A$		931.4812 MeV		
Electron rest mass	m_e	5.4858026	10^{-4} u	10^{-4} u
Proton rest mass	m_p	1.007276470	u	u
Neutron rest mass	m_n	1.008664904	u	u
Bohr radius	a_0	5.2917706	10^{-11} m	10^{-9} cm
Electron radius (classical)	r_e	2.817939	10^{-15} m	10^{-13} cm
Compton wavelength of electron	h/m_ec	2.4263089	10^{-12} m	10^{-10} cm
Compton wavelength of proton	h/m_pc	1.3214099	10^{-15} m	10^{-13} cm
Bohr magneton	$\mu_B = \dfrac{he}{2m_ec}$	9.274078	10^{-24} JT^{-1}	10^{-21} erg G^{-1}

Nuclear magneton	$\mu_N = \frac{he}{2m_pc}$	5.050824	10^{-27} JT^{-1}	10^{-23} erg G^{-1}
Fine structure constant	$\propto^{-1} = \frac{hc}{e^2}$	137.03604		
Compton wavelength of neutron	$\frac{h}{m_nc}$	1.3195909	10^{-15} m	10^{-13} cm

Conversion Factors

1 atomic mass unit = 1.66×10^{-27} kg

= 931.48 MeV

1 tesla = 10^4 gauss

1A = 10^{-10} metre

1 eV = 1.6×10^{-19} joule

1 curie = 3.7×10^{10} sec^{-1}

1 fermi = 10^{-15} metre.

Appendix II

List of Elements

Z		Name	Z		Name
1	H	hydrogen	2	He	helium
3	Li	lithium	4	Be	beryllium
5	B	boron	6	C	carbon
7	N	nitrogen	8	O	oxygen
9	F	fluorine	10	Ne	neon
11	Na	sodium	12	Mg	magnesium
13	Al	aluminium	14	Si	silicon
15	P	phosphorus	16	S	sulphur
17	Cl	chlorine	18	Ar	argon
19	K	potassium	20	Ca	calcium
21	Sc	scandium	22	Ti	titanium
23	V	vanadium	24	Cr	chromium
25	Mn	manganese	26	Fe	iron
27	Co	cobalt	28	Ni	nickel
29	Cu	copper	30	Zn	zinc
31	Ga	gallium	32	Ge	germanium
33	As	arsenic	34	Se	selenium
35	Br	bromine	36	Kr	krypton
37	Rb	rubidium	38	Sr	strontium
39	Y	yttrium	40	Zr	zirconium
41	Nb	niobium	42	Mo	molybdenum
43	Tc	technetium	44	Ru	ruthenium
45	Rh	rhodium	46	Pd	palladium
47	Ag	silver	48	Cd	cadmium

49	In	indium	50	Sn	tin
51	Sb	antimony	52	Te	tellurium
53	I	iodine	54	Xe	xenon
55	Cs	caesium	56	Ba	barium
57	La	lanthanum	58	Ce	cerium
59	Pr	praseodymium	60	Nd	neodymium
61	Pm	promethium	62	Sm	samarium
63	Eu	europium	64	Gd	gadolinium
65	Tb	terbium	66	Dy	dysprosium
67	Ho	holmium	68	Er	erbium
69	Tm	thulium	70	Yb	ytterbium
71	Lu	lutetium	72	Hf	hafnium
73	Ta	tantalum	74	W	tungsten
75	Re	rhenium	76	Os	osmium
77	Ir	iridium	78	Pt	platinum
79	Au	gold	80	Hg	mercury
81	Tl	thallium	82	Pb	lead
83	Bi	bismuth	84	Po	polonium
85	At	astatine	86	Rn	radon
87	Fr	francium	88	Ra	radium
89	Ac	actinium	90	Th	thorium
91	Pa	protactinium	92	U	uranium
93	Np	neptunium	94	Pu	plutonium
95	Am	americium	96	Cm	curium
97	Bk	berkelium	98	Cf	californium
99	Es	einsteinium	100	Fm	fermium
101	Md	mendelevium	102	No	nobelium
103	Lr	lawrencium	104	Rf	rutherfordium
105	Ha	hahnium			

Appendix III

Masses of Neutral Atoms

In the fifth column of the table an asterisk on the mass number indicates a radioactive isotope, the half-life of which is given in the seventh column.

Z	*Element*	*Symbol*	*Chemical atomic weight*	*A*	*Mass* (u)	$T_{1/2}$
0	(Neutron)	n		1*	1.008665	12 min
1	Hydrogen	H	1.0079	1	1.007825	
	Deuterium	D		2	2.014102	
	Tritium	T		3*	3.016030	12.26 yrs
2	Helium	He	4.0026	3	3.016030	
				4	4.002603	
				6*	6.018892	0.802 s
3	Lithium	Li	6.939	6	6.015125	
				7	7.016004	
4	Beryllium	Be	9.0122	7*	7.016929	53.4 days
				9	9.012186	
				10*	10.013534	$2{:}7 \times 10^6$ yrs
5	Boron	B	10.811	10	10.012939	
				11	11.009305	
6	Carbon	C	12.01115	12	12.000000	
				13	13.003354	
				14*	14.003242	5730 yrs
7	Nitrogen	N	14.0067	14	14.003074	
				15	15.000108	
8	Oxygen	O	15.9994	15*	15.003070	122 s
				16	15.994915	
				17	16.999133	
				18	17.999160	
9	Fluorine	F	18.9984	19	18.998405	
10	Neon	Ne	20.183	20	19.992440	
				21	20.993849	
				22	21.991385	

Element	*Symbol*	*Chemical atomic weight*	*A*	*Mass* (u)
Sodium	Na	22.9898	22*	21.994437
			23	22.989771
Magnesium	Mg	24.312	23*	22.994125
			24	23.985042
			25	24.986809
			26	25.982593
Aluminium	Al	26.9815	26*	25.986892
			27	26.981539
Silicon	Si	28.086	28	27.976929
			29	28.976496
			30	29.973763
			32*	31.974020
Phosphorus	P	30.9738	31	30.973765
Sulphur	S	32.064	32	31.972074
			33	32.971462
			34	33.967865
			36	35.967089
Chlorine	Cl	35.453	35	34.968851
			36*	35.968309
			37	36.965898
Argon	A	39.948	36	35.967544
			38	37.962728
			39*	38.964317
			40	39.962384
			42*	41.963048
Potassium	K	39.102	39	38.963710
			40*	39.964000
			41	40.961832
Calcium	Ca	40.08	39*	38.970691
			40	39.962589
			41*	40.962275
			42	41.958625
			43	42.958780
			44	43.955492
			46	45.953689
			48	47.952531
Scandium	Sc	44.956	45	44.955920
			50*	49.951730
Titanium	Ti	47.90	44*	43.959572
			46	45.952632
			47	46.951768
			48	47.947950
			49	48.947870
			50	49.944786
Vanadium	V	50.942	50*	49.947164
			51	50.943961
Chromium	Cr	51.996	50	49.946055

Z	Element	Symbol	Chemical atomic weight	A	Mass (u)	$T_{1/2}$
				52	51.940513	
				53	52.940653	
				54	53.938882	
25	Manganese	Mn	54.9380	50*	49.954215	0.29 s
				55	54.938050	
26	Iron	Fe	55.847	54	53.939616	
				55*	54.938299	2.4 yrs
				56	55.939395	
				57	56.935398	
				58	57.933282	
				60*	59.933964	≈ 10^5 yrs
27	Cobalt	Co	58.9332	59	58.933189	
				60*	59.933813	5.24 yrs
28	Nickel	Ni	58.71	58	57.935342	
				59*	58.934342	8×10^4 yrs
				60	59.930787	
				61	60.931056	
				62	61.928342	
				63*	62.929664	92 yrs
				64	61.927958	
29	Copper	Cu	63.54	63	62.929592	
				65	64.927786	
30	Zinc	Zn	65.37	64	63.929145	
				66	65.926052	
				67	66.927145	
				68	67.924857	
				70	69.925334	
31	Gallium	Ga	69.72	69	68.925574	
				71	70.924706	
32	Germanium	Ge	72.59	70	69.924252	
				72	71.922082	
				73	72.923462	
				74	73.921181	
				76	75.921405	
33	Arsenic	As	74.9216	75	74.921596	
34	Selenium	Se	78.96	74	73.922476	
				76	75.919207	
				77	76.919911	
				78	77.917314	
				79*	78.918494	7×10^4 yrs
				80	79.916527	
				82	81.916707	
35	Bromine	Br	79.909	79	78.918329	
				81	80.916292	
36	Krypton	Kr	83.80	78	77.920403	
				80	79.916380	
				81*	80.916610	2.1×10^5 yrs

Z	*Element*	*Symbol*	*atomic weight*	*A*	*Mass* (*u*)	*Chemical* $T_{1/2}$
				82	81.913482	
				83	82.914131	
				84	83.911503	
				85*	84.912523	10.76 yrs
				86	85.910616	
37	Rubidium	Rb	85.47	85	84.911800	
				87*	86.909186	5.2×10^{10} yrs
38	Strontium	Sr	87.62	84	83.913430	
				86	85.909285	
				87	86.908892	
				88	87.905641	
				90*	89.907747	28.8 yrs
39	Yttrium	Y	88.905	89	88.905872	
40	Zirconium	Zr	91.22	90	89.904700	
				91	90.905642	
				92	91.905031	
				93*	92.906450	9.5×10^{5} yrs
				94	93.906313	
				96	95.908286	
41	Niobium	Nb	92.906	91*	90.906860	(long)
				92*	91.907211	$\approx 10^{7}$ yrs
				93	92.906382	
				94*	93.907303	2×10^{4} yrs
42	Molybdenum	Mo	95.94	92	91.906810	
				93*	92.906830	$\approx 10^{4}$ yrs
				94	93.905090	
				95	94.905839	
				96	95.904674	
				97	96.906021	
				98	97.905409	
				100	99.907475	
43	Technetium	Te		97*	96.906340	2.6×10^{6} yrs
				98*	97.907110	1.5×10^{6} yrs
				99*	98.906249	2.1×10^{5} yrs
44	Ruthenium	Ru	101.07	96	95.907598	
				98	97.905289	
				99	98.905936	
				100	99.904218	
				101	100.905577	
				102	101.904348	
				104	103.905430	
45	Rhodium	Rh	102.905	103	102.905511	
46	Palladium	Pd	106.4	102	101.905609	
				104	103.904011	
				105	104.905064	
				106	105.903479	
				107*	106.905132	7×10^{6} yrs

Z	*Element*	*Symbol*	*Chemical atomic weight*	*A*	*Mass (u)*	$T_{1/2}$
				108	107.903891	
				110	109.905164	
47	Silver	Ag	107.870	107	106.905094	
				109	108.904756	
48	Cadmium	Cd	112.40	106	105.906463	
				108	107.904187	
				109*	108.904928	453 days
				110	109.903012	
				111	110.904188	
				112	111.902762	
				113	112.904408	
				114	113.903360	
				116	115.904462	
49	Indium	In	114.82	113	112.904089	
				115*	114.903871	6 × 10^4 yrs
50	Tin	Sn	118.69	112	111.904835	
				114	113.902773	
				115	114.903346	
				116	115.901745	
				117	116.902958	
				118	117.901606	
				119	118.903313	
				120	119.902198	
				121*	120.904227	25 yrs
				122	121.903441	
				124	123.905272	
51	Antimony	Sb	121.75	121	120.903816	
				123	122.904213	
				125*	124.905232	2.7 yrs
52	Tellurium	Te	127.60	120	119.904023	
				122	121.903064	
				123*	122.904277	1.2 × 10^{13} yrs
				124	123.902842	
				125	124.904418	
				126	125.903322	
				128	127.904476	
				130	129.906238	
53	Iodine	I	126.9044	127	126.904070	
				129*	128.904987	1.6 × 10^7 yrs
54	Xenon	Xe	131.30	124	123.906120	
				126	125.904288	
				128	127.903540	
				129	128.904784	
				130	129.903509	
				131	130.905085	
				132	131.904161	
				134	133.905815	
				136	135.907221	

Z	*Element*	*Symbol*	*Chemical atomic weight*	*A*	*Mass* (*u*)	$T_{1/2}$
55	Caesium	Cs	132.905	133	132.905355	
				134*	133.906823	2.1 yrs
				135*	134.905770	2×10^{6} yrs
				137*	133.906770	30 yrs
56	Barium	Ba	137.34	130	129.906245	
				132	131.905120	
				133*	132.905879	7.2 yrs
				134	133.904612	
				135	134.905550	
				136	135.904300	
				137	136.905500	
				138	137.905000	
57	Lanthanum	La	138.91	137*	136.906040	6×10^{4} yrs
				138*	137.906910	1.1×10^{11} yrs
				139	138.906140	
58	Cerium	Ce	140.12	136	135.907100	
				138	137.905830	
				140	139.905392	
				142*	141.909140	5×10^{15} yrs
59	Praseodymium	Pr	140.907	141	140.907596	
60	Neodymium	Nd	144.24	142	141.907663	
				143	142.909779	
				144*	143.910039	2.1×10^{15} yrs
				145	144.912538	
				146	145.913086	
				148	147.916869	
				150	149.920960	
61	Promethium	Pm		145*	144.912691	18 yrs
				146*	145.914632	1600 days
				147*	146.915108	2.6 yrs
62	Samarium	Sm	150.35	144	143.911989	
				146*	145.912992	1.2×10^{8} yrs
				147*	146.914867	1.08×10^{11} yrs
				148*	147.914791	1.2×10^{13} yrs
				149*	148.917180	4×10^{14} yrs
				150	149.917276	
				151*	150.919919	90 yrs
				152	151.919756	
				154	153.922282	
63	Europium	Eu	151.96	151	150.919838	
				152*	151.921749	12.4 yrs
				153	152.921242	
				154*	153.923053	16 yrs
				155*	154.922930	1.8 yrs
64	Gadolinium	Gd	157.25	148*	147.918101	85 yrs
				150*	149.918605	1.8×10^{6} yrs

Z	*Element*	*Symbol*	*Chemical atomic weight*	*A*	*Mass (u)*	$T_{1/2}$
				152*	151.919794	1.1 × 10^{14} yrs
				154	153.920929	
				155	154.922664	
				156	155.922175	
				157	156.924025	
				158	157.924178	
				160	159.927115	
65	Terbium	Tb	158.925	159	158.925351	
66	Dysprosium	Dy	162.50	156*	155.923930	1.2 × 10^3 yrs
				158	157.924449	
				160	159.925202	
				161	160.926945	
				162	161.926803	
				163	162.928755	
				164	163.929200	
67	Holmium	Ho	164.930	165	164.930421	
				166*	165.932289	1.2 × 10^3 yrs
68	Erbium	Er	167.26	162	161.928740	
				164	163.929287	
				166	165.930907	
				167	166.932060	
				168	167.932383	
				170	169.935560	
69	Thulium	Tm	168.934	169	168.934245	
				171*	170.936530	1.9 yrs
70	Ytterbium	Yb	173.04	168	167.934160	
				170	169.935020	
				171	170.936430	
				172	171.936360	
				173	172.938060	
				174	173.938740	
				176	175.942680	
				173*	172.938800	1.4 yrs
71	Lutetium	Lu	174.97	175	174.940640	
				176*	175.942660	2.2 × 10^{10} yrs
72	Hafnium	Hf	178.49	174*	173.940360	2.0 × 10^{15} yrs
				176	175.941570	
				177	176.943400	
				178	177.943880	
				179	178.946030	
				180	179.946820	
73	Tantalum	Ta	180.948	180	179.947544	
				181	180.948007	
74	Wolfram (Tungsten)	W	183.85	180	179.947000	
				182	181.948301	
				183	182.950324	
				184	183.951025	
				186	185.954440	

Z	*Element*	*Symbol*	*Chemical atomic weight*	*A*	*Mass* (*u*)	$T_{1/2}$
75	Rhenium	Re	186.2	185	184.953059	
				187*	186.955833	5×10^{10} yrs
76	Osmium	Os	190.2	184	183 952750	
				186	185.953870	
				187	186.955832	
				188	187.956081	
				189	188.958300	
				190	189.958630	
				192	191.961450	
				194*	193.965229	6.0 yrs
77	Iridium	Ir	192.2	191	190.960640	
				193	192.963012	
78	Platinum	Pt	195.09	190*	189.959950	7×10^{11} yrs
				192	191.961150	
				194	193.962725	
				195	194.964813	
				196	195.964967	
				198	197.967895	
79	Gold	Au	196.967	197	196.966541	
80	Mercury	Hg	200.59	196	195.965820	
				198	197.966756	
				199	198.968279	
				200	199.968327	
				201	200.970308	
				202	201.970642	
				204	203.973495	
81	Thallium	Tl	204.19	203	202.972353	
				204*	203.973865	3.75 yrs
				205	204.974442	
		Ra E″		206*	205.976104	4.3 min
		Ac C″		207*	206.977450	4.78 min
		Th C″		208*	207.982013	3.1 min
		Ra C″		210*	209.990054	1.3 min
82	Lead	Pb	207.19	202*	201.927997	3×10^5 yrs
				204*	203.973044	1.4×10^{17} yrs
				205*	204.974480	3×10^7 yrs
				206	205.974468	
				207	206.975903	
				208	207.976650	
		Ra D		210*	209.984187	22 yrs
		Ac B		211*	210.988742	36.1 min
		Th B		212*	211.991905	10.64 hrs
		Ra B		214*	213.999764	26.8 min
83	Bismuth	Bi	209.980	207*	206.978438	30 yrs
				208*	207.979731	3.7×10^5 yrs
				209	208.980394	
		Ra E		210*	209.984121	5.1 days

Element	*Symbol*	*Chemical atomic weight*	*A*	*Mass (u)*
	Th C		211*	210.987300
			212*	211.991876
	Ra C		214*	213.998686
			215*	215.001830
Polonium	Po		209*	208.982426
	Ra F′		210*	209.982876
	Ac C′		211*	210.986657
	Th C′		212*	211.989629
	Ra C′		214*	213.995201
	Ac A		215*	214.999423
	Th A		216*	216.001790
	Ra A		218*	218.008930
Astatine	At		215*	214.998663
			218*	218.008607
			219*	219.011290
Radon	Rn			
	An		219*	219.009481
	Tn		220*	220.011401
	Rn		222*	222.017531
Francium	Fr			
	Ac K		223*	223.019736
Radium	Ra	226.0		
	Ac X	232.08	223*	223.018501
	Th X		224*	224.020218
	Ra		226*	226.025360
	$MsTh_1$		228*	228.031139
Actinium	Ac		227*	227.027753
	$MsTh_2$		228*	228.031080
Thorium	Th	232.038		
	RdAc		227*	227.027706
	RdTh		228*	228.028750
			229*	229.031652
	Io		230*	230.033087
	UY		231*	231.036291
	Th		232*	232.038124
	UX_1	231.0359	234*	234.043583
Protoactinium	Pa	238.03	231*	231.035877
	UZ		234*	234.043298
Uranium	U		230*	230.033937
			231*	231.036264
			232*	232.037168
			233*	233.039522
			234*	234.040904
	Ac U		235*	235.043915
			236*	236.045637
	UI		238*	238.048608
Neptunium	Np	237.0480	235*	235.044049
			236*	236.046624

Z	*Element*	*Symbol*	*Chemical atomic weight*	*A*	*Mass* (u)	$T_{1/2}$
94	Plutonium	Pu	239.0522	237*	237.048056	2.14 × 10^6 yrs
				236*	236.046071	2.85 yrs
				238*	238.049511	89 yrs
				239*	239.052146	24360 yrs
				240*	240.053882	6700 yrs
				241*	241.056737	13 yrs
				242*	242.058725	3.79 × 10^5 yrs
				244*	244.064100	7.6 × 10^7 yrs

Appendix IV

The Concept of Cross-Section for a Nuclear Reaction

Consider a mono-energetic beam of particles incident on a target shown in Fig. (App. IV.1). Let the beam be uniform and contain n particles per unit volume moving with a velocity v, w.r.t. to the stationery target. Clearly the product nv gives number of particles crossing a unit area perpendicular to the beam per unit time. It defines the *flux* F of the particles in the incident beam.

$$F = nv.$$

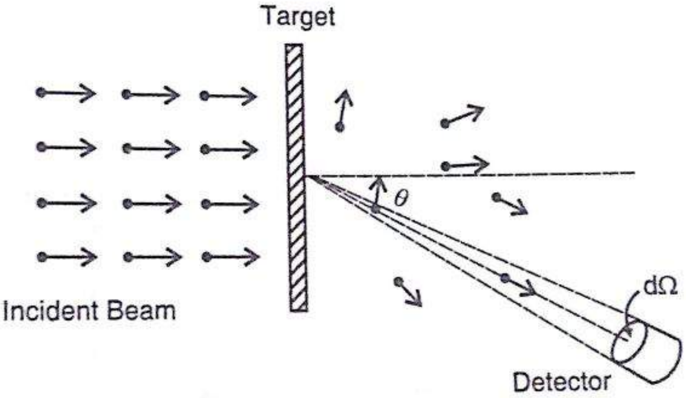

Fig. (App. IV. 1).

It is customary to normalise the number of particles to one particle per volume V.

$$\therefore \qquad n = \frac{1}{V}$$

The detector detects all particles scattered through an angle θ, into the solid angle $d\Omega$. Th number of particles $d\bar{\mathbf{N}}$ detected per unit time depends on the following factors:

(*i*) flux of incident beam, F

(*ii*) the solid angle $d\Omega$ and

(*iii*) the number of independent scattering centres in the target that are intercepted by t beam. Let these be **N**.

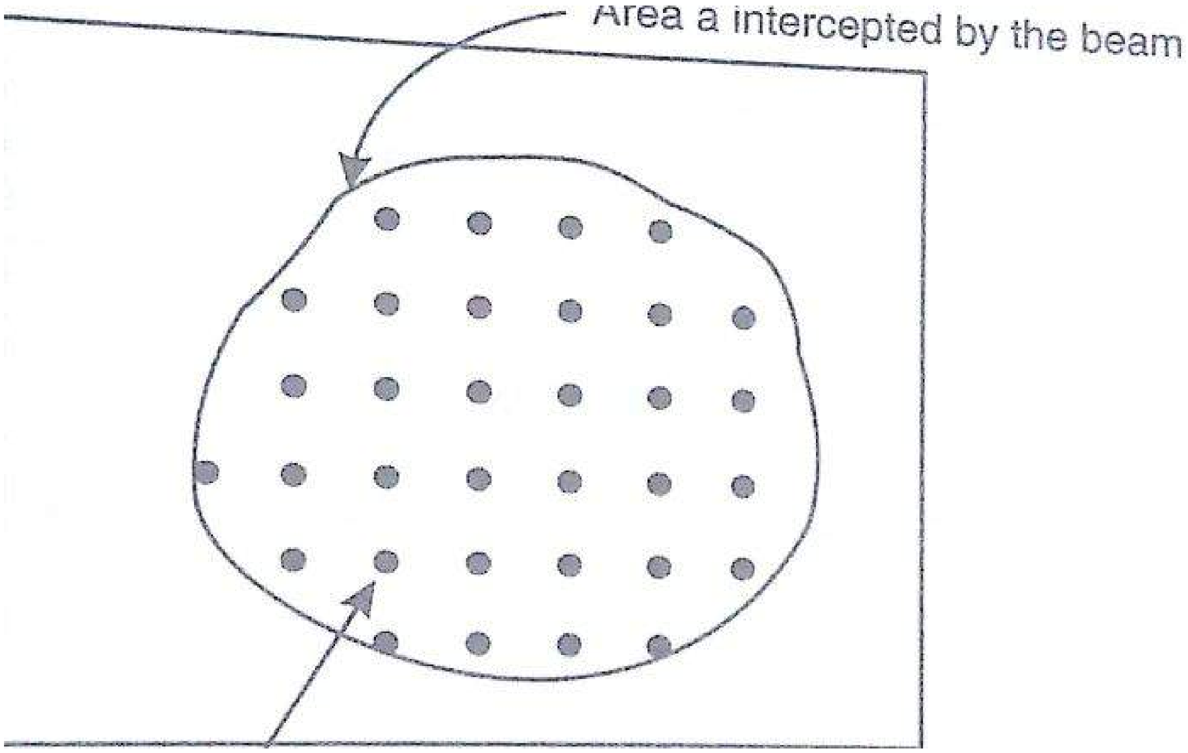
Area a intercepted by the beam

$$\bar{\mathbf{N}}_{\text{scattered}} = F\mathbf{N}\sigma_{\text{total}}$$

$$\therefore \qquad \frac{\bar{\mathbf{N}}_{\text{scattered}}}{\bar{\mathbf{N}}_{\text{incident}}} = \frac{\mathbf{N}\sigma_{\text{total}}}{a}$$

This expression is transparent. It implies that the fraction of particles scattered is equal to the effective fraction of total area occupied by the scattering centres. In other words, the total cross-section σ_{total} is equal to the *area effective in scattering for one scattering centre.*